

# **AIR SLIDE BASIC MODELLING**

by

Serena Carmen Valciu

A thesis submitted in partial fulfilment of the requirements for the  
award of the degree of Doctor of Philosophy

This research was carried out at The Wolfson Centre for Bulk  
Solids Handling Technology  
University of Greenwich

September 2015

## DECLARATION

I certify that this work has not been accepted in substance for any degree, and is not currently being submitted for any degree other than that of PhD being studied at the University of Greenwich. I also declare that this work is the result of my own investigations except where otherwise identified by references and that I have not plagiarised another's work.

---

Serena Carmen Valciu

PhD candidate

---

Prof. M. S. A. Bradley

Supervisor

---

Dr. R. Berry

Supervisor

---

Dr. A. Dyrøy

Supervisor

## **ACKNOWLEDGEMENTS**

I would like to express my gratitude to my supervisors and to the staff at Hydro, POSTEC and the Wolfson Centre for Bulk Solids Handling Technology without whom this project could not have been undertaken. No technical research programme such as this which involved several large measurements programmes test rig configurations and redesign would ever get far without the input and support of Are Dyrøy, Morten Karlsen and the contagious drive of Richard Farnish. Great thanks are extended to Caroline Chapman for her organizational skills and to my other supervisors for their help and encouragement.

My friend Prof. Bernt Lie at the Telemark University College, although not directly involved in this project was a great source of inspiration and mental support during the modelling work.

## **Air slide basic modelling**

### **SYNOPSIS**

This thesis addresses the evaluation, modification and modelling of a mass flow feeding silo, stand pipe and standard air slide system for use in handling and transporting alumina in the aluminium smelting industry. Stability and repeatability of gravitational flow rates from feeding silos and stand pipes (addressed as interfaces) is crucial from operational point of view and needs to be achieved before one can further estimate and model the flow of alumina and the capacity of an air slide. Although techniques for design of storage vessels (based on the flow characteristics of particulates) have been in the public domain since the 1960's, they have been slow to gain acceptance in the industry (due to a lack of awareness of their existence amongst engineers). The use of the stand pipe concept to increase flow rates during gravity discharge and to achieve stability of flow has been examined experimentally in a small rig at Tel-Tek department of POSTEC. The stand pipe should be integrated into the mechanical design of an air slide, because if the material cannot be delivered (discharged) properly from the feeding unit onto the air slide, there will be no stable conveying conditions. It has been found by Gu, Arnold and McLean (1993) that the stand pipe is efficient only if it is kept full of powder - the feeding silo acting more as a buffer for the stand pipe. Their concept was implemented in practice during the tests conducted at POSTEC by monitoring the weight of material in the stand pipe and the flow rates of alumina in real time by using LabView software and weighing cells. What makes the research work reported in this document unique is the integration of different mechanical and modelling concepts from different engineering fields (continuum and soil mechanics, fluid dynamics, rheology, cybernetics and powder technology).

Previous work undertaken by Haugland (1998) for Hydro focused the flow of alumina as a Newtonian fluid and was itself based on the modelling work of Woodcock (1978). Yet, besides their work, no accurate mathematical model has been developed which could be used to predict the velocity and mass flow rates of alumina flow and capacity of an air slide for a range of alumina qualities. Such a model would be extremely useful when designing new air slide systems, as the capacity of air slides could be predicted from the rheology of powder and the knowledge of bulk particulate characteristics.

Previous research, measurement campaigns and extensive literature studies, all point out that in terms of controlling discharge from gravity flow equipment (and after studying the transport behaviour of an air slide), it is often the gravity discharge approach that generates the greatest degree of variability, in terms of both consistency and repeatability. The root of the problem of inconsistent discharge rates has been identified to lie with the flow channel development within the feeding silo and/or the stand pipe (discharge head). The potential causes of flow irregularities are even more critical to be aware of, in the cases where mass flow principles are intended to be applied - especially in the case of highly segregable materials like alumina blends.

This thesis is aimed at developing a reliable means for predicting the average velocity of alumina flow and capacity and also to understand the mechanisms that govern the flow behaviour. To enable online estimation and further modelling of full-scale air slide capacity, a small-scale rig with adjustable length was built at POSTEC in 2012 and further modified in 2013. Air slide capacity (alumina flow rates) for different lengths of 3 m, 7 m and 15 m and inclination angles from 0 to 3.1 degrees of air slide were measured by using pressurized air in the range of 3 to 6.5 barg. Empirical models have been developed from test results as a first step. It was found based on empirical models that the velocity of alumina bed has a power law behaviour. However, these models would require the use of expensive and time-consuming air slide trials to determine the values of the power law coefficients for each alumina quality.

The degree of segregation when handling and transporting alumina has proven to be quite considerable, in terms of undesirable effects on the production process. This thesis was prompted by several measurement programmes of work undertaken for Hydro by the author with the aim of mapping the performance of volumetric feeders and the degree of segregation in a feeding air slide rig at The Reference Centre in Årdal. Sampling from feeders and chemical analysis of the samples have clearly shown the degree of segregation, especially when fluidizing and transporting binary mixtures of alumina and aluminium fluoride. Pressure measurement results showed pressure drops along the air supply tube, which also have been found to have an impact on segregation. Fluidization and shearing trials have been conducted both on alumina and binary mixtures in order to establish a benchmark procedure for powder characterisation that could be used as an operational support tool. Currently the minimum fluidization

velocity for all Hydro Aluminium plants is set to 2.0 cm/s, which is much higher than what it is actually needed to achieve an optimal fluidization.

There is a strong analogy with the flow of Newtonian or non – Newtonian fluids in an open channel that can be applied to the flow of fluidized alumina on an air slide. In this thesis, the hydrological non- Newtonian model developed from the general Saint-Venant model of open channel in a rectangular channel has been applied as a second step. Such theoretical mechanistic models, based on the mass and momentum balance with bottom friction along the powder bed, are numerically challenging to solve. The model requires use of rheometrical benchmark tests to determine the flow index coefficients for a specific quality of alumina for a given initial inlet bed depth and steady state estimated capacity. The use of an Ordinary Differential Equations (ODE) solver in MATLAB to predict the height and the velocity of alumina bed in an open channel seemed promising and showed similar trends when compared to the alumina bed results obtained from the air slide tests conducted at POSTEC. Results obtained so far indicate that a more detailed analysis needs to be conducted in order to find out how to ‘fine tune’ the model parameters to further improve the model fit to measurement data. Although more experimental data is needed, e.g. shear stress measurements and flow coefficients at different fluidization velocities and for different alumina qualities, the correlation between measurements and the model obtained so far confirmed that further investigation would be justified.

Thus, the effect of interfaces, the feeding silo and the stand pipe should be considered and included into further design approaches for mechanical equipment, by balancing headroom availability in pot rooms versus increase in transport capacity of bulk solids to optimize production.

## CONTENTS

<b>1</b>	<b>Introduction.....</b>	<b>1</b>
1.1	What is fluidization? .....	1
1.2	Aluminium production and relevance of the project to industry.....	3
1.3	Objectives of the project and approaches to study .....	5
1.4	Project preview.....	6
<b>2</b>	<b>Background concepts and literature review .....</b>	<b>9</b>
2.1	Review of early air slide studies: the steady uniform Newtonian approach .....	9
2.1.1	Woodcock and Mason.....	9
2.1.2	Model proposed by Keuncke (1965) (as cited by Haugland (1998)).....	14
2.1.3	Model proposed by Woodcock and Haugland .....	16
2.2	Formulation of the hypothesis: fluid like non- Newtonian behaviour of alumina ..	19
2.2.1	Theoretical concepts .....	19
2.2.2	Results and discussion small scale open channel viscometer experiments, non Newtonian approach.....	27
2.2.3	Savage and Oger (2013) - two part investigation study of air slides.....	31
2.3	Gupta et al.....	39
2.4	Discussion of flow regimes .....	40
2.5	Links between fluidization, rheological and reometry results .....	43
2.5.1	Saint Venant – shallow water equations.....	44
2.6	Concluding remarks .....	45
<b>3</b>	<b>Survey of powder flow behaviour .....</b>	<b>46</b>
3.1	Introduction.....	46
3.2	The electrolysis process .....	46
3.3	Feeding alumina and aluminium fluoride to the electrolysis cells .....	47
3.4	Motivation for this PhD .....	50
3.4.1	Programme of work on the alumina rig.....	53
3.4.2	Execution of the test programme .....	55
3.4.3	Series 1: test 1 to 6.....	57
3.4.4	Inventory of sample bags and weighing buckets - closed alumina refill valve... 60	
3.4.5	Series 1 test results: mass balance (buckets) based on dump weights versus bags/sample chemical analysis.....	61
3.4.6	Series 2 test results: mass balance (buckets) based on dump weights versus bags/sample chemical analysis.....	63
3.4.7	Test 13 .....	67
3.4.8	Test 13 – results .....	68
3.4.9	Performance of feeders.....	70
3.4.10	Summary of the verification programme on the alumina rig .....	74
3.5	Minimum fluidization velocity.....	75
3.5.1	The Geldard classification of powders.....	76
3.6	Powder characterisation .....	77
3.6.1	Fluidization of binary mixtures of alumina and fines.....	77
3.6.2	Test equipment.....	78
3.7	Test design - preparation of the test powders .....	80
3.8	Measuring powder flowability .....	82
3.8.1	Bulk flow property measurements .....	83
3.8.2	Sample preparation .....	86
3.8.3	Presentation of the results .....	86
3.9	Powder characterisation and segregation in an aluminium plant .....	89
3.10	Conclusions.....	91
<b>4</b>	<b>Silo outlet design and interfaces to an air slide .....</b>	<b>93</b>
4.1	Introduction.....	93
4.2	Air slide test rig 2012: scale up of feeder concept.....	94

4.2.1	Design of the test rig 2012 .....	95
4.2.2	Measurements .....	100
4.2.3	Test procedure.....	102
4.2.4	Observation of the flow .....	102
4.2.5	Experimental results and discussion .....	103
4.2.6	Cloth-iris-valve flow restriction and short stand pipe.....	105
<b>5</b>	<b>Modified and improved air slide test rig 2013 .....</b>	<b>108</b>
5.1	Preliminary silo outlet modelling .....	109
5.1.2	Data acquisition and analysis .....	124
5.2	Pressure drop in pipes.....	125
5.2.1	Verification of the pressure transducers .....	127
5.2.2	Pressure readings in a 3 m long air slide segment for all downward inclinations 130	
5.2.3	Bed heights and capacity tests in a 3 m long air slide segment.....	131
5.2.4	Pressure readings in a 7 m long air slide for all downward inclinations.....	135
5.2.5	Bed heights and capacity tests in a 7 m long air slide segment.....	137
5.2.6	Pressure readings in a 15 m long air slide for all downward inclinations .....	139
5.2.7	Bed heights and capacity tests in a 15 m long air slide segment .....	143
5.2.8	Conclusions .....	145
5.2.9	Further work: scale down to support feeder concept and design.....	146
<b>6</b>	<b>Empirical modelling .....</b>	<b>147</b>
6.1	Data analysis and building models .....	148
6.1.1	Criterion of fit and model .....	149
6.1.2	Model Validation.....	150
6.2	Effects of downward inclination angle, $\theta$ and dimensionless coefficient of velocity, <b><math>UOUm_f</math></b> on average bed velocity.....	152
6.2.1	3 m - effect of inclination angle, $\theta$ on average bed velocity at different distances away from inlet and at different dimensionless coefficient of velocity <b><math>UOUm_f</math></b> .....	156
6.2.2	3 m - Further investigation of the effect of power law exponent - bed velocity slope <b><math>K(\theta)</math></b> , versus distance from inlet at different <b><math>UOUm_f</math></b> .....	166
6.2.3	7 m long air slide segment .....	176
6.2.4	7 m - effect of inclination angle, $\theta$ on bed velocity at different distances away from inlet and at different dimensionless coefficient of velocity <b><math>UOUm_f</math></b> .....	176
6.2.5	7 m - bed velocity slope <b><math>K\theta</math></b> , versus distance from inlet at different <b><math>UOUm_f</math></b> .	191
6.2.6	15 m - effect of inclination angle, $\theta$ on bed velocity at different distances away from inlet and at different dimensionless coefficient of velocity <b><math>UOUm_f</math></b> .....	193
6.2.7	15 m - bed velocity slope <b><math>K\theta</math></b> , versus distance from inlet at different <b><math>UOUm_f</math></b>	207
6.3	Conclusions.....	210
<b>7</b>	<b>Mathematical modelling .....</b>	<b>212</b>
7.1	Solid flow for air slide systems .....	213
7.2	One dimensional Saint Venant model assumptions.....	214
7.2.1	Air slide powder flow model using Saint Venant .....	215
7.2.2	Flow resistance.....	221
7.2.3	Saint Venant steady state .....	224
7.2.4	Rheometrical experiments at share rate ramp- up.....	225
7.2.5	Boundary and initial conditions .....	229
7.3	MATLAB simulations .....	230
7.4	Simulation results .....	232
7.4.1	The effects of inclination angle and air velocity on resistance slope .....	233
7.4.2	The effects of inlet configuration on resistance slope .....	238
7.5	Conclusions.....	240
<b>8</b>	<b>CONCLUSIONS .....</b>	<b>242</b>
<b>9</b>	<b>FURTHER WORK .....</b>	<b>247</b>
	<b>REFERENCES .....</b>	<b>250</b>



<b>APPENDIX A 3 M AIR SLIDE CAPACITY TESTS .....</b>	<b>258</b>
<b>APPENDIX B 7 M AIR SLIDE CAPACITY TESTS .....</b>	<b>270</b>
<b>APPENDIX C 15 M AIR SLIDE CAPACITY TESTS .....</b>	<b>290</b>
<b>APPENDIX D VELOCITY CALCULATIONS .....</b>	<b>306</b>
<b>APPENDIX E DATA SHEETS .....</b>	<b>326</b>
<b>APPENDIX F ALUMINA RIG.....</b>	<b>347</b>
<b>APPENDIX G FURTHER WORK RHEOMETRY .....</b>	<b>388</b>

## List of Figures

Figure 1 ALSTOM Norway. Plant layout. ....	3
Figure 2 Experimental design: Scale – up: technology verification and scale – down: knowledge transfer. ....	6
Figure 3 Cement unloading test equipment used by CP Technologies, reprinted from Hilgraf (2011). Aerated silo and wedge shaped box placed between the slide gate valve and the inlet section of the short air slide conveyor. ....	13
Figure 4 Haugland (1998) Drag coefficient as a function of the hydraulic diameter. .	15
Figure 5 Haugland (1998). Results of tests conducted at 1°. Bed height profiles for different mass flow rates. ....	16
Figure 6 Haugland (1998). Method of estimating K1 and K2. ....	17
Figure 7 Haugland (1998). Results of tests conducted at 1° with one average value at different mass flow rates. ....	17
Figure 8 Haugland (1998). Results of tests conducted at 1°. Values from measurement points at positions 2 to 5 away from the inlet of the air slide at different mass flow rates. ....	18
Figure 9 Shear deformation of a fluid. ....	21
Figure 10 Rheograms for newtonian and Bingham plastic flows as described by Bingham. (Source: Wikipedia). ....	25
Figure 11 Botterill et al. (1971). Bauxilite rheograms. Torque vs. shear rate for fluidised 102 $\mu\text{m}$ Bauxilite in 140 mm diam. bed of 20 mm packed height. ....	28
Figure 12 Botterill et al. (1971). Bauxilite rheograms. Effect of channel width and depth on stress- strain relationship measured for fluidised 102 $\mu\text{m}$ Bauxilite, 3.5 x $U_{mf}$ . ....	29
Figure 13 Botterill and Besant (1973). Sand rheograms. Variation in shear stress/shear rate curves with channel width for 200 - $\mu\text{m}$ diameter sand. ....	30
Figure 14 Layout of flow system rig (reprinted from Savage and Oger (2013)). ....	32
Figure 15 Savage and Oger (2013). FlexPDE finite element predictions of power law, for n equal to 0.53 and 0.66, compared to the experimental data points of Boterill and Besant (1976). ....	33
Figure 16 Savage and Oger (2013). FlexPDE finite element predictions of velocity distribution based on a power law viscosity exponent n = 0.65. ....	34

Figure 17 Mass flow rates versus the bed inclination angle $\theta$ and three gate openings. .....	34
Figure 18 Flow depth versus $\theta$ and three gate openings; reprinted from Oger and Savage (2013). .....	35
Figure 19 Rheometry curves: Coulomb material versus Bingham fluid, when the material is subject to a simple shear experiment (Ancy (2007)). .....	41
Figure 20 Simplified diagram of Ancy (2007) flow regimes. ....	42
Figure 21 Lay out and the three levels of ADS (Karlsen (2002), Dyrøy (2006), Øystese (2015)). Two parallel rows of electrolysis pots. ....	48
Figure 22 Mechanical components of a feeding air slide, volumetric feeder and feeder interfaces. ....	51
Figure 23 a) Alumina rig: feeders 1 to 8 (diamond shaped), feeding air slide and feeding silos on the wall; the fluoride silo for the rig is not visible on the picture. ....	52
Figure 24 Illustration of the alumina rig: feeding silos, feeding air slide and volumetric feeders. ....	53
Figure 25 Knife valves on the outlets of the feeding silos for opening & closing alumina & fluoride supply to the feeding air slide and for manual sampling of fluoride.....	54
Figure 26 a) Simens Simatic Panel used for filling and level controls of the feeding silos supplying alumina and aluminium fluoride to the feeding air slide; b) Bench scale used for weighing the dumps from the feeders. ....	55
Figure 27 Displacements of buckets under each feeder, scales to measure the accumulated weights and weights of sample bags.....	57
Figure 28 Total powder weight used per cycle per test and series 1 average. Series 1: test 1 to 6, run with closed valve for alumina refill. ....	59
Figure 29 a) Test 4: inventory of sample bags, dump weights; b) Alumina and fluoride mass balance through the air slide. Feeders 1 - 4 got empty during cycle 7. ....	61
Figure 30 Test 4 a) Alumina and fluoride mass balance through the air slide. Mass increase above the average cycle. b) Test 4 results of chemical analysis. ....	63
Figure 31 Total powder weight used per cycle per test and series 2 average. Series 2: test 7 to 12, run with open valve for alumina refill.....	65
Figure 32 Test 9 Alumina and fluoride mass balance through the feeding air slide. .	65

Figure 33 Test 9 a) Alumina and fluoride mass distribution through the air slide. Mass increase above the average cycle. b) Test 9 results of chemical analysis. ....	66
Figure 34 Test 13 Alumina and fluoride mass balance through the feeding air slide. ....	69
Figure 35 Test 13 a) Alumina and fluoride mass distribution through the air slide. Mass increase above the average cycle. b) Test 9 results of chemical analysis. ....	70
Figure 36 Specific pressure drop vs. air velocity chart for alumina. ....	76
Figure 37 Fluidisation column rig (originally located at POSTEC). ....	78
Figure 38 Layout of the fluidization column. ....	80
Figure 39 Fluidization velocities of alumina and fluoride. ....	81
Figure 40 Brookfield Powder flow tester (PFT) and test components. a) PFT tester (reprinted from Brookfield's customer leaflet); b) PFT accessories. ....	84
Figure 41 Flow function test results with the Brookfield PFT– Alumina powder. Mohr stress circles for steady – state flow at different consolidation stresses. Steady – state yield locus is approximated by a straight line. ....	85
Figure 42 a) Bulk density results produced by the Flow Function test; b) Bulk density results produced by the Bulk Density test. ....	87
Figure 43 Flow function test results with the Brookfield PFT. Differences between the angles of effective and static internal friction as an indication of the degree of cohesiveness. Individual components and binary mixtures. ....	88
Figure 44 Pyrex wall friction test results for alumina: wall friction angle, $\phi_w$ as a function of the normal stress $\sigma_N$ . Data obtained from the Brookfield PFT. ....	89
Figure 45 Dyrøy (2006): Geldart's classification chart. Changes of alumina characteristics from A-powder [1] to C-powder [2]. ....	90
Figure 46 Dyrøy (2006): Air slide capacity for alumina when fines content and operational velocity increase. ....	91
Figure 47 Fluidized feeder layout. ....	94
Figure 48 a) Volumetric feeder and air slide, choked flow condition due to interfacing and dosing operation. b) Feeding silo, iris valve and air slide, free fall conditions (gravity discharge). ....	95
Figure 49 Plan of the alumina rig, batch wise operation. ....	96
Figure 50 Test rig layout. ....	98
Figure 51 Interface silo outlet/air slide inlet, a, c) front and b) side view. ....	99

Figure 52 Additional air exhaust system and cyclone for capturing of fines.....	100
Figure 53 a) Pressure controller, b) nozzle, air distribution through the bottom of the air slide. ....	100
Figure 54 Cross section of an air slide channel a) porous membranes membranes and b) flow visualization, dead zone, effect of unfluidized edge. ....	103
Figure 55 Variation of alumina mass flow rates with dimensionless air velocity factor at different air slide inclinations. ....	105
Figure 56 a) Outlet configuration of the initial rig built in 2012 cloth - iris valve and short standpipe; b) 2013 configuration: longstandpipe, 7 x D and flexible joint. ....	106
Figure 57 Vertical stand pipe. a) Equipment design at the Wolfson Centre (consultancy work) and b) modified silo outlet at POSTEC (2013). ....	108
Figure 58 “Mock-up” tests at the Wolfson Centre to verify Gu’s et al (1993) concepts. ....	110
Figure 59 Janssen efect for stress distribution in silos: a) stress distribution in the vertical section of a silo for different wall friction angles; b) The method of differential slices: stresses on a cylindrical element inside the standpipe ( a),b) re-printed from the Wolfson Centre short course presentation). ....	111
Figure 60 Janssen’s effect for a series of feeding silo diameters, from D = 200 mm down to D = 140 mm for lengths of standpipe from 0 up to 7 x D. ....	113
Figure 61 Final solution chosen for the modified rig 7.5 x D long standpipe; Janssen’s effect for a feeding silo diameter with D = 140 mm for lengths of standpipe from 0 up to 7.5 x D. ....	113
Figure 62 Modifications to the feeding silo outlet: a) Step 1: 2012: iris valve, short standpipe, D = 204 mm; Step 2: 2013: 7.5 D long standpipe, D = 140 mm. ....	114
Figure 63 a) Feeding silo outlet (2012); b) New design (2013). ....	115
Figure 64 Measurements of the downward angle of inclination at several points along the air slide. ....	116
Figure 65 a) Cutting pieces of air slide to make room for b) bed height measurements. ....	116
Figure 66 Schematic view of the alumina rig and signal sampling.....	118
Figure 67 Example of LabView instantaneous discharge rates used in the test result analysis. ....	119

Figure 68 Pre-weighing for calibration of beam cells.....	121
Figure 69 a) 3 x HBM model HLCB 1C3 shear beam load cells arrangement; b) Junction box electrical input to HBM Clip AE 301 and LabView. ....	122
Figure 70 a) HBM model HLCB 1C3 550 kg shear beam load cells; b) Wiring code for each load cell. Pictures are taken from the operational manual (see Appendix for details).....	122
Figure 71 a) Junction box and input signal to b) measuring amplifier, HBM Clip AE 301 and b) amplifier connections (operating voltage zero and supply-voltage are internally connected); terminal 5 of the Clip amplifier was grounded according to the operating manual.....	123
Figure 72 a) Control cabinet set up, “something new, something old” - hardware and input signals from transducers used to measure feeding silo and air slide capacities, flow rates and pressure drops; b) HBM RM 4220 amplifier attached to the support rails of the scales. ....	123
Figure 73 a) NI 9203 8 - channel AI Module; b) NI 9239 4 - channel AI Module; c) NI cDAQ 9174 chassis. ....	125
Figure 74 Wiring diagram.....	125
Figure 75 Moody and Princeton (1944) diagram. ....	127
Figure 76 a) “Pillow”nozzle - just below the stand dpipe outlet to accelerate flow for 3 seconds: 1.2 mm, PT0: 1.4 mm, PT1 - PT5: 1.6 mm nozzles; b) 3 - 4 m fluidization elements with one nozzle inlet/element.....	128
Figure 77 Arrangement of flowmeter, pressure controller, pressure transducers for calibration measurements; 1.4 and 1.6 mm nozzles used for air exit. ....	129
Figure 78 Test rig setup: scaffolding, feeding silo, stand pipe/control box, 3m air slide segment.....	130
Figure 79 a) Bed heights measurements; b) Air slide capacity, 100% capacity.....	132
Figure 80 a) Bed heights measurements; b) Air slide capacity, 25 % capacity.....	134
Figure 81 Test rig setup: scaffolding, feeding silo, stand pipe/controlbox, 3 + 4 m air slide segment. ....	136
Figure 82 a) Bed heights measurements, b) Air slide 100% capacity.....	137
Figure 83 a) Print screen of LabView showing pressure drop from 4.96 to 4.05 in a 15 m long air slide segment. Complete set of data given in the tables above; b) Gain in	

weight (receiving bin) and loss in weight (feeding silo) in kg; c) Air slide and feeding silo capacity in t/hr. ....	140
Figure 84 Different set up configuration of P0 to investigate the pressure drop: a) initial configuration PT0 placed beneath an elbow and the air supply tube, b) PT0 moved above the tube, no elbow, c) PT0 moved above an elbow, aT and the tube.....	140
Figure 85 a) FluidSim model of an air slide; b) Comparison of measured and simulated values using FluidSim (Øystese (2015)). ....	142
Figure 86 a) Bed heights measurements; b) Air slide 100% capacity.....	143
Figure 87 a) Bed heights measurements; b) Air slide capacity, 25 % capacity.....	144
Figure 88 a) Feeding silo, standpipe and air slide, free fall conditions (gravity discharge);.....	146
Figure 89 The empirical modeling loop. ....	148
Figure 90 Linear trend lines fitted to experimental data in: a) 3 m; b) 7 m; c) 15 m long air slide segment. Bed velocity based on measurements of bed height at last point in each of the segments. ....	151
Figure 91 Linear trend lines fitted to experimental data at 1.6 downward inclination in: a) 3 m b) 15 m long air slide segment. ....	152
Figure 93 Power law trend lines fitted to experimental data in a: a) 3 m; b) 7 m; c) 15 m long air slide segment. Bed velocity based on measurements of bed height at last point in each of the segments. ....	153
Figure 93 Exponential law trend lines fitted to experimental data in a: a) 3 m; b) 7 m; c) 15 m long air slide segment. Bed velocity based on measurements of bed height at last point in the segment. ....	154
Figure 94 Power law trend lines fitted to the experimental data of average bed velocity as a function of angle of inclination, $\theta = 0..30$ at different $U0Umf = 0.99 \dots 2.14$ . ....	158
Figure 95 Investigation of the effect of changing power law exponent, $P\theta$ for $U0Umf = 0.99$ and $U0Umf = 2.14$ . Ten percent error bars showing the goodness of the mathematical method for all ranges of $U0Umf$ from 0.99 to 2.14.....	165
Figure 96 Values of $R^2$ expressing the goodnes of the fit when using Avg $P\theta$ instead of $P\theta$ into the power trend lines fitted to experimental data. ....	166
Figure 97 a) Exponential and b) power law trend lines fitted to the slope of average bed velocity as a function of angle of inclination, $\theta = 0..3.10$ , $K(\theta)$ , versus distance from inlet, at different $U0Umf = 0.99 \dots 2.14$ . ....	168

Figure 98 Power law trend lines fitted to experimental data for different air slide segments: a) 3 m, b) 7 m, c) 15 m. ....	171
Figure 99 Exponential law trend lines fitted to experimental data for different air slide segments: a) 3 m, b) 7 m, c) 15 m. ....	172
Figure 100 Comparison of $R^2$ values for exponential and power law equations for a) 3 m, b) 7 m and c) 15 m long air slide segments.....	173
Figure 101 Full capacity bed heights profiles in a) 3 m, b) 7 m, c) 15 m long air slide segment.....	175
Figure 102 Power law trend lines fitted to experimental data of average bed velocity as a function of angle of inclination, $\theta = 0.3, 1, 0$ at different $U_0/U_{mf} = 0.99 \dots 2.14$ . ....	181
Figure 103 Investigation of the effect of changing power law exponent, $P_\theta$ for $U_0/U_{mf} = 0.99$ and $U_0/U_{mf} = 2.14$ . Ten percent error bars showing the goodness of the mathematical method for all ranges of $U_0/U_{mf}$ from 0.99 to 2.14.....	190
Figure 104 Values of $R^2$ expressing the goodness of the fit when using $AvgP_\theta$ instead of $P_\theta$ into the power trend lines fitted to experimental data. ....	191
Figure 105 a) Exponential and b) power law trend lines fitted to the slope of average bed velocity as a function of angle of inclination, $\theta = 0.3, 1, 0$ , $K(\theta)$ , versus distance from inlet, at different $U_0/U_{mf} = 0.99 \dots 2.14$ . ....	193
Figure 106 Power law trend lines fitted to experimental data of average bed velocity as a function of angle of inclination, $\theta = 0.1, 0.6, 0$ at different $U_0/U_{mf} = 0.99 \dots 1.97$ . ....	198
Figure 107 Investigation of the effect of changing power law exponent, $P_\theta$ for $U_0/U_{mf} = 0.99$ and $U_0/U_{mf} = 2.14$ . Ten percent error bars showing the goodness of the mathematical method for all ranges of $U_0/U_{mf}$ from 0.99 to 2.14.....	205
Figure 108 Values of $R^2$ expressing the goodness of the fit when using $AvgP_\theta$ instead of $P_\theta$ into the power law trend lines fitted to the experimental data. ....	206
Figure 109 a) Exponential and b) power law trend lines fitted to the slope of average bed velocity as a function of angle of inclination, $\theta = 0.1, 0.6, 0$ , $K(\theta)$ , versus distance from inlet, at different $U_0/U_{mf} = 0.99 \dots 1.97$ . ....	208
Figure 110 Comparison of $K_\theta$ and $AvgP_\theta$ for different segments of air slide lengths: 3 m, 7 m, 15 m representing different flow regimes: acceleration and steady state...	209
Figure 111 Bruni (2004). Alumina rheogram and calculated values for the Herschel-Bulkley model parameters. ....	226



Figure 112 Fluidization column and Brookfield reometer to study the behaviour of alumina.....	227
Figure 113 Alumina rheogram. Test 1 Power law model results.....	227
Figure 114 Alumina rheogram. Raw data Test 1.....	228
Figure 115 Alumina rheogram. Test 2 Power law model results.....	228
Figure 116 Alumina rheogram. Test 3 Power law model results.....	228
Figure 117 Diagram of the model implemented in MATLAB.....	230
Figure 118 Flow profiles at 4 bar: a) Bed height measurements compared to model results; b) Velocity measurements compared to model results. Model parameters: $K = 1.35$ , $n = 0.51$ , $\theta = 1.10$ , $\tau_y = 12.5e-3$ , $h_0 = 0.111m$ , $Q_0 = 0.0062m^3s$ .....	231
Figure 119 Flow profiles at 4 bar. Spline function to interpolate the average of three measurements (red) and model results (blue). Model parameters: $K = 1.35$ , $n = 0.51$ , $\theta = 1.10$ , $\tau_y = 12.5e-3$ , $h_0 = 0.111m$ , $Q_0 = 0.0062m^3s$ . a) Bed heights, b) average velocity profiles. ....	231
Figure 120 Bed heights profiles a) no gate b) gate.....	232
Figure 121 Simulation results for $\theta = 1.1$ and $1.6$ degrees, measured versus predicted. Left: 10- 13% pressure drop, right: pressure drop adjusted.....	237
Figure 122 Values of $R^2$ expressing the goodnes of the fit for the power law models. ....	238
Figure 123 Simulation results for $\theta = 1.1$ and $1.6$ degrees, measured versus predicted, gate and no restriction gate. ....	240
Figure 124 System capacity: 3 m – 2. 6 degrees – 2. 5 bar .....	258
Figure 125 System capacity: 3 m – 2.6 degrees – 3.0 bar .....	259
Figure 126 System capacity: 3 m – 2.6 degrees – 3.5 bar .....	260
Figure 127 System capacity: 3 m – 2.6 degrees – 4.0 bar .....	260
Figure 128 System capacity: 3 m – 2.6 degrees – 4.5 bar .....	261
Figure 129 System capacity: 3 m – 2.6 degrees – 5.0 bar .....	262
Figure 130 System capacity: 3 m – 2.6 degrees – 5.5 bar .....	263
Figure 131 System capacity: 3 m – 2.6 degrees – 6.0 bar .....	264
Figure 132 System capacity: 3 m – 2.6 degrees – 6.5 bar .....	265
Figure 133 System capacity: 3 m – 3.1 degrees – 2.5 bar .....	266

Figure 134 System capacity: 3 m – 3.1 degrees – 3.0 bar .....	266
Figure 135 System capacity: 3 m – 3.1 degrees – 3.5 bar .....	266
Figure 136 System capacity: 3 m – 3.1 degrees – 4.0 bar .....	267
Figure 137 System capacity: 3 m – 3.1 degrees – 4.5 bar .....	267
Figure 138 System capacity: 3 m – 3.1 degrees – 5.0 bar .....	267
Figure 139 System capacity: 3 m – 3.1 degrees – 5.5 bar .....	267
Figure 140 System capacity: 3 m – 3.1 degrees – 6.0 bar .....	268
Figure 141 System capacity: 3 m – 3.1 degrees – 6.5 bar .....	268
Figure 142 System capacity: 3 m – 0.6 degrees – 3.0 bar .....	268
Figure 143 System capacity: 3 m – 0.6 degrees – 3.5 bar .....	268
Figure 144 System capacity: 3 m – 0.6 degrees – 4.0 bar .....	269
Figure 145 System capacity: 3 m – 0.6 degrees – 4.5 bar .....	269
Figure 146 System capacity: 7 m – 0.0 degrees – 2.5 bar .....	271
Figure 147 System capacity: 7 m – 0.0 degrees – 3.0 bar .....	271
Figure 148 System capacity: 7 m – 0.0 degrees – 3.5 bar .....	271
Figure 149 System capacity: 7 m – 0.0 degrees – 4.5 bar .....	271
Figure 150 System capacity: 7 m – 0.0 degrees – 5.0 bar .....	272
Figure 151 System capacity: 7 m – 0.0 degrees – 5.5 bar .....	272
Figure 152 System capacity: 7 m – 0.0 degrees – 6.0 bar .....	272
Figure 153 System capacity: 7 m – 0.0 degrees – 6.5 bar .....	272
Figure 154 System capacity: 7 m – 0.6 degrees – 2.5 bar .....	273
Figure 155 System capacity: 7 m – 0.6 degrees – 3.0 bar .....	273
Figure 156 System capacity: 7 m – 0.6 degrees – 3.5 bar .....	273
Figure 157 System capacity: 7 m – 0.6 degrees – 4.0 bar .....	273
Figure 158 System capacity: 7 m – 0.6 degrees – 4.5 bar .....	274
Figure 159 System capacity: 7 m – 0.6 degrees – 5.0 bar .....	274
Figure 160 System capacity: 7 m – 0.6 degrees – 5.5 bar .....	274
Figure 161 System capacity: 7 m – 0.6 degrees – 6.0 bar .....	274
Figure 162 System capacity: 7 m – 0.6 degrees – 6.5 bar .....	275

Figure 163 System capacity: 7 m – 1.1 degrees – 2.5 bar .....	275
Figure 164 System capacity: 7 m – 1.1 degrees – 3.0 bar .....	275
Figure 165 System capacity: 7 m – 1.1 degrees – 3.5 bar .....	275
Figure 166 System capacity: 7 m – 1.1 degrees – 4.0 bar .....	276
Figure 167 System capacity: 7 m – 1.1 degrees – 4.5 bar .....	276
Figure 168 System capacity: 7 m – 1.1 degrees – 5.0 bar .....	276
Figure 169 System capacity: 7 m – 1.1 degrees – 5.5 bar .....	276
Figure 170 System capacity: 7 m – 1.1 degrees – 6.0 bar .....	277
Figure 171 System capacity: 7 m – 1.1 degrees – 6.5 bar .....	277
Figure 172 System capacity: 7 m – 1.6 degrees – 2.5 bar .....	277
Figure 173 System capacity: 7 m – 1.6 degrees – 3.0 bar .....	277
Figure 174 System capacity: 7 m – 1.6 degrees – 3.5 bar .....	278
Figure 175 System capacity: 7 m – 1.6 degrees – 4.0 bar .....	278
Figure 176 System capacity: 7 m – 1.6 degrees – 4.5 bar .....	278
Figure 177 System capacity: 7 m – 1.6 degrees – 5.0 bar .....	278
Figure 178 System capacity: 7 m – 1.6 degrees – 5.5 bar .....	279
Figure 179 System capacity: 7 m – 1.6 degrees – 6.0 bar .....	279
Figure 180 System capacity: 7 m – 1.6 degrees – 6.5 bar .....	279
Figure 181 System capacity: 7 m – 2.1 degrees – 2.5 bar .....	280
Figure 182 System capacity: 7 m – 2.1 degrees – 3.0 bar .....	280
Figure 183 System capacity: 7 m – 2.1 degrees – 3.5 bar .....	281
Figure 184 System capacity: 7 m – 2.1 degrees – 4.0 bar .....	281
Figure 185 System capacity: 7 m – 2.1 degrees – 4.5 bar .....	281
Figure 186 System capacity: 7 m – 2.1 degrees – 5.0 bar .....	281
Figure 187 System capacity: 7 m – 2.1 degrees – 5.5 bar .....	282
Figure 188 System capacity: 7 m – 2.1 degrees – 6.0 bar .....	282
Figure 189 System capacity: 7 m – 2.1 degrees – 6.5 bar .....	282
Figure 190 System capacity: 7 m – 2.6 degrees – 2.5 bar .....	283
Figure 191 System capacity: 7 m – 2.6 degrees – 3.0 bar .....	284

Figure 192 System capacity: 7 m – 2.6 degrees – 3.5 bar .....	284
Figure 193 System capacity: 7 m – 2.6 degrees – 4.0 bar .....	284
Figure 194 System capacity: 7 m – 2.6 degrees – 4.5 bar .....	285
Figure 195 System capacity: 7 m – 2.6 degrees – 5.0 bar .....	286
Figure 196 System capacity: 7 m – 2.6 degrees – 5.5 bar .....	286
Figure 197 System capacity: 7 m – 2.6 degrees – 6.0 bar .....	286
Figure 198 System capacity: 7 m – 2.6 degrees – 6.5 bar .....	286
Figure 199 System capacity: 7 m – 3.1 degrees – 2.5 bar .....	287
Figure 200 System capacity: 7 m – 3.1 degrees – 3.0 bar .....	287
Figure 201 System capacity: 7 m – 3.1 degrees – 3.5 bar .....	287
Figure 202 System capacity: 7 m – 3.1 degrees – 4.0 bar .....	287
Figure 203 System capacity: 7 m – 3.1 degrees – 4.5 bar .....	288
Figure 204 System capacity: 7 m – 3.1 degrees – 5.0 bar .....	289
Figure 205 System capacity: 7 m – 3.1 degrees – 5.5 bar .....	289
Figure 206 System capacity: 7 m – 3.1 degrees – 6.0 bar .....	289
Figure 207 System capacity: 7 m – 3.1 degrees – 6.5 bar .....	289
Figure 208 System capacity: 15 m – 0.0 degrees – 3.5 bar .....	290
Figure 209 System capacity: 15 m – 0.0 degrees – 4.0 bar .....	290
Figure 210 System capacity: 15 m – 0.0 degrees – 5.0 bar .....	290
Figure 211 System capacity: 15 m – 0.0 degrees – 5.5 bar .....	290
Figure 212 System capacity: 15 m – 0.0 degrees – 6.0 bar .....	291
Figure 213 System capacity: 15 m – 0.6 degrees – 3.0 bar .....	291
Figure 214 System capacity: 15 m – 0.6 degrees – 3.5 bar .....	291
Figure 215 System capacity: 15 m – 0.6 degrees – 4.0 bar .....	291
Figure 216 System capacity: 15 m – 0.6 degrees – 4.5 bar .....	292
Figure 217 System capacity: 15 m – 0.6 degrees – 5.0 bar .....	293
Figure 218 System capacity: 15 m – 0.6 degrees – 5.5 bar .....	293
Figure 219 System capacity: 15 m – 0.6 degrees – 6.0 bar .....	293
Figure 220 System capacity: 15 m – 1.1 degrees – 3.0 bar .....	293

Figure 221 System capacity: 15 m – 1.1 degrees – 3.5 bar .....	293
Figure 222 System capacity: 15 m – 1.1 degrees – 4.0 bar .....	294
Figure 223 System capacity: 15 m – 1.1 degrees – 4.5 bar .....	294
Figure 224 System capacity: 15 m – 1.1 degrees – 5.0 bar .....	294
Figure 225 System capacity: 15 m – 1.1 degrees – 5.5 bar .....	294
Figure 226 System capacity: 15 m – 1.1 degrees – 6.0 bar .....	295
Figure 227 System capacity: 15 m – 1.6 degrees – 3.0 bar .....	295
Figure 228 System capacity: 15 m – 1.6 degrees – 3.5 bar .....	295
Figure 229 System capacity: 15 m – 1.6 degrees – 4.0 bar .....	295
Figure 230 System capacity: 15 m – 1.6 degrees – 4.5 bar .....	296
Figure 231 System capacity: 15 m – 1.6 degrees – 5.0 bar .....	296
Figure 232 System capacity: 15 m – 1.6 degrees – 5.5 bar .....	296
Figure 233 System capacity: 15 m – 1.6 degrees – 6.0 bar .....	296
Figure 234 System capacity: 15 m – 0.0 degrees – 4.5 bar .....	297
Figure 235 System capacity: 15 m – 0.0 degrees – 5.0 bar .....	297
Figure 236 System capacity: 15 m – 0.0 degrees – 5.5 bar .....	297
Figure 237 System capacity: 15 m – 0.0 degrees – 6.0 bar .....	297
Figure 238 System capacity: 15 m – 0.6 degrees – 3.5 bar .....	298
Figure 239 System capacity: 15 m – 0.6 degrees – 4.0 bar .....	298
Figure 240 System capacity: 15 m – 0.6 degrees – 4.5 bar .....	298
Figure 241 System capacity: 15 m – 0.6 degrees – 5.0 bar .....	298
Figure 242 System capacity: 15 m – 0.6 degrees – 5.5 bar .....	299
Figure 243 System capacity: 15 m – 0.6 degrees – 6.0 bar .....	299
Figure 244 System capacity: 15 m – 1.1 degrees – 3.0 bar .....	299
Figure 245 System capacity: 15 m – 1.1 degrees – 3.5 bar .....	299
Figure 246 System capacity: 15 m – 1.1 degrees – 4.0 bar .....	300
Figure 247 System capacity: 15 m – 1.1 degrees – 4.5 bar .....	300
Figure 248 System capacity: 15 m – 1.1 degrees – 5.0 bar .....	300
Figure 249 System capacity: 15 m – 1.1 degrees – 5.5 bar .....	300

Figure 250 System capacity: 15 m – 1.1 degrees – 6.0 bar .....	301
Figure 251 System capacity: 15 m – 1.6 degrees – 3.0 bar .....	301
Figure 252 System capacity: 15 m – 1.6 degrees – 3.5 bar .....	301
Figure 253 System capacity: 15 m – 1.6 degrees – 4.0 bar .....	301
Figure 254 System capacity: 15 m – 1.6 degrees – 4.5 bar .....	302
Figure 255 System capacity: 15 m – 1.6 degrees – 5.0 bar .....	302
Figure 256 System capacity: 15 m – 1.6 degrees – 5.5 bar .....	302
Figure 257 System capacity: 15 m – 1.6 degrees – 6.0 bar .....	302
Figure 262 Power law models of average bed velocity as a function of $U/U_{mf} = 0.99 \dots 2.14$ at different angles of inclination, $\theta = 0.3, 10$ .....	310
Figure 263 Exponential and power law models fitted to the slope of average bed velocity as a function of $U/U_{mf} = 0.99 \dots 2.14$ , $K(U/U_{mf})$ , versus distance from inlet, at different angles of inclination, $\theta = 0.3, 10$ .....	312
Figure 264 Power law models of average bed velocity as a function of $U/U_{mf} = 0.99 \dots 2.14$ at different angles of inclination, $\theta = 0.3, 10$ .....	317
Figure 265 Exponential and power law models fitted to the slope of average bed velocity as a function of $U/U_{mf} = 0.99 \dots 2.14$ , $K(U/U_{mf})$ , versus distance from inlet, at different angles of inclination, $\theta = 0.3, 10$ .....	319
Figure 262 Power law models of average bed velocity as a function of $U/U_{mf} = 0.99 \dots 1.97$ at different angles of inclination, $\theta = 0.1, 60$ .....	323
Figure 263 Exponential and power law models fitted to the slope of average bed velocity as a function of $U/U_{mf} = 0.99 \dots 1.97$ , $K(U/U_{mf})$ , versus distance from inlet, at different angles of inclination, $\theta = 0.1, 60$ .....	324
Figure 264 a) Fluidization elements; b) Flow regimes in converging - diverging nozzles based on M number.....	325
Figure 265 Test 1: Samples inventory.....	349
Figure 266 Test 2: Samples inventory.....	351
Figure 267 Test 3: Samples inventory.....	353
Figure 268 Test 4: Samples inventory.....	356
Figure 269 Test 5: Sample inventory .....	360
Figure 270 Test 6: Sample inventory .....	363

Figure 271 Alumina and fluoride distribution from feeder 1 to 8. ....	367
Figure 272 Alumina and fluoride distribution from feeder 1 to 8. ....	371
Figure 273 Alumina and fluoride distribution from feeder 1 to 8. ....	375
Figure 274 Alumina and fluoride distribution from feeder 1 to 8. ....	379
Figure 275 Alumina and fluoride distribution from feeder 1 to 8. ....	383
Figure 276 Alumina and fluoride distribution from feeder 1 to 8. ....	387
Figure 277 Position of the spindle a) bottom - middle of the column b) bottom – wall. .....	388
Figure 278 Middle of the column measurements with two spindle lengths: 330 and 180 mm. ....	390
Figure 279 At the wall of the column measurements with two spindle lengths: 330 and 180 mm. ....	390

## List of Tables

Table 1 Total powder weight [kg] used per test. Mass balance series 1, test 1 to 6, closed valve for alumina refill. ....	58
Table 2 Alumina and fluoride total mass balance per cycle per test [kg], series 1 test 1 to 6. Closed valve for alumina refill. Tests 3 and 6 empty feeding air slide during cycle 6. ....	60
Table 3 Total powder weight used per test. Mass balance series 2, test 7 to 12, opened valve for alumina refill. ....	64
Table 4 Alumina and fluoride total mass balance per cycle per test [kg], series 2 test 7 to 12. Open valve for alumina refill. ....	64
Table 5 Feeder data. Cycle 1, only alumina in the feeding air slide. ....	71
Table 6 Test 9. Feeder data, accumulated dump weights [g]. Cycles 2 - 4, alumina and fluoride in the feeding air slide. ....	73
Table 7 Characteristic values of $Al_2O_3$ and $AlF_3$ . ....	81
Table 8 Dimensions of the air slide. ....	98
Table 9 Capacity and coefficients of variation for different segments of air slide at 1.1 degrees downward inclination. ....	119
Table 10 Pressure ramp up using 1.4 and 1.6 mm nozzles for air exit. ....	129
Table 11 Pressure loss tests conducted with and without alumina in the air slide. .	130
Table 12 Capacity tests: air slide and feeding silo based on 100% capacity, from 2.5 to 6.5 bar pressure, for downward inclinations from 0 to 1.1°. ....	132
Table 13 Capacity tests: air slide and feeding silo based on 100% capacity, from 2.5 to 6.5 bar pressure, for downward inclinations from 1.6 to 2.1°. ....	133
Table 14 Capacity tests: air slide and feeding silo based on 100% capacity, from 2.5 to 6.5 bar pressure, for downward inclinations from 2.6 to 3.1°. ....	133
Table 15 Capacity tests: air slide and feeding silo based on 25 % capacity, from 2, 5 to 6, 5 bar pressure, for downward inclinations from 0 to 1,1°. ....	135
Table 16 Capacity tests: air slide and feeding silo based on 25 % capacity, from 2, 5 to 6, 5 bar pressure, for downward inclinations from 1,6 to 2,1°. ....	135
Table 17 Pressure loss tests conducted without alumina in the air slide. ....	136
Table 18 Pressure loss tests conducted with alumina in the air slide. ....	137



Table 19 Capacity tests: air slide and feeding silo based on 100 % capacity, from 2.5 to 6.5 bar pressure, for downward inclinations from 0 to 1.1°.	138
Table 20 Capacity tests: air slide and feeding silo based on 100 % capacity, from 2.5 to 6.5 bar pressure, for downward inclinations from 1.6 to 2.1°.	138
Table 21 Capacity tests: air slide and feeding silo based on 100 % capacity, from 2.5 to 6.5 bar pressure, for downward inclinations from 2.6 to 3.1°.	138
Table 22 Pressure loss tests conducted without alumina in the air slide.	139
Table 23 Pressure loss tests conducted with alumina in the air slide.	139
Table 24 Capacity tests: air slide and feeding silo based on 100 % capacity, from 2.5 to 6.0 bar pressure, for downward inclinations from 0 to 0.6°.	143
Table 25 Capacity tests: air slide and feeding silo based on 100 % filling degree, from 2, 5 to 6, 0 bar pressure, for downward inclinations from 1, 1 to 1,6°.	144
Table 26 Capacity tests: air slide and feeding silo based on 25 % capacity, from 2.5 to 6.0 bar pressure, for downward inclinations from 0 to 0.6°.	144
Table 27 Capacity tests: air slide and feeding silo based on 25 % capacity, from 2.5 to 6.0 bar pressure, for downward inclinations from 1.1 to 1.6°.	145
Table 28 Power law trend lines fitted to experimental data for average bed velocity at all angles of inclination, $\theta$ , at different $U_{0Umf}$ for each measurement point from 0.5 to 2.5 m. $K(\theta)$ is the coefficient and $P\theta$ is the exponent of power law.	159
Table 29 Results of power law trend lines fitted to the experimental data by using single average power exponent, $AvgP\theta$ , a summary of Table 28.	167
Table 30 Power law trend lines fitted to experimental data for average bed velocity at all angles of inclination, $\theta$ , at different $U_{0Umf}$ for each measurement point from 0.5 to 5.5 m. $K(\theta)$ is the coefficient and $P\theta$ is the exponent of power law.	182
Table 31 Results of power law trend lines fitted to the experimental data by using single average power exponent, $AvgP\theta$ , a summary of Table 30.	192
Table 32 Power law trend lines fitted to experimental data for average bed velocity at all angles of inclination, $\theta$ , at different $U_{0Umf}$ for each measurement point from 0.5 to 12.6 m. $K(\theta)$ is the coefficient and $P\theta$ is the exponent of power law.	198
Table 33 Results of power law trend lines fitted to the experimental data by using single average power exponent, $AvgP\theta$ , a summary of Table 32.	207

Table 34 Flow resistance - open channel approach models (Naef et al. (2006) updated)	221
Table 35 Lengths of acceleration zones as a function of $U_0/U_{mf}$ and $\theta$ and calibration values of $\tau_y$	237
Table 36 Summary of Figure 124: power law equations for 1.1 and 1.6 degrees downward inclination at $U_0/U_{mf} = 1.31 \dots 1.97$	238
Table 37 Capacity, 3 m air slide segment, no gate	303
Table 38 Velocity calculations ( $U_0/U_{mf}$ ), 3 m air slide, 0.5 m from inlet	306
Table 39 Velocity calculations ( $U_0/U_{mf}$ ), 3 m air slide, 1.0 m from inlet	306
Table 40 Velocity calculations ( $U_0/U_{mf}$ ), 3 m air slide, 1.5 m from inlet	306
Table 41 Velocity calculations ( $U_0/U_{mf}$ ), 3 m air slide, 2.0 m from inlet	307
Table 42 Velocity calculations ( $U_0/U_{mf}$ ), 3 m air slide, 2.5 m from inlet	307
Table 43 Velocity calculations, 3 m air slide, 0.5 m from inlet	307
Table 44 Velocity calculations, 3 m air slide, 1.0 m from inlet	308
Table 45 Velocity calculations, 3 m air slide, 1.5 m from inlet	308
Table 46 Velocity calculations, 3 m air slide, 2.0 m from inlet	308
Table 47 Velocity calculations, 3 m air slide, 2.5 m from inlet	308
Table 48 3 m air slide, bed velocity slopes	310
Table 49 Bed velocity slope coefficients	311
Table 50 Velocity calculations ( $U_0/U_{mf}$ ), 7 m air slide, 0.5 m from inlet	312
Table 51 Velocity calculations ( $U_0/U_{mf}$ ), 7 m air slide, 1.0 m from inlet	312
Table 52 Velocity calculations ( $U_0/U_{mf}$ ), 7 m air slide, 1.5 m from inlet	312
Table 53 Velocity calculations ( $U_0/U_{mf}$ ), 7 m air slide, 2.0 m from inlet	312
Table 54 Velocity calculations ( $U_0/U_{mf}$ ), 7 m air slide, 2.5 m from inlet	313
Table 55 Velocity calculations ( $U_0/U_{mf}$ ), 7 m air slide, 3.0 m from inlet	313
Table 56 Velocity calculations ( $U_0/U_{mf}$ ), 7 m air slide, 3.5 m from inlet	313
Table 57 Velocity calculations ( $U_0/U_{mf}$ ), 7 m air slide, 4.0 m from inlet	314
Table 58 Velocity calculations ( $U_0/U_{mf}$ ), 7 m air slide, 4.5 m from inlet	314
Table 59 Velocity calculations ( $U_0/U_{mf}$ ), 7 m air slide, 5.0 m from inlet	314
Table 60 Velocity calculations ( $U_0/U_{mf}$ ), 7 m air slide, 5.5 m from inlet	315

Table 61 Bed velocity slopes, 7 m. ....	318
Table 62 Velocity calculations, 7 m air slide, 0.5 m from inlet.....	319
Table 63 Velocity calculations, 7 m air slide, 1.0 m from inlet.....	319
Table 64 Velocity calculations, 7 m air slide, 1.5 m from inlet.....	319
Table 65 Velocity calculations, 7 m air slide, 2.0 m from inlet.....	319
Table 66 Velocity calculations, 7 m air slide, 2.5 m from inlet.....	320
Table 67 Velocity calculations, 7 m air slide, 3.0 m from inlet.....	320
Table 68 Velocity calculations, 7 m air slide, 3.5 m from inlet.....	320
Table 69 Velocity calculations, 7 m air slide, 4.0 m from inlet.....	320
Table 70 Velocity calculations, 7 m air slide, 4.5 m from inlet.....	321
Table 71 Velocity calculations, 7 m air slide, 5.0 m from inlet.....	321
Table 72 15 m air slide,bedvelocity slope. ....	323
Table 73 Data Sheet HMB RM4220.....	326
Table 74 HBM HLC data sheet .....	328
Table 75 HLMB Certificate of Approval .....	334
Table 76 Technical information flow measuring system .....	343
Table 77 Test 1: Closed valve for refilling of alumina from the silo, cycle 1 not weighted, Alumina and fluoride dump weights: [grams] / feeder / cycle. Cycle 1 only alumina, cycle 2 to 7 alumina mixed with fluoride.....	347
Table 78 Test 1: Closed valve for refilling of alumina from the silo, cycle 1 not weighted, estimated to 145 kg (same as cycle 2). Alumina and fluoride mass balance: [kg] / feeder / cycle. ....	348
Table 79 Test 1: Alumina and fluoride total mass balance: 1074 [kg] material used / test.....	348
Table 80 Test 2: Closed valve for refilling of alumina from the silo. Alumina and fluoride accumulated dump weights: [grams] / feeder / cycle. Cycle 1 only alumina, cycle 2 to 7 alumina mixed with fluoride.....	350
Table 81 Test 2: Closed valve for refilling of alumina from the silo. Alumina and fluoride mass balance: [kg] / feeder / cycle.....	350
Table 82 Test 2: Alumina and fluoride total mass balance: 1089 [kg] material used / test.....	351

Table 83 Test 3: Closed valve for refilling of alumina from the silo. Alumina and fluoride accumulated and individual dump weights: [grams] / feeder / cycle. Cycle 1 only alumina, cycle 2 to 6 alumina mixed with fluoride.....	351
Table 84 Test 3: Closed valve for refilling of alumina from the silo. Alumina and fluoride mass balance: [kg] / feeder / cycle. ....	353
Table 85 Test 3: Alumina and fluoride total mass balance: 914 [kg] material used / test. ....	353
Table 86 Test 4: Closed valve for refilling of alumina from the silo. Alumina and fluoride accumulated and individual dump weights: [grams] / feeder / cycle. Cycle 1 only alumina, cycle 2 to 6 alumina mixed with fluoride.....	354
Table 87 Test 4: Closed valve for refilling of alumina from the silo. Alumina and fluoride mass balance: [kg] / feeder / cycle. ....	356
Table 88 Test 4: Alumina and fluoride total mass balance: 1082 [kg] material used / test.....	356
Table 89 Test 4 Average alumina and fluoride [kg/feeder/cycle] .....	357
Table 90 Test 4 Method of calculation. Cycle 1, only alumina is considered the 0 line on the X axis. ....	357
Table 91 Test 5: Closed valve for refilling of alumina from the silo. Alumina and fluoride accumulated and individual dump weights: [grams] / feeder / cycle. Cycle 1 only alumina, cycle 2 to 6 alumina mixed with fluoride.....	357
Table 92 Test 5: Closed valve for refilling of alumina from the silo. Alumina and fluoride mass balance: [kg] / feeder / cycle. ....	360
Table 93 Test 5: Test 5: Alumina and fluoride total mass balance: 1076 [kg] material used / test. ....	360
Table 94 Test 6: Closed valve for refilling of alumina from the silo. Alumina and fluoride accumulated and individual dump weights: [grams] / feeder / cycle. Cycle 1 only alumina, cycle 2 to 5 alumina mixed with fluoride.....	361
Table 95 Test 6: Closed valve for refilling of alumina from the silo. Alumina and fluoride mass balance: [kg] / feeder / cycle. ....	362
Table 96 Test 6: Alumina and fluoride total mass balance: 879 [kg] material used / test. ....	363
Table 97 Test 7: Open valve for refilling of alumina from the silo. Alumina and fluoride mass balance: [kg] / feeder / cycle. ....	364

Table 98 Test 7: Open valve for refilling of alumina from the silo. Alumina and fluoride accumulated and individual dump weights: [grams] / feeder / cycle. Cycle 1 only alumina, cycle 2 to 8 alumina mixed with fluoride.....	364
Table 99 Test 8: Open valve for refilling of alumina from the silo. Alumina and fluoride mass balance: [kg] / feeder / cycle. ....	367
Table 100 Test 8: Open valve for refilling of alumina from the silo. Alumina and fluoride accumulated and individual dump weights: [grams] / feeder / cycle. Cycle 1 only alumina, cycle 2 to 8 alumina mixed with fluoride.....	368
Table 101 Test 9: Open valve for refilling of alumina from the silo. Alumina and fluoride mass balance: [kg] / feeder / cycle. ....	371
Table 102 Test 9: Open valve for refilling of alumina from the silo. Alumina and fluoride accumulated and individual dump weights: [grams] / feeder / cycle. Cycle 1 only alumina, cycle 2 to 8 alumina mixed with fluoride.....	372
Table 103 Test 10: Open valve for refilling of alumina from the silo. Alumina and fluoride mass balance: [kg] / feeder / cycle. ....	375
Table 104 Test 10: Open valve for refilling of alumina from the silo. Alumina and fluoride accumulated and individual dump weights: [grams] / feeder / cycle. Cycle 1 only alumina, cycle 2 to 8 alumina mixed with fluoride. ....	376
Table 105 Test 11: Open valve for refilling of alumina from the silo. Alumina and fluoride mass balance: [kg] / feeder / cycle. ....	379
Table 106 Test 11: Open valve for refilling of alumina from the silo. Alumina and fluoride accumulated and individual dump weights: [grams] / feeder / cycle. Cycle 1 only alumina, cycle 2 to 8 alumina mixed with fluoride. ....	380
Table 107 Test 12: Open valve for refilling of alumina from the silo. Alumina and fluoride mass balance: [kg] / feeder / cycle. ....	383
Table 108 Test 12: Open valve for refilling of alumina from the silo. Alumina and fluoride accumulated and individual dump weights: [grams] / feeder / cycle. Cycle 1 only alumina, cycle 2 to 8 alumina mixed with fluoride. ....	384

## Nomenclature

$h$	Height of the bed [m]
$b$	Width of the channel in general and of the air slide [m]
$\alpha$	Inclination of the channel [degrees]
$\rho$	Fluid density [kg/m <sup>3</sup> ]
$g$	Gravitational acceleration 9.81 [m/s <sup>2</sup> ]
$\tau_w$	Average shear stress at the side walls [Pa]
$\tau_b$	Average shear stress at the bottom walls [Pa]
$u_{av}$	Average solids flow velocity [m/s]
$U_0$	Operational velocity air slide [cm/s]
$U_{mf}$	Minimum fluidization velocity [cm/s]
$\delta l$	Elemental section length [m]
$Q$	Flow rate [m <sup>3</sup> /s]
$\lambda_F$	Drag coefficient
$P_{wett}$	The wetted perimeter [m]
$K1, K2$	Experimental constants used by Haugland (1998)
$\mu$	Fluid viscosity [Pa.s]
$\frac{\mu}{\rho}$	Kinematic viscosity [m <sup>2</sup> /s]
$\tau$	Shear stress [Pa]
$\dot{\gamma}$	Shear rate (strain) [reciprocal seconds]
$\tau_c$	Bingham yield stress [Pa]

$k$	Consistency coefficient (flow index) [Pa.s <sup>n</sup> ] (
$n$	Fluid consistency index (shear rate exponent) [-]
Re	Reynold number
$L$	Characteristic linear dimension (travelled length of the fluid)
$D$	Pipe diameter (circular geometry) [m]
$D_H$	Hydraulic diameter (rectangular channel) [m]
$R_H$	Hydraulic radius (rectangular channel) [m]
$P$	Pressure [Pa]
$F$	Force [N]
$F_b$	Body force [N]
$F_f$	Frictional force [N]
$F_p$	Pressure force [N]
$f_D$	Darcy frictional factor [-]
$h_f$	Frictional head loss [m]
$S_f$	Frictional slope
$t$	Time [s]
$x$	Distance [m]
$\beta$	Momentum correction coefficient [-]

### Operators

$\Delta$	Increment
$\Sigma$	Summation

$\frac{\partial}{\partial}$  Partial derivative

$\int$  Integral



## **1 Introduction**

This thesis will continue the work of Dyrøy (2006) carried out on the development, evaluation and modelling of an anti-segregation system “AS- System” for use in large silos handling alumina in the aluminium industry. An anti-segregation tube was designed at Tel-Tek’s Department of Powder Science and Technology (POSTEC). The design was based on theory for pressure drop in pneumatic conveying and a non-linear model called Solid Surface Body Drag Model (SSBDM) was developed and verified against measurements from a test rig. This work will take Dyrøy’s (2006) work one step forward, further downstream for the AS system, focusing on the effect of interfaces (feeding silo and stand pipe) and challenges when fluidizing and transporting alumina in an air slide. The work of Farnish (2006) on stand pipes (referred in his work as “dispensing head”) was of great inspiration and was used as support and basis for the mechanical modifications undertaken on the air slide rig at POSTEC during this project. Within the context of this thesis the term “stand pipe” refers to a circular pipe attached at the outlet of a gravity discharge feeding silo, used to control and regulate the flow of alumina into an air slide.

### **1.1 What is fluidization?**

Fluidization is the operation by which solid particles are transformed into a fluid like state through suspension in a gas or liquid (Kuni and Levenspiel (1991)). In the aluminium industry, as in many other industries, pressurised air at a certain velocity, 2.0 cm/s is introduced by nozzles through the bottom of kilometres long air slide networks. The air flows upwards, passes through elements of fixed lengths assembled together, each element consisting of a porous membrane and a nozzle and which when in contact with the bed of alumina particles facilitates bed expansion and flow.

Interfaces such as an alumina feeding silo and stand pipe discharging alumina to the air slide need to be included into the modelling work in order to understand their relationship with, and their impact upon, the operational stability and reliability of an air slide.

The primary factor influencing fluidized bed transport is airflow. There are different stages and regimes of fluidization in an alumina bed, depending on the upward velocity of air (exiting the nozzle relative to the surface of the membrane to be activated) used for operating a network of air slides. If the upward velocity of air, equally distributed

throughout the area of the membrane, is low, the gas will merely be distributed through the void spaces between stationary alumina particles. This is a fixed/packed bed situation where the alumina bed still behaves as a static bulk solid. This packed bed condition can occur in the control box, right above the discharge from the feeding silo, through a standpipe, where the gravity forces and hydrostatic pressure (Janssen effect from the stand pipe, to be explained in further chapters) are dominant. An upward air velocity (higher than the minimum fluidization velocity,  $U_{mf}$ ) is needed to overcome frictional forces between alumina particles. This is achieved in daily operations by briefly activating a much smaller nozzle called “pillow”, with a diameter of 1.2 mm thus providing a locally higher air velocity than the 2 cm/s used in the rest of the air slide. The multitude of interactions between the solid alumina particles will then induce an internal pressure that may generate an increase of the mean free distance between the solid particles that will result in a reduction of the frictional resistance between them (Pudasaini and Hutter (2007)). At still higher velocity (within the area delimited by the control box), lower than that provided by the pillow, but higher than the rest of the network, a point is reached where the alumina particles become buoyant in the upward flowing air. This condition defines the onset of fluidisation, when the frictional force between alumina particles and air is counterbalancing the weight of the particles, the vertical compressive force between adjacent particles disappears and the pressure drop balances the net downward forces (gravity minus buoyancy forces) on the alumina bed. The bed is considered to be just fluidized and is referred to as an alumina bed at **minimum fluidization velocity**. The alumina is fed and transported from the control box into the air slide under both the effect of gravity discharge from the stand pipe pushing the alumina forward, pillow effect to activate the flow, and further transported inside the air slide at flow rates above minimum fluidization velocity. An increase in air flow rate above minimum fluidization velocity will result in a smooth expansion of the bed. Such a bed is called **homogenously fluidized bed, or smoothly fluidized bed** (Kuni and Levenspiel (1991)). At even higher flow rates, the bed will not expand more beyond its expansion at minimum fluidization velocity (instead bubbling and agitation can be observed) at which point the bed is referred to as a **bubbling bed**. When the bed of alumina is fluidised at sufficiently high air flow rates, the terminal velocity of alumina particles will be exceeded, and instead of bubbles, clusters of solid alumina particles or voids of gas will be observed. This known as a turbulent **fluidized bed**. The

solid alumina particles will be carried out of the bed with the gas through the venting pipes placed along the air slide network. In this state the bubbling bed has been transformed into a **pneumatic transport of solids** mode, an extreme situation that should be controlled and avoided as much as possible in operations.

## 1.2 Aluminium production and relevance of the project to industry

In the aluminium industry, as in many other process industries, one of the main goals is to manufacture the end product, aluminium metal, at lowest possible costs energy wise, while satisfying and maintaining product quality performance when it comes to raw materials (e.g.: alumina). Results from previous measurement campaigns from The Reference Centre in Årdal showed how changes in alumina quality (e.g. increase in amount of fines) quickly affect the capacity of the feeding air slide and point out the need for better understanding of the fluidized rheology of the powders, flow regimes and transport behaviour. While determining and testing air slide systems, it became clear that interfaces ( e.g. the outlet of a feeding silo discharging onto the control box attached to the inlet of an air slide) also have a great influence on the design of the transport system.

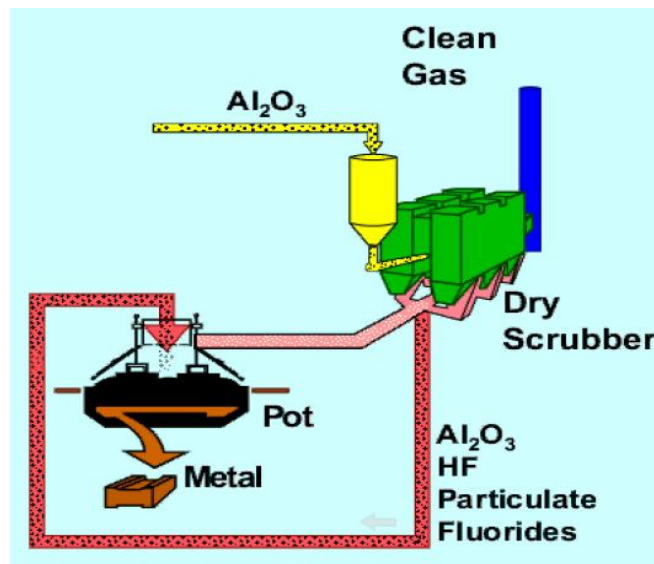


Figure 1 ALSTOM Norway. Plant layout.

Approximately two tonnes of alumina are needed in order to produce one tonne of aluminium. Thus, the storage silos have to supply alumina at a rate of almost twice (1.93 times) the aluminium production. Hydro Aluminium uses air slides for transport

of alumina over short to long distances (kilometres), for the production of aluminium. Their length depends very much on the powder handling equipment they are connected to. In modern smelters air slides are used to convey the primary alumina internally from the main silo to the day bins (buffer silos). Downstream from the main primary alumina storage silos there are the fume treatment plants as shown in Figure 1, where both primary and secondary alumina (recycled, which previously had reacted with the exhaust gas from the pots, hydrogen fluoride (HF) and particulate fluoride) are used in the transport loop, up to six to seven times. The recycled alumina is then transported to the secondary alumina silo and from there conveyed to the potrooms and the electrolysis pots. During the process of making aluminium (which will not be explained here), both secondary alumina  $\text{Al}_2\text{O}_3$  and aluminium fluoride  $\text{AlF}_3$  (in small quantities) are fed to the pot. Each pot has its own  $\text{Al}_2\text{O}_3$  and  $\text{AlF}_3$  feeding silos. The interface, or the end point, between the kilometres long transport air slides and the electrolysis pots where the alumina is melted, consists of a feeding air slide with multiple discharge outlets (alumina and fluoride feeders, pre-set to feed the binary mixture batch wise to the pot, continuously during the pot's life cycle). Capacity and powder quality go hand in hand with the mechanical design of the air slide, the design of the feeders and the robustness of the control system. Ideally, changes in the alumina quality should immediately be picked up by the online measurement equipment, sent to and corrected for by the control system, based on a general powder model incorporated into the control system. Thus the control system should be prepared to make the adequate corrections for each alumina quality. Such a general powder model does not currently exist. When a new alumina quality is to be distributed through the system, manual measurements are taken by the operators by opening the hoods on the pots and directly taking dump weight measurements from the feeders. The results are then communicated to the control group who then make manually adjustments to the control system. Direct rheometrical experiments in an operating air slide to capture changes in powder quality are not easy to perform in a full scale plant; so other ways of interpreting alumina flow behaviour and differentiating between the different flow regimes are needed. One way is interpreting the traces of past events (e.g. shape and heights of the alumina bed when there is no air on in the air slide, frozen bed) or controlled small-scale experiments using weigh scales and pressure sensors ( thus making it possible to draw analogies with idealized materials).

### **1.3 Objectives of the project and approaches to study**

Objectives of the project were specified as follow:

- To develop a characterisation technique to observe the behaviour of powder under air fluidised conditions in an air slide;
- To produce an economic, robust and easy to verify mathematical model to help with further optimizing of air slide design or the more economical operation of air slides.

The model should be able to predict following parameters for air slide conveyors:

- aeration requirements;
- transport capacity;
- flow velocities;

Figure 2 shows how the work in this thesis was thought, organized and conducted. Previous tests conducted in Årdal as part of a technology verification programme on existing feeder technology built up the motivation for this project. In this project, the initial approach to study the behaviour of alumina flow was to replicate and scale - up an alumina feeder and transport system (based on existing technology) and install it in the form of an air slide rig at POSTEC. A study of feeder operation and performance was initially not an integral element of this thesis. However, it became clear after analysing the results from the first round of air slide capacity tests conducted at POSTEC in 2012 (indicated as Step 1 in Figure 2), that in order to achieve the initial objectives of the project “Air slide basic modelling”, one should include the impact that air slide interfaces: e.g. feeders and feeders outlet design have on the capacity of an air slide. Initial test results conducted in 2012 showed a high instability of flow rates of alumina and clearly indicated that the original design of the rig was not optimal. The design of the feeding silo outlet was modified (as shown in Step 2: 2013 in Figure 2) and a stand pipe was attached to the system and new tests were conducted with satisfactory results.

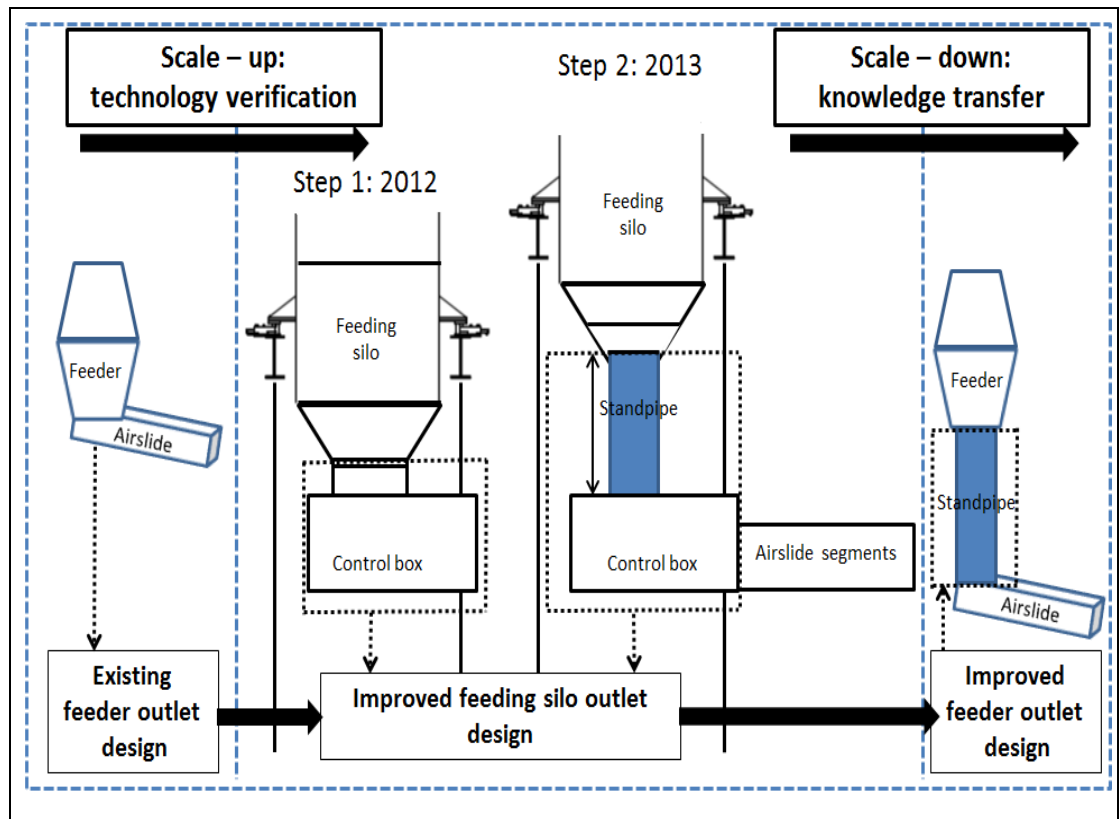


Figure 2 Experimental design: Scale – up: technology verification and scale – down: knowledge transfer.

The concepts and scale- up, scale down phases applied to the experimental design, as shown in Figure 2, will be explained chapter wise in the next section. The results from this project are planned to be used further in Hydro Aluminium as knowledge transfer and further modelling work on existing and new feeder systems.

#### 1.4 Project preview

Chapter 2 gives a review of background concepts and available literature relevant for air slide modelling. There is no equipment resemblance or standard method for modelling alumina flow in an air slide other than the measurements and analysis of Haugland (1998), Oger and Savage (2013) and Savage and Oger (2013). The measurement and analysis methods used by Haugland (1998) and Oger and Savage (2013) and Saint Venant shallow water equations used together with Jin and Fread (1997) flow resistance term have been selected as a starting point for the modelling work in this thesis.

Chapter 3 starts with a basic overview of the aluminium production. Then it describes the various stages of powder characterisation methods conducted in this research

project, focusing on the key parameters in air slide and feeder operation, in order to give the reader a better understanding of the factors considered to affect equipment operation. The development of powder characterization methods were aimed at finding a pragmatic approach to be used in modelling the alumina flow inside the standpipe and air slide. One of the objectives of this project was to better understand the behaviour of alumina under fluidized conditions. Alumina and binary mixtures of alumina and aluminium fluoride at different concentrations were tested in a fluidization column in order to find out the minimum fluidization velocity,  $U_{mf}$ . This parameter will be used together with the operational air velocity of the air slide rig,  $U_0$  calculated (as explained in Chapter 4) using nozzle isentropic conditions and area of the air slide membrane in Chapters 4 and 5. The ratio between operational and minimum fluidization velocity,  $U_0/U_{mf}$  will be used as input for the empirical model in Chapter 6. The existing feeder outlet design operation and performance analysis, as part of a technology verification programme, will provide the reader with the background for understanding the reason for the scale - up phase and for further improvements described in Chapter 4 and 5.

Chapter 4 describes what in Figure 2 is referred to as Step 1: 2012. The initial approach to study the behaviour of alumina flow was to replicate an alumina handling and transport system and install it in the form of an air slide rig at POSTEC. Trials were undertaken to quantify the repeatability of discharges. Through literature surveys and analysing the high variation in the test results it became clear that the mechanical design chosen for the rig (i.e. short standpipe equipped with an iris valve) was the bottleneck in achieving stability of discharges and operation.

Chapter 5 describes what in Figure 2 as referred to as Step 2: 2013. The mechanical modifications implemented were aimed at modifying the flow patterns generated from the air slide interface and extending through the feeding silo. By using a longer stand pipe combined with monitoring the loss in weight of the feeding silo an acceptable stability of discharges was finally established. The stand pipe was found to be efficient only if it was kept full of powder (the feeding silo acting more as a buffer for the stand pipe). This can be achieved in practice by monitoring the weight of material in the stand pipe and the flow rates of alumina on line.

Chapter 6 presents the experimental results of the different tests undertaken at different operational parameters. It also presents the empirical model based on a power law.

Chapter 7 describes the mathematical model used to model air slide capacity based on experience from Chapter 6. This project also investigated some other areas related to alumina flow in air slides such as acceleration zones and steady state flow. Tests performed using air slide segments of different lengths showed that there is a minimum length of air slide required immediately after the stand pipe, in order to get steady state flow. This research considered these length effects in a systematic manner with respect to changes in air flow rates and angle of downward inclination for 3, 7 and 15 m long air slide segments. The average powder bed velocity modelled by using Saint Venant model follows a power law behaviour, similar to the empirical model.

Chapter 8 presents the conclusions from this project and this project's contribution to knowledge. Based upon the lessons learned during this part of the project, it has been established that the stand pipe should be integrated into the mechanical design of an air slide, because if the material cannot be delivered (discharged at stable capacity rates with low coefficients of variation) properly from the feeding unit, there can be no stable conveying. Scale-up: technology verification phase. The development of the silo outlet was not only focused on improving an existing system, as part of technology verification and implementing the new design: e.g. stand pipe and powder lock concept back to existing feeders, but also tried to establish a basic understanding of the mechanisms governing the alumina flow behaviour. The knowledge transfer will be made by proposing a mathematical model which can be applied to a holistic diagnosis of the system.

Chapter 9 proposes recommendations for further work in order to advance the outcomes produced from this investigation.



## **2 Background concepts and literature review**

Fluidized bed gravity conveying is variously known as air assisted gravity conveying or air slide conveying, where gravity is the driving force. Originally designed and used for the transport of cement, many other types of particulate materials are now handled by air slides: coal, fly ash, plastic, metal powders, washing powders, sand and alumina. One of the objectives of this project was to understand the flow behaviour of alumina in an air slide and determine how it could be modelled mathematically. The approach to reach this objective is to establish a basic understanding by reviewing previous work undertaken on air slides and then build on the basic understanding using new knowledge obtained from experimental work. Thirty-nine years have elapsed since Woodcock & Mason (1976) wrote “Fluidized bed conveying - Art or Science?”. The design and dimensioning of air assisted gravity conveyors still remains empirically based. In this time a great deal of literature has been published, concerned with fluidization, flow properties and rheological behaviour of fluidized particulate materials. Several other investigations of air slides, presenting both experiments and models were undertaken four decades ago. Results of Newtonian and non-Newtonian approaches from flow of fluidized particulate solids using an analogy with the flow of fluids in pipes and open channels have been originally reported by Siemes and Hellmer (1962), Keunecke (1965), Botterill and his co-workers, Woodcock and Mason (1976), Latkovik and Levy (1991), Haugland (1998) and many others. Recently the early work of Botterill et al. (1970), (1971), Botterill and der Kolk (1971), Botterill and Bessant (1973), (1976), Botterill and Abdul Halim (1978), (1979), Singh et al. (1978) has been cited extensively by Savage and Oger (2013) and by Gupta et al. (2006), (2009) and (2010) in their study of air slides.

### **2.1 Review of early air slide studies: the steady uniform Newtonian approach**

#### **2.1.1 Woodcock and Mason**

Woodcock and Mason (1976) performed fluidized particulate measurements on a test rig developed in the Powder Handling Laboratory at Thames Polytechnic. Woodcock applied fluidized rheometry observations from stationary beds to air slides in order to predict the flowability of a powder. The relationships between the powder mass flow rate, conveyor’s inclination, velocity of the fluidizing air and the depth of the flowing

bed were investigated in his PhD work. Thus, based on knowledge of the density and particle size distribution of the powder to be used, an estimate of the minimum fluidization velocity could be made.

The conveying channel was 6 m long and 10 cm wide and could be adjusted for inclination between 0 and 12 degrees, having a porous distributor base of 'Vyon' type. The particulate material used for the experiments was 'Corvic', a p.v.c powder (a high molecular weight of homopolymer of vinyl chloride) having a mean particle diameter of 140  $\mu\text{m}$  and a density of approximately 1.4 kg/m<sup>3</sup>. The bulk density was 500 kg/m<sup>3</sup> and the fluidizing velocity measured in a small rig was found to be about 2.3 cm/s for this material. Air supply to the upper (feeding) and lower (receiving) hoppers and to the conveying channel was supplied by a Roots type blower, the flow rate was indicated by rotameters. The return of the powder to the upper level hopper was provided by an Entecon "Floveyor". A series of preliminary tests were then run to establish a basic understanding of the flow behaviour. It was found that at any given inclination angle there was an optimum airflow rate for conveying. Any reduction in air supply below this optimal value would result in a rapid thickening of the fluidized bed, where the powder flow would become erratic and then cease. Any increase beyond the critical value for the air supply would not give an advantage and resulted in unnecessary energy consumption. The cases where the inclination was 5 up to 7 degrees seemed to be most appropriate for conveying the pvc. They also found that the average bed depth increased with increasing mass flow rate of the material, but that the relationship was not linear. The authors documented the challenges they faced during the measurement programme. It was found after the first test runs that powder flow was time-dependent. An examination of the powder indicated an increasing significance of the inter-particle forces, associated, according to the authors with electro-static charging of the particles during transport through the test rig. The most obvious effect was a reduction in the free-flow behaviour of the material, having an impact on the nature of the flow in the conveying channel. After fifteen to twenty consecutive test runs, the results gave good repeatability. But, if the material was left undisturbed over a period of several days, and the tests were repeated, then again they showed a wide variation in measurements.

Woodcock and Mason (1978) proposed a flow model based on a momentum balance on an elemental section assuming a steady uniform flow in an inclined channel to calculate the flow rate  $Q$ .

$$(2\tau_w h + \tau_b b)\delta l - \rho g h b \delta l \sin \alpha = 0$$

Equation 1

Rearranged as in

Equation 2:

$$h = \frac{b \tau_b}{\rho g b \sin \alpha - 2\tau_w}$$

Equation 2

Where the variables are defined as:

- $h$  Height of the bed
- $b$  Width of the channel
- $\alpha$  Inclination of the channel
- $\rho$  Fluid density
- $g$  Gravitational acceleration
- $\tau_w$  Average shear stress at the side walls
- $\tau_b$  Average shear stress at the bottom walls
- $u_{av}$  Average solids flow velocity
- $\delta l$  Elemental section length
- $Q$  Flow rate

Extra they considered:

$$\tau_w = k_w u_{av} = k_w \left( \frac{Q}{bh} \right)$$

Equation 3

$$\tau_b = k_b u_{av} = k_b \left( \frac{Q}{bh} \right)$$

Equation 4

for the following cases:

1. Constant shear stress at the channel base and wall shear stress proportional to  $u_s$ ,  $Q$  becomes:

$$Q = \frac{\rho^3 g b^2 h \sin \alpha}{2k_w} - \frac{\rho^2 b 2\tau_b}{2k_w} \quad \text{Equation 5}$$

For  $\tau_b = 0$  (total slip at the channel base)

$$Q = \frac{\rho^3 g b^2 h \sin \alpha}{2k_w} \quad \text{Equation 6}$$

2. Shear stresses at sidewalls and the channel base proportional to  $u_s$ .

$$Q = \frac{\rho^3 g b^2 h^2 \sin \alpha}{(2k_w h + k_b b)} \quad \text{Equation 7}$$

3. Constant shear stress at sidewalls and shear stress at base proportional to  $u_s$ .

$$Q = (\rho^2 g b \sin \alpha - 2\rho\tau_w) \frac{h^2}{\rho k_b} \quad \text{Equation 8}$$

Haugland (1998), a PhD candidate registered at the University of Greenwich and TelTek/Postec and previous Norsk Hydro employee, also conducted some research on the flow behaviour of fluidized material in air slides based on Keuneke and Woodcock's work. The main objective of Haugland's work, was to establish the relationship between design parameters, the operating conditions, the powder flow rates and powder characteristics for an air slide. There are no pictures available of the design that was used by Haugland (1998) in his work. A similar design to that employed by Haugland (1998) used for his rig was found in Hilgraf (2011) and is shown in Figure 3. Figure 3 shows test installation equipment for cement unloading used by Claudius Peters Technologies (CP), showing the supply of cement to a vertical screw inlet. The cement is supplied from an aerated silo and fed via a short air slide segment directly to a vertical screw. Haugland (1998) used similar CP aerated feeding silo, slide valve and wedge shaped box concepts as inlet design and interfaces to a long air slide. The test rig that Haugland used was 19 m long with a width of 90 mm. Special attention was given to the interfaces between: feeding silo/ air slide inlet and air slide outlet/receiving bin for alumina. The feeding silo was mounted on load cells which required the silo to be mechanically de-coupled from the air slide. A flexible connection was used between

silo and the air slide. This allowed the measurement of mass flow into the air slide, discharge rates from the feeding silo to be measured. A slide gate valve was mounted at the discharge outlet of the silo in order to retain the material in the silo between the tests and during the filling of the silo. A wedge shaped box was placed between the slide gate valve and the inlet section of the conveyor. Its purposes were:

- to increase the flow rate into the conveyor beyond what it was possible for a regular joint;
- the geometry of the box allowed for fluidizing elements to be placed at angles up to 45 degrees downward inclination to the horizontal under the outlet from the silo;



**Figure 3** Cement unloading test equipment used by CP Technologies, reprinted from Hilgraf (2011). Aerated silo and wedge shaped box placed between the slide gate valve and the inlet section of the short air slide conveyor.

The material in the feed silo could be fluidized by activating fluidizing elements mounted inside the hopper section. A dense phase conveyor for return of material to the feeding silo was used. The air slide was connected to an exhaust air system equipped with a filter to allow the separated material to be recovered for further use when testing. A pressure transmitter was mounted on the plenum chamber in order to estimate the

pressure drop across the fluidized bed. Tests were undertaken at angles of inclination of 1 to 3 degrees. The magnitude of operational air velocities used for the tests was not recorded in Haugland's work.

In his work Haugland presented a description of two models: Woodcock and Keuneke's and performed a numerical comparison between his own experimental data and the two models. Haugland's approach is shown below.

### 2.1.2 Model proposed by Keunecke (1965) (as cited by Haugland (1998))

Keunecke (1965) focused on the relationship between air velocity, pressure loss due to increase in height of layer, viscosity and resistance coefficient (as cited by Haugland (1998)). The materials used were: thomasphosphate, cement, gypsum, potash salt, flour, food additive flour, wholemeal, wheat, wheat, sand, barley wholemeal and oats wholemeal. He carried out measurements of local bed velocities by measuring the force on a thin metal plate, perpendicular to the flow direction, submerged in the fluidized bed. A strain gauge, mounted on the plate, measured the force applied on the plate by the moving fluidized bed. The model proposed by Keunecke is based on flow of fluidized material in chutes. A transformation to account for rectangular geometry was made. The model is based on the Bernoulli equation:

$$u_s = \sqrt{\tan \alpha \frac{2g}{\lambda_F} \frac{4A}{P_{wett}}} \quad \text{Equation 9}$$

where  $\lambda_F$  is the drag coefficient and  $P_{wett}$  the wetted perimeter. The wetted perimeter for a channel is the total perimeter of all channel walls that are in contact with the flow.

Haugland (1998) investigated the model proposed by Keunecke using the expression proposed by Keunecke to calculate the drag coefficient:

$$\lambda_F = 8\rho^3 b^3 h^3 \sin(\alpha) \left[ \frac{g}{\cos(\alpha)(Q^2(2h+b))} \right] \quad \text{Equation 10}$$

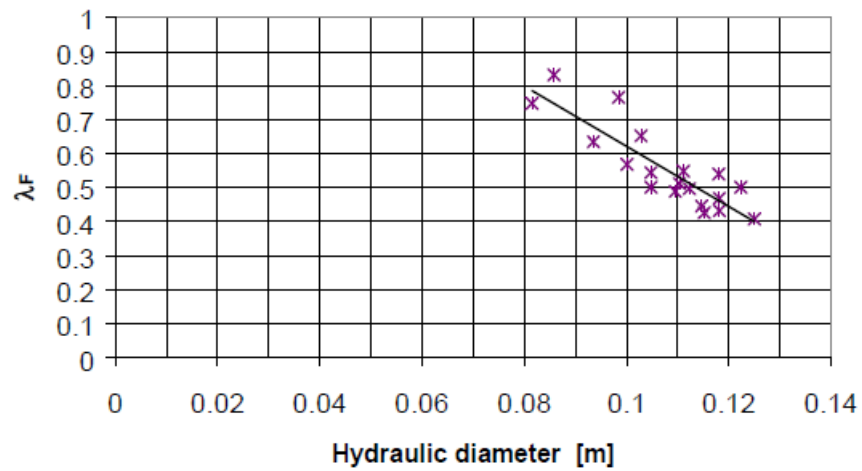


Figure 4 Haugland (1998) Drag coefficient as a function of the hydraulic diameter.

Haugland used an empirical relationship to fit a straight line to the data in Figure 4:

$$\lambda_F = -8.86D_H + 1.51 \quad \text{Equation 11}$$

and to solve the following equation for the mass flow rates expressed in kg/s shown in Figure 5:

$$\frac{Q}{\rho} = 2\sqrt{2} \frac{\sqrt{\sin(\alpha)}}{\sqrt{\cos(\alpha)}} \frac{\sqrt{g}}{\sqrt{\lambda_F}} h^{\frac{3}{2}} \frac{b^{\frac{3}{2}}}{\sqrt{2h+b}} \quad \text{Equation 12}$$

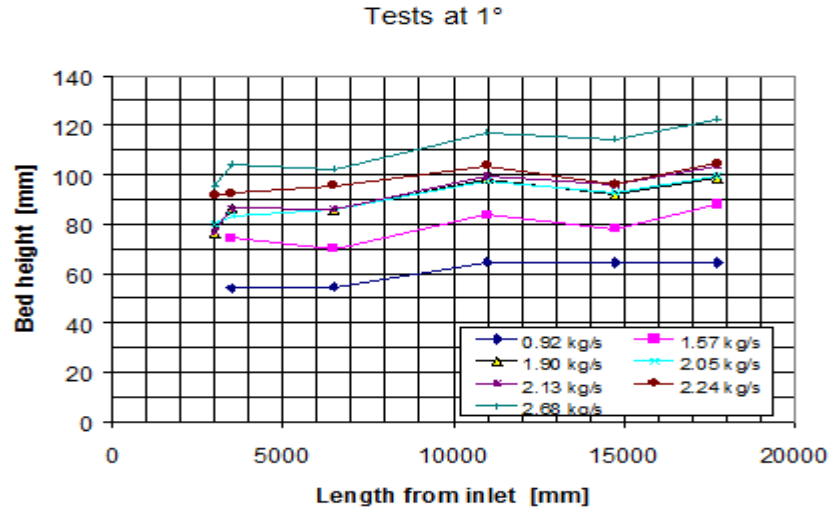


Figure 5 Haugland (1998). Results of tests conducted at 1°. Bed height profiles for different mass flow rates.

### 2.1.3 Model proposed by Woodcock and Haugland

Woodcock proposed following model assuming constant shear stress at sidewalls and shear stress at base proportional to  $u_s$  :

$$Q = (\rho^2 g b \sin \alpha - 2\rho\tau_w) \frac{h^2}{\rho k_b} \quad \text{Equation 13}$$

Woodcock rearranged the Equation 13 as:

$$\frac{Q}{h^2} = K_1 \rho^2 (\rho g b \sin \alpha - K_2) \quad \text{Equation 14}$$

introducing following set of parameters  $(K_1, K_2)$ , where:  $K_1 = \frac{1}{k_b}$  and  $K_2 = 2\tau_w$ .

Haugland (1998) determined the values of the two parameters:

$$(K_1, K_2) = (78.13 \text{Ns} / \text{m}^3, -5.45 \text{N} / \text{m}^2),$$

using experimental data from the test he had carried out. His method of estimation is shown in Figure 6, Figure 7 and Figure 8. A straight line was fitted to the points (experimental data) using the least square method.



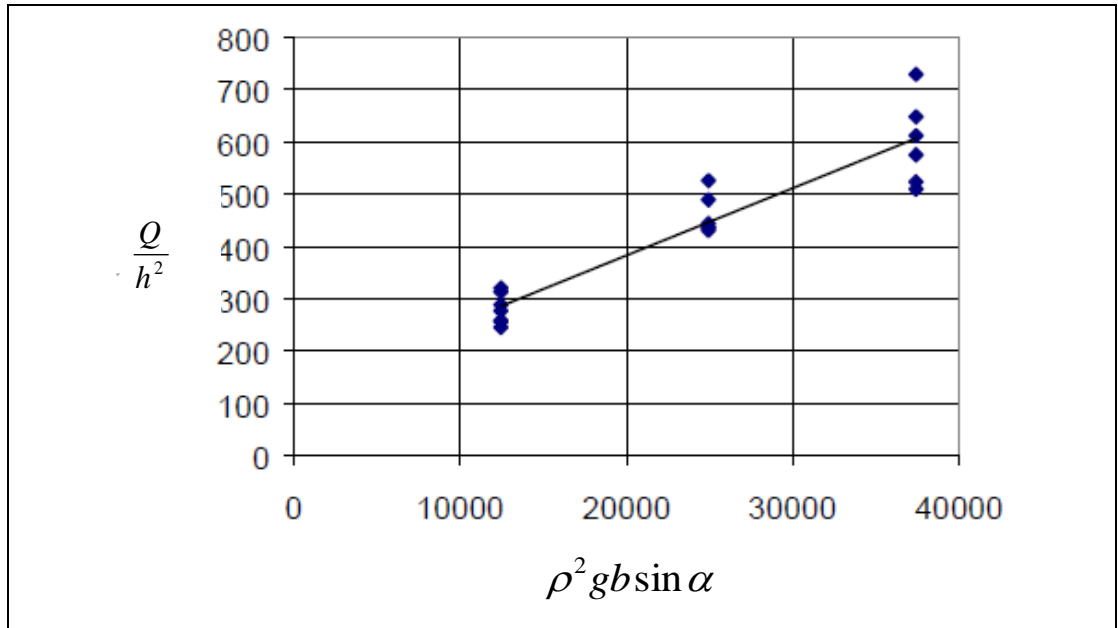


Figure 6 Haugland (1998). Method of estimating  $K_1$  and  $K_2$ .

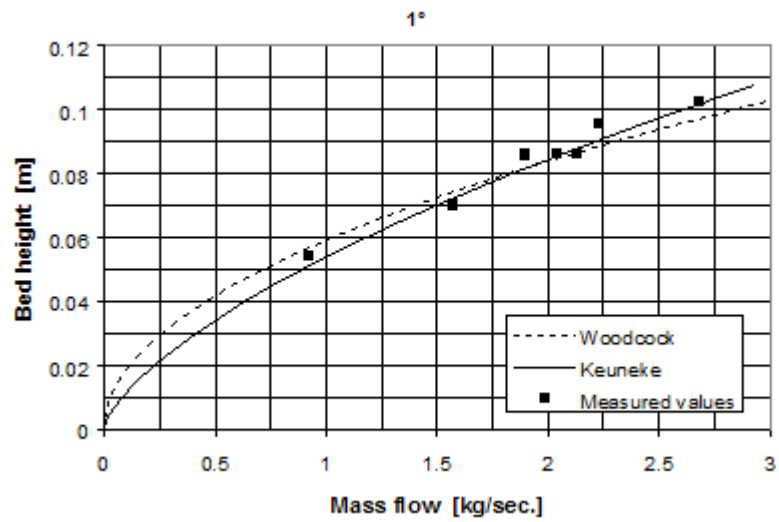
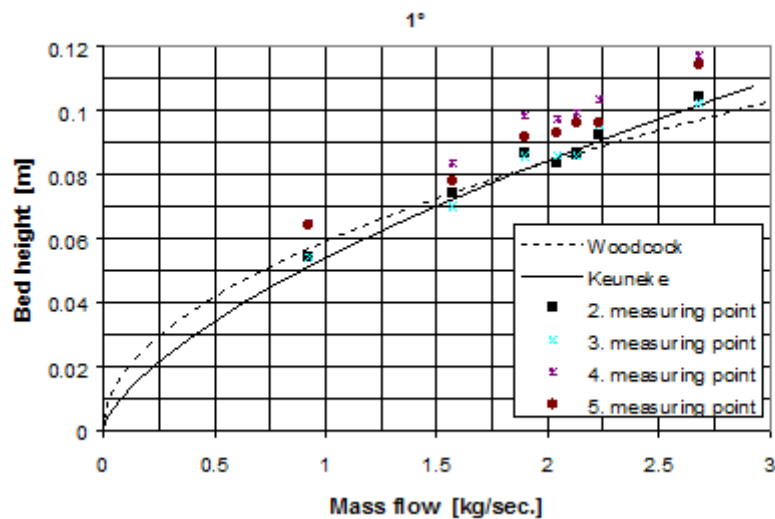


Figure 7 Haugland (1998). Results of tests conducted at  $1^\circ$  with one average value at different mass flow rates.



**Figure 8 Haugland (1998). Results of tests conducted at 1°. Values from measurement points at positions 2 to 5 away from the inlet of the air slide at different mass flow rates.**

A possible explanation, supporting Haugland's conclusions, explaining why the accuracy of the models deteriorates as shown in Figure 8, was given by Singh et al. (1978). Singh et al. (1978) reviewed Keuncke's work establishing that similar results to Keuncke's had been obtained by Siemes and Hellmer (1962). Further comments made by Singh et al. were:

- both Keuncke's and Siemes and Hellmer's approaches were based on shallow beds (up to 40 mm) with a flow behaviour analysed in terms of Newtonian liquids; based on a power-law approach, their way of interpretation meant that  $n$  was always equal to one;
- Keuncke, and Siemes had used dimensionless air velocity factor  $U_0/U_{mf}$  in the range of 2.5 to 6; neither the operational air velocity, nor the dimensionless velocity factor was mentioned in Haugland's work;
- Discrepancies between models could result from the nature of the distributors used by different authors;
- For deep beds models, above 40 mm as Haugland tested in his work, Singh et al. (1978) recommended the analogy to non-Newtonian fluids, similar to the approach used by Botterill and his co-workers. This implies measurements of viscosity at different bed heights and different fluidization velocities.

All the models selected were based on the assumption of uniform flow. Haugland's main contribution was the analysis of flow behaviour by looking at the straight lines fitted to the measured data: bed heights versus length from inlet, indicating an acceleration of the bed through the air slide and demonstrated that the flow was not uniform. Other models are needed, for non Newtonian behaviour and models which allow for the possibility of varying bed depth when modelling the flow behaviour.

## **2.2 Formulation of the hypothesis: fluid like non- Newtonian behaviour of alumina**

There is a strong analogy with the flow of Newtonian or non – Newtonian fluids in an open and closed channel which can be applied to the flow of fluidized alumina in an air slide. Haugland (1998) conducted his research based on a steady uniform Newtonian flow approach, similar to the work of Siemes and Helmer (1962), Keunecke (1965) and Woodcock (1976). Results from his experimental work pointed out that the flow of alumina was not uniform over the length of the air slide and that a non – Newtonian approach would have to be considered in further studies. A new approach based on the rheology of non-Newtonian fluids will be developed in this thesis.

To support a good understanding of the following chapters, some basic review of fluid dynamics and a classification of fluid behaviour, using basic concepts explained by Metzner and Reed (1955), Hutter et al. (1996), Coussot and Meunier (1996), Pouliquen and Forterre (2001), Pudashaini and Hutter (2007), Ancey et al. (2004) - (2013), will be introduced next. The concept of plasticity and two plastic theories common in fluid dynamics: Coulomb plasticity and visco-plasticity will be the focus of this chapter, as plasticity and fluid approach have been used in this thesis to model the flow of alumina in air slides.

### **2.2.1 Theoretical concepts**

The objective of this section is to explain the concept of plasticity and how plasticity has been used in engineering and geophysical fluid dynamics. Viscoplastic models such as the Herschel - Bulkley model has been extensively used in engineering as an idealization of materials that behave as solids when at rest, but like fluids when sufficient stress is applied (Ancey et al (2012)). Rapid and huge mass movements such as occurring in snow and rock avalanches, debris and lava flows, dam break in rivers,

all are examples of gravity- driven geophysical phenomena involving slurries or solid particles within an interstitial fluid (air or water). They take the appearance of a viscous fluid flowing down a slope. Traditionally, the bulk behaviour of these materials has been modelled as plastic behaviour described as: “a plastic material yields and starts to flow once its stress state has significantly departed from equilibrium” (Ancy (2007), (2012)). Other notions and concepts mentioned in this chapter will be: yield surface, flow associated with a plastic behaviour, flow regimes, and the Saint Venant (depth-averaging) equations.

### **2.2.1.1 Shear stress in fluids**

A gas fluidized alumina bed looks very much like a boiling liquid, once submerged into the bed and released, any object will pop up and float on the surface of the bed. When we tip a fluidizing column, the surface of the alumina bed will remain horizontal. The difference in pressure between any two vertical ordinates in the bed is equal to the height of column of bed between these points. The liquid like behaviour of a flowing alumina bed allows the formulation of a fluid like non Newtonian behaviour for further modelling of alumina in an air slide.

In order to characterize a fluid, such as water, for example, it requires two material properties: density ( $\rho$ ) and viscosity ( $\mu$ ). The density represents the mass of fluid per unit volume. Materials with the characteristics of a fluid will flow when subjected to a stress, which is defined as the force per area. The viscosity is a measure of the resistance of the fluid to deformation by shearing. Any fluids (liquids and gases included) flowing along a solid boundary such as the walls of an air slide, in this case, will produce a shear stress on that boundary, as shown schematic in Figure 9. The concept of “no slip” means that the speed at the boundary (at the wall ( $y = 0$ )) = 0. The region between these two points, the wall (bottom) and some chosen distance  $y$  from the wall (bottom) is referred to as the boundary layer.

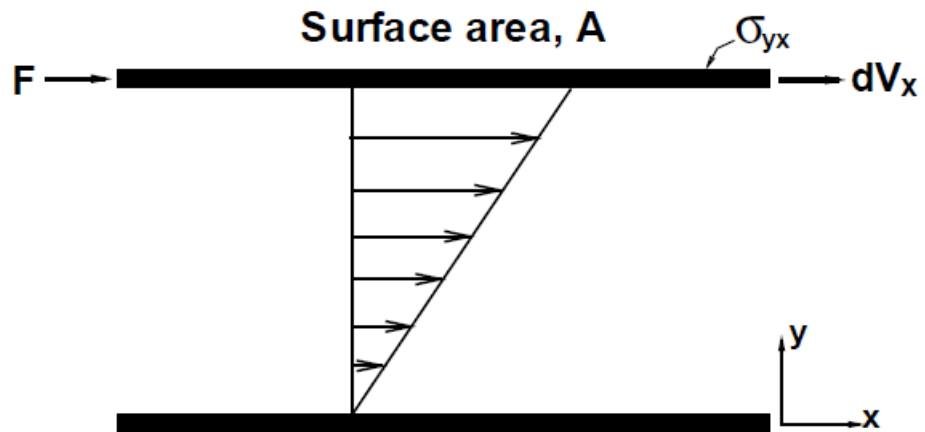


Figure 9 Shear deformation of a fluid.

### 2.2.1.2 Newtonian laminar and turbulent flow

Depending on the cross sectional geometry of the transport channel (pipe or open channel), rates of discharge and transport capacity as well as the material properties of the fluid flowing in the channel, fluid flow can be characterized as laminar or turbulent. If the flow is laminar, then one layer slides over the next one in a streamlined motion. An element of a flowing fluid (liquid or gas) will suffer forces from the surrounding fluid, including viscous stress forces that cause it to gradually deform over time. These forces can be mathematically approximated to first order by a viscous stress tensor, which is usually denoted by  $\tau(y)$ . In the late seventeenth century, Isaac Newton stated that shear stress in a fluid is linearly proportional to the time rate of strain,  $\dot{\gamma}$ , i.e., velocity gradients, denoted  $\dot{\gamma} = \frac{\partial u_x}{\partial y}$  where the dynamical viscosity of the fluid (shear viscosity)  $\mu$ , is the constant of proportionality in Equation 15. Such fluids are called Newtonian fluids and they have a Newtonian fluid behavior. In the case of a Newtonian fluid, the shear stress at a surface element parallel to a flat wall, at the distance  $y$ , is given by:

$$\frac{F}{A} = \tau_{yx}(y) = \mu \left( \frac{\partial u_x}{\partial y} \right) \quad \text{Equation 15}$$

This relationship is linear and it is applicable only to the laminar flow region. The shear stress  $\tau_{yx}(y)$  is equal to the force exerted on the fluid per unit area and the shear rate  $\frac{\partial u}{\partial y}$  is the change in velocity with respect to  $y$ , which is measured normal to the plane

(Schulze(2008)). The ratio  $\frac{\mu}{\rho}$  is known as the kinematic viscosity. Fluids in which  $\tau_{yx}(y)$  is not proportional to the velocity gradients are called non-Newtonian fluids and they have a non-Newtonian fluid behaviour. In turbulent flow the fluid particles flow in erratic paths, which make the velocity components to fluctuate. These fluctuations create momentum changes, which result in large increases in shear stresses (Metzner and Reed (1955)). Reynolds was the first to study these flow regimes and developed the following equation, known as Reynolds number:

$$\text{Re} = \frac{\rho u L}{\mu} \quad \text{Equation 16}$$

where  $\rho$  is the density of the fluid,  $u$  is the mean flow velocity,  $L$  is a characteristic linear dimension or travelled length of the fluid, and  $\mu$  is the viscosity of the fluid. The Reynolds number is proportional to the ratio between inertial and viscous forces. For pipe flow (cylindrical geometry)  $L$  becomes the inside pipe diameter  $D$ , thus:

$$\text{Re} = \frac{\rho u D}{\mu} \quad \text{Equation 17}$$

### 2.2.1.3 Open channel flow

An open flow is a channel (of any shape) with a free surface open to the atmosphere where the flow is dominated by the effect of gravity. For shapes such as rectangular ducts, the characteristic dimension for flow is taken to be the hydraulic diameter,  $D_H$  defined as  $D_H = 4A/P$ , where  $A$  is the cross sectional area of the channel and  $P$  is the wetted perimeter. As mentioned before,  $P$  for a channel is the total perimeter of all channel walls that are in contact with the flow. This means that the length of the rectangular channel exposed to air (free surface) is not included in the wetted parameter formula. For open channel flow  $L$  becomes the hydraulic radius  $R_h$ . Thus the Reynolds number is given as:

$$\text{Re} = \frac{\rho u R_H}{\mu} \quad \text{Equation 18}$$

#### **2.2.1.4 Steady and unsteady flow**

Open channel flow is steady when the flow depth does not change with time (during a time interval). Unsteady flow occurs when the flow depth changes with time.

#### **2.2.1.5 Uniform and varied flow**

The flow is uniform when the flow depth is the same over a section of the channel. The flow is varied when the flow depth varies over the length of the channel.

Steady uniform Newtonian flow has been used to analyse the flow of fluidized solids in inclined, open channels by Siemes and Hellmer (1965), Keunecke (1965) and Haugland (1998). Non-Newtonian flow was studied by Metzner and Reed (1955), Botterill and his co-workers, Singh et al. (1977), Latkovik and Levy (1991).

This thesis will be based on the non-Newtonian steady state approach and will study the rheological behaviour of the fluids.

#### **2.2.1.6 Rheometry and rheological models**

It must be mentioned that the flow behaviour presented below is only for time independent fluids. That means that the flow behaviour of the fluid does not change over time. There are four time-independent models presented in this investigation describing the rheological behaviour of fluids: one Newtonian and three non-Newtonian ones.

#### **2.2.1.7 Newtonian model**

The simplest rheological model is the Newtonian model, having a single rheological parameter  $\mu$ . For all Newtonian fluids the relationship between the shear stress ( $\tau$ )

proportional to the shear rate  $\frac{\partial u}{\partial y}$  in the fluid, as explained earlier:  $\tau(y) = \mu \frac{\partial u}{\partial y}$ , is

known as the rheogram, according to Wilson et al. (2006). As shown in Figure 10 it follows that the rheogram of a Newtonian fluid is a straight line which passes through the origin and has slope  $\mu$ . The data points required for plotting rheograms can be obtained by using a fluid rheometer, then further work needs to be done, as mathematical functions need to be fitted to the experimentally determined points plotted on the rheograms.

Figure 10 shows a graph of the behaviour of an ordinary Newtonian fluid, for example in a pipe (or a fluidized air slide). If the pressure at one end of the pipe is increased, this

will have an impact on the fluid; it will produce a shear stress on the fluid, making it move. A secondary effect will be a proportional increase in the volumetric flow rate in the pipe.

### 2.2.1.8 Bingham plastic model

A Bingham plastic is a viscoplastic material that behaves as a rigid body (elastic solid) at low stresses, but flows as a viscous fluid at high stress. It is named after Eugene C. Bingham who proposed its mathematical form. It is used as a mathematical model of mud flow in drilling engineering, for the oil industry. Rheograms for non Newtonian fluids are not so simple, as they do not pass through the origin and the viscosity no longer represents the slope of the rheogram itself. Figure 10 shows a graph with the behaviour of a Bingham plastic versus a Newtonian fluid. If for example, the pressure at one end in the same pipe or fluidized air slide, is increased, as before, stress is applied, but the fluid will not flow, until a certain critical, minimum value, the yield stress  $\tau_c$  is reached. The fluid is an elastic solid for shear stress less than this minimum value. Once this minimum value is reached and exceeded, the flow rate will increase proportionally with increasing shear stress. The material will then flow in such a way, that the shear rate  $\frac{\partial u}{\partial y}$  is directly proportional to the amount by which the applied shear stress exceeds the yield stress. Wilson et al. (2006) describe it's rheogram as linear, passing through the Bingham yield stress  $\tau_c$  at  $\frac{\partial u}{\partial y} = 0$  and having a slope  $\mu$  called plastic viscosity, thus:

$$\tau = \tau_c + \mu \frac{\partial u}{\partial y}$$

Equation 19



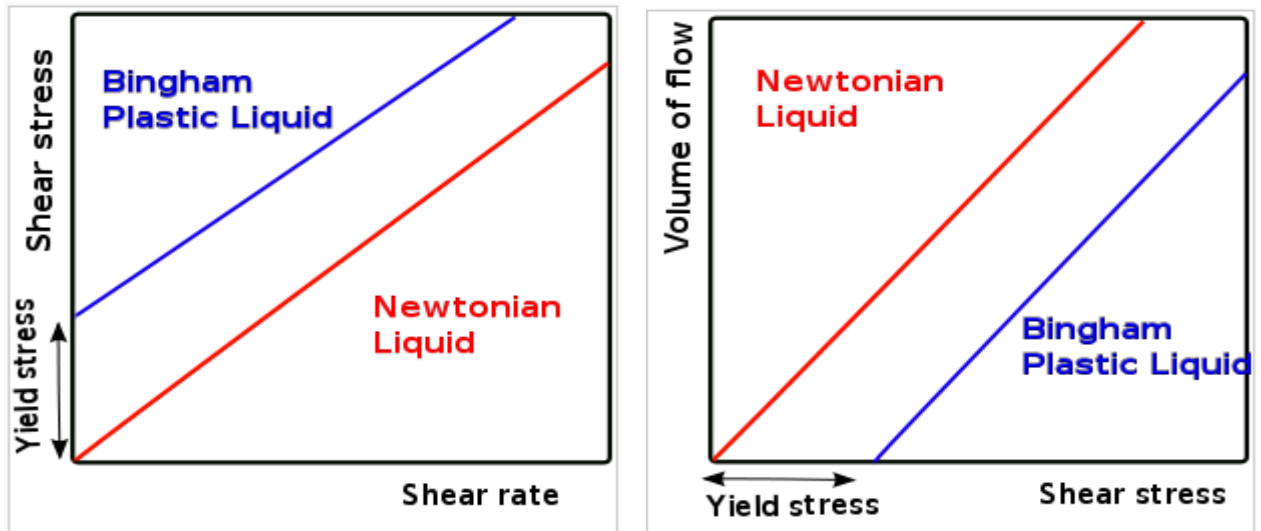


Figure 10 Rheograms for newtonian and Bingham plastic flows as described by Bingham. (Source: Wikipedia).

#### 2.2.1.9 Power law: Oswald de Waele model

Ideal fluids have a rheogram passing through origin; however the rheogram may not be a straight line as in the case of single parameter Newtonian model. The power law model is a two parameter  $k$  and  $n$  model and is expressed by the equation:

$$\tau = k \left( \frac{\partial u}{\partial y} \right)^n \quad \text{Equation 20}$$

where  $k$  is the consistency coefficient (flow index) and  $n$  is shear rate exponent. The two parameters  $k$  and  $n$  are empirical curve fitting parameters.

When the shear rate increases more than linearly with the shear stress, the material is said to show a pseudoplastic or shear- thinning behaviour, e.g. slurry flows, with  $n < 1$ . If  $n = 1$  the equation reverts back to the Newtonian model, with  $k = \mu$ .

#### 2.2.1.10 The Metzner - Reed model

The approach of Metzner and Reed (1955) by simplifying the Rabinowitsch - Mooney equation is based on a power law model for non-Newtonian pipe flow, which relates

the shear stress  $\tau$  and the shear rate  $\left( \frac{\partial u}{\partial y} \right)$  at the wall as:

$$\tau_w = k' \frac{4n'}{1+3n'} \left( \frac{\partial u_w}{\partial y_w} \right)^{n'} \quad \text{Equation 21}$$

where the shear rate at the wall  $\frac{\partial u_w}{\partial y_w}$  is given as:

$$\frac{\partial u_w}{\partial y_w} = \frac{1+3n'}{4n'} \frac{8u}{D} \quad \text{Equation 22}$$

and  $n'$  and  $k'$  are the flow factors and  $u$  is the mean velocity over cross section of flow and  $D$  is the pipe diameter. The parameter  $k'$  is reported to give an indication of consistency of the fluid: the larger the value of  $k'$ , the more viscous the fluid. The parameter  $n'$  defines the degree of non-Newtonian behaviour of the fluid. According to Metzner and Reed (1955) and Metzner and Park (1964) it reflects the degree to which the rheological properties of a purely viscous fluid, at any chosen value of the wall stress  $\tau_w$ , diverge from the properties of Newtonian fluids. This model was used by Latkovik and Levy (1991) to study the flow characteristics of fluidized magnetite powder in an inclined open channel.

#### 2.2.1.11 Herschel - Bulkley or the yield - pseudoplastic model

If a Bingham fluid exhibits a non-linear relationship, then the yield pseudoplastic three constant model can be used (Haldenwang et al. (2003) – (2012), Fitton (2007), Ancy (2012), (2013). Introducing additional parameters apparently improves the fit of the model to the rheological data, according to Wilson et al. (2006), but they also point out that in practice it is very difficult to obtain a proper calibration of a three-parameter model. As it can be seen from the equation of the model:

$$\tau = \tau_c + k \left( \frac{\partial u}{\partial y} \right)^n \quad \text{Equation 23}$$

it can be simplified to the power-law model in the absence of shear stress (if  $\tau = 0$ ), to the Bingham model if  $n = 1$  and to the Newtonian model when both conditions apply ( $\tau = 0$  and  $n = 1$ ). This model was used by Bruni (2004) to characterize the flow behaviour of fines of alumina and silica.

### **2.2.2 Results and discussion small scale open channel viscometer experiments, non Newtonian approach**

Botterill et al. (1971) carried out a series of viscometer experiments in the Department of Mechanical Engineering at the University of Aston, using a Brookfield Synchroelectric instrument with a type of cylindrical rotor. The samples had been previously tested in large scale flow situations. They investigated whether or not the viscometer element disturbed the fluidisation behaviour, in the small scale equipment, questioning the use of results for prediction with good accuracy of the same effect in full scale applications of flow. Further assumptions and tests were made. They checked whether slip between the surface of the rotor and the fluidized solids was occurring, changing from a rotor with polished surface to one with serrations to match the same size as the fluidized solids. This change had no effect on the shear stress for a pre-set rotor speed; therefore it was presumed that the rotor slip could be ignored. In the absence of established theory for the type of rotor they used, they doubted whether the shear rate could be calculated for their system. To solve the problem, they calibrated the equipment against a standard fluid of known viscosity, a 65 % sugar solution, whose viscosity at 25° C was 0.14 Pa s. Another point considered in detail was the possible differences in behaviour of the fluidized solids on the vertical walls and on the fluidized base.

Figure 11 shows the results of measured torque versus shear rate for different fluidisation velocities.

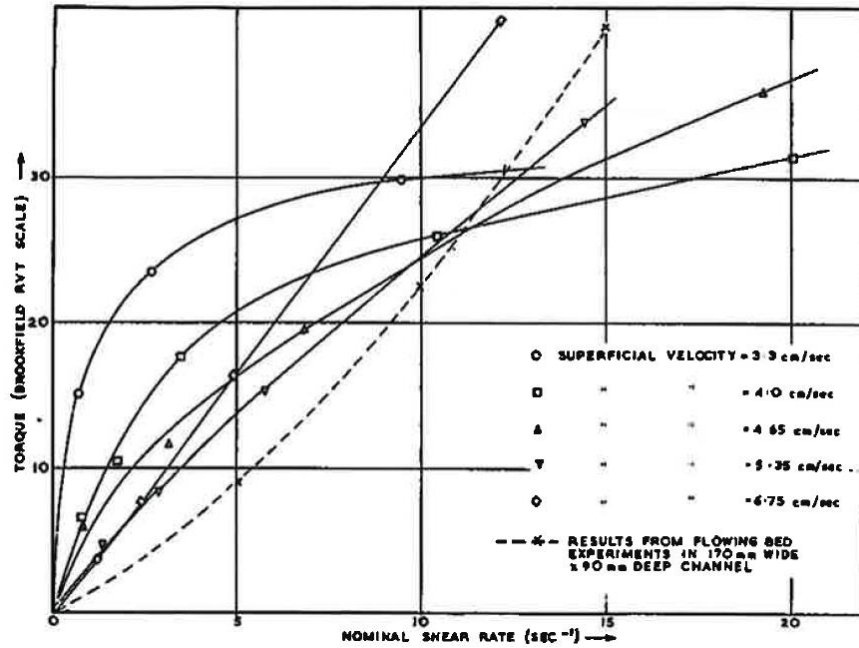


Figure 11 Botterill et al. (1971). Bauxilite rheograms. Torque vs. shear rate for fluidised  $102 \mu\text{m}$  Bauxilite in 140 mm diam. bed of 20 mm packed height.

From the rheograms of bauxilite it was found that at low fluidising velocities the flow is non-Newtonian. One curve for a 90 - mm- deep full scale bed (dotted line) fluidized at  $2 \times U_{mf}$  was also shown, following a similar pattern as the rheograms from small scale.

### 2.2.2.1 Botterill et al.

Botterill et al. (1970), (1971) performed fluidized particulate measurements on a test rig developed at University of Birmingham. The equipment consisted of the fluidized bed contained within an open, closed- loop horizontal channel with porous tile distributors, impellers for driving the fluidized solids round the channel, a blower to supply the fluidization air, with an overall length of the rig of 3 m. A series of paddles mounted at right angles to strips of belt stretched between two pulleys and driven by a motor, made the fluidized bed to flow round the channel. The channel width was adjusted by a 2.5 m long test section, made from walls held vertical and parallel by spacers to allow variations of the channel width. Pressure drops were measured between probe points using a micromanometer. Local flow velocity was measured using a small turbine element having a 6 mm diameter rotor. The effect of varying the bed depth  $h$

and width  $w$  was also investigated. Figure 12 shows the results of calculated stress  $\Delta P D_H / 4L$  versus calculated shear rate  $8V / D_H$  at  $3 \times U_{mf}$ , where:

$$D_H = \frac{4 \times \text{flow\_area}}{\text{base} + 2 \times \text{height}}$$

Equation 24

$L$  Distance between the pressure probes

$\Delta P$  Pressure loss as measured

$V$  Velocity as measured

The bauxilite rheograms showed a non-Newtonian flow behaviour.

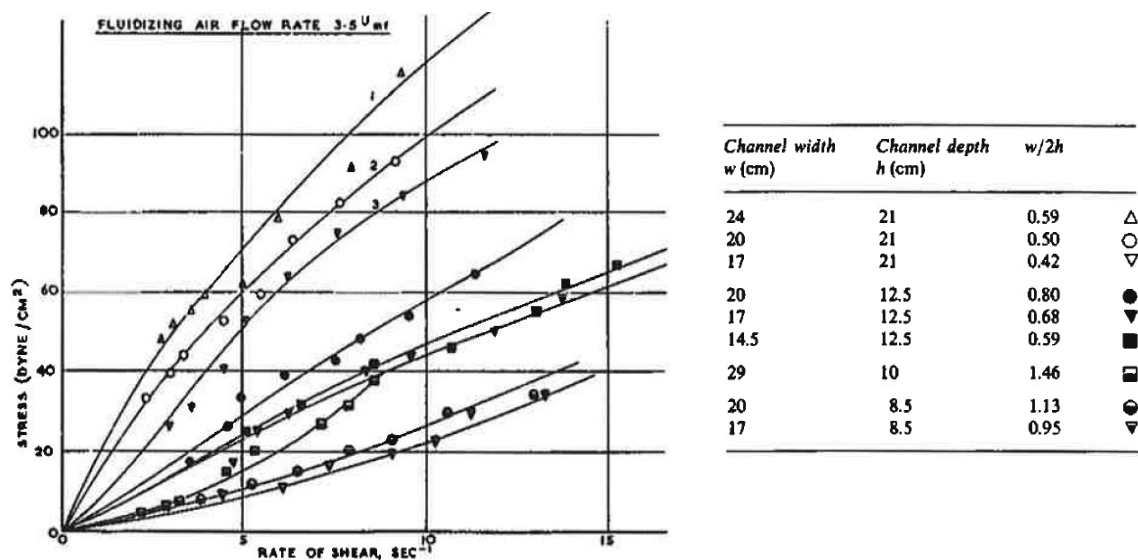


Figure 12 Botterill et al. (1971). Bauxilite rheograms. Effect of channel width and depth on stress- strain relationship measured for fluidised  $102 \mu m$  Bauxilite,  $3.5 \times U_{mf}$ .

Work on the rheological properties of fluidized solids done by Botterill and van der Kolk (1971) showed that  $185 - \mu m$  diameter sand displayed Bingham plastic properties which were particularly pronounced at low fluidizing velocities and that its plastic viscosity passed through a minimum at  $3 \times U_{mf}$ . Sand of  $138 - \mu m$  and bauxilite of  $102 - \mu m$  diameter displayed a range of behaviour from dilatant to pseudoplastic, dependent on the bed dimensions. Variations of the bed depth and width showed the effects of drag forces along the vertical wall and over the distributor. It was also believed that an

air slide effect occurred above the porous tile distributor, and that the resistance to bed flow at the distributor was expected to increase with an increase in bed velocity.

### 2.2.2.2 Botterill and Bessant

Botterill and Bessant (1973) reported the results of experimental measurements of the non-Newtonian flow behaviour of a 200  $\mu\text{m}$  diameter sand. The velocity profiles were estimated using a turbine element. It was pointed out that the real non-Newtonian flow properties were more difficult to study because of the varying degree of influence presented by the distributor (base) and the vertical walls on the flow behaviour. The varying degree of influence was again a function of the fluidizing air flow rate and the material shear flow rate through the channel.

Changes in the sand rheograms for a fluidized bed at  $2 \times U_{mf}$ , with 118 mm constant bed height and for different channel widths: 100, 140 and 180 mm were also investigated.

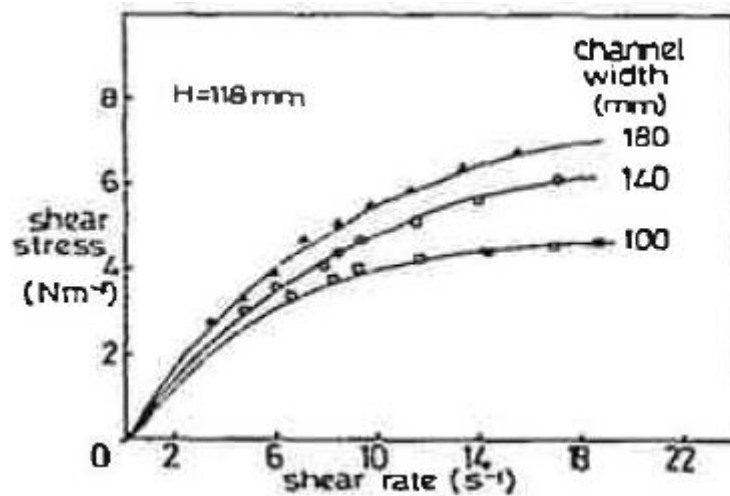


Figure 13 Botterill and Bessant (1973). Sand rheograms. Variation in shear stress/shear rate curves with channel width for 200 -  $\mu\text{m}$  diameter sand.

In the study the velocity profiles were considered as a function of the channel aspect ratio and it was shown how they could be predicted from a power law model, assuming similar influence of the drag across the distributor and the vertical walls on the flow. Thus using a power law model for a pseudoplastic fluid:

$$\tau = k \left( \frac{\partial u}{\partial y} \right)^n$$

Equation 25

estimations for the constants  $k$  and  $n$  were obtained from the data shown in Figure 11 to Figure 13. The next step in the evaluation of the shear stress / shear rate characteristics was the use of the equivalent diameter formula, as used earlier by Botterill et al. (1971) shown in Equation 24:

$$D_H = \frac{4bh}{b + 2h}$$

Equation 26

where  $\tau = \Delta P D_H / 4L$  and  $\frac{\partial u}{\partial y} = \frac{8V}{D_H}$ .

Botterill and Bessant (1976) performed experimental measurements in of 200 -  $\mu m$  diameter sand, using bed heights of 77 and 118 mm and two channel widths 140 and 180 mm, varying the fluidization conditions from 1.75 up to  $2 \times U_{mf}$ . Again they addressed their own previous work, pointing out the impracticability of applying the equivalent diameter concept as a link between open channel flow and rotating viscometer measurements, due to the variability of the drag across the distributor. They reported that at lower bed flow rates and closer to the minimum fluidizing velocity, there was a higher drag across the distributor than that measured at the vertical channel walls. Another important effect was the influence of bed height on apparent viscosity.

### 2.2.2.3 Botterill and Abdul Halim

Botterill and Abdul Halim (1978) corrected earlier assumptions presented by Botterill et al. (1971) and confirmed previous work done by Botterill and Bessant (1976). Botterill and Abdul Halim (1979) extended the experiments of Botterill and Bessant (1976) by using catalyst, sand and ash for several channel widths and heights.

### 2.2.3 Savage and Oger (2013) - two part investigation study of air slides

The initial experiments had been conducted in a fluidized flow channel constructed by Savage and his co-workers at McGill University in 1978. Experiments were carried out by Liot (1978) and Chan (1979) (cited by Savage and Oger (2013)). A diagram of the flow channel is given in Figure 14. The aluminium channel was 2.4 m long, 0.101 m wide and 0.051 m high. Air was supplied to the channel by three vacuum fans, each

having a  $0.14 \text{ m}^3\text{s}^{-1}$  capacity. All the experiments were conducted with a vertical air velocity of  $0.434 \text{ ms}^{-1}$  using a ‘Dynamopore’ plate as membrane. The granular material supplied to the flow channel by an upper feed hopper was controlled by a gate at three gate heights:  $H_g = 12.7 \text{ mm}$ ,  $19.1 \text{ mm}$  and  $25.4 \text{ mm}$ . For each gate opening and bed inclination angle between  $3$  and  $8^\circ$  measurements of mass flow rate and depth of the material were recorded. Boterill and Besant’s (1976) reometry measurement and velocity profile results were used by Savage and Oger (2013) ( as in Figure 15) together with a finite element model implemented in FlexPDE (finite element package) based on a power law and non-Newtonian viscosity model computations.

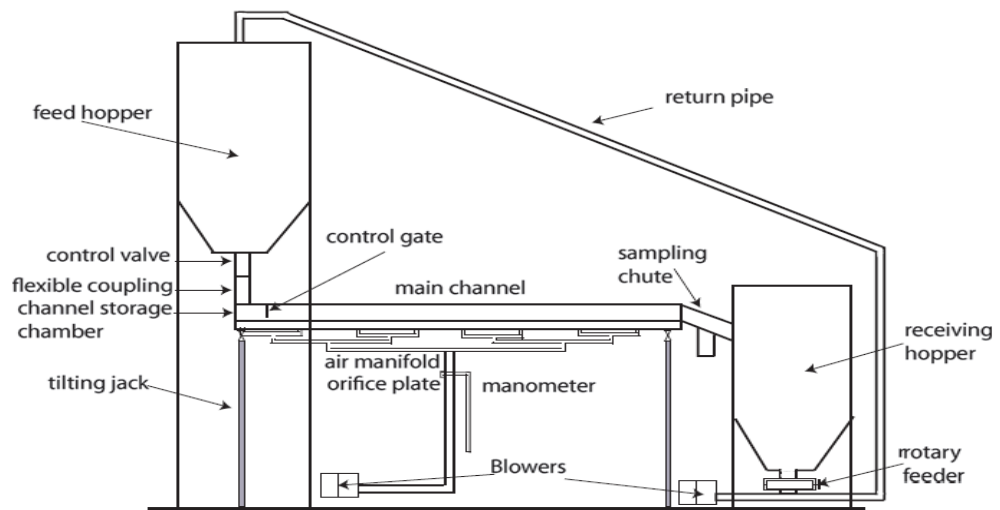


Figure 14 Layout of flow system rig (reprinted from Savage and Oger (2013)).

They noted that Botterill and Bessant (1976)’s approach could not be regarded as a “truly predictive model” since the values of  $n$  had not been linked to the fluidizing air or other flow properties. But they pointed out that this approach could be regarded as a good curve fit to the experimental data.



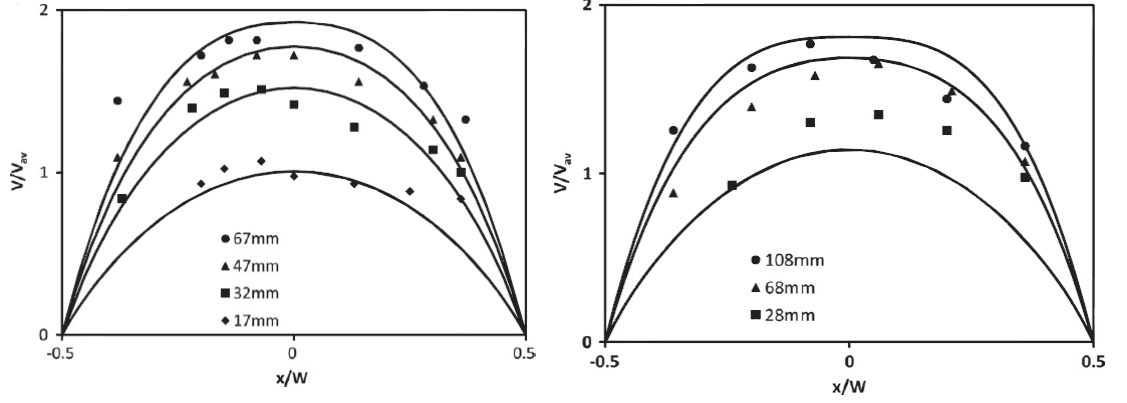


Figure 15 Savage and Oger (2013). FlexPDE finite element predictions of power law, for  $n$  equal to 0.53 and 0.66, compared to the experimental data points of Boterill and Besant (1976).

Savage and Oger (2013) used an analogous analysis method from the field of processing of polymeric materials, presented by Han (2007, page 10). The method allowed the determination of the velocity field developed by a non-Newtonian fluid in a rectangular channel of constant cross section. Han (2007) (as cited by Savage and Oger (2013)) assumed that the streamwise velocity  $v_z$  in the axial  $z$  direction depended only on  $x$  and  $y$ , then used the momentum equation as:

$$-\frac{\partial p}{\partial z} + \frac{\partial}{\partial x} \left( \mu \frac{\partial v_z}{\partial x} \right) + \frac{\partial}{\partial y} \left( \mu \frac{\partial v_z}{\partial y} \right) = 0 \quad \text{Equation 27}$$

where  $p$  is the pressure in the power law fluid and the power-law non-Newtonian viscosity was given by:

$$\mu = \mu_0 \left[ \left( \frac{\partial v_z}{\partial x} \right)^2 + \left( \frac{\partial v_z}{\partial y} \right)^2 \right]^{(n-1)/2} \quad \text{Equation 28}$$

where  $\mu_0$  is a viscosity constant and  $n$  is the viscosity exponent with values between 0 and 1. Oger and Savage (2013) assumed no slip boundary conditions and zero shear stress at the upper free surface for a rectangular channel of given height  $H$  and width  $W$ ,  $v_z = 0$  at the walls,  $x = \pm W/2$  and  $y = \pm H/2$ . Figure 16 shows the front of velocity profiles for the partial differential equation system by using the finite element package FlexPDE 6, for a free surface flow in a channel 8.8 cm wide and 4 cm deep, based on a viscosity exponent  $n = 0.65$ .

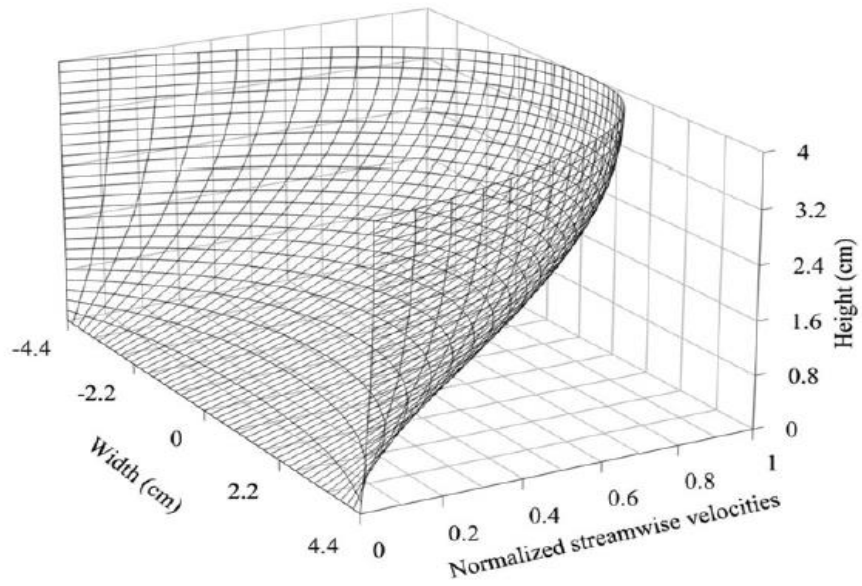


Figure 16 Savage and Oger (2013). FlexPDE finite element predictions of velocity distribution based on a power law viscosity exponent  $n = 0.65$ .

Further they interpreted the results of Liot (1978) and Chan (1979) as shown in Figure 17 and Figure 18 by using an open channel approach and hydraulics backwater analysis.

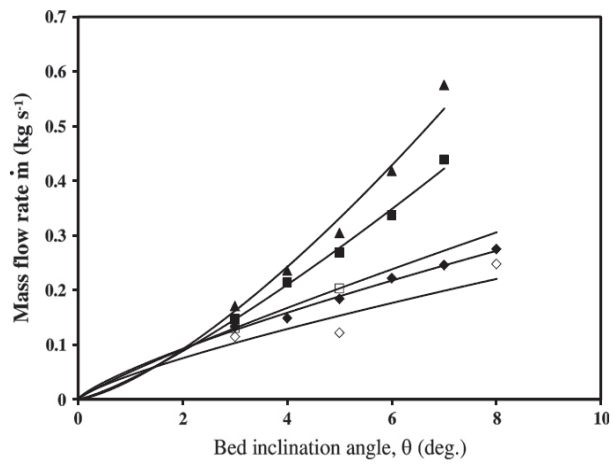


Figure 17 Mass flow rates versus the bed inclination angle  $\theta$  and three gate openings.

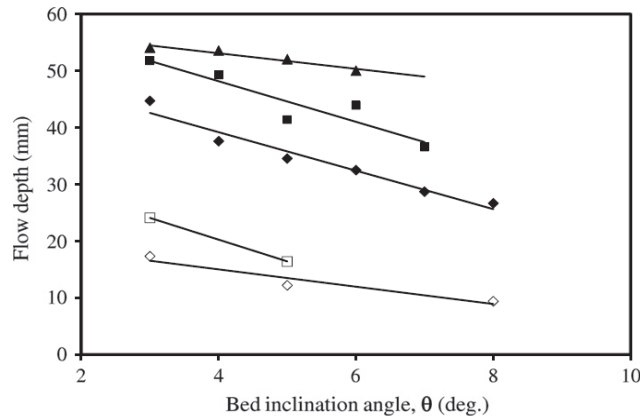


Figure 18 Flow depth versus  $\theta$  and three gate openings; reprinted from Oger and Savage (2013).

### 2.2.3.1 Singh et al. (1978)

Other early investigators cited by Savage and Oger (2013) and by Gupta et al. (2010) were Singh et al. (1978) and Latkovik and Levi (1991). Singh et al. (1978) developed a model for the flow of Newtonian and non-Newtonian liquids in an open channel for laminar flow. The validity of the model was tested using oils, coal-water slurry and carboxymethylcellulose solution. Then the model was used to determine the flow behaviour and parameters of fluidized silica sand. For the fluidization of sand a new design of distributor named “Pneudistributor” and air slide with a V shaped bottom named “Pneuair slide” was used. The total length of the slide was 9.15 m with a channel width of 150 mm. Sand was fed under gravity by a common rectangular chute from two hoppers above the channel. A slide valve was provided in the common feed chute, thus allowing for the flow of sand to be diverted away from the channel into a hopper for measurement of flow rate. Sand discharged from the slide was carried back to the feed end by two conveyor belts with a nominal capacity of 50 t/h sand each. Air through the top of the channel was discharged through a 100 mm diameter flexible hose to a dust collector and thus vented to the atmosphere. Ten pressure probes located 50 mm above the top of the distributor pipe were placed along the length of the air slide. The sand used in their test had a minimum fluidization velocity of 3.9 cm/s. Their dimensionless air velocity factor  $U_0/U_{mf}$  was in the range of 1.3 to 2.8. Tests were carried out with two sets of orifice diameters of 2.8 and 4 mm in the distributor. The angles of inclination were varied from 0 to 30 degrees (downward inclination). Sand flow rates in the range of 5 to 100 t/h were achieved. They combined the following assumptions:

- Flow of liquids and solutions: for laminar regime in an circular pipe, the liquid was assumed to adhere to both walls and the bottom of the channel; the model applied to both accelerating and uniform flows;

- The rheological behaviour of the liquid could be expressed by the power law:

$$\tau = k \left( \frac{\partial u}{\partial y} \right)^n$$

where the consistency index,  $k$  and flow behaviour index,  $n$ , were assumed to be constants;

- The validity of model was tested in the accelerating regime for both Newtonian and non- Newtonian fluids;

- Flow of fluidized solids: to determine the flow parameters of fluidized sand along a channel;

- By using the Botterill and Besant (1978)'s suggestion of hydraulic diameter:

$$D_H = \frac{4bh}{Kb + 2h} \quad \text{Equation 29}$$

where  $K$  is a function of the distributor and its value would range between 0 (complete slippage) and 1 (no slip), depending of the degree of slippage at the distributor. The results indicated that:

- a continuous decrease in hydrostatic pressure together with observations of bed heights indicated that uniform flow conditions were not attained;
- the flow parameters were influenced by the design of the distributor; in Singh's study air was not distributed over the entire cross-section of the channel;
- the mass flow rates became stable at a dimensionless air velocity factor  $U_0/U_{mf}$  of 2.2 for all angles of inclination; this flow behaviour was similar to the results reported in the work of Botterill and his co-workers or as in the studies reported by Keunecke (1965) and Siemes and Helmer (1962).
- the flow parameters  $k$  and  $n$  were varying more with the angles of variation for  $K = 0$ ; for  $K = 1$ ,  $k$  and  $n$  were independent of the angles of inclination; the authors concluded that for the type of the distributor used in their rig, the assumption of no slip at the distributor ( $K = 1$ ) was more correct then the assumption complete slip ( $K = 0$ ). Singh et al. (1965) presented a procedure for the design of a flow channel, pointing out that there was a theoretically lower limit for the minimum height of free surface of the fluid falling freely under gravity,  $H_m$  :

$$H_m = \left[ \frac{\rho Q}{\beta b g} \right]^{\frac{1}{2}} \quad \text{Equation 30}$$

where:

$Q$  Flow rate

$\beta$  Correction factor in the kinetic energy term, dimensionless, determined as:

$$\beta = \frac{(2n + 1)(5n + 3)}{3(3n + 1)^2} \quad \text{Equation 31}$$

### 2.2.3.2 Latkovik and Levy (1991)

Latkovik and Levy (1991) studied the flow characteristics of a fluidized bed of 139  $\mu\text{m}$  and 169  $\mu\text{m}$  magnetite particles, with  $U_{mf}$  values of 3.2 and 2.3 cm/s using a similar data analysis approach as presented by Botterill and his co-workers. The experiments were undertaken in 100 mm wide open channels with a total length of 2.3 m, similar length as used by Keuncke (1965) and Siemes and Helmer (1962). The slope of the channel was varied between 1 and 30 degrees downward inclination during the tests. The parameters which were monitored during each test were the bed depth, mass feed rate of solids, superficial gas velocity and channel inclination. They observed that the flow behaviour varied with the operating conditions, thus a shift from Bingham plastic to pseudoplastic flow properties occurred with an increase in bed depth. They observed accelerated flows at low shear rates with a large increase in bed depth at the channel inlet compared to the discharge. At high shear rates, the flow was uniform with no changes in bed depth along the length of the fluidized channel. For certain operating conditions at values of superficial air velocity in the range of 1.7 to 3.5  $U_{mf}$  they applied liquid analogy approach based on the laminar flow of non – Newtonian fluids in pipes to the flowing bed of magnetite. A friction factor versus generalized Reynolds number correlation, characterized by a power law model developed by Metzner and Reed (1955), showed a good agreement with the experimental data. Their theoretical approach was as following:

- The pipe diameter  $D$  was replaced by the hydraulic diameter  $D_H$  defined as :

$$D_H = \frac{4 \times \text{flow\_area}}{\text{width} + 2 \times \text{height}} \quad \text{Equation 32}$$

- From the equation of motion for open – channel flow the wall shear stress was expressed as:

$$\tau_w = \frac{D_H \rho_{bfl} g}{4} \sin \alpha \quad \text{Equation 33}$$

- The mean flow velocity of the flowing bed was evaluated from:

$$u_{av} = \frac{Q}{\rho_{bfl} w h_{av}} \quad \text{Equation 34}$$

- The fluidized bulk density  $\rho_{bfl}$  of the bed was obtained from measurements in a 150 – mm diameter batch fluidized bed.
- The change of bed depth (bed expansion), h was recorded for two different packed bed depths: 35 mm and 70 mm.
- The fluidized bulk density was evaluated using the expression:

$$\rho_{bfl} = \frac{m}{\frac{D_b^2 \pi}{4} h} \quad \text{Equation 35}$$

- The shear stress at the wall was expressed in terms of Darcy friction factor  $f_D$  and was applied to the Metzner-Reed (1955) model:

$$f_D = \frac{4\tau_w}{\frac{\rho_{bfl} u_{av}^2}{2}} = \frac{8k'8^{n'}}{\rho_{bfl} D_H^{n'} u_{av}^{2-n'}} \quad \text{Equation 36}$$

- Using the relationship  $f_D=64/Re'$  as for Newtonian fluids in laminar flow, the generalized Reynolds number was defined as:

$$Re' = \frac{D_H^{n'} u_{av}^{2-n'} \rho_{bfl}}{k' x 8^{n'-1}} \quad \text{Equation 37}$$

- The factor 64 corresponds to pipe flow and it has to be replaced by a factor  $Ce$  for the aspect ratio of the channel. The test results obtained for uniform flow at 40 mm ( $Ce = 59$ ) and 55 mm ( $Ce = 58$ ), were correlated and compared with the relationship for laminar flow

The flowing bed of 139  $\mu m$  magnetite showed different non-Newtonian characteristics, depending on the superficial gas velocity and depth of the bed. For a superficial gas velocity of 2.3  $U_{mf}$  and 40 mm bed depth, the bed behaved as a Bingham plastic fluid, while at a 55 mm bed depth the flow showed pseudoplastic behaviour. Their results were in close agreement to those reported by Botterill and van der Kolk (1971). Botterill

and Bessant (1976) reported similar non-Newtonian flow characteristics for sand, where the flow behaviour changed from Bingham plastic toward Newtonian behaviour, depending on the fluidization conditions.

### **2.3 Gupta et al.**

Gupta et al. (2006) reported the performance characteristics of a 3.7 m long fluidized motion conveying system at both horizontal, upward and downward inclination. Coal ash of median particle size of  $108 \mu\text{m}$  and minimum fluidization velocity of 2.5 cm/s was used as the conveyed material. The depths of the conveying channel section and plenum chamber were 150 mm and 75 mm respectively. The plenum chamber pressure was measured with a U-tube manometer. Six collection vessels were used to collect the material at the exit. They used the same methods as Botterill and Besant (1976) (as cited by Gupta et al.) to categorize the flow pattern on the basis of non-dimensional superficial air velocity  $U_0/U_{mf}$  for two material supply valve openings 50 % and 65 %, at different angle of inclination of the channel. The conveyor inclination was varied from 1.75 (downward) to -1.68 (upward) at increments of 0.50 degrees. The non-dimensional superficial air velocity  $U_0/U_{mf}$  was varied from 0.85 to 4.28.  $U_0$  is the air flow rate divided by the area of the porous membrane of the conveying channel expressed in cm/s and  $U_{mf}$  is the minimum fluidization velocity in cm/s. They found out that the material mass flux reached a stable saturation level at  $U_0/U_{mf}$  values around 1.5 to 1.7 for all conveyor inclination.

The maximum material mass flux at 50 % material supply valve opening was 1.69 kg/s, while for 65 % it reached 3.27 kg/s. The time averaged bed depth was observed at two fixed locations along the channel length for a given material supply valve and three conveyor inclinations: 1.75, 0.0 and -1.68 degrees. The solids mass flow decreased as the conveyor orientation changed from downward to upward direction. Further the upward inclination required a higher operating superficial air velocity to allow the material flow, and led to an increase of the material bed depth in the channel.

Gupta et al. (2009) extended the conveying channel from 3.7 to 5.5 and 7.5 m. A partition made of Perspex sheet was fixed inside the plenum chamber to divide it into two compartments, in order to maintain the same pressure in both compartments. Thus they used a single plenum chamber for the first 3.7 m channel length and two compartments for the rest of the channel length. A roots blower with air delivery of 340

$\text{m}^3/\text{h}$  was used to supply the airflow to a reservoir connected to the air inlets of the two plenum chamber compartments. They observed that the saturation levels of the material mass flow rates were falling with increasing channel length, due to what they assigned to be the back pressure developed by the air flow. It was also pointed out that the required operating superficial air velocity for a given mass flow rate increased with the increasing channel length. They attempted to give a prediction of material mass flux and operating air velocity by using the models reported by Woodcock and Mason (1978). The models did not work for their study due to following:

- the models reported by Woodcock and Mason (1978) assumed constant viscosity and density of the fluidized bed and laminar flow of the liquids, which is not always the case, as shown by Botterill and Abdul Halim (1979), Haugland (1998) and Oger and Savage (2013);
- the models considered steady state uniform flow of material that maintained a fixed bed height throughout the length of the channel;
- the models were not able to handle zero (horizontal), and negative (upward) channel inclinations.

#### **2.4 Discussion of flow regimes**

In the literature studies presented above, depending on the flow pressures (pressure gradients), the hydrodynamic conditions varied from dilute flow (rapid transport) to very dense flow (slow flow) in which frictional contacts predominate. The high concentration slow flow has received extensive attention in soil mechanics literature.

It is of practical interest, taking one more theoretical step further, the possibility to combine rheology and continuum mechanics in order to characterize the flow of materials, which poses a combination of elastic, viscous and plastic behaviour, by combining elasticity and fluid dynamics/mechanics. Ancy et al (2012), (2013) investigated the dam break problem for Herschel-Bulkley fluids by releasing a polymeric gel called Carbol ultrez down an inclined flume. DiCristo et al. (2013) used Ancy et al.'s (2012) approach to model waves dynamics in a linearized mud-flow shallow model, both for subcritical and supercritical flows.

Bingham and Coulomb behaviours are idealized representations of true materials related to the pioneering work done by Coulomb and Bingham. The differences between the two materials are shown in Figure 19. An important concept that needs to



be clarified is the **shear-rate dependence** for the two material representations. In the Coulomb representation the shear stress  $\tau$  is independent of the shear rate  $\dot{\gamma} = \left(\frac{\partial u}{\partial y}\right)$ , whereas in the Bingham fluid  $\tau$  is linearly dependent on  $\dot{\gamma}$ . Another concept is the **normal-stress dependence**. For a Coulomb material the shear stress is a linear function of the normal stress  $\sigma$ , whereas for a Bingham fluid  $\tau$  is independent of  $\sigma$ . The concept of **yielding** separates Coulomb materials from Bingham fluids: when  $\tau$  is below a threshold, called the yield stress,  $\tau_y$ , then they have very little in common and behave either like rigid or elastic materials. When the threshold is reached and exceeded, then the materials yield and start flowing:  $\tau = \tau_c + \mu\dot{\gamma}^n$ . Thus for a Coulomb material:  $\mu = 0$ ,  $\tau = (\tan\delta)p$ , according to a Coulomb type friction law for the basal shear traction with bed friction angle  $\delta$  and a hydrostatic pressure distribution,  $p$ , for which pore pressure and friction play the key role in bulk dynamics (Pudasaini and Hutter (2007) and Ancy (2007)). The concept of Coulomb plasticity has been used to characterize this material behaviour.

Bingham fluid:  $n = 1$ ,  $\tau_c$  is constant, the material exhibits a viscous behaviour after yielding. The concept of viscoplasticity has been used to characterize this fluid behaviour (Ancy (2007)).

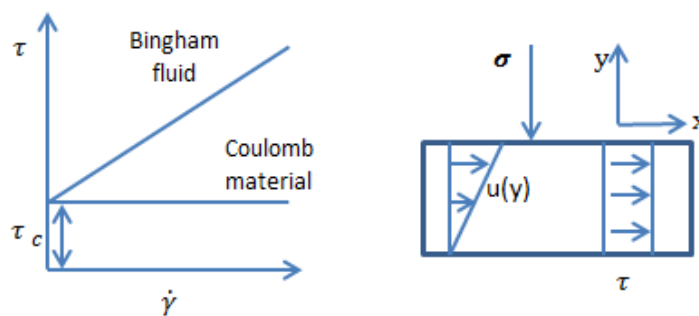


Figure 19 Rheometry curves: Coulomb material versus Bingham fluid, when the material is subject to a simple shear experiment (Ancy (2007)).

The concept of **yield surface** comes from soil mechanics and rheology fields and requires a detailed explanation. For concentrated particle suspensions/beds, the stress

at the particle surface is related to particle interactions. Flow initiation or yielding is a direct consequence of changes in these interactions. A simplified diagram of flow regimes as depicted in Figure 20 has been built up by Ancy (2007), where the transitions between regimes have been described by using dimensionless numbers. For concentrated particle suspensions, the stress at the surface is directly related to particle interactions, yielding being a consequence of changes in these interactions. In rheology, three flow regimes (illustrated as E-G in Figure 20) are known at high solid concentrations, where significant changes occur due to shear stresses and dilatancy of powder. Reynolds (cited by Ancy (2007)) described dilatancy in 1885 as a relationship between the applied stress and the voidage between particles filled with fluid or gas, stating that if an array of spherical particles is subject to a load, so as to cause a shear deformation, then the particles will ride one another, resulting in an increase in bulk density.

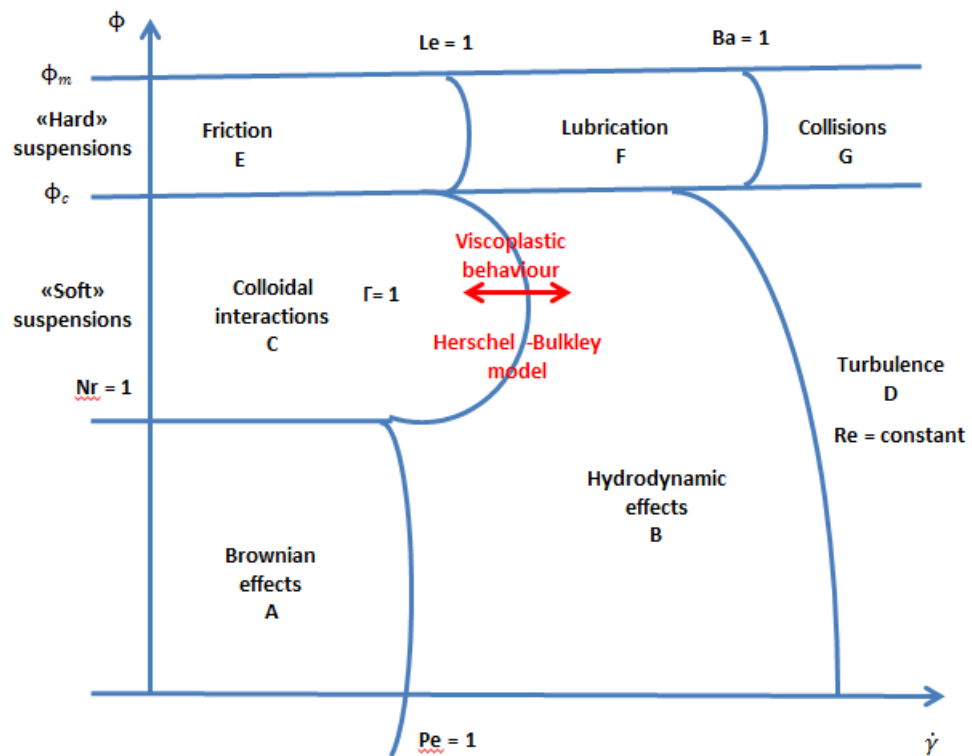


Figure 20 Simplified diagram of Ancy (2007) flow regimes.

From rheological point of view, the variation of particle sizes and types results in different flow behaviours. A key issue is the viscoplastic transition between zone B and

C, since it corresponds to viscoplastic regime and it can be described by using the Herschel - Bulkley model.

## 2.5 Links between fluidization, rheological and reometry results

It has been widely documented by Anjaneyulu and Khakhar (1995), Bruni (2005), Bruni et al. (2007 a & b) that fluidization behaviour of powders of different particle size distribution is affected by their rheological properties traditionally characterised by shear testers.

1. Anjaneyulu and Khakhar (1995) carried out experiments in a gas fluidized bed of glass beads by using a Brookfield Synchro - Lectric viscometer recording the torque on a vertical rotating cylinder. A relation between the wall shear stress and the rotational speed of the cylinder was fitted to the experimental data to obtain the rheological parameters. The data was interpreted from a momentum balance in cylindrical coordinates, using a Bingham plastic model. Bruni et al. (2004) studied the flow properties of alumina powder having a mean particle diameter of  $46 \mu\text{m}$  and a density of approximately  $1.7 \text{ kg m}^{-3}$ , for different fluidization velocities. A mechanically stirred Fluidized Bed Rheometer (msFBR) built and commissioned at University College London was used for the experiments. A 140 x 300 mm tall Pyrex vessel fitted with a steel distributor plate was used as a fluidising vessel. Nitrogen was used as fluidizing gas, flow rate was controlled by a set of rotameters, the pressure drop across the bed was measured by pressure differential sensors. The agitator consisted of a 165 mm long stainless steel shaft, fitted with a two-flat bladed paddle (36 mm x 7 mm x 0.7 mm thickness). A shear rate versus shear stress relationship was derived from the experimental torque profiles and a rheological model was fitted to the data. Results are presented in Chapter 7.

Bruni (2007 a) used a Contraves Rheomat 30 equipped with a steel shaft, fitted with two – flat - bladed paddles in her work. The data was interpreted by using Janssen's analysis to model stress distributions in the fluidizing column for mixtures of alumina and fines fluidized below  $U_{mf}$ . A review of the powders and bulk solids literature was undertaken to find modelling examples of stress distribution in a fluidizing column subjected to an upward gas flow. Nedderman (1992) and Schulze (2008) gave a detailed explanation of the Janssen effect. Bruni et al. (2007 a, b) used Janssen's analysis

(presented in Chapter 5) to model stress distributions in a fluidizing column for mixtures of alumina and fines fluidized below  $U_{mf}$ . In order to further investigate the links between fluidization, rheology and flow properties a small fluidization column was commissioned by the author at the Wolfson Centre. Results will be presented in Chapter 7.

### 2.5.1 Saint Venant – shallow water equations

The unsteady state flow of a fluid in an open channel can be described by the one dimensional Saint Venant equations (Ancy et al. (2012), Cristo et al. (2013)) based on single - phase mass and momentum conservation principles:

$$\frac{\partial A}{\partial t} + \frac{\partial(Q)}{\partial x} = 0$$

Equation 38

$$\frac{\partial Q}{\partial t} + \frac{\partial(\beta Q^2/A)}{\partial x} = Ag\sin\theta - Ag\cos\theta \frac{\partial h}{\partial x} - AgS_f$$

Equation 39

where: Q is the volume flow rate, A is flow cross sectional area,  $\theta$  is the angle of downward inclination of the channel, g is acceleration due to gravity,  $\beta$  is the momentum correction coefficient and  $S_f$  is the frictional slope. The formulation of flow resistance for fluid flow in an open channel is equivalent to that of pipe flow. Based on the Darcy- Weisbach equation for pipe flow:

$$h_f = f_D \frac{L V^2}{D 2g}$$

Equation 40

where  $h_f$  is the frictional head loss and  $f_D$  is the Darcy friction factor, then the frictional slope (also known as the flow resistance term) can be defined as:

$$S_f = \frac{h_f}{L} = \frac{f_D V^2}{D 2g}$$

Equation 41

The flow resistance term  $S_f$  will be discussed in detail in Chapter 7. Mathematical equations and different models assuming different flow layers and regimes have been proposed for the flow resistance term  $S_f$  (Jin and Fread (1997) and Naef et al. (2006),

Savage and Hutter (2008)) in geophysical flow studies. Geophysical flows ( such as debris flows, snow avalanches, dam break in rivers) involve massive movement of solid particles carried by a fluid and behave as the motion of a fluid down a slope and are analysed with hybrid methods both from fluid and soil mechanics.

## **2.6 Concluding remarks**

The investigation into methods and modelling approaches to estimate flow rates show that a number of researchers in the past have used different approaches to model material flow in an open channel. The theories that have been established either for fluidization or for the gravity flow of bulk solids are specific for each mechanical design and do not describe fully the behaviour of the material flow on the air slide. This is a major drawback for comparing results with other researchers test data. There is no equipment resemblance or standard method for modelling alumina flow in an air slide other than the measurements and analysis of Haugland (1998) and Oger and Savage (2013). In this work the measurement and analysis methods used by Haugland (1998) and Oger and Savage (2013) and Saint Venant shallow water equations have been selected to be used together with Jin and Fread (1997) flow resistance term as a starting point for the modelling work.

### **3 Survey of powder flow behaviour**

#### **3.1 Introduction**

This chapter covers a technology verification programme and standard powder characterisation techniques undertaken in order to build up basic understanding on which the research methodology and modelling strategies outlined in Chapter 6 and 7 are based on. The key objective of this project is to develop a modelling strategy to predict bed velocity and capacity in an air slide. To meet this objective, it is required to characterize the bulk flow properties using standard techniques commonly used in industry, as the main objective is to develop a model for aluminium industry. This chapter gives a short presentation of the electrolysis process and of the alumina distribution system (ADS). It then presents the methodology and the results of a verification programme undertaken in Årdal, which was the motivation for doing this PhD work. Test procedures for characterising alumina, fluoride and binary mixtures of the two powders, through fluidization and shear testing were conducted to build up basic understanding about powder behaviour and to fill the gaps of industrial knowledge between previous work done by Dyrøy (2006) and knowledge required by newer technological applications implemented at the Reference Centre in Årdal (e.g. the alumina rig).

#### **3.2 The electrolysis process**

Aluminium metal is obtained from alumina powder or aluminium oxide  $\text{Al}_2\text{O}_3$ , by electrolytic reduction in electrolytic cells connected in series to a power source. The fundamental concept of aluminium production is to reduce alumina to aluminium and oxygen by melting the alumina powder. The aim of the aluminium industry is to achieve stable electrolysis cell conditions during daily operations. A considerable amount of work has been published on both process modelling related topics and on aluminium production in general. Yet the number of publications focusing on alumina flow behaviour and design of feeding equipment is small. This may be due to high cost associated to with experimental investigations to assess the robustness and performance of such equipment or due to intellectual property confidentiality restrictions imposed by the various companies on this type of technology.

The electrolysis process and bath temperature dynamics have been explained in detail by Drengstig (1997) and Dyrøy (2006), this section giving only a very short overview.

An electrolytic cell consists of a rectangular steel box lined with isolating and refractory bricks and carbon blocks acting as the cathode. The melting point of alumina is close to 2030°C. In order to produce aluminium metal at a lower operating temperature, cryolite,  $\text{Na}_3\text{AlF}_6$  is used as a solvent for alumina. Alumina powder is fed and melted into the molten electrolyte, “bath”, contained within the isolated box. The bath is an extremely corrosive mixture of cryolite,  $\text{Na}_3\text{AlF}_6$ , a double salt consisting of sodium fluoride and aluminium fluoride. A number of anodes are suspended in the bath, acting as electrical conductors for the electric current. It takes approximately two kilograms of alumina to make one kilogram of aluminium metal, the Hydro Primary Metal business area having a total annual production capacity of more than 2 million tons primary aluminium.

Aluminium fluoride,  $\text{AlF}_3$ , is added to the cell in small quantities, from time to time as additive, to improve bath properties such as: temperature, reduced aluminium solubility, improved current efficiency and lower density. Cryolite’s melting point is at 1010°C, but the addition of aluminium fluoride,  $\text{AlF}_3$  reduces its melting point. The ability of cryolite to dissolve alumina is about 10 %, depending on bath temperature and the addition of extra additives.

### **3.3 Feeding alumina and aluminium fluoride to the electrolysis cells**

The alumina aerated distribution system (ADS) shown in Figure 21 is part of any electrolysis pot room, utilising basic principles as powder fluidization to convey alumina from the feeding silos to the electrolysis pots. The ADS is divided into three levels (Karlsen (2002)) and consists of inclined conveyor rectangular boxes (air slides) equipped with aeration elements (nozzles and membranes) to fluidize and transport alumina from the main alumina supply silo to the electrolysis pots.

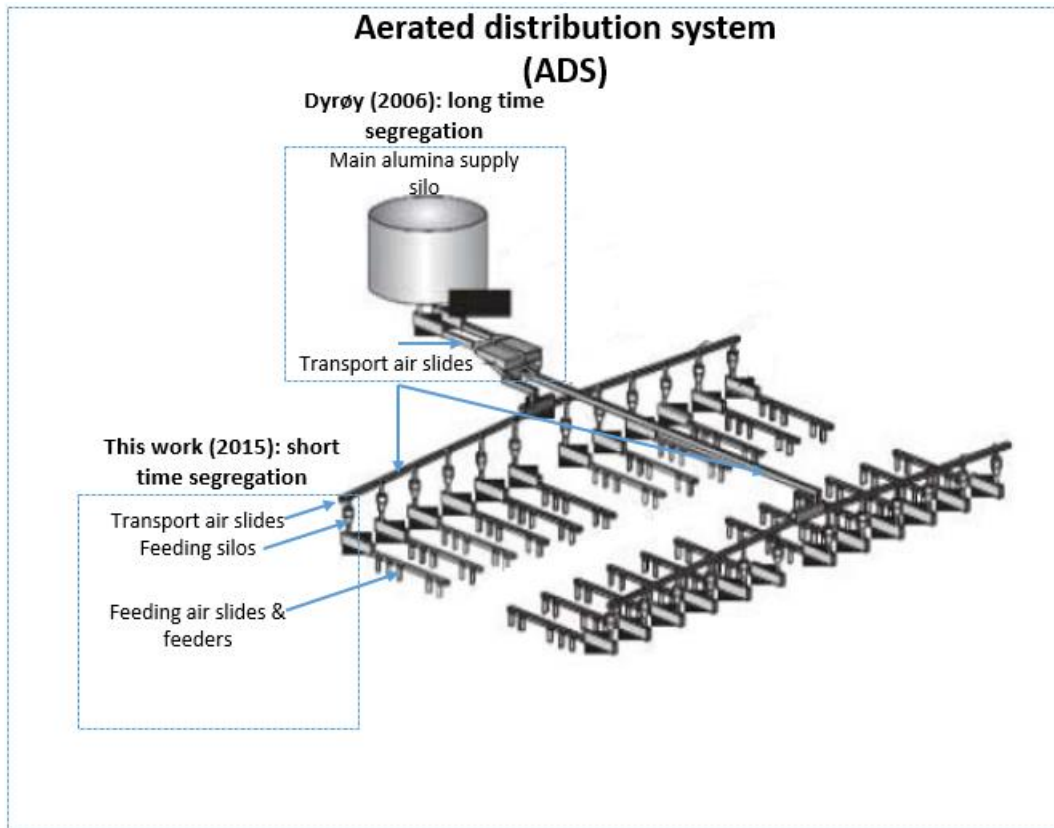


Figure 21 Lay out and the three levels of ADS (Karlsen (2002), Dyrøy (2006), Øystese (2015)). Two parallel rows of electrolysis pots.

The ADS is divided into three levels (Karlsen (2002)). The first level, defined as the conveying system from the main alumina supply silo and transport air slides into the pot rooms, was the main topic in Dyrøy's (2006) work. The second level is the transport air slide system inside the pot room conveying and distributing to the feeding silos allocated to each electrolysis pot. The third level is the part of the ADS distributing alumina and aluminium fluoride into the electrolysis cell through feeding air slides and volumetric feeders and together with air slide basic modelling, is the main topic of this thesis. Traditionally alumina powder is fed to the cell by volumetric dosing from a 12 up to 16.5 meters long feeding air slide (depending on cell design) with various point feeders (also called volumetric feeders) connected to it. Each electrolysis cell has a feeding air slide with 1 degree fixed inclination angle set by design. Aluminium fluoride (from a separate feeding silo on the pot room wall) is mixed in small quantities with alumina in the feeding air slide and fed to the cell together with the alumina, through the same feeders. Pressurized air distributed through nozzles to the membrane segments on the bottom of the air slide fluidize the powder bed and make it flow.



Although initially not an integral element of this thesis, as mentioned in Section 1.3, it became clear that in order to understand the behaviour of powder under air fluidised conditions in an air slide, one should study the impact that air slide interfaces e.g. feeding silos and silo outlet design have on the capacity of an air slide. A small feeder and its short air slide outlet is a scaled down concept of a bigger feeding silo discharging into a long feeding air slide. In order to understand the discharge patterns from big feeding silos as interfaces and input to air slides, small feeders from an alumina rig in Årdal were used as case study. Dyrøy (2006) defined segregation mechanisms as localized events, which lead to the separation of one type of component or size class of a powder or a binary mixture from another. A segregation process is a situation in which one or more of the mechanisms can become active, for example the discharging of a feeding silo or a feeder, or the fluidized transport of powders in air slides and their subsequent discharge. This work was conducted to fill the gaps of industrial knowledge, also the gaps between long time segregation processes (as in main storage facilities, see Figure 21) and short time segregation (as in smaller feeding silos, feeders and air slides). As pointed out by Dyrøy (2006) long time segregation can only be handled by the main storage facilities. Short time segregation starts where the powder is fed to the pots, from the feeding air slides to volumetric feeders through the feeders discharge rates (dumps) and directly affects the electrolysis pots. The feeding system is programmed as a high frequency small filling system for each electrolysis cell and whole sections of cells, where dump weights (feeder discharge) should be as equal as possible. Ideally, one should keep the alumina and the binary mixtures as homogeneous as possible in order to get low variation of dump weights. The feeders act more or less as a buffer/mini feeding silo. What one wants to control is their discharge rates (dumps) which should be as constant as possible throughout the operational life of a electrolysis cell. The design of the feeders should be so optimal that the feeding system should be able to cope both with changes in alumina quality, changes in fines content and in binary mixtures concentration, without too high variations in dump weights (discharge rates). The main feeding parameters that one needs to control are the optimal frequency of the powder doses and their optimal weights (dump weights), determined as a function of bath temperature and power consumption. Between 13 to 15 kWh per kilogram of aluminium produced is consumed in the process. Another control aim is to prolong cell life and minimize the use of expensive additives as aluminium fluoride  $\text{AlF}_3$ . According

to Dyrøy (2006) up to 1% of the current efficiency, hence the effect consumption of producing aluminium metal is lost due to quality variations in powders fed to the cell. It is then powder characterisation and studies of powder flow behaviour become important, serving as a reduction tool for power consumption.

### **3.4 Motivation for this PhD**

The entire survey work presented in this thesis has been motivated mainly from industrial points of view and tried to fill the knowledge gaps between previous work as investigated by Dyrøy (2006) and new challenges provided by newer technology implementations (e.g. the alumina rig in Årdal). Section 3.3 describes in details a measurement programme that built up the motivation for this PhD work. A new feeding air slide/alumina rig have been commissioned at Reference Centre in Årdal and tests for tuning alumina feeding parameters had been carried out between June – November 2009 and April 2015. The alumina dosing operation has been met on the rig by interfacing diamond shaped volumetric feeders and short air slide segments. Mechanical components of a feeding air slide are shown in Figure 22 and Figure 23. The volumetric feeder system operates on the same principles as a feeding silo and a feeding air slide system. One air slide segment supplies alumina to the feeder while a discharge (emptying) air slide feeds alumina to the cell. Each air slide is equipped with two nozzles supplying air to the fluidizing membrane, only one nozzle being activated during the tests in this programme. The deaeration tubes (black colour in Figure 22 b) on the two air slide segments lead the excess air back to the feeding air slide. The philosophy behind the dosing operation on the alumina rig consisted in emptying a pre-set number of volumetric feeders at equal time intervals in order to get twenty equal doses (during one cycle of operation) from each feeder.

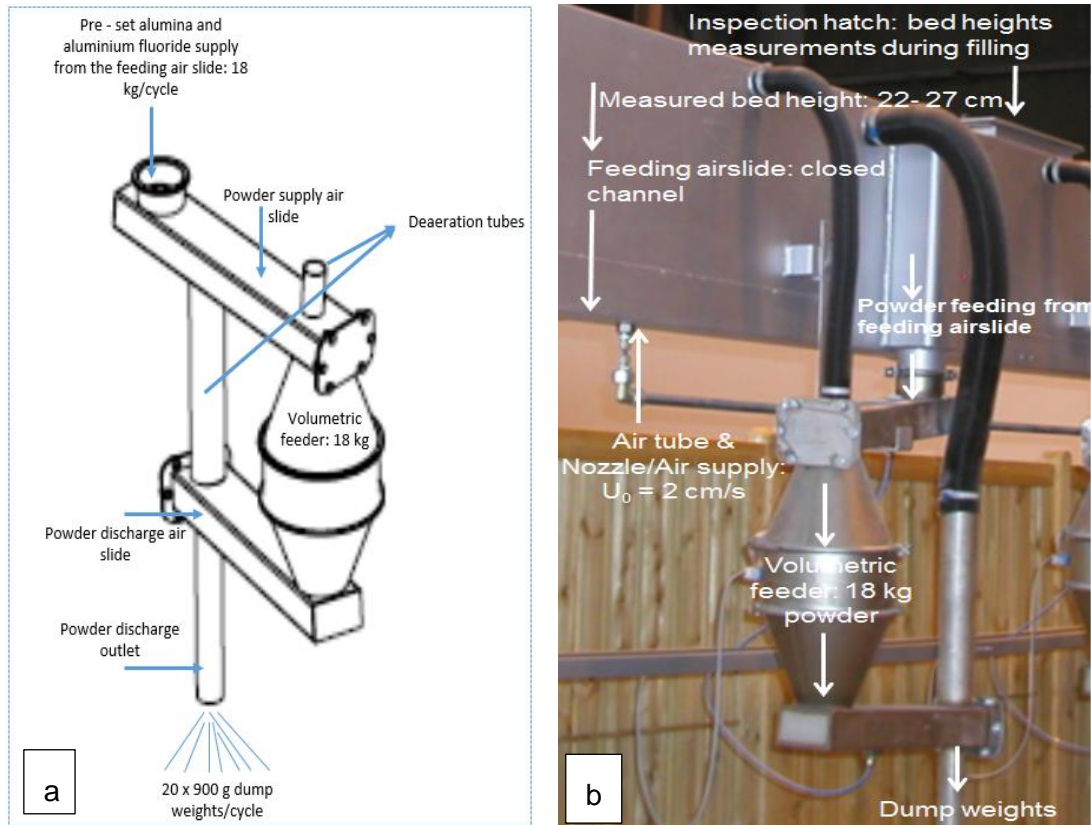


**Figure 22 Mechanical components of a feeding air slide, volumetric feeder and feeder interfaces.**

For alumina the real density values, determined by the actual density of the grains within a given powder sample, are between 3450 and 3600 kg/m<sup>3</sup> and can be measured by a pycnometer. The mechanical design of the feeders was chosen based on the loose bulk density of alumina, measured to be around 950 - 1000 kg/m<sup>3</sup>. The loose bulk density is defined as the mass of a powder sample divided by the total volume the sample occupies. In order to keep track of how much alumina is distributed to the cells at any time, a diamond shaped geometry was chosen for the feeders. It was then calculated based on the loose bulk density of alumina and the fixed control volume (geometry) of the feeder, that each feeder will store 18 kg of alumina powder for each cycle of operation and that 20 discharge dumps each dump weighing 900 g would be necessary to empty each feeder. This design approach and the control philosophy were right when taking in consideration only the loose bulk density of alumina. The aluminium fluoride is denser, having a loose bulk density of 1500 kg/m<sup>3</sup>. When distributed through the feeders, within the same control volume, it will result in higher

dump weights, above the 900 g average alumina weight. Each volumetric feeder (see Figure 23) is filled up with a binary mixture of powder from the main feeding air slide.



**Figure 23 a) Alumina rig: feeders 1 to 8 (diamond shaped), feeding air slide and feeding silos on the wall; the fluoride silo for the rig is not visible on the picture.**

Due to differences in loose bulk densities between the two powders and due to distribution patterns of the fluoride within the feeding air slide, each feeder will receive a different composition of binary mixture from the powder bed above. A deviation in the control volume due to changes in the composition of the binary mixture will have a large effect on the 20 doses varying between being either too large or too small. It is mainly this distribution pattern of the fluoride into the alumina bed through the feeding air slide and then through feeders into the cell, that was referred to as short time segregation earlier in Section 3.2. The accuracy of dump weights, as close to 900 g as possible (set by design) and with as little degree of variation as possible is essential for potroom operations in order to keep a stable bath chemistry into the electrolysis cells. A higher  $\text{AlF}_3$  distribution through feeders to certain areas of the cell will disturb the chemical balance of the bath, which is not desirable from control and operational point of view. Once the rig was tuned in, new tests were performed during September – November 2010 and April 2011 to check the behaviour of the system when filling  $\text{AlF}_3$  in addition to  $\text{Al}_2\text{O}_3$ . Experiments were aimed to investigate the robustness of the new mechanical design and feeders performance by analysing the repeatability of dump

weights from each individual feeder during six to eight consecutive run cycles as well as the mixing degree and distribution of  $\text{AlF}_3$  into the system as  $\text{AlF}_3$  wt % (weight percent) in secondary alumina powder. The results of this programme, presented in the next sections, served as part of technology verification of Hydro's alumina and fluoride distribution programme built on new technology cells.

### 3.4.1 Programme of work on the alumina rig

The test material used in the test programme was secondary alumina, the same alumina used by test electrolysis cells in operation, as the test rig and the cells are sharing the same distribution air slide. Alumina was fed to the feeding air slide by measuring the fluidized bed height. Alumina supply from the buffer silo on the wall (see Figure 24) was considered to be enough for the tests when the fluidized bed in the feeding air slide would reach 33 - 35 cm, measured from the bottom of the fluidizing membrane to the surface of the bubbling bed.

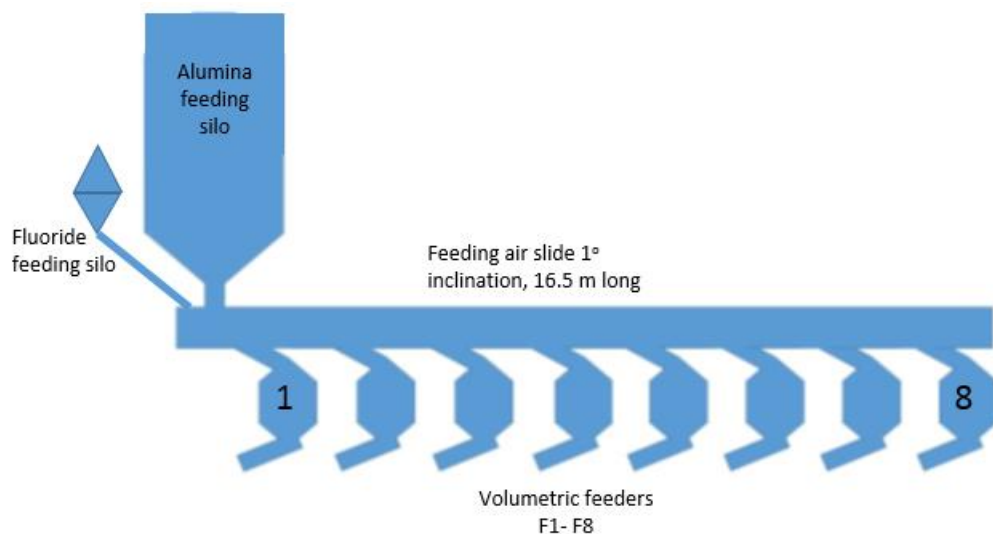


**Figure 24 Illustration of the alumina rig: feeding silos, feeding air slide and volumetric feeders.**

Based on the volume of the alumina bed in the feeding air slide and the bulk density of fluidized alumina, the amount needed for each test was estimated to be around 850 – 900 kg of powder. Thirteen tests were conducted totally; an amount of ca. 13 tons of powder was used in total. The work programme had clear objectives: to investigate the fluoride distribution, 150 kg into 900 kg of alumina for each test, both with closed and open valve for alumina supply from the silo on the wall.

Six tests, called series 1, were performed with a closed valve for alumina supply on the feeding silo and by supplying 150 kg of  $\text{AlF}_3$  at once, on the top of alumina bed. The powder was then supplied to all feeders and the content of each feeder was emptied into buckets, powder samples were taken and accumulated dump weights registered manually. Powder samples were sent to the Hydro lab for chemical analysis of the components in the powder (XRF analysis). Another six tests were then conducted, called series 2, where the same amount of fluoride was added to the system, but this time the valve for alumina supply was kept open. One wanted to investigate the fluoride distribution onto the alumina bed during various cycles of operation and the effects of having the alumina supply valve open (Figure 25) and how continuously supplying alumina to the feeding air slide will influence the fluoride distribution in the feeding air slide and across all feeders.



**Figure 25 Knife valves on the outlets of the feeding silos for opening & closing alumina & fluoride supply to the feeding air slide and for manual sampling of fluoride.**

A single test was performed at the end of the programme, Test 13, to investigate what the situation would be in real operations. The challenge was to be able to track the added fluoride from the supply silo because of the low concentration changes in normal operation. The lowest amount of added  $\text{AlF}_3$  in one shot was estimated to the same

volume as one feeding apparatus, i.e. 8 liters or 12 kg. At the same time it was important to add  $AlF_3$  partly continuously to simulate the real operational mode.

### 3.4.2 Execution of the test programme

Next sections describe the test programme conducted on the alumina rig and the test results. The method presented below is the only way to test capacity of a feeding air slide and map volumetric feeder capacity and performance, standard operational procedure at the Reference Centre. The alumina and fluoride supply to the feeding air slide was controlled through a Simens Simatic panel as shown in Figure 26 a. The panel had level indicators for the feeding silos indicating when the silos had to be refilled from the main transport air slides. Other input parameters such as number of dumps (doses) per feeder and run time for the feeding element needed to be set before starting the tests. A bench scale from Metter Toledo (Figure 26 b) with a maximum capacity of 15 kg was used to weigh the dumps from each feeder.

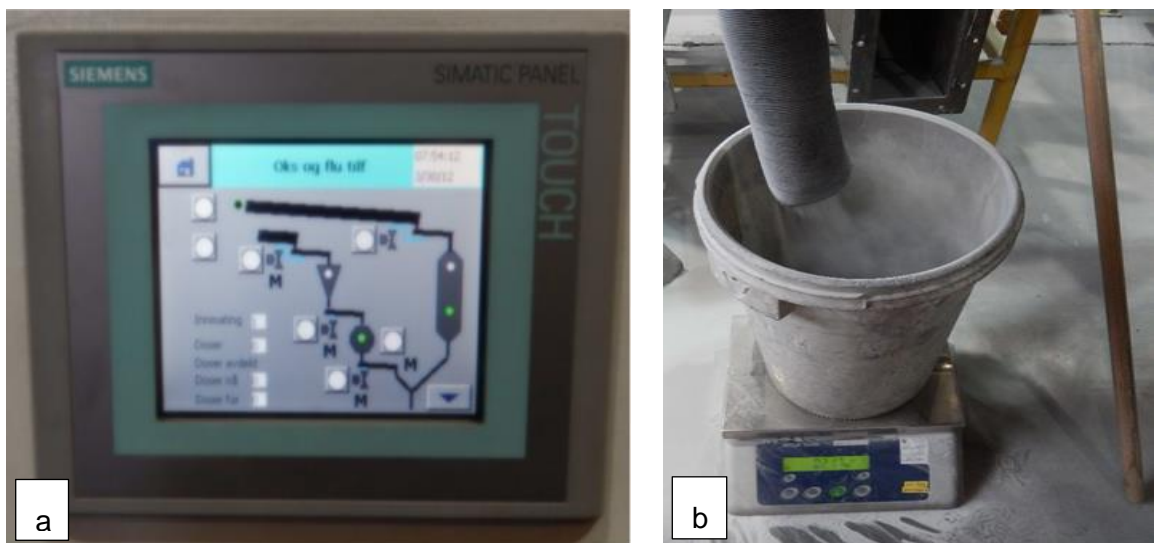


**Figure 26 a) Simens Simatic Panel used for filling and level controls of the feeding silos supplying alumina and aluminium fluoride to the feeding air slide; b) Bench scale used for weighing the dumps from the feeders.**

One cycle of operation for a volumetric feeder means 20 dumps, discharging in theory 18 kg of powder. Powder dumps (doses) weighing 900 g each were discharged 20 times from each feeder, the flow of powder being choked (stopped) by the PLS after the discharge of each dump. Parameters used for the Simens Programmable Logical Controller (PLS) control panel were:

- 20 dumps/cycle (used for each one of eight feeders).
- Valve (dump) opening time 2600 - 2900 mseconds.
- 6 to 8 consecutive cycles were run for each test.

Each test was executed in the following sequence controlled from the PLS panel: first dump out of twenty dumps will be discharged from the first feeder into the bucket, then first dump from the second feeder and so on until the eighth feeder. Then again, the second dump will be discharged from the first feeder and the sequence will go on until the twentieth dump will be discharged from the last feeder. At the end of each cycle the rig will be stopped manually, the buckets weighed and emptied into the garbage bin and the sequence for filling of the feeding air slide started. Same procedures will be repeated six to eight times (cycles) during one test. Each dump weighs from 850 to 1400 grams, depending on the fluoride density in the alumina bed into the feeding air slide above the feeder and the powder density supplied to the feeder. One test consists of: 1 to 6 up to 8 cycles, one series consists of 6 tests. Thus, the requirements for the first test series, which included tests 1 to 6, were defined as following:

- To start by emptying and vacuum cleaning the alumina distribution and feeding air slides, since the rig had not been in use for a while;
- Empty the feeding alumina silo on the wall (shown in Figure 25), discharge the powder through the feeders, throw the old powder into the garbage bin and fill the feeding silo with fresh alumina from the main air slide;
- Filled feeding air slide: approximately 800 kg secondary alumina corresponding to a height of product in the air slide of 33 - 34 cm measured manually through the inspection hatches situated on the top between feeder no.6 and 7 and 22- 23 cm measured between no. 3 and 4. Closed valve for refilling of the unit from the alumina feeding silo on the wall.
- Fill 150 kg  $\text{AlF}_3$  as fast as possible in the first section of the air slide and close the valve, thus no possibility for further feeding of  $\text{AlF}_3$ .
- Adjust the feeding rate to fit the sampling rate and numbering for the people (two) involved so they can cope with the tempo.
- Run the feeding and filling cycle 48 times (8 feeders, 6 cycles) to be sure that the  $\text{AlF}_3$  would be supplied and distributed through all feeders.
- Take samples for analysis from all apparatus and mark them accordingly: date, time, cycle and dump number; do not sample from the first and the last two



dumps as it was seen from the pre tuning tests that they deviate from the cycle average. Total samples for each run are 64 out of 976 dosages.

- Alumina and fluoride removed: 976 x 0.9 kg secondary alumina plus 150 kg  $AlF_3$ , altogether approximate 1028 kg powder.

Figure 27 a shows the buckets used to weigh the discharged powder from the feeders. Each bucket is left under the feeder during one cycle. At the end of each cycle all buckets are weighted on the scales and emptied into a garbage bin.



**Figure 27 Displacements of buckets under each feeder, scales to measure the accumulated weights and weights of sample bags.**

Figure 27 b shows the sample bags (blue). Empty sample bags were placed by each feeder at the beginning of the test with cycle and dump number: 4, 6, 8...16 and 17 written on. At the end of each test sample bags were weighted and packed down into storage boxes for further chemical analysis at the lab. Complete results of the alumina rig programme are presented in the Appendix, in Table 77 to Figure 276.

### 3.4.3 Series 1: test 1 to 6

Following the instructions as described above, six tests, with 6 (some tests with only 5) cycles each, were run. A mass balance including sample bags weights, bucket accumulated weight and powder left in the air slide at the end of each test is shown in Table 1. Tests 3 and 6 were completed after five cycles only, due to too little powder supplied to the feeding air slide. This was due to not enough alumina being supplied to

the air slide, as indicated by the powder height measurements above feeder 2 (F2: 22 cm in Table 1). Measurements of the powder height in the air slide were conducted at the beginning at each test at two inspection hatches situated on the top of the air slide above feeders 2 and 5 (F2 and F5 in Table 1). All powder left in the feeding air slide at the end of each test round was emptied through the feeders and extracted from the mass balance. Results of tests 1 to 6 run with closed valve of alumina refill from the feeding silo, presenting dump weights for a whole cycle and dump weights from an inventory of the sample bags are presented in Appendix in Table 77 to Figure 270.

**Table 1 Total powder weight [kg] used per test. Mass balance series 1, test 1 to 6, closed valve for alumina refill.**

Test	Nr. of cycles	Powder height in the airslide	Total amount of alumina & fluoride [kg]	Powder left in the airslide [kg]
1	7	F5: 33 cm, F2: 23 cm	1074 - 30 = 1044 kg , cycle 7 not complete: 102 kg	30
2	7	F5: 34 cm, F2: 27 cm	1089 - 39 = 1050 kg , cycle 7 not complete: 124 kg	39
3	6	F5: 31 cm, F2: 22 cm	914 - 35 = 879 kg , cycle 6 not complete: 109 kg	35
4	7	F5: 34.5 cm, F2: 27 cm	1082 - 34 = 1048 kg , cycle 7 not complete: 111 kg	34
5	7	F5: 33 cm, F2: 27 cm	1076 - 28 = 1048 kg , cycle 7 not complete: 95 kg	28
6	5	F5: 35 cm, F2: 22 cm	879 - 104 = 775 kg , airslide emptied before cycle 6	104

Since only sample bags from one test out of six would be sent to the lab for chemical analysis, due to the high costs of such analysis, an overview by studying the test results was made to help choosing from which test they should be sent. Figure 28 shows a clear test pattern. The accumulated bucket weights for Cycles 1 and 2 in each test are lower than those for Cycles 3 to 6 (5). During cycle 1, for each test, only secondary alumina was used. It is also very close to the series 1 average result. E.g.: the buckets with powder from feeder 1 to 8 weigh 152 kg (test 4). Buckets were getting heavier during cycle 3, 4, 5 reaching gradually 166 kg, as for test 1, cycle 5, due to higher fluoride distribution through the air slide. Buckets weigh 158 kg after cycle 6. Eight cycles instead of six, should have been run to show the bucket weight decrease after cycle 5.

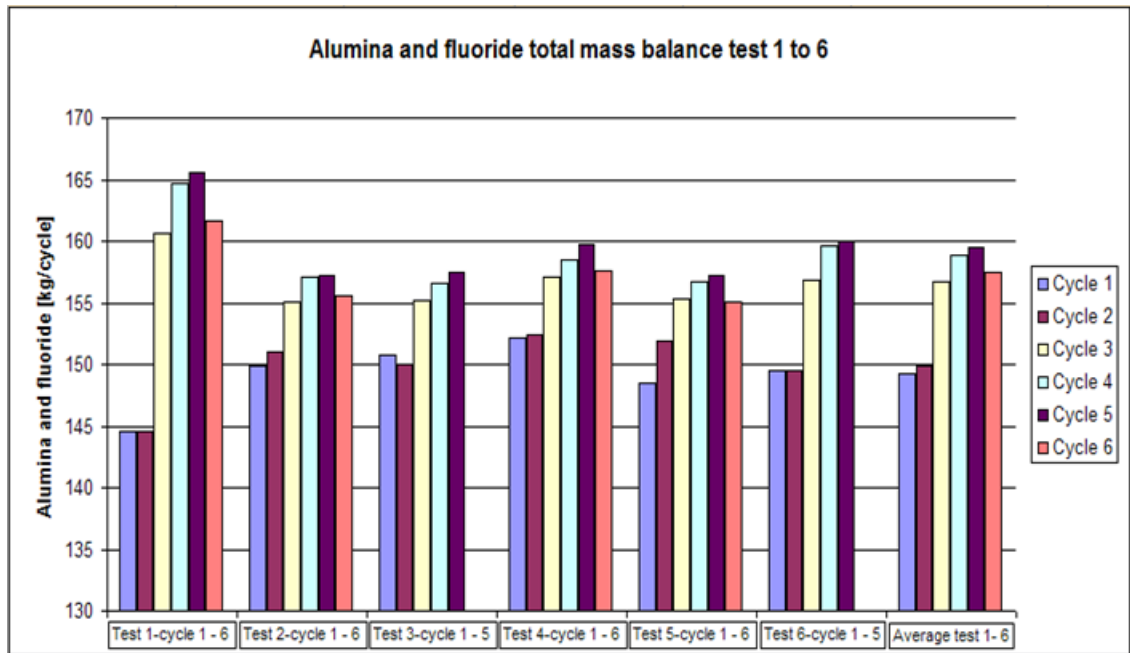


Figure 28 Total powder weight used per cycle per test and series 1 average. Series 1: test 1 to 6, run with closed valve for alumina refill.

In order to check the repeatability and the robustness of the rig, coefficients of variation for each cycle in each test were calculated as shown in Table 2.

Basic statistic theory has been used to analyse the results. The average value  $\bar{X}$  of a series of  $i = 1 \dots n$  cycles, with  $n = 5 \dots 8$

$$\bar{X} = \frac{1}{n} \sum_{i=1}^n X_i$$

and the standard deviation:

$$St\ dev = \sqrt{\frac{\sum_{i=1}^n (X_i - \bar{X})^2}{n - 1}}$$

have been used to calculate the coefficients of variation of a series of  $i = 1 \dots n$  cycles:

$$Coeff\ of\ variation = \frac{St\ dev}{\bar{X}}$$

The coefficients of variation were calculated as standard deviation divided by average bucket weight (re- including the weight of the sample bags). As it can be seen, the

variation is very low, +/- 1 % to 2 % within cycle 1, for example, for all tests 1 to 6. Test 1 had the highest coefficient of variation +/- 6 %, so it was not that representative. Tests 2, 4 and 5 showed the same mass distribution pattern, with equal numbers of cycle run. That is why test 4 was chosen to be sent to the lab in Tangen for chemical analysis.

**Table 2 Alumina and fluoride total mass balance per cycle per test [kg], series 1 test 1 to 6. Closed valve for alumina refill. Tests 3 and 6 empty feeding air slide during cycle 6.**

Test number	Cycle 1 [kg]	Cycle 2 [kg]	Cycle 3 [kg]	Cycle 4 [kg]	Cycle 5 [kg]	Cycle 6 [kg]	Coeff. of variation
1	145	145	161	165	166	162	6 %
2	150	151	155	157	157	156	2 %
3	151	150	155	157	157		2 %
4	152	152	157	158	160	158	2 %
5	148	152	155	157	157	155	2 %
6	150	149	157	160	160		3 %
<b>Average</b>	<b>149</b>	<b>150</b>	<b>157</b>	<b>159</b>	<b>160</b>	<b>157</b>	
<b>Coeff. of variation</b>	<b>2 %</b>	<b>2 %</b>	<b>1 %</b>	<b>2 %</b>	<b>2 %</b>	<b>2 %</b>	

#### 3.4.4 Inventory of sample bags and weighing buckets - closed alumina refill valve

For each test, an inventory of the weight of the sample bags per cycle per feeder was made. Results from Test 4 are shown in Figure 29 a and b. It is clearly shown how most of the fluoride is distributed from the air slide to feeders 1 to 4. The test was run with 6 complete cycles. Although feeders 1 to 4 got empty in the middle of the cycle 7, samples have been taken. The weight of a sample bag can vary between 780 and 1380 grams. Sample bags dump weights were re- included (summed up) to the weight of the buckets, in order to get the total alumina and fluoride mass balance. It shows that most of fluoride is distributed through feeders 1 to 3. Thus having the information acquired from mass balance, it was very interesting to compare it to results from the chemical analysis. Sample bags content from the test has been split 50 – 50 % and only half of the content has been sent to the lab, the rest has been stored for further use, as backup, in case something would go wrong with the samples and the lab will require more samples.

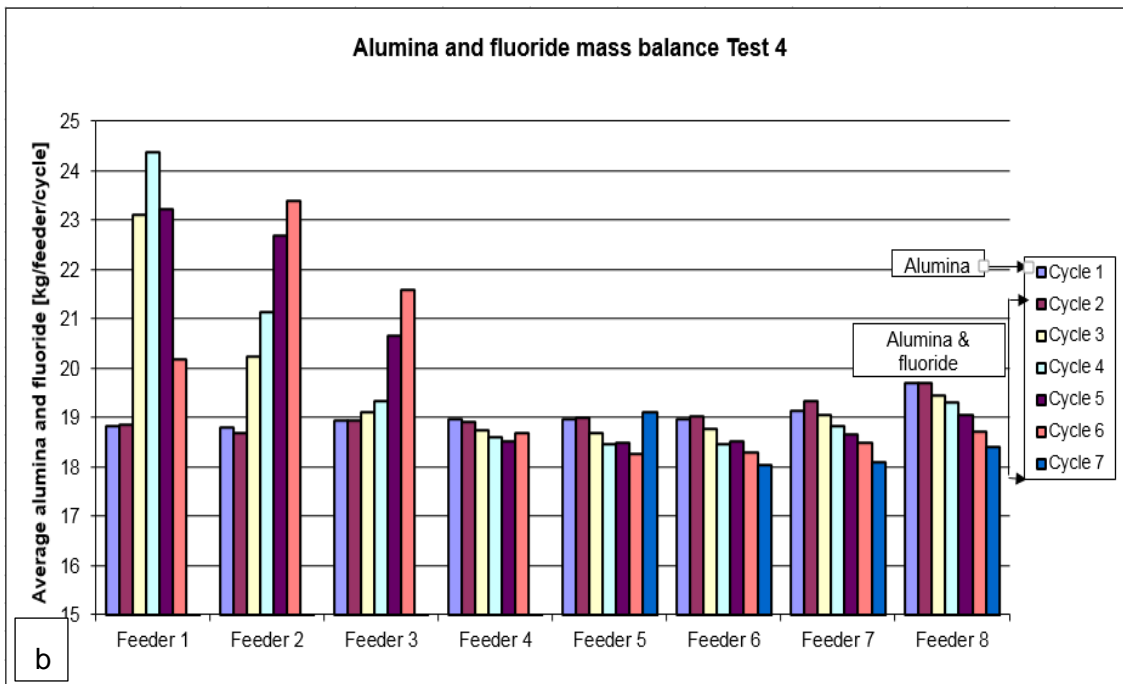
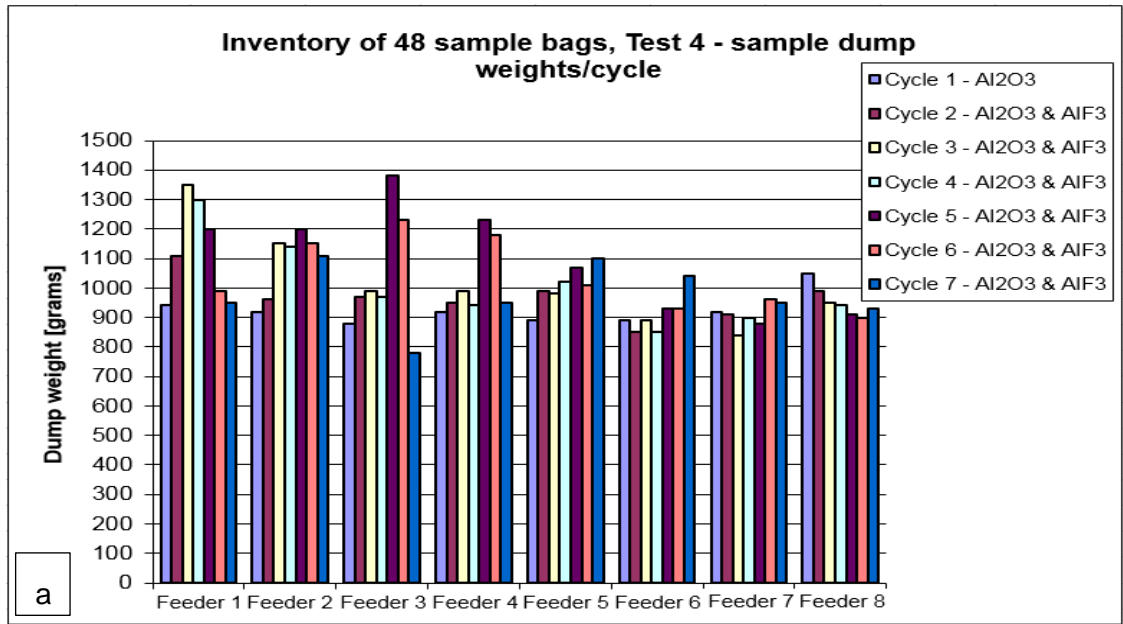


Figure 29 a) Test 4: inventory of sample bags, dump weights; b) Alumina and fluoride mass balance through the air slide. Feeders 1 - 4 got empty during cycle 7.

### 3.4.5 Series 1 test results: mass balance (buckets) based on dump weights versus bags/sample chemical analysis

Figure 29 b has been adjusted (shown as Figure 30 a) in order to make it easier to directly compare the mass balance to the chemical results (Figure 30 b). The average, considered as being Cycle 1, only alumina, is represented as the 0 line on the X – axis (Figure 30 b). All values above average are due to fluoride distribution into the feeding

air slide, through the feeders. Figure 29 a and b show a higher mass increase around feeders 1 and 3, coming from a higher concentration of fluoride into the alumina fed and discharged from feeders 1 and 3. Having a higher bulk density than alumina, the fluoride tends to “sink” instead of being transported all the way to feeder no. 8. Results from mass balance based on average test values show similar trends, thus a strong correlation with chemical results based on the inventory of sample bags sent to the lab: Figure 30 b), Feeder 1, Cycle 3, 4, 5: sample bags with high percentage of fluoride in the range of 60 to 75 wt %  $\text{AlF}_3$ . Figure 30 a), Feeder 1, Cycle 3, 4, 5 shows a similar mass increase above average (cycle 1 only alumina).

Results of the tests with closed valve for alumina supply from the feeding silo showed that fluoride, having a higher bulk density than alumina, was distributed only through feeders 1 to 3. In the absence of fresh alumina supply to the feeding air slide to push the fluoride further, towards the end of the feeding air slide, the fluoride will “sink” into the alumina bed above feeders 1 to 3. Low concentrations of fluoride from the sample bags (results from chemical analysis of the components in the powder) taken from feeders 4 to 8 and no increase in alumina and fluoride mass from the average cycle 1 (mass balance of the accumulated weight of sample bags and buckets) strongly confirmed this.

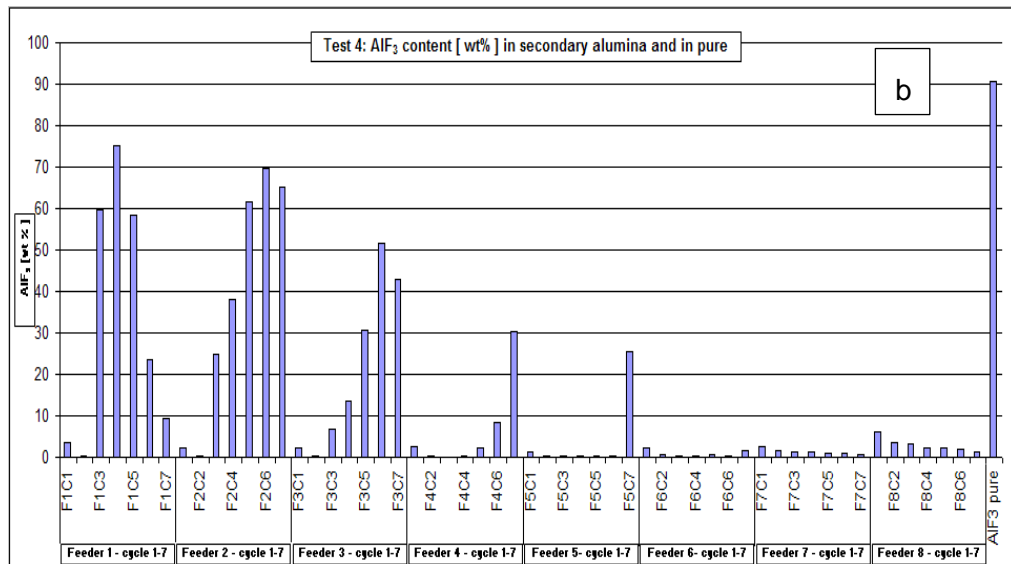
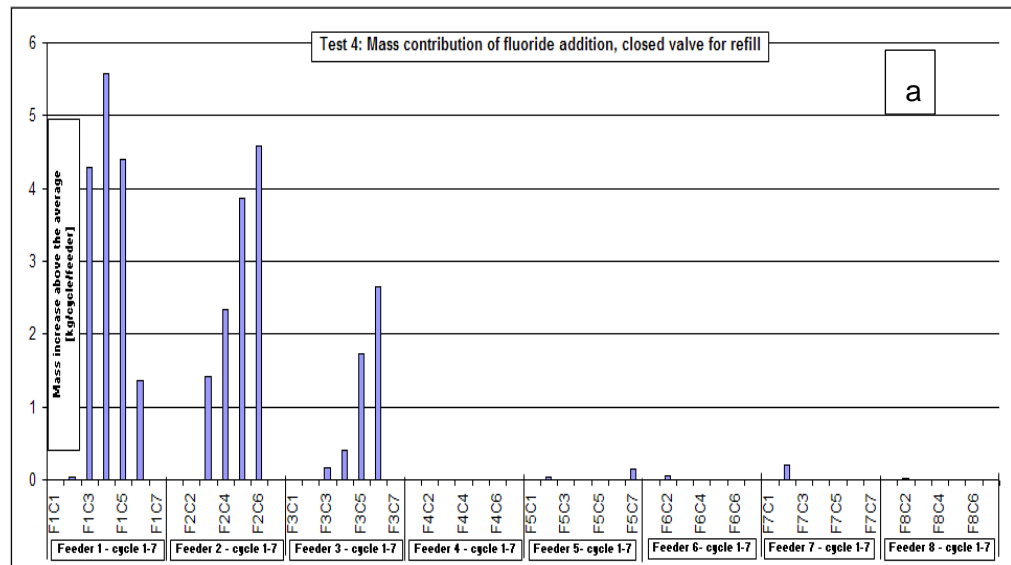


Figure 30 Test 4 a) Alumina and fluoride mass balance through the air slide. Mass increase above the average cycle. b) Test 4 results of chemical analysis.

### 3.4.6 Series 2 test results: mass balance (buckets) based on dump weights versus bags/sample chemical analysis

Same parameters for the PLS control panel and the same method for test set-up and execution was used for series 2, tests 7 to 12, but the tests were run with open valve for alumina refill, thus all tests were run with the same amount of powder (as shown in Table 3). Based on the experience from the previous tests, eight cycles were run instead of six this time, to better show the fluoride distribution through the feeding air slide and feeders. Results of tests 7 to 12 run with open valve of alumina refill from the feeding silo, presenting dump weights for a whole cycle and dump weights from an inventory of the sample bags are presented in Appendix in Table 97 to Figure 276. As it can be

seen from Table 4, the variation between tests 7 to 12 calculated for each cycle 1 to 8 is very low, +/- 1 % to 2 % .

**Table 3 Total powder weight used per test. Mass balance series 2, test 7 to 12, opened valve for alumina refill.**

Test	Nr. of cycles	Powder height in the airslide	Total amount of alumina & fluoride [kg]	Powder left in the airslide [kg]
7	8	Open valve, no need	1232 kg	Open valve, no need
8	8		1217 kg	
9	8		1220 kg	
10	8		1231 kg	
11	8		1216 kg	
12	8		1228 kg	

**Table 4 Alumina and fluoride total mass balance per cycle per test [kg], series 2 test 7 to 12. Open valve for alumina refill.**

Test number	Cycle 1 [kg]	Cycle 2 [kg]	Cycle 3 [kg]	Cycle 4 [kg]	Cycle 5 [kg]	Cycle 6 [kg]	Cycle 7 [kg]	Cycle 8 [kg]	Coeff. of variation
7	151	152	157	159	159	155	151	150	2 %
8	149	149	157	159	153	151	150	149	3 %
9	147	150	155	159	156	153	150	149	3 %
10	149	152	156	157	160	155	153	151	2 %
11	148	150	156	159	153	151	150	149	3 %
12	149	155	156	156	156	155	152	149	2 %
<b>Average [kg]</b>	<b>149</b>	<b>151</b>	<b>156</b>	<b>158</b>	<b>156</b>	<b>153</b>	<b>151</b>	<b>149</b>	
<b>Coeff. of variation</b>	<b>1 %</b>	<b>1 %</b>	<b>0 %</b>	<b>1 %</b>	<b>2 %</b>	<b>1 %</b>	<b>1 %</b>	<b>1 %</b>	

All tests except Test 12 showed the same mass distribution pattern as seen in Figure 31, with equal numbers of cycle runs. That is why test 9 was chosen to be sent to the lab for chemical analysis.



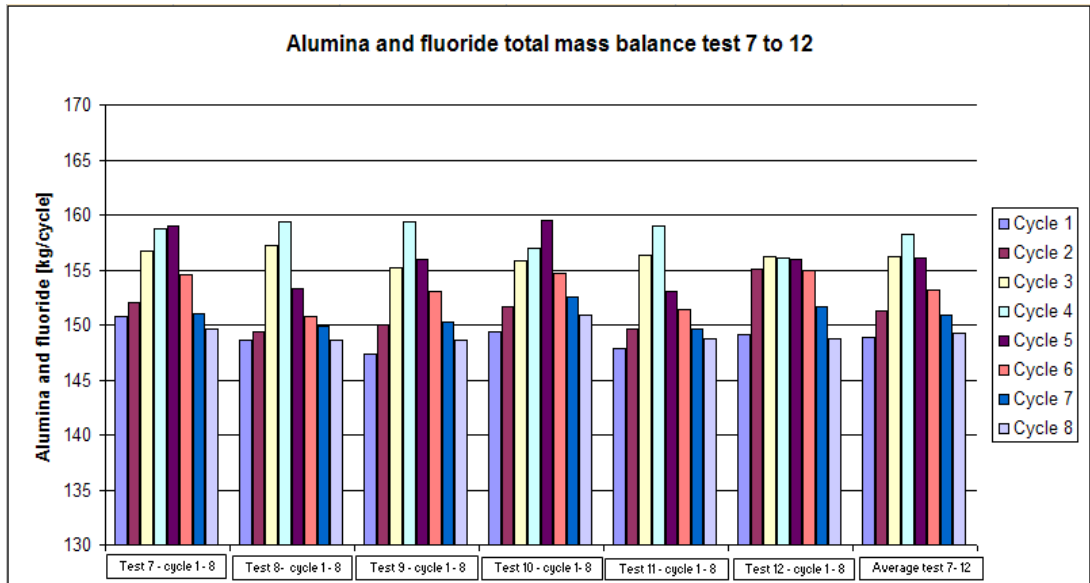


Figure 31 Total powder weight used per cycle per test and series 2 average. Series 2: test 7 to 12, run with open valve for alumina refill.

It can be seen from Figure 31 that the total powder weight used per cycle per test is increasing during cycles 3, 4, 5 reaching its maximum during cycle 4 and decreases again after cycle 6. This gives a strong indication about the fluoride distribution during operation of the feeders.

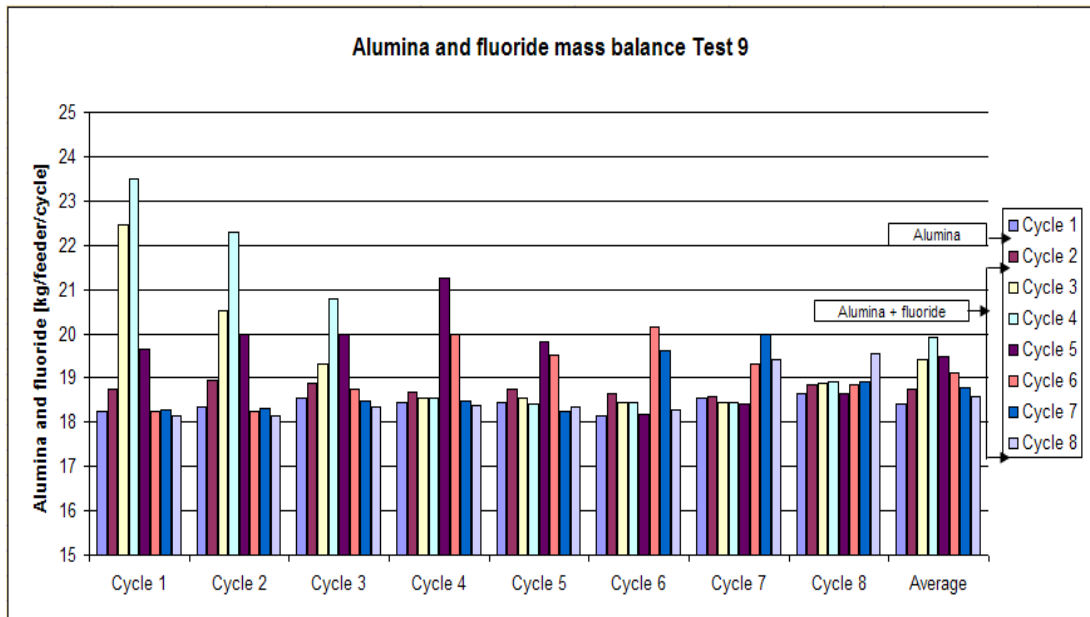


Figure 32 Test 9 Alumina and fluoride mass balance through the feeding air slide.

When comparing Test 4 (Figure 30 a and b) to Test 9 (Figure 33 a and b), one can see a different pattern, although the same amount of fluoride was used. The difference is in keeping the valve for alumina refill open. This contributes to a better distribution of the fluoride throughout the entire feeding air slide, not only around feeders 1 to 3 as shown in the previous test. This is also how the Hydro test cells are running during daily operations.

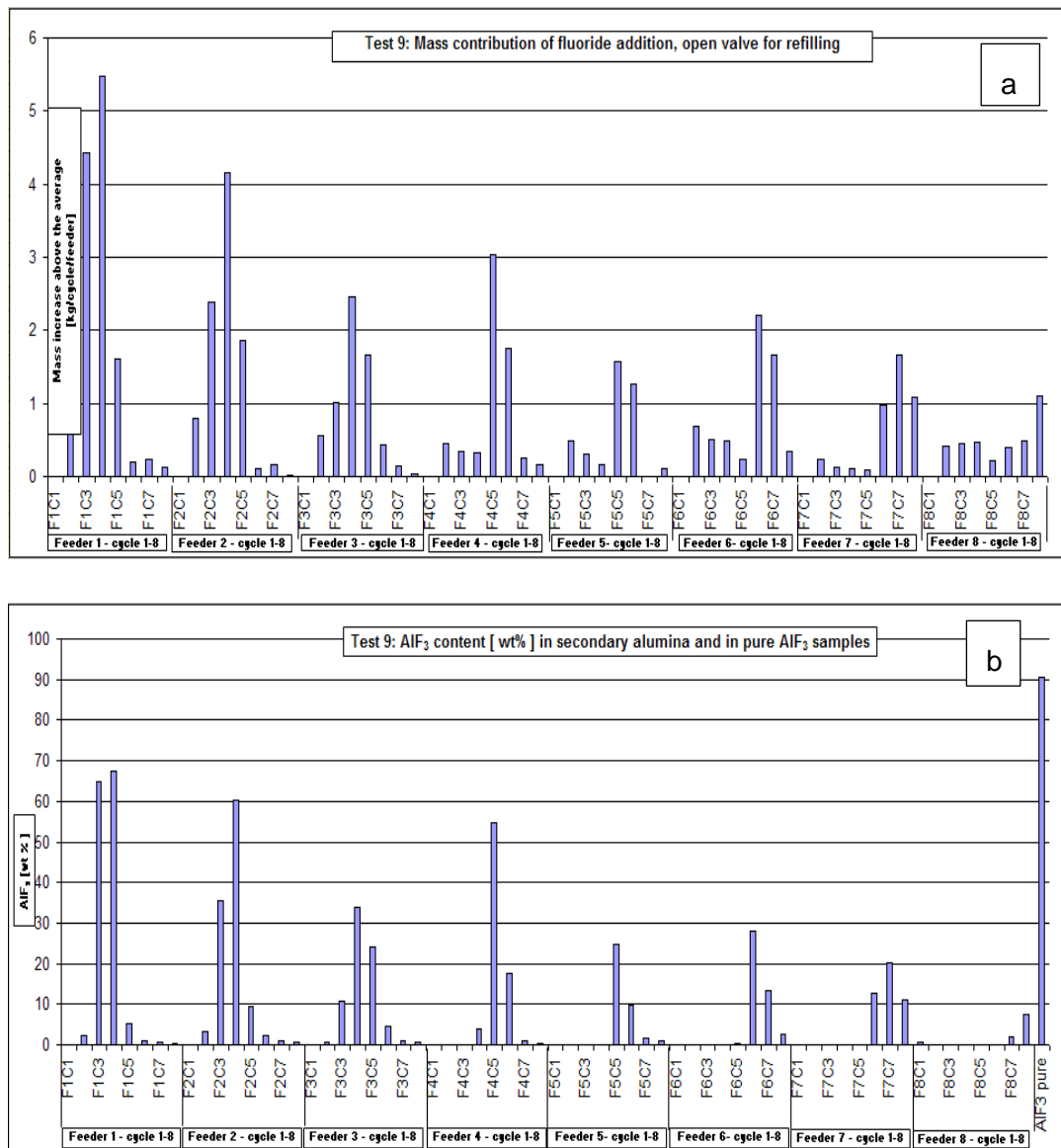


Figure 33 Test 9 a) Alumina and fluoride mass distribution through the air slide. Mass increase above the average cycle. b) Test 9 results of chemical analysis.

Results of the tests in series 2 presented above showed a better distribution of fluoride through the system. Feeders 1 and 2 still received high loads of the fluoride, during

cycle 3 and 4, but the difference from previous test, was that the fluoride was pushed forward towards the end of the air slide due to continuously supplying of alumina to the air slide and slowly distributed to the other feeders. The open valve allowed a continuous feeding of alumina into the air slide, thus slowly pushing the fluoride mass further to the end of the feeding air slide.

#### 3.4.7 Test 13

Same parameters as for the previous two series were used for the PLS control panel, but with a different feeding strategy for the fluoride. Only one test was conducted between the 12/13 th. of April 2011.

The last test was performed in such a way to simulate the real flow of fluoride into the feeding air slide. The challenge was to be able to track the added fluoride because of the low concentration changes in normal operation. The lowest amount of added  $\text{AlF}_3$  in one shot was estimated to the same volume as one feeder, i.e. 8 liters or 12 kg. At the same time it is important to add  $\text{AlF}_3$  continuously to simulate the real operational mode. The compromise solution to detect and simulate the real operational mode is to use 6 feeders or one buffer silo and spread the addition over three distinct time laps or feeding cycles. Tests were executed according to the following procedure:

- Fill up the air slide (approx. 800kg) and open the valve for refilling of the air slide from the buffer silo at the wall.
- Set the feeding rate to fit the sampling rate and numbering for the people involved so that they can cope with the tempo, same procedure as in Test 1
- Take dosage for analysis for the feeders and mark them accordingly: time, feeder number and dosage number in the interval 3 to 18 ( do not include the 2 first and 2 last in the feeding cycle of the apparatus of 20 dosages)
- Discharge 6 fluoride feeding silos (from the feeding silo on the wall) or 75 kg  $\text{AlF}_3$  (F1  $\text{AlF}_3$  – F6  $\text{AlF}_3$ ) into the feeding air slide in the following sequence of cycles:
  - Cycle 1: Open the valve for refilling of the feeding air slide from the buffer silo on the wall. Take samples for the first filling, i.e. ordinary secondary alumina, from each feeder 1 to 8.
  - Cycle 2: Fill up the  $\text{AlF}_3$  feeding silo on the wall and dump it to the feeding air slide intake and (F1  $\text{AlF}_3$ ). In order to distribute the fluoride towards the end of

the feeding air slide fill up feeders 8 to 5 first with a binary mixture of  $\text{Al}_2\text{O}_3$  and  $\text{AlF}_3$ . Stop the filling sequence. Fill next dump of  $\text{AlF}_3$  to the feeding air slide intake ( $\text{F2 AlF}_3$ ). Fill up feeders 4 to 1 with a mixture of  $\text{Al}_2\text{O}_3$  and  $\text{AlF}_3$ . Stop the filling sequence. Take samples from the feeding units.

- Cycle 3: Fill up the  $\text{AlF}_3$  feeding silo and dump it to the feeding air slide intake, ( $\text{F3 AlF}_3$ ). Fill up feeders 8 to 5 with a mixture of  $\text{Al}_2\text{O}_3$  and  $\text{AlF}_3$ . Stop the filling sequence. Fill next dump of  $\text{AlF}_3$  to the feeding air slide intake ( $\text{F4 AlF}_3$ ). Fill up feeders 4 to 1 with a mix of  $\text{Al}_2\text{O}_3$  and  $\text{AlF}_3$ . Stop the filling sequence. Take samples from the feeding units.
- Cycle 4: Fill up the  $\text{AlF}_3$  feeding silo and dump it to the feeding air slide intake, ( $\text{F5AlF}_3$ ). Fill up feeders 8 to 5 with a mixture of  $\text{Al}_2\text{O}_3$  and  $\text{AlF}_3$ . Stop the filling sequence. Fill next dump of  $\text{AlF}_3$  to the feeding air slide intake ( $\text{F6 AlF}_3$ ). Fill up feeders 4 to 1 with a mix of  $\text{Al}_2\text{O}_3$  and  $\text{AlF}_3$ . Stop the filling sequence. Take samples from the feeding units.
- Cycle5: Run the rig in normal mode and take samples from each feeding unit or apparatus 1-8.
- Cycle 6: Run the rig in normal mode and take samples from each feeding unit or apparatus 1-8.
- Cycle 7: Run the rig in normal mode and take samples from each feeding unit or apparatus 1-8.
- Cycle 8: Run the rig in normal mode and take samples from each feeding unit or apparatus 1-8. Test run finished. Take sample of pure  $\text{AlF}_3$  for chemical analysis.

#### 3.4.8 Test 13 – results

Only half of the fluoride, 75 kg compared to previous tests was used for this last test. The last test was performed in such a way to simulate the real flow of fluoride into the feeding air slide, as it is fed to the cells in daily operations. In order to push the  $\text{AlF}_3$  towards the end of the feeding air slide and achieve a more even distribution of the  $\text{AlF}_3$  through feeders, feeders 8 to 5 were filled first followed by feeders 4 to 1. Figure 34 shows the alumina and fluoride distribution through feeders and air slide. One can see that there is a uniform distribution. When comparing Figure 35 a and b, one can see equal distributions of fluoride through the feeding air slide, as indicated by both mass balance and chemical analysis of the sample bags delivered to the lab.

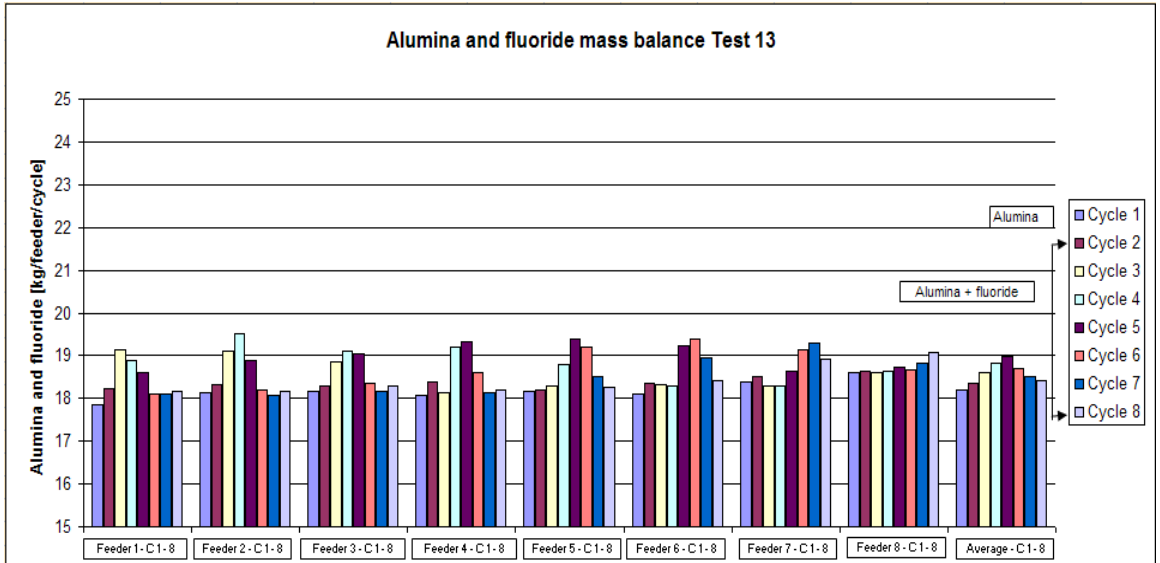
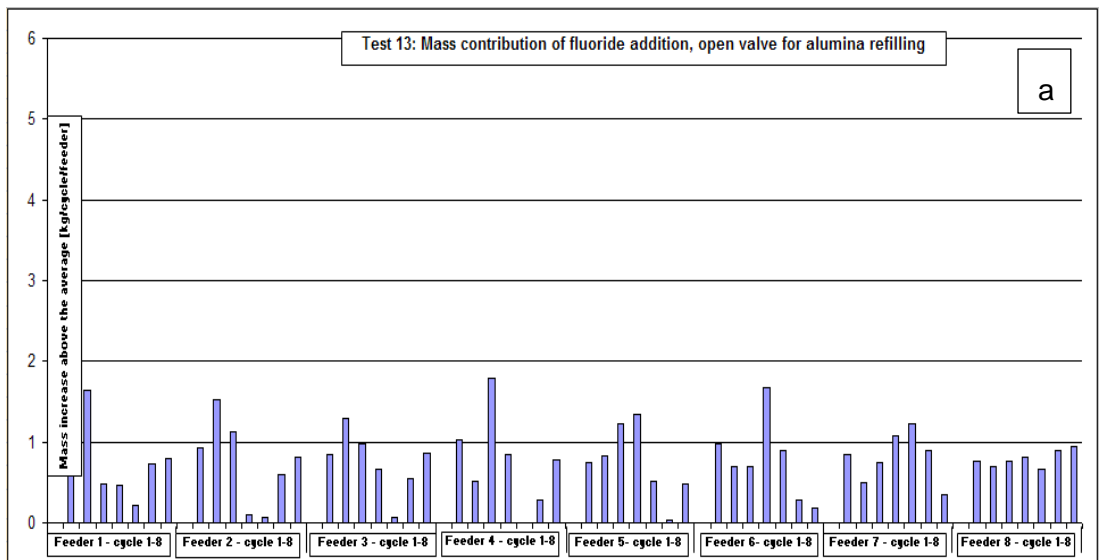


Figure 34 Test 13 Alumina and fluoride mass balance through the feeding air slide.



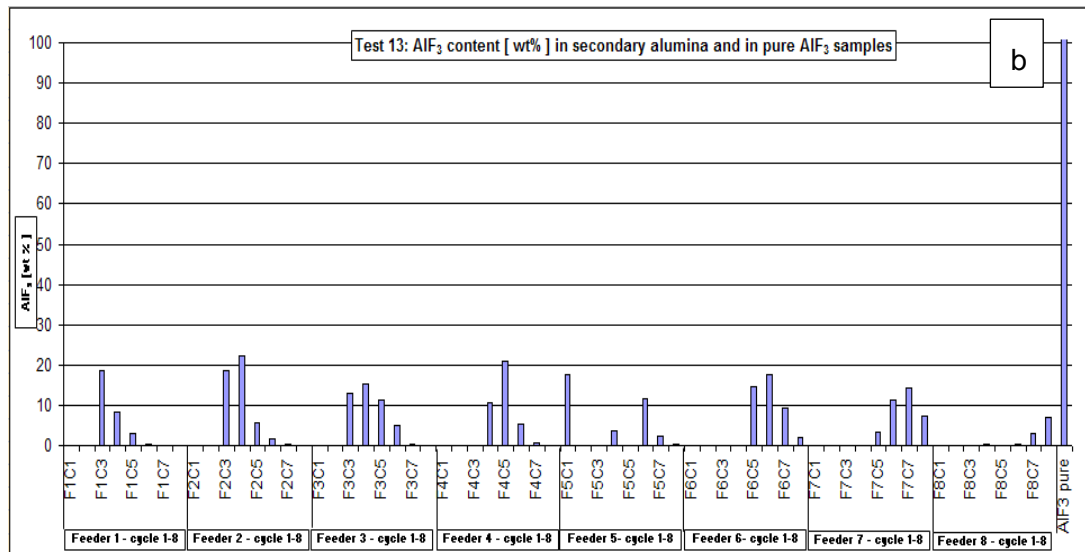


Figure 35 Test 13 a) Alumina and fluoride mass distribution through the air slide. Mass increase above the average cycle. b) Test 9 results of chemical analysis.

A better distribution pattern of AlF<sub>3</sub> to the feeders was achieved by Test 13. Results of this test showed a very good distribution of the fluoride through all the feeders throughout the whole length of the feeding air slide. Results of both mass balance and chemical analysis matched very well in all cases. All tests that have been conducted showed an overall good repeatability of the chosen mechanical equipment, both when testing with alumina and when using binary mixtures: alumina and fluoride. The analysis of the results showed strong correlation between mass balance and chemical analysis. Good repeatability from the test results addresses fluoride distribution patterns through the feeding air slide and through the feeders, but from mechanical point of view it does not necessarily mean good performance of the feeders. This topic will be covered in the next section.

### 3.4.9 Performance of feeders

Dump weights from feeders were measured after careful tuning of opening valve time of each feeder, in order to analyse performance of feeders. This can be visualised by calculating the coefficients of variation between each dump weight, from 1 to 20. Table 5 shows an example of the data gathered, e.g. from Test 11, Cycle 1, meaning only alumina (no fluoride) was supplied to the feeding air slide from the feeding silo on the wall. Numbers in bold represent the weight of the random samples (dump number) taken from each feeder (feeder number) during each run cycle.

Table 5 Feeder data. Cycle 1, only alumina in the feeding air slide.

Test 11: Alumina / Cycle 1								
	Accumulated [g]	Dump weight [g]	Accumulated [g]	Dump weight [g]	Accumulated [g]	Dump weight [g]	Accumulated [g]	Dump weight [g]
Dump nr.	Feeder 1 / Cycle 1	Feeder 1 / Cycle 1	Feeder 2 / Cycle 1	Feeder 2 / Cycle 1	Feeder 3 / Cycle 1	Feeder 3 / Cycle 1	Feeder 4 / Cycle 1	Feeder 4 / Cycle 1
1	760	760	600	600	630	630	710	710
2	1690	930	1430	830	1360	730	1540	830
3	2610	920	2240	810	2170	810	2350	810
4	3550	<b>940</b>	3070	<b>830</b>	3020	<b>850</b>	3200	850
5	4470	920	3910	840	3870	850	4030	830
6	5380	910	4790	880	4710	840	4860	830
7	6300	920	5870	1080	5520	810	5690	830
8	7280	980	6780	910	6410	890	6550	860
9	8270	990	7630	850	7230	820	7380	830
10	9640	1370	8470	840	8060	830	8230	<b>850</b>
11	10140	500	9320	850	8890	830	9160	930
12	11090	950	10150	830	9700	810	9990	830
13	12020	930	11040	890	10500	800	10820	830
14	12930	910	11890	850	11320	820	11610	790
15	13880	950	12710	820	12210	890	12430	820
16	14880	1000	13580	870	13060	850	13250	820
17	15920	1040	14480	900	13980	920	14210	960
18	16910	990	15430	950	15050	1070	15110	900
19	17620	710	16420	990	16080	1030	16090	980
20	<b>18180</b>	560	<b>18350</b>	1930	<b>18330</b>	2250	<b>18300</b>	2210
Average		909		918		917		915
Stdev		180		255		327		311
Coeff of var		20 %		28 %		36 %		34 %

Complete tables from all the tests are given in the Appendix. A total overview of the tables in the Appendix shows coefficients of variation between 12 and 52 % for Cycle 1, for all tests, both with closed valve for refill and open valve. Thus the valve, continuous supply of alumina to the feeding air slide (open valve), or batch wise supply (closed valve), upstream for the feeding air slide, does not have any influence on the performance of the feeders. The coefficients of variation for cycle 2 to 8 (e.g. Cycle 2 to 4 shown in Table 6), when aluminium fluoride is fed to the system and mixed with the alumina are in the same range 6 to 52 %, which is quite interesting. This proves that is not the difference in loose bulk density alone that is causing the high coefficient of variation, but there are other parameters that cause the variations. A detailed assessment of the parameters causing the dump variations needs to be undertaken. What is best for operations in terms of reliable dump weights during one cycle of operation or during many cycles of operation is an important question to ask and answer. The amount of alumina fed to an electrolysis cell over time is essential in maintaining a stable bath concentration in the cell, too large or too small dump weights can have an impact on the stability and on the alumina concentration in the bath. In the case of too small dump weights, the cell will not receive enough alumina over time, a situation resulting in anode effects. The case of too large dump weights will result in sludge formation with a bath concentration close to saturation. One possible parameter could be the fluidizing air to the discharge air slides connected to the feeders. Other parameter causing the

variations could be introduced by the operating concept of the feeders and their mechanical design.



Table 6 Test 9. Feeder data, accumulated dump weights [g]. Cycles 2 - 4, alumina and fluoride in the feeding air slide.

Test 9: Alumina + Fluoride / Cycle 2								
Dump nr.	Accumulated [g]	Dump weight [g]	Accumulated [g]	Dump weight [g]	Accumulated [g]	Dump weight [g]	Accumulated [g]	Dump weight [g]
	Feeder 1 / Cycle 2	Feeder 1 / Cycle 2	Feeder 2 / Cycle 2	Feeder 2 / Cycle 2	Feeder 3 / Cycle 2	Feeder 3 / Cycle 2	Feeder 4 / Cycle 2	Feeder 4 / Cycle 2
1	800	800	810	810	830	830	920	920
2	1680	880	1570	760	2180	1350	1800	880
3	2590	910	2430	860	3180	1000	2710	910
4	3510	920	3310	880	4090	910	3660	950
5	4440	930	4210	900	4970	880	4590	930
6	5300	860	5050	840	5800	830	5480	890
7	6170	870	5910	860	6660	860	6400	920
8	7170	<b>980</b>	6880	970	7490	830	7300	900
9	8080	910	7780	900	8420	930	8190	890
10	9000	920	8780	<b>900</b>	9280	860	9060	870
11	9900	900	9620	840	10170	890	9960	900
12	10800	900	10440	820	11170	<b>910</b>	10840	880
13	11760	960	11300	860	12060	890	11840	<b>940</b>
14	12700	940	12380	1080	12940	880	12730	890
15	13650	950	13310	930	13830	890	13570	840
16	14650	1000	14210	900	14710	880	14510	940
17	15700	1050	15180	970	15680	970	15580	1070
18	16730	1030	16260	1080	16720	1040	16650	1070
19	17720	990	17300	1040	17700	980	17610	960
20	<b>18730</b>	1010	<b>18930</b>	1630	<b>18880</b>	1180	<b>18680</b>	1070
Average		936		942		940		931
Stdev		62		184		128		67
Coeff of var		7 %		19 %		14 %		7 %

Test 9: Alumina + Fluoride / Cycle 3								
Dump nr.	Accumulated [g]	Dump weight [g]	Accumulated [g]	Dump weight [g]	Accumulated [g]	Dump weight [g]	Accumulated [g]	Dump weight [g]
	Feeder 1 / Cycle 3	Feeder 1 / Cycle 3	Feeder 2 / Cycle 3	Feeder 2 / Cycle 3	Feeder 3 / Cycle 3	Feeder 3 / Cycle 3	Feeder 4 / Cycle 3	Feeder 4 / Cycle 3
1	910	910	740	740	730	730	810	810
2	1700	790	1700	960	1550	820	1670	860
3	3540	1840	2730	1030	2470	920	2610	940
4	4880	1340	3820	1090	3390	920	3530	920
5	6230	1350	4910	1090	4300	910	4480	950
6	7600	1370	6020	1110	5210	910	5420	940
7	9010	1410	7060	1040	6130	920	6310	890
8	10010	<b>1170</b>	8090	1030	7080	950	7180	870
9	11380	1370	9160	1070	7990	910	8420	1240
10	12720	1340	10210	1050	8990	<b>1020</b>	9410	990
11	14090	1370	11190	980	9970	980	10310	900
12	15450	1360	12190	<b>1010</b>	10860	890	11250	940
13	16790	1340	13260	1070	11850	990	12150	900
14	18220	1430	14290	1030	12810	960	13150	<b>980</b>
15	19650	1430	15390	1100	13740	930	14040	890
16	20950	1300	16490	1100	14680	940	14960	920
17	21850	900	17660	1170	15670	990	16030	1070
18	22250	400	18730	1070	16790	1120	17120	1090
19	22410	160	19640	910	17810	1020	17940	820
20	<b>22460</b>	50	<b>20520</b>	880	<b>19330</b>	1520	<b>18560</b>	620
Average		1132		1027		968		927
Stdev		462		96		152		122
Coeff of var		41 %		9 %		16 %		13 %

Test 9: Alumina + Fluoride / Cycle 4								
Dump nr.	Accumulated [g]	Dump weight [g]	Accumulated [g]	Dump weight [g]	Accumulated [g]	Dump weight [g]	Accumulated [g]	Dump weight [g]
	Feeder 1 / Cycle 4	Feeder 1 / Cycle 4	Feeder 2 / Cycle 4	Feeder 2 / Cycle 4	Feeder 3 / Cycle 4	Feeder 3 / Cycle 4	Feeder 4 / Cycle 4	Feeder 4 / Cycle 4
1	1140	1140	960	960	810	810	800	800
2	2660	1520	2190	1230	1850	1040	1730	930
3	4070	1410	3490	1300	2960	1110	2660	930
4	5500	1430	4830	1340	4080	1120	3600	940
5	6900	1400	6130	1300	5180	1100	4540	940
6	8370	1470	7430	1300	6300	1120	5460	920
7	9740	1370	8740	1310	7390	1090	6380	920
8	11090	1350	10130	1390	8810	1420	7370	990
9	12480	1390	11410	1280	9950	1140	8290	920
10	13930	1450	12680	1270	11070	1120	9230	940
11	15330	1400	13950	1270	12160	1090	10150	920
12	16330	<b>1400</b>	15190	1240	13310	1150	11080	930
13	17750	1420	16500	1310	14440	1130	11990	910
14	19210	1460	17500	<b>1340</b>	15530	1090	12900	910
15	20740	1530	18860	1360	16730	1200	13870	970
16	21830	1090	20060	1200	17730	<b>1330</b>	14870	<b>1060</b>
17	22920	1090	21260	1200	19000	1270	15850	1080
18	23220	300	21940	680	19920	920	17040	1090
19	23360	140	22200	260	20500	580	17910	870
20	<b>23500</b>	140	<b>22290</b>	90	<b>20780</b>	280	<b>18550</b>	640
Average		1195		1132		1056		931
Stdev		450		364		254		96
Coeff of var		38 %		32 %		24 %		10 %

#### 3.4.10 Summary of the verification programme on the alumina rig

On the alumina rig the requirement for reliable and consistent discharge rates from a feeding air slide through volumetric feeders applied to alumina and fluoride dosing operation has been met by interfacing diamond shaped volumetric feeders and short air slide segments. The philosophy behind the dosing operation consisted in emptying eight volumetric feeders each one designed for 18 kg powder, at equal time intervals in order to get twenty equal doses from each feeder.

The following conclusions could be drawn from the work programme on the alumina rig:

- Results of the tests with closed valve for alumina supply from the feeding silo, tests 1 to 6 showed that fluoride, having a higher bulk density than alumina, was distributed only through the first three feeders.
- Results of the tests in series 2 with open valve for alumina supply showed a better distribution of fluoride through the system, from feeder one to eight.
- Results from Test 13 with open valve for alumina supply and controlled distribution of  $AlF_3$  in an organized pattern promoted distribution of the powder with higher bulk density more evenly towards the entire length of the feeding air slide.
- Results from Test 13 showed (based on results from mass balance correlated with results from chemical analysis) improved mixing of fluoride and alumina and distribution of binary mixtures in a feeding air slide and through the feeders. The results led to the conclusion that the feeding air slide is delivering a more homogenous powder when fluoride is pushed towards the end of the feeding air slide and
- fed into an organised pattern, to the last four feeders first (feeder 8 to 5) and then to the first four (feeders 4 to 1).
- Next challenge, adopting a top down approach, would be to study the behaviour of the fluidized feeders alone, isolated from the feeding air slide. If not the difference in bulk density between alumina and aluminium fluoride is causing the main variation in dump weights, what else is causing this variation? This was an important question that needed to be answered and it was the main motivation for this work.

After carefully analysing the results following thoughts for further work emerged. As a consequence of the operation that was required, dosing of powder, the equipment: feeder and mini air slides had to operate in a fully choked condition, i.e. the material was not in free fall condition. The choked condition was identified to be one of the sources to dosing irregularities in this work, thus subject to further investigation. Meanwhile a deeper analysis needs to be done before drawing final conclusions. A parameter causing the dump weights variations could be the operating concept of the feeders and their mechanical design. They are designed and built as a control volume, acting as a buffer silo discharging into an air slide. To address the high coefficients of variations found during this measurement programme for all feeders, deeper studies into flow patterns from silos and silo design need to be conducted. This again would require more knowledge about the fluidization behaviour of basic components:  $\text{Al}_2\text{O}_3$ ,  $\text{AlF}_3$ , alumina fines and binary mixtures at different concentrations of the three components.

Based on the conclusions from the work programme on the alumina rig, some attempts to characterize the behaviour of alumina and binary mixtures have been undertaken and are described below. Geldard's (1973) fluidisation criteria and previous work done by Dyrøy (2006) were used as a starting point.

### **3.5 Minimum fluidization velocity**

Following the conclusions from the previous section, more knowledge about the fluidization behaviour of basic components:  $\text{Al}_2\text{O}_3$ ,  $\text{AlF}_3$ , alumina fines and binary mixtures at different concentrations was needed. Geldard (1973) classified powders based on test results from a fluidization column. Minimum fluidization velocity  $U_{mf}$  is the most important measurement needed for design of fluidisation and transport systems of powder. The minimum fluidization velocity is visualised together with the pressure drop across the bed of powder as shown in Figure 36. Figure 36 Specific pressure drop vs. air velocity chart for alumina. At low airflow rates the pressure drop  $\Delta p$  is proportional to the operational air velocity,  $U_0$  and is higher than the static pressure of the bed. A further increase in  $U_0$  will cause an increase in bed voidage, thus a decrease in pressure drop which will now equal the static pressure of the bed.

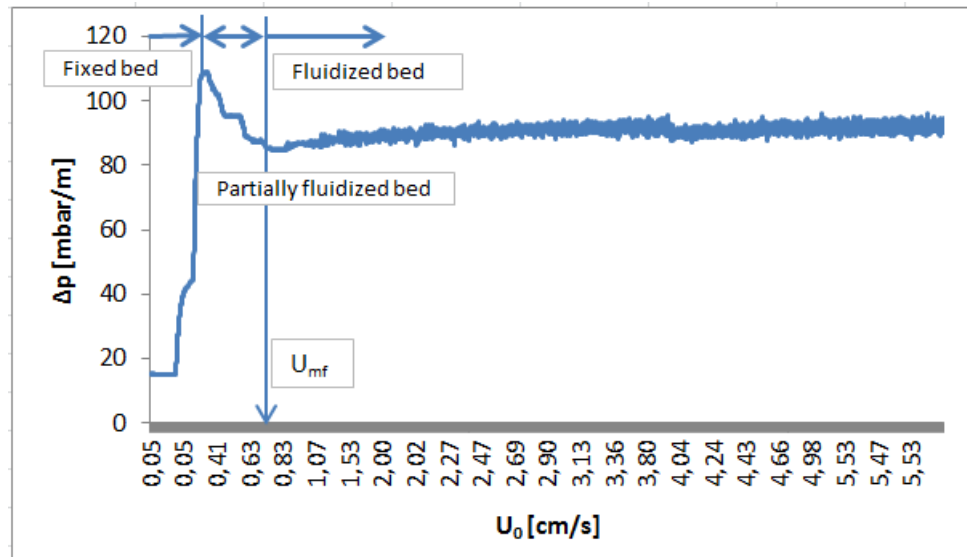


Figure 36 Specific pressure drop vs. air velocity chart for alumina.

### 3.5.1 The Geldart classification of powders

By observing the fluidization behaviour of a series of sorts and sizes of particles, Geldart came up with four types of particle behaviour. They are described below, ranged from smallest to largest type of particles:

- Group C: cohesive and very fine powders. They are difficult to fluidize, due to strong interparticle forces. In fluidized beds they tend to rise as a plug of solids and cracks in the plug, from the membrane to the surface of the bed, appear when high fluidization velocities are applied to the bed.
- Group A: aeratable powders, having a low particle density, below  $1.4 \text{ g/cm}^3$  characterized by the fact that they fluidize easily with a homogeneous expansion throughout the whole bed.
- Group B: sandlike, bubbly, coarser than A powders, with density in the range of  $1.4$  to  $4.0 \text{ g/cm}^3$ . According to Kunii and Levenspiel (1991) bubbles form as soon as the gas velocity exceeds the minimum fluidization velocity. Bubble size increases linearly with the distance above the top of the membrane.
- Group D: coarse powders that spout easily when fluidized above minimum fluidization velocity.

### **3.6 Powder characterisation**

When discussing powder flow behaviour and modelling approaches, either empirical or analytical, the most important analysis is characterisation of powder. If the information about the performance of the full scale equipment in terms of variation of capacity and knowledge about what is causing the variation is not complete or accurate, further modelling of alumina flow and optimization of the production (electrolysis) process will not be realistic. Particle size analysis, as a characterisation method, has not been the scope of this thesis, as Dyrøy (2006) had looked at it in previous work. In this work alumina  $\text{Al}_2\text{O}_3$  and combinations of  $\text{Al}_2\text{O}_3$  and aluminium fluoride  $\text{AlF}_3$  have been tested in a cylindrical fluidization column to better understand the results previously obtained in a feeding air slide on the alumina rig at the Reference Centre in Årdal during 2009 – 2011 presented in previous sections.

#### **3.6.1 Fluidization of binary mixtures of alumina and fines**

Norheim and Dyrøy (2009) conducted fluidization work using the same fluidization column as the one used in this thesis. Their preliminary results showed a potential for air consumption reduction for all HAL's fluidisation equipment estimated at around 30%. It was estimated at that time that for Qatalum alone, with 17 km of air slides, this would give a reduction in air consumption equivalent to 3.7 MNOK/ year, given a price of 0.10 NOK/m<sup>3</sup> air. The alumina used in their experiments was secondary alumina from Sunndalsøra. The experiments were performed to clarify the relationship between the amount of fine particles (different amount of particles smaller than 45 µm) and the minimum fluidisation velocity. The experiments showed that the particle size had a significant effect on the minimum fluidisation velocity and that the minimum fluidization velocity increases with increasing particle size. The average minimum fluidisation velocity for alumina with approximately 25 to 30% of the particles less than 45 µm was 0.40 cm/s while for alumina containing 5% of the particles less than 45 µm in size it was 0.66 cm/s. Thus a variation in content of fines from 5% to 25 to 30% caused a drop in fluidization velocity requirements from 0.7 to 0.4 cm/s. This clearly demonstrated that whenever the material changes in nature from an A to a C powder (e.g. higher amount of fines, particles less than 45 µm), then the operating air velocity required will be lower. Currently the minimum fluidization velocity for all HAL plants is set to 2.0 cm/s, which is much higher than what it is actually needed to achieve an optimal fluidization. The ability to predict and regulate the extent of mixing will give

the possibility to optimize air supply rates needed for fluidization, thus high potential for reducing the air consumption at the plants.

### 3.6.2 Test equipment

A fluidization column 220 mm wide and 1000 mm high was used for the experiments in this thesis. The main function of the fluidisation rig is to measure the pressure variations, air flow and velocity simultaneously in order to determine the right fluidisation velocity and deaeration time for a given powder or mixture of solids. The alumina used in the experiments was primary alumina from the C-hall in Årdal.

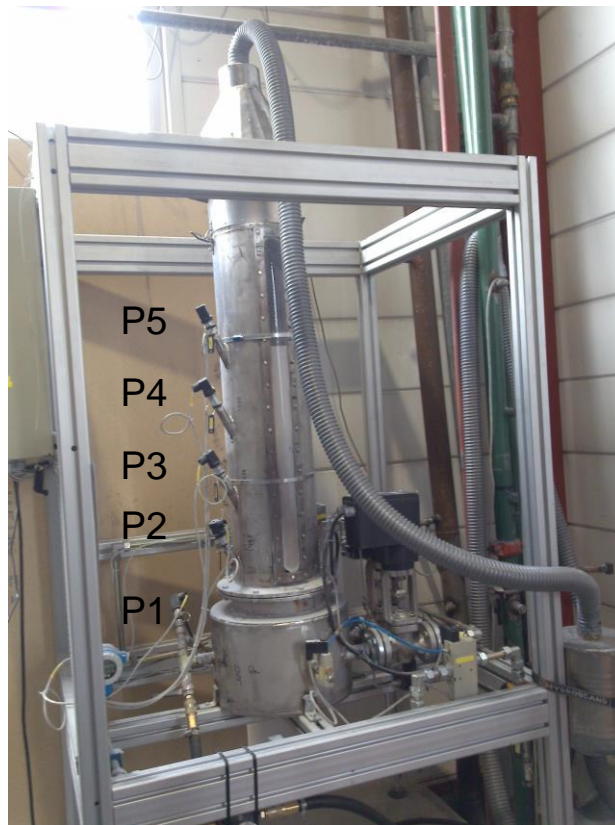


Figure 37 Fluidisation column rig (originally located at POSTEC).

The fluidisation rig is provided with 6.0 to 6.5 bar pressurized air directly from the plant compressor. To cover a wider range of the air flow rate, the rig was originally equipped with two parallel air supply lines with valves and air flow transmitters. The lower range of air supply valve and air flow transmitter was called “the 1. line”, while the higher air flow transmitter and air supply valve was called “the 2. line”. Preliminary tests at Postec quickly showed no need for the “2. line”, as the “1. line” provided enough air for the

tests. Thus the 2. line was disconnected from the software (but not removed from the rig). When the column was moved from Postec to Årdal in 2011 new challenges arose. The original pressure transmitters, P1 - P5 (see Figure 37) were affected by the strong magnetic field at the Reference Centre in Årdal, thus they were replaced by new ones with ceramic components. Figure 38 shows the fluidisation rig layout, with only one air supply, as it was programmed to be further used for this PhD study. The pressurized air is supplied to the plenum chamber of the column through a valve connected to a flow transmitter. A mechanical actuator (black box in Figure 37) is controlling the valve opening, restricting the amount of air supplied to the plenum chamber. When the program is run, the operator can choose the air supply rate from the plant compressor displayed as percentage [%]: 100% means fully opened, 0 % means closed valve for air supply. The minimum fluidization velocity for primary alumina 0.6 cm/s corresponds to a valve opening of 51 %. When fluoride is mixed into the column, it requires 52 % opening of the valve, corresponding to 0.8 cm/s. It then opens gradually and the pressure at the bottom of the column (P2) increases respectively. The air velocity increases until it reaches the fluidisation velocity of the powder or binary mixture and it remains constant. Then the operator can decrease the valve opening until the air velocity drops. The release valve has to be opened by the operator after each test in order to release the air from the air chamber. There are four pressure transmitters P2 - P4 on the side of the fluidisation column situated at equal distances of 0.2 m from each other and one on the side of the air chamber, P1, as shown in Figure 38. The user calculates the specific pressure drop between the four transmitters by taking the difference  $P3 - P2$ ,  $P4 - P3$ ,  $P5 - P4$  and divided it by the distance between them.

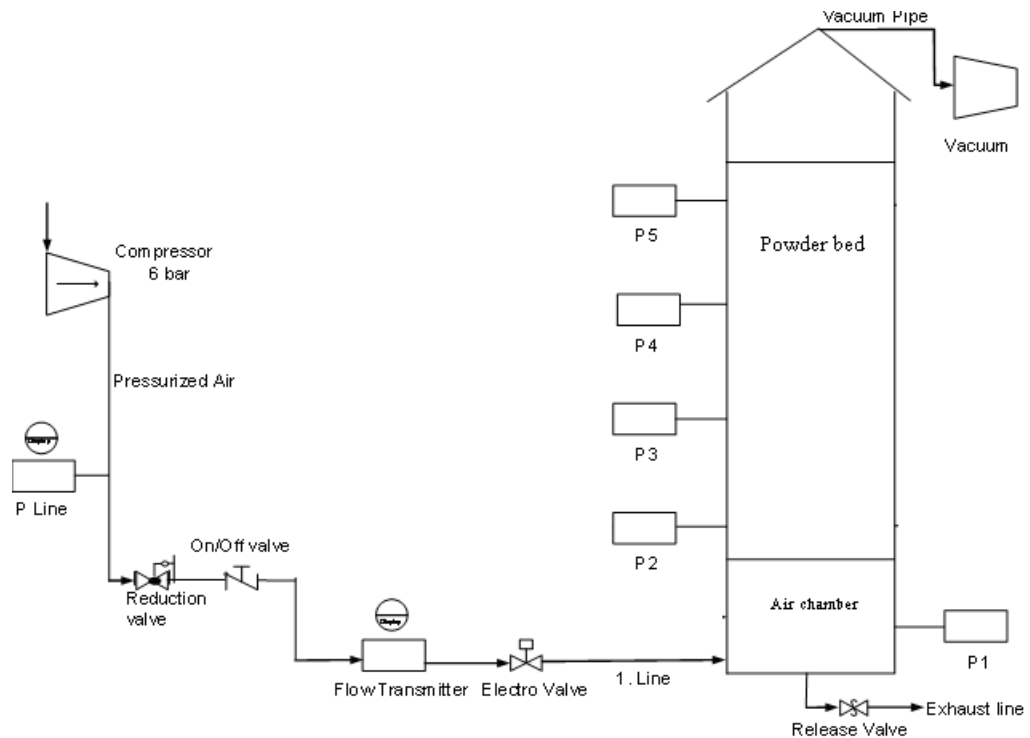


Figure 38 Layout of the fluidization column.

### 3.7 Test design - preparation of the test powders

The experiments were aimed to address many questions around dump weights variations that had come up during previous work on the alumina rig at Årdal as presented in previous section. The first task to be solved was to establish the individual fluidization ranges for primary alumina and aluminium fluoride. Although minimum fluidization velocity for secondary alumina had been previously tested at Postec by Nordheim (2009) and found out to be 0.66 cm/s, all the tests showing good repeatability, new tests were conducted for this project. The operational fluidization velocity is currently set to 2.0 cm/s in Hydro plants. There is no previous work done prior to this report in Hydro, as known by the author, to document the fluidization velocity of fluoride and that of binary mixtures. By binary mixtures is meant mixtures of alumina and fluoride at different concentrations. Loading method of the powder into the column was the same for all experiments in order to achieve good repeatability. The binary mixtures were loaded separately, as two batches, using a bucket and scales to weigh the powder. At the beginning of each fluidization test, the binary mixture was completely segregated (used as Phase S in Table 7). The bed consists of two distinct layers: 1)  $\text{Al}_2\text{O}_3$  on the bottom and  $\text{AlF}_3$  on the top or 2)  $\text{AlF}_3$  and  $\text{Al}_2\text{O}_3$  on the top. The



height of the bottom layer was kept constant at 51 cm, only varying the height of the top layers. At the end of each fluidization cycle the column was vacuum cleaned.

The aim of the experiments, once the two components had been fluidized separately, was to establish more understanding about their fluidization behaviour as a binary mixture at different concentrations and at different air supply rates. A series of initial tests were conducted to determine the behaviour of the two components alumina  $\text{Al}_2\text{O}_3$  and aluminium fluoride  $\text{AlF}_3$  separately and establish basic knowledge about each of them. Bed height was kept constant; 51 cm of powder was used in both cases. The results of three tests using 25 kg alumina and three tests using 38 kg fluoride are presented in Figure 39. Table 7 summarizes the results.

**Table 7 Characteristic values of  $\text{Al}_2\text{O}_3$  and  $\text{AlF}_3$ .**

Component name	Nr. of tests	Concentration [%]	Phase	Mass [kg]	Bed height [cm]		Air flow rates [ $\text{Nm}^3/\text{h}$ ]	Fluidization velocity [cm/s]	Pressure drops [mbar/m]		
					Unfluidized	Fluidized			P2-P3	P3-P4	P4-P5
Alumina	3	100	S	25	51	57,5	1	0,6	86		
Fluoride	3	100	S	37		53,5	1,3-1,4	0,7-0,8	133-137		

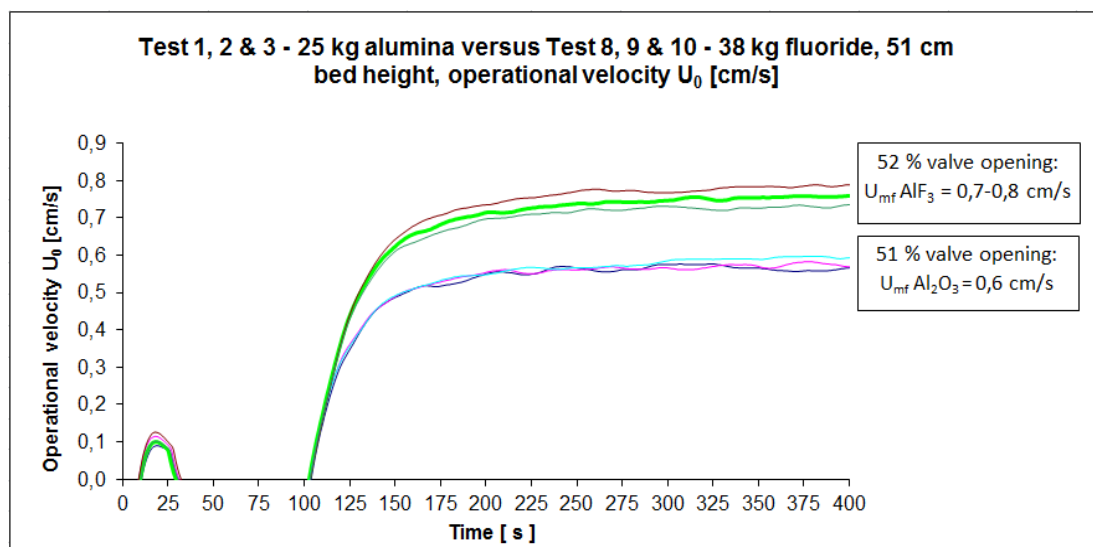


**Figure 39 Fluidization velocities of alumina and fluoride.**

Based on knowledge about behaviour of binary mixtures from fluidization tests, operational velocity  $U_0$  was reduced from 2.0 cm/s down to 1.2 cm/s on one test cell in operation, L32. The change has been implemented by the Cell Design Team in Årdal by reducing the dimension of the membrane in the short air slide segment interfacing the volumetric feeders. This has been a conservative choice, with the pot operating in a

safe zone. Next step would be to implement the change on other pots and eventually in full scale operation, wherever control valves allow this change, e.g. Qatalum plant.

This part of survey has shown the fluidization behaviour of alumina and aluminium fluoride as basic components and as binary mixtures. Binary mixture situation occurs in a feeding air slide. During all tests the bed expanded by 10 % of its initial height. A fluidization velocity around 0.8 cm/s it is enough in order to fluidize the binary mixture for any concentration of fluoride from 0 to 79 %. As an optimal and very good safety interval, 1.0 to 1.2 cm/s should be used in full scale systems alumina and fluoride distribution systems. Higher rates of fluidization velocities are unnecessary, due to waste of energy and higher contribution to dusting/ loss of fines through the venting pipes.

### **3.8 Measuring powder flowability**

A common cause of irregularity of discharges in industry is the misapplication of equipment types that are not properly suited to the flow characteristics of the material in use (e.g. alumina feeders designed for and suited for a free flowing product being used with a fine powder like alumina fines). In this thesis the term “powder flowability” will be used to define the ability of alumina and binary mixtures to flow when they are transported or discharged: e.g. discharged through feeders on the alumina rig or transported through an air slide. Clearly when the quality of alumina becomes poor due to high content of fines, optimization of the equipment to suit every material to be handled is not a viable option. However, if a “universal feeder” can be developed, that can cope with a wide range of alumina qualities and binary mixtures, then considerable savings could be brought to the aluminium industry.

Very often the flow properties of continuously transported and handled alumina vary: when a new shipment arrives, when a silo is emptied, a lot of fines are introduced to the system. For knowing which deviations can be accepted it is necessary to measure the flow function accurately. In order to understand and clarify questions around high coefficients of variation when analysing feeder performance (see Section 3.4 and Section 3.5) and to further optimize mechanical design and test feeders' performance as recommended in Section 3.6, the best method to design silos for flow is the method developed by Janike (1961 & 1964). The method for measuring the flow function accepted by academia and industry is to use a shear tester. The approach to powder flow

property measurements used in this thesis was to measure the flow function and the bulk density.

The concepts of flow function and results of measurements will be explained in detail below. The value of bulk density is a key parameter and will be further used in preliminary modelling of silo outlet using Janssen's analysis in Section 5.1, in empirical and mathematical modelling Chapters 6 and 7 for calculations of velocity and capacity.

### 3.8.1 Bulk flow property measurements

Currently a great number of methods and shear cell testers are available to determine the strength and flow properties of bulk solids as presented by Schwedes (2003), Berry and Bradley (2010), Berry et al. (2010) and Pinzon (2012). An automated annular shear tester developed at the Wolfson Centre in collaboration with Brookfield Viscometers known as the Brookfield Powder Flow Tester (PFT) was used to determine the powder properties reported in this work. The PFT as shown in Figure 40, is the first fully-robotised powder shear tester integrating both testing and analytical functions in embedded software, also amenable to undertaking multiple measurements per powder sample. It follows the ASTM D61228-00 standard test method for shear testing of bulk solids using the Jenike shear cell. The method covers both the apparatus and procedures for measuring the cohesive strength of bulk solids during continuous flow and after storage at rest. This standard is applicable to testing bulk solids that reach the steady state requirement within the movement limit of the shear cell. The information provided by the tests can then be used for storage bins and hoppers design to prevent flow stoppages due to arching and ratholing. The test values expressed in SI units are to be regarded as standard.

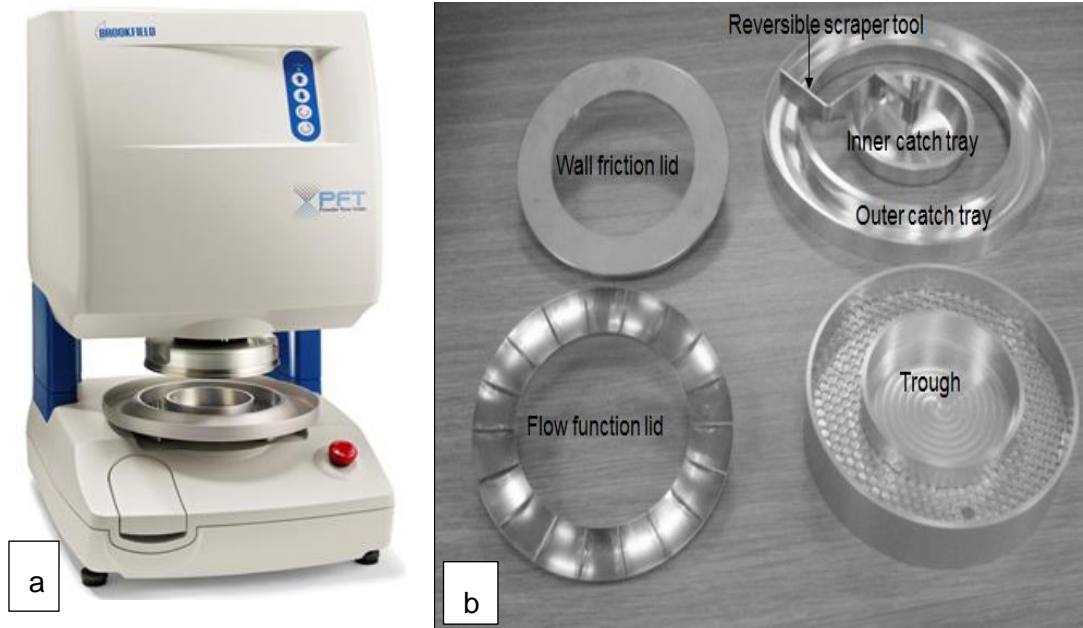


**Figure 40 Brookfield Powder flow tetser (PFT) and test components. a) PFT tester (reprinted from Brookfield’s customer leaflet); b) PFT accessories.**

The design principles and applicability of the PFT have been presented in detail by Berry and Bradley (2010) and widely applied by Pinzon (2012) in his work. The powder sample is weighed and stored in an annular, 155 mm diameter open base (trough) (Figure 40 b) enclosed with a matching 152 mm diameter annular lid. A known normal load is applied to the lid to produce the required normal stress within the powder in the base. The base is then rotated forward (0.5 degrees rotation), while the lid is prevented from rotating by a torque measuring system, and backward (to reduce torque to zero). Thus the rotation of the base relative to the fix lid produces a horizontal shear/failure plane within the powder sample. The shear load acting on this shear/failure plan is then calculated, for a given geometry of the cross section area of the base where the sample is stored. The lid has 18 equal spaced radial vanes (called “pocket geometry” design). The normal and the shear stresses are determined by the area of the lid. The test procedure is as follows: initially the powder sample is consolidated to the critical consolidation and then shared which causes the material to flow under consolidation stress until the shear forces reaches a steady value (achieves steady state). Figure 41 shows a normal stress/shear stress diagram.

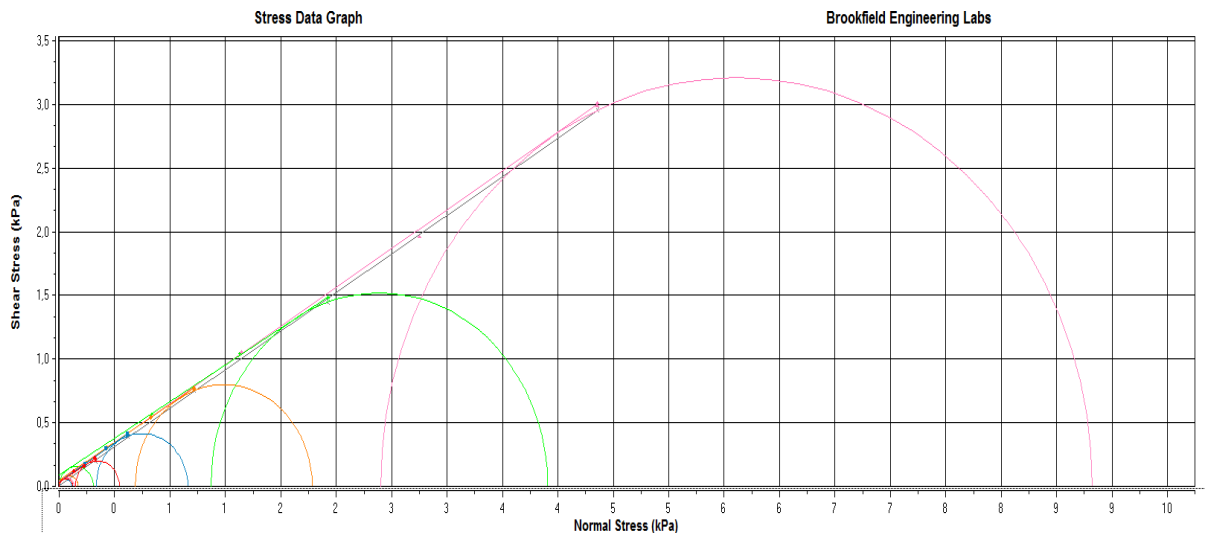


Figure 41 Flow function test results with the Brookfield PFT– Alumina powder. Mohr stress circles for steady – state flow at different consolidation stresses. Steady – state yield locus is approximated by a straight line.

A straight line drawn through the origin and tangential to the consolidation Mohr semi circles is called the effective failure locus. The angle between this failure locus and the horizontal axis of the diagram in Figure 41 is called the effective angle of internal friction. The effective angle of internal friction represents the ratio of the major and minor principal stresses during steady state flow. Both the angle of effective internal friction and the bulk density vary with the consolidating stress.

Characterization of a powder (one test) takes approximately 45 minutes and requires attendance for around 5 minutes during sample preparation, at the start and at the end of the test.

Three basic tests were run on the machine:

- **Flow Function:** this is a measurement undertaken in around 35 minutes of the internal resistance to flow of a powder; and is the result of a series of tests of unconfined failure strength,  $\sigma_c$ , as a function of major principal stress  $\sigma_1$ .
- **Wall Friction:** measures the friction developed between the powder and a constraining surface: e.g. the walls of a feeding silo. The friction controls the flow pattern which forms when the feeding silo discharges, as well as the tendency for the powder to flow or to hang on the surface of a chute, according to Berry and Bradley (2010).

- **Bulk Density and compressibility:** another property to be measured, characterised as a compression curve.

### 3.8.2 Sample preparation

The powders tested are representative of those used in the aluminium industry. The binary mixtures' concentration choice was based on previous analysis results from samples of dump weights taken using the alumina rig at the Reference Centre in Årdal. All tests were undertaken at ambient conditions of temperature and humidity in the laboratories at The Wolfson Centre: 15 to 20 °C and 45 to 50 % HR. The laboratories are equipped with a climate chamber used to prepare, weigh and mix the test samples. The alumina and the fluoride was sent to Wolfson from Årdal in airtight containers. The main objective of the testing was to acquire enough knowledge about the powders and the binary mixtures previously used in the alumina rig tests and to create a data base of particle and bulk flow properties to be further used in industry (and not only for this thesis). It was investigated whether different sample preparation techniques, as segregated and fully mixed layers of powders may lead to different results.

The filling of the powder into the through has been undertaken in two ways:

- two distinct layers of powder: fluoride (bottom) and alumina (top);
- fully mixed powders (as binary mixtures) at different concentrations.

### 3.8.3 Presentation of the results

Bulk flow properties of alumina, fluoride and binary mixtures such as flow function and bulk density (Figure 42 a and b), internal friction (Figure 43) and friction function (Figure 44) were measured with the PFT shown in Figure 40. The tests were undertaken using a standard volume cell (263 cc volume and 150 mm outer diameter) with an upper limit for the particle size of 2 mm and a maximum consolidation normal stress limit of 4.8 kPa. Hydro has already purchased a PFT machine for further use in industry. The test results are presented on the PC connected via an USB cable to the PFT. The data files have been exported to Excel and analysed. From Figure 42 a and b it can be seen that the preparation method of the powder sample, as segregated or mixed layers has no influence on the test results.

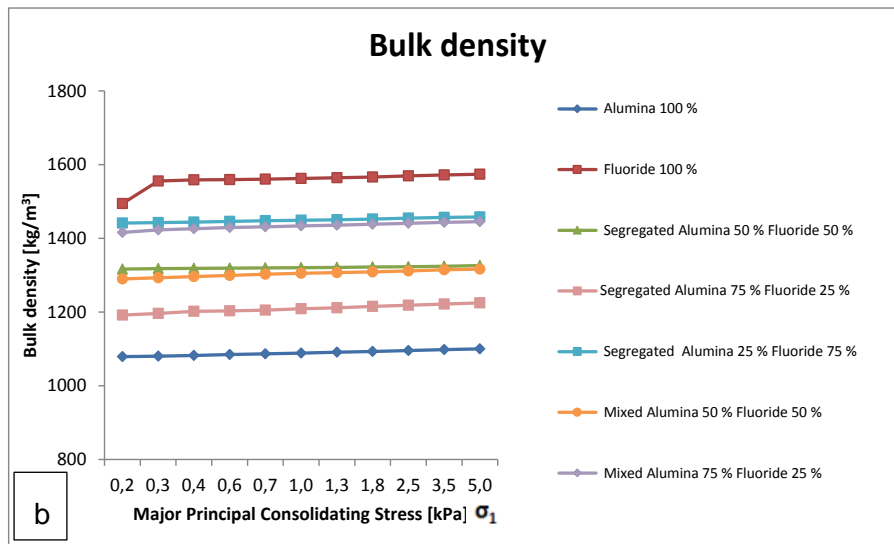
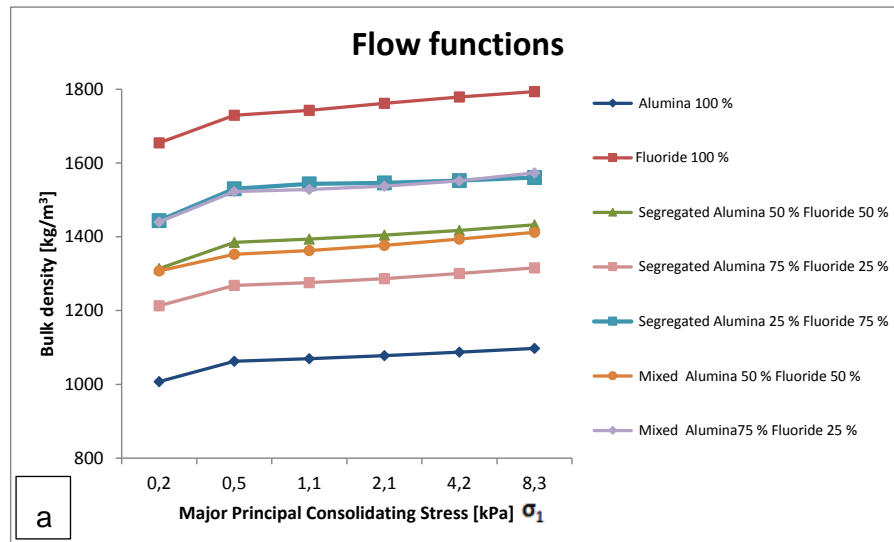


Figure 42 a) Bulk density results produced by the Flow Function test; b) Bulk density results produced by the Bulk Density test.

The internal friction of the powders is another important bulk flow property to be measured. As mentioned in earlier sections, knowing the flow properties of a powder is necessary for design of bulk solid handling equipment (e.g. feeders and silos) for reliable flow and discharge. The same tests used to measure the flow function properties are used to measure the internal friction of the powders.

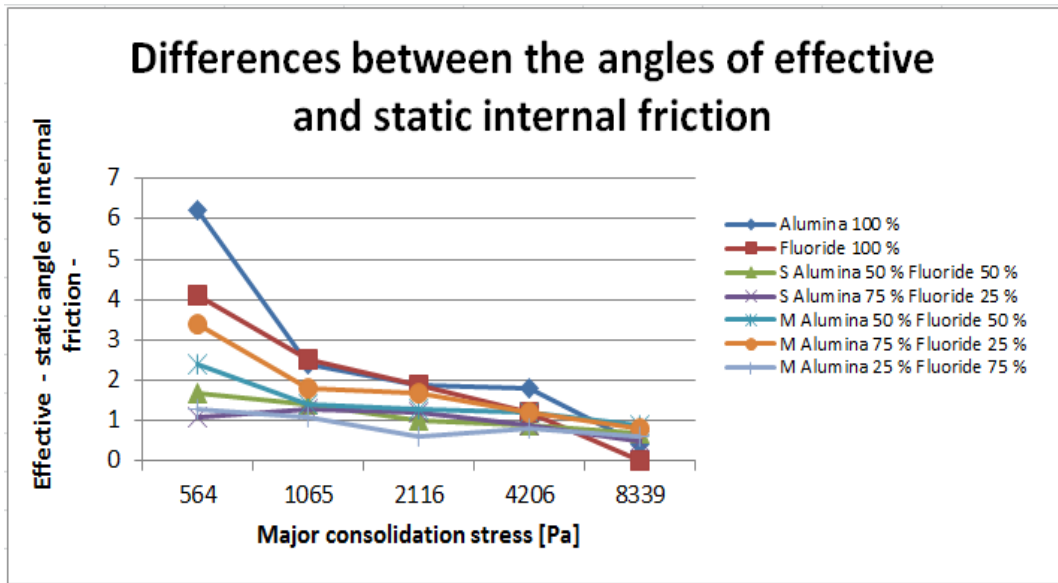


Figure 43 Flow function test results with the Brookfield PFT. Differences between the angles of effective and static internal friction as an indication of the degree of cohesiveness. Individual components and binary mixtures.

The design of a mass flow feeder or silo requires information about the friction between the powder and the silo wall. The feeders or silos at Hydro have a standard steel finish, this material was not available at Wolfson, and instead a Pyrex layer finish was used for the tests. In the future, different wall materials could be considered for different silo design and other vessel applications. Figure 44 shows the results of a series of tests using standard wall friction test for alumina with a Pyrex layer surface finish. The wall friction angle,  $\phi_w$ , is presented as function of the normal stress and has a value of  $24^\circ$ . The finishing on the volumetric feeders inner wall surface on the alumina rig differs quite a lot from the Pyrex finish used for the wall friction test on the PFT. In Chapter 5 a value of  $\phi_w = 20^\circ$  was used for preliminary silo outlet modelling.



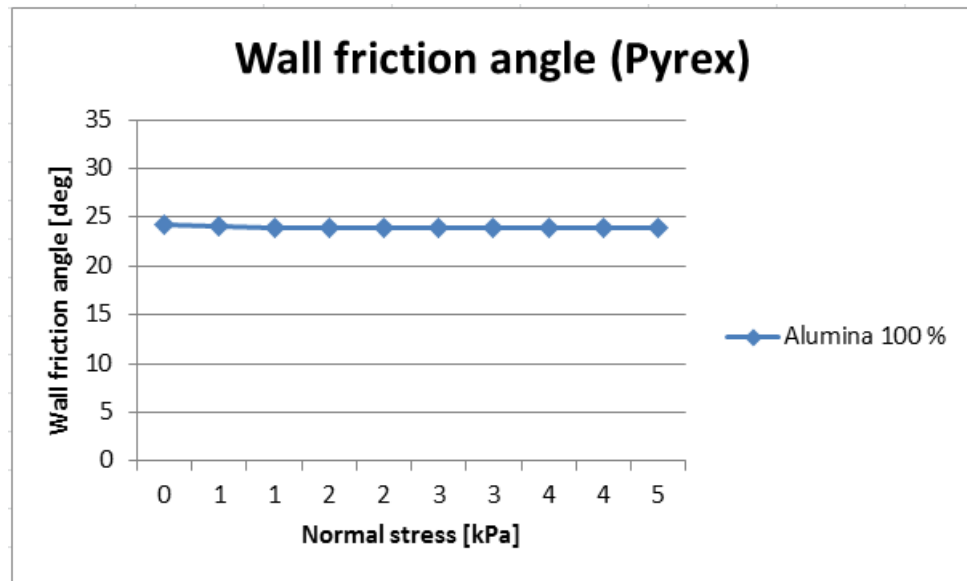


Figure 44 Pyrex wall friction test results for alumina: wall friction angle,  $\phi_w$  as a function of the normal stress  $\sigma_N$ . Data obtained from the Brookfield PFT.

Further work needs to be done in order to determine the exact value of  $\phi_w$  for the same wall surface as the volumetric feeders on the alumina rig used in Årdal or the feeding silo used at POSTEC.

### 3.9 Powder characterisation and segregation in an aluminium plant

A key issue from rheological point of view applied to fluidized alumina in an open/closed channel, is the effect of increase in fine fraction content. To test the effect of fines content changes in fluidized alumina, tests measuring the changes in capacity for a 12 m long air slide were conducted by Dyrøy (2006).

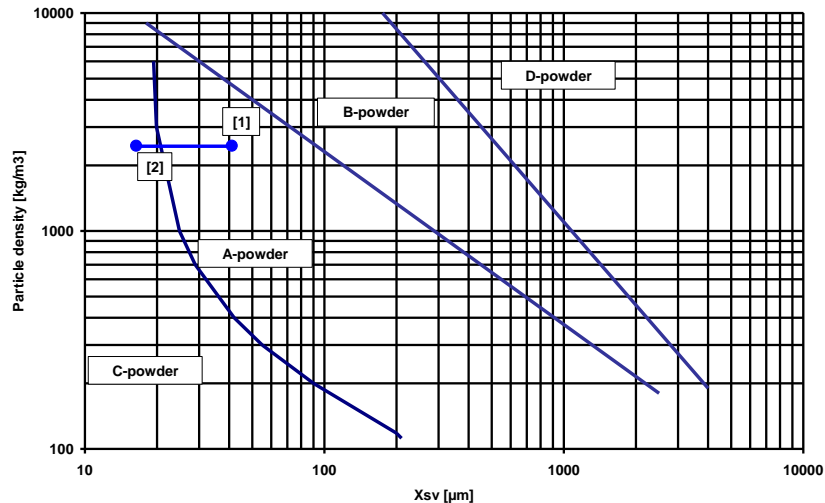


Figure 45 Dyrøy (2006): Geldart's classification chart. Changes of alumina characteristics from A-powder [1] to C-powder [2].

From Geldart's classification chart and Dyrøy's (2006) work results that the coarser alumina fraction belongs to region A, while the fines rich fraction belongs to region C, as shown in Figure 45. Kuni and Levenspiel (1991) refer at this AC classification for the same powder as an "extension" of the Geldart's chart. In an uncertain transition region [1] to [2], between Geldart group A and group C, the alumina will flow well when fluidized (A behaviour) but then it will defluidize in the air slide creating a plug (C behaviour). Dyrøy (2006) showed the effects of using high operating velocities, in the range of 2.0 to 3.4 cm/s, with the alumina powder changed from A to C. As shown in Figure 46, due to a "plug" formation in the air slide, the capacity will drop or worse, the system will stop transporting. It would have been interesting to investigate the effects of fines content on the air slide capacity at lower operating air velocities, in the range of 1.0 to 2.0 cm/s.

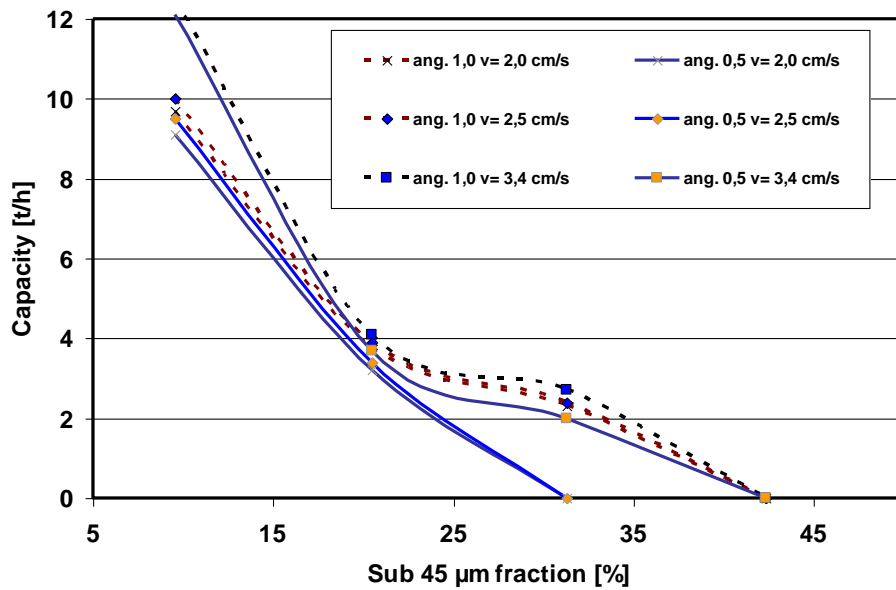


Figure 46 Dyrøy (2006): Air slide capacity for alumina when fines content and operational velocity increase.

### 3.10 Conclusions

As the main objective of the project is to develop a mathematical model to predict bed velocity and transport capacity in an air slide, the knowledge of powders and binary mixtures when fluidized and the flow function properties play an important role in this research work. The characterization of powders and understanding of flow behaviour are the most important measures in both fighting segregation and when further optimizing powder handling systems. Without proper information about powders and their flow behaviour one cannot succeed in eliminating the short time segregation. Anti-segregation measures have been successfully implemented for the main storage facilities to minimize long time segregation. However there are still short time segregation effects present where the powder is fed to the pots, from the feeding air slides, measured as dump weights through discharges from the volumetric feeders. The extensive working programme done on the alumina rig and the data analysis performed on the variation of the dump weights not only has yielded a distribution of powder and feeder performance verification study. The work on the alumina rig in Årdal showed high coefficients of variation in dump weights and addressed the need to better understand the flow behaviour of binary mixtures and the need to optimize feeder design further. This analysis has uncovered equipment interfacing and chocked flow as

a possible bottleneck in achieving repeatability from feeders. The academic challenge was to select the necessary testing methodology and to develop a practical understanding of the results. The results of the fluidization and flow functions tests were used to create basic knowledge on which the modification of the air slide rig at POSTEC described in Chapter 5 and the modelling strategies described in Chapters 5 and 6 are based on.

## **4 Silo outlet design and interfaces to an air slide**

### **4.1 Introduction**

This chapter presents the research methodology and the initial design of the air slide rig at POSTEC applied in this work, as a direct result of the verification programme on the alumina rig in Årdal presented in Chapter 3. After a thorough analysis of the results in last chapter it has become clearer that in order to study and model flow behaviour in an air slide, one cannot ignore the effects of interfaces: feeding silo outlet and transition to control box and air slide inlet. Chocked flow (as output from a volumetric feeder) conditions and further as input to an air slide was identified in Chapter 3 as one of the bottleneck in achieving reliable discharges (doses). Air used to transport powder to the feeder and out of the feeder is fed back to the feeding air slide through venting pipes. The bottleneck interfacing is shown in Figure 47, as volumetric feeder – air slide 2. Interfacing: air slide 1 outlet – inlet to volumetric feeder will not be addressed in this work. Before one can model the behaviour of flow in an air slide, short or large, stability of discharges needs to be established first. A better alternative to chocked conditions (doses) is free fall under gravity discharge. In order to understand and clarify questions around high coefficients of variation when analysing feeder performance and to further optimize mechanical design and test feeders' performance a topic to further study from mechanical point of view and analyse would be silo/vessel design using Farnish's (2006) analysis approach. Farnish (2006) had reviewed a few industrial practice cases with flow in chocked conditions and addressed the issues caused by equipment interfacing and dosing irregularities and variations.

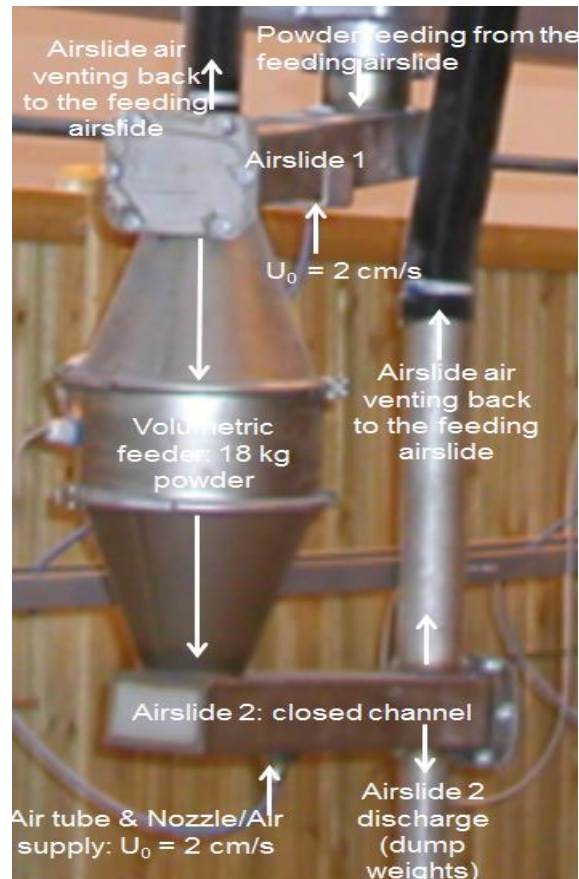


Figure 47 Fluidized feeder layout.

#### 4.2 Air slide test rig 2012: scale up of feeder concept

The meaning with “scaling up” was not to scale up the feeder and build up a bigger twin feeder test rig with proportional dimensions. The purpose was to use the concept: feeder and air slide and try to eliminate the choked conditions at the inlet of the air slide pointed out as bottleneck in Chapter 3. The free fall condition was implemented by placing an iris valve at the outlet of the feeding silo continued by a short portion of pipe into the control box (inlet to the air slide). As powder from the receiving bin was to be used to manually feed the feeding silo at the beginning of each test, there was need for a service valve, to open and close the outlet of the silo. The iris valve was needed in order to prevent both dusting and flooding of the air slide during filling of the feeding silo with powder from the receiving bin. Once the choked flow condition at the inlet of the air slide was eliminated, it was important to identify the other bottlenecks (if any) to be controlled in order to achieve reliable discharges from the air slide.



a



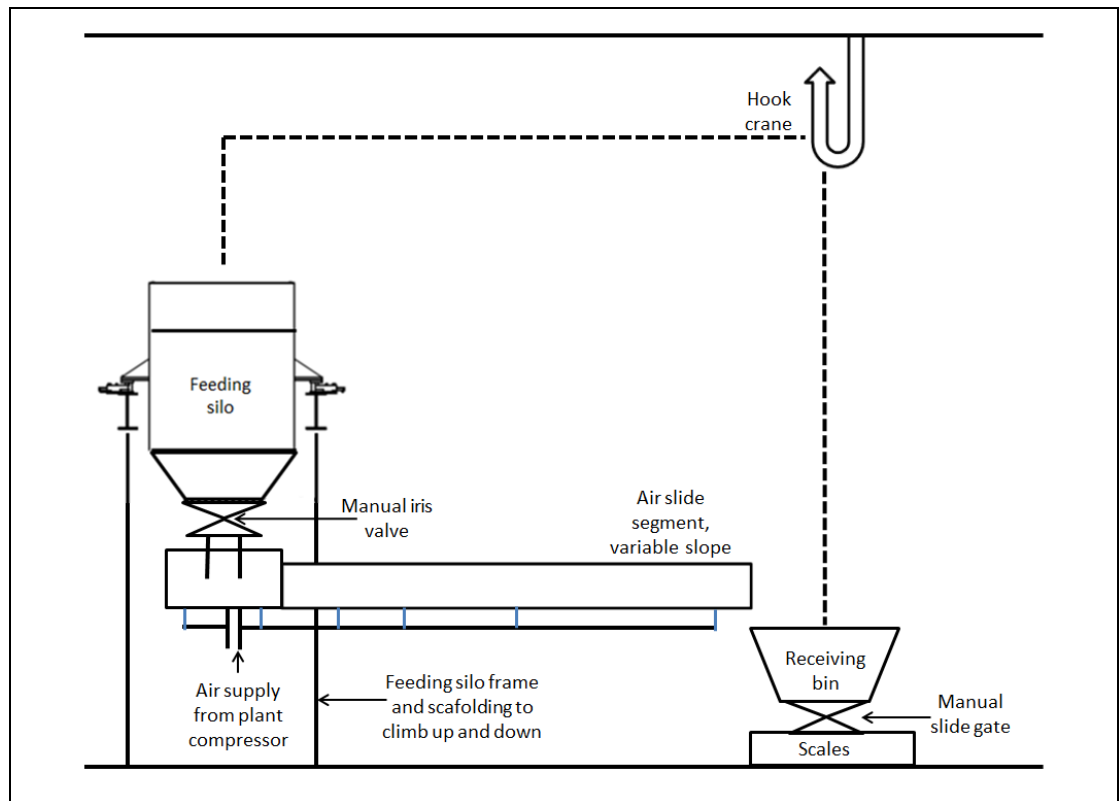
b

Figure 48 a) Volumetric feeder and air slide, chocked flow condition due to interfacing and dosing operation. b) Feeding silo, iris valve and air slide, free fall conditions (gravity discharge).

#### 4.2.1 Design of the test rig 2012

The overall purpose of the alumina rig was to enable empirical studies to be made of fluidized flow of alumina under conditions representative (if not identical) of those that would occur in an industrial situation. One of the main decisions that were made when planning the rig was whether it should have continuous circulation of alumina or to operate batch wise. Previous investigators used both methods. Keuneke (1965), Liot and Chan (1979) and Haugland (1998) constructed their rig for continuous flow of powder, whereas Siemes and Hellmer (1962), Woodcock (1978), Gupta et al. (2006) and Dyrøy (2006) chose to operate batch wise. The main argument against an alumina rig for continuous operation equipped with a conveying system to convey alumina from the discharge end of the air slide back to the top of the feeding silo (at a rate corresponding to the capacity of the air slide) was the high price of the pieces of equipment necessary for such a system and the need to keep expenditure within reasonable limits. Other arguments against such a conveying system were the floor space and headroom availability at POSTEC and the requirement to keep enough space

for other ongoing research activities. So it was decided to opt for a system based on batch wise operation. The test rig has been built at POSTEC in cooperation with Hydro Aluminium and it consists of a feeding silo with a capacity of 550 kg alumina, a control box, a 12 meters long air slide segment and a receiving bin, as seen in Figure 49, Figure 50 a and b and Table 8.



**Figure 49 Plan of the alumina rig, batch wise operation.**

The length of the air slide was chosen to be the same as the length of a full scale feeding air slide, while the channel width was fixed at 150 mm, following Hydro standards. Another argument for maintaining the channel width fixed was related to the maximum capacity of the air slide. The main target was to operate the air slide at various pressurized air supply rates and to be able to achieve its maximum capacity.

Before using batch wise operation it was necessary to estimate and make sure that the maximum flow rate of alumina could be maintained in the air slide for a period of time long enough to provide stable flow. Another requirement was the size of the feeding silo and receiving bin, which would allow continuous discharge of alumina at all flow rates. A capacity of 500 kg was considered to be sufficient to comply with the test



conditions. The air slide was mounted on brackets adjustable in height, this to allow for variations of the angle of inclination. A plan of the alumina rig is shown in Figure 50 and its dimensions are given in Table 8.

The main features of the test rig may be summarized as:

- upstream feeding silo of sufficient capacity to allow for the alumina flow in the air slide to be maintained for a period of time until it becomes stable;
- manual iris valve: means of closing the discharge from the feeding silo to the air slide inlet during filling of the feeding silo;
- short stand pipe consisting of iris valve and feeding silo outlet;
- control box as interface between the stand pipe and air slide inlet;
- air slide segment: conveying channel of fixed width and variable slope;
- downstream receiving bin and scales for the determination of discharge mass flow rates;
- powder return system to convey alumina from the receiving bin to the feeding silo, to ensure a short break between test runs;
- variable air supply to the channel and pressure controller;

Table 8 Dimensions of the air slide.

Material	Mild steel
Length	12 m
Width	150 mm
Height	200 mm
Height control box	300 mm
Distributor/fluidizing fabric	Fluitex E800
Angle of inclination	0-2.1°

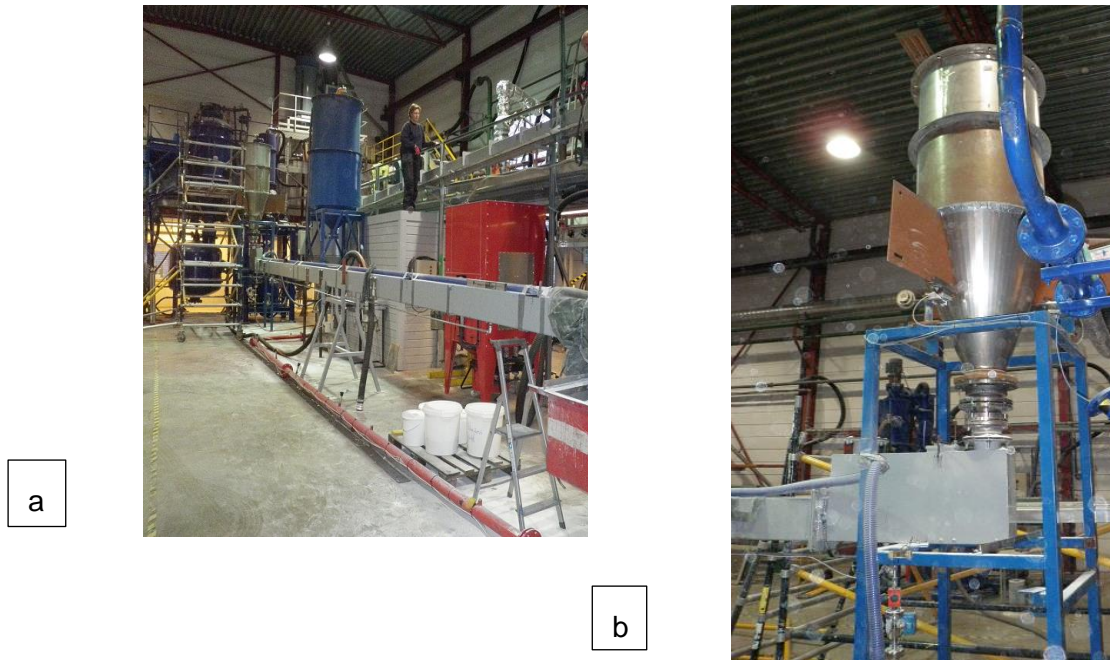


Figure 50 Test rig layout.

Test runs at downward inclination of the air slide above 2.1 degrees could not be conducted due to unavailable vertical space between the discharge end of the air slide and the edge of the receiving bin. To prevent dusting of the test facilities the discharge end of the air slide and the receiving bin were sealed by a plastic cover. The plastic cover was the only alternative to minimize dusting, one constant source of irritation stemmed from the amount of alumina on the floor and the daily amount of time spent on housekeeping. In this investigation the dispensing head device presented by Farnish (2006) in his work consists of an iris valve and the feeding silo outlet, as shown in

Figure 50 b and was built as interface between the feeding silo and the control box/inlet of the air slide. Alumina was fed under gravity through the dispensing head with open iris valve during discharge. The iris valve was closed during refilling of the feeding silo. Figure 51 a, b and c shows a front and a side view of the silo outlet with the stand pipe and the control box. In Figure 51 b the top of the restriction plate can be seen, tests being conducted with the restriction plate inserted into the alumina bed down to approximately 170 and 240 mm from the fluidization membrane on the bottom of the air slide. The objective of using a restriction plate inserted into the powder bed was to simulate the impact of a lower filling degree (shorter distance between the silo outlet and the top of the fluidizing membrane) on the capacity of the air slide. The metallic edge of a fluidization membrane segment can be seen in Figure 51 c.

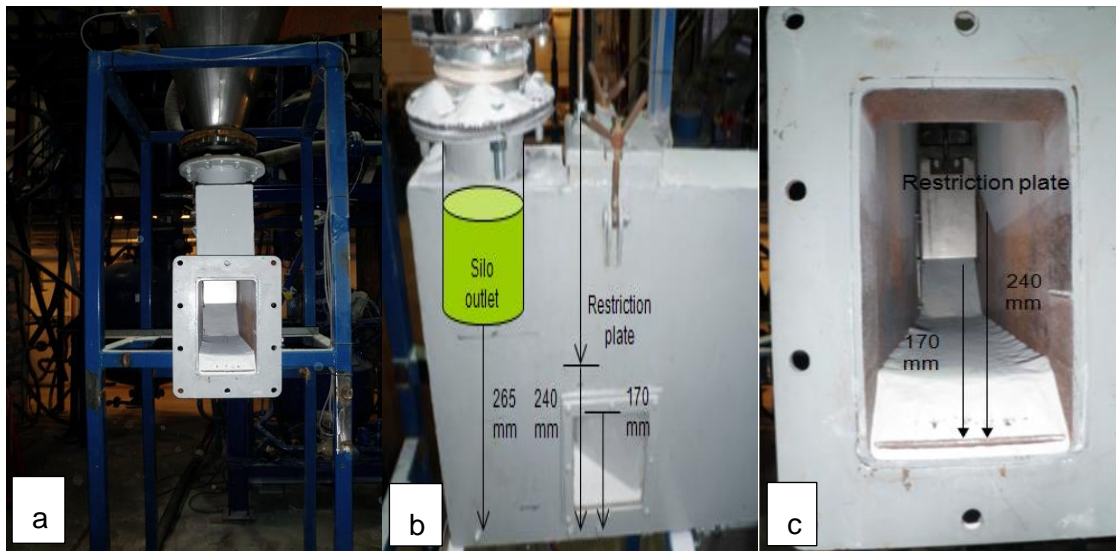


Figure 51 Interface silo outlet/air slide inlet, a, c) front and b) side view.

The air slide outlet was connected to the main air exhaust system through plastic hoses, in order to reduce dusting from experiment. Five holes were made on the upper face at the air slide to allow bed height measurements. This allowed also fines to be captured by an additional air exhaust system and redirected to the cyclone shown in Figure 52.



Figure 52 Additional air exhaust system and cyclone for capturing of fines.

Air from the main compressor was supplied to the rig through a tube connected to five nozzles situated at equal distances along the bottom of the air slide (Figure 53 a and b).

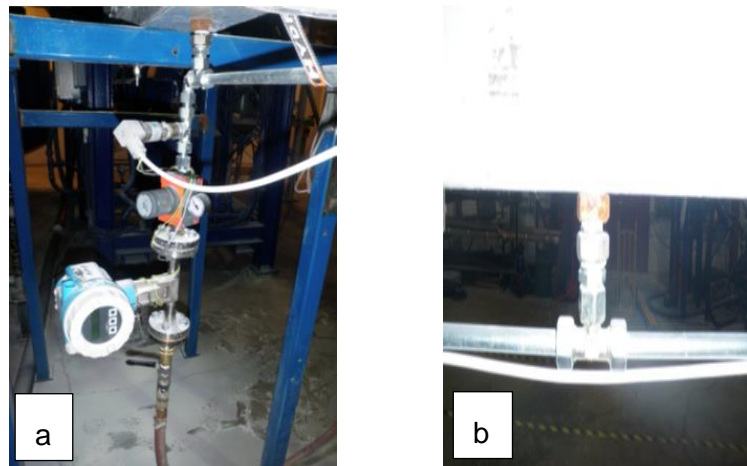


Figure 53 a) Pressure controller, b) nozzle, air distribution through the bottom of the air slide.

#### 4.2.2 Measurements

Measurements were taken at angles of downward inclination of 0.0, 0.6, 1.1, 1.6 and 2.1 degrees. At each inclination four tests were conducted for each pressure rate from 2.5 up to 6.5 bars at increments of 0.5 bars. This range of pressure rates corresponded

to a dimensionless air velocity factor  $U_0/U_{mf}$  from 1.0 up to 2.5, results are presented in Figure 55 a and b. The operating parameters were the air flow rate, the restriction plate (with/without) and the air slide inclination angle. The restriction plate acted as a material supply controller influencing the material supply degree. Two distances from the bottom of the restriction plate to the top of the distributor were tested: 240 and 170 mm, as shown in Figure 51 b and c. Experiments performed with and without restriction plate for all inclination angles from 0 to 2.1 degrees (horizontal to downward inclination) have been conducted to investigate the effect of the interfaces, feeding silo outlet/ inlet, on the material mass flow and bed heights. A total of 480 tests were performed for each case:

- Case 1: restriction plate, 170 mm distance between restriction plate and distributor, 160 tests;
- Case 2: restriction plate, 240 mm distance between restriction plate and distributor, 160 tests;
- Case 3: no restriction plate, 265 mm distance between silo outlet (stand pipe) and distributor, 160 tests;

Three big bags (one tone each) of primary alumina sent to POSTEC from Årdal Reference Centre were used. Two types of measurements were carried out during the tests. One type was measurements of the weight of the receiving bin in order to calculate the discharge mass flow rates (the capacity of the air slide). The other type was measurements of the bed heights at five locations. The bed heights were measured at the end of each test under unfluidized conditions. From the literature reviewed it became clear that the measurement of the depth of the flowing bed apparently had caused difficulties in previous experimental studies. Some of the researchers cited by Woodcock (1978) did not measure them directly, but deduced them from a pressure drop correlation with readings from a small stationary bed. Keuneke (cited by Woodcock (1978)) determined the bed depth as an average of three direct measurements using sight glasses. Due to bubbling or waves in the alumina bed during flow, direct measurements of the bed heights cannot be accurate, especially if one wants to have values at different distances away from the inlet. Woodcock (1978) attached five vertical scales to the channel walls of a Perspex rig at equal intervals along its length and used the readings of the middle three scales in estimating the average depth of the flowing bed. The approach used in this present work combined previous

empirical knowledge from observations of flow in a deep feeding air slide and from work with a fluidization column where bed expansion was measured carefully and where it had been concluded that the expansion of the bed would not be higher than 8 up to 10 %. Vertical scales were glued to the walls of the air slide channel and values of static bed heights at five positions away from the inlet were recorded manually for each test run.

#### **4.2.3 Test procedure**

For the tests two persons were required: one to operate the crane and to control the rig and collect data using LabView, while the other person adjusted the pressure air rates and climbed up and down the scaffolding after every two tests to empty the receiving bin into the feeding silo. In the absence of a transport system to convey the alumina back to the feeding silo, this had to be done by hook crane. Two tests could be conducted at the time, before the receiving bin had to be emptied into the filling silo. Tests have been conducted by following same procedure each time. At the start of each test the data recording equipment was switched on, the vacuum system was switched on to remove the dust from the air slide and from the receiving bin placed on scales at the end of the air slide. The main compressor to supply air to the air slide remained switched on during the whole day. At the end of each test the air was first switched off then the data recording was stopped and the data saved as 'txt.' files. Each of the LabView features with the various refinements used for the instrumentation of the rig will be described in detail in the next chapter.

#### **4.2.4 Observation of the flow**

Figure 54 a and b illustrate the cross section of the air slide channel showing the way the 3 m long porous membranes are attached to the bottom of the channel.

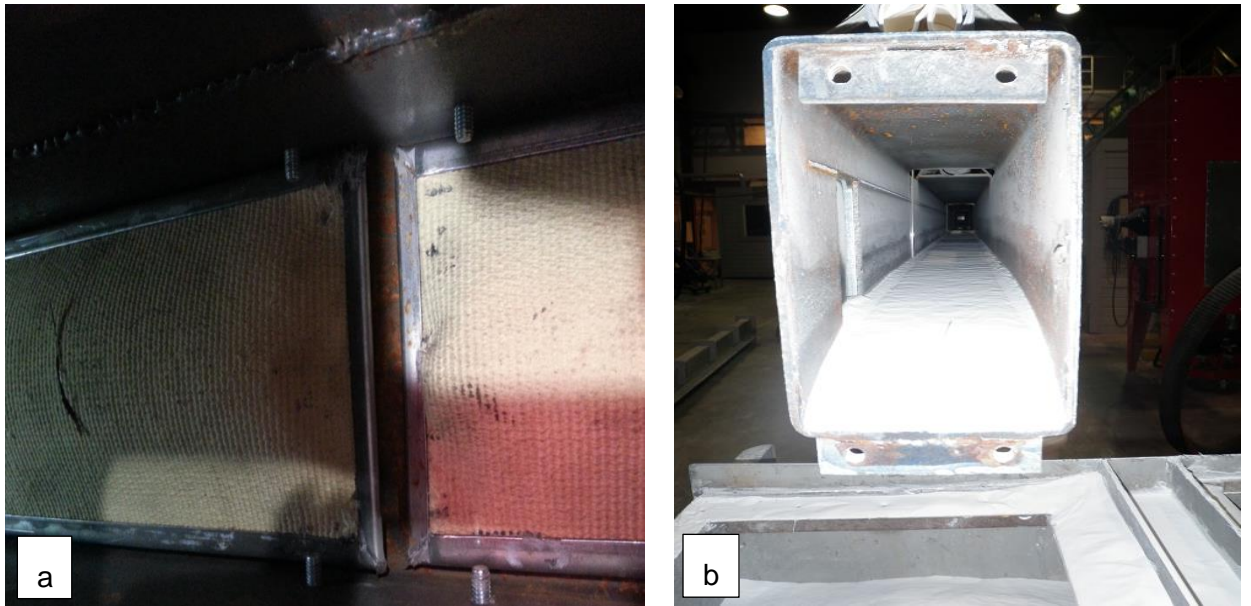


Figure 54 Cross section of an air slide channel a) porous membranes membranes and b) flow visualization, dead zone, effect of unfluidized edge.

There is a gap of 1.5 cm between the short ends of the membranes. Figure 54 b shows a cross section of the channel taken at the discharge end right above the receiving bin showing some interesting static bed profiles, after the supply air had been switched off. Due to the metal edges of the membranes dead zones of unfluidized materials of 0.5 cm width could be observed when conveying at low pressure, below 3 bars. At higher pressure, the edges become fluidized.

#### 4.2.5 Experimental results and discussion

The objective of the tests was to investigate the parameters affecting the capacity of the air slide and record any observations that will help understanding the behaviour of the flow. The results are given below as material mass flow and material bed depths.

Gupta et al. (2006) found that the plenum chamber pressure was independent of the flow resistance offered by the moving material, being linearly dependent only on the supply air flow rate into the plenum.

In this investigation the dimensionless air velocity factor  $U_0/U_{mf}$  has been varied from the start up value of 1.0, which corresponds to the minimum fluidization velocity of alumina powder,  $U_{mf}$  of 0.68 cm/s, up to an upper limit of the compressed air supply of 2.5. Gupta et al. (2006) had used an interval of 0.8 to 3.3, their material having a  $U_{mf}$  of 2.5 cm/s, while Botterill and Besant (1976) operated with an upper interval in the range

of 3.0. Singh et al. (1978) conducted their tests in the range of 1 to 2.8, their material having a  $U_{mf}$  of 3.9 cm/s.

In good agreement with the work of Botteril (1979), Singh et al. (1978), Latkovik (1991) and Gupta et al. (2010) it was found that a minimum fluidization velocity needs to be exceeded to start the flow of material in the conveyor. Above a dimensionless air velocity factor  $U_0/U_{mf}$  of 1.5 the alumina mass flow rate became independent of the operational air velocity. Similar behaviour was observed for all angles of inclination. Similar behaviour occurs as the one reported by Singh (1978) and Gupta (2010): an initial sharp increase in the material mass flow occurs for  $U_0/U_{mf}$  in the range of 1-1.5. In this region, flow behaviour is affected by operational air velocity through its influence on the viscosity. According to Siemes and Hellmer (1962), Botterill and Besant (1979), an increase of the operational air velocity after the material flow start-up caused an increase of the bed voidage and a decrease in viscosity. At levels of  $U_0/U_{mf}$  above 1.5 the mass flow curves reach a saturation level. Only the curves in Figure 55 a) for angles of inclination of 0.5 degrees and b) for angles of inclination of 2.1degrees show stable levels of  $U_0/U_{mf}$  above 1.4 - 1.5. At this level material flow is independent of operational air velocity as it has little effect on the viscosity (Singh et al. (1978)). As pointed out by Gupta et al. (2010) and Kalman and Rabinovich (2008) in their studies of threshold velocities in pneumatic conveying, conveying velocities above what is necessary can lead to wasted energy, particle attrition and pipe erosion. On the other hand, high operational air velocities increase the probability of the fines to be carried out by the air stream and further to the venting pipes. This should have been the case for all mass flow rates shown in Figure 55, but unfortunately, the variation in the results is high, with a coefficient of variation of 46 %. Although suspicion about variations in flow rates was aroused early in the test programme, it was decided to complete the test programme first and then based on the analysed data to identify the causes of the variations.

At this stage it was believed that the variation in the discharge rates happened due to segregation effects during gravity discharge and varying level of fines in the alumina used for the tests, as shown by Dyrøy (2006) and possibly restrictions of the flow discharged from the feeding silo as reported by Farnish (2006).



Improvements of the test rig are necessary. Segregation of the alumina under gravity discharge occurs at all stages, showing the negative effect of interfaces on the operational stability of the rig:

- as alumina is discharged from the big bags into the feeding bin;
- as alumina is discharged from the feeding silo into the air slide;
- as alumina is discharged from the outlet of the air slide to the receiving bin;
- as alumina is transported back by crane and discharged from the receiving bin to the feeding silo.
- difficulties in operating the iris valve at the outlet of the feeding silo and blockages of the valve during filling of the feeding silo, could have changed the mass flow into core flow as previously investigated by Farnish (2006) in his work.

After a careful analysis of the data it was concluded that the control of gravity discharge of powder through the manual operation of an iris valve and the accuracy of such an approach was not optimal. Even when being fully opened, the iris valve can cause an intrusion across the outlet of the feeding silo.

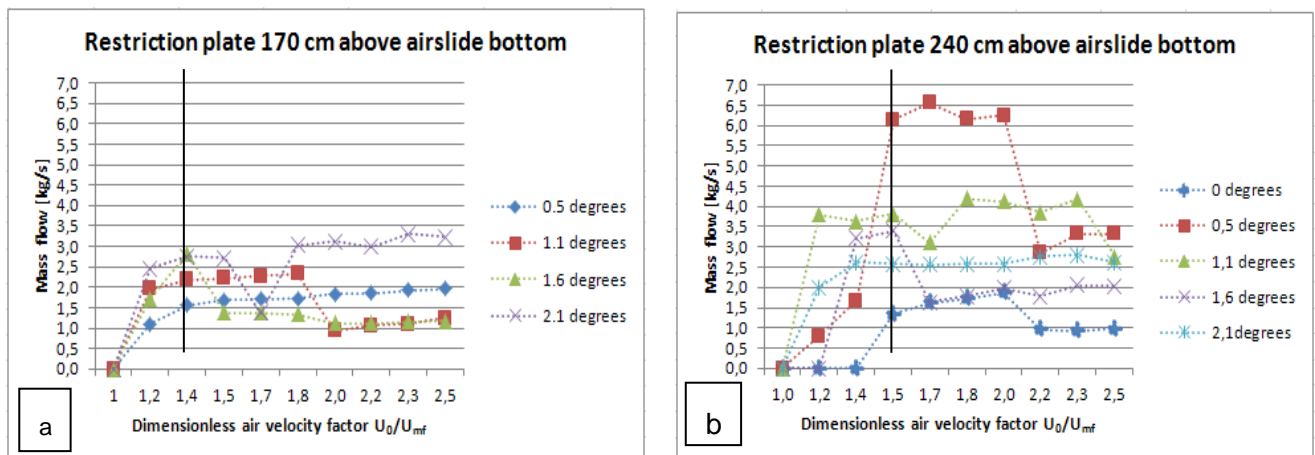


Figure 55 Variation of alumina mass flow rates with dimensionless air velocity factor at different air slide inclinations.

#### 4.2.6 Cloth-iris-valve flow restriction and short stand pipe

The initial configuration (2012) of the rig was not optimal. As with any experimental programme of this size it was difficult to assess the design of the silo outlet until it had been in use for some time, it soon became clear that there were some parts of the rig in

which modification and improvements could be made. Then it became clear that the mechanical design of the outlet from the feeding silo as shown in Figure 56 was again the bottleneck in trying to establish stable feed conditions into the air slide. From all literature reviewed the work of Farnish (2006) was a great starting point in understanding the source of all flow irregularities and discharge variations. Farnish (2006) had reviewed few industrial practice cases with flow in chocked conditions and addressed the issues caused by equipment interfacing and dosing irregularities and variations. His findings were a great source of inspiration for the interpretation of results and approaches in this work.



**Figure 56 a) Outlet configuration of the initial rig built in 2012 cloth - iris valve and short standpipe; b) 2013 configuration: longstandpipe, 7 x D and flexible joint.**

Although the free fall condition for alumina discharge from the feeding silo had been implemented on the rig, it did not provide stability and repeatability of discharges. Farnish and Bradley (2006) discussed the design faults present in this configuration in

terms of discharge equipment and the overall system design commonly found in industrial applications, pointing out that consistency and repeatability of discharge from vessels was the keystone to the efficiency and profitability of many types of processes. Although techniques for design of storage vessels based on the flow characteristics of particulates have been in the public domain since the 1960's, they have been slow to gain acceptance in the industry (mainly through a lack of awareness of their existence amongst engineers). According to the authors, in terms of controlling discharge from gravity flow equipment, it was often the gravity discharge approach which generated the greatest degree of variability, in terms of both quantity and repeatability. The root of the problem of inconsistent discharge rates was identified to lie with the flow channel development within the feeding silo or the discharge head (stand pipe). The potential causes of flow irregularities were even more critical to be aware of, in the cases where mass flow principles were to be applied, especially in the case of easy to segregate materials. Thus on systems that operated on a discharge basis that uses an adjustable outlet aperture, the development of a flow channel subject to minimal shear at its boundaries is essential. In many cases the outlet aperture relied upon the insertion of devices such as iris valves or gate valves (acting perpendicular or nearly so) to the path of the flow channel. In such cases static material would be supported from the leading edge of the valve to the nearest wall of the discharge head or vessel outlet. This supported material could extend for some distance from the outlet and generate a major shear plane of powder on powder, which again, would induce inconsistent discharge rates from the outlet – mainly by imposing core flow discharge conditions (which are characterized by inconsistency in flow rate and exaggerated segregation effects).

## 5 Modified and improved air slide test rig 2013

In industry the strategy has been to increase the limiting flow rates without reducing the storage capacity of the feeding mass flow silos. From the short courses attended at the Wolfson Centre, without going too much into detail, it was learned that with mass flow, the bulk solid is in motion at every point of the silo whenever any material is allowed to flow through the outlet.



**Figure 57 Vertical stand pipe. a) Equipment design at the Wolfson Centre (consultancy work) and b) modified silo outlet at POSTEC (2013).**

Two case studies were undertaken by Farnish (2006) in his extensive review of discharge problems. The bulk handling systems in his work had then been replicated and installed in the form of an instrumented test rig at the laboratories of the Wolfson Centre for Bulk Solids Handling Technology, University of Greenwich. The term

“dispensing head” or “stand pipe” were used in his work to refer to a device that is used to control or regulate the flow of powdered solid material in bulk from a gravity discharge vessel or chute. In addition to the requirement for the rig to measure discharge rates from the dispensing head, was the need to be able to quantify transient flow rate effects. Following measuring program was then initiated by Farnish (2006):

- measure loss in weight for the hopper;
- measure instantaneous mass flow rate and study flow transition effects;
- take powder samples over a number of repeated discharges;

Typical mass flow bins with stand pipes attached to them are shown in Figure 57. Vertical stand pipes as shown in Figure 57 often have limited application in industry due to headroom constraints commonly found in pot rooms (not enough room for cranes, rails and receiving silo/bin). For a given bulk material to flow in gravity discharge a set of geometrical parameters are required such as minimum outlet dimension and the angle of converging portion of the silo for a given wall material. As pointed out in the previous Chapter, a single piece of equipment to suit for a wide range of alumina qualities and binary mixtures might require a range of geometries that cannot be implemented in a single design and in the same piece of equipment.

### **5.1 Preliminary silo outlet modelling**

In the bulk solids community the work of Gu et al (1993) is well known. They provided experimental and theoretical evidence of the use of stand pipes to increase gravity flow rates of both sand and alumina powders from mass flow bins. Their results on relatively small bore standpipes ( $D = 44.5$  mm) indicated that the effects of a stand pipe attached under a bin/ feeding silo outlet would become more significant as the particle size of the bulk solid reduces and the length of the stand pipe increased - provided that the stand pipe would remain full of material during operation. The bulk solid discharging from the feeding silo under the effect of gravity has a self-limiting flow rate that is primarily attributed to the self-generated negative air pressure gradient within the inter-particle voids in the region of the outlet of the feeding silo. Additional observations from “mock up” trials undertaken at the Wolfson Centre enriched the research and made an important change in the direction of investigation. “Mock –up” tests as shown in Figure 58 have been conducted at the Wolfson Centre to verify Gu’s concepts. The diameters of the pipes were 40 mm and 100 mm with a hopper half - angle of 20 degrees.

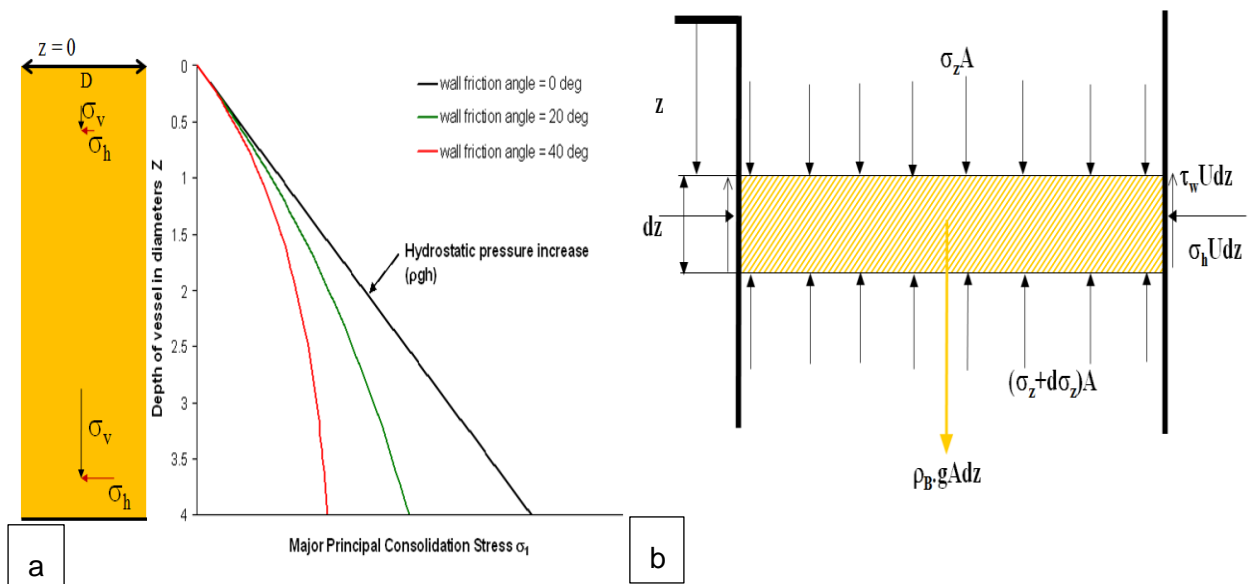
Tests were started with  $8x D$  and the pipes were cut down to  $7xD$ ,  $6xD$ ,  $5xD \dots 1xD$ . Repeatability of flow rates from discharging 15 kg of alumina/test became less critical already at  $5xD$ , where flow rates varied from 7 to 11 t/hr. Best stability was achieved for  $6xD$ ,  $7xD$  and  $8xD$ . The trials gave an indication that for an improved silo outlet design, in order to achieve stability and good repeatability of discharges, a minimum  $6xD$  long standpipe would be a safe choice.



Figure 58 “Mock-up” tests at the Wolfson Centre to verify Gu’s et al (1993) concepts.

Based on the previous work of Gu et al (1993) and Farnish et al (2006 - 2012) fresh measurements were carried out on a modified alumina rig at POSTEC during 2013 from which the iris valve was removed and the silo outlet pipe extended to  $7.5x D$  following Janssen’s (1895) work. Janssen (1895) presented in his paper the saturation effect in granular silos and developed a one dimensional differential slice method to describe the distribution of internal stresses in the vertical section of a silo. The saturation of pressure with depth in a static powder system confined by vertical silo walls is therefore known as Janssen effect. The process of silo discharge through a vertical stand pipe was taught to be further modelled using analytical techniques from soil mechanics and

powder technology based on the work of Janssen (1895), Arnold et al. (1982), Nedderman (1992) and Schulze (2008). The Janssen effect principle directly applied to a vertical stand pipe is illustrated in Figure 59 a. When the feeding silo and the stand pipe are filled with alumina without any friction against the walls, the stress distribution will be dominated by the hydrostatic pressure,  $\rho_b g h$  and will increase linearly with the depth in the stand pipe, from  $= 0$  , at the inlet of the stand pipe, throughout the entire length of the stand pipe. If there is wall friction between alumina and the walls of the stand pipe, then there will be an exponential decrease in stresses as shown by the green and red curves, proportional to the length of the stand pipe. The stress ratio,  $K = \frac{\sigma_h}{\sigma_v}$ , is defined as the ratio between the horizontal stress,  $\sigma_h$  at the wall to the mean vertical stress,  $\sigma_v$  (Schweddes (2003) , Schulze (2008), Pinzon (2012)). The stress ratio,  $K$  of a powder varies between 0.3 and 0.6 being 1.0 for liquids.



**Figure 59 Janssen effect for stress distribution in silos: a) stress distribution in the vertical section of a silo for different wall friction angles; b) The method of differential slices: stresses on a cylindrical element inside the standpipe ( a),b) reprinted from the Wolfson Centre short course presentation).**

Figure 59 b shows the method of differential slices, a name given by Hancock (1970) (cited by Nedderman (1992)) to an approximate analysis of the Janssen effect. According to Walker’s (1966) (cited by Nedderman (1992)) improvement of Janssen’s analysis, it is assumed that the material is sliding down the wall and that there will be an upward shear stress  $\tau_w$  exerted by the wall on the material. A force balance has been

performed on an elemental slice of thickness  $dz$  at depth  $z$ . There is a downward force  $A\sigma_z$  on the top surface of the element that is open to the atmosphere and an upward force  $A(\sigma_z + d\sigma_z)$  on the bottom.  $A$  is the cross section area of the standpipe, given by  $A = \pi D^2$ . It will be assumed that the top surface is subjected to a uniform surcharge  $P_{v0}$  at  $z = 0$ . The force exerted by the weight of the material is  $\rho_b g A dz$ .

A force balance on the slice element gives:

$$A\sigma_z + \rho_b g A dz = \tau_w U dz + A(\sigma_z + d\sigma_z)$$

To demonstrate that the length of stand pipe does have an effect on the pressure distribution and stabilization, following formula implemented in Excel was used on alumina:

$$P_v = \frac{\rho_b g D}{4\mu_w k_J} \left[ 1 - e^{-\frac{4\mu_w k_J z}{D}} \right] + P_{v0} e^{-\frac{4\mu_w k_J z}{D}}$$

where for a cylindrical standpipe:

$$\frac{D}{4} = \frac{A}{U}$$

$U$  is the perimeter;

$P_{v0}$  is the surcharge pressure at the inlet at the standpipe,  $z = 0$ ,

$\mu_w = \tan \phi_w = 0.364$ , the coefficient of wall friction, calculated based on

$\phi_w = 20^\circ$  the angle of wall friction

$k_J = 0.7$  is the Janssen constant, identical to Rankine's coefficient of earth pressure and

$\rho_b = 1000$  the bulk density.

Without surcharge stress at the inlet, the pressure distribution becomes:

$$P_v = \frac{\rho_b g D}{4\mu_w k_J} \left[ 1 - e^{-\frac{4\mu_w k_J z}{D}} \right]$$

Figure 60 and Figure 61 show the results of Janssen's effect for a feeding silo with an outlet diameter varying from 200 mm down to 140 mm along a standpipe from 0 up to 7.5 times the outlet diameter.



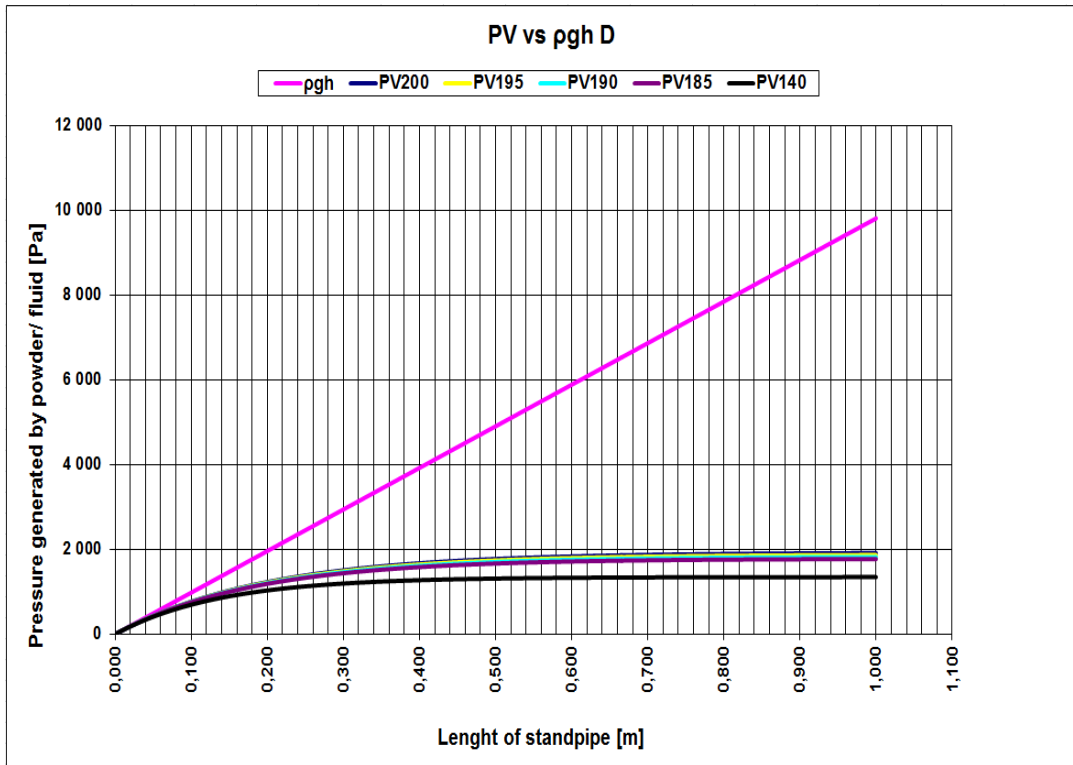


Figure 60 Janssen's effect for a series of feeding silo diameters, from  $D = 200$  mm down to  $D = 140$  mm for lengths of standpipe from 0 up to  $7 \times D$ .

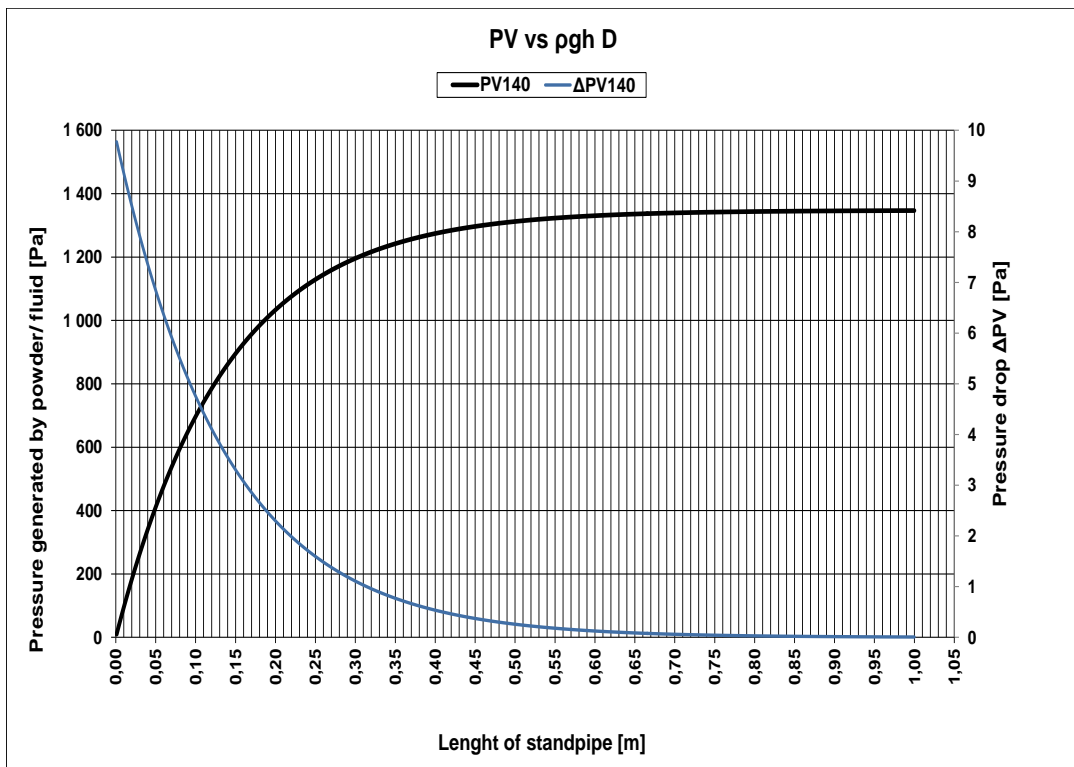


Figure 61 Final solution chosen for the modified rig  $7.5 \times D$  long standpipe; Janssen's effect for a feeding silo diameter with  $D = 140$  mm for lengths of standpipe from 0 up to  $7.5 \times D$ .

Inspired by the work of Gu et al. (1993) and Farnish (2006) changes to silo outlet design and in measurements were implemented once again to the test rig in 2013. The irregular discharge behaviour created from using an iris valve resulting in shear planes incorporating static product has been mitigated by removing the valve and redesigning the outlet area of the silo. The outlet diameter of the feeding silo was modified from 204 mm to 140 mm as shown in Figure 62.

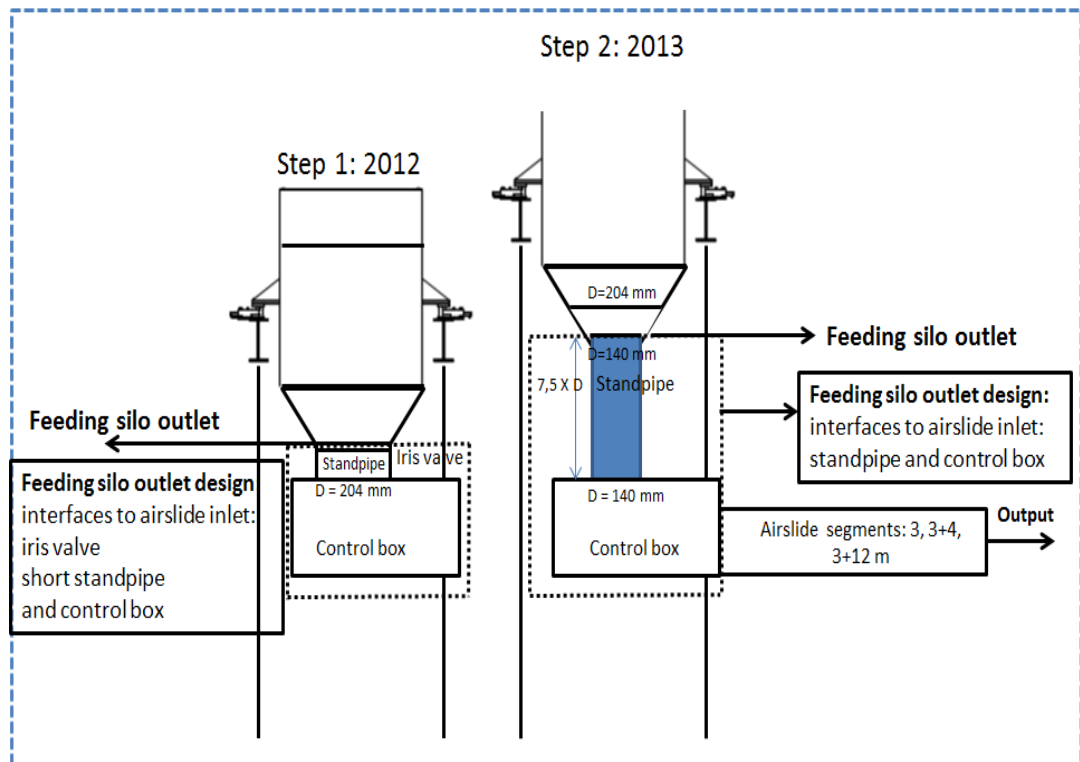


Figure 62 Modifications to the feeding silo outlet: a) Step 1: 2012: iris valve, short standpipe,  $D = 204$  mm; Step 2: 2013:  $7.5 D$  long standpipe,  $D = 140$  mm.

A 140 mm diameter stand pipe was installed at the outlet of the mass flow silo as shown in Figure 63. In order to be able to implement the mechanical changes, the upper ring of the feeding silo had to be removed due to headroom restrictions. A schematic view of the new rig is shown in Figure 66 b. The stand pipe had a length to diameter ratio ( $L/D$ ) of 7.5 and was connected to standard air slide segments of 3 m, 7 m and 15 m. The joint between the stand pipe and control box was flexible to allow for testing at different downward inclinations of the air slide and it was sealed using glue and tape.



Figure 63 a) Feeding silo outlet (2012); b) New design (2013).

The modification of the rig gave time to reflect upon the outcome of the project and the opportunity to include the measurement of some more variables: loss in weight from the feeding silo, pressure measurements and tests with different air slide segments, which had not been taken into account previously. The maximum length of 15 m was set by the space available at POSTEC, although one more 4 m segment was available to extend the channel further up to 19 m. A further extension would have required to move the receiving bin and scales outside the test building, outside the direct reach of the hook crane and to expose the alumina to outdoor ambient conditions.

Air slide capacity for 0 to 3.1 degrees of downward inclination was to be measured for each segment by using pressurized air in the range of 3 to 6.5 bar. In an attempt to ensure that the air supplied to the plenum chamber beneath the porous membrane of the air slide was uniformly distributed, pressure transmitters were placed right under each nozzle supplying air to each individual membrane segment. Each set of data taken during a run consisted of:

- the length of the air slide segment;
- the slope (downward inclination) of the air slide channel;
- the operational velocity calculated from pressure data recorded by the pressure sensors;

- the mass flow of alumina recorded on line, as capacity of both feeding silo (loss in weight of the feeding silo) and air slide (gain in weight of the receiving bin);
- the average depth of the static bed.



Figure 64 Measurements of the downward angle of inclination at several points along the air slide.

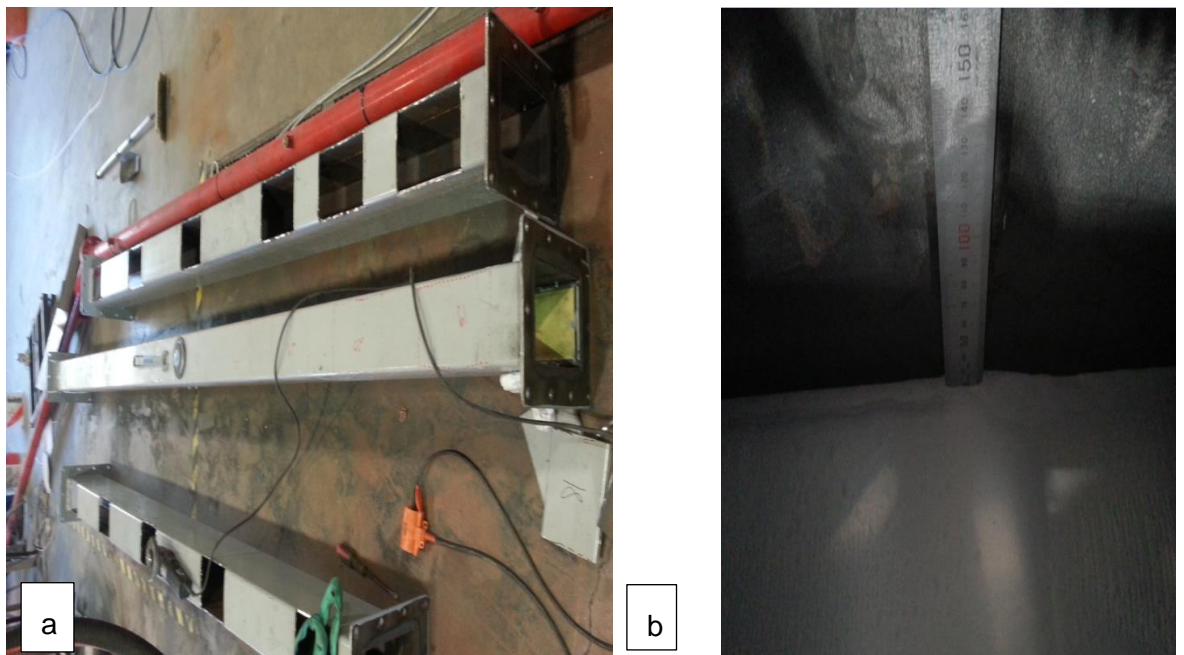


Figure 65 a) Cutting pieces of air slide to make room for b) bed height measurements.

Air pressure was adjusted by using a small pressure controller. Five tons alumina supplied by the Reference Centre in Årdal were used for conducting all the tests, around 500 kg being used per test round. The flow properties of alumina were measured by using a Brookfield Powder Flow Tester with V1.2 Build 19 software.

Three consecutive tests were conducted for each operational condition (a given air pressure at a given air slide downward inclination). A hook crane was used to lift up and transport the receiving bin back and forth to the feeding silo for each test round. At the completion of each test run, one operator would switch off the data recording in LabView, hook up the receiving bin to the crane and convey it to the top of the feeding silo. A butterfly valve had to manually be opened and closed for emptying alumina from the receiving bin into the feeding silo. The other operator would switch off the supply air, climb up the scaffolding, open the slide gate on the bottom of the receiving bin and wait for the alumina to be discharged. Once emptied the bin, the operator would climb down and measure the static bed heights at different distances from the inlet, while the crane operator would place the bin back on scales, seal it and make ready for the next test run. During the test runs, the operation of the rig generally presented no problems, the only major area of difficulty being the dusting from the discharge end of the air slide. The sealing cover and the central vacuum cleaning system could not cope and prevent dusting, all the equipment in the test facility being covered in a thin layer of alumina during all seven weeks of commissioning and test runs.

LabView was used to record and display data from the flow meter, pressure sensors, weight beam cells and scales. Shear beam load cells and scales, most common used in industry, are simple weighing devices, thus the values of loss and gain in weight have been calculated by filtering the electrical signals from load cells.

It was known from previous work that the stand pipe had to remain full of product at any time during operation in order to achieve stability and good repeatability of test work. It was found that the weight of the powder in a full stand pipe was approximately 50-60 kg, thus each test was to be run until 60-70 kg of powder would remain in the system and then manually switch off the pressurized air and stop the test. The previous work of Gu (1993) played an important role in showing how the main parts: feeding silo, stand pipe and air slide of a transport system are integrated together. The stand pipe is an important part of the system acting as interface between the feeding silo and the air slide. An example of on line measured capacities for a given set of specified

parameters for a test round: 7 m long segment, 1.1degrees downward inclination, air supply from 3 to 6.5 bar, same amount of powder for all tests, is shown in Figure 66.

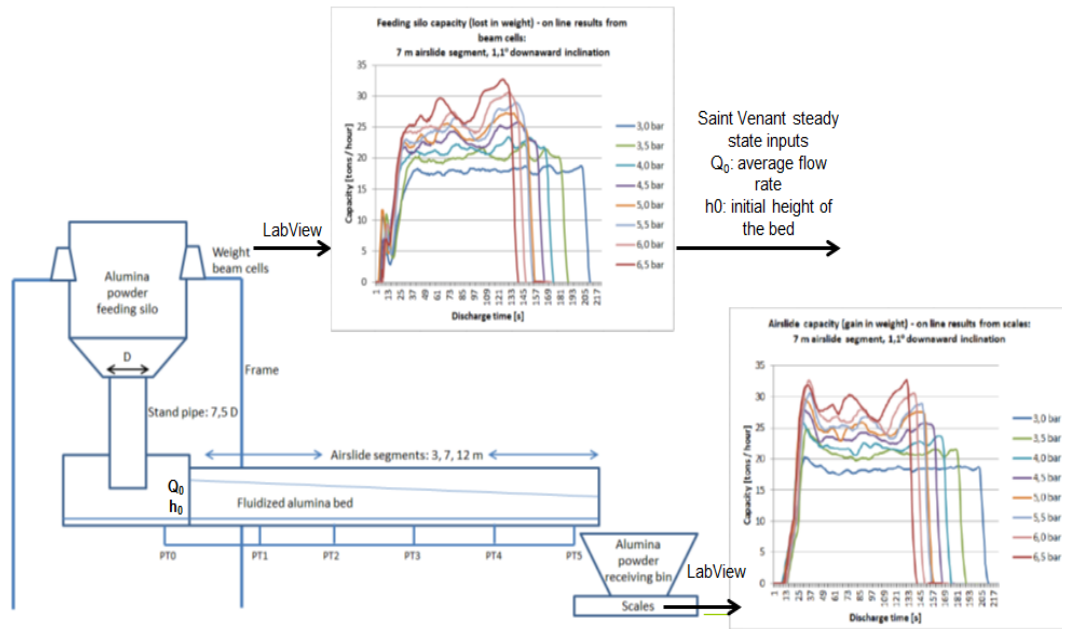


Figure 66 Schematic view of the alumina rig and signal sampling.

The variability of the discharge rates from the test equipment logged via LabView was analysed in Excel. The values of one test are presented in Figure 67. The signals from the load cells and scales have been plotted together to study the behaviour of the feeding silo, stand pipe and air slide system. Initiation of gravity discharge for each test was initiated by first running LabView and then by adjusting the compressed air regulator at the desired pressure rate. After forty seconds from start-up the system is reaching steady state condition. When there are 60 - 70 kg of powder left in the system, corresponding to full stand pipe, the compressed air is shut down and two more tests are conducted with the same operational parameters. The average values from a succession of tests for a set of given operational parameters were then processed using the ratio between standard deviation and average in order to calculate the coefficients of variation used as stability and performance indicators. It is then the capacity average value for three tests during the steady state condition,  $Q_0$ , that is used further in the Saint Venant model.

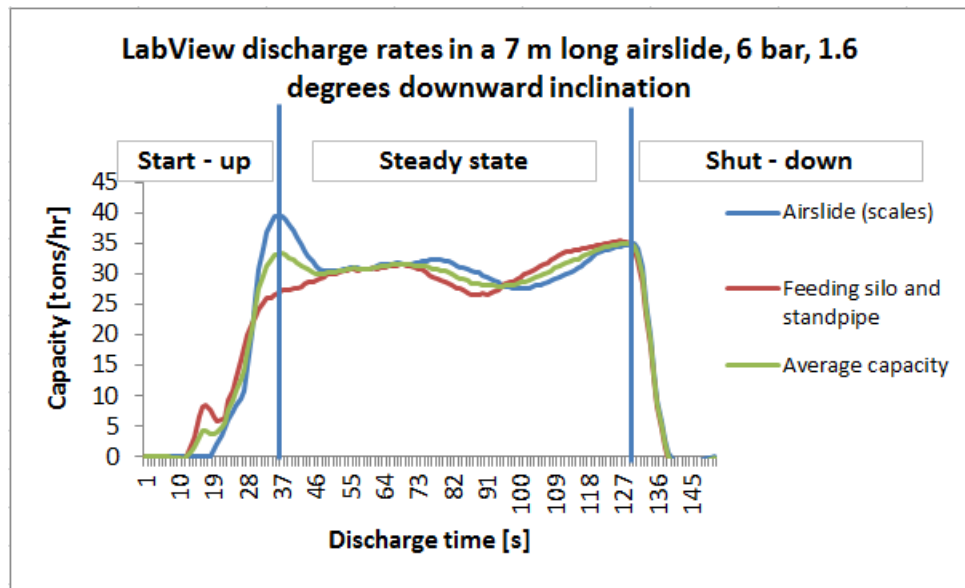


Figure 67 Example of LabView instantaneous discharge rates used in the test result analysis.

An example of results of capacities of the feeding silo and air slide calculated as average values from LabView and coefficients of variation for segments of three lengths: 3 m, 7 m and 15 m are shown in Table 9.

Table 9 Capacity and coefficients of variation for different segments of air slide at 1.1 degrees downward inclination.

1,1 degrees													
$U_d/U_{mf}$	3 m				7 m				15 m				
	Capacity [t/hr]		Coefficient of variation [%]		Capacity [t/hr]		Coefficient of variation [%]		Capacity [t/hr]		Coefficient of variation [%]		
	Airslide	Feeding silo	Airslide	Feeding silo	Airslide	Feeding silo	Airslide	Feeding silo	Airslide	Feeding silo	Airslide	Feeding silo	
0,99	13,1	13,2	2,1	2,1	17,9	17,7	3,1	1,6	18,4	17,0	5,0	0,6	
1,16	16,8	16,9	1,1	1,1	20,9	20,4	0,1	0,5	20,0	19,3	5,6	0,7	
1,31	19,3	19,5	1,5	1,7	22,3	21,7	1,3	1,0	21,5	20,6	3,1	1,3	
1,49	20,2	20,3	1,6	1,8	23,8	23,1	0,5	0,8	22,9	21,4	1,3	1,6	
1,64	21,3	21,4	2,8	2,8	24,9	24,3	0,4	0,1	23,9	22,7	1,1	1,1	
1,81	21,8	21,9	0,4	0,2	26,1	25,2	1,6	0,9	25,1	23,6	0,5	0,1	
1,97	22,9	22,9	1,0	0,9	27,0	26,2	0,6	0,7	25,8	24,2	0,5	0,6	
2,14	23,1	23,2	2,1	1,2	28,4	27,6	0,6	0,7					

Examination of the coefficients of variation show good repeatability between the tests and prove the strong operational stability of the stand pipe concept used for outlet design. Before achieving the good results shown in Table 9, some calibration of the transducers had to be done as described in the next sections.

#### **5.1.1.1 Weighing system and calibration of shear beam load cells**

A load cell is a transducer that is used to create an electrical signal having a magnitude proportional to the force being measured. The force being sensed deforms four strain gauges. Shortly explained, the strain gauges measure the strain (deformation) as a change in electrical resistance, which is a measure of strain and hence the applied force.

The support weighing structure, installation and calibration of load cells were vital for a successful implementation of feeding silo weighing system and powder lock concept. The load cell positioning is important to avoid differences in loads and selection of correct capacity (550 kg each) is important for optimal utilisation of the cells and for a stable electrical signal. The method chosen was calibration by reference weight. Other more detailed methods of calibration can be found in Marklev (1996). Scales used to record the gain in weight of the receiving bin in order to measure air slide capacity and the receiving bin were used as reference weight equipment. The uncertainty of calibration from feeding silo and standpipe system will thus depend of the calibration uncertainty of the reference weighing system: receiving bin and scales. Otherwise the two systems would not influence each other, since they were physically disconnected and in addition they used different input hardware modules inside the control cabinet.

Calibration procedure was following:

- with the load cells installed in the weighing system (empty feeding silo and standpipe) and no load applied, the zero (dead load) was established;
- the pre-weighed alumina from the receiving bin was emptied into the feeding silo; the system was allowed to stabilize at each step before readings were taken and the average result was recorded;
- the material was removed and the procedure was repeated three times for quantities of: 60 kg, 250 kg, 500 kg (full capacity of the receiving bin);
- a four point: 0 – 60 – 250 - 500 kg increasing linearity test was performed and used as calibration curve input in LabView;

The change in resistance of the strain gauges provided an electrical value change that was calibrated to the weight of the empty feeding silo and then to the weight of powder lock: empty feeding silo with a full stand pipe as shown in Figure 68. The optimal amount of powder that would give full standpipe was found by trial and error and visual



inspection from the top platform of scaffolding. Tests in the range of 40 to 100 kg were conducted, 60 kg was found to be the optimal powder weight for the powder lock. An alarm was implemented in LabView, so the operator would know by inspecting the loss in weight from online trends, when to stop the test. According to Gu's concept, in order to achieve stability and repeatability, the standpipe should remain full of powder, meaning that each test should be stopped when the amount of powder left in the feeding silo and standpipe will approach 60 kg.

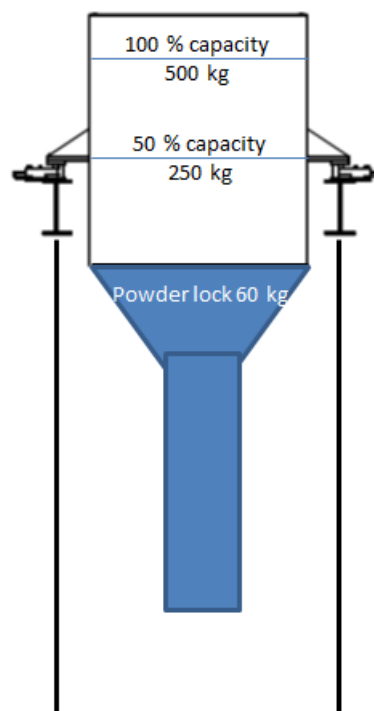


**Figure 68 Pre-weighing for calibration of beam cells.**

The loss in weight for the feeding silo mounted on a frame equipped with beam cells, as shown in Figure 69 and gain in weight for the receiving bin placed on scales were recorded by measuring the mass variation in the feeding silo/stand pipe and receiving bin versus discharge time. The feeding silo and air slide (receiving bin) capacities calculated by differentiating the mass curves with respect to time were displayed online in LabView.

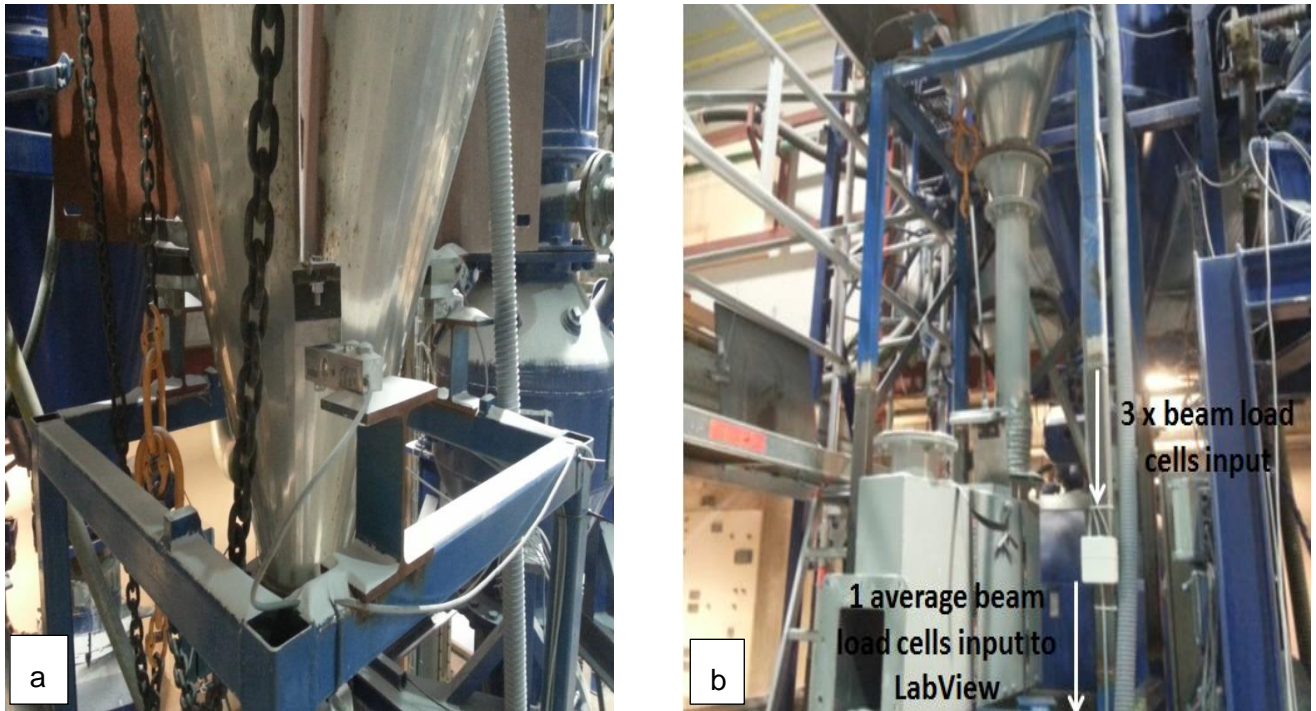


Figure 69 a) 3 x HBM model HLCB 1C3 shear beam load cells arrangement; b) Junction box electrical input to HBM Clip AE 301 and LabView.

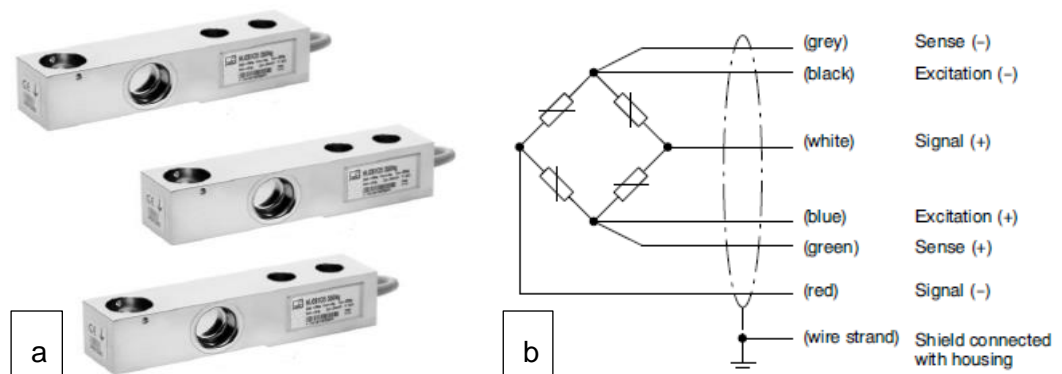


Figure 70 a) HBM model HLCB 1C3 550 kg shear beam load cells; b) Wiring code for each load cell. Pictures are taken from the operational manual (see Appendix for details).

A signal amplifier is an electric device suitable for the measurement of mechanical quantities such as force, weight, torque, pressure, displacement, strain and acceleration. An industrial measuring amplifier Clip Electronic in cast housing from Hottinger Baldwin Messtechnik, HBM Clip AE 301 as shown in Figure 71 b was used to connect with the beam load cells from the feeding silo.

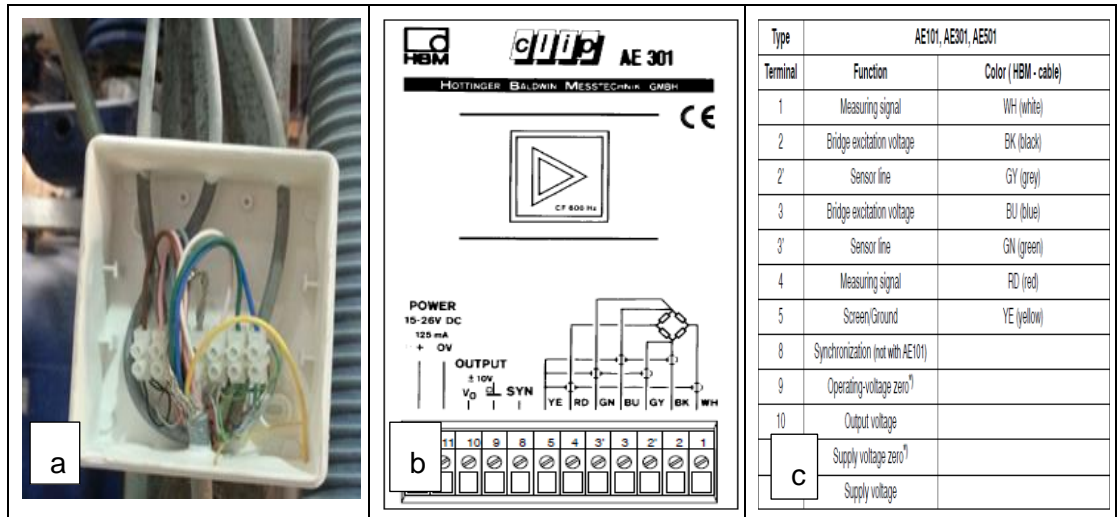


Figure 71 a) Junction box and input signal to b) measuring amplifier, HBM Clip AE 301 and b) amplifier connections (operating voltage zero and supply-voltage are internally connected); terminal 5 of the Clip amplifier was grounded according to the operating manual.

The housing was installed onto mounting rails into the control cabinet shown in Figure 72 a.

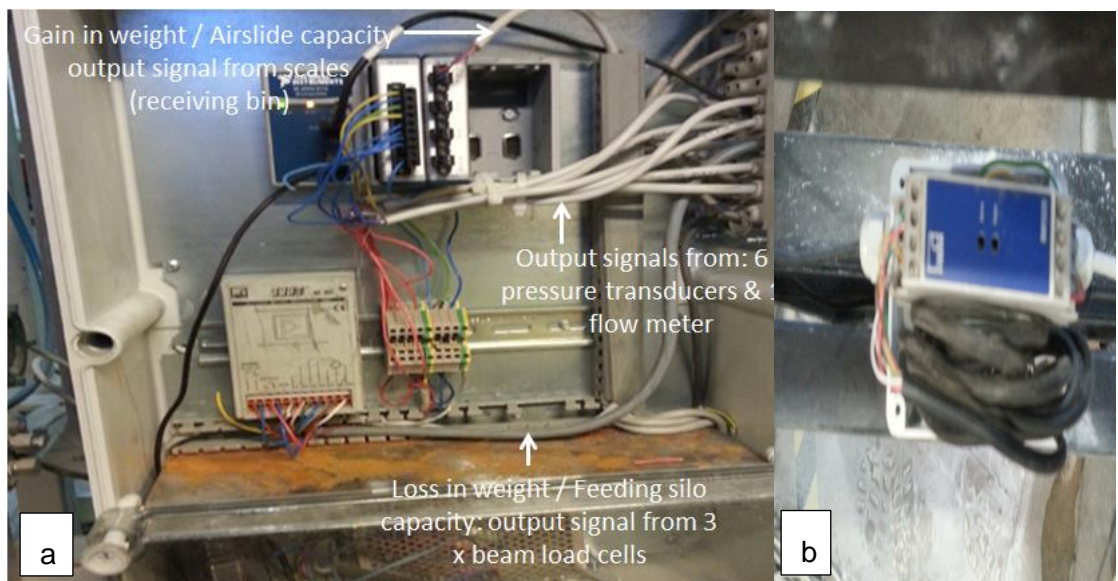


Figure 72 a) Control cabinet set up, "something new, something old" - hardware and input signals from transducers used to measure feeding silo and air slide capacities, flow rates and pressure drops; b) HBM RM 4220 amplifier attached to the support rails of the scales.

An HBM RM 4220 amplifier for strain gauge transducers with 4 mA to 20 mA output signal was attached directly to the support rails of the scales in water proof housing as shown in Figure 72 b. The signal was used to measure gain in weight of the receiving bin (air slide capacity).

### 5.1.2 Data acquisition and analysis

In order to collect the data from the tests, a data acquisition system was designed and built. The program for the test rig was written in National Instrument's LabView software, created to store and display the data during the tests. The LabView program uses NI's Data Acquisition hardware to process signals from the transducers. A laptop PC running LabView 13 software was used for data acquisition and processing. The total data collection time for each test depended on the amount of pressurized air and the angle of air slide inclination used for the test.

All transducers and hardware had been previously calibrated and used by POSTEC in previous projects; the NI modules were borrowed from other test rigs not being in use. A NI 9203 8 - input channel, +/- 20 mA, 16 bit Analog Input (AI) module from National Instruments was used to connect the current signals from scales, flowmeter and pressure transducers via HBM RM4220. As seen in Figure 73 a, each channel has an AI terminal to which the current signals were connected as shown in Figure 74. The NI9203 also has a common terminal, COM, internally connected to the isolated ground reference of the module.

NI 9239 module is a 4 - channel, +/- 10 V, 24 bit simultaneous channel to channel isolated analog input module was used to collect the voltage signal from beam shear load cells via HBM Clip AE 301 and convert them to digital. According to the operation manual, the NI 9239 uses a combination of analog and digital filtering to provide accurate representation of in - band signals while rejecting out- of band signals. More information about installing, configuring, specifications and terminal assignments can be found in the operating manuals for each module on NI's homepage.

The NI 9203 and NI 9239 modules were then inserted into the slots of a NI cDAQ - 9174 chassis mounted inside the control cabinet, which integrated all signals and transferred them to the computer via a USB cable. The LabView program on the computer processed the data and provided output '.txt' files which imported to Excel were analysed offline. The test results are presented in the next sections.

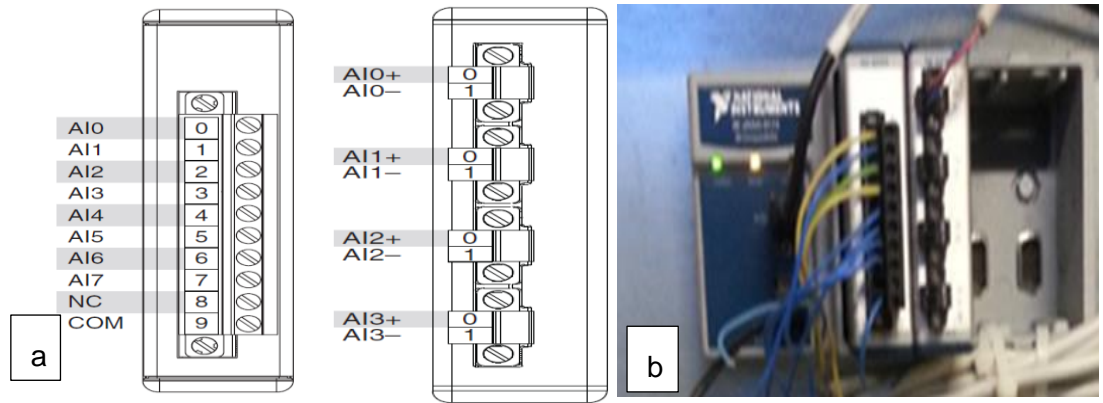


Figure 73 a) NI 9203 8 - channel AI Module; b) NI 9239 4 - channel AI Module; c) NI cDAQ 9174 chassis.

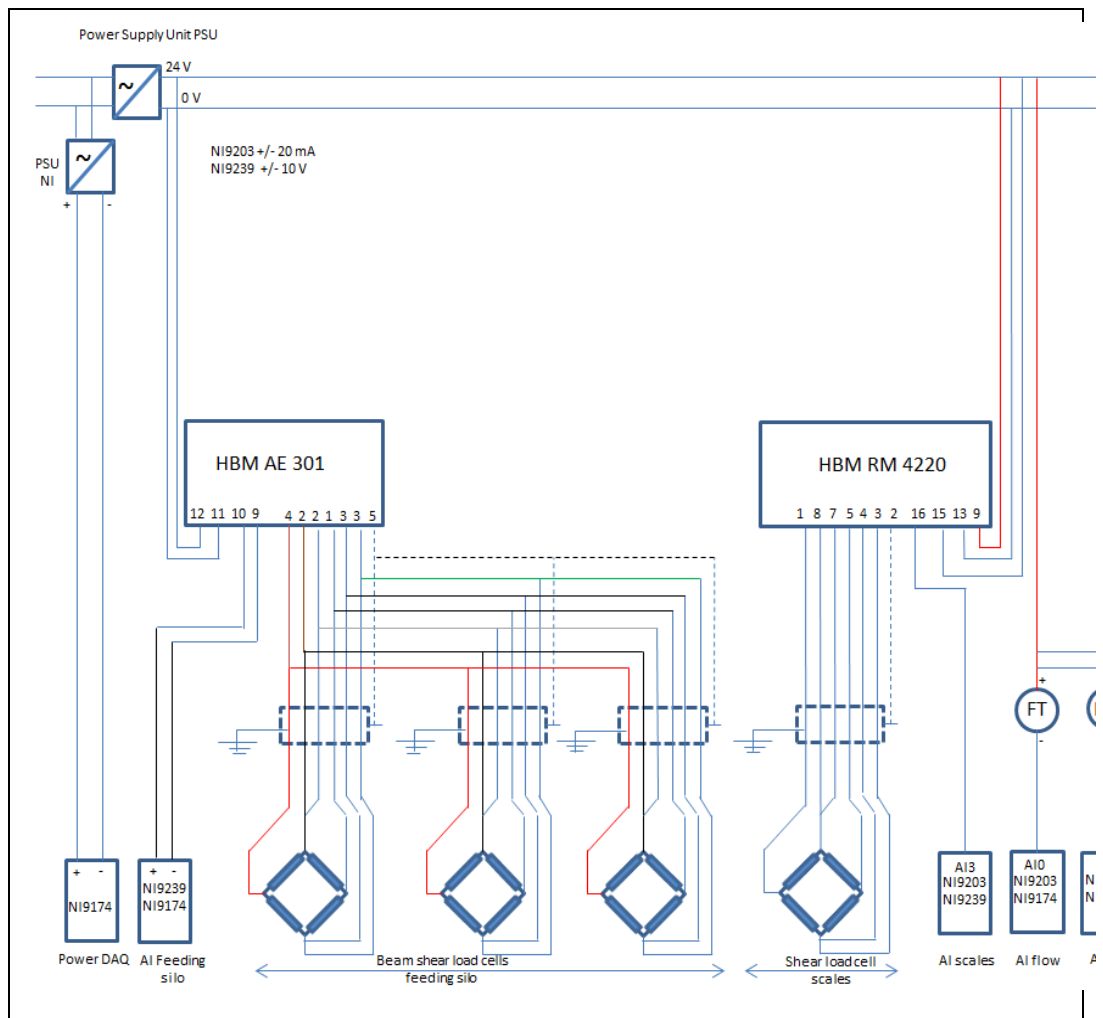


Figure 74 Wiring diagram.

## 5.2 Pressure drop in pipes

The operational velocity  $U_0$  has been calculated using the inlet pressure of a nozzle. The pressure is an important parameter for the ADS system, used to calculate required nozzle and supply air tubes for the distribution system. A pressure drop in the system

will cause lower operational velocity,  $U_0$ , resulting in a lower transport rate of the fluidized alumina bed, thus lower transport capacity of the air slide. However the earlier calculation of  $U_0$  did not take pressure drop along the air tube length due to frictional parameters into consideration. Pressure drop along the tube supplying pressurized air to the bottom of the fluidizing membrane was not investigated in the previous programme of work on the air slide rig at POSTEC, as the main objective had been stability of air slide capacity and design modifications. Once the design modifications were implemented, it became important to investigate the effect of pressure drop on the air slide system. Basic theoretical concepts for laminar and turbulent flow were explained in Chapter 2. To calculate the pressure drop in a pipe for air, Reynolds number,  $Re$ , which is a ratio between inertial and viscous forces, is used to distinguish the turbulent and laminar flows. The Darcy - Weissbach equation for pipe flow is:

$$h_f = f_D \frac{L v^2}{D 2g}$$

Equation 42

where  $h_f$  is the frictional head loss,  $L$  and  $D$  the length and the pipe diameter,  $v$  is the average fluid velocity,  $g$  is the gravitational acceleration and  $f_D$  is the Darcy friction factor, commonly used to predict the pressure drop. The Darcy friction factor,  $f_D$  in Equation 42 for laminar flow ( $Re < 2320$ ) is:

$$f_D = \frac{64}{Re}$$

Equation 43

For turbulent flow ( $Re > 2320$ ) the values of  $f_D$  can be calculated using the transformed Colebrook – White equation:

$$\frac{1}{\sqrt{f_D}} = -2 \log_{10} \left( \frac{2.51}{Re \sqrt{f_D}} + \frac{0.269\epsilon}{D} \right)$$

Equation 44

where  $\epsilon$  is the roughness coefficient and  $D$  is the pipe diameter. The friction factor as a function of Reynolds number can be calculated from the Moody diagram (Moody and Princeton (1944)) shown in Figure 75. The pressure drop for circular pipes,  $\Delta p$  can then be calculated by using Equation 45 and Equation 46.

$$h_f = f_D \frac{L v^2}{D 2g}$$

Equation 45

$$\Delta p = \rho g h_f$$

Equation 46

The formulation of  $h_f$  for pipe flow will be used again in Chapter 7 for fluid flow in an open channel.

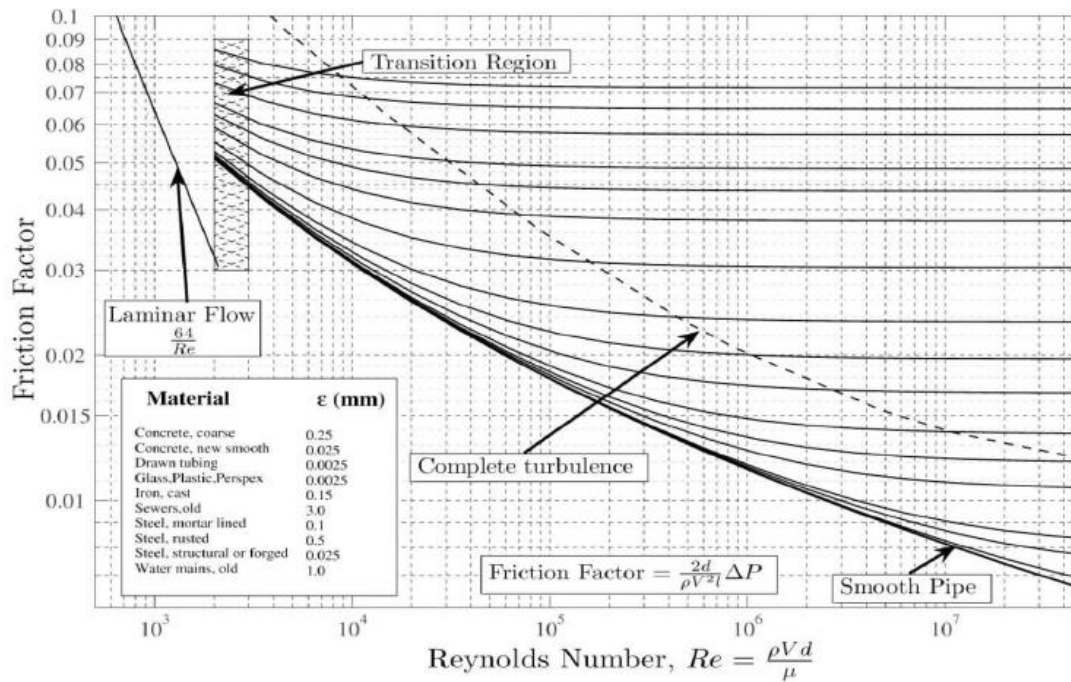


Figure 75 Moody and Princeton (1944) diagram.

Tests to directly measure the pressure in the air supply pipe were carried out using pressure transducers mounted below each nozzle. The tests were carried out in 3 m, 7 m and 15 m long air slide segments both with powder and no powder in the air slide. The results of pressure measurements and pressure loss for the different segments of air slide length are presented in the next sections. Measurement results from the 15 m long air slide segment validated by Øystese (2015) against simulated results using the theoretical concepts presented in this section will be presented in next sections.

### 5.2.1 Verification of the pressure transducers

Six pressure transducers from Endress & Hauser with an electronic output of 4 to 20 mA, labelled PT0 – PT5, connected to the NI 9203 module were used. Each transducer

had been calibrated by the manufacturer, but the calibration certificates were missing from POSTEC. To check their accuracy and eliminate any doubts, measurements with a pressure ramp up were performed and the results recorded in LabView using the test rig software explained in the previous section. As shown in Figure 77 the six transducers were connected to a short 10.7 mm diameter tube section borrowed from the rig, terminated with a 1.4 mm nozzle for the air exit. Pressure was varied from 2.1 to 6.5 bars using a pressure controller to read and adjust the pressurized air from the main compressor. The tests were repeated for a 1.6 mm nozzle. The calibration test results are presented in Table 10. The different nozzle sizes can be seen in Figure 76 a, each nozzle supplying air to a 3 or 4 m long fluidizing element ( Figure 76 b ).

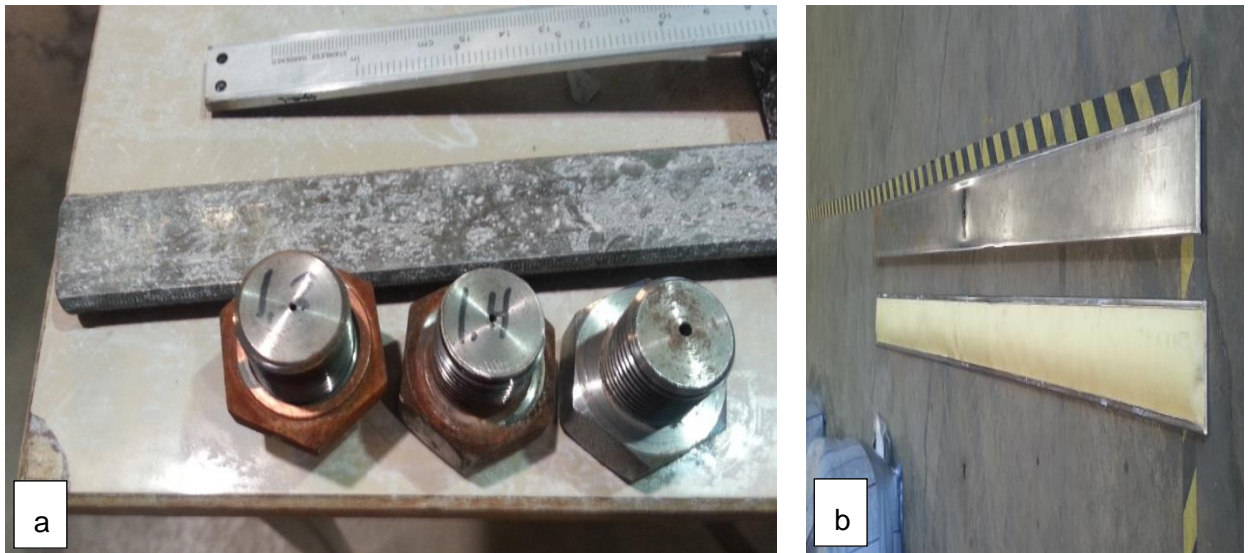


**Figure 76 a) “Pillow” nozzle - just below the stand dpipe outlet to accelerate flow for 3 seconds: 1.2 mm, PT0: 1.4 mm, PT1 - PT5: 1.6 mm nozzles; b) 3 - 4 m fluidization elements with one nozzle inlet/element.**





**Figure 77** Arrangement of flowmeter, pressure controller, pressure transducers for calibration measurements; 1.4 and 1.6 mm nozzles used for air exit.

The tests carried out using pressure transducers mounted below each nozzle conducted both with no powder and powder in the air slide are shown in Table 10.

**Table 10** Pressure ramp up using 1.4 and 1.6 mm nozzles for air exit.

Calibration of the sensors with 1,4 mm nozzle						Calibration of the sensors with 1,6 mm nozzle					
Preassure readings [bar]						Preassure readings [bar]					
PT0	PT1	PT2	PT3	PT4	PT5	PT0	PT1	PT2	PT3	PT4	PT5
2,13	2,14	2,15	2,15	2,15	2,14	2,11	2,11	2,12	2,11	2,11	2,11
2,61	2,62	2,63	2,63	2,63	2,63	2,61	2,60	2,61	2,61	2,61	2,61
3,06	3,07	3,09	3,08	3,09	3,08	3,05	3,05	3,06	3,05	3,05	3,05
3,48	3,49	3,50	3,50	3,51	3,50	3,56	3,56	3,57	3,56	3,56	3,56
4,05	4,05	4,07	4,07	4,07	4,06	4,06	4,05	4,06	4,06	4,06	4,06
4,46	4,47	4,48	4,48	4,49	4,48	4,53	4,52	4,53	4,53	4,53	4,53
5,06	5,07	5,09	5,09	5,09	5,08	4,98	4,98	4,99	4,99	4,99	4,98
5,51	5,52	5,54	5,53	5,54	5,53	5,48	5,47	5,48	5,48	5,48	5,48
6,02	6,03	6,04	6,04	6,04	6,04	6,01	6,00	6,02	6,02	6,01	6,01
6,50	6,50	6,52	6,52	6,52	6,51	6,56	6,56	6,57	6,57	6,57	6,57

It can be seen from the test results in Table 10 that there were very little / no difference in the pressure readings provided by the transducers. Although the calibration certificates were missing, it was decided that they could safely be used for this project.

### 5.2.2 Pressure readings in a 3 m long air slide segment for all downward inclinations

The beam shear load cells and the pressure transducers had been calibrated and LabView software with implemented powder lock concept for the feeding silo and stand pipe had been tested and ready to use. Next step was to connect interfaces: the feeding silo and the stand pipe/control box to air slide segments of different lengths: 3 m, 3 + 4 m and 3 + 12 m. First series of tests were conducted using a 3 m long air slide segment as shown in Figure 78.



Figure 78 Test rig setup: scaffolding, feeding silo, stand pipe/control box, 3m air slide segment.

Table 11 Pressure loss tests conducted with and without alumina in the air slide.

No powder in the airslide			Powder in the airslide		
Control box	3 m		Control box	3 m	
1,4 mm nozzle	1,6 nozzle	System pressure loss	1.4 mm nozzle	1.6 mm nozzle	System pressure loss
Pressure [bar]			Pressure [bar]		
PT0	PT1	PT1-PT0	PT0	PT1	PT1-PT0
2,7	2,7	0 %	2,5	2,5	0 %
3,1	3,1		3,0	3,0	
3,6	3,6		3,5	3,5	
4,0	4,0		4,0	4,0	
4,5	4,5		4,4	4,5	
5,0	5,0		5,0	5,0	
5,5	5,5		5,4	5,4	
6,0	6,0		6,0	6,0	
6,6	6,6		6,7	6,7	

Two pressure transducers labelled PT0 and PT1 were used for the tests. PT0 measured the air pressure received by the control box air slide segment through a 1.4 mm nozzle, while PT1 situated at 18.8 cm away from P0, in the 3 m air slide segment, measured the pressure through a 1.6 mm nozzle. Operational air velocity calculations through a nozzle and membrane were presented in Chapter 4. Pressure tests performed in this section, and system pressure loss expressed in % by calculating the pressure difference between two sensors, were aimed to ensure that the rig will get same pressurized air flow rates throughout the whole length of the 10.7 mm air tube supplying the air slide segment with pressurized air, which is essential for a stable powder transport capacity. Table 11 shows the results of tests with both alumina and without alumina in the air slide, for pressurized air ranging from 2.5 to 6.5 bar. The system pressure loss was 0, which means no pressure loss was measured through the system.

### 5.2.3 Bed heights and capacity tests in a 3 m long air slide segment

As stated earlier one of the main objectives of the current programme of work was to establish the relationship amongst the significant variables governing the flow of alumina in the air slide. In order to investigate the influence of the inlet configuration on capacity, tests were conducted at two conditions, similar to the tests conducted previously in 2012: no restriction plate (no gate, giving 100 % capacity) and with the restriction plate lowered into the bed of alumina down to 170 mm above the air slide bottom (gives 25 % capacity). Bed heights have been measured with the supply air switched off as mentioned in earlier sections. At each angle of inclination, test runs were conducted in the range of 0.99 to 2.14  $U_0/U_{mf}$  corresponding to an air pressure from 2.5 to 6.5 bar. Measurements were taken at six points along the air slide segment. The measurements at the sixth point was influenced by the discharge end of the air slide segment, having coefficients of variation above 10 %, and was therefore not used as material further in the analysis of the data. Results show that the bed heights do not change with increasing air supply velocity, the coefficient of variation being less than 8.6 %. Based on the analysis of the coefficients of variation of the bed heights, it was decided to plot only the average of all bed heights at  $U_0/U_{mf}$  from 0.99 to 2.14 at each measurement point for all inclinations of the air slide. Same method has been used for all lengths of air slide segments. Figure 79 a shows that bed heights are independent of the downward inclination of the air slide and that they slowly decrease with increasing distance away from the inlet. Figure 79 b shows that capacity is dependent of the

inclination of the channel and is increasing with increasing operational air velocity, a clear suggestion that the flow is accelerating.

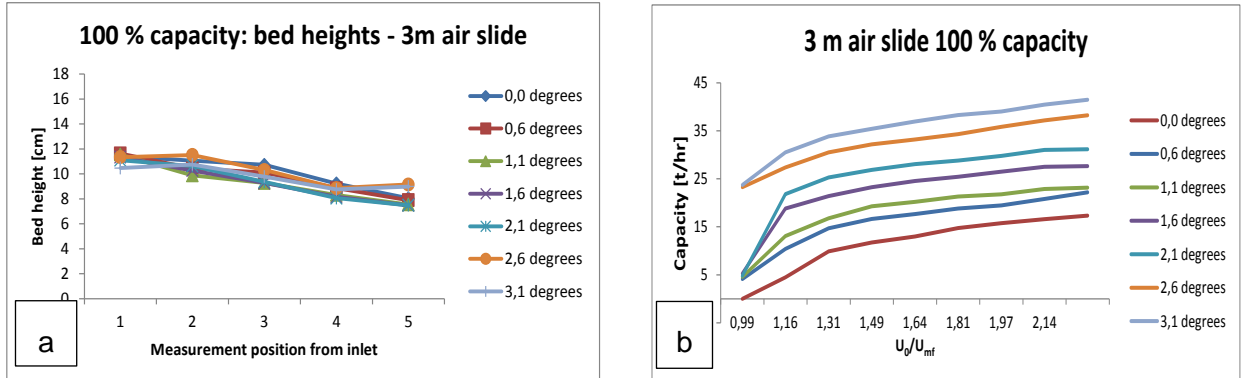


Figure 79 a) Bed heights measurements; b) Air slide capacity, 100% capacity.

Table 12, Table 13 and Table 14 show results of capacity tests and coefficients of variation for both air slide and feeding silo.

Table 12 Capacity tests: air slide and feeding silo based on 100% capacity, from 2.5 to 6.5 bar pressure, for downward inclinations from 0 to 1.1°.

Pressure [bar]	0				0,6				1,1			
	Capacity [t/hr]		Coefficient of variation [%]		Capacity [t/hr]		Coefficient of variation [%]		Capacity [t/hr]		Coefficient of variation [%]	
	Airslide	Feeding silo	Airslide	Feeding silo	Airslide	Feeding silo	Airslide	Feeding silo	Airslide	Feeding silo	Airslide	Feeding silo
2,5	0,0	0,0			4,1	4,1	3,4	3,7	4,6	4,5	8,7	8,8
3	4,5	4,5	4,8	4,8	10,4	10,8	6,9	6,9	13,1	13,2	2,1	2,1
3,5	9,9	9,9	0,8	0,9	14,7	14,9	1,4	1,1	16,8	16,9	1,1	1,1
4	11,7	11,8	0,8	0,8	16,6	16,7	0,9	1,2	19,3	19,5	1,5	1,7
4,5	13,0	13,2	1,8	1,5	17,7	17,9	1,3	0,4	20,2	20,3	1,6	1,8
5	14,7	14,8	0,4	0,7	18,8	18,9	1,1	1,3	21,3	21,4	2,8	2,8
5,5	15,8	15,9	2,2	1,6	19,5	19,9	1,0	0,5	21,8	21,9	0,4	0,2
6	16,6	16,7	2,7	2,4	20,8	21,0	1,6	1,3	22,9	22,9	1,0	0,9
6,5	17,3	17,4	1,6	1,5	22,2	22,3	1,9	1,8	23,1	23,2	2,1	1,2

**Table 13 Capacity tests: air slide and feeding silo based on 100% capacity, from 2.5 to 6.5 bar pressure, for downward inclinations from 1.6 to 2.1°.**

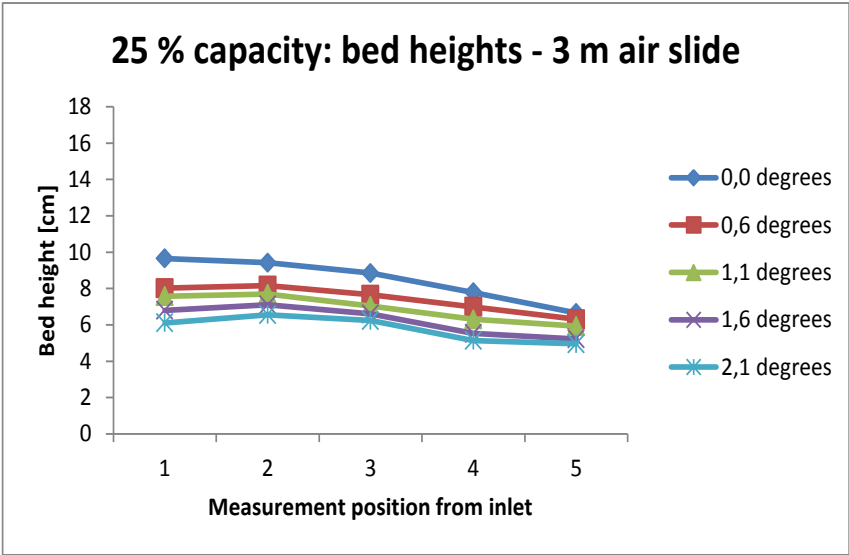
Pressure [bar]	1,6				2,1			
	Capacity [t/hr]		Coefficient of variation [%]		Capacity [t/hr]		Coefficient of variation [%]	
	Airslide	Feeding silo	Airslide	Feeding silo	Airslide	Feeding silo	Airslide	Feeding silo
2,5	5,3	5,2	2,8	3,0	4,8	4,7	1,9	1,8
3	18,8	18,9	3,3	3,5	21,8	21,7	0,8	0,6
3,5	21,4	21,5	1,2	1,3	25,3	25,2	1,1	1,9
4	23,3	23,4	1,1	0,9	26,9	26,7	0,9	0,7
4,5	24,6	24,7	0,4	0,4	28,1	27,8	0,6	1,0
5	25,4	25,6	0,7	0,6	28,8	28,6	0,9	0,7
5,5	26,5	26,7	1,3	1,3	29,8	29,6	0,7	0,6
6	27,5	27,8	1,0	0,8	31,0	30,8	1,8	1,5
6,5	27,6	27,6	2,1	1,7	31,2	30,8	0,6	0,3

**Table 14 Capacity tests: air slide and feeding silo based on 100% capacity, from 2.5 to 6.5 bar pressure, for downward inclinations from 2.6 to 3.1°.**

Pressure [bar]	2,6				3,1			
	Capacity [t/hr]		Coefficient of variation [%]		Capacity [t/hr]		Coefficient of variation [%]	
	Airslide	Feeding silo	Airslide	Feeding silo	Airslide	Feeding silo	Airslide	Feeding silo
2,5	23,2	23,1	3,3	3,9	23,7	23,4	0,7	1,1
3	27,4	27,1	0,7	0,7	30,5	29,9	0,9	0,8
3,5	30,5	30,1	0,3	0,7	33,8	33,0	1,3	1,1
4	32,2	31,8	1,2	0,8	35,4	34,6	0,9	0,5
4,5	33,2	32,8	0,8	0,6	36,9	36,0	0,8	0,7
5	34,3	33,9	1,1	1,1	38,3	37,4	1,4	0,9
5,5	35,8	35,2	0,9	0,3	39,0	38,0	0,5	0,3
6	37,2	36,5	0,8	0,5	40,4	39,4	0,6	0,7
6,5	38,2	37,5	1,2	1,4	41,5	40,4	1,1	0,8

Figure 80, Table 15 and Table 16 show capacity results recorded with the restriction gate inserted into the air slide channel.

a



b

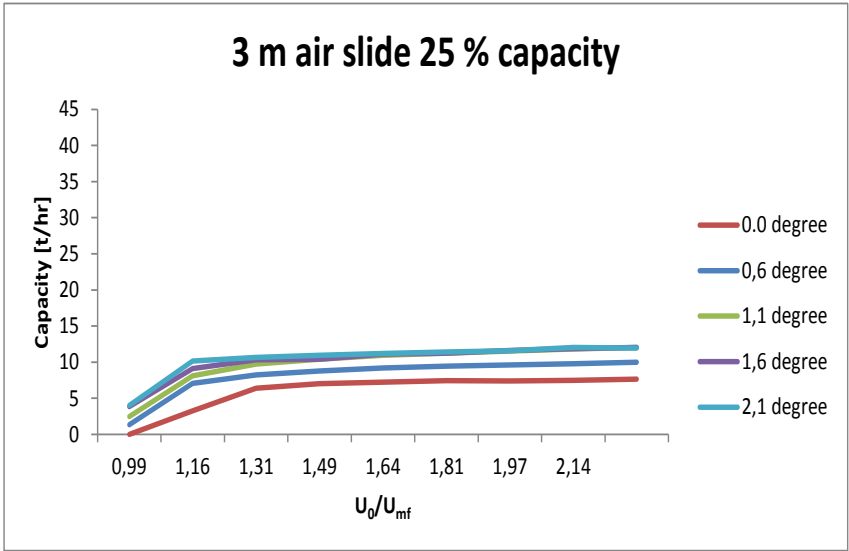


Figure 80 a) Bed heights measurements; b) Air slide capacity, 25 % capacity.

**Table 15 Capacity tests: air slide and feeding silo based on 25 % capacity, from 2, 5 to 6, 5 bar pressure, for downward inclinations from 0 to 1,1°.**

Pressure [bar]	0				0,6				1,1			
	Capacity [t/hr]		Coefficient of variation [%]		Capacity [t/hr]		Coefficient of variation [%]		Capacity [t/hr]		Coefficient of variation [%]	
	Airslide	Feeding silo	Airslide	Feeding silo	Airslide	Feeding silo	Airslide	Feeding silo	Airslide	Feeding silo	Airslide	Feeding silo
2,5												
3	3,3	3,2			7,1	7,0	1,1	1,1	8,1	7,9	6,5	6,7
3,5	6,4	6,3	1,8	1,7	8,2	8,1	0,5	0,3	9,7	9,6	0,2	0,8
4	7,1	6,9	0,6	0,6	8,8	8,6	0,4	0,4	10,4	10,2	0,8	0,6
4,5	7,3	7,2	1,0	1,1	9,2	9,0	0,5	0,6	11,0	10,7	0,7	0,9
5	7,5	7,3	1,7	1,8	9,5	9,3	0,4	0,3	11,3	10,9	0,7	0,9
5,5	7,4	7,3	1,7	1,6	9,6	9,5	0,6	1,4	11,6	11,3	1,3	1,6
6	7,5	7,4	0,9	0,9	9,8	9,6	0,5	0,7	11,8	11,6	0,5	0,6
6,5	7,6	7,5	0,6	0,6	10,0	9,9	0,4	0,2	12,1	11,8	1,4	1,4

**Table 16 Capacity tests: air slide and feeding silo based on 25 % capacity, from 2, 5 to 6, 5 bar pressure, for downward inclinations from 1,6 to 2,1°.**

Pressure [bar]	1,6				2,1			
	Capacity [t/hr]		Coefficient of variation [%]		Capacity [t/hr]		Coefficient of variation [%]	
	Airslide	Feeding silo	Airslide	Feeding silo	Airslide	Feeding silo	Airslide	Feeding silo
2,5	3,9	3,8	4,4	4,4	4,0	3,9	5,1	5,1
3	9,1	8,9	0,8	0,9	10,1	9,9	1,6	1,9
3,5	10,3	10,1	0,4	0,8	10,7	10,4	0,5	0,5
4	10,4	10,2	0,6	0,7	10,9	10,7	0,1	0,2
4,5	11,1	10,9	1,4	1,1	11,2	11,0	0,7	0,5
5	11,3	11,0	1,7	1,0	11,4	11,2	0,7	0,4
5,5	11,6	11,3	1,0	1,1	11,6	11,3	1,6	1,4
6	11,9	11,6	1,0	0,9	12,0	11,8	0,2	0,3
6,5	12,0	11,7	0,9	1,0	12,0	11,8	3,1	2,4

#### 5.2.4 Pressure readings in a 7 m long air slide for all downward inclinations

A four meter air slide segment was added to the existing 3 meter segment and the air supply tube was extended accordingly. Figure 81 shows the seven meters long air slide channel.



Figure 81 Test rig setup: scaffolding, feeding silo, stand pipe/controlbox, 3 + 4 m air slide segment.

One extra pressure transmitter PT3 was added to the system. Preliminary test runs were again conducted to monitor the system pressure loss in the air supply tube. Results in Table 17 and Table 18 show the system pressure loss was in the range of 0 to 5 %, which is within acceptable limits.

Table 17 Pressure loss tests conducted without alumina in the air slide.

No powder in the airslide						
Control box	3 m	4 m			System pressure loss	
1,4 mm nozzle	1,6 nozzle					
Pressure [bar]					PT1-PT3	PT0-PT3
PT0	PT1	PT2	PT3			
2,5	2,5	2,5	2,5		0 %	0 %
3,0	3,0	2,9	2,9		3 %	3 %
3,5	3,4	3,4	3,4		0 %	3 %
4,0	3,9	3,8	3,8		3 %	5 %
4,5	4,4	4,3	4,3		2 %	4 %
5,0	4,9	4,8	4,8		2 %	4 %
5,5	5,4	5,3	5,3		2 %	4 %
6,0	5,9	5,8	5,8		2 %	3 %
6,5	6,4	6,3	6,3		2 %	3 %

\*1 x 1,6 nozzle, PT1 sensor on the 3 m airslide (attached when testing with powder)



Table 18 Pressure loss tests conducted with alumina in the air slide.

Powder in the airslide						
Control box	3m	4 m			System pressure loss	
1.4 mm nozzle	1.6 mm nozzle					
Pressure [bar]						
PT0	PT1	PT2	PT3		PT1-PT3	PT0-PT3
2,0		Little or no powder transport				
2,5	2,5	2,4	2,4		4 %	4 %
3,0	3,0	2,9	2,9		3 %	3 %
3,5	3,4	3,4	3,4		0 %	3 %
4,0	3,9	3,8	3,8		3 %	5 %
4,4	4,3	4,3	4,3		0 %	2 %
5,0	4,9	4,8	4,8		2 %	4 %
5,3	5,2	5,2	5,2		0 %	2 %
5,9	5,8	5,7	5,7		2 %	3 %
6,5	6,5	6,4	6,4		2 %	2 %

\*1 x 1,6 nozzle, PT1 sensor on the 3 m airslide (attached when testing with powder)

### 5.2.5 Bed heights and capacity tests in a 7 m long air slide segment

Bed heights were taken at twelve measurement points, due to disturbance from the open discharge end of the channel, only eleven degrees points were used. Some new trends can be seen in Figure 82 a, which is different from what it was noticed in the 3 m long air slide segment. At all inclination angles except at 0 degrees, the bed heights become stable after 5.5 m away from the inlet, which offers a strong indication that the flow has stopped accelerating and that it is getting stable. Capacity follows the same trends, it increases smoothly as a function of both  $U_0/U_{mf}$  and inclination.

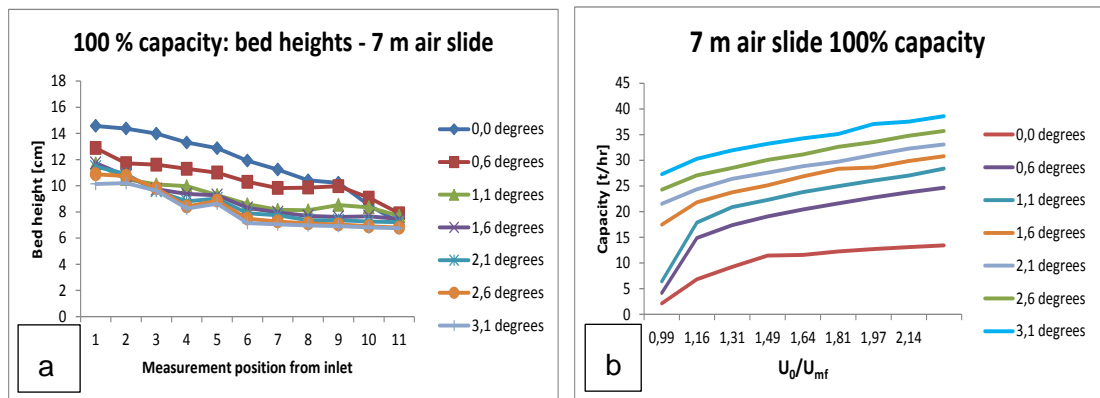


Figure 82 a) Bed heights measurements, b) Air slide 100% capacity.

**Table 19 Capacity tests: air slide and feeding silo based on 100 % capacity, from 2.5 to 6.5 bar pressure, for downward inclinations from 0 to 1.1°.**

Pressure [bar]	0				0,6				1,1			
	Capacity [t/hr]		Coefficient of variation [%]		Capacity [t/hr]		Coefficient of variation [%]		Capacity [t/hr]		Coefficient of variation [%]	
	Airslide	Feeding silo	Airslide	Feeding silo	Airslide	Feeding silo	Airslide	Feeding silo	Airslide	Feeding silo	Airslide	Feeding silo
2,5	2,1	2,1	7,4	7,2	4,2	4,1	1,3	0,6	6,4	6,2	2,8	1,7
3	6,8	6,8	1,6	2,4	14,9	14,8	4,0	2,1	17,9	17,7	3,1	1,6
3,5	9,2	9,2	0,7	0,4	17,4	17,1	0,2	0,3	20,9	20,4	0,1	0,5
4	11,4	11,4	0,3	0,3	19,1	18,7	0,8	0,7	22,3	21,7	1,3	1,0
4,5	11,6	11,5	0,3	0,5	20,4	20,1	0,7	0,8	23,8	23,1	0,5	0,8
5	12,3	12,2	2,1	1,8	21,6	21,2	1,1	1,3	24,9	24,3	0,4	0,1
5,5	12,7	12,7	0,9	1,3	22,7	22,5	0,7	0,8	26,1	25,2	1,6	0,9
6	13,1	13,0	1,5	1,1	23,8	23,2	1,0	0,5	27,0	26,2	0,6	0,7
6,5	13,4	13,4	0,5	0,4	24,7	24,6	1,4	1,3	28,4	27,6	0,6	0,7

**Table 20 Capacity tests: air slide and feeding silo based on 100 % capacity, from 2.5 to 6.5 bar pressure, for downward inclinations from 1.6 to 2.1°.**

Pressure [bar]	1,6				2,1			
	Capacity [t/hr]		Coefficient of variation [%]		Capacity [t/hr]		Coefficient of variation [%]	
	Airslide	Feeding silo	Airslide	Feeding silo	Airslide	Feeding silo	Airslide	Feeding silo
2,5	17,5	17,2	6,6	6,7	21,5	21,0	0,5	0,4
3	21,8	21,4	0,2	0,2	24,4	23,9	1,5	0,8
3,5	23,8	23,4	0,3	0,1	26,4	25,9	1,3	0,9
4	25,1	24,7	0,6	0,4	27,6	27,0	0,5	0,4
4,5	26,8	26,1	1,6	0,9	28,8	28,2	1,1	0,8
5	28,4	27,3	1,9	1,6	29,7	29,0	1,1	0,6
5,5	28,6	27,7	1,2	1,3	31,0	30,1	1,5	0,4
6	29,9	28,8	1,7	1,4	32,3	31,3	0,4	0,6
6,5	30,8	29,8	0,8	0,7	33,1	32,2	1,7	1,7

**Table 21 Capacity tests: air slide and feeding silo based on 100 % capacity, from 2.5 to 6.5 bar pressure, for downward inclinations from 2.6 to 3.1°.**

Pressure [bar]	2,6				3,1			
	Capacity [t/hr]		Coefficient of variation [%]		Capacity [t/hr]		Coefficient of variation [%]	
	Airslide	Feeding silo	Airslide	Feeding silo	Airslide	Feeding silo	Airslide	Feeding silo
2,5	24,3	23,9	0,7	0,8	27,3	27,1	1,4	0,8
3	27,1	26,8	0,5	0,9	30,3	29,7	0,5	0,3
3,5	28,5	28,2	1,0	0,6	31,9	31,6	1,2	0,7
4	30,1	29,5	1,8	0,8	33,2	33,1	2,6	1,6
4,5	31,2	30,8	0,8	1,3	34,3	34,0	0,3	0,2
5	32,6	31,9	0,5	0,2	35,1	34,9	1,9	1,6
5,5	33,5	32,6	0,4	1,9	37,1	36,4	0,6	0,6
6	34,8	33,9	0,6	0,3	37,5	37,1	2,8	2,0
6,5	35,7	34,7	1,3	1,0	38,6	37,8	2,3	2,1

Due to budget and time limitation, test runs were conducted for 100 % capacity only.

### 5.2.6 Pressure readings in a 15 m long air slide for all downward inclinations

Once again the test rig was modified, the 4 m air slide segment and air supply tube were removed and a 12 m long segment was connected to the 3 m segment. Adjustments were made to the air supply tube and new pressure transmitters were connected to the tube.

Table 22 Pressure loss tests conducted without alumina in the air slide.

No powder in the airslide							
Control box	3m	12 m				Total pressure loss	
1,4 mm nozzle	1,6 nozzle						
Pressure [bar]							
PT0	PT1	PT2	PT3	PT4	PT5	PT1-PT5	PT0-PT5
2,0	1,9	1,7	1,7	1,6	1,6	16 %	20 %
2,5	2,4	2,1	2,1	2,0	2,0	17 %	20 %
3,0	2,8	2,6	2,5	2,5	2,5	11 %	17 %
3,5	3,3	3,0	3,0	2,9	2,9	12 %	17 %
4,0	3,8	3,5	3,4	3,4	3,3	13 %	18 %
4,5	4,3	4,0	3,9	3,8	3,8	12 %	16 %
5,0	4,8	4,4	4,3	4,3	4,2	13 %	16 %
5,5	5,3	4,9	4,8	4,7	4,7	11 %	15 %
6,0	5,8	5,3	5,2	5,2	5,1	12 %	15 %
*1 x 1,6 nozzle, PT1 sensor on the 3 m airslide (not attached when testing with powder)							

Table 23 Pressure loss tests conducted with alumina in the air slide.

Powder in the airslide							
Control box	3m	12 m				System pressure loss	
1.4 mm nozzle	1.6 mm nozzle						
Pressure [bar]							
PT0	*PT1	PT2	PT3	PT4	PT5	*PT1-PT5	PT0-PT5
2,0		Little or no powder transport					
2,5	2,4	2,1	2,0	2,0	2,0	18 %	20 %
3,0	2,7	2,5	2,5	2,4	2,4	12 %	20 %
3,5	3,2	2,9	2,9	2,8	2,8	16 %	20 %
4,0	3,7	3,4	3,3	3,3	3,2	14 %	20 %
4,5	4,0	3,7	3,7	3,6	3,6	15 %	20 %
5,0	4,7	4,3	4,2	4,2	4,1	16 %	18 %
5,5	5,1	4,7	4,6	4,6	4,5	14 %	18 %
6,0	5,7	5,2	5,1	5,0	5,0	15 %	17 %
*Estimated value, PT1 on the 3 m airslide (not attached when testing with powder)							

Table 22 and Table 23 show the test run results conducted to monitor the system pressure loss in the air supply tube. The pressure loss has been calculated from pressure online data recorded in LabView as shown in Figure 83. The pressure losses are much higher than in the 7 m long air slide segment, in the range of 12 to 18 % on the last nozzle element, which is significantly higher than what should be considered as an acceptable value. Due to the fact that the nozzles are dimensioned using the equations presented in Chapter 4 for calculating the operational velocity,  $U_0$ , the pressure loss along the tube should be as little as possible, it is important that the pressure at the end of the tube does not deviate from the inlet pressure.

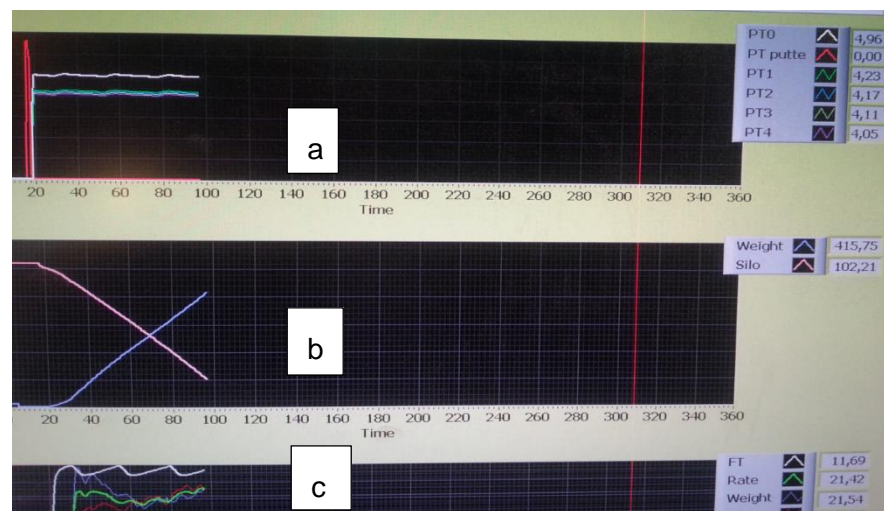


Figure 83 a) Print screen of LabView showing pressure drop from 4.96 to 4.05 in a 15 m long air slide segment. Complete set of data given in the tables above; b) Gain in weight (receiving bin) and loss in weight (feeding silo) in kg; c) Air slide and feeding silo capacity in t/hr.

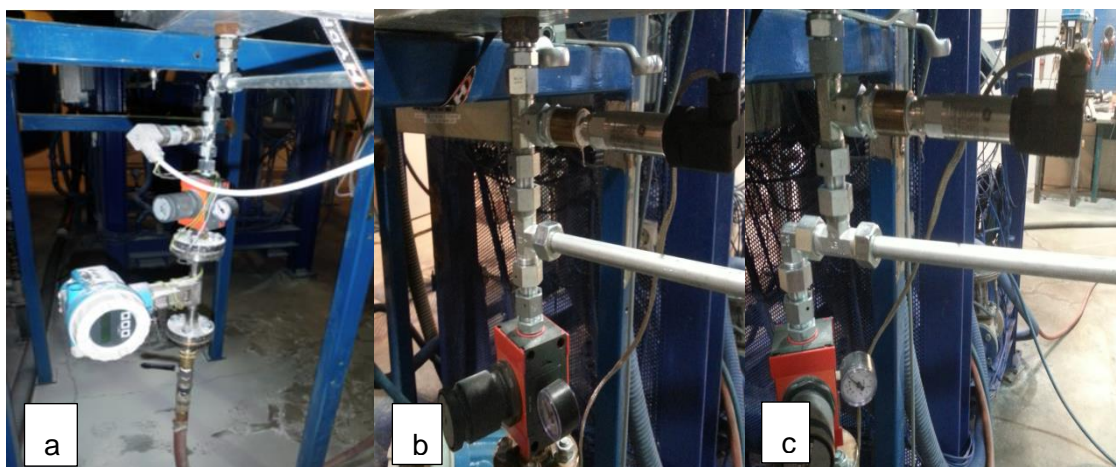


Figure 84 Different set up configuration of P0 to investigate the pressure drop: a) initial configuration PT0 placed beneath an elbow and the air supply tube, b) PT0 moved above the tube, no elbow, c) PT0 moved above an elbow, aT and the tube.

To begin with, it was believed that the new set up configuration as shown in Figure 84, e.g. PT0 placed just before a tube bend would cause the pressure loss in the system.

Two new configurations (Figure 84 b and c) were tested in order to check the resistance coefficients if of any relevance) in elbows and T-s, with no improvements in the pressure loss results. Finally, it was understood that it was the diameter of the air supply tube, 10.7 mm, which was too small for the air slide system. Øystense (2015) used the measurement results from the 15 m long air slide segment with 6 bar input and 5.2 bar towards the end of the tube (as shown in Table 22 and Table 23) to validate them against simulated results. A model of the air slide system was created using FluidSim Pneumatics software (Figure 85 a) to validate the measurement results. The software requires inputs of measured pressure and volumetric airflow in order to predict the operational velocity,  $U_0$  and the pressure. Nine nozzles, P0 – P8 were considered in the model compared to only six used on the air slide rig.

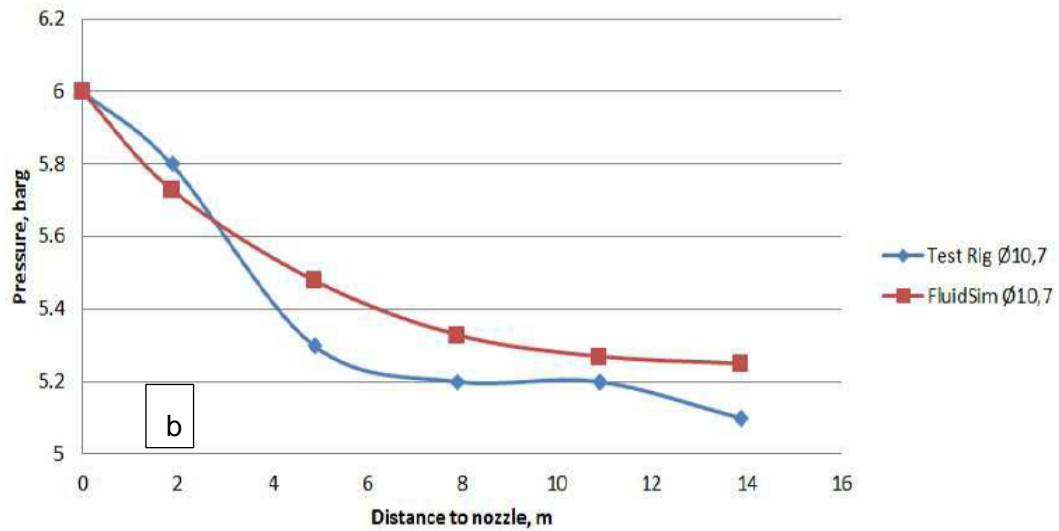
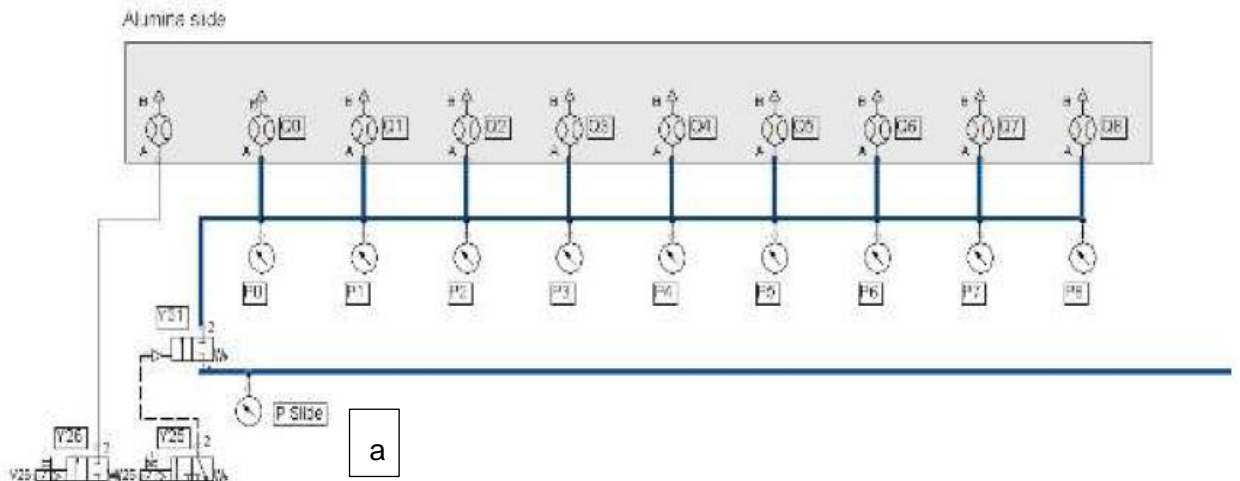


Figure 85 a) FluidSim model of an air slide; b) Comparison of measured and simulated values using FluidSim (Øystese (2015)).

In order to prevent pressure loss in in long air supply tubes, 19 mm diameter should be used, not 10.7 mm, according to the simulations conducted by Øystese (2015)). This conclusion could not be validated through new modifications to the air slide system, due to both budget and time restrictions, thus the conclusion is based only on simulated pressure data for 10.7 mm, 15 mm and 19 mm diameter tubes conducted by Øystese (2015).

### 5.2.7 Bed heights and capacity tests in a 15 m long air slide segment

Tests results (Figure 86 a) show that at all inclination angles except at 0 degrees, the bed heights become stable after 5.5 m away from the inlet, which offers a strong indication that the flow has stopped accelerating and that it is getting stable, the same trend as in the 7 m long segment. Capacity follows the same trends, it increases smoothly as a function of both  $U_0/U_{mf}$  and inclination.

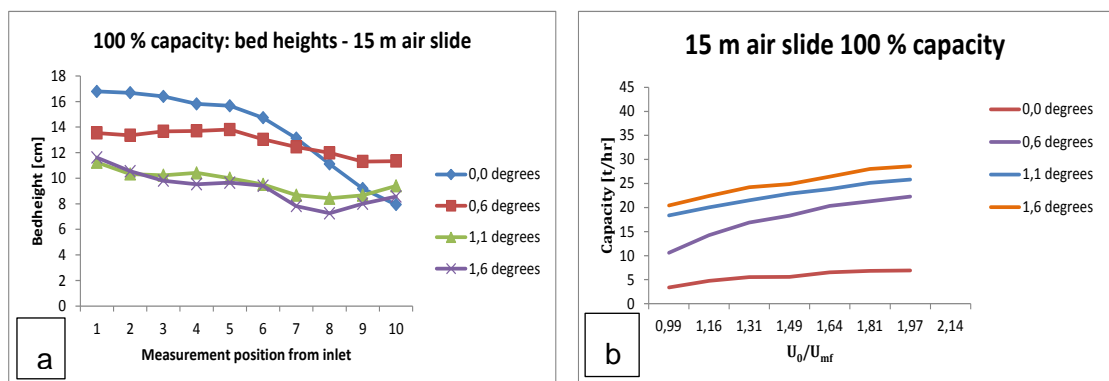


Figure 86 a) Bed heights measurements; b) Air slide 100% capacity.

Table 24 and Table 25 show results of capacity recorded with no restriction gate.

Table 24 Capacity tests: air slide and feeding silo based on 100 % capacity, from 2.5 to 6.0 bar pressure, for downward inclinations from 0 to 0.6°.

Pressure [bar]	0				0,6			
	Capacity [t/hr]		Coefficient of variation [%]		Capacity [t/hr]		Coefficient of variation [%]	
	Airslide	Feeding silo	Airslide	Feeding silo	Airslide	Feeding silo	Airslide	Feeding silo
2,5	3,4	3,4	8,85	8,64	2,5	2,6	5,2	11,4
3	4,8	4,7	1,9	2,1	10,6	10,3	1,3	0,5
3,5	5,5	5,5	0,3	0,3	14,3	14,0	0,5	0,3
4	5,6	5,5	1,4	0,9	16,9	16,4	0,4	0,5
4,5	6,4	6,3	1,5	1,5	18,3	17,8	0,7	0,4
5	6,5	6,5	3,6	3,6	20,4	19,5	0,3	0,6
5,5	6,8	6,7	1,8	1,7	21,3	20,4	1,2	0,8
6	6,9	6,8	0,2	0,6	22,3	21,2	0,9	0,8
6,5								

Table 25 Capacity tests: air slide and feeding silo based on 100 % filling degree, from 2, 5 to 6, 0 bar pressure, for downward inclinations from 1, 1 to 1,6°.

Pressure [bar]	1,1				1,6			
	Capacity [t/hr]		Coefficient of variation [%]		Capacity [t/hr]		Coefficient of variation [%]	
	Airslide	Feeding silo	Airslide	Feeding silo	Airslide	Feeding silo	Airslide	Feeding silo
2,5	13,0	13,3	2,1	10,9	17,8	17,8	9,9	4,1
3	18,4	17,0	5,0	0,6	20,4	19,8	0,4	0,4
3,5	20,0	19,3	5,6	0,7	22,4	21,4	1,2	1,3
4	21,5	20,6	3,1	1,3	24,2	23,0	0,6	0,7
4,5	22,9	21,4	1,3	1,6	24,9	24,1	2,7	0,8
5	23,9	22,7	1,1	1,1	26,5	25,0	2,2	0,9
5,5	25,1	23,6	0,5	0,1	28,0	26,2	0,3	0,1
6	25,8	24,2	0,5	0,6	28,6	26,7	1,8	1,6
6,5								

Figure 87 a and b, Table 26 and Table 27 show capacity results recorded with the restriction gate inserted into the air slide channel.

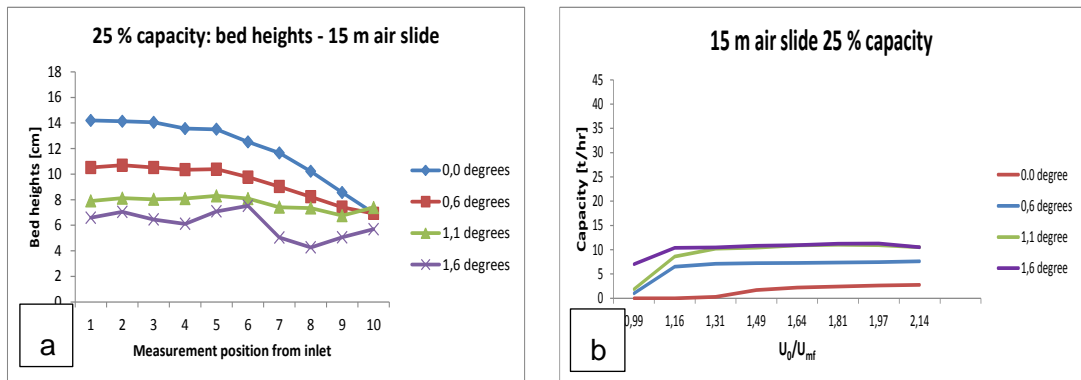


Figure 87 a) Bed heights measurements; b) Air slide capacity, 25 % capacity.

Table 26 Capacity tests: air slide and feeding silo based on 25 % capacity, from 2.5 to 6.0 bar pressure, for downward inclinations from 0 to 0.6°.

Pressure [bar]	0				0,6			
	Capacity [t/hr]		Coefficient of variation [%]		Capacity [t/hr]		Coefficient of variation [%]	
	Airslide	Feeding silo	Airslide	Feeding silo	Airslide	Feeding silo	Airslide	Feeding silo
2,5					4,1	3,7		
3					6,5	6,3	8,6	7,4
3,5					7,2	6,8	0,1	0,2
4	1,7	1,6	12,7	12,8	7,3	7,0	0,4	0,6
4,5	2,2	2,2	1,4	2,0	7,3	7,1	0,6	0,8
5	2,4	2,4	1,7	1,2	7,4	7,1	0,9	0,6
5,5	2,6	2,6	0,5	0,3	7,5	7,2	0,4	0,1
6	2,8	2,7	1,0	1,1	7,6	7,4	0,7	0,6
6,5								



Table 27 Capacity tests: air slide and feeding silo based on 25 % capacity, from 2.5 to 6.0 bar pressure, for downward inclinations from 1.1 to 1.6°.

Pressure [bar]	1,1				1,6			
	Capacity [t/hr]		Coefficient of variation [%]		Capacity [t/hr]		Coefficient of variation [%]	
	Airslide	Feeding silo	Airslide	Feeding silo	Airslide	Feeding silo	Airslide	Feeding silo
2,5	1,9	1,9	7,7	3,0	7,0	6,9	6,4	11,1
3	8,6	8,1	4,8	0,9	10,4	9,8	4,1	1,2
3,5	10,2	9,3	6,2	0,4	10,5	10,0	1,2	1,7
4	10,4	9,9	1,2	1,7	10,8	10,2	2,0	1,5
4,5	10,9	10,4	0,5	1,0	10,9	10,4	2,8	2,9
5	11,0	10,5	0,9	0,8	11,2	10,6	3,1	2,7
5,5	10,9	10,2	5,0	5,4	11,3	10,8	1,1	0,9
6	10,5	10,0	1,0	1,0	11,3	10,9	1,6	0,5
6,5								

### 5.2.8 Conclusions

This chapter presented the methods for design of a long stand pipe and implementation of the powder lock concept. The modifications made to the feeding silo outlet covered in this chapter corrected problems that had developed as a direct result of flow disturbances due to inadequate mechanical configuration and material on material shear within the outlet of the silo. The results demonstrate the effects of inadequate interfacing and the effects this problem can have on the repeatability of discharge rates, thus on air slide capacity. In the first case the use of iris valve and short standpipe gave poor repeatability. Stability of discharge rates and with different standpipe lengths from  $1xD$  up to  $8xD$  had been tested at the Wolfson Centre by using a “mock up”. It was first when tested at POSTEC and after analysing the results of both feeding silo capacity and air slide one could see the effect of interfaces on the air slide and the interdependence between mechanical equipment. The final solution involved the use of Gu’s (1993) powder lock concept and a long stand pipe, 7.5 times the diameter of the feeding silo, which gave very good repeatability of discharge rates. The main advantages of this type of outlet design and interfacing to an air slide were the ability to produce a self-regulating system and to achieve stability and repeatability of gravity discharge rates. A considerable amount of experimental data has been presented on the graphs discussed in the preceding sections providing a useful overall picture of the alumina behaviour in inclined air slide segments of different lengths. For modelling purposes it was essential to achieve stability of discharges, before one could set up any

model at all. The results of this final part of the programme have been analysed in a superficial manner, focus being put on the mechanical design. In order to complete the work a closer analysis at the relationships observed will be performed in Chapter 6 and 7.

### 5.2.9 Further work: scale down to support feeder concept and design

Conclusions drawn from the studies undertaken on the small feeders in Årdal and on the rig at POSTEC, they all point out in the same direction: modifications to the feeder outlet are necessary in order to achieve better repeatability and reduce the high coefficients of variation.



Figure 88 a) Feeding silo, standpipe and air slide, free fall conditions (gravity discharge);

b) Volumetric feeder and air slide, chocked flow condition due to interfacing and dosing operation.

The powder lock concept and long stand pipe shown in Figure 88 a together with all test results presented in this chapter they all show so far that the concepts have a good potential for further implementation on the feeders on the alumina rig in Årdal.

## **6 Empirical modelling**

A model is defined as a representation of a real system or event of interest. Although this is a quite short and general definition, the modelling of transport capacity in an air slide falls under this definition. The type of the model to be used is very much determined by the final purpose of the model, for example for process optimization and quality control, a static (steady state) model might be suitable. The two types of models investigated in this thesis are empirical or data based, covered by this chapter and mechanistic as presented in the next chapter. Empirical models are mainly based on experience and statistics and are used to find a suitable mathematical law to reproduce the data. When we interact with a system, we need some concept of how its variables relate to each other. With a broad definition, we shall call such an assumed relationship among observed signals, a model of the system, according to Ljung (1999). For certain systems it is appropriate to predict their behaviour or describe their properties using numerical tables and plots. This has been the approach in this chapter, where models are shown graphically, in order to show how variables such as angle of inclination and dimensionless coefficient of velocity relate to each other and how they influence the bed height and average bed velocity. Mechanistic models on the other hand try to give an explanation of the mechanisms that lie behind and govern the behaviour of a system. They are based on the application of well-established and known physical laws of mass, energy and momentum to the physical system being investigated. Some might argue that mechanistic models are empirical or semi-empirical, because the mechanisms are derived from previous experience of the behaviour of a system. This is also true, since in order to model a system, it is easier to split it into stable subsystems and interfaces, whose properties are verified or at least well understood from earlier empirical experience. In conclusion, purely mechanistic models are rare, since input and output signals from the system and other experimental data are required in order to find expressions for certain terms of the physical laws or for the values of certain parameters in the model. The approach in this thesis is a holistic approach. Based on previous empirical work from small scale feeders, a full scale system was built. The design of the rig was optimized in order to achieve system stability. It became clear that further modeling work would not have been possible without the standpipe concept and without paying attention to interfaces and inlet design. The empirical model approach was inspired by the work of Chaudhry (2006). In his thesis he carried out a detailed

empirical analysis for prediction of bend pressure losses in lean phase pneumatic during steady state conditions conveying for ten test materials.

### 6.1 Data analysis and building models

Basically, when building an empirical model it has to be constructed from observed data and by use of graphical models made up from a set of measurements, as explained in previous section. Figure 89 illustrates the approach strategy to empirical modelling used in this thesis. Prior system knowledge through experimental measurements and system design have been described in previous chapters. Three data sets have been chosen: data from 3 m, 7 m and 15 m long air slide segments. In addition, changes in capacity as a function of inlet configuration were monitored in the 3 m and 15 long segments. Tests were conducted with two inlet configurations: “no gate” meaning original design with no restriction plate and “gate” (restriction plate).

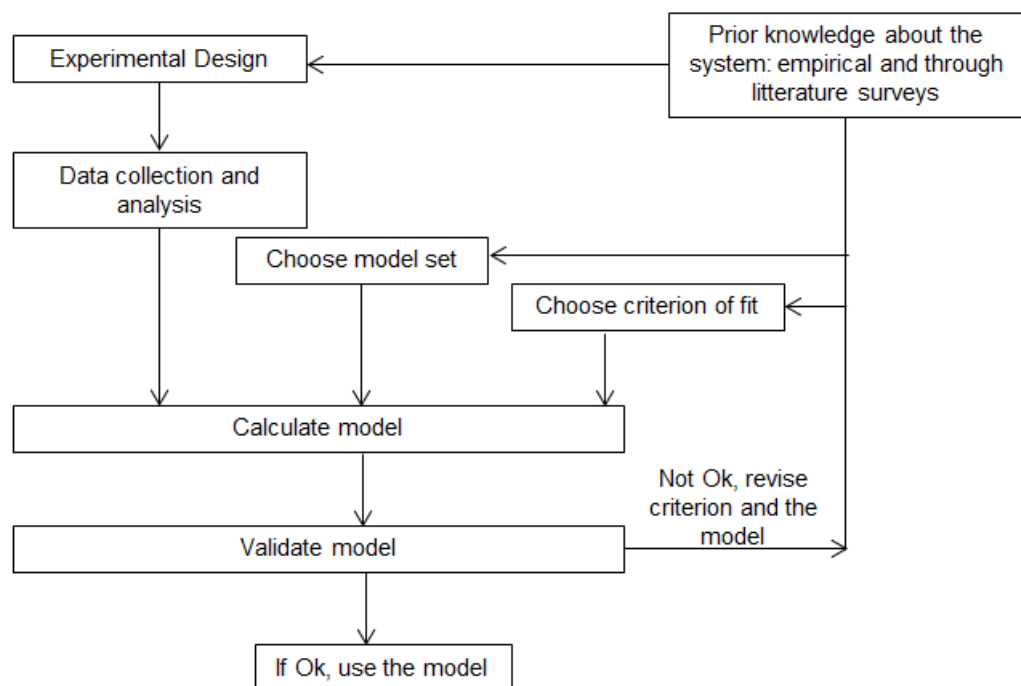


Figure 89 The empirical modeling loop.

Determining the best model to universally fit the three model sets is based on how well they will perform and how well they reproduce the measured data. The data analysis

results for 3 m, 7 m and 15 m long air slide segment showed that there is a strong correlation between:

- average bed velocity and dimensionless coefficient of velocity,  $U_0/U_{mf}$ , for all angles of inclination  $\theta$ ;
- bed velocity and distance from inlet for all dimensionless coefficients of velocity  $U_0/U_{mf}$  for all angles of inclination;
- average bed velocity and length of air slide segment as strong indicator of flow regime: acceleration or steady state flow.

### 6.1.1 Criterion of fit and model

Curve fit equations are shown together with the plots in order to fit correlations between bed velocity and different process variables. A graphical approach was adopted in order to seek the empirical correlations. Each data point represents the average of three consecutive tests.

The average bed velocity versus  $U_0/U_{mf}$  and versus  $\theta$  at different distances from inlet were showing similar trends, but in order to find the best fit model for all lengths of air slide segments, three mathematical models were fitted to all data:

- Linear
- Exponential
- Power

The comparison between these models and further evaluation of the best model was based on the values of  $R^2$  (R –squared) which is a statistical function in Excel that will give some information about the goodness of the fit of a model. Its values are between 0 and 1, an  $R^2$  of 1 indicating that the regression line perfectly fits the data. Following question needed to be answered: given values of an unknown function  $f$ , corresponding to certain values of  $x$  (measurement range), what would be the behaviour of the function  $f$ ? To answer this question, the strategy was to find an equation (law) that fits a selected set of points  $(x_i, f(x_i))$  and then study the behaviour of the equation and the function over the  $x_i$  interval, where  $i$  represented a measurement point. It was first expected that values of a first degree polynomial should give a reliable estimate of the values of the function in question. A linear fit line was forced through all data, resulting in a first degree polynomial and the model was applied for all segments: 3 m, 7 m and 15 m. The

fitted line plots in Figure 90 Linear trend lines fitted to experimental data in: a) 3 m; b) 7 m; c) 15 m long air slide segment. Bed velocity based on measurements of bed height at last point in each of the segments.

show that the  $Y$ - data follows a nice function and that the  $R$  - squared values,  $R^2$  are high, which looked pretty promising to begin with. Meanwhile, a drawback and a limitation with relying too much on  $R^2$ , is that it does not indicate whether a regression model is adequate or not, since it cannot determine whether the predictions are biased. A good model can have a low  $R^2$  value, or can have a high  $R^2$  value that does not fit the data, which is why the residual plots must be assessed. A model fits the data well, if the residuals, by definition expressed as the difference between the observed values and the fitted (predicted) values, are small and unbiased.

### 6.1.2 Model Validation

We follow the steps indicated by arrows in Figure 89 further. After settling on an “universal” model, that will say a model that describes the measurement data according to a chosen criterion of fit,  $R^2$ , the next step will be to determine whether the model is good enough or not. The method that will determine whether the model is good enough, that is whether the model is valid or not for its purpose is known as model validation (Ljung (1999)). The method involves various data analysis and mathematical procedures to assess how the model relates and fits to the measured data, to prior knowledge and to its further use. Initially a linear fit was chosen. The linear fit shown in Figure 90 Linear trend lines fitted to experimental data in: a) 3 m; b) 7 m; c) 15 m long air slide segment. Bed velocity based on measurements of bed height at last point in each of the segments.

was used for 3 m, 7 m and 15 m lengths of air slide segments. Based on  $R^2$  values, as the criterion of fit, it looked promising in a 3 m long segment, except for 0 degrees case. If  $R^2$  is greater than 0.80, there is a good fit to the data.  $R^2$  of 0.80 means that 80 % of the variation in average bed velocity can be explained by  $U_0/U_{mf}$  at different angle of inclination  $\theta$ .

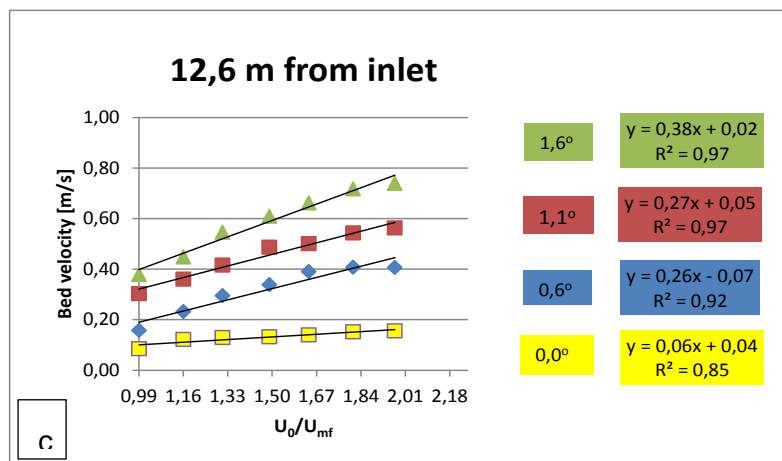
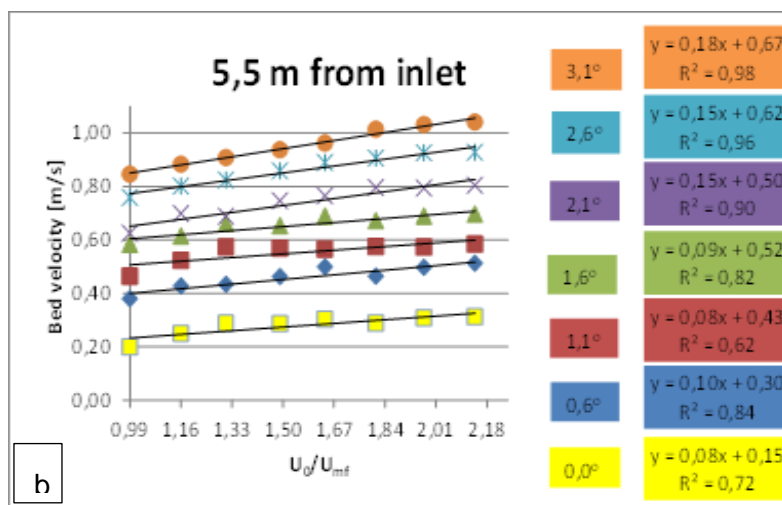
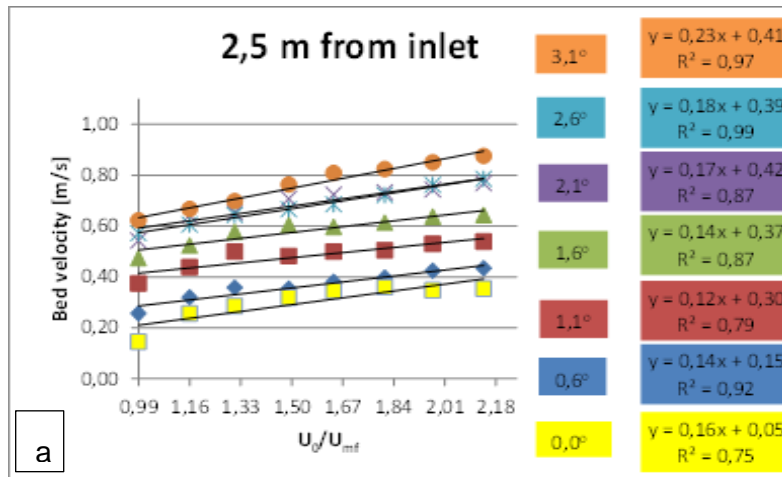


Figure 90 Linear trend lines fitted to experimental data in: a) 3 m; b) 7 m; c) 15 m long air slide segment. Bed velocity based on measurements of bed height at last point in each of the segments.

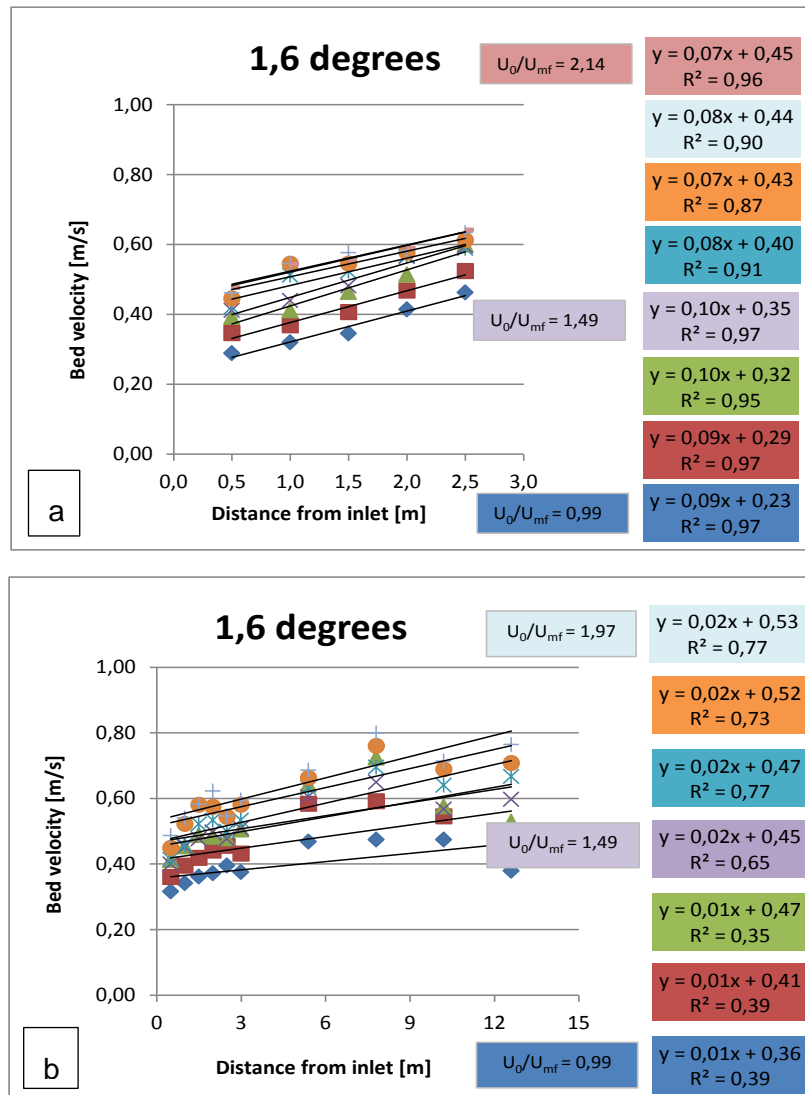


Figure 91 Linear trend lines fitted to experimental data at 1.6 downward inclination in: a) 3 m b) 15 m long air slide segment.

A deeper analysis into the effects of velocity changes as a function of distance from inlet used for two model sets: a 3 m and a 15 m long air slide segment at a 1.6 degree inclination, as shown in Figure 91, shows that the linear trend lines fit well the first data set, but it does not fit the second data set. The scope of empirical modelling is to find a model to fit all three data sets, based on the same criterion of fit.

## 6.2 Effects of downward inclination angle, $\theta$ and dimensionless coefficient of velocity, $U_0/U_{mf}$ on average bed velocity

Two other models: power law and exponential law were studied as shown in Figure 92 and Figure 93. Bed velocity power and exponential models as a function of  $U_0/U_{mf}$  do not perform very well for angles below 1.6 degrees.



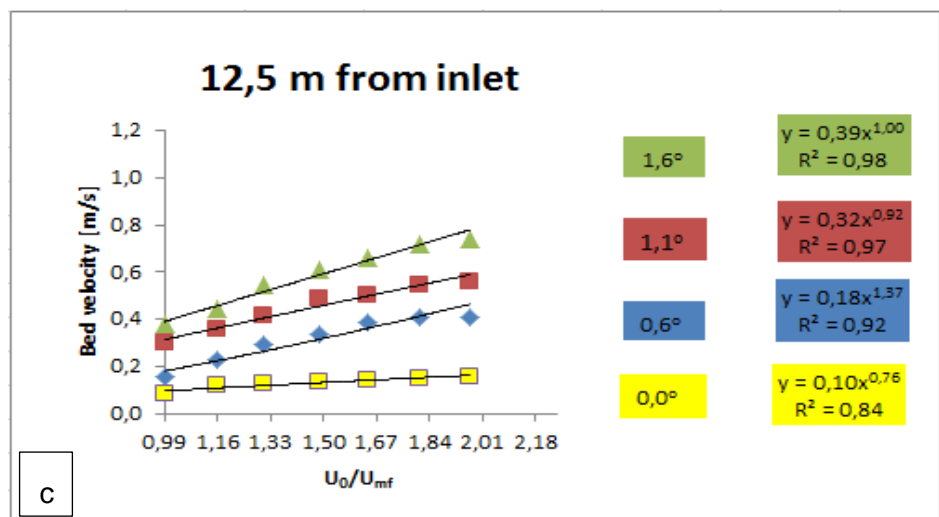
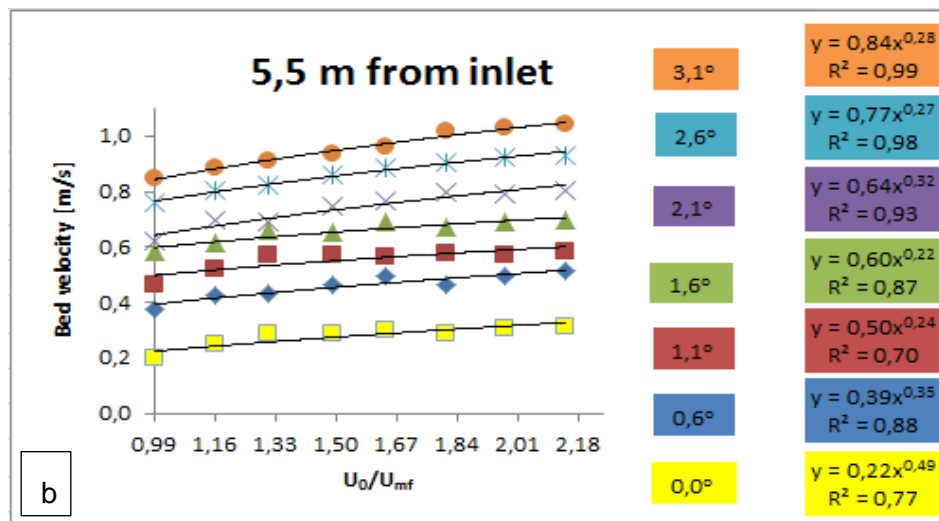
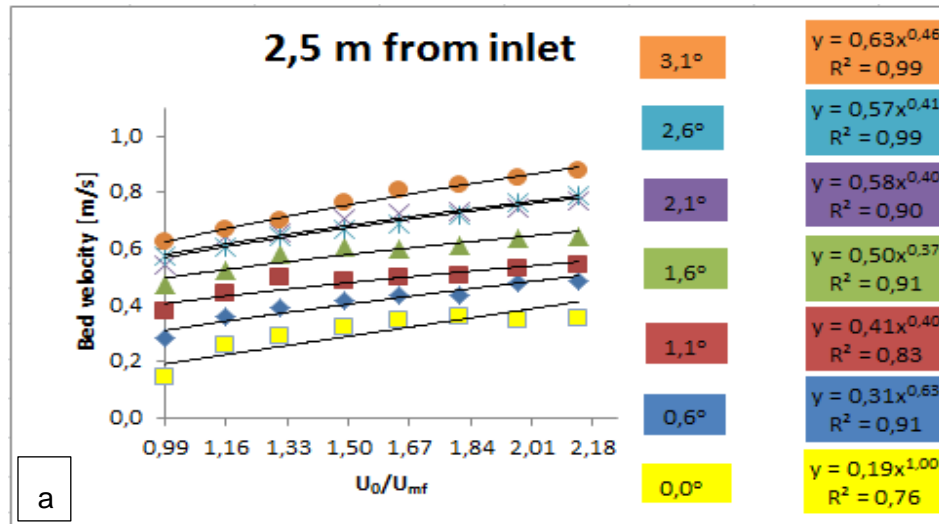


Figure 92 Power law trend lines fitted to experimental data in a: a) 3 m; b) 7 m; c) 15 m long air slide segment. Bed velocity based on measurements of bed height at last point in each of the segments.

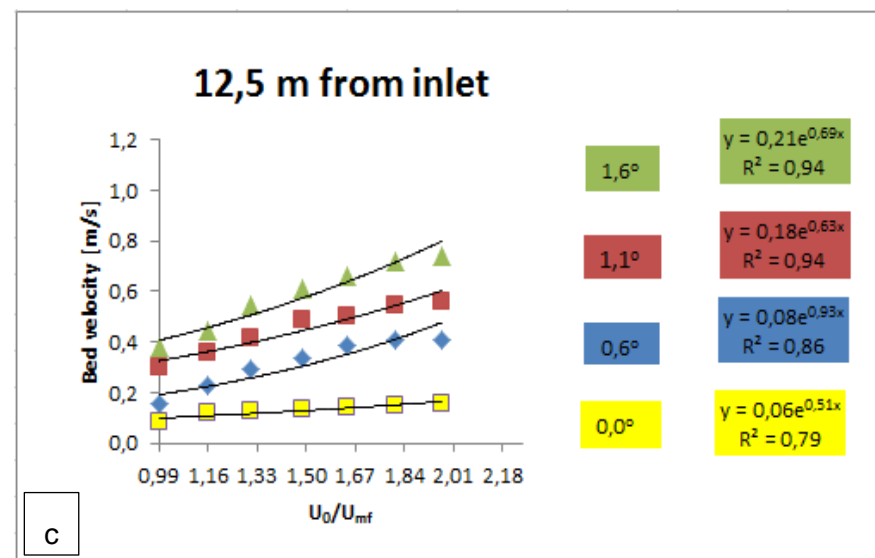
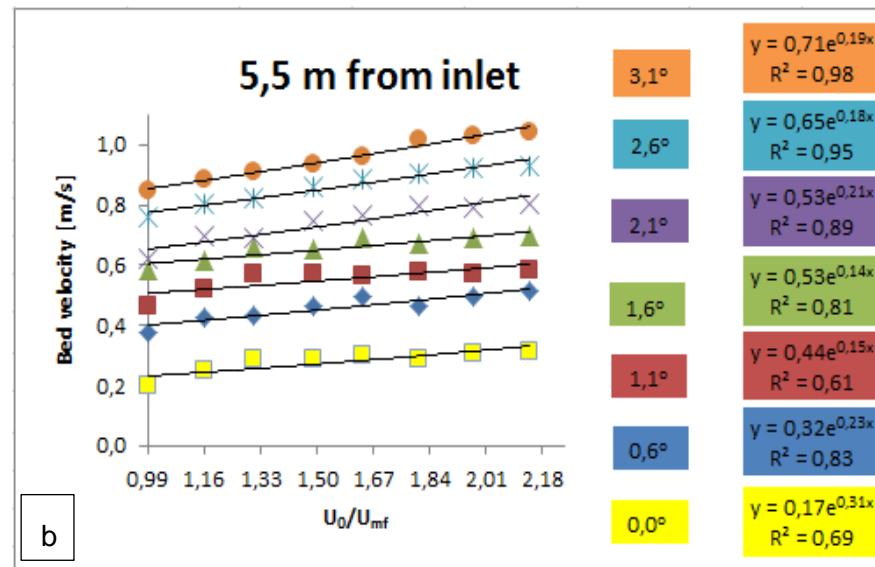
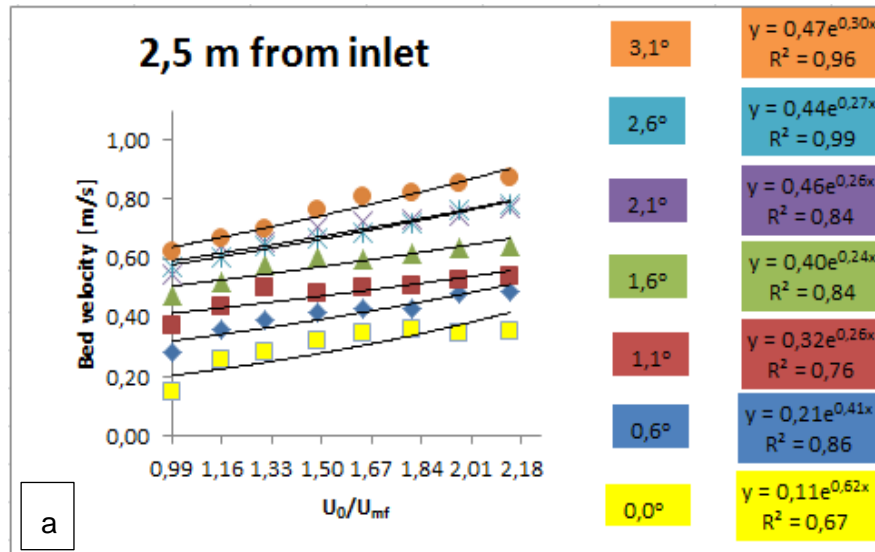


Figure 93 Exponential law trend lines fitted to experimental data in a: a) 3 m; b) 7 m; c) 15 m long air slide segment. Bed velocity based on measurements of bed height at last point in the segment.

Since the flow is mainly driven by gravity, one does not expect any acceleration when the inclination is zero as concluded by Savage and Oger (2013). The results in this thesis show that there is an accelerating trend even when the bed inclination angle approaches zero. In order to understand the behaviour of average bed velocity, indirectly calculated from measurements of bed height, the slopes of bed velocity as a function of both  $U_0/U_{mf}$  and  $\theta$  need to be studied. The results of average bed velocity in the next subsections come from direct measurements of bed heights and discharge rates performed with no restriction gate, meaning full capacity of the system using original inlet configuration. The average bed velocity has been calculated as:  $v = Q/\rho A$ , where  $Q$  is the measured solids flow rate,  $\rho$  fluidized bulk density and  $A$  the cross sectional area of the bed. The fluidized density, measured in a fluidized column, has been kept constant,  $\rho = 1000$  for all values of  $U_0/U_{mf}$ . There are two cases that need to be investigated, depending on the length of air slide segments involved in the transport of alumina and the availability of headroom. One can thus try to investigate and answer Woodcock's 39 years old question: "Fluidized bed conveying – Art or science?" To answer his question we can start by asking ourselves, "Air slide modelling - intuition or knowledge?". Anyway, in order to be able to answer the questions, two cases need in depth investigation:

**Case 1:** effect of inclination angle,  $\theta$  on average bed velocity,  $v$  at different distances away from inlet and at different dimensionless coefficient of velocity  $U_0/U_{mf}$ . This is a case where we have a given range of inclination angles  $\theta$  and we want to model and predict the average bed velocity and its slope at different  $U_0/U_{mf}$ . This case is suitable for short segments of air slide. In long air slide segments this case is "expensive" due to headroom availability, where head loss depends on the length of the air slide and the sine of the inclination angle,  $\theta$ . The longer the air slide, the higher the head loss. Case 1 is the subject of next sections and is the base for mathematical modelling in the next chapter.

**Case 2:** effect of  $U_0/U_{mf}$  on average bed velocity at different distances away from inlet and at different angles of inclination,  $\theta$ . This is a case where we have a given range of  $U_0/U_{mf}$  values and we want to predict the values of average bed velocity and its slope at different values of  $\theta$ . As mentioned above, due to headroom availability one can choose a low  $\theta$  and compensate in order to increase capacity, by increasing

$U_0/U_{mf}$ . This is a case suitable for long air slide segments. Preliminary results for Case 2 were shown in Figure 92 and Figure 93, results showing that bed velocity power and exponential models as a function of  $U_0/U_{mf}$  do not perform very well for angles below 1.6 degrees.

The calculated values of average bed velocity versus  $\theta$  and  $U_0/U_{mf}$  for case 1 and 2 were fitted by power laws having the general expression  $v = a\theta^b$  and  $v = c(U_0/U_{mf})^d$ . The same method was applied in all air slide segment lengths 3 m, 7 m and 15 m for all measurement points from 0.5 to 2.5, 5.5 and 12.5 m distance from inlet at all angles of downward inclination from 0 to 3.1 degrees and for all ranges at dimensionless coefficient of velocity  $U_0/U_{mf}$  in the range of 0.99 to 2.14.

### 6.2.1 3 m - effect of inclination angle, $\theta$ on average bed velocity at different distances away from inlet and at different dimensionless coefficient of velocity $U_0/U_{mf}$

An analysis of the calculated average velocity over the cross section of the bed (bed velocity [m/s]) at various locations along the 3 m long air slide segment showing its dependence of both dimensionless coefficient of velocity  $U_0/U_{mf}$  and downward inclination angle  $\theta$  is shown in Figure 94. Each data point represents the average of three consecutive tests. A power law curve fit was forced through all data as illustrated in Figure 94. From the analysis of the data it became clear that power rather than linear fit equations were giving the best fit over the whole range of data at all distances from inlet and for all air slide segment lengths. The same method was applied for all measurement points from 0.5 to 2.5 m distance from inlet at all angles of downward inclination from 0 to 3.1 degrees and for all ranges at dimensionless coefficient of velocity  $U_0/U_{mf}$  in the range of 0.99 to 2.14. The calculated values of average bed velocity versus  $\theta$  and  $U_0/U_{mf}$  were fitted by a power law having the expression:  $y = K \cdot x^P$ , where  $y$  is the average bed velocity,  $x$  is the angle of inclination,  $K$  is the coefficient of and  $P$  is the power exponent. Results of power fit equations and values of  $R^2$  for each  $U_0/U_{mf}$  are given together with the graphs. On analysing the data in Figure 94 at each point of measurement, it can be seen that the slope value in each graph for the increasing values of  $\theta$  is increasing with increasing  $U_0/U_{mf}$ . Another interesting observation is that the value of the same slope is increasing with increasing distance away from the inlet, which is a clear indication that the flow is accelerating, and that a

3 m long air slide segment is not long enough for the flow to achieve steady state. Power values results of the analysis shown graphically in Figure 94 are presented in Table 28 as summary, for all the measurement points from 0.5 m to 2.5 m distance from inlet. If  $R^2$  is greater than 0.80, there is a good fit to the data.  $R^2$  of 0.80 means that 80 % of the variation in average bed velocity at each measurement point away from the inlet can be explained by the angle of inclination  $\theta$  at different  $U_0/U_{mf}$ .

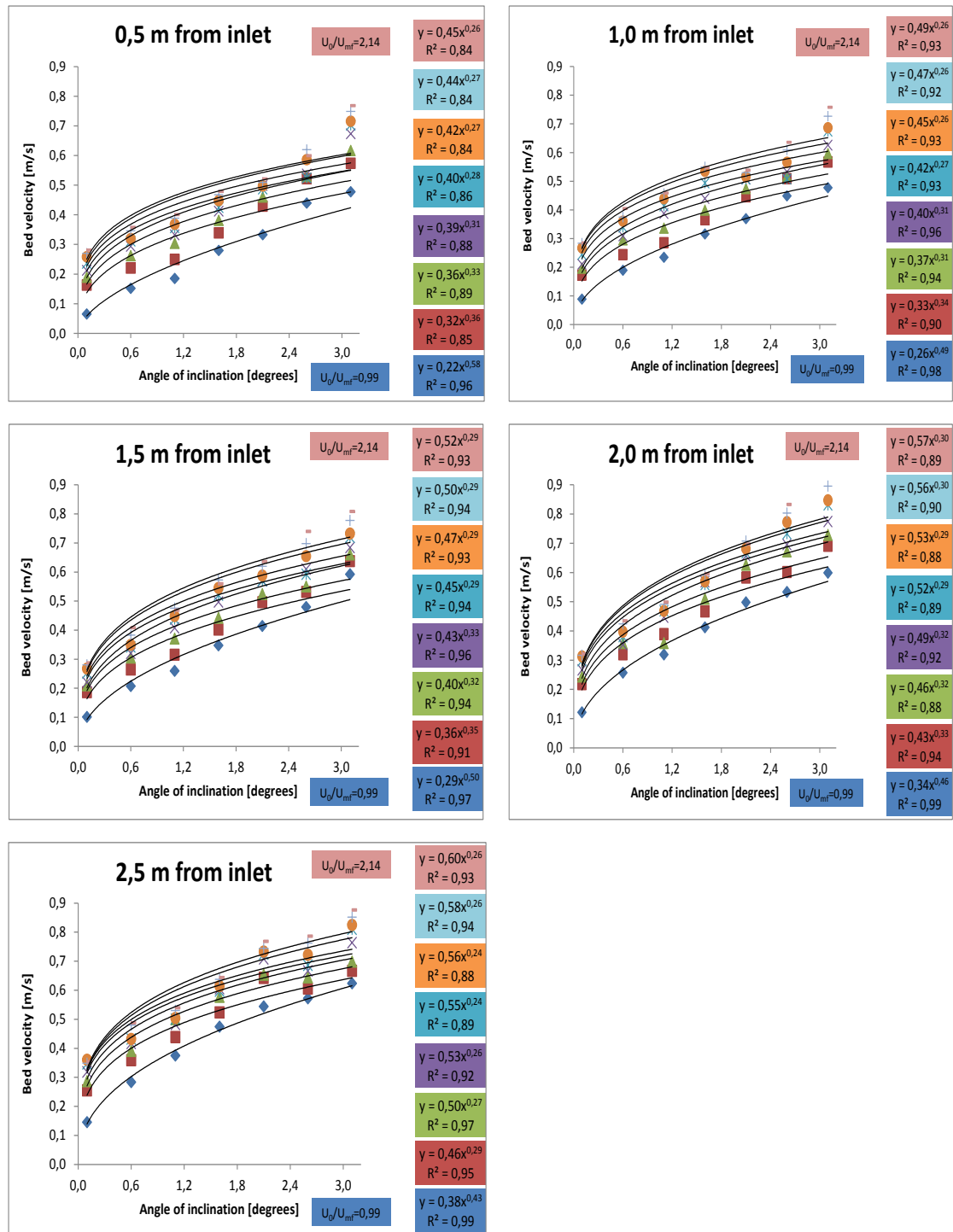


Figure 94 Power law trend lines fitted to the experimental data of average bed velocity as a function of angle of inclination,  $\theta = 0..3^0$  at different  $U_0/U_{mf} = 0.99 \dots 2.14$ .

At this stage of data analysis the results looked very promising showing there is a strong correlation between average bed velocity and angle of inclination for each  $U_0/U_{mf}$ . This gave a strong indication that both  $U_0/U_{mf}$  and  $\theta$  had a simultaneous influence on

bed velocity. Since bed velocity has been calculated from measured static bed height at different measurement points away from inlet of the air slide, then both  $U_0/U_{mf}$  and  $\theta$  will have a simultaneous influence on height and thus on air slide capacity. The strategy is to try to connect the slopes of bed velocities shown in Figure 94 together, in order to express velocity profiles at all distances from inlet for each  $U_0/U_{mf}$  in one graph. The starting point for the slopes of bed velocity was to express them as in Figure 94, in terms of the inclination angle, and for keeping this starting point as a condition for building up of an empirical model, the symbols  $K(\theta)$  for the coefficient of power law at all angles of inclination and  $P(\theta)$  for the exponent of power law at all angles of inclination will be used further.

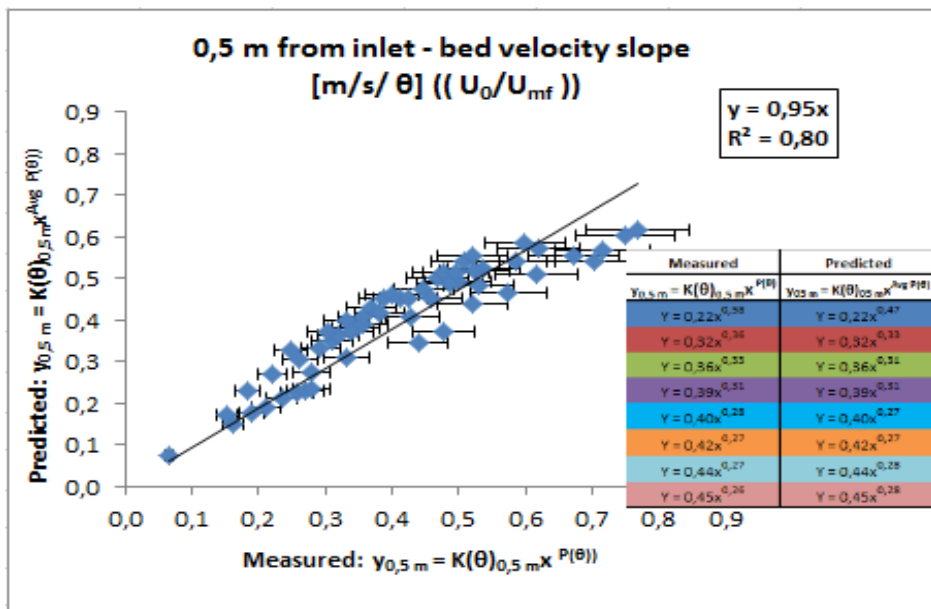
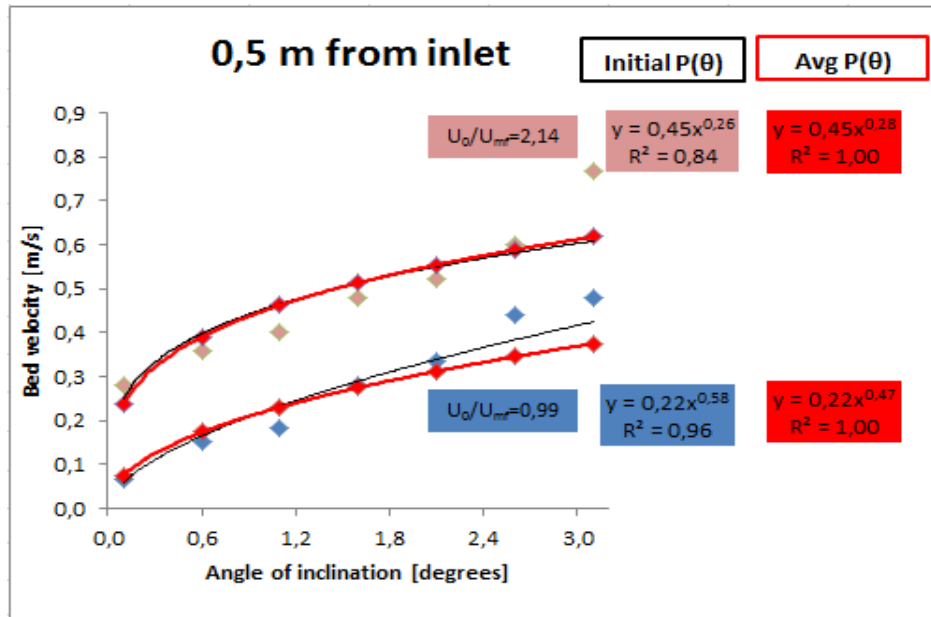
**Table 28 Power law trend lines fitted to experimental data for average bed velocity at all angles of inclination,  $\theta$ , at different  $U_0/U_{mf}$  for each measurement point from 0.5 to 2.5 m.  $K(\theta)$  is the coefficient and  $P(\theta)$  is the exponent of power law.**

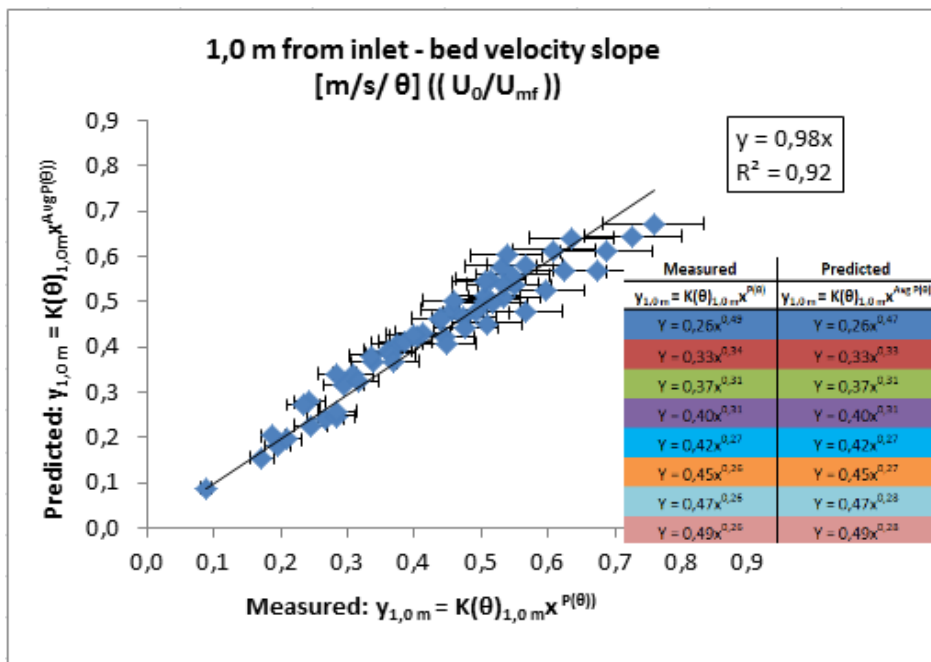
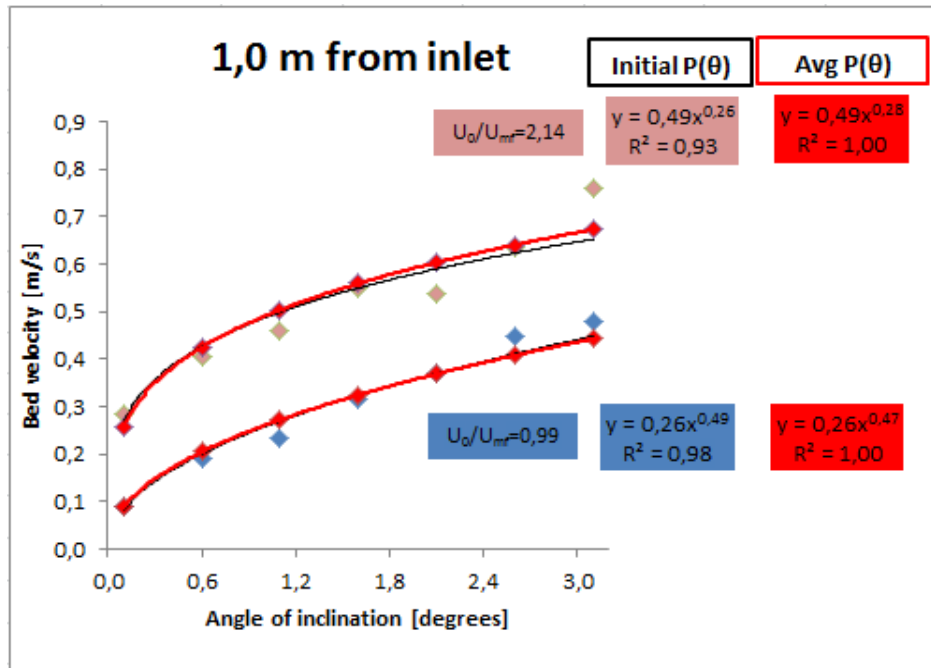
3 m - $K(\theta)$ - Bed velocity slope [m/s/ $\theta$ ] ( $(U_0/U_{mf})$ )																	
$U_0/U_{mf}$	$R^2$	$K(\theta)_{0,5m}$	$P(\theta)_{0,5m}$	$R^2$	$K(\theta)_{1,0m}$	$P(\theta)_{1,0m}$	$R^2$	$K(\theta)_{1,5m}$	$P(\theta)_{1,5m}$	$R^2$	$K(\theta)_{2,0m}$	$P(\theta)_{2,0m}$	$R^2$	$K(\theta)_{2,5m}$	$P(\theta)_{2,5m}$	Avg $P(\theta)$	Stdev/Avg $P(\theta)$
0,99	0,96	0,22	0,58	0,98	0,26	0,49	0,97	0,29	0,50	0,99	0,34	0,46	0,99	0,38	0,43	0,47	7 %
1,16	0,85	0,32	0,36	0,90	0,33	0,34	0,91	0,36	0,35	0,94	0,43	0,33	0,95	0,46	0,29	0,33	8 %
1,31	0,89	0,36	0,33	0,94	0,37	0,31	0,94	0,40	0,32	0,88	0,46	0,32	0,97	0,50	0,27	0,31	8 %
1,49	0,88	0,39	0,31	0,96	0,40	0,31	0,96	0,43	0,33	0,92	0,49	0,32	0,92	0,53	0,26	0,31	10 %
1,64	0,86	0,40	0,28	0,93	0,42	0,27	0,94	0,45	0,29	0,89	0,52	0,29	0,89	0,55	0,24	0,27	9 %
1,81	0,84	0,42	0,27	0,93	0,45	0,26	0,93	0,47	0,29	0,88	0,53	0,29	0,88	0,56	0,24	0,27	9 %
1,97	0,84	0,44	0,27	0,92	0,47	0,26	0,94	0,50	0,29	0,90	0,56	0,3	0,94	0,58	0,26	0,28	7 %
2,14	0,84	0,45	0,26	0,93	0,49	0,26	0,93	0,52	0,29	0,89	0,57	0,30	0,93	0,60	0,26	0,28	7 %
Avg $P(\theta)$		0,30	0,29			0,29			0,31			0,31			0,26		0,29
Stdev/Avg $P(\theta)$		13 %	10 %			11 %			8 %			5 %			7 %		8 %

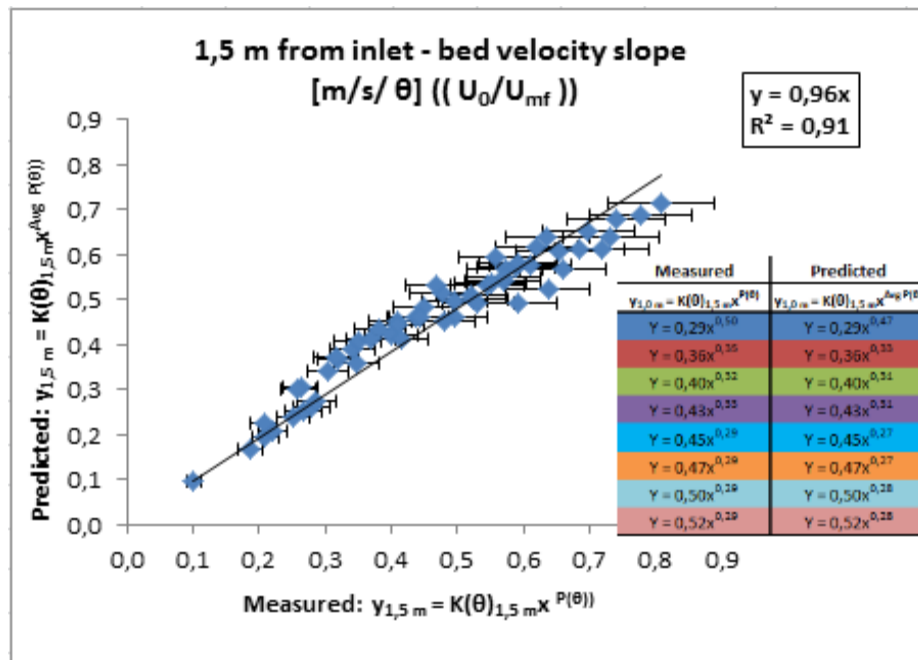
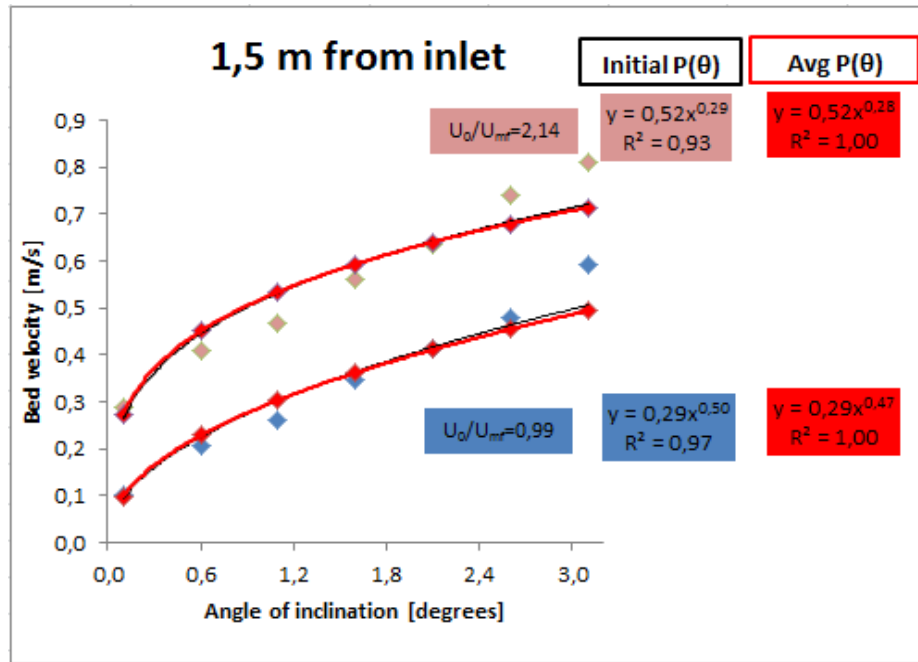
From an analysis of Table 28 it was interesting to note that for each  $U_0/U_{mf}$ , while the values of  $K(\theta)$  are constantly increasing with increasing distance away from the inlet, the values of  $P(\theta)$  are more stable. Two values were not following this trend and they are highlighted in red:  $P(\theta)_{0,5m} = 0.58$  at  $U_0/U_{mf} = 0.99$  and  $P(\theta)_{0,5m} = 0.36$  at  $U_0/U_{mf} = 1.16$ . It is believed that at low operational air velocity close to the inlet at the air slide, the influence of inlet configuration is strong, thus influencing the bed heights. An average  $P(\theta)$  was calculated excluding these two values. The thought of this exercise was to investigate whether a single average power exponent could be used for the entire length of air slide segment in order to predict bed velocity, “for philosophy has to do with things that can be demonstrated and are eternally the same” according to Aristotle (Barnes (1994)). A similar method was used by Chaudry (2006) in his

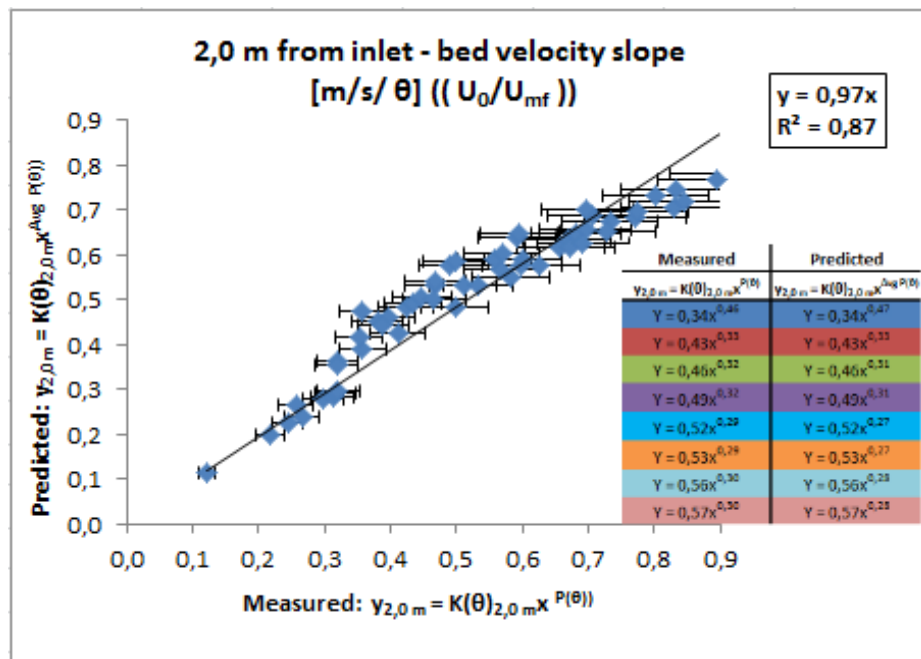
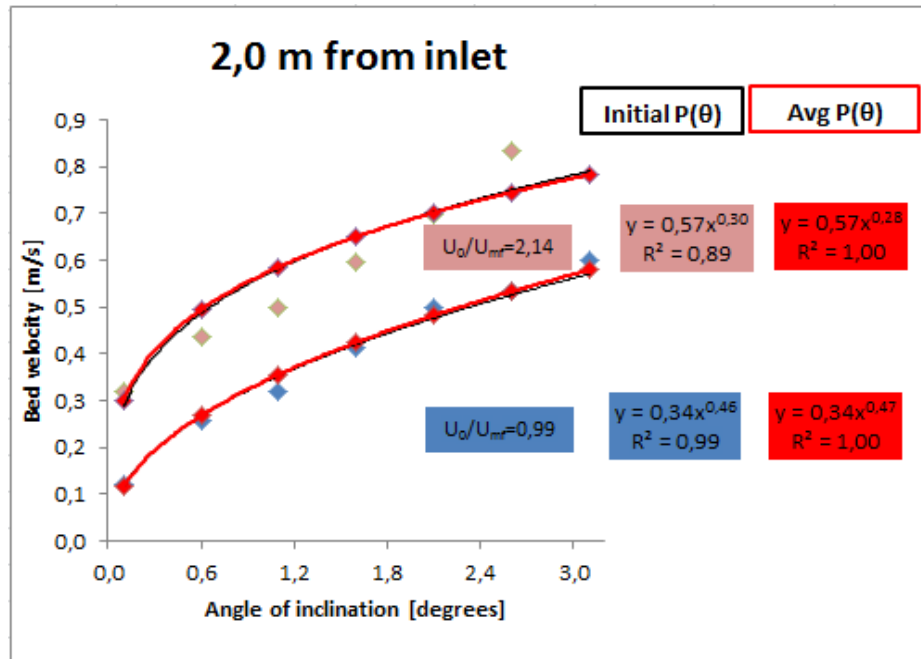
empirical modelling approach used to fit a power equation to bend pressure drop versus suspension density in a pneumatic conveying line, with the difference that in his study only changing the exponent value did not achieve the required objective. Now, back to the initial thought, values of bed velocities at minimum and maximum  $U_0/U_{mf} = 0.99$  and  $U_0/U_{mf} = 2.14$  are plotted in Figure 95. Taking  $U_0/U_{mf} = 0.99$  at 0.5 m away from inlet, for example, the blue points represent the initial measurements with the initial power law equation:  $y = 0.22x^{0.58}$ . Using the average  $P(\theta)$ , the bed velocity was recalculated using the modified law  $y = 0.22x^{0.47}$  based on  $AvgP(\theta)$  on the initial data. The new bed velocity data points (red colour) and the new trend line based on  $y = 0.22x^{0.47}$  (red colour) were plotted together with the initial data (blue) and initial law (black) to show the effect of changing the exponent of power law. Figure 95 shows this exercise for all distances from 0.5 to 2.5 m away from the inlet. The initial power law under-predicted the bed velocity at high  $\theta$  values, the new power law based on average exponent provides a mathematical correction of the under or over-predicted initial measurement values. Ten percent error bars were applied to the predicted (based on  $AvgP(\theta)$ ) versus measured (based on  $P(\theta)$ ) data points and no points have been omitted from the analysis.











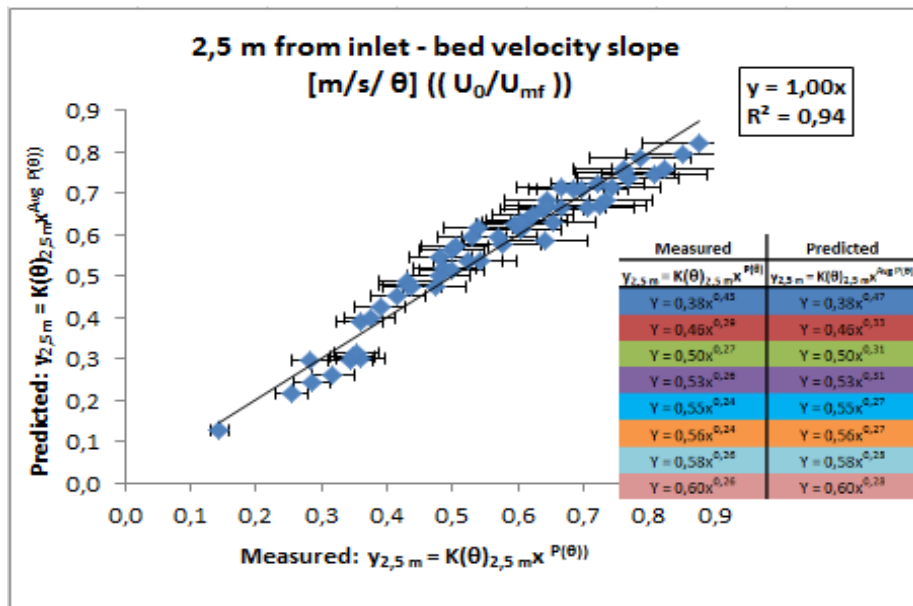
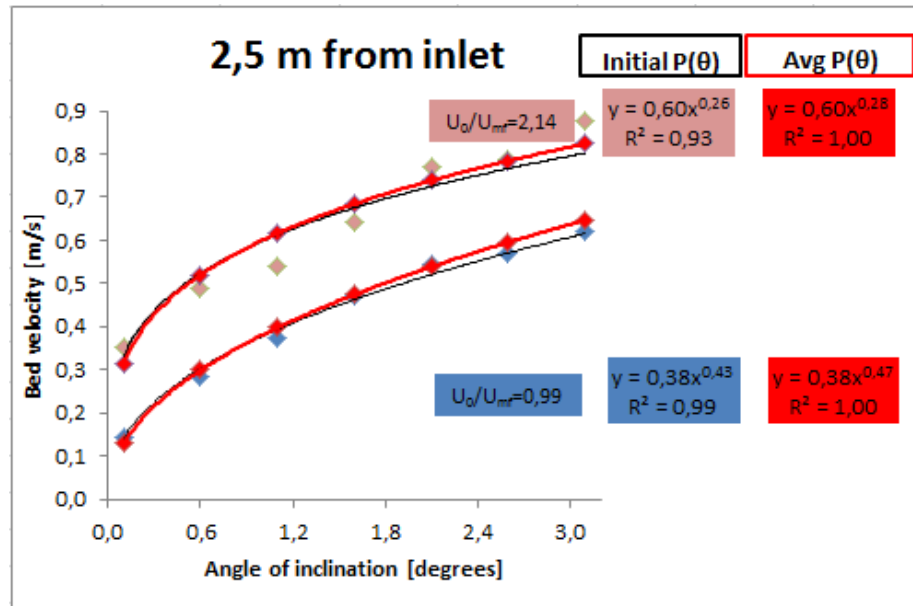


Figure 95 Investigation of the effect of changing power law exponent,  $P(\theta)$  for  $U_0/U_{mf} = 0.99$  and  $U_0/U_{mf} = 2.14$ . Ten percent error bars showing the goodness of the mathematical method for all ranges of  $U_0/U_{mf}$  from 0.99 to 2.14.

Figure 96 presents values of  $R^2$  from using  $Avg P(\theta)$  power law exponent presented graphically in Figure 95. If  $R^2$  is greater than 0.80, there is a good fit to the data. This means that between 80 to 97 % of the variation of the bed velocity data can be explained by a bed velocity power law based on  $g P(\theta)$ .

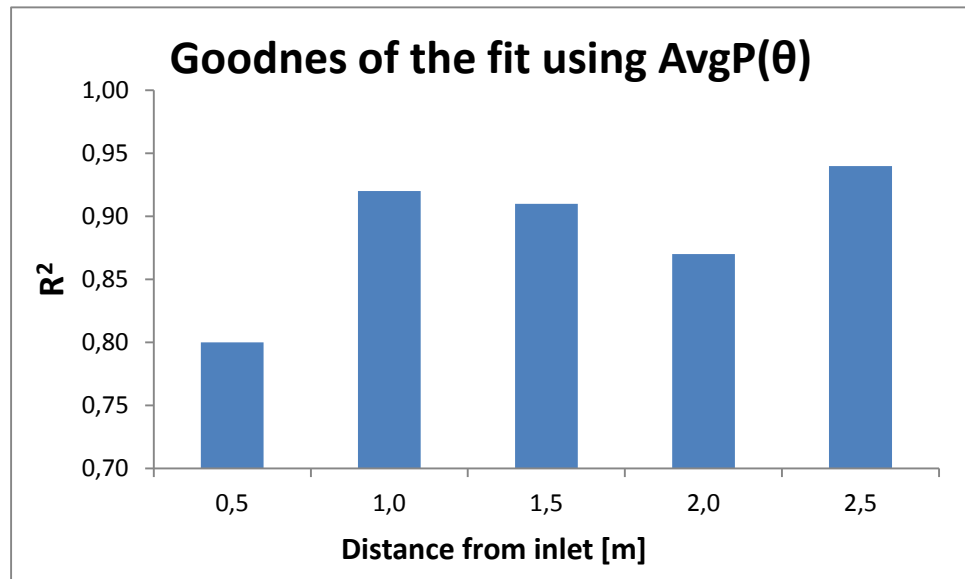


Figure 96 Values of  $R^2$  expressing the goodness of the fit when using  $AvgP(\theta)$  instead of  $P(\theta)$  into the power trend lines fitted to experimental data.

### 6.2.2 3 m - Further investigation of the effect of power law exponent - bed velocity slope $K(\theta)$ , versus distance from inlet at different $U_0/U_{mf}$

Again the scope of this exercise is to investigate whether a single average power exponent could be used for the entire length of air slide segment in order to predict average bed velocity. Results of power law model by using single average power exponent,  $AvgP(\theta)$ , a summary of Table 29, replacing  $P(\theta)$  by  $AvgP(\theta)$  is given in Table 29. So far we have only investigated the effect of power law coefficient,  $AvgP(\theta)$ . To be able to compare the goodness of the fit of the power law models in each air slide segment: 3 m, 7 m and 15 m we need to express the average bed velocity as a function of distance from inlet. Again, to be able to do this, the effect of the power law coefficient,  $K(\theta)$  needs to be investigated.

**Table 29 Results of power law trend lines fitted to the experimental data by using single average power exponent,  $AvgP(\theta)$ , a summary of Table 28.**

3 m - $K(\theta)$ - Bed velocity slope [m/s/ $\theta$ ] ( $(U_0/U_{mf})$ )					
$U_0/U_{mf}$	$Y_{0,5\text{ m}} = K(\theta)_{0,5\text{ m}} X^{AvgP(\theta)}$	$Y_{1,0\text{ m}} = K(\theta)_{1,0\text{ m}} X^{AvgP(\theta)}$	$Y_{1,5\text{ m}} = K(\theta)_{1,5\text{ m}} X^{AvgP(\theta)}$	$Y_{2,0\text{ m}} = K(\theta)_{2,0\text{ m}} X^{AvgP(\theta)}$	$Y_{2,5\text{ m}} = K(\theta)_{2,5\text{ m}} X^{AvgP(\theta)}$
0,99	$Y = 0,22x^{0,47}$	$Y = 0,26x^{0,47}$	$Y = 0,29x^{0,47}$	$Y = 0,34x^{0,47}$	$Y = 0,38x^{0,47}$
1,16	$Y = 0,32x^{0,33}$	$Y = 0,33x^{0,33}$	$Y = 0,36x^{0,33}$	$Y = 0,43x^{0,33}$	$Y = 0,46x^{0,33}$
1,31	$Y = 0,36x^{0,31}$	$Y = 0,37x^{0,31}$	$Y = 0,40x^{0,31}$	$Y = 0,46x^{0,31}$	$Y = 0,50x^{0,31}$
1,49	$Y = 0,39x^{0,31}$	$Y = 0,40x^{0,31}$	$Y = 0,43x^{0,31}$	$Y = 0,49x^{0,31}$	$Y = 0,53x^{0,31}$
1,64	$Y = 0,40x^{0,27}$	$Y = 0,42x^{0,27}$	$Y = 0,45x^{0,27}$	$Y = 0,52x^{0,27}$	$Y = 0,55x^{0,27}$
1,81	$Y = 0,42x^{0,27}$	$Y = 0,45x^{0,27}$	$Y = 0,47x^{0,27}$	$Y = 0,53x^{0,27}$	$Y = 0,56x^{0,27}$
1,97	$Y = 0,44x^{0,28}$	$Y = 0,47x^{0,28}$	$Y = 0,50x^{0,28}$	$Y = 0,56x^{0,28}$	$Y = 0,58x^{0,28}$
2,14	$Y = 0,45x^{0,28}$	$Y = 0,49x^{0,28}$	$Y = 0,52x^{0,28}$	$Y = 0,57x^{0,28}$	$Y = 0,60x^{0,28}$

We start by analysing the data in the first row, columns 1 to 5 from Table 29. Average bed velocity at each measurement point  $Y_{measurement}$  is expressed as  $Y_{measurement} = K(\theta)x^{AvgP(\theta)}$ . If we replace the value of  $x^{0,47}$ , where  $x$  was the angle of inclination,  $\theta$ , by  $X$ , where  $X$  is the same at every measurement point, then we get  $Y_{measurement} = K(\theta)X(\theta)$ . Now the initial power law coefficient,  $K(\theta)$  has become the average bed velocity slope as a function of distance from inlet.

Results of the bed velocity slopes, the initial power law coefficients,  $K(\theta)$  presented in Table 29 have been plotted in Figure 97. To find the best fit model two mathematical models were again fitted to all  $K(\theta)$  from Table 29:

- Exponential
- Power

All data points follow the trends, and no data points have been corrected for or omitted from the analysis. The bed velocity slopes as a function of  $\theta$ , named  $K(\theta)$ , were plotted against distance from inlet at various  $U_0/U_{mf}$ . The data plotted in Figure 97 shows increasing coefficient of power law,  $K'(\theta)$ , values with increasing distance from inlet and increasing  $U_0/U_{mf}$ . The exponential law is derived from the power law data by changing the trend/regression type in Excel from “Power” to “Exponential”. A quick look at the two graphs in Figure 97 where the equations and the values of  $R^2$  are displayed, indicates that the exponential law has higher  $R^2$  values than the power law values, but is it better to apply the exponential law than the power law? Will this exponential law still be best to apply to predict the average bed velocity when the flow

regimes will change, as we already know, from accelerating to steady state? To answer the questions raised above, an analysis of both exponential and power law slope values and values of  $R^2$  will have to be performed first.

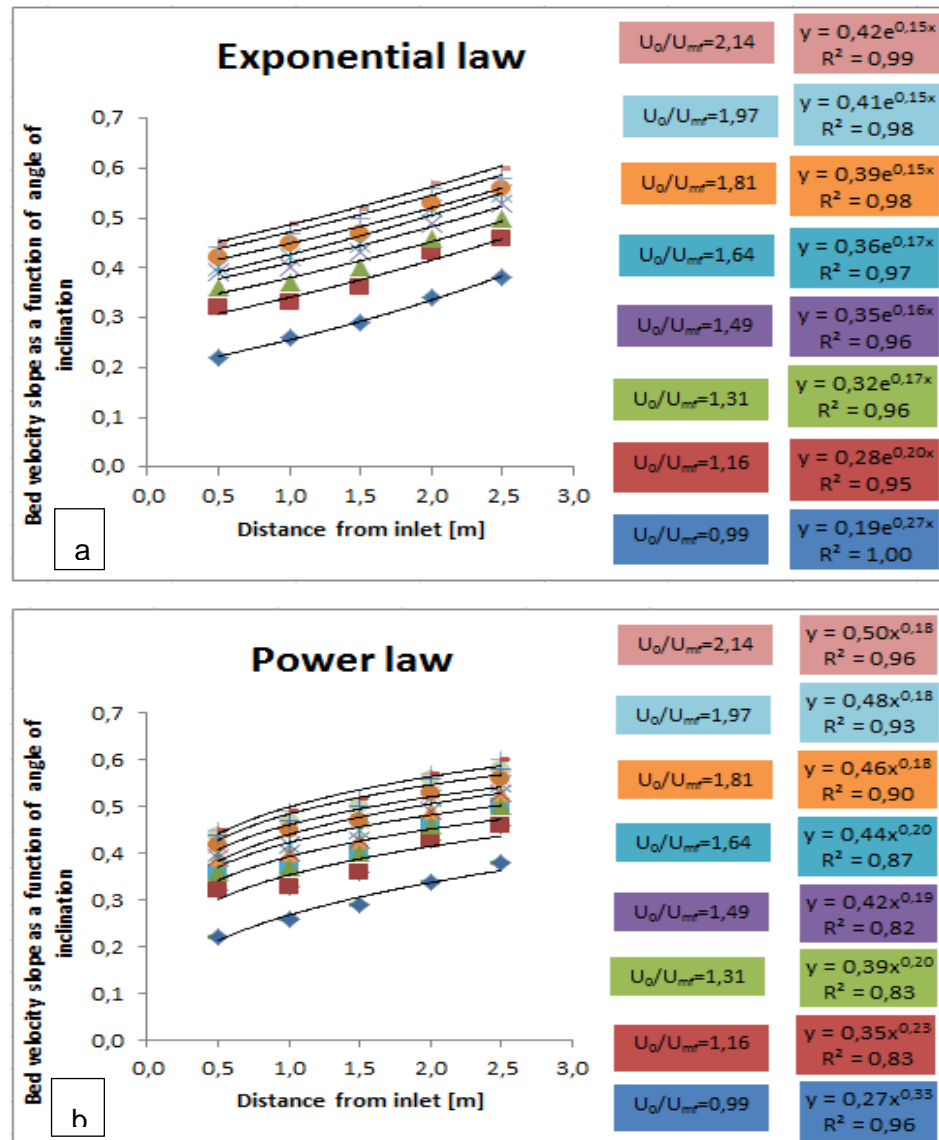


Figure 97 a) Exponential and b) power law trend lines fitted to the slope of average bed velocity as a function of angle of inclination,  $\theta = 0..3.1^0$ ,  $K(\theta)$ , versus distance from inlet, at different  $U_0/U_{mf} = 0.99 \dots 2.14$ .

Already at this stage of analysis some intuitive mechanisms have been triggered by the analysis. The scope of this empirical modelling approach is to develop a model that should be applicable for each air slide segment length given two possible mathematical laws: exponential and power. The applicability of a single average power exponent used for the entire length of a 3 m air slide segment in order to predict average bed velocity was demonstrated and proved to be a robust tool in order to achieve the scope. This



analysis approach and the mathematical slope correction based on  $AvgP(\theta)$  are quite demanding so before applying it to the 7 m and 15 m long segments, we take a closer look at the behaviour at both power law and exponential law, to understand the difference between them. Again the thought behind this approach is inspired by Aristotle's *Magna Moralia* (Barnes (1994), page 1894). "Philosophy is composed of knowledge and intuition. For philosophy has to do both with the principles and what it can be proved from the principles, with which knowledge deals. In so far, then, as it deals with the principles, it itself partakes of intuition, but in so far as it deals with demonstrative conclusions from the principles, it partakes of knowledge. So that is evident that philosophy is compounded of intuition and knowledge, so that it will deal with the same things with which intuition and knowledge do." Now having this clearly in mind, the scope of further analysis will be to find a mathematical law applicable in all segment lengths of air slide based on a single average power exponent used for the entire length of each air slide segment in order to predict bed velocity, "for philosophy has to do with things that can be demonstrated and are eternally the same." Once this analysis will be completed, it will cover the part of this thesis, based on intuition, estimation and determination. Once more, "intuition has to do with the first principles of things, intelligible and real. For knowledge has to do with things that admit of demonstration, but the principles are indemonstrable, so that it will not be knowledge but intuition that is concerned with the principles" (Barnes (1994), page 1894). Once the empirical model will be completed, then the focus will be on the knowledge part of this thesis (next chapter), to find a model based on physical laws that are demonstrable and try to link the empirical model (based on intuition), to the physical model (based on knowledge). Based on Aristotle's thinking presented in *Magna Moralia*, it will be the link and the goodness of the fit between empirical and physical models, indemonstrable versus demonstrable, that will then lift up this thesis to a philosophical level.

Now, back on track, the question to be answered is: "given two models: exponential and power law, which of them is the best to choose and why"? With the experience from the results from linear model fit in mind, where  $R^2$  decreased gradually from the 3 segment to the 12 m segment, thus disqualifying the linear model in favour of power law model valid for all lengths, both models: exponential and power for the slope data will now be studied. The results for all segment length are shown in Figure 98 and

Figure 99 and a comparison  $R^2$  of the two models is given in Figure 100. A careful study of the graphs and their equations in Figure 98 and Figure 99 and was undertaken. Acceleration zone has been defined in this thesis as the distance after the inlet of the air slide required to accelerate the alumina particles in the bed to the average transport velocity of the alumina bed. A theory is that a 3 m long air slide segment is not long enough for the flow to achieve steady state.

The exponential law is clearly the best one to predict the average bed velocity in a 3 m segment. In a 7 m long segment, at high  $U_0/U_{mf}$  values the flow is reaching steady state after 4.5 – 5 m. If we have a closer look at bed height profiles in Figure 101, we can see that in the 7 m long air slide segment stable bed heights occur already at 3.5 m away from the inlet. The  $R^2$  values of the power law trend lines increase compared to the values in the 3 m segment, indicating a change in flow regime, accelerating in the first 4.5 - 5.0 m away from inlet, and steady state in the last part of the segment. Both models can be used for prediction.

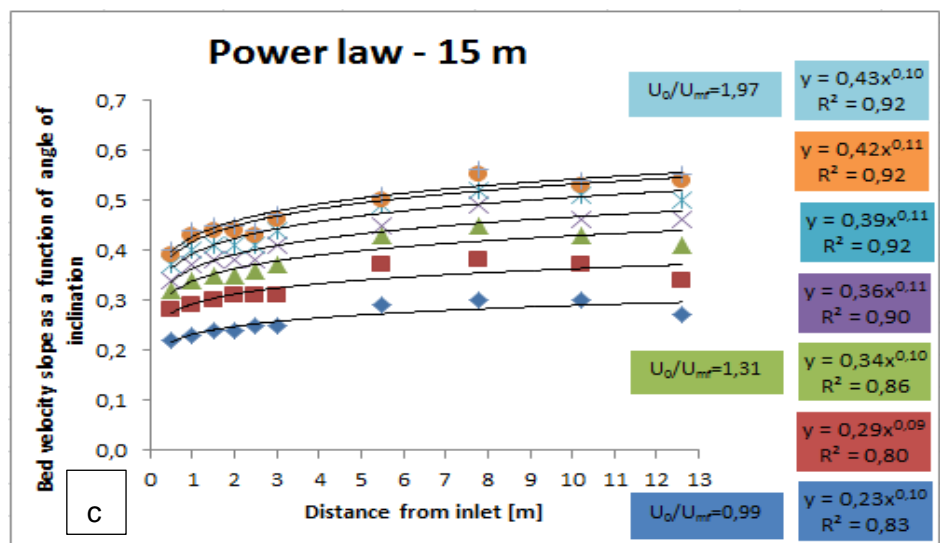
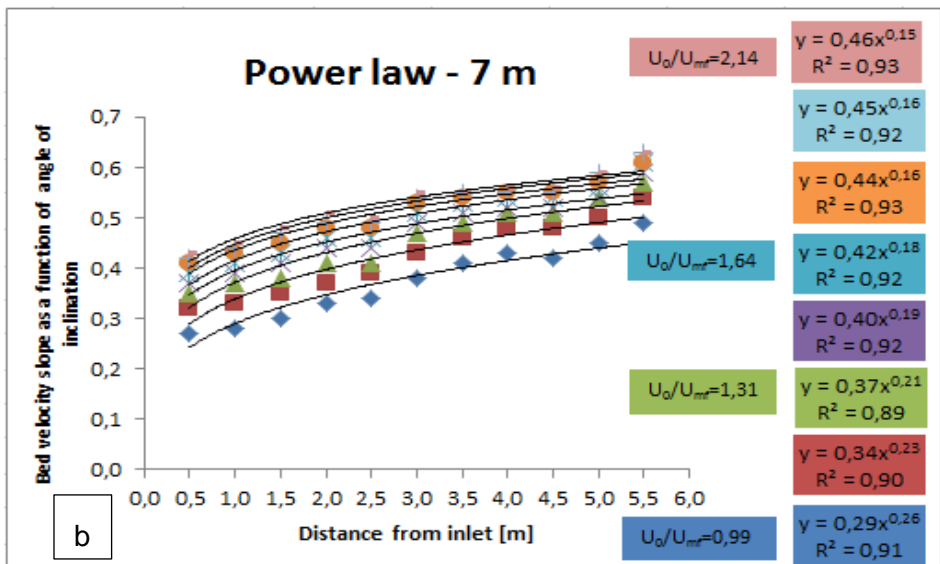
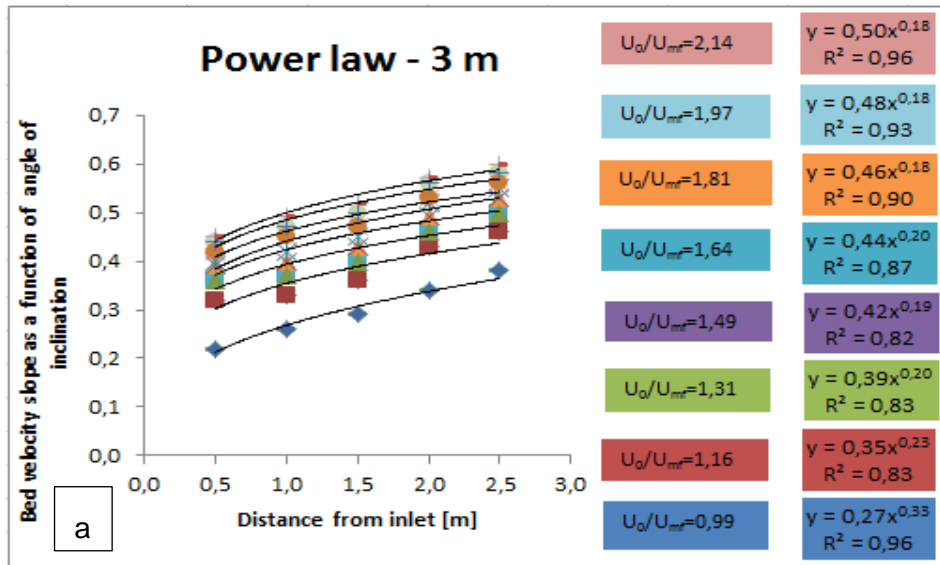


Figure 98 Power law trend lines fitted to experimental data for different air slide segments: a) 3 m, b) 7 m, c) 15 m.

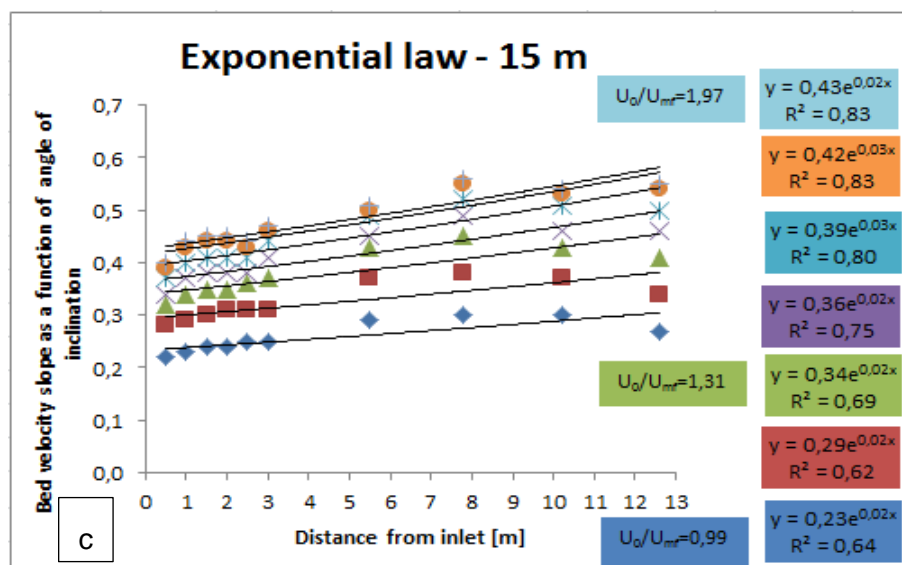
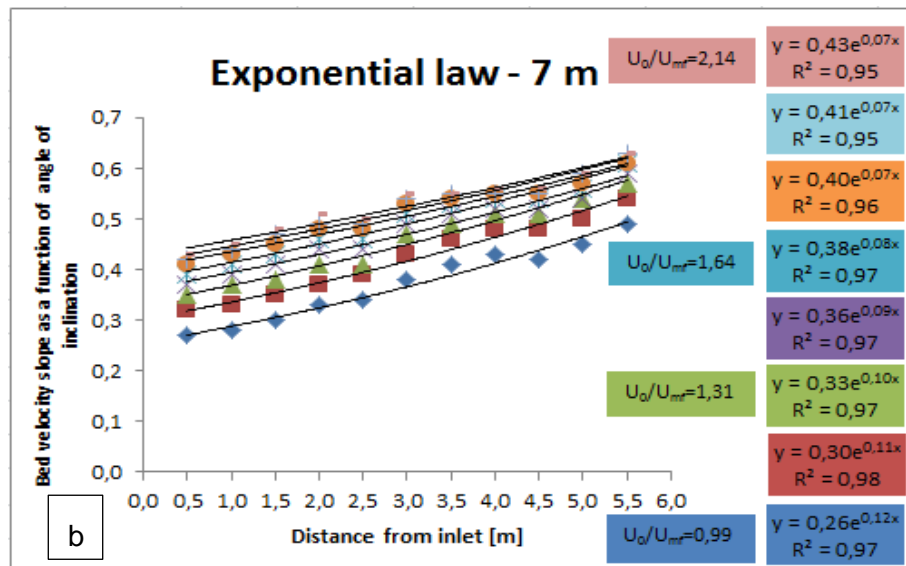
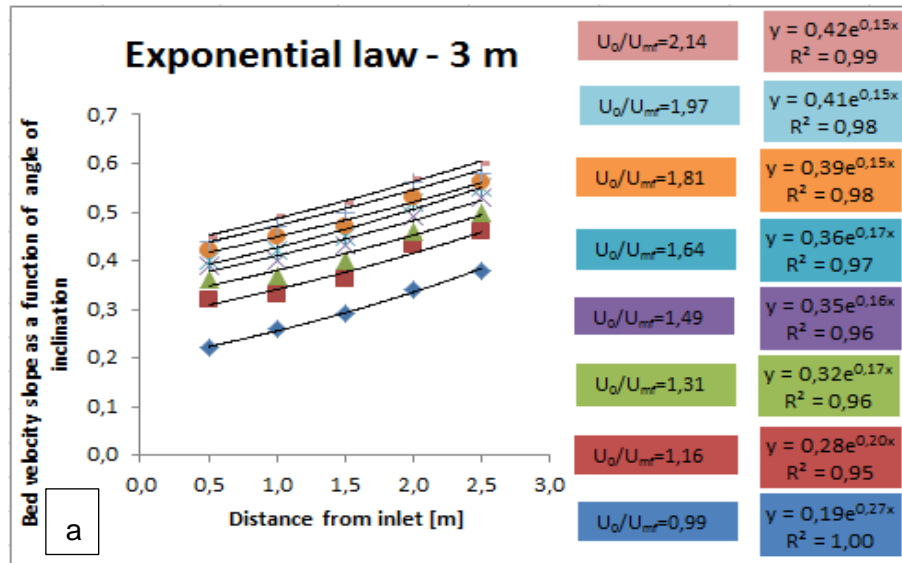


Figure 99 Exponential law trend lines fitted to experimental data for different air slide segments: a) 3 m, b) 7 m, c) 15 m.

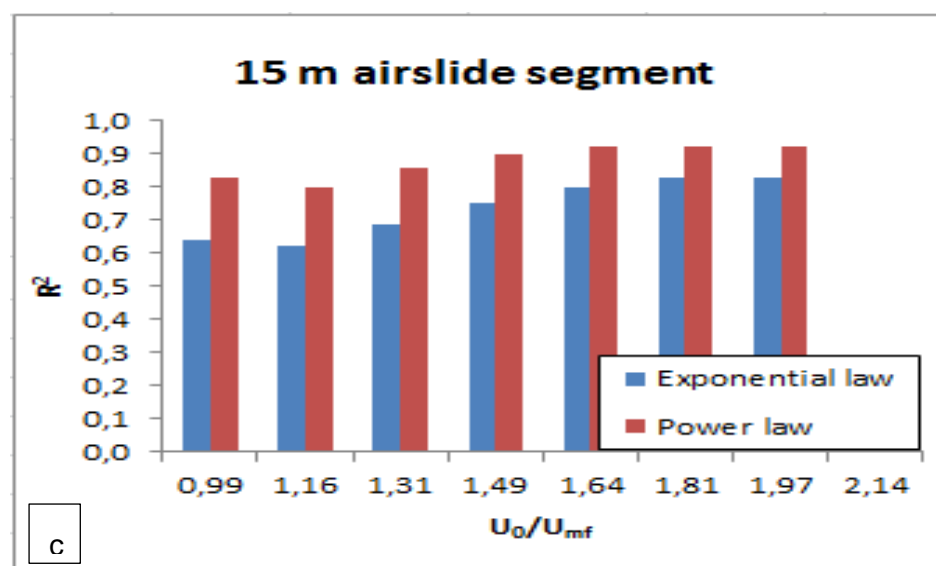
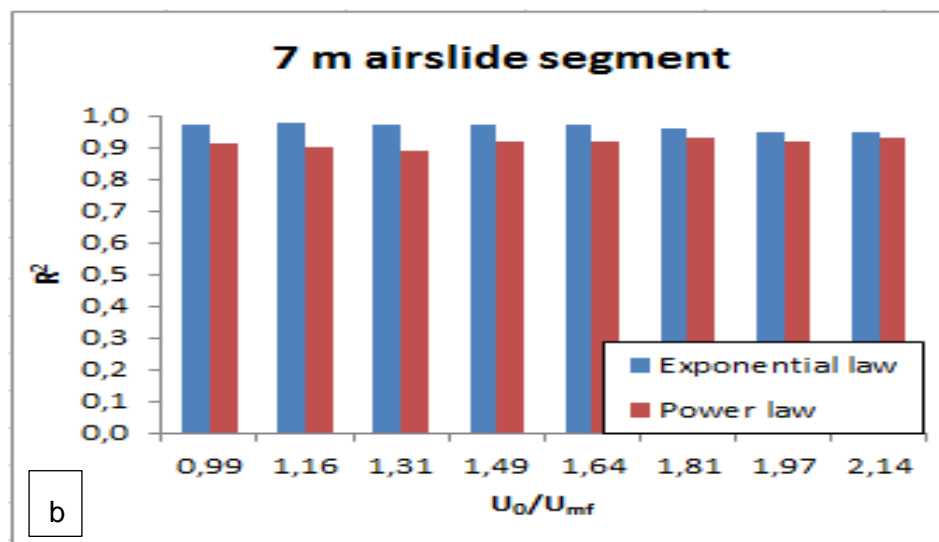
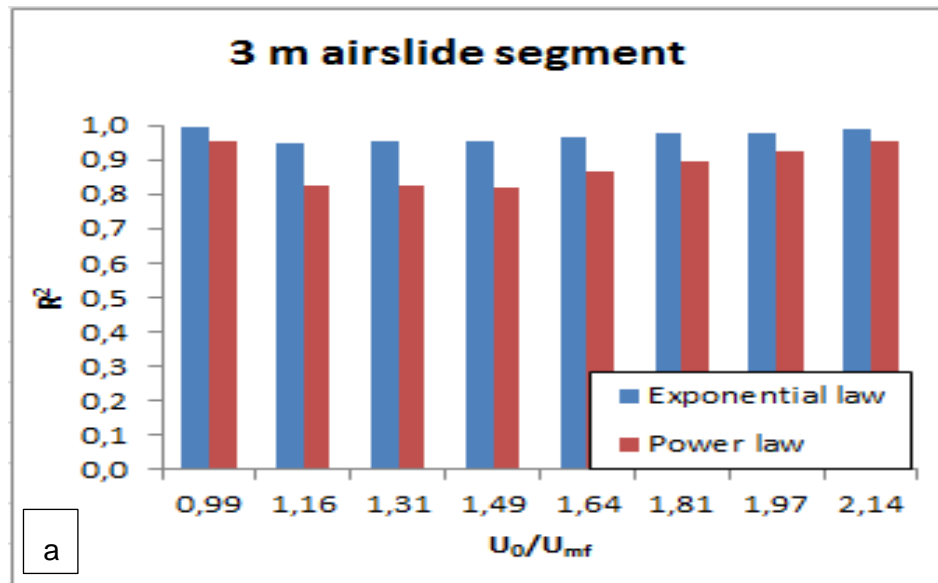
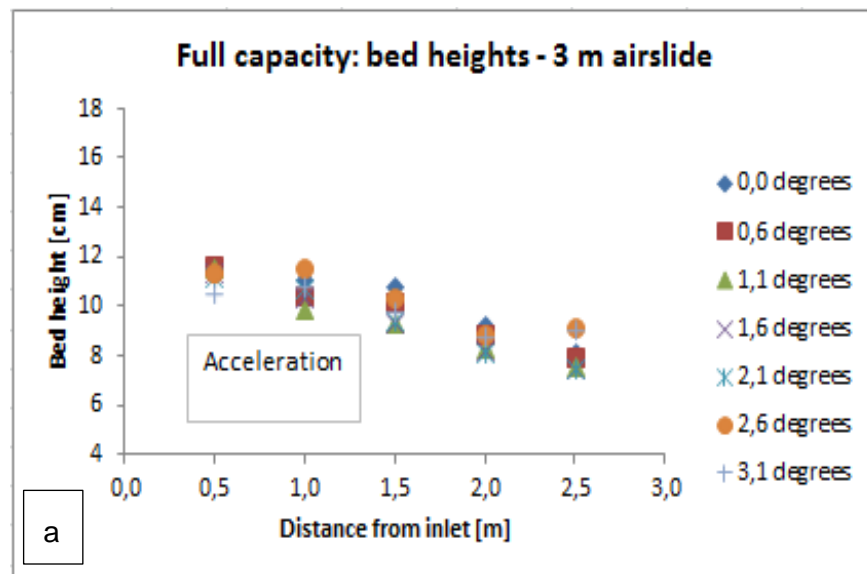


Figure 100 Comparison of  $R^2$  values for exponential and power law equations for a) 3 m, b) 7 m and c) 15 m long air slide segments.

The flow regime changes in a 15 m long air slide segment as it can be seen from Figure 100, where the values of the  $R^2$  decrease below 0.7 at low air velocities and below 0.8 at high air velocities in the exponential law model while they increase in the power law model. Bed height profiles in Figure 101 support this theory. One can see clearly from the measurement points that there is hardly any change in average bed velocity after 5.0 - 5.5 m away from the inlet in the 12 m long air slide segment. It should be mentioned that no measurements were taken in the 12 m long air slide segment in the region between 3 m and 5.5 m, so the steady state flow regime could have occurred at a shorter distance from inlet than 5.0 - 5.5 m. In the absence of measurement points in the region 3 m - 5.5 m from the inlet, one cannot draw any conclusion based on estimation or speculate, so that why we stick to 5.0 – 5.5 m. As it can be seen from Figure 101 when the length of the steady state zone becomes longer than the length of the acceleration zone, the exponential model cannot be used to predict average bed velocity as it is not optimal longer.



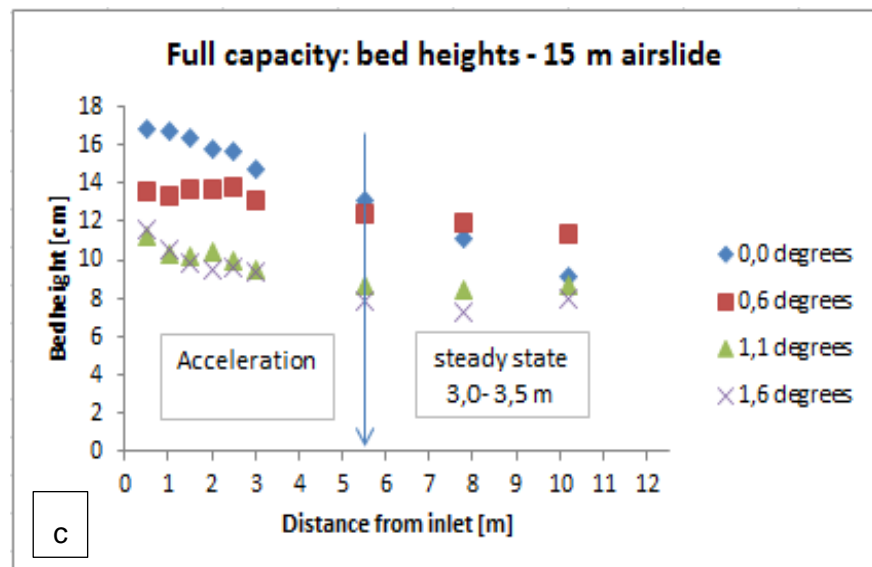
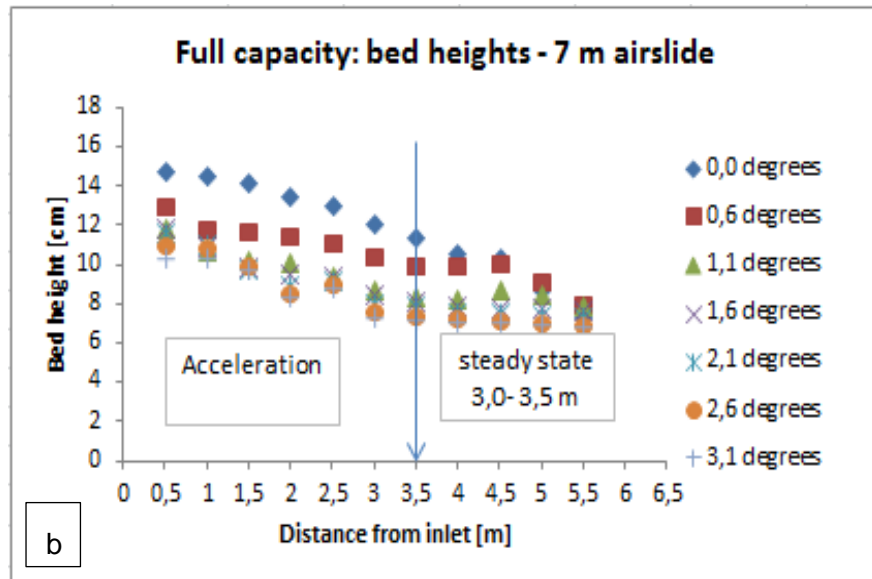


Figure 101 Full capacity bed heights profiles in a) 3 m, b) 7 m, c) 15 m long air slide segment.

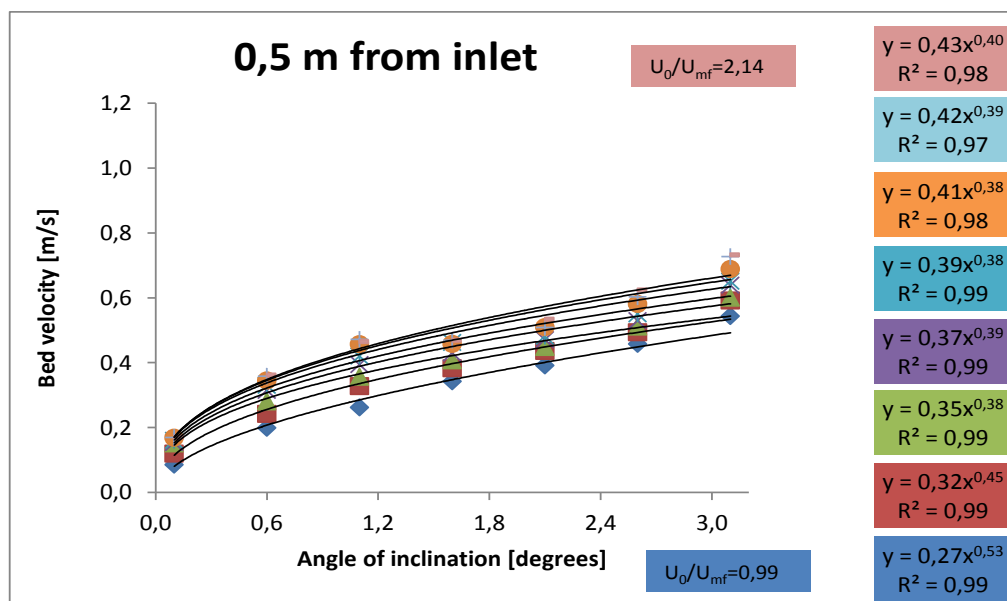
The exponential model could be applied only in short air slides where the acceleration zone is dominant. As a conclusion, the scope of analysis to find a mathematical law applicable in all segment lengths of air slide based on a single average power exponent used for the entire length of each air slide segment in order to predict bed velocity was achieved. The power law can thus be applied for all air slide segments, so the same analysis approach for predicting average bed velocity will be used in the 7 m and 15 m air slide segments. A model to predict bed heights will not be addressed at this stage, it will be addressed in the next chapter and will be based on physical modelling.

### 6.2.3 7 m long air slide segment

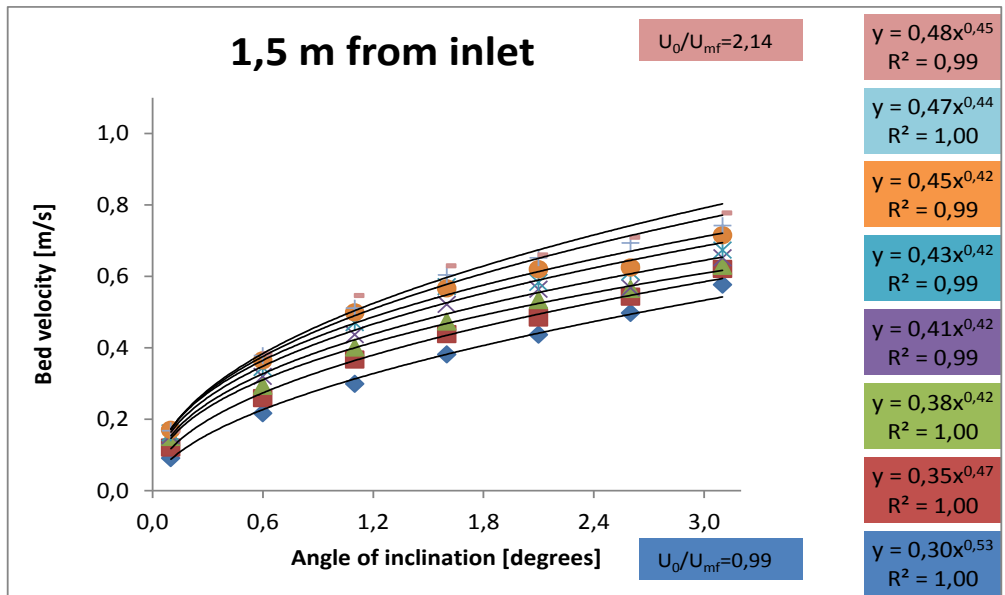
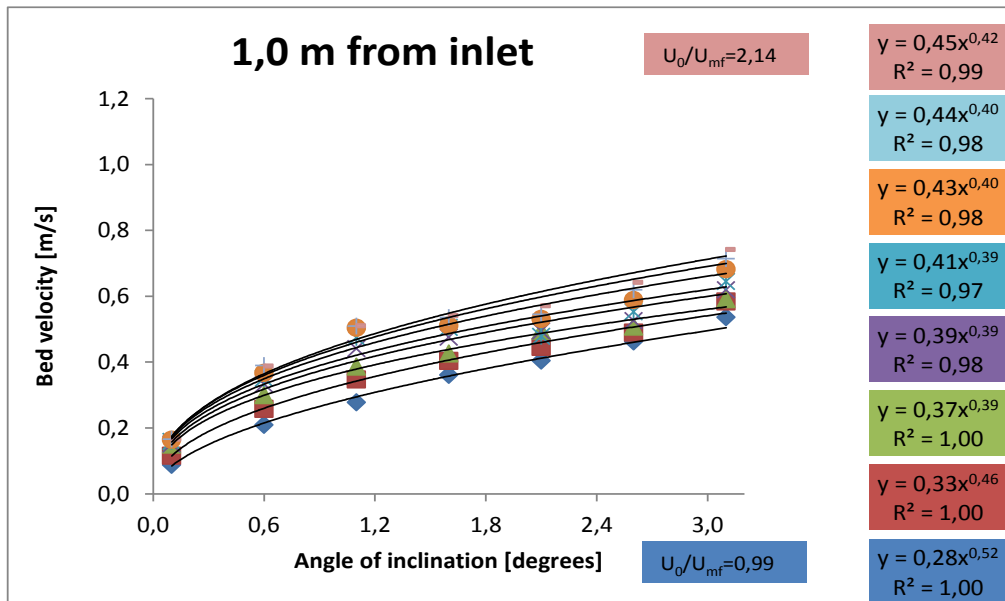
Data analysis in a 3 m long air slide segment showed that flow rates were accelerating, the length of the air slide was too short for the flow to achieve steady state. A 4 m air slide segment has been attached to the existing 3 m segment in order to investigate the relationship between acceleration and steady state zone lengths and the length of air slide segment. A similar analysis of the data as described in the last section will be performed on the 7 m air slide segment. The same method was applied for all measurement points from 0.5 to 7 m distance from inlet at all angles of downward inclination from 0 to 3.1 degrees and for all ranges at dimensionless coefficient of velocity in the range of 0.99 to 2.14.

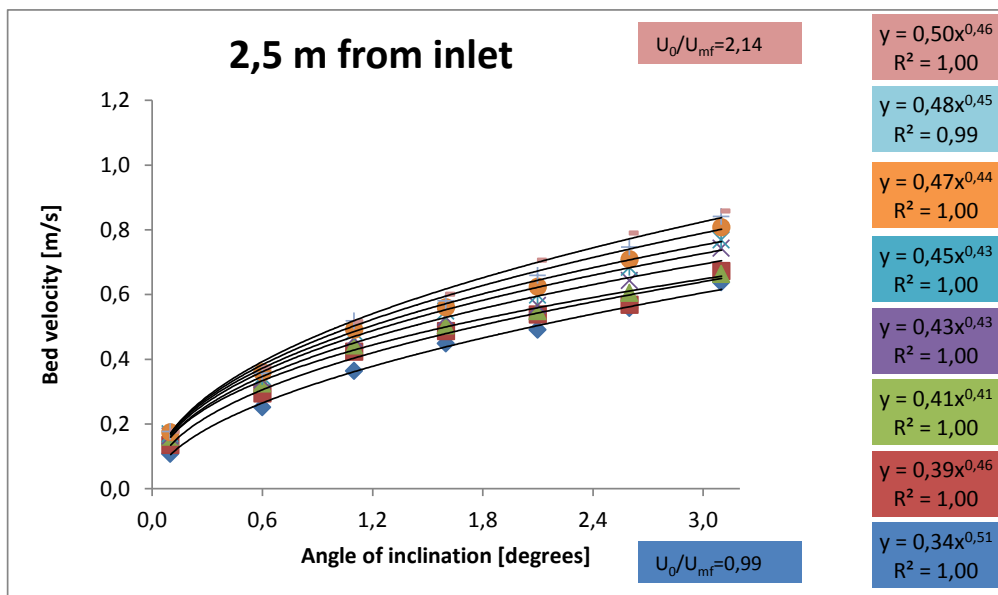
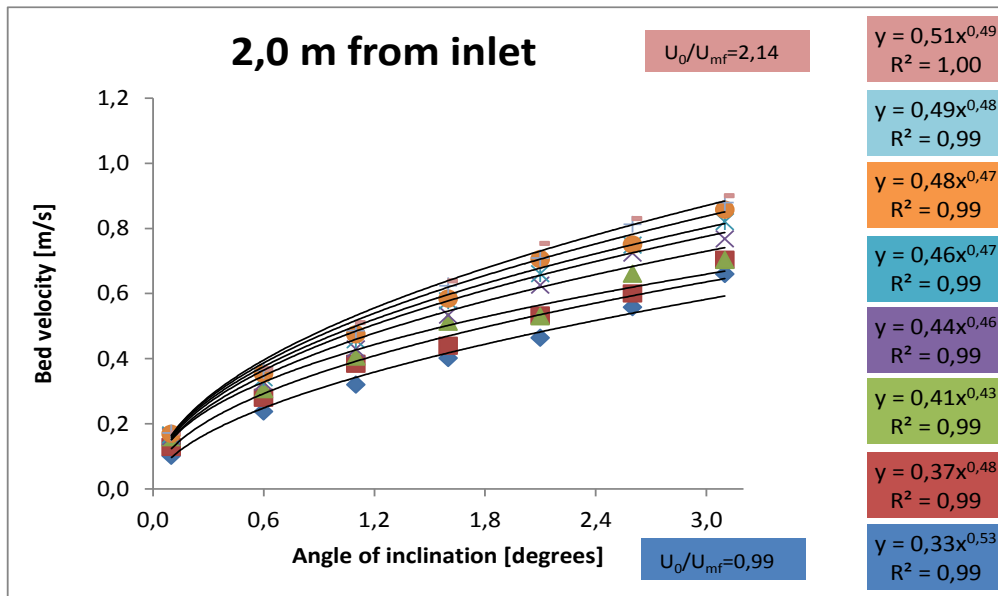
### 6.2.4 7 m - effect of inclination angle, $\theta$ on bed velocity at different distances away from inlet and at different dimensionless coefficient of velocity $U_0/U_{mf}$

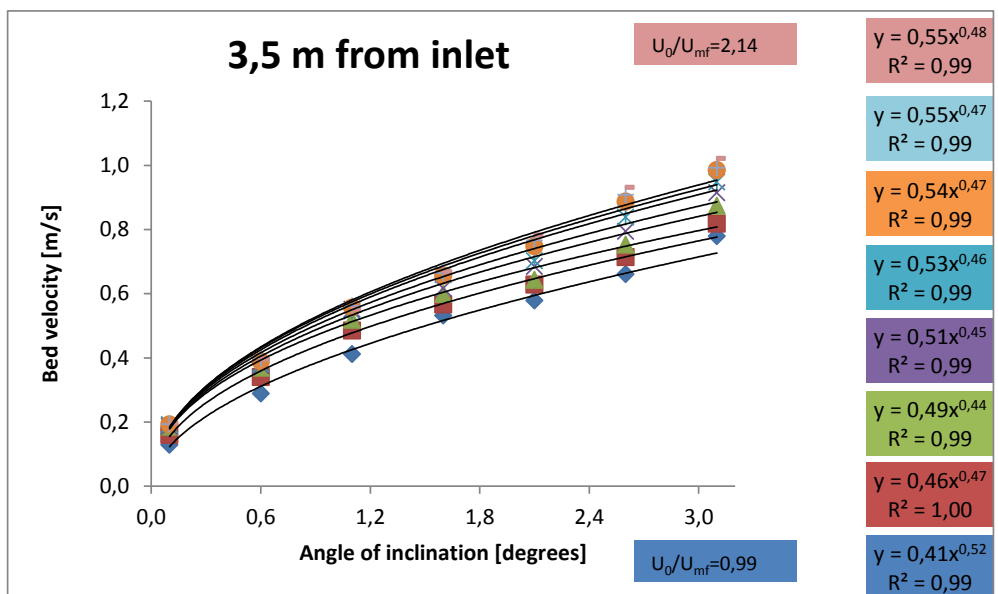
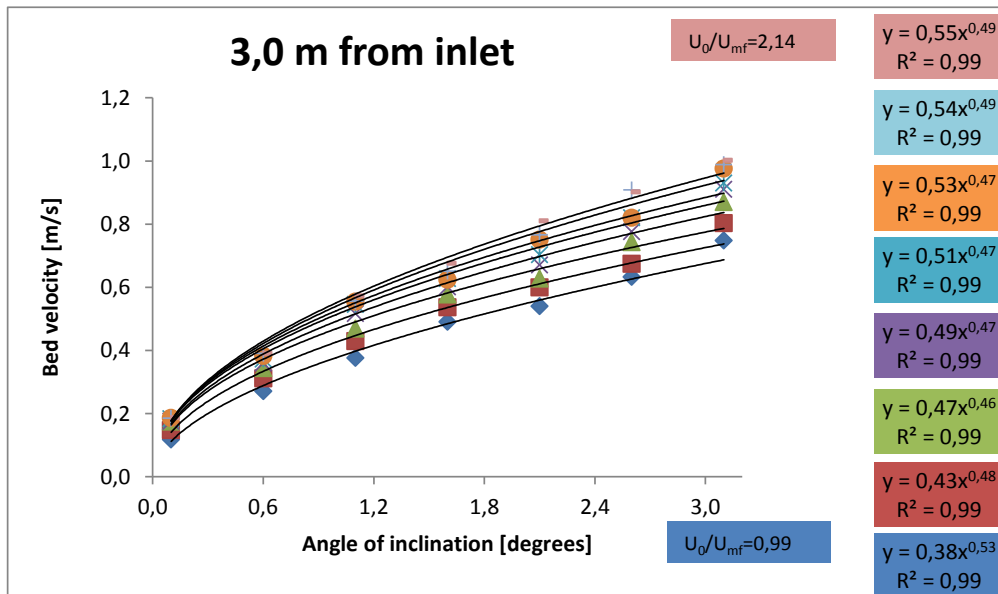
Power law curve fits were forced through all data as illustrated in Figure 102.

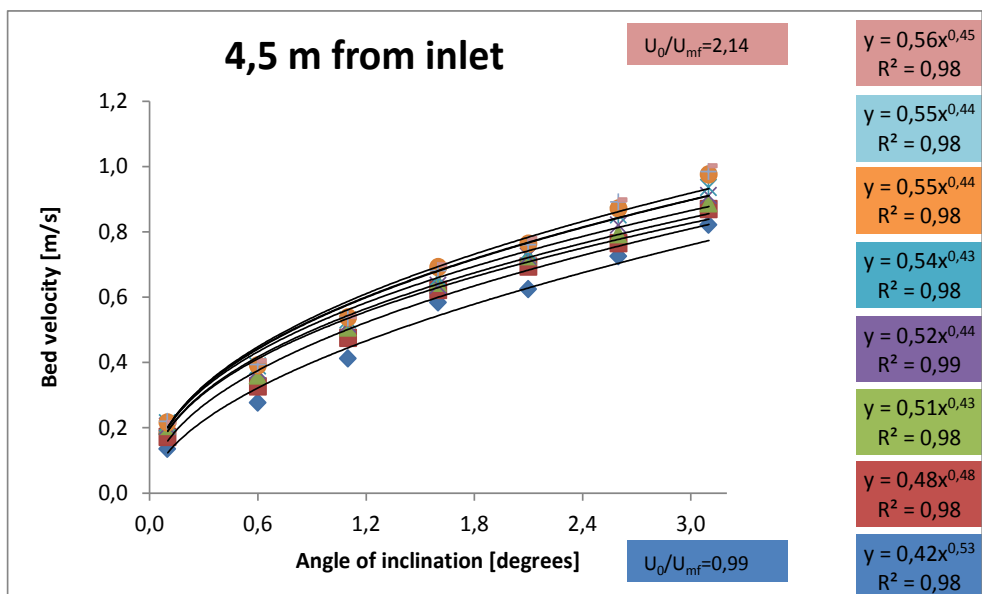
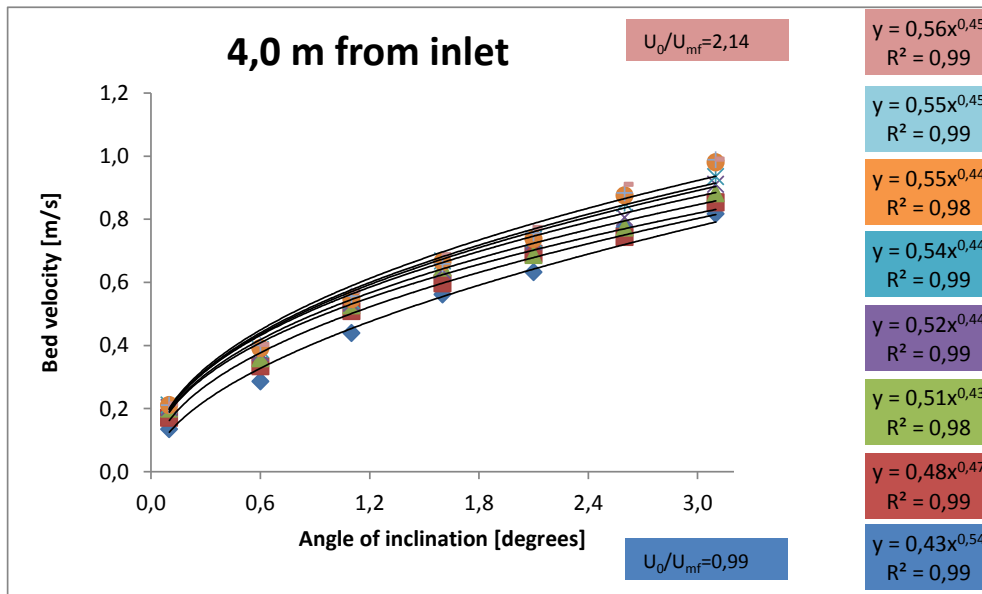












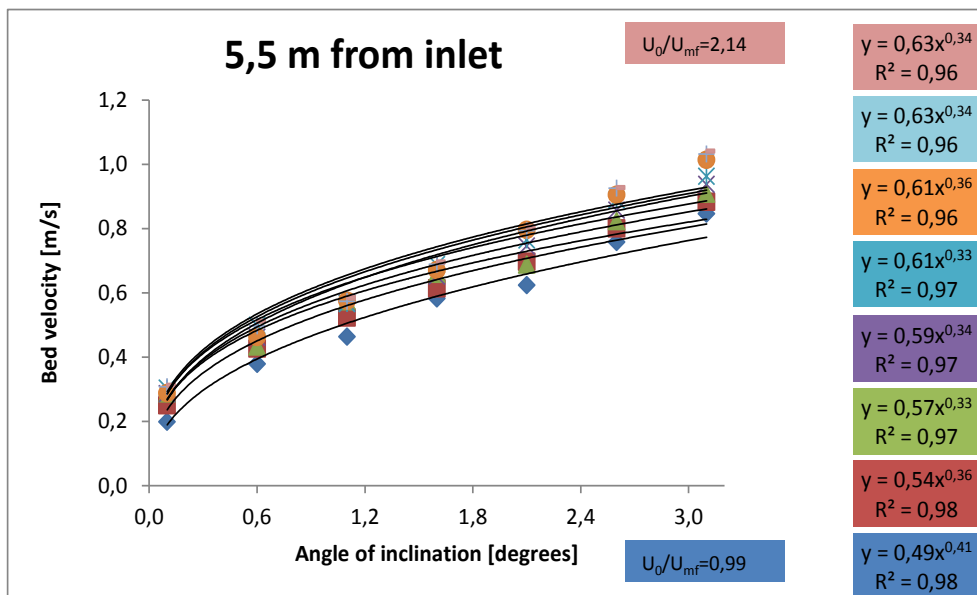
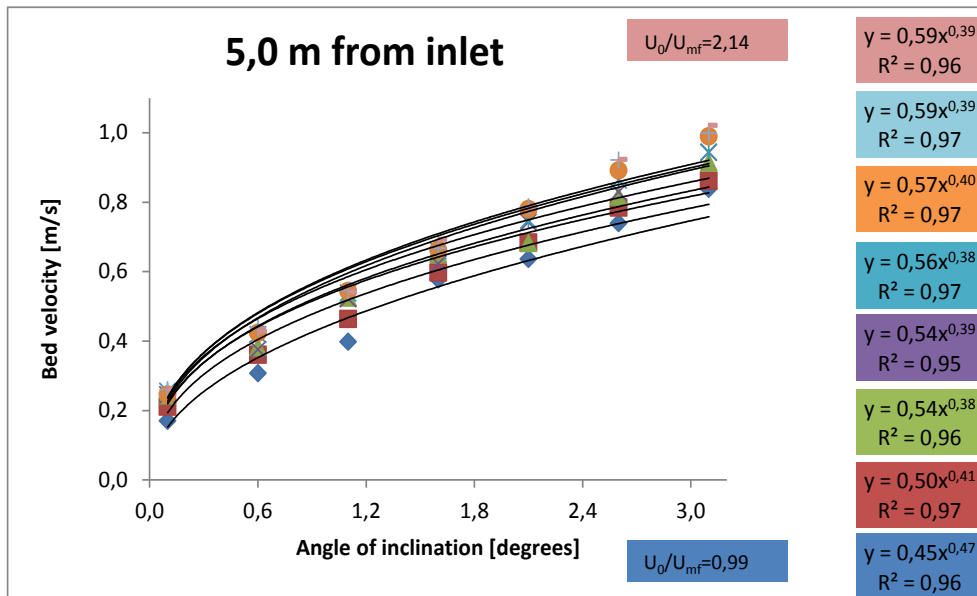
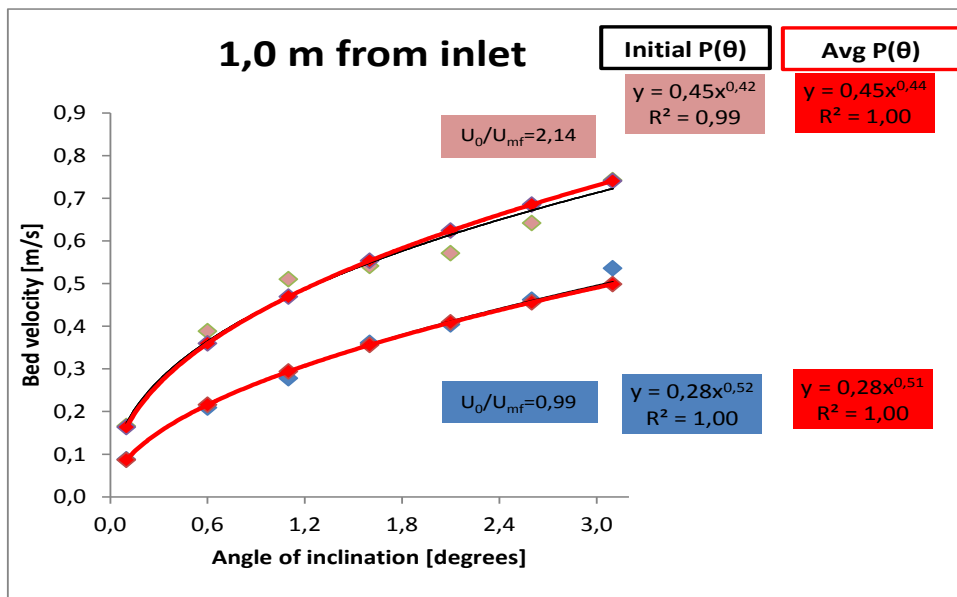
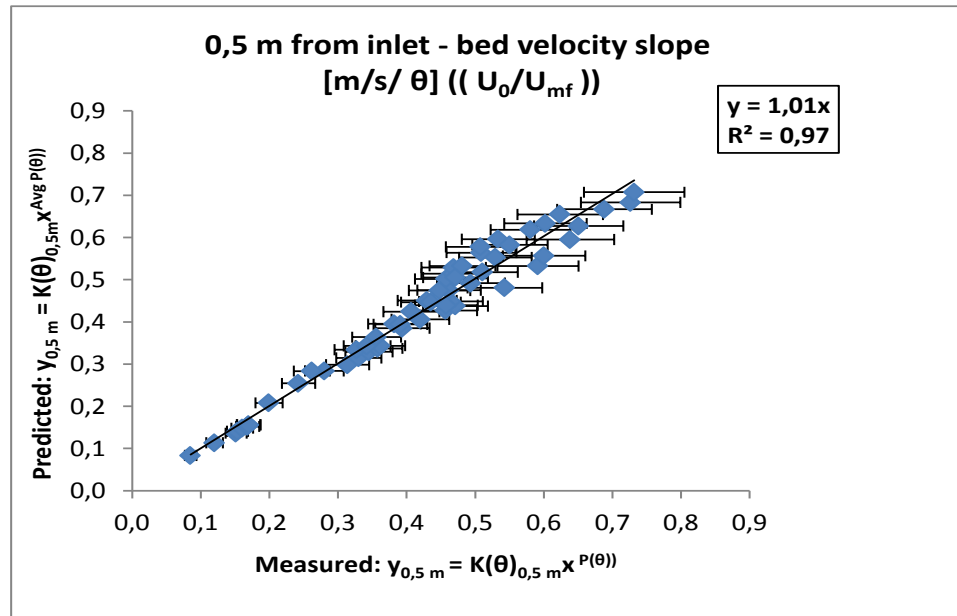
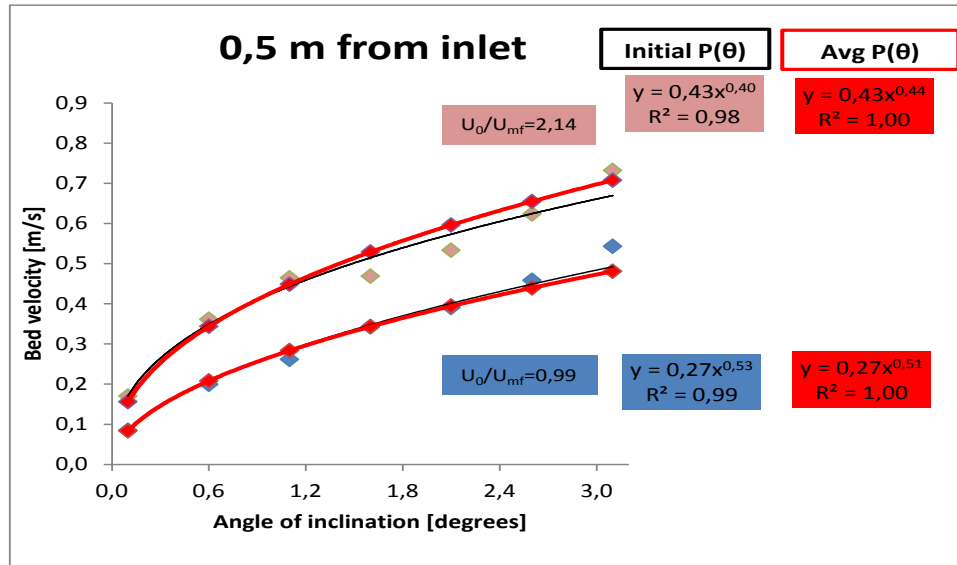


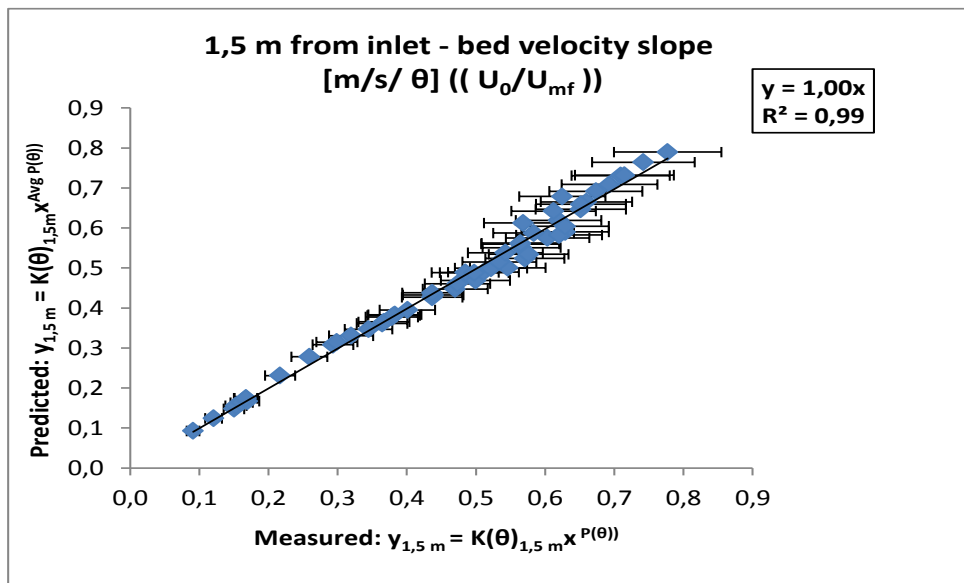
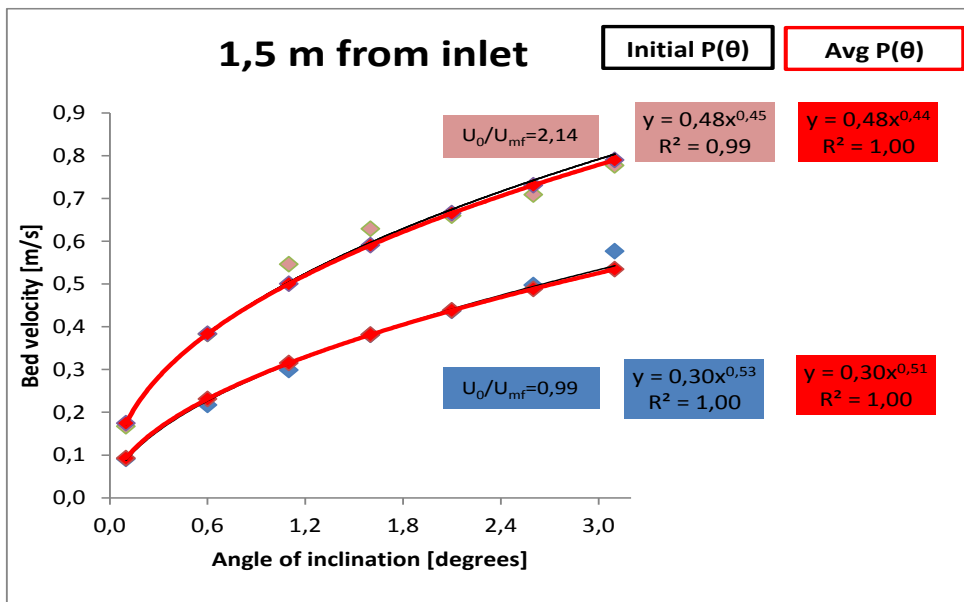
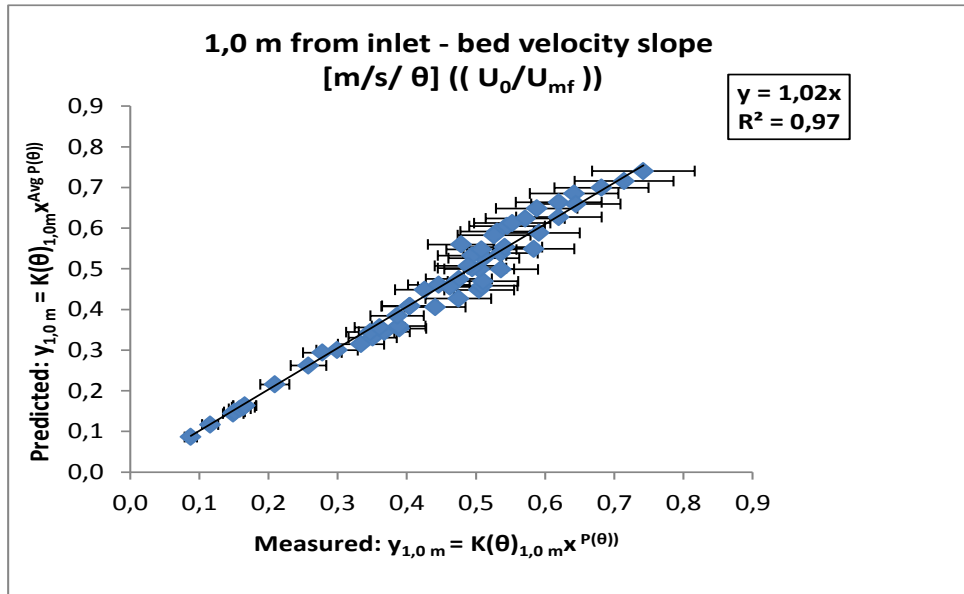
Figure 102 Power law trend lines fitted to experimental data of average bed velocity as a function of angle of inclination,  $\theta = 0.3 \cdot 10^0$  at different  $U_0/U_{mf} = 0.99 \dots 2.14$ .

Figure 102 shows similar trends as Table 28, for the 3 m segment.

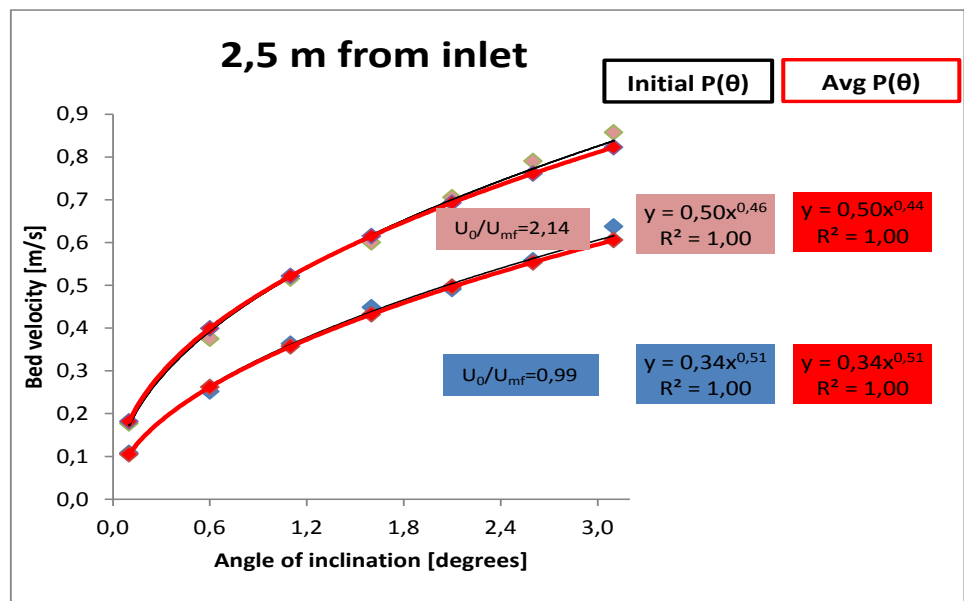
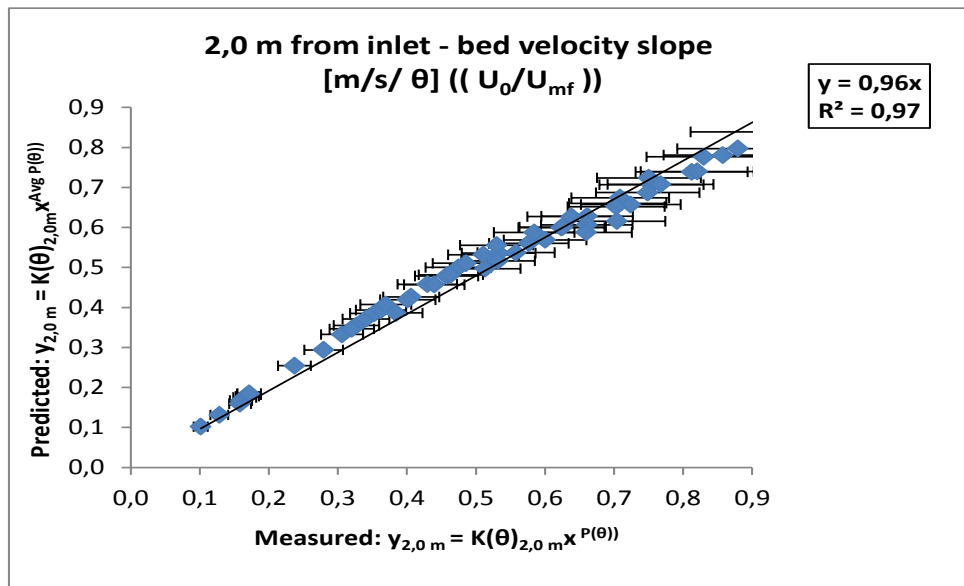
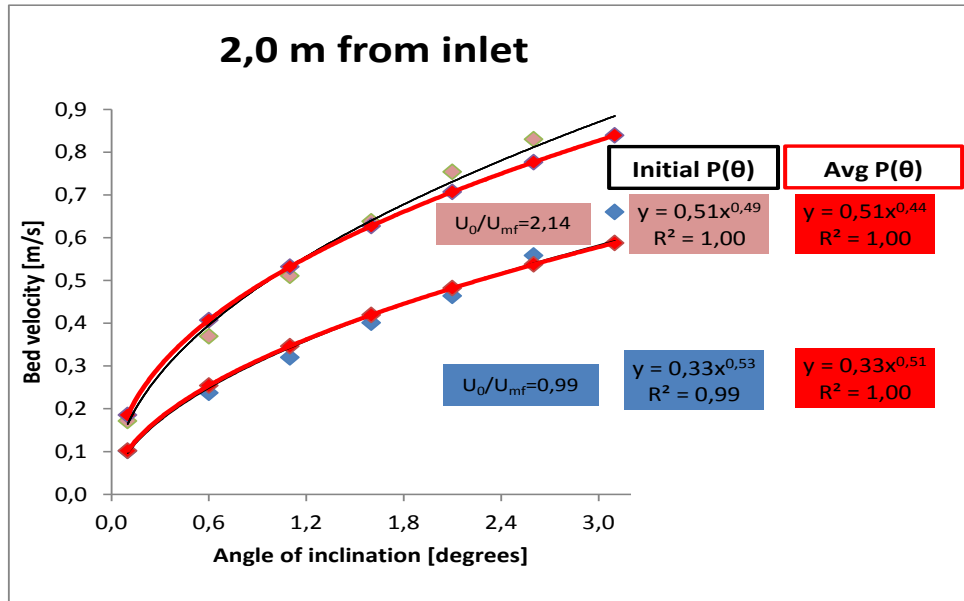
**Table 30 Power law trend lines fitted to experimental data for average bed velocity at all angles of inclination,  $\theta$ , at different  $U_0/U_{mf}$  for each measurement point from 0.5 to 5.5 m.  $K(\theta)$  is the coefficient and  $P(\theta)$  is the exponent of power law.**

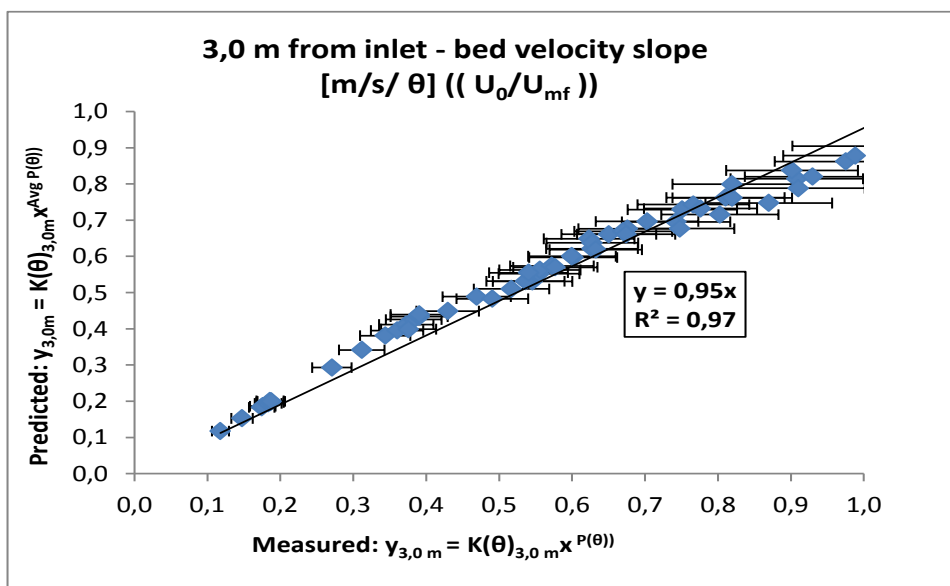
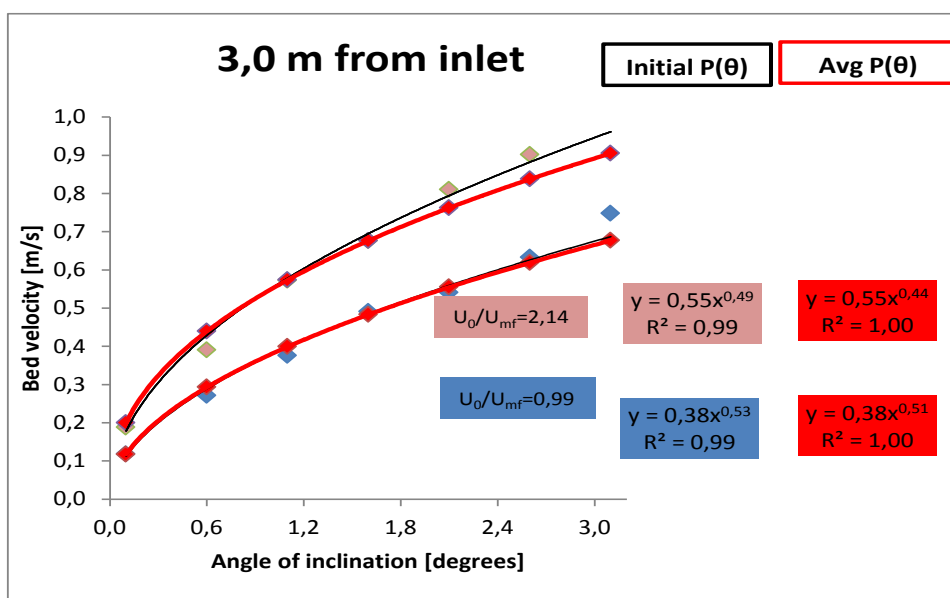
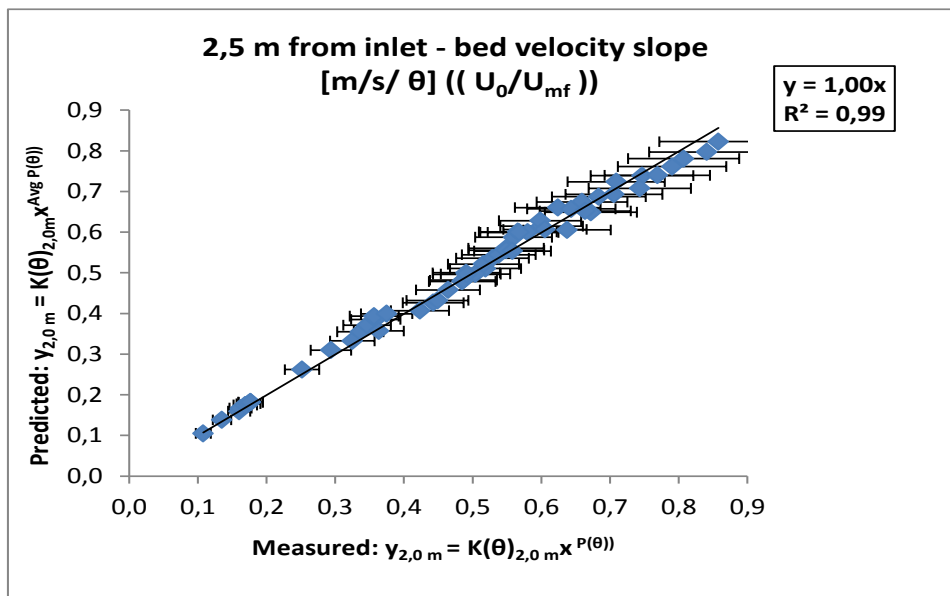
7 m - $K(\theta)$ - Bed velocity slope [m/s/ $\theta$ ] (( $U_0/U_{mf}$ ))																		
$U_0/U_{mf}$	$R^2$	$K(\theta)_{0.5\text{ m}}$	$P(\theta)_{0.5\text{ m}}$	$R^2$	$K(\theta)_{1.0\text{ m}}$	$P(\theta)_{1.0\text{ m}}$	$R^2$	$K(\theta)_{1.5\text{ m}}$	$P(\theta)_{1.5\text{ m}}$	$R^2$	$K(\theta)_{2.0\text{ m}}$	$P(\theta)_{2.0\text{ m}}$	$R^2$	$K(\theta)_{2.5\text{ m}}$	$P(\theta)_{2.5\text{ m}}$	$R^2$	$K(\theta)_{3.0\text{ m}}$	$P(\theta)_{3.0\text{ m}}$
<b>0,99</b>	0,99	0,27	0,53	1,00	0,28	0,52	1,00	0,30	0,53	0,99	0,33	0,53	1,00	0,34	0,51	0,99	0,38	0,53
<b>1,16</b>	0,99	0,32	0,45	1,00	0,33	0,46	1,00	0,35	0,47	0,99	0,37	0,48	1,00	0,39	0,46	0,99	0,43	0,48
<b>1,31</b>	0,99	0,35	0,38	1,00	0,37	0,39	1,00	0,38	0,42	0,99	0,41	0,43	1,00	0,41	0,41	0,99	0,47	0,46
<b>1,49</b>	0,99	0,37	0,39	0,98	0,39	0,39	0,99	0,41	0,42	0,99	0,44	0,46	1,00	0,44	0,43	0,99	0,49	0,47
<b>1,64</b>	0,99	0,39	0,38	0,97	0,41	0,39	0,99	0,43	0,42	0,99	0,46	0,47	1,00	0,46	0,43	0,99	0,51	0,47
<b>1,81</b>	0,98	0,41	0,38	0,98	0,43	0,4	0,99	0,45	0,42	0,99	0,48	0,47	1,00	0,48	0,44	0,99	0,53	0,47
<b>1,97</b>	0,97	0,42	0,39	0,98	0,44	0,4	1,00	0,47	0,44	0,99	0,49	0,48	0,99	0,49	0,45	0,99	0,54	0,49
<b>2,14</b>	0,98	0,43	0,4	0,99	0,45	0,42	0,99	0,48	0,45	1,00	0,51	0,49	1,00	0,50	0,46	0,99	0,55	0,49
$U_0/U_{mf}$	$R^2$	$K(\theta)_{3.5\text{ m}}$	$P(\theta)_{3.5\text{ m}}$	$R^2$	$K(\theta)_{4.0\text{ m}}$	$P(\theta)_{4.0\text{ m}}$	$R^2$	$K(\theta)_{4.5\text{ m}}$	$P(\theta)_{4.5\text{ m}}$	$R^2$	$K(\theta)_{5.0\text{ m}}$	$P(\theta)_{5.0\text{ m}}$	$R^2$	$K(\theta)_{5.5\text{ m}}$	$P(\theta)_{5.5\text{ m}}$	Avg $P(\theta)$	Stdev/Avg $P(\theta)$	
<b>0,99</b>	0,99	0,41	0,52	0,99	0,43	0,54	0,98	0,42	0,53	0,96	0,45	0,47	0,98	0,49	0,41	<b>0,51</b>	<b>5%</b>	
<b>1,16</b>	1,00	0,46	0,47	0,99	0,48	0,47	0,98	0,48	0,48	0,97	0,50	0,41	0,98	0,54	0,36	<b>0,45</b>	<b>6%</b>	
<b>1,31</b>	0,99	0,49	0,44	0,98	0,51	0,43	0,98	0,51	0,43	0,96	0,54	0,38	0,97	0,57	0,33	<b>0,41</b>	<b>7%</b>	
<b>1,49</b>	0,99	0,51	0,45	0,99	0,52	0,44	0,99	0,52	0,44	0,95	0,54	0,39	0,97	0,59	0,34	<b>0,42</b>	<b>7%</b>	
<b>1,64</b>	0,99	0,53	0,46	0,98	0,54	0,44	0,98	0,54	0,43	0,97	0,56	0,38	0,97	0,61	0,33	<b>0,42</b>	<b>9%</b>	
<b>1,81</b>	0,99	0,54	0,47	0,99	0,55	0,44	0,98	0,55	0,44	0,97	0,57	0,40	0,96	0,61	0,36	<b>0,43</b>	<b>8%</b>	
<b>1,97</b>	0,99	0,55	0,47	0,99	0,55	0,45	0,98	0,55	0,44	0,97	0,59	0,39	0,96	0,63	0,34	<b>0,43</b>	<b>9%</b>	
<b>2,14</b>	0,99	0,55	0,48	0,99	0,56	0,45	0,98	0,56	0,45	0,96	0,59	0,39	0,96	0,63	0,34	<b>0,44</b>	<b>9%</b>	

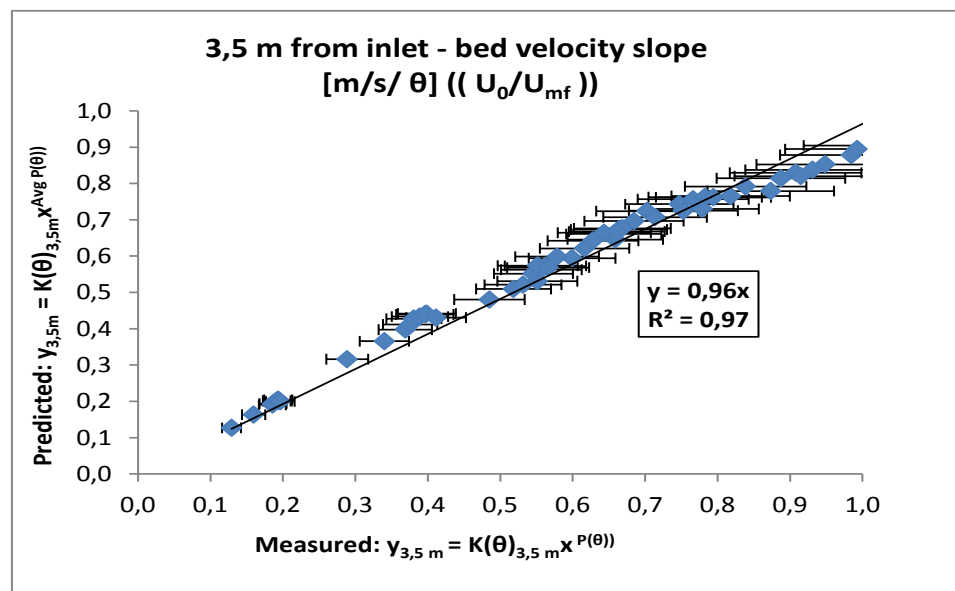
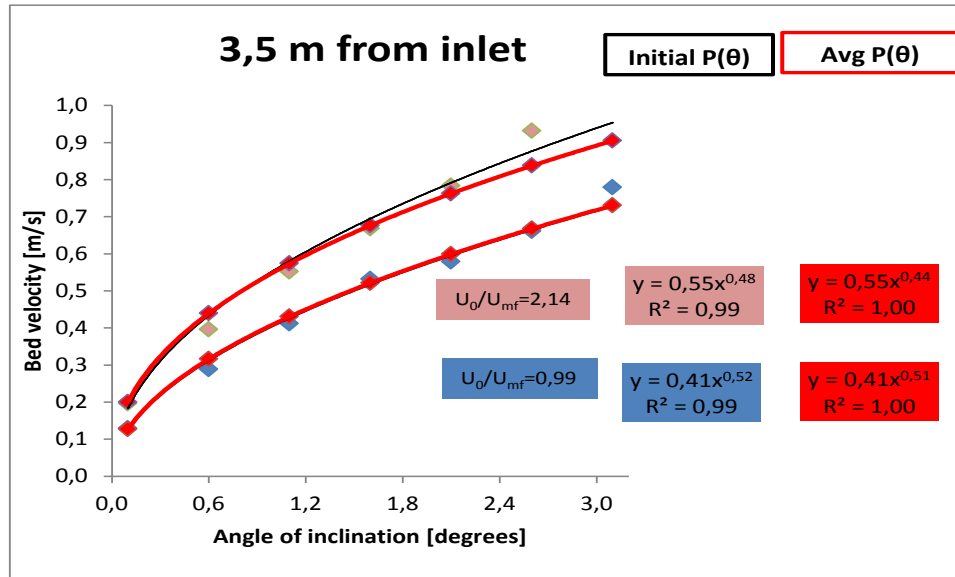


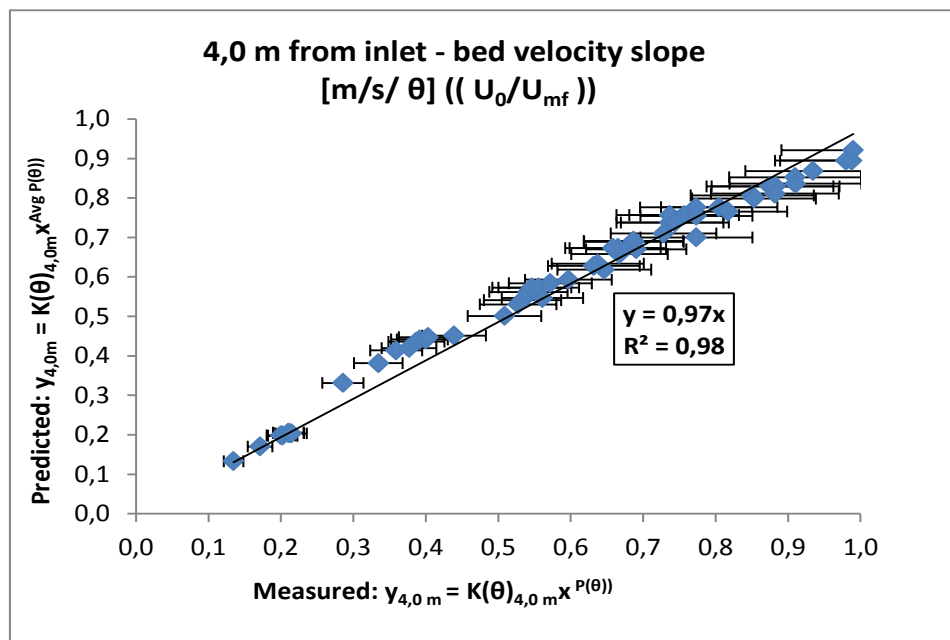
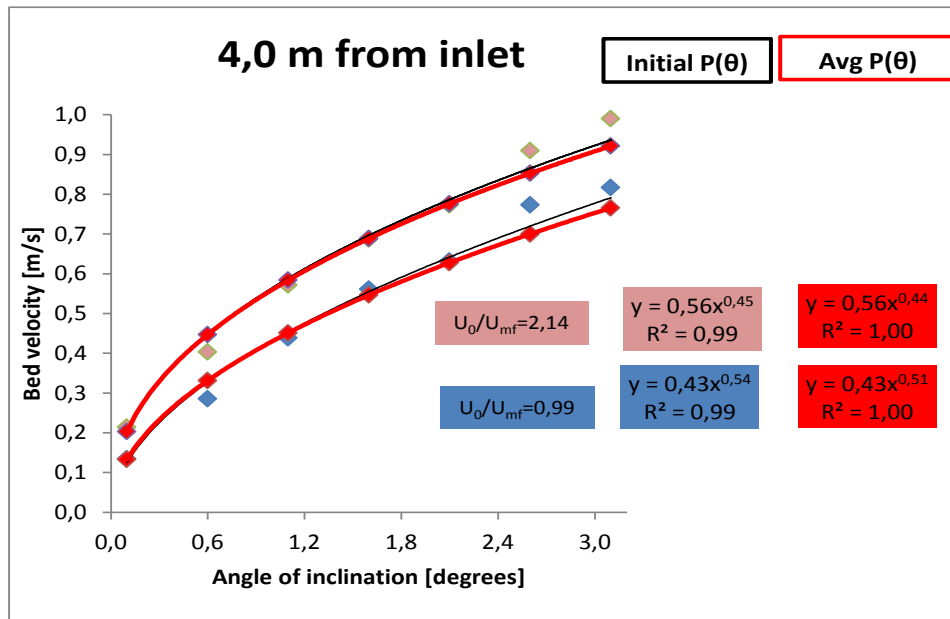


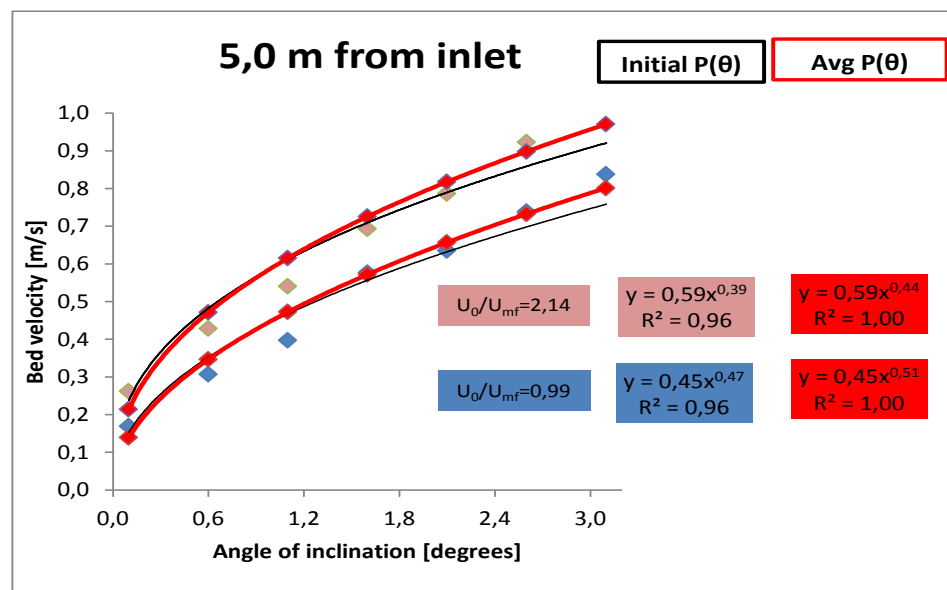
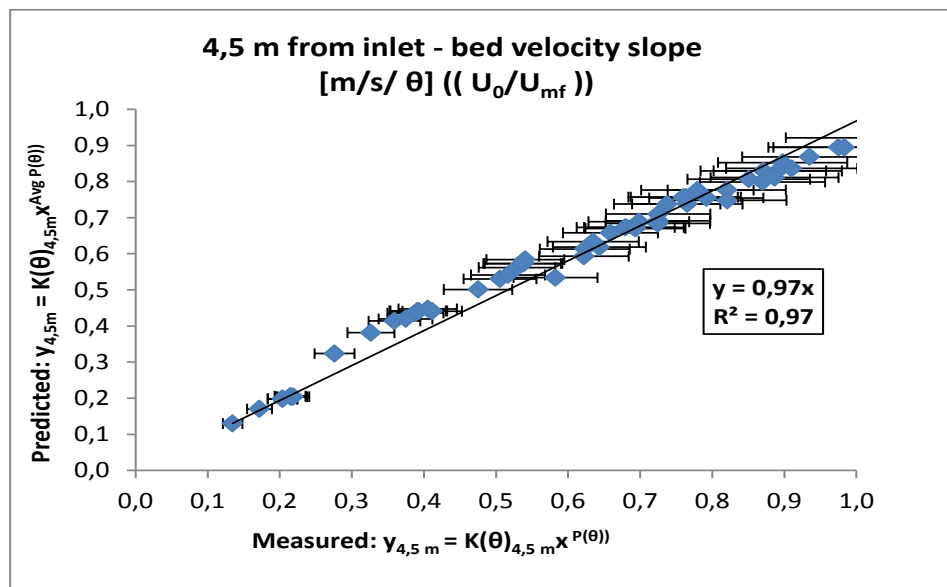
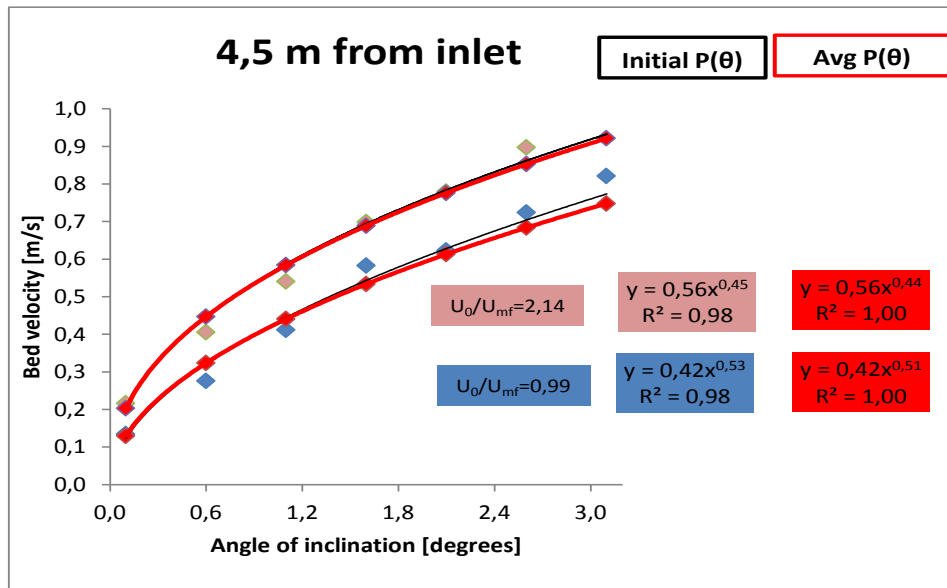












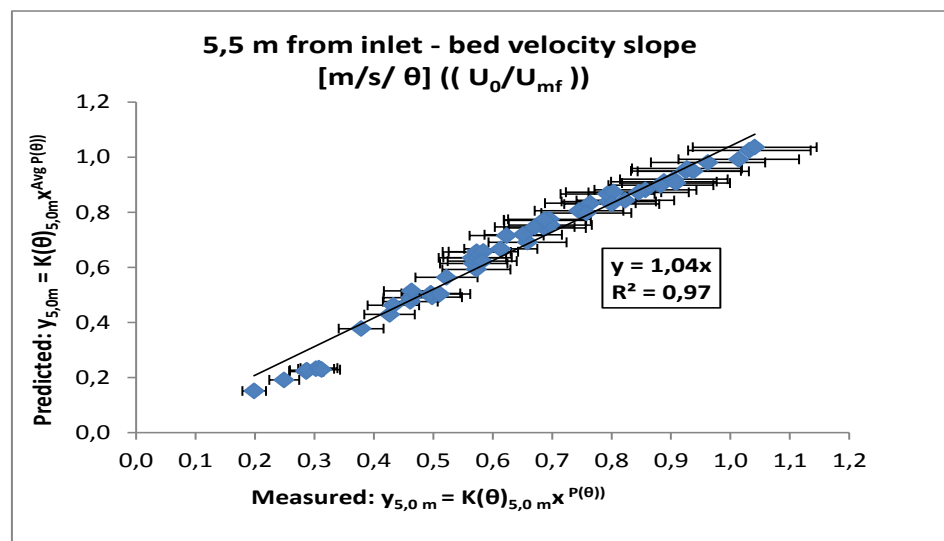
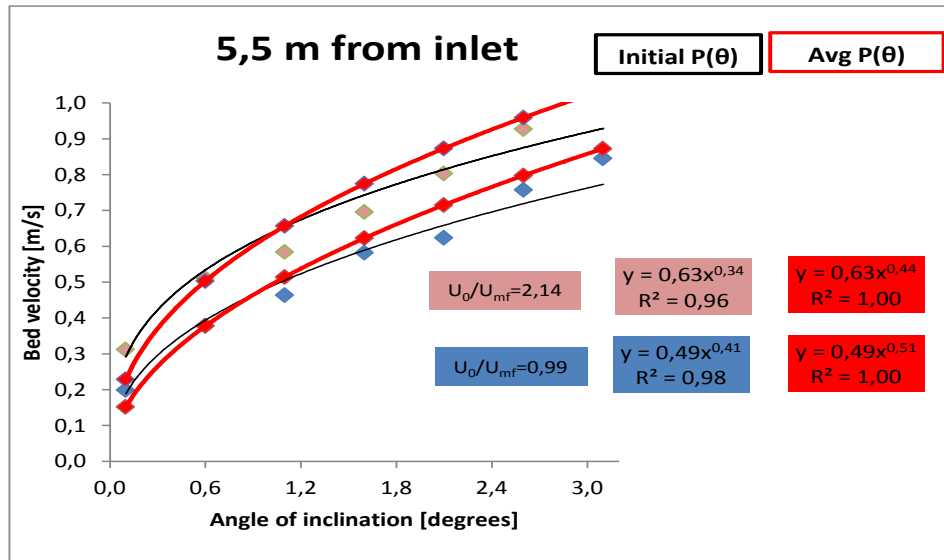
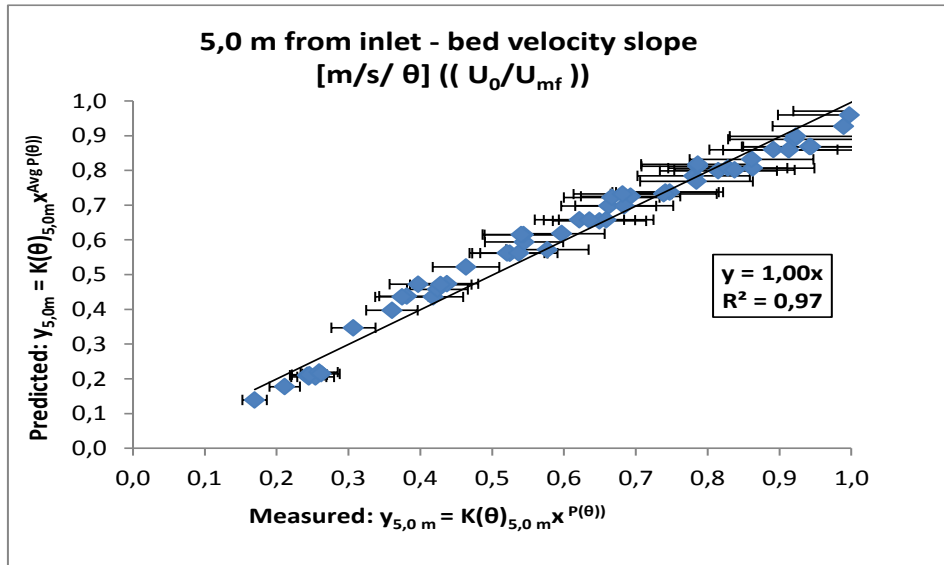


Figure 103 Investigation of the effect of changing power law exponent,  $P(\theta)$  for  $U_0/U_{mf} = 0.99$  and  $U_0/U_{mf} = 2.14$ . Ten percent error bars showing the goodness of the mathematical method for all ranges of  $U_0/U_{mf}$  from 0.99 to 2.14.

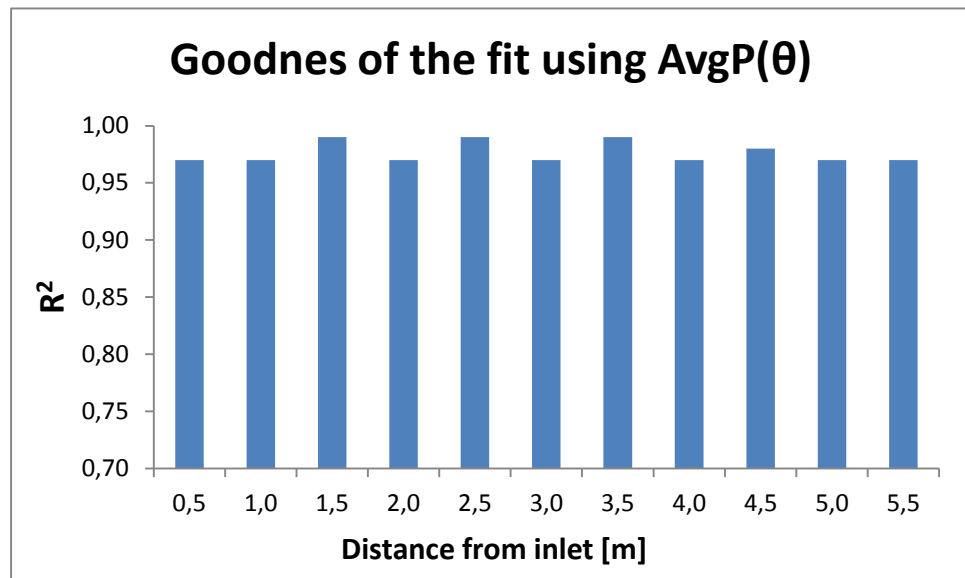


Figure 104 Values of  $R^2$  expressing the goodnes of the fit when using  $AvgP(\theta)$  instead of  $P(\theta)$  into the power trend lines fitted to experimental data.

The scope of the analysis was again, as in the 3 m long air slide segment, to find a mathematical law applicable in all segment lengths of air slide based on a single average power exponent used for the entire length of each air slide segment in order to predict bed velocity. Figure 104 presents values of  $R^2$  from using  $Avg P(\theta)$  power law exponent presented graphically in Figure 103. If  $R^2$  is greater than 0.80, there is a good fit to the data. This means that between 97 to 99 % of the variation of the bed velocity data can be explained by a bed velocity power law based on  $P(\theta)$ .

#### 6.2.5 7 m - bed velocity slope $K(\theta)$ , versus distance from inlet at different $U_0/U_{mf}$

Table 31 shows results of power law model by using single average power exponent,  $AvgP(\theta)$ , a summary of both Figure 102 and Figure 103.

**Table 31 Results of power law trend lines fitted to the experimental data by using single average power exponent,  $Avg P(\theta)$ , a summary of Table 30.**

<b>7 m - <math>K(\theta)</math> - Bed velocity slope [m/s/ <math>\theta</math>] (<math>(U_o/U_{mf})</math>)</b>						
<b><math>U_o/U_{mf}</math></b>	<b><math>Y_{0,5 m} = K(\theta)_{0,5 m} X^{Avg P(\theta)}</math></b>	<b><math>Y_{1,0 m} = K(\theta)_{1,0 m} X^{Avg P(\theta)}</math></b>	<b><math>Y_{1,5 m} = K(\theta)_{1,5 m} X^{Avg P(\theta)}</math></b>	<b><math>Y_{2,0 m} = K(\theta)_{2,0 m} X^{Avg P(\theta)}</math></b>	<b><math>Y_{2,5 m} = K(\theta)_{2,5 m} X^{Avg P(\theta)}</math></b>	<b><math>Y_{3,0 m} = K(\theta)_{3,0 m} X^{Avg P(\theta)}</math></b>
<b>0,99</b>	$Y = 0,27x^{0,51}$	$Y = 0,28x^{0,51}$	$Y = 0,30x^{0,51}$	$Y = 0,33x^{0,51}$	$Y = 0,34x^{0,51}$	$Y = 0,38x^{0,51}$
<b>1,16</b>	$Y = 0,32x^{0,45}$	$Y = 0,33x^{0,45}$	$Y = 0,35x^{0,45}$	$Y = 0,37x^{0,45}$	$Y = 0,39x^{0,45}$	$Y = 0,43x^{0,45}$
<b>1,31</b>	$Y = 0,35x^{0,41}$	$Y = 0,37x^{0,41}$	$Y = 0,38x^{0,41}$	$Y = 0,41x^{0,41}$	$Y = 0,41x^{0,41}$	$Y = 0,47x^{0,41}$
<b>1,49</b>	$Y = 0,37x^{0,42}$	$Y = 0,39x^{0,42}$	$Y = 0,41x^{0,42}$	$Y = 0,44x^{0,42}$	$Y = 0,44x^{0,42}$	$Y = 0,49x^{0,42}$
<b>1,64</b>	$Y = 0,39x^{0,42}$	$Y = 0,41x^{0,42}$	$Y = 0,43x^{0,42}$	$Y = 0,46x^{0,42}$	$Y = 0,46x^{0,42}$	$Y = 0,51x^{0,42}$
<b>1,81</b>	$Y = 0,41x^{0,43}$	$Y = 0,43x^{0,43}$	$Y = 0,45x^{0,43}$	$Y = 0,48x^{0,43}$	$Y = 0,48x^{0,43}$	$Y = 0,53x^{0,43}$
<b>1,97</b>	$Y = 0,42x^{0,43}$	$Y = 0,44x^{0,43}$	$Y = 0,47x^{0,43}$	$Y = 0,49x^{0,43}$	$Y = 0,49x^{0,43}$	$Y = 0,54x^{0,43}$
<b>2,14</b>	$Y = 0,43x^{0,44}$	$Y = 0,45x^{0,44}$	$Y = 0,48x^{0,44}$	$Y = 0,51x^{0,44}$	$Y = 0,50x^{0,44}$	$Y = 0,55x^{0,44}$
<b><math>U_o/U_{mf}</math></b>	<b><math>Y_{3,5 m} = K(\theta)_{3,5 m} X^{Avg P(\theta)}</math></b>	<b><math>Y_{4,0 m} = K(\theta)_{4,0 m} X^{Avg P(\theta)}</math></b>	<b><math>Y_{4,5 m} = K(\theta)_{4,5 m} X^{Avg P(\theta)}</math></b>	<b><math>Y_{5,0 m} = K(\theta)_{5,0 m} X^{Avg P(\theta)}</math></b>	<b><math>Y_{5,5 m} = K(\theta)_{5,5 m} X^{Avg P(\theta)}</math></b>	
<b>0,99</b>	$Y = 0,41x^{0,51}$	$Y = 0,43x^{0,51}$	$Y = 0,42x^{0,51}$	$Y = 0,45x^{0,51}$	$Y = 0,49x^{0,51}$	
<b>1,16</b>	$Y = 0,46x^{0,45}$	$Y = 0,48x^{0,45}$	$Y = 0,48x^{0,45}$	$Y = 0,50x^{0,45}$	$Y = 0,54x^{0,45}$	
<b>1,31</b>	$Y = 0,49x^{0,41}$	$Y = 0,51x^{0,41}$	$Y = 0,51x^{0,41}$	$Y = 0,54x^{0,41}$	$Y = 0,57x^{0,41}$	
<b>1,49</b>	$Y = 0,51x^{0,42}$	$Y = 0,52x^{0,42}$	$Y = 0,52x^{0,42}$	$Y = 0,54x^{0,42}$	$Y = 0,59x^{0,42}$	
<b>1,64</b>	$Y = 0,53x^{0,42}$	$Y = 0,54x^{0,42}$	$Y = 0,54x^{0,42}$	$Y = 0,56x^{0,42}$	$Y = 0,61x^{0,42}$	
<b>1,81</b>	$Y = 0,54x^{0,43}$	$Y = 0,55x^{0,43}$	$Y = 0,55x^{0,43}$	$Y = 0,57x^{0,43}$	$Y = 0,61x^{0,43}$	
<b>1,97</b>	$Y = 0,55x^{0,43}$	$Y = 0,55x^{0,43}$	$Y = 0,55x^{0,43}$	$Y = 0,59x^{0,43}$	$Y = 0,63x^{0,43}$	
<b>2,14</b>	$Y = 0,55x^{0,44}$	$Y = 0,56x^{0,44}$	$Y = 0,56x^{0,44}$	$Y = 0,59x^{0,44}$	$Y = 0,63x^{0,44}$	



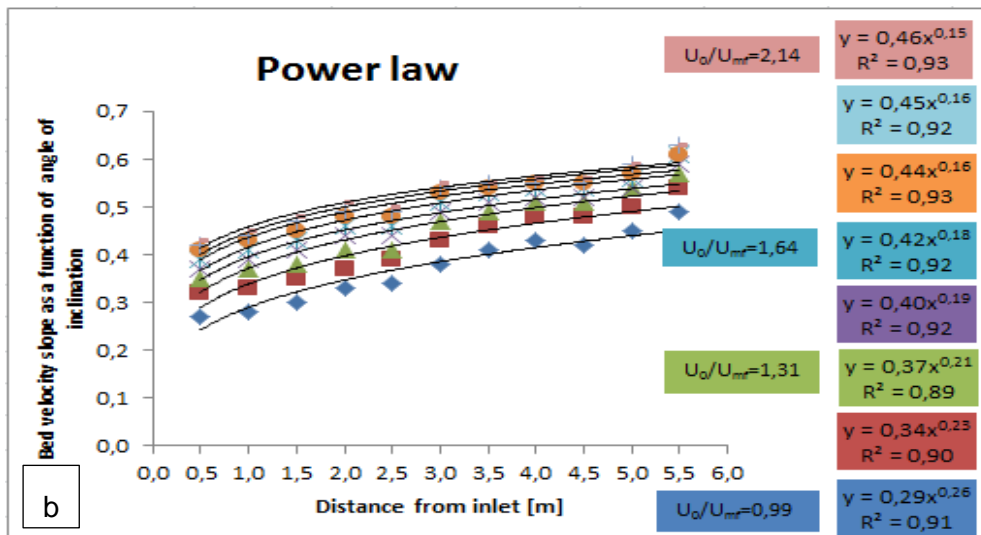
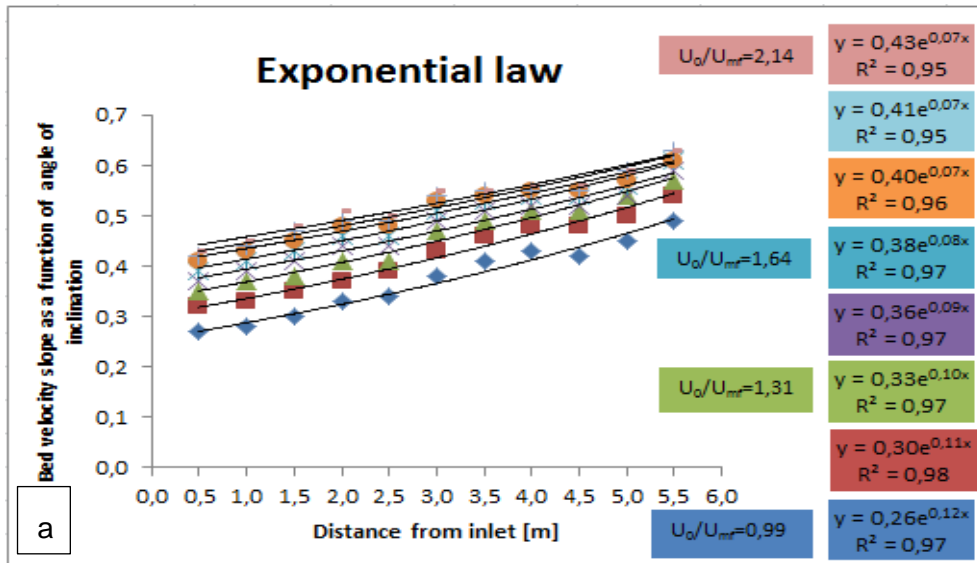
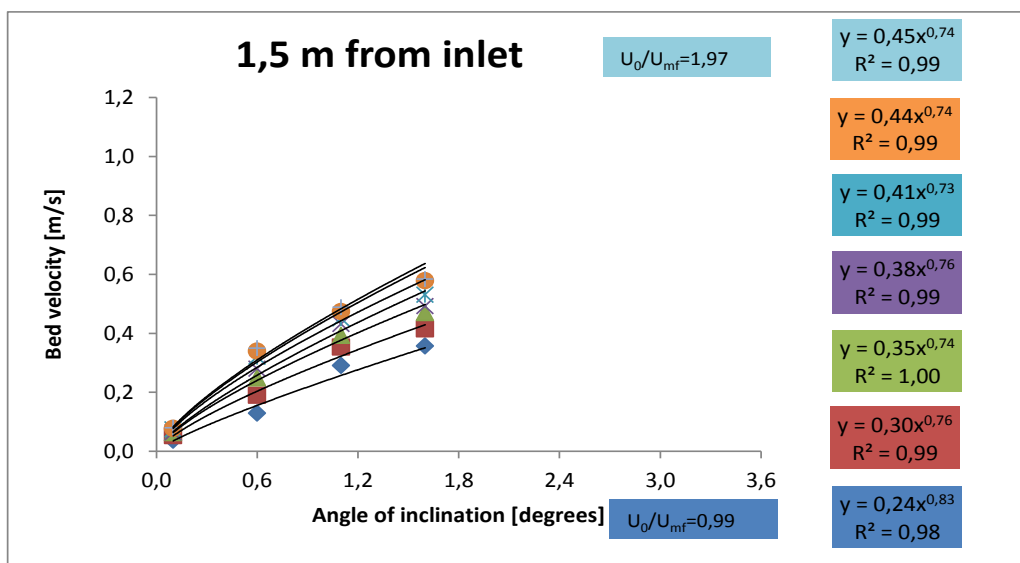
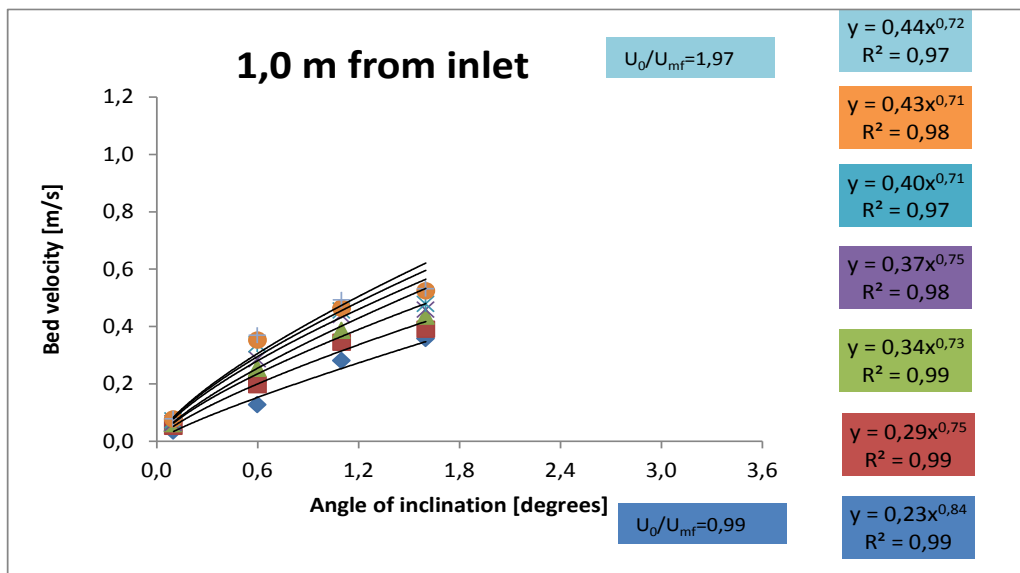
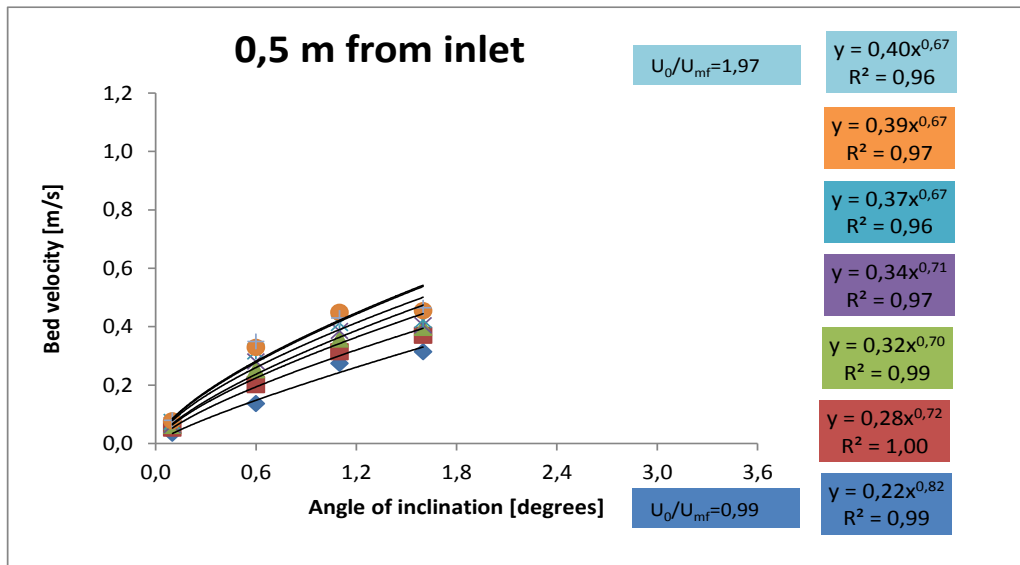
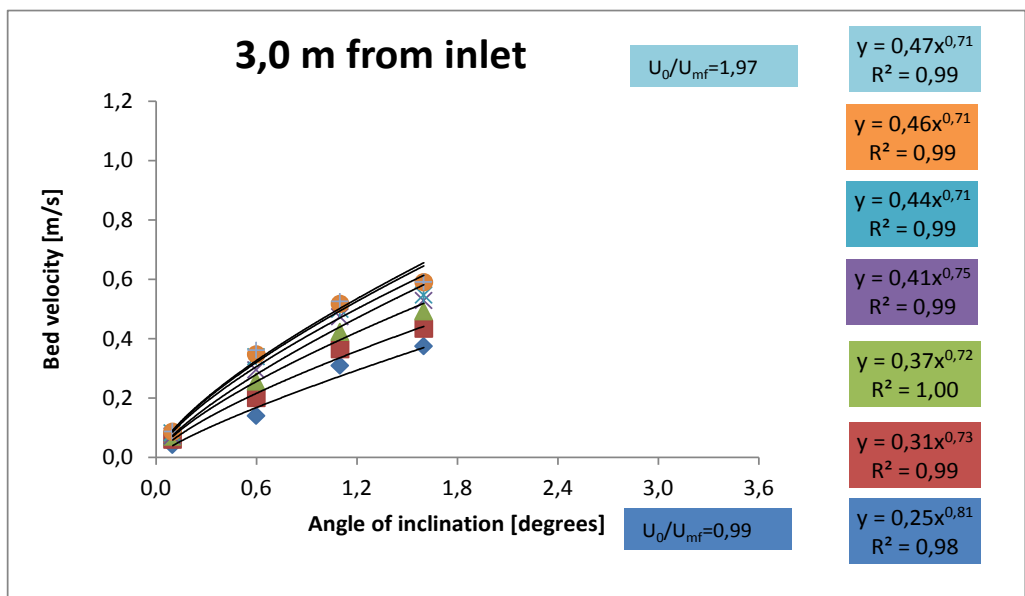
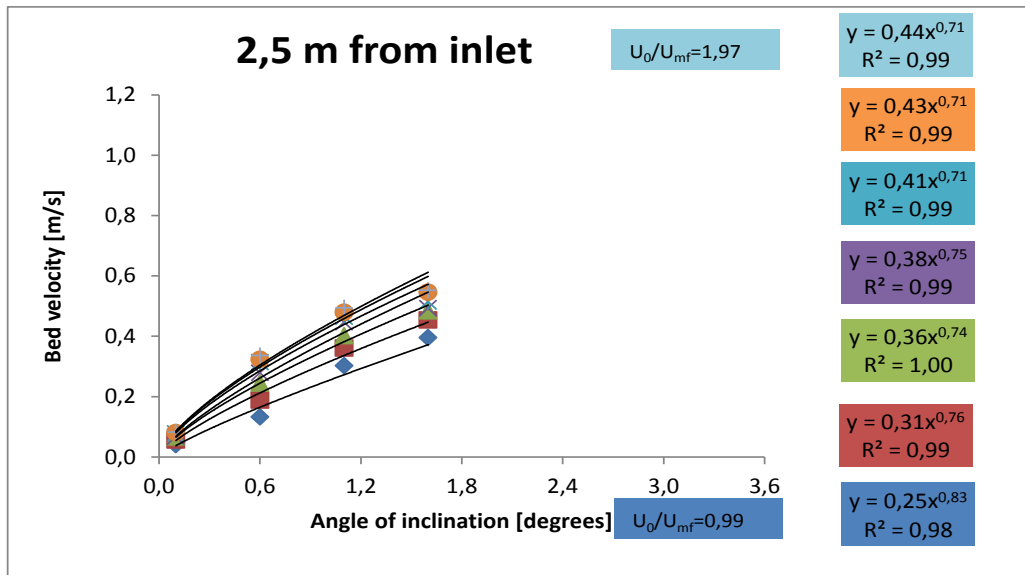
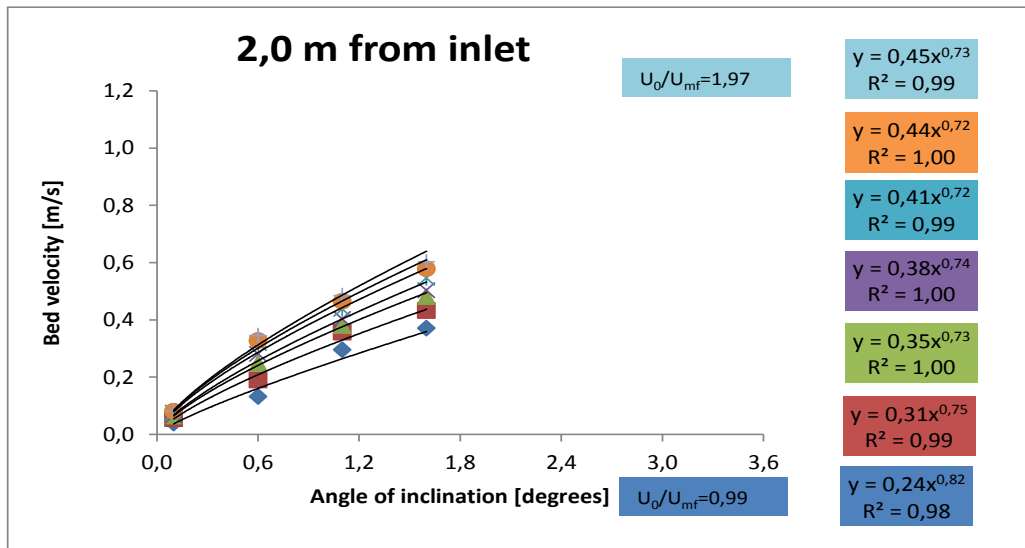


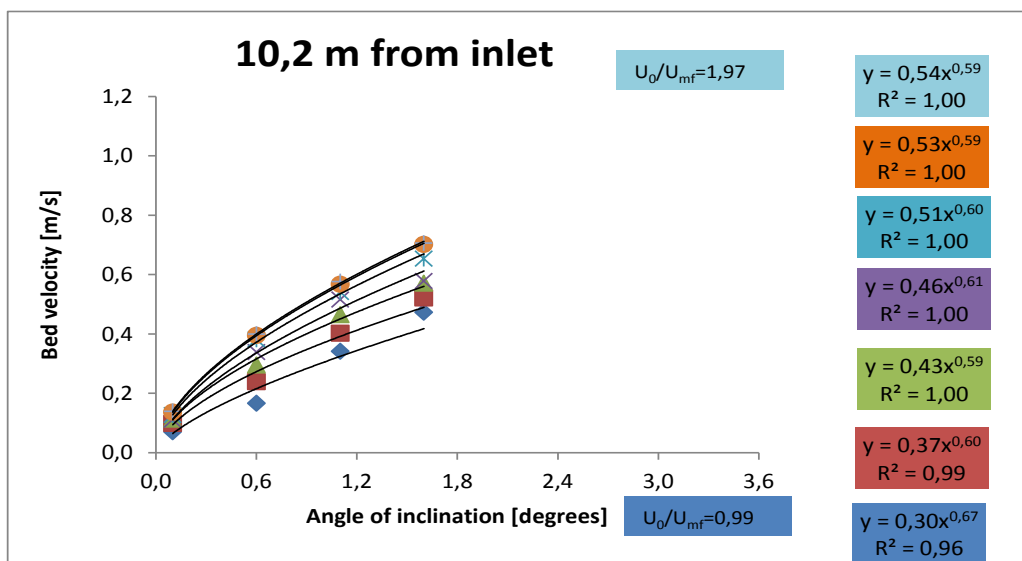
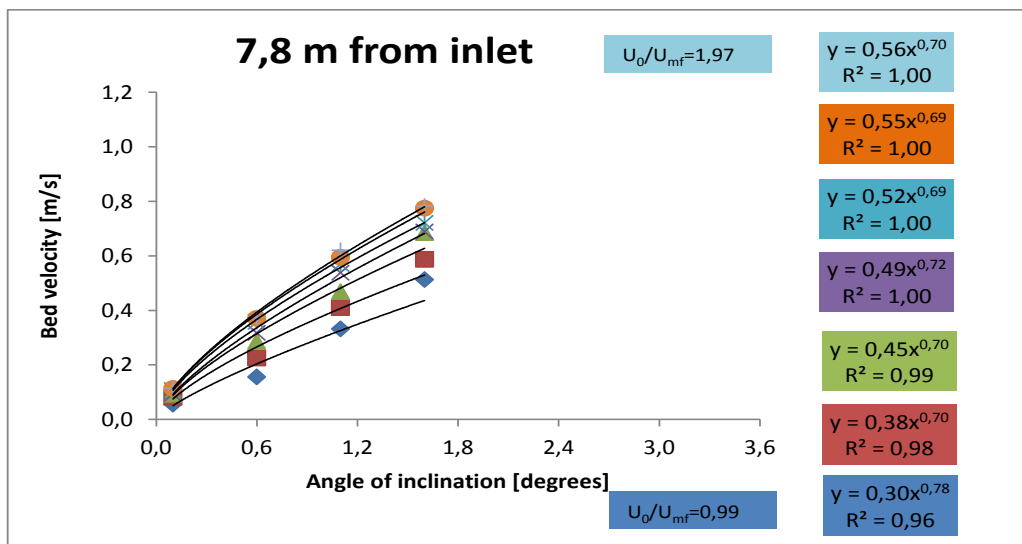
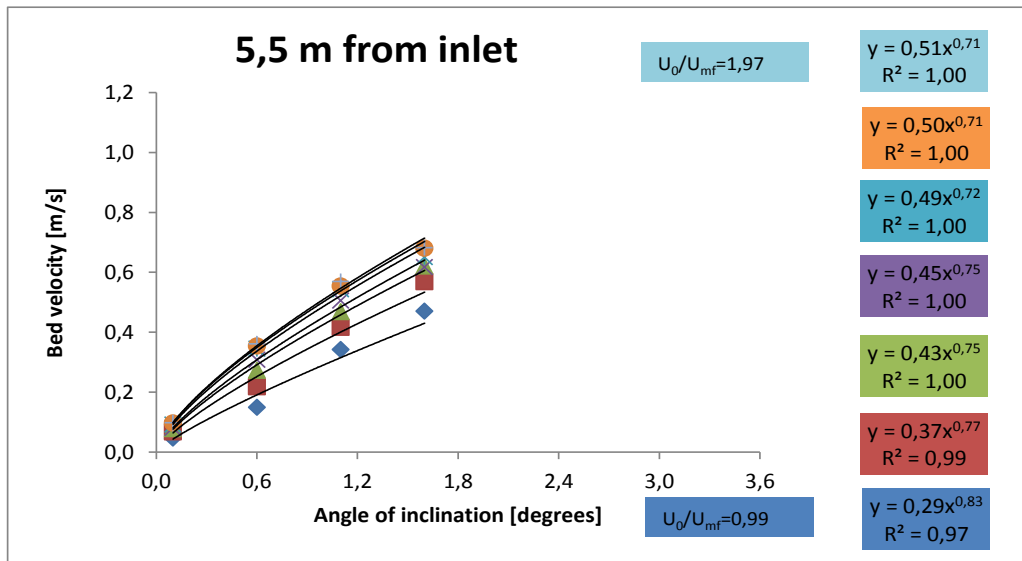
Figure 105 a) Exponential and b) power law trend lines fitted to the slope of average bed velocity as a function of angle of inclination,  $\theta = 0..3.1^0$ ,  $K(\theta)$ , versus distance from inlet, at different  $U_0/U_{mf} = 0.99 \dots 2.14$ .

6.2.6 **15 m - effect of inclination angle,  $\theta$  on bed velocity at different distances away from inlet and at different dimensionless coefficient of velocity  $U_0/U_{mf}$**

For the third model set, the 15 m long air slide segment, the same method of analysis has been used as for the previous two data sets, 3 m and 7 m. Table 32 shows results of power law model, a summary of both Figure 106 and Figure 107.







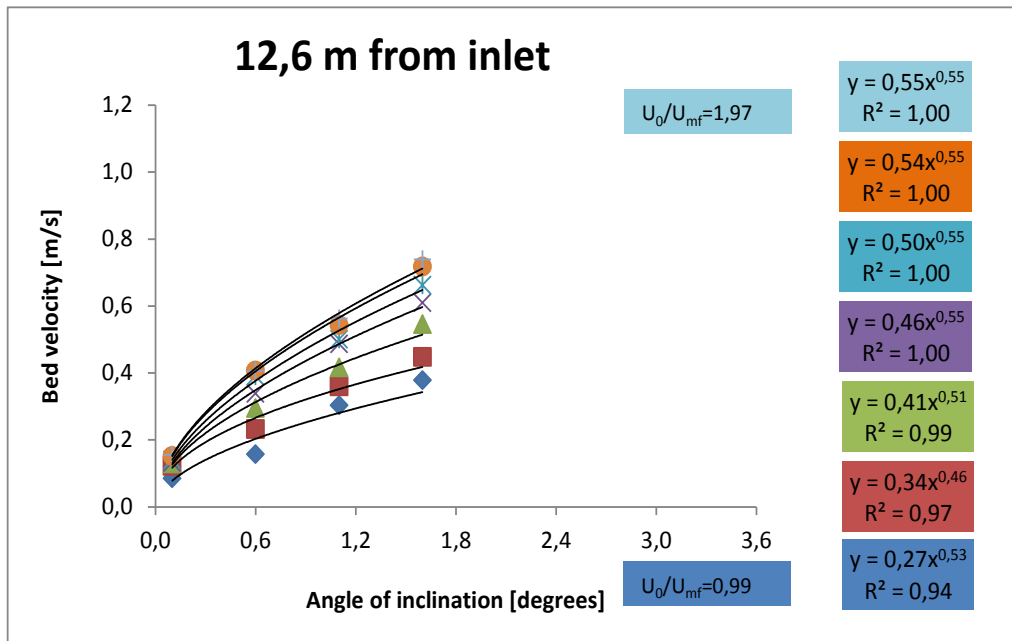
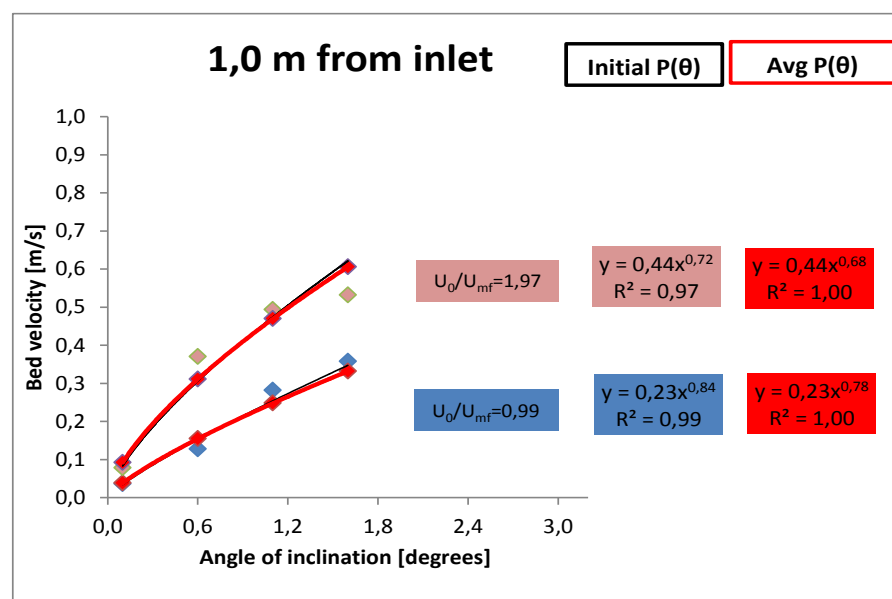
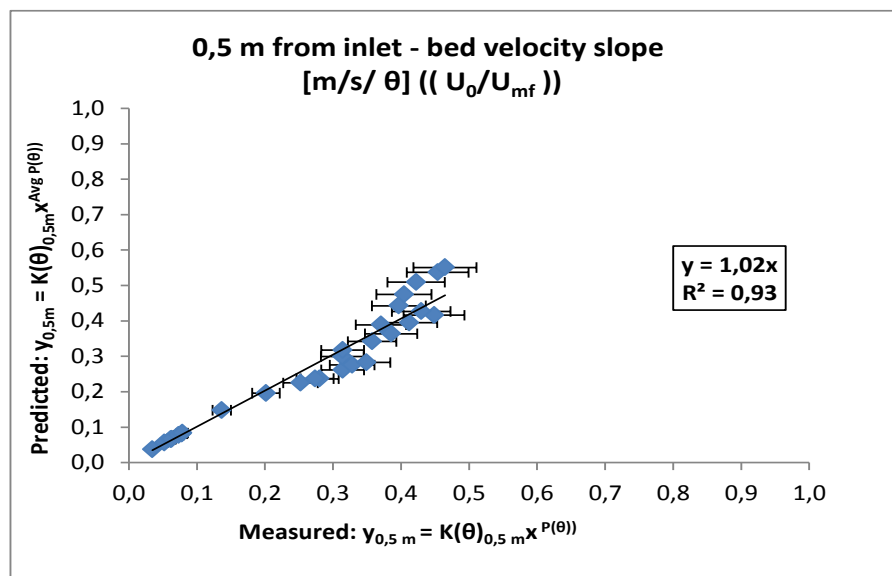
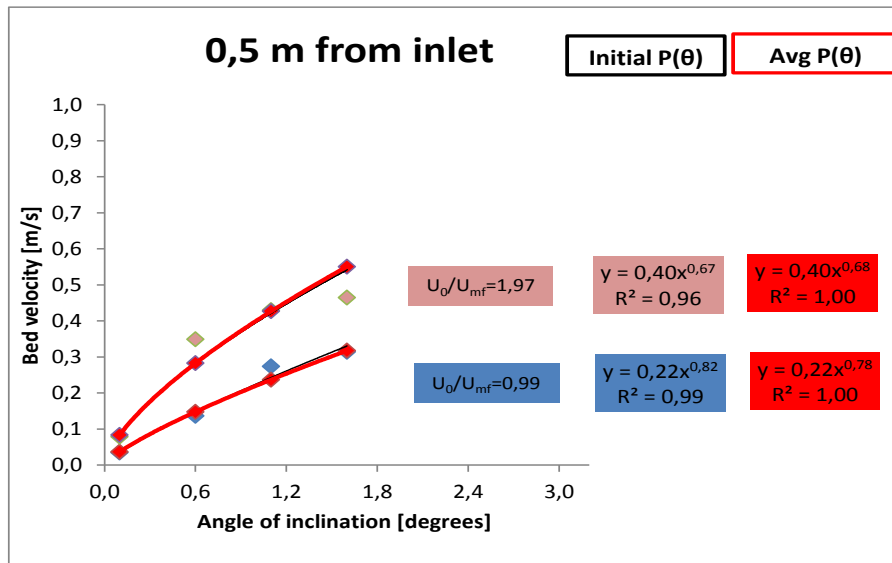
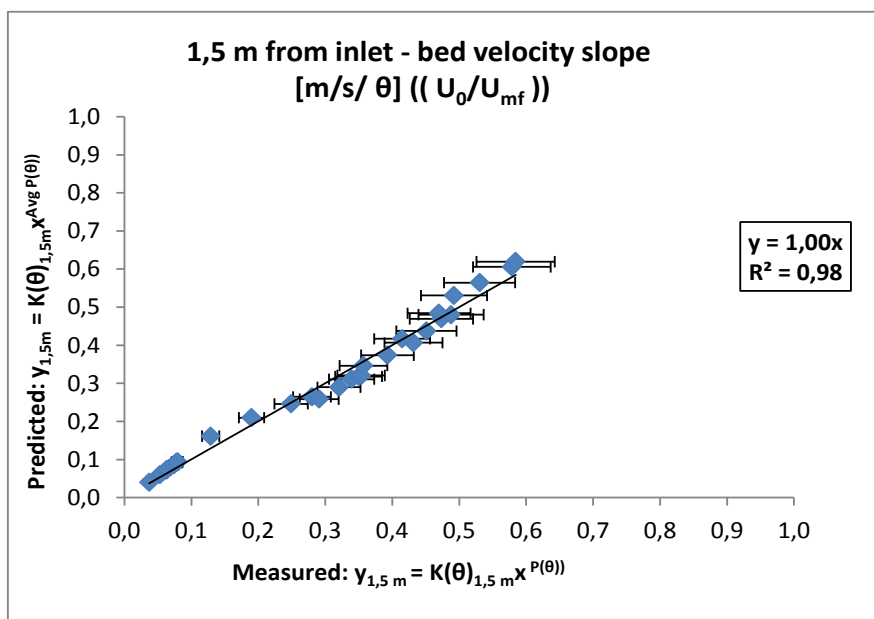
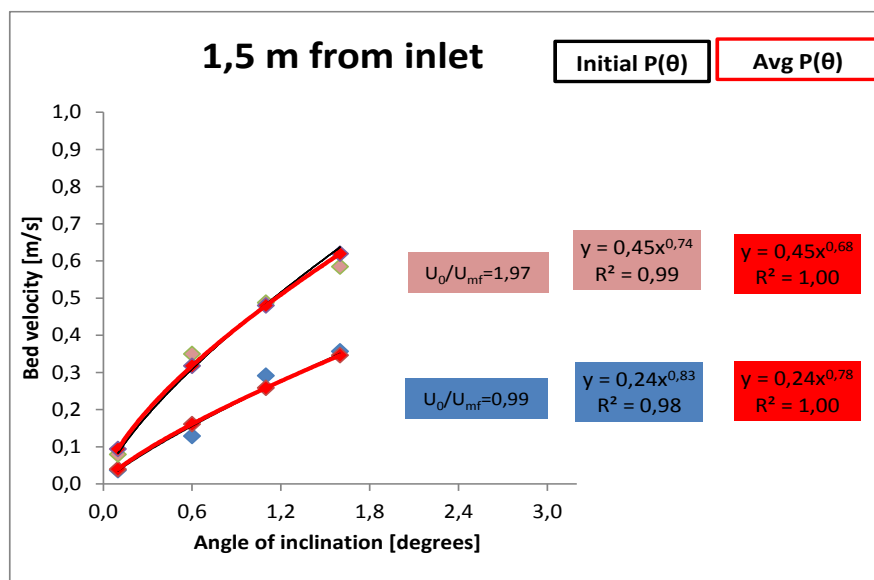
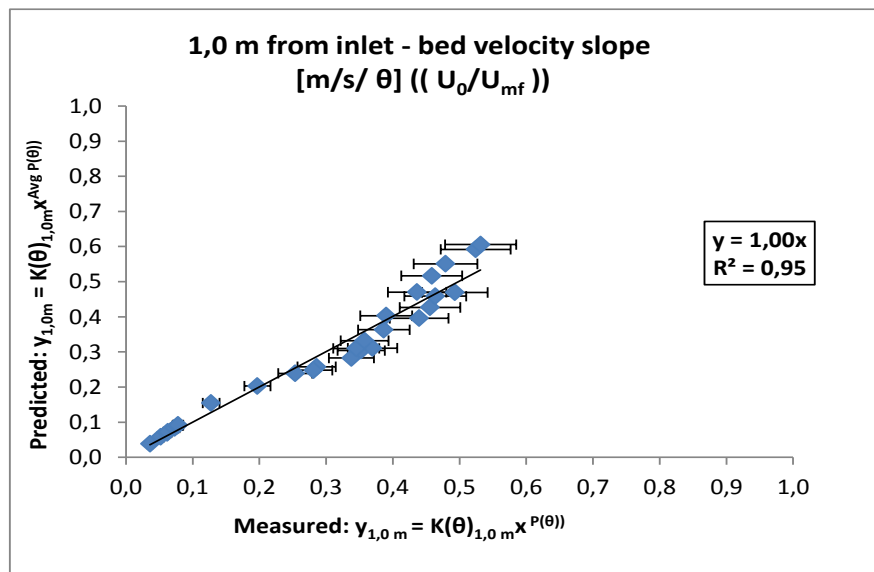


Figure 106 Power law trend lines fitted to experimental data of average bed velocity as a function of angle of inclination,  $\theta = 0.1, 6^\circ$  at different  $U_0/U_{mf} = 0.99 \dots 1.97$ .

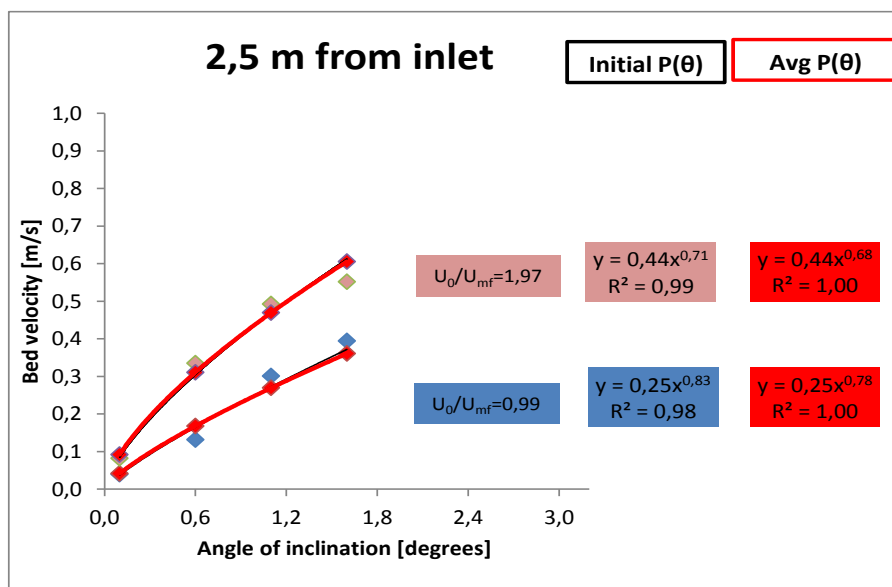
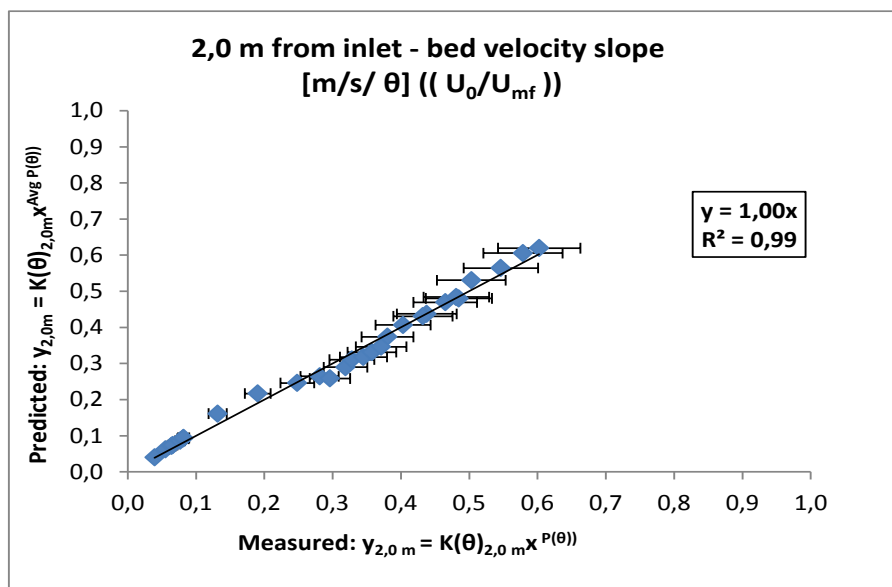
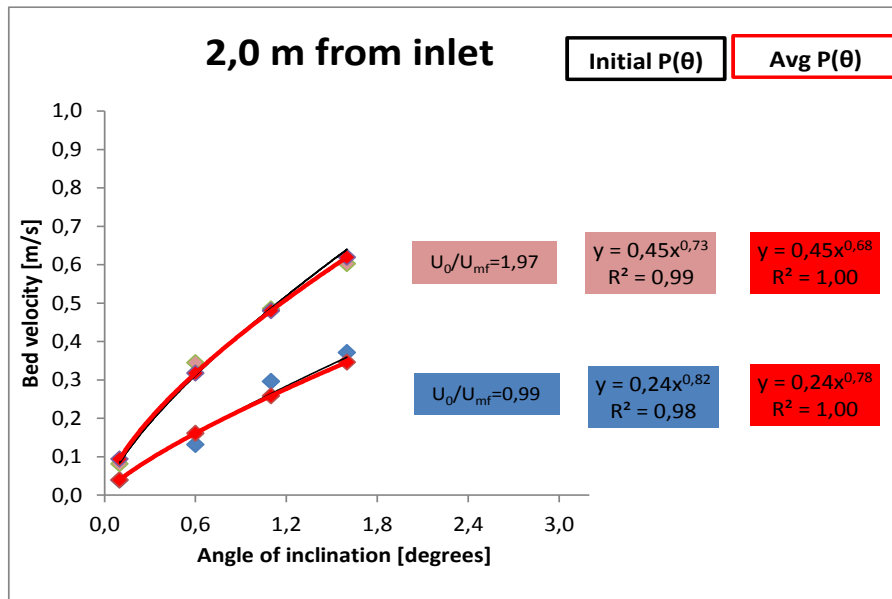
Table 32 Power law trend lines fitted to experimental data for average bed velocity at all angles of inclination,  $\theta$ , at different  $U_0/U_{mf}$  for each measurement point from 0.5 to 12.6 m.  $K(\theta)$  is the coefficient and  $P(\theta)$  is the exponent of power law.

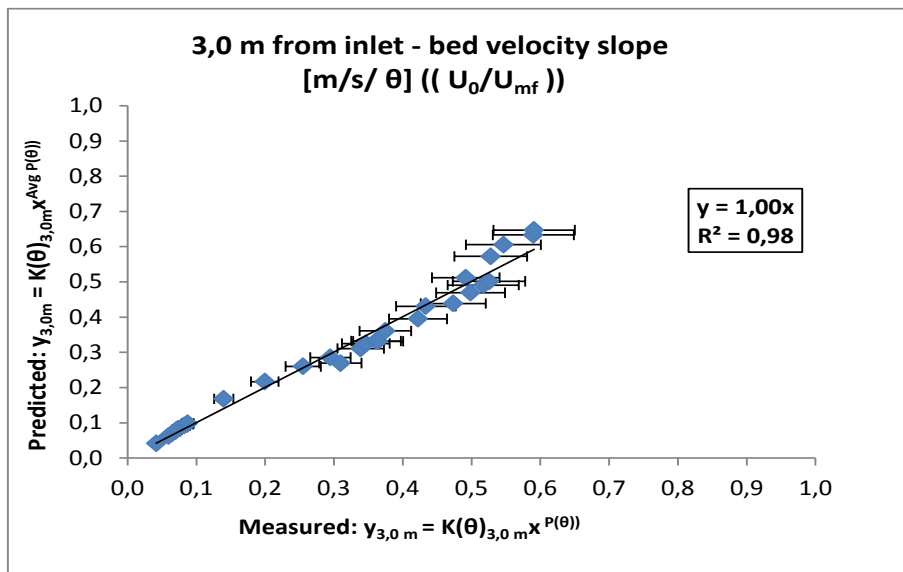
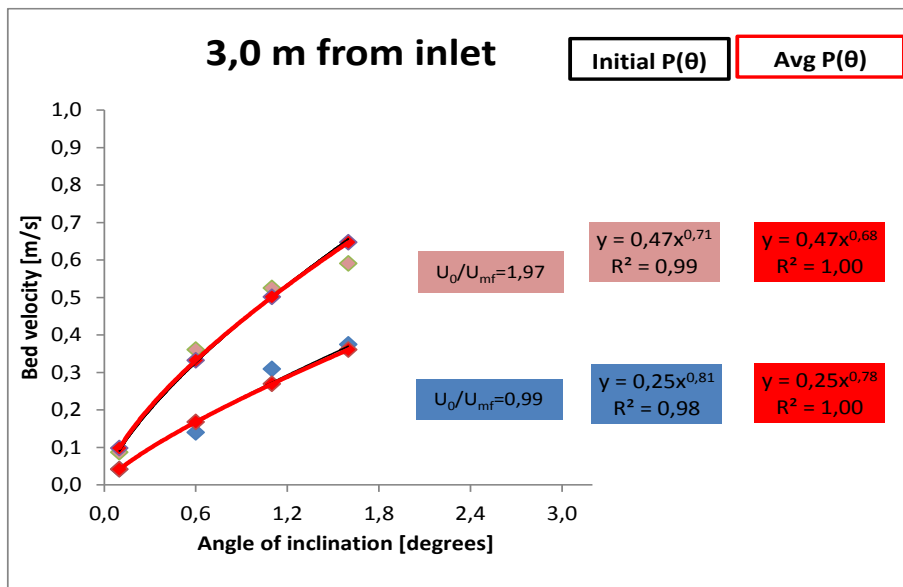
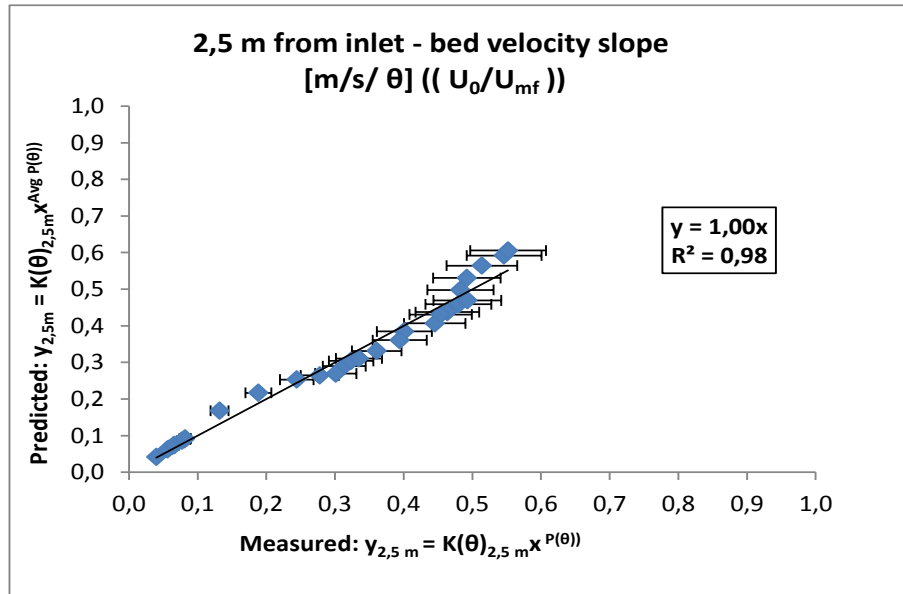
12 m - $K(\theta)$ - Bed velocity slope [m/s/ $\theta$ ] ( $U_0/U_{mf}$ )																		
$U_0/U_{mf}$	$R^2$	$K(\theta)_{0.5\text{ m}}$	$P(\theta)_{0.5\text{ m}}$	$R^2$	$K(\theta)_{1.0\text{ m}}$	$P(\theta)_{1.0\text{ m}}$	$R^2$	$K(\theta)_{1.5\text{ m}}$	$P(\theta)_{1.5\text{ m}}$	$R^2$	$K(\theta)_{2.0\text{ m}}$	$P(\theta)_{2.0\text{ m}}$	$R^2$	$K(\theta)_{2.5\text{ m}}$	$P(\theta)_{2.5\text{ m}}$	$R^2$	$K(\theta)_{3.0\text{ m}}$	$P(\theta)_{3.0\text{ m}}$
<b>0,99</b>	0,99	0,22	0,82	0,99	0,23	0,84	0,98	0,24	0,83	0,98	0,24	0,82	0,98	0,25	0,83	0,98	0,25	0,81
<b>1,16</b>	1,00	0,28	0,72	0,99	0,29	0,75	0,99	0,30	0,76	0,99	0,31	0,75	0,99	0,31	0,76	0,99	0,31	0,73
<b>1,31</b>	0,99	0,32	0,70	0,99	0,34	0,73	1,00	0,35	0,74	1,00	0,35	0,73	1,00	0,36	0,74	1,00	0,37	0,72
<b>1,49</b>	0,97	0,34	0,71	0,98	0,37	0,75	0,99	0,38	0,76	1,00	0,38	0,74	0,99	0,38	0,75	0,99	0,41	0,75
<b>1,64</b>	0,96	0,37	0,67	0,97	0,40	0,71	0,99	0,41	0,73	0,99	0,41	0,72	0,99	0,41	0,71	0,99	0,44	0,71
<b>1,81</b>	0,97	0,39	0,67	0,98	0,43	0,71	0,99	0,44	0,74	1,00	0,44	0,72	0,99	0,43	0,71	0,99	0,46	0,71
<b>1,97</b>	0,96	0,40	0,67	0,97	0,44	0,72	0,99	0,45	0,74	0,99	0,45	0,73	0,99	0,44	0,71	0,99	0,47	0,71
$U_0/U_{mf}$	$R^2$	$K(\theta)_{5.5\text{ m}}$	$P(\theta)_{5.5\text{ m}}$	$R^2$	$K(\theta)_{7.8\text{ m}}$	$P(\theta)_{7.8\text{ m}}$	$R^2$	$K(\theta)_{10.20\text{ m}}$	$P(\theta)_{10.20\text{ m}}$	$R^2$	$K(\theta)_{12.60\text{ m}}$	$P(\theta)_{12.60\text{ m}}$	Avg $P(\theta)$		Stdev/Avg $P(\theta)$			
<b>0,99</b>	0,97	0,29	0,83	0,96	0,30	0,78	0,96	0,30	0,67	0,94	0,27	0,53	<b>0,78</b>	<b>13 %</b>				
<b>1,16</b>	0,99	0,37	0,77	0,98	0,38	0,70	0,99	0,37	0,60	0,97	0,34	0,46	<b>0,70</b>	<b>14 %</b>				
<b>1,31</b>	1,00	0,43	0,75	0,99	0,45	0,70	1,00	0,43	0,59	0,99	0,41	0,51	<b>0,69</b>	<b>11 %</b>				
<b>1,49</b>	1,00	0,45	0,75	1,00	0,49	0,72	1,00	0,46	0,61	1,00	0,46	0,55	<b>0,71</b>	<b>10 %</b>				
<b>1,64</b>	1,00	0,49	0,72	1,00	0,52	0,69	1,00	0,51	0,6	1,00	0,50	0,55	<b>0,68</b>	<b>9 %</b>				
<b>1,81</b>	1,00	0,50	0,71	1,00	0,55	0,69	1,00	0,53	0,59	1,00	0,54	0,55	<b>0,68</b>	<b>9 %</b>				
<b>1,97</b>	1,00	0,51	0,71	1,00	0,56	0,70	1,00	0,54	0,59	1,00	0,55	0,55	<b>0,68</b>	<b>9 %</b>				

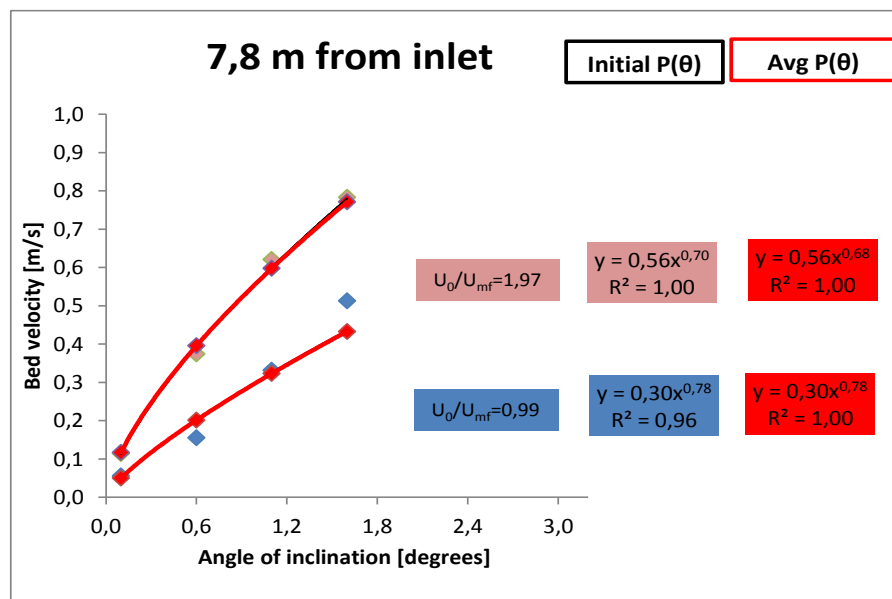
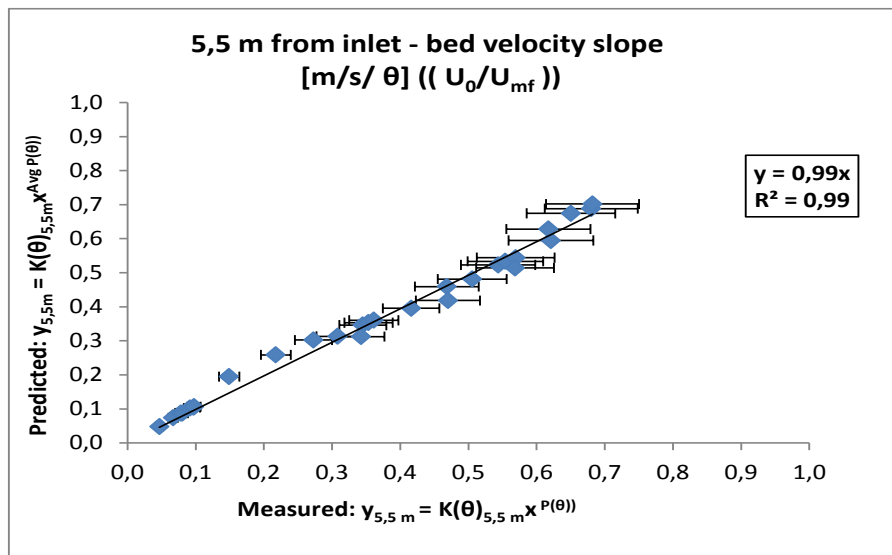
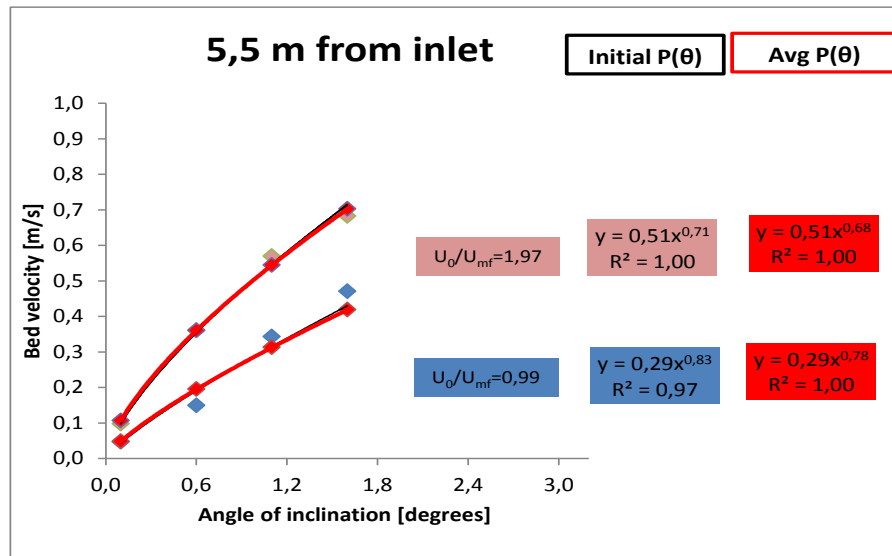


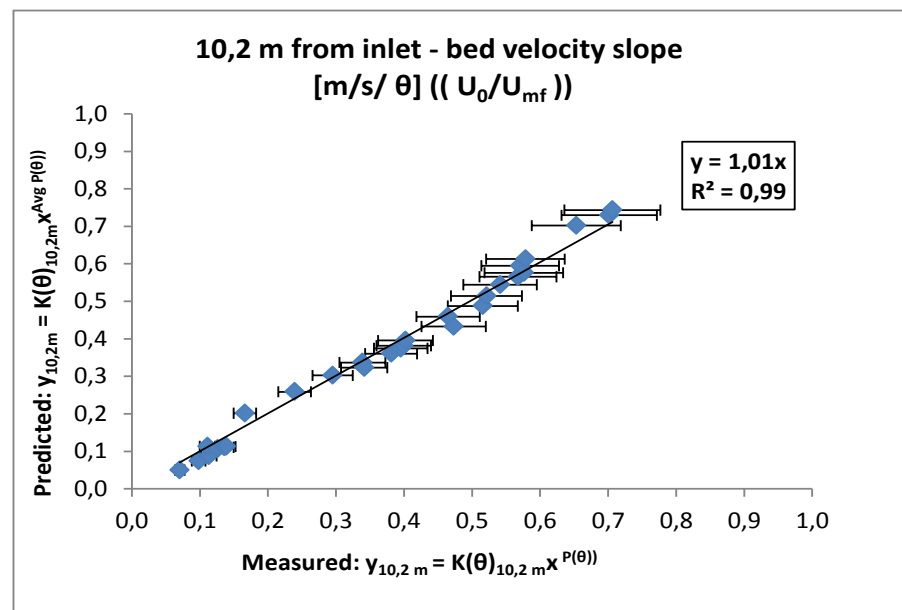
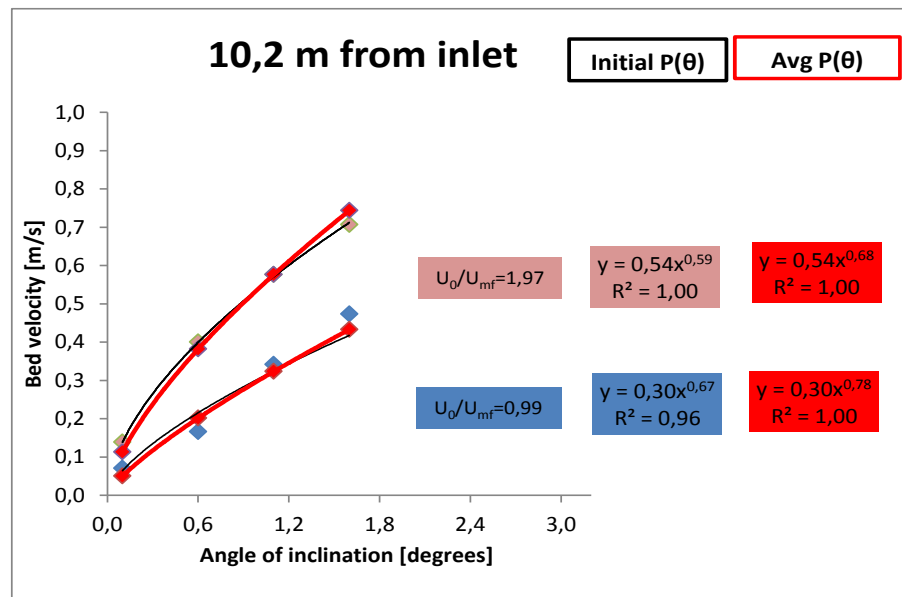
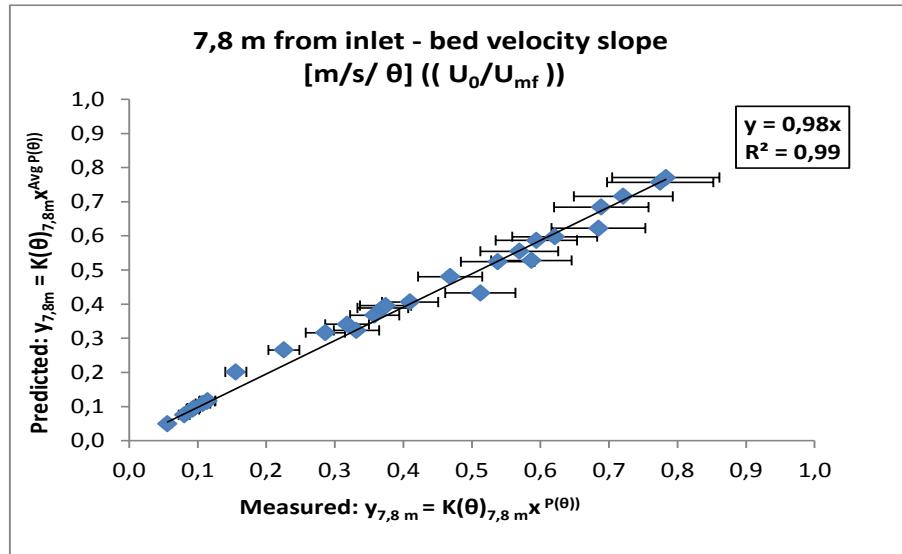












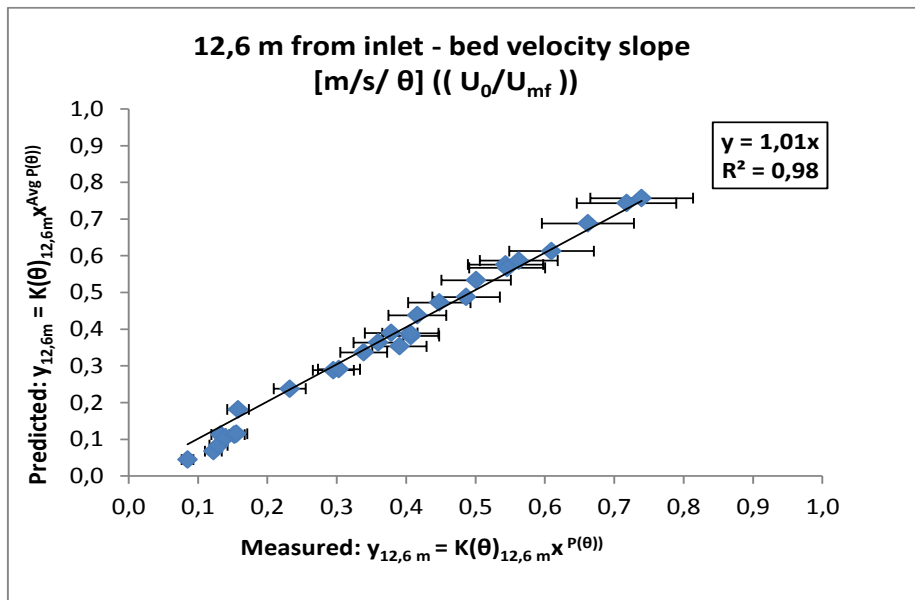
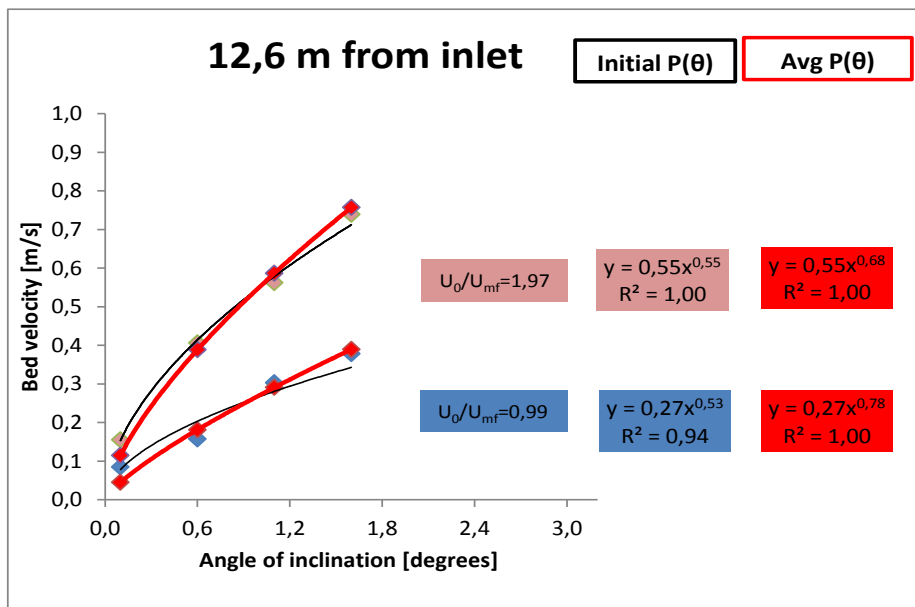


Figure 107 Investigation of the effect of changing power law exponent,  $P(\theta)$  for  $U_0/U_{mf} = 0.99$  and  $U_0/U_{mf} = 2.14$ . Ten percent error bars showing the goodness of the mathematical method for all ranges of  $U_0/U_{mf}$  from 0.99 to 2.14.

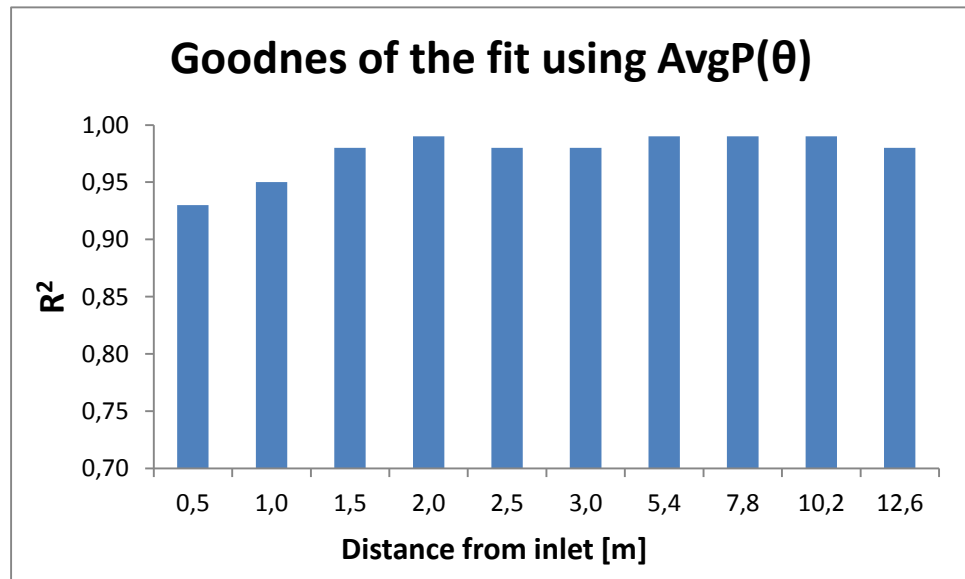


Figure 108 Values of  $R^2$  expressing the goodness of the fit when using  $AvgP(\theta)$  instead of  $P(\theta)$  into the power law trend lines fitted to the experimental data.

Figure 108 presents values of  $R^2$  from using  $Avg P(\theta)$  power law exponent presented graphically in Figure 107. If  $R^2$  is greater than 0.80, there is a good fit to the data. This means that between 93 to 99 % of the variation of the bed velocity data can be explained by a bed velocity power law based on  $P(\theta)$ . The scope of the analysis was again, as in the 3 m and 7 m long air slide segments, to find a mathematical law applicable in all segment lengths of air slide based on a single average power exponent used for the entire length of each air slide segment in order to predict bed velocity.

6.2.7 15 m - bed velocity slope  $K(\theta)$ , versus distance from inlet at different  $U_0/U_{mf}$

Table 33 Results of power law trend lines fitted to the experimental data by using single average power exponent,  $Avg P(\theta)$ , a summary of Table 32.

15 m - $K(\theta)$ - Bed velocity slope [m/s/ $\theta$ ] ( $(U_0/U_{mf})$ )					
$U_0/U_{mf}$	$Y_{0,5\text{ m}} = K(\theta)_{0,5\text{ m}}^{Avg P(\theta)}$	$Y_{1,0\text{ m}} = K(\theta)_{1,0\text{ m}}^{Avg P(\theta)}$	$Y_{1,5\text{ m}} = K(\theta)_{1,5\text{ m}}^{Avg P(\theta)}$	$Y_{2,0\text{ m}} = K(\theta)_{2,0\text{ m}}^{Avg P(\theta)}$	$Y_{2,5\text{ m}} = K(\theta)_{2,5\text{ m}}^{Avg P(\theta)}$
0,99	$Y=0,22x^{0,78}$	$Y=0,23x^{0,78}$	$Y=0,24x^{0,78}$	$Y=0,24x^{0,78}$	$Y=0,25x^{0,78}$
1,16	$Y=0,28x^{0,70}$	$Y=0,29x^{0,70}$	$Y=0,30x^{0,70}$	$Y=0,31x^{0,70}$	$Y=0,31x^{0,70}$
1,31	$Y=0,32x^{0,69}$	$Y=0,34x^{0,69}$	$Y=0,35x^{0,69}$	$Y=0,35x^{0,69}$	$Y=0,36x^{0,69}$
1,49	$Y=0,34x^{0,71}$	$Y=0,37x^{0,71}$	$Y=0,38x^{0,71}$	$Y=0,38x^{0,71}$	$Y=0,38x^{0,71}$
1,64	$Y=0,37x^{0,68}$	$Y=0,40x^{0,68}$	$Y=0,41x^{0,68}$	$Y=0,41x^{0,68}$	$Y=0,41x^{0,68}$
1,81	$Y=0,39x^{0,68}$	$Y=0,43x^{0,68}$	$Y=0,44x^{0,68}$	$Y=0,44x^{0,68}$	$Y=0,43x^{0,68}$
1,97	$Y=0,40x^{0,68}$	$Y=0,44x^{0,68}$	$Y=0,45x^{0,68}$	$Y=0,45x^{0,68}$	$Y=0,44x^{0,68}$
$U_0/U_{mf}$	$Y_{3,0\text{ m}} = K(\theta)_{3,0\text{ m}}^{Avg P(\theta)}$	$Y_{5,5\text{ m}} = K(\theta)_{5,5\text{ m}}^{Avg P(\theta)}$	$Y_{7,8\text{ m}} = K(\theta)_{7,8\text{ m}}^{Avg P(\theta)}$	$Y_{10,2\text{ m}} = K(\theta)_{10,2\text{ m}}^{Avg P(\theta)}$	$Y_{12,6\text{ m}} = K(\theta)_{12,6\text{ m}}^{Avg P(\theta)}$
0,99	$Y=0,25x^{0,78}$	$Y=0,29x^{0,78}$	$Y=0,30x^{0,78}$	$Y=0,30x^{0,78}$	$Y=0,27x^{0,78}$
1,16	$Y=0,31x^{0,70}$	$Y=0,37x^{0,70}$	$Y=0,38x^{0,70}$	$Y=0,37x^{0,70}$	$Y=0,34x^{0,70}$
1,31	$Y=0,37x^{0,69}$	$Y=0,43x^{0,69}$	$Y=0,45x^{0,69}$	$Y=0,43x^{0,69}$	$Y=0,41x^{0,69}$
1,49	$Y=0,41x^{0,71}$	$Y=0,45x^{0,71}$	$Y=0,49x^{0,71}$	$Y=0,46x^{0,71}$	$Y=0,46x^{0,71}$
1,64	$Y=0,44x^{0,68}$	$Y=0,49x^{0,68}$	$Y=0,52x^{0,68}$	$Y=0,51x^{0,68}$	$Y=0,50x^{0,68}$
1,81	$Y=0,46x^{0,68}$	$Y=0,50x^{0,68}$	$Y=0,55x^{0,68}$	$Y=0,53x^{0,68}$	$Y=0,54x^{0,68}$
1,97	$Y=0,47x^{0,68}$	$Y=0,51x^{0,68}$	$Y=0,56x^{0,68}$	$Y=0,54x^{0,68}$	$Y=0,55x^{0,68}$

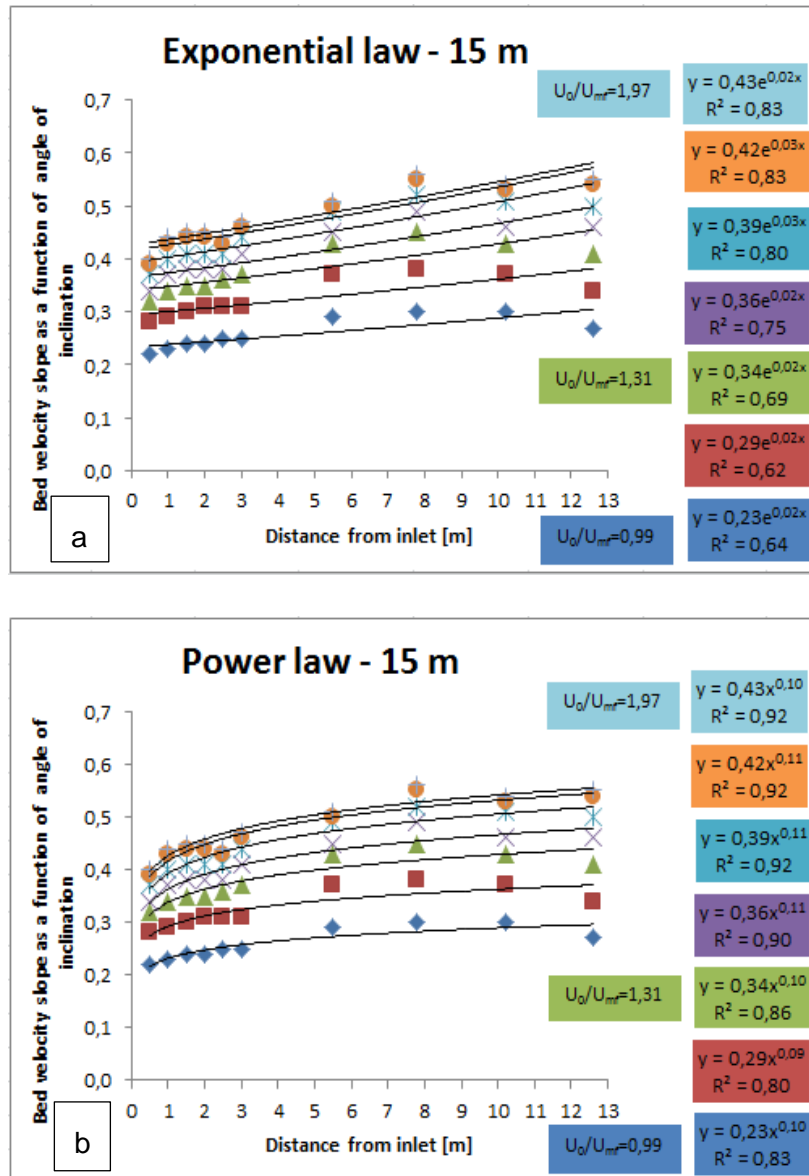


Figure 109 a) Exponential and b) power law trend lines fitted to the slope of average bed velocity as a function of angle of inclination,  $\theta = 0..1.6^\circ$ ,  $K(\theta)$ , versus distance from inlet, at different  $U_0/U_{mf} = 0.99 \dots 1.97$ .

The empirical modeling loop presented in Figure 89 has been completed; the power law model has been validated using three model sets, data from a 3 m, 7 m and a 15 m long air slide segment. For each of the three model sets same power law and same criterion of fit based on  $AvgP(\theta)$  and values of  $R^2$  above 0.80 were used successfully. Figure 110 shows a graphical summary of the results presented in this chapter. The average bed velocity as a function of both  $U_0/U_{mf}$  and  $\theta$  was best modelled as a power law, where average bed velocity at each measurement point  $Y_{measurement}$  was expressed as  $Y_{measurement} = K(\theta)x^{AvgP(\theta)}$ .



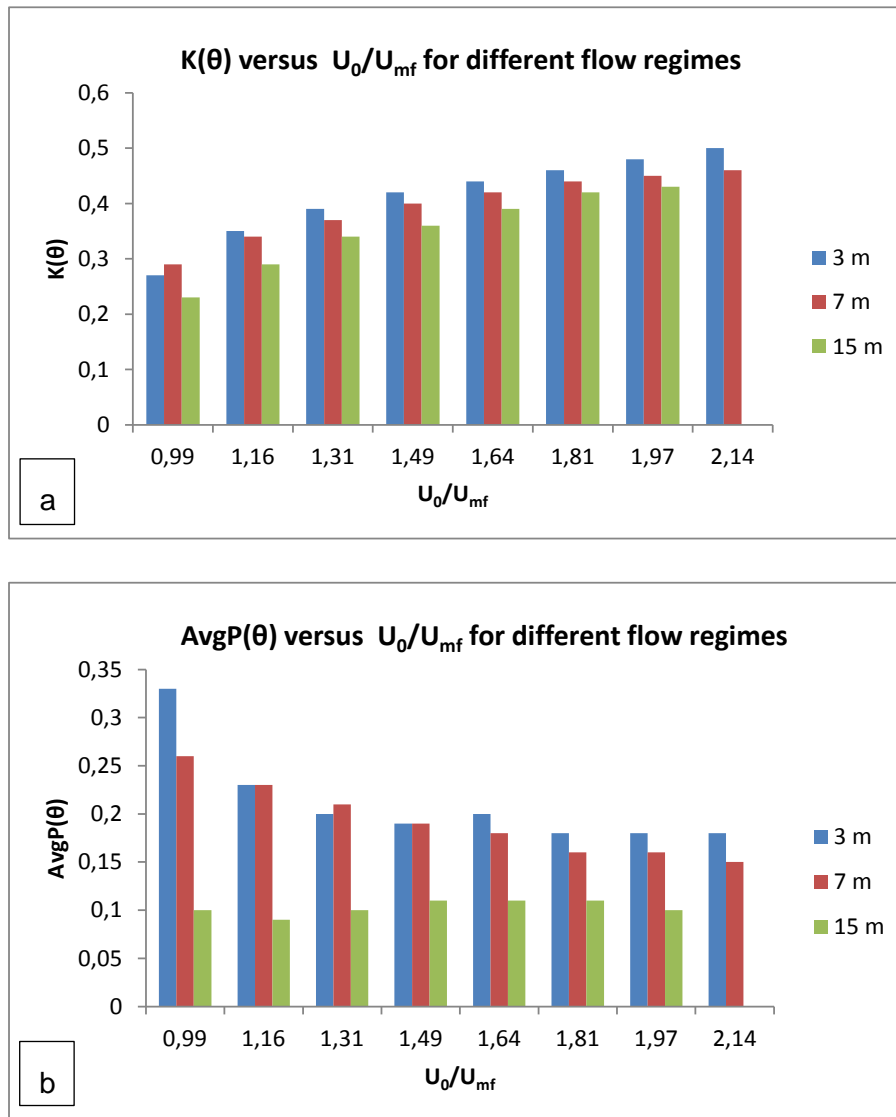


Figure 110 Comparison of  $K(\theta)$  and  $AvgP(\theta)$  for different segments of air slide lengths: 3 m, 7 m, 15 m representing different flow regimes: acceleration and steady state.

So how to interpret the model based on results from Figure 110? The values of  $K(\theta)$  are unique for each flow regime: acceleration or steady state and they increase with increasing  $U_0/U_{mf}$ . The values of the power coefficient  $AvgP(\theta)$  behave differently. Both in a 3 m long acceleration zone and 7 m acceleration zone and steady state with a 50/50 ratio the plots show decreasing trends with increasing  $U_0/U_{mf}$ . In a 15 m long air slide segment where the steady state zone is at least three times longer than the acceleration zone, the values of  $AvgP(\theta)$  remain constant for all values of  $U_0/U_{mf}$ . One can argue that the empirical model is not fully developed since it is based only on one powder quality and that will not yield for another powder, which is true. Work carried out by Chaudhry (2006) by conveying ten test materials at a wide

range of lean phase conveying conditions, although not in a fluidized air slide, has shown that particle properties (size, shape, density) had a great influence towards the pressure drop created by the material. In his power law model the values of his  $K$  and  $P$  at different conveying velocities were unique for every material and he concluded that they had to be determined experimentally. There are few experimental data on fluidized air slides that can be used for comparison with models. Newly in their review of air slides experiments, Savage and Oger (2013) related their modeling work on experiments of Botterill and Bessant (1976), Liot (1979) and Chan (1979) (cited by Savage and Oger (2013)). Their measurements of mass flow rate versus  $\theta$  were fitted by a power law expression. A standard open channel flow hydraulics approach was used to model the fluidized solids flow. An open channel method similar to their work, with modifications, will be shown in the next chapter.

### 6.3 Conclusions

The data analysis performed in this chapter has both yielded an average bed velocity model and looked at lengths of acceleration and steady state zones. A detailed and extensive data analysis and investigation has been conducted in order to model average bed velocity at each measurement point as a function of process parameters such as  $U_0/U_{mf}$  and  $\theta$ . The analysis has shown that average bed velocity as a function of both  $U_0/U_{mf}$  and  $\theta$  is best modelled as a power law, where average bed velocity,  $Y_{measurement}$ , at each measurement point,  $x$ , is expressed as  $Y_{measurement} = K(\theta)x^{AvgP(\theta)}$ . It was observed that the values of  $K(\theta)$  and  $AvgP(\theta)$  changed with changing air slide segment lengths. It should be noted that  $AvgP(\theta)$  is not a natural value, but an imposed value obtained by averaging different exponents from different data sets. It was found out that in an air slide segment, the first 3.5 m correspond to acceleration zone and that the flow regime gets stable after the first 3.5 meters and reaches steady state. There was no literature available for air slides to support this theory; the theory is based on empirical analysis of test results conducted using one alumina powder quality only.

Next, in order to understand the behaviour of the alumina bed, we need a mathematical interpretation of the empirical findings based on knowledge from physical mechanisms of alumina transport in the air slide. What kind of mathematical model will be suitable?

One needs to look for a model to incorporate both expressions of  $\frac{\partial h}{\partial x}$  and  $\frac{\partial v}{\partial x}$  to model changes in bed heights and average bed velocity as a function of changing distance from inlet. In addition, the mathematical model will have to incorporate a power law expression having a constant power law exponent  $AvgP(\theta)$  as shown by the empirical analysis conducted in the 15 m long air slide segment. Savage and Oger (2013) used a standard open channel flow hydraulics approach for their model, pointing out that based on previous work of Botterill and van der Kolk (1971) and Botterill et al. (1972) changes in fluidizing velocity and bed heights could result in changes in viscosity of the fluidized material. A non-Newtonian viscosity power law model was considered by Botterill and Besant (1976) to provide good approximations to their measured velocity profiles. Again, the main difference is that they conducted their experiments in a closed system with flow driven by paddles rather than by gravity as in this work. In conclusion, the detailed discussion of the analytical modelling of the flow of fluidized bulk solids in inclined channels undertaken in the literature study and the results from empirical analysis led up to the suggestion that an approach based on a simple force balance equation for steady uniform flow might be the way to go further. If the model is to be of practical use, it would be expected that values could be found for the parameters  $K(\theta)$  and  $AvgP(\theta)$  such that curves plotted from the model would match the curves obtained experimentally.

## 7 Mathematical modelling

In the previous chapter power law trends fitted to experimental data to predict average bed velocity in an air slide were investigated. One of the objectives of the experimental work carried out in this programme was to obtain enough data with which to test the modelling approach referred to in this chapter for a series of operational and design parameters. In this chapter a theoretical model and the correlation between the experimental data and the model have been investigated. The scope of this chapter is to find a mathematical law applicable in all segment lengths of air slide based on a single average power exponent (as investigated in Chapter 6) used for the entire length of each air slide segment in order to predict bed velocity, for philosophy has to do with things that can be demonstrated and are eternally the same. The modelling approach presented in this thesis started originally with the analysis of the alumina Solids Surface Body Drag Model (SSBDM) developed by Dyrøy (2006) for calculation of the expression of capacity through a vertical Anti Segregation Tube (AST). Two other modelling approaches have then been studied: the Savage and Hutter - SH model used for avalanche dynamics as presented by Pudasaini and Hutter (2007) and classical Saint Venant shallow water equations. Savage and Hutter (2007) developed the first continuum mechanical theory in 1989 to describe the behaviour of a finite mass of a granular material and its velocity distribution as it slides down an inclined surface. The basic one dimensional flow equations expressing hydraulic principles were formulated by Saint Venant and Bousinesque in the 19<sup>th</sup> century.

No matter what they model: powder flow, debris flow from volcanic eruptions, avalanche of snow and rocks, dam break in rivers, all models have in common the fundamental physical principles:

- mass is conserved;
- Newton's second law;
- energy is conserved;

The investigation into methods and modelling approaches to estimate flow rates showed that a number of researchers in the past have used different approaches to model flow in an open channel. The theories that have been established either for fluidization or for gravity flow of bulk solids are specific for each mechanical design and do not describe fully the behaviour of the flow. This author has selected the measurement and analysis methods used by Haugland (1998) and Oger and Savage (2013) and Saint Venant

shallow water equations used together with Jin and Fread (1997) flow resistance term as a starting point for the modelling work. The concepts used by Jin and Fread (1997) to model mud/debris floods need a short explanation. Mud/debris floods are caused by a landslide of mud-debris flow or a dam-break failure of a debris dam. A unique characteristic of this type of flow is that is unsteady with flow changing rapidly and the flow properties of the moving fluid mixture: mud/debris and water are different from those of water.

Originally the shallow water Matlab software was used by Lie and Agu (2014) and Agu (2014) to model water flow in an open channel in various projects for the Intelligent mud drilling research group in Statoil, Porsgrunn. The author of this thesis after having investigated Pudasaini and Hutter (2007) and Oger and Savage's (2013) work was convinced based on both own intuition and acquired theoretical knowledge that a shallow water approach will be suitable for modelling alumina flow in an air slide. The author does not claim to be an expert in shallow water modelling, support to adjust the Matlab scripts to flow of alumina in an air slide was given by Lie and Agu and this resulted in a conference paper presented by Valciu, Dyrøy, Farnish, Agu and Lie (2014) at SIMS 2014 – the 55<sup>th</sup> International Conference on Simulation and Modelling. Another argument for using shallow water approach in this work was author's holistic approach to system design and operation of air slide systems as explained in Section 1.3, Figure 2 and further in Chapter 4. The final target will be scale down and knowledge transfer, both design concepts and modelling approaches, in order to optimize feeder operation and performance in a feeding air slide.

## **7.1 Solid flow for air slide systems**

When fluidising alumina powder by use of pressurized air, collisions between the powder particles will occur, thus the distance between particles will increase as they move apart, but the bed density at given air velocities and downward inclinations of the air slide will be the same in all sections of the bed, according to Pudasaini and Hutter (2007). The solid phase, alumina, will behave more or less like a fluid (liquids and gases included) under the action of “upward pushing” by the current of gas moving through the bed of solid alumina particles. In the bed layer above the fluidization membrane in the air slide, due to collisions between particles, an internal pressure will be induced into the bed that will further increase the free distance between the particles, reducing the frictional resistance between them. Fluidisation will start at the point where the

pressure drop on each single particle will be balanced by the gravity minus buoyancy forces (drag forces) and will be transmitted throughout the whole powder bed. Once air will be blown through the bed, the fluidised mass will be in motion, like a liquid and displacements will be generated within its entire volume.

## **7.2 One dimensional Saint Venant model assumptions**

Several other simplified assumptions have been made for the flow of alumina based on the Saint Venant model:

- The alumina flow is in isothermal, incompressible, viscous and homogeneous state;
- The bulk density of the fluidized alumina is constant;
- The shear stresses at the air slide walls, lateral to the flow direction can be neglected; instead roughness coefficients can be used, based on any of the resistance laws applied to steady state flow;

The alumina flow is strictly one dimensional, although this does not apply in real life; this means that the flow velocity and other transport properties vary only in the longitudinal direction of the flow along the air slide;

- The fluidized bed velocity is uniform over the cross section and the alumina level across the section can be represented by a horizontal line;
- The vertical acceleration is negligible and the pressure can be considered hydrostatic, in the direction of the flow depth;
- The alumina bed height and width are very small compared to the length of the air slide;

This model is based on an oversimplified approach and has its limitations. The following topics were not covered; however they need to be considered in further work:

- Sensitivity of alumina flow behaviour to different fines content;
- The effect of channel wall roughness on the alumina flow behaviour;
- Changes in bed velocity profiles from the channel bottom and walls.

The assumption of incompressible flow needs an additional explanation. This assumption is valid in steady state regime when the bed velocity becomes constant and the bulk density does not change. During design and operation of air slides the focus has been to keep the overpressure over the alumina bed as close to atmospheric pressure

as possible. To achieve this in close channels, venting pipes are used to transport the fluidization air once it has passed the alumina bed back to the system. This operation philosophy that in a closed air slide system the pressure is kept as closed to atmospheric as possible through venting has inspired the author to use the shallow water model, originally used for open channel flow.

### 7.2.1 Air slide powder flow model using Saint Venant

The Saint Venant equations describe the flow behaviour for a set of two dependent parameters that are functions of space,  $x$  and time,  $t$  :

- flow rate:  $Q(x, t) = \text{alumina bed velocity} \times \text{cross sectional area} [m^3/s]$ ;
- cross sectional area:  
 $A(x, t) = \text{height of the alumina bed} \times \text{width of the air slide} [m^2]$ ;

#### The continuity equation

The continuity equation is obtained by applying mass conservation principle over the left and right faces of the fixed element in **Error! Reference source not found.**, which re perpendicular to the  $x$  axis, with the alumina bed moving through it. The area of these faces is the cross sectional area of the bed within the air slide,  $A$ . The element volume has a fixed length  $\Delta x$  in the flow direction. By convention the flow mean velocity,  $u$ , is positive in the positive  $x$  direction. Thus the contributions of inflow and outflow of mass through the sides of the element are as modelled by Versteeg and Malalasekera (2007),

Szymkiewicz (2010), Agu and Lie (2014), assuming that the flow properties are differentiable, hence continuous:

- the mass inside the fluid element is:  $\rho A \Delta x$
- the time rate of mass decrease, contributing to the dynamic behaviour of the whole system, is expressed in Equation 47 :

$$-\frac{\partial(\rho A \Delta x)}{\partial t} = -\rho \Delta x \frac{\partial A}{\partial t} \quad \text{Equation 47}$$

- the mass flow through the front (left) face:  $\approx \rho u A = \rho Q$
- the mass flow through the back (right) face:  $\approx \rho u A + \frac{\partial(\rho u A)}{\partial x} \Delta x = \rho(Q + \frac{\partial(Q)}{\partial x} \Delta x)$

- a net outflow of mass in the x direction as a positive quantity (also known as the convective flux out of the system, across the boundaries) will give:

$$\rho \left( Q + \frac{\partial(Q)}{\partial x} \Delta x \right) - \rho Q = \rho \frac{\partial(Q)}{\partial x} \Delta x$$

Thus the physical principle that the mass is conserved applied to the fixed element requires that the mass flow out of the fluid element must equal the time rate of decrease of mass inside the fluid element:

$$\rho \frac{\partial(Q)}{\partial x} \Delta x = -\rho \Delta x \frac{\partial A}{\partial t}$$

Equation 48

Dividing by  $\rho \Delta x$  on both sides and moving all terms to the left gives the unsteady one dimensional continuity equation for incompressible flow in an open channel:

$$\frac{\partial A}{\partial t} + \frac{\partial(Q)}{\partial x} = 0$$

Equation 49

### **The momentum equation**

Another physical principle that governs the flow is Newton's second law of motion:  $F_x = ma_x$ , saying that the net force on the fluid element is equal to its mass times the acceleration of the element in the x direction,  $a_x$ . In open channel flow momentum is treated as a one dimension longitudinal quantity in the direction of the flow and is expressed as momentum per unit time, as the product of mass flow rate and mean velocity (or  $ma_x$ ), having units of force. Balance of momentum states that the time rate of change of x momentum of the fluid element equals the convected flux into and out of the fluid element plus the sum of forces acting on the fluid element (Pudasaini and Hutter (2007)):

***Rate of increase of momentum of fluid element***

***= Sum of forces on the fluid element***

***Rate of increase of momentum of fluid element***

***= Rate of increase of momentum in fluid element***

***+ Net rate of flow of momentum out of fluid element***

Considering first the right hand side of Newton's law, where:



- the mass of the fluid element is:  $m = \rho A \Delta x$
- the acceleration of the fluid element in the  $x$  direction,  $a_x$ , is the time rate of change of its mean velocity:  $a_x = \frac{\partial u_x}{\partial t}$ , then momentum per unit time equals  $ma$  and is equivalent to:

$$\begin{aligned} \text{Rate of increase of momentum in fluid element} &= \rho A \Delta x \frac{\partial u_x}{\partial t} \\ &= \rho \Delta x \frac{\partial Q}{\partial t} \end{aligned}$$

The concepts of net rate of flow of momentum are illustrated in **Error! Reference source not found.** :

- the rate of momentum into the fluid element at the left face, given by the product of mass flow rate and mean velocity is:  $\rho Qu$
- the rate of momentum out of the fluid element at the right face is:  $\rho Qu + \frac{\partial(\rho Qu)}{\partial x} \Delta x$
- a net outflow of momentum in the  $x$  direction as a positive quantity will give:

$$\left( \rho Qu + \frac{\partial(\rho Qu)}{\partial x} \Delta x \right) - \rho Qu \quad \text{Equation 50}$$

thus:

$$\text{Net rate of flow of momentum out of fluid element} = \frac{\partial(\rho Qu)}{\partial x} \Delta x$$

Considering the left hand side of Newton's law, the force in the  $x$  direction,  $F_x$  consists mainly of two contributions:

- body forces, acting directly on the volumetric mass of the fluid element, such as gravitational force,  $F_b$ ;
- surface forces acting directly on the surface of the fluid element such as pressure,  $F_p$ , viscous forces and boundary friction forces,  $F_f$ ;

The balance of forces can be written as in Equation 51:

$$\sum F_x = F_b + F_p + F_f \quad \text{Equation 51}$$

**Error! Reference source not found.** illustrates the concepts explained above. The driving force is the downslope component of the gravity force in the  $x$  direction,  $F_b$ , (counteracted by the frictional force,  $F_f$ ) equal to:

$$F_b = mg \sin \theta = \rho A \Delta x g \sin \theta \quad \text{Equation 52}$$

The pressure force  $F_p$  acts across the boundary of the fluid element in the  $x$  direction and is given by:

$$\frac{dF_p}{dA} = P - \left( P + \frac{\partial P}{\partial x} \Delta x \right) = -\frac{\partial P}{\partial x} \Delta x \quad \text{Equation 53}$$

To express the pressure, a force balance in the vertical direction yields a hydrostatic pressure distribution  $P_y = -g$ , where the hydrostatic pressure decreases with increasing height.  $P_y$  is zero at the free surface at the fluid element and maximum at the bottom of the channel:

$$\frac{\partial P}{\partial y} = -\rho g \cos \theta \quad \text{Equation 54}$$

Integration over the depth of the fluid element from the bottom at  $y = 0$  to the top at  $y = h(x)$  gives:

$$0 - P = \int_0^{h(x)} (-\rho g \cos \theta) dy \quad \text{Equation 55}$$

$$P = \rho g h \cos \theta \quad \text{Equation 56}$$

Substitution of  $P$  into  $\frac{dF_p}{dA}$  gives:

$$\frac{dF_p}{dA} = -\frac{\partial(\rho g h \cos \theta)}{\partial x} \Delta x = -\rho g \cos \theta \frac{\partial(h)}{\partial x} \Delta x \quad \text{Equation 57}$$

Integration over the cross sectional area gives:

$$F_p = -\rho g \cos \theta \Delta x \int \frac{\partial h}{\partial x} dA \quad \text{Equation 58}$$

$$F_p = -\rho g \cos\theta \Delta x \int \frac{\partial h}{\partial x} dA \quad \text{Equation 59}$$

Since the change in the height of the flow over the fluid element length  $\Delta x$  is small,  $\frac{\partial h}{\partial x}$  is assumed to be constant, which results in the final expression of the pressure force:

$$F_p = -\rho g \cos\theta A \Delta x \frac{\partial h}{\partial x} \quad \text{Equation 60}$$

The frictional force,  $F_f$ , acts in the x direction opposite to the flow direction. Supposing that the flow resistances by the sidewalls are negligible to those on the bottom, then:

$$F_f = -\tau_f P_{wetted} \Delta x \quad \text{Equation 61}$$

And

$$\tau_f = \rho g R_h S_f = \rho g \frac{D_H}{4} S_f \quad \text{Equation 62}$$

where  $S_f$  is the friction slope or the flow resistance term. Substitution of  $\tau_f$  into  $F_f$  gives:

$$F_f = -\rho g A S_f \Delta x \quad \text{Equation 63}$$

Finally, the sum of forces acting on the fluid element is:

$$\sum F_x = \rho A \Delta x g \sin\theta - \rho g \cos\theta A \Delta x \frac{\partial h}{\partial x} - \rho g A S_f \Delta x \quad \text{Equation 64}$$

and the momentum balance can be written as:

$$\begin{aligned} & \rho \Delta x \frac{\partial Q}{\partial t} + \frac{\partial(\rho Q u)}{\partial x} \Delta x \\ & = \rho A \Delta x g \sin\theta - \rho g \cos\theta A \Delta x \frac{\partial h}{\partial x} \\ & - \rho g A S_f \Delta x \end{aligned} \quad \text{Equation 65}$$

Division on both sides by  $\rho \Delta x$  gives the final expression of the momentum equation:

$$\frac{\partial Q}{\partial t} + \frac{\partial(Qu)}{\partial x} = Ag\sin\theta - Ag\cos\theta \frac{\partial h}{\partial x} - AgS_f$$

Equation 66

One of the important assumptions in shallow water equations is the independence of the velocity distribution on the vertical coordinate. In deriving the momentum equation the pressure distribution has been assumed to be hydrostatic and the effect of non-uniform cross sectional velocity distribution has been assumed to be small. Xia and Yen (1994), Orgaz and Chanson (2013), Emeka (2014) and many other researchers have introduced momentum correction coefficients in order to take into account flow non-uniformity (i.e., Boussinesq coefficient),  $\beta_x$ , defined as:

$$\beta_x = \frac{1}{u^2 A} \int_0^A U^2 dA$$

Equation 67

where  $u$  is the mean flow velocity and  $U$  is the local velocity. Since the value of the actual distribution of velocity  $U$  is not known, an estimated value of  $\beta_x$  ranging from 1.03 to 1.07 will be used instead (Wali (2013), Orgaz and Chanson (2013) and Emeka (2014)). Xia and Yen (1994) analysed the effects of the coefficients and confirmed that the values of the effects of the coefficients were relatively small when the flow was nearly steady state and uniform and that their effects increased with unsteadiness of the flow. They concluded that the correction coefficients had a greater impact on the solution for velocity than for depth. Summing up the continuity and using the Boussinesq coefficient into the momentum equation gives the unsteady state Saint Venant system of partial differential equations:

$$\frac{\partial A}{\partial t} + \frac{\partial Q}{\partial x} = 0$$

Equation 68

$$\frac{\partial Q}{\partial t} + \frac{\partial(\beta Q^2/A)}{\partial x} = Ag\sin\theta - Ag\cos\theta \frac{\partial h}{\partial x} - AgS_f$$

Equation 69

Naef et al. (2006) presented a systematic comparison of one phase flow resistance relations shown in Table 34 for debris flow using the same finite element solution method for different previously proposed resistance laws.

### 7.2.2 Flow resistance

The formulation of flow resistance for fluid flow in an open channel is equivalent to that of pipe flow presented in Chapter 5 and used to predict and validate pressure losses in a 15 m long air slide segment against measurement results. Table 34 shows flow resistance factors used in literature to model debris flows. In debris flows the solid fluid mixtures are considered as a quasi-homogeneous fluid and have been modelled as single – phase flows by Naef et al. (2006) using shallow water equations together with a finite element solution method.

**Table 34 Flow resistance - open channel approach models (Naef et al. (2006) updated)**

Authors	Flow resistance model	Friction slope (flow resistance term) $S_f$
Jin & Fread (1997) Agu and Lie (2014)	Mud/debris and water flow:	$S_f = \frac{\tau_y}{\rho g R_h} \left[ 1 + \left( \frac{(\epsilon + 1)(\epsilon + 2) V }{(0.74 + 0.65\epsilon) \left(\frac{\tau_y}{k}\right)^\epsilon R_h} \right)^{\frac{1}{\epsilon + 0.15}} \right]$
Naef et al. (2006)	Full Bingham	$S_f = \frac{\tau_0}{\rho g h}, \text{ where } 2\tau_0^3 - 3\left(\tau_y + 2\frac{\mu_{Bq}}{h^2}\right)\tau_0^2 + \tau_y^3 = 0$
	Simplified Bingham	$S_f = \frac{\tau_0}{\rho g h}, \text{ where } \tau_0 = 1,5 \tau_y + 3\frac{\mu_{Bq}}{h^2}$
	Voellmy	$S_f = \frac{q\sqrt{q^2}}{h^2 C^2 h_r} + \cos \alpha \tan \delta$
	Turbulent & Coulomb	$S_f = \frac{n^2 q \sqrt{q^2}}{h^2 h_r^{\frac{4}{3}}} + \cos \alpha \tan \delta$
	Turbulent & Yield	$S_f = \frac{n^2 q \sqrt{q^2}}{h^2 h_r^{\frac{4}{3}}} + \frac{\tau_y}{\rho g h}$

	Turbulent, Coulomb & Yield	$S_f = \frac{n^2 q \sqrt{q^2}}{h^2 h_r^{\frac{4}{3}}} + \frac{\tau_i}{\rho g h} \text{ with } \tau_i: \min(\tau_y; \rho g h \cos \alpha \tan \delta)$
	Quadratic	$S_f = \frac{n^2 q \sqrt{q^2}}{h^2 h_r^{\frac{4}{3}}} + \frac{\kappa \eta q}{8 h^3 \rho g} + \frac{\tau_y}{\rho g h}$
	Coulomb viscous	Full Bingham with $\tau_y = \rho g h \cos \alpha \tan \delta$

Based on the Darcy- Weissbach equation for pipe flow:

$$h_f = f_D \frac{L}{D} \frac{v^2}{2g}$$

Equation 70

where  $h_f$  is the frictional head loss and  $f_D$  is the Darcy friction factor, then the frictional slope can be defined as:

$$S_f = \frac{h_f}{L} = \frac{f_D}{D} \frac{v^2}{2g}$$

Equation 71

Di Cristo et al. (2013), Agu (2014) following the work of Ancy et al. (2007), Ancy et al. (2012), combined the equation of shear distribution through the depth  $y$  of a one dimensional steady uniform open channel flow, assuming no slip at the bottom for the velocity in the direction of the flow ( $v(0) = 0$ ):

$$\tau(y) = \rho g (h - y) \sin \theta = \rho g S_f (R_h - y)$$

Equation 72

and the rheological power law equation of non-Newtonian fluids (Herschel-Bulkley model):

$$\tau = \tau_y + k \left( \frac{\partial u}{\partial y} \right)^n$$

Equation 73

and obtained:

$$\tau = \rho g S_f (R_h - y) = \tau_y + k \left( \frac{\partial u}{\partial y} \right)^n \quad \text{Equation 74}$$

in which  $\tau$  is the internal shear stress,  $\tau_y$  is the yield shear stress,  $y$  is the height of the bed,  $\partial u / \partial y$  is the longitudinal velocity in the  $x$  direction of the flow,  $k$  and  $n$  are flow factors to be determined from rheometric experiments,  $\rho$  is the bulk density of the fluid/mixture,  $g$  is the gravity constant and  $R_h$  the hydraulic radius of the channel.

A condition for steady uniform flow, necessary, since bed heights and the alumina flow through the air slide measured by the load cells showed stable flow, is according to Ancy et al. (2012) that the bottom shear stress  $\tau_b$  should be larger than  $\tau_y$ , otherwise no steady uniform flow would take place. In an attempt to derive an expression for  $\tau_b$  as a function of the average bed velocity and bed height,  $\rho g S_f$  is substituted by  $\tau_f / R_h$  and Equation 74 is integrated twice to obtain the final Ancy et al. (2012) nonlinear implicit expression for the bottom shear stress:

$$\left( \frac{K}{\tau_y} \right)^{\frac{1}{n}} \frac{2n + 1}{n} \frac{V}{n} = \left( \frac{\tau_f}{\tau_y} \right)^{\frac{1}{n}} \left( 1 - \frac{\tau_y}{\tau_f} \right)^{1 + \frac{1}{n}} \left( 1 + \frac{n}{n + 1} \frac{\tau_y}{\tau_f} \right) \quad \text{Equation 75}$$

Equation 75 cannot be used in this form. Jin and Fread (1997) in their FLDAW dynamic flood routing model proposed following expression (cited by Agu and Lie (2014), Agu (2014) in Table 34):

$$S_f = \frac{\tau_y}{\rho g R_h} \left[ 1 + \left( \frac{(\epsilon + 1)(\epsilon + 2)|V|}{(0.74 + 0.65\epsilon) \left( \frac{\tau_y}{k} \right)^\epsilon R_h} \right)^{\frac{1}{\epsilon + 0.15}} \right] = \frac{h_f}{f_D} \quad \text{Equation 76}$$

In their model Jin and Fread (1997) used a one dimensional dynamic unsteady flow equation by adding the frictional slope term  $S_f$  in the momentum Saint Venant equation, based on rheological properties of the flowing mud/debris – water mixtures. Their technique involves determining the friction slope of mud/debris flow based on a semi-empirical rheological power-law equation. The derivation of the friction slope term  $S_f$  of the flow will thus depend on the rheological model for shear stress vs shear rate of the non – Newtonian fluid Equation 79 will be used in this thesis as flow

resistance factor for modelling air slide capacity. Other flow resistance factors are given in Table 34 and can be used, but they do not include a rheological kernel.

### 7.2.3 Saint Venant steady state

At steady state  $\lim_{t \rightarrow \infty} \frac{\partial A}{\partial t} = 0$  and  $\lim_{t \rightarrow \infty} \frac{\partial Q}{\partial t} = 0$ . Thus from the continuity equation it results that  $Q = Au$  constant and then differentiating with respect to  $x$ :

$$A \frac{\partial u}{\partial x} + u \frac{\partial A}{\partial x} = 0 \quad \text{Equation 77}$$

$$\frac{\partial A}{\partial x} = b \frac{\partial h}{\partial x} + h \frac{\partial b}{\partial x} \quad \text{Equation 78}$$

Letting  $\frac{\partial b}{\partial x}$  be equal to the constant,  $C$ :

$$\frac{\partial A}{\partial x} = b \frac{\partial h}{\partial x} + hC \quad \text{Equation 79}$$

Substitution back into the continuity equation gives:

$$u \left( b \frac{\partial h}{\partial x} + hC \right) + A \frac{\partial u}{\partial x} = 0 \quad \text{Equation 80}$$

Expressing  $\frac{\partial u}{\partial x}$  as a function of  $\frac{\partial h}{\partial x}$ :

$$\frac{\partial u}{\partial x} = - \frac{uhC + ub \frac{\partial h}{\partial x}}{A} \quad \text{Equation 81}$$

Substitution into the momentum equation gives:

$$\frac{\partial \left( \frac{\beta Q^2}{A} \right)}{\partial x} = Ag \sin \theta - Ag \cos \theta \frac{\partial h}{\partial x} - Ag S_f \quad \text{Equation 82}$$

$$\beta Q \frac{\partial u}{\partial x} = \frac{Q}{u} g \sin \theta - \frac{Q}{u} g \cos \theta \frac{\partial h}{\partial x} - \frac{Q}{u} g S_f \quad \text{Equation 83}$$

Multiplication by  $\frac{u}{Q}$  on both sides gives:



$$\beta u \frac{\partial u}{\partial x} + g \cos \theta \frac{\partial h}{\partial x} = g(\sin \theta - S_f) \quad \text{Equation 84}$$

$$-\beta u \left( \frac{uhc + ub \frac{\partial h}{\partial x}}{A} \right) + g \cos \theta \frac{\partial h}{\partial x} = g(\sin \theta - S_f) \quad \text{Equation 85}$$

$$\frac{\partial h}{\partial x} = \frac{Ag(\sin \theta - S_f) + \beta u^2 hC}{Ag \cos \theta - \beta u^2 b}$$

Equation 86

The denominator of  $\frac{\partial h}{\partial x}$  characterizes the flow, the flow becomes critical when the denominator approaches zero value Agu and Lie (2014):

$$Ag \cos \theta - \beta u^2 b \geq 0 \quad \text{Equation 87}$$

Multiplication by  $A^2$  gives:

$$A^3 g \cos \theta - \beta Q^2 b \geq 0 \quad \text{Equation 88}$$

Thus the expression for flow rate, Q becomes:

$$Q \leq \frac{(\cos \theta)^{\frac{1}{2}} g^{\frac{1}{2}} b h^{\frac{3}{2}}}{\beta^{\frac{1}{2}}} \quad \text{Equation 89}$$

What is interesting to point out is that the capacity that the model is predicting for critical flow is proportional to the cosine of the angle of downward air slide inclination  $\cos \theta$ , at the power of 0.5, width  $b$  and the height of the bed  $h$  at the power of 1.5. A similar proportionality  $Q \propto b h^{\frac{3}{2}}$  was found by Dyrøy (2006) in his SSBD model when designing the anti-segregation system for a rectangular tube.

#### 7.2.4 Rheometrical experiments at share rate ramp- up

The author built up and used a small fluidisation column together with a Brookfield rheometer at the Wolfson Centre, in order to conduct some simple rheometry tests. The motivation for conducting the experiments was based on three strong arguments; first argument being that results from empirical modelling showed average bed velocity could be modelled as a power law. From empirical modelling results in Chapter 6 Figure 110, it became clear that in an 15 long air slide segment with short accelerating zone where the flow reaches steady state after, 3.5 - 5 m, the exponent of power low

model was constant for all range of  $U_0/U_{mf}$ , independent of bed height changes and air slide inclination. The values of the power law coefficient, on the other side, had increasing trends with increasing value of  $U_0/U_{mf}$ . Another solid argument for using rheometry was that shallow water equations using Jin and Fread's (1997) formula needed a rheological kernel. Another argument was the work of Bruni et al. (2005) showing that a power law model could be successfully fitted to the shear rate/shear stress curves at different rates of fluidization of alumina.

The general equation of the Herschel-Bulkley model used by Bruni et al. (2005) is:

$$\tau = \tau_y + k \left( \frac{\partial u}{\partial y} \right)^n \quad \text{Equation 90}$$

The Herschel-Bulkley model in Equation 90 was fitted to the curves presented in Figure 111 for each rate of aeration and then values for the model parameters were calculated. The results showed that the alumina powder had yield stress behaviour at fluidization velocities below  $U_{mf}$  (minimum fluidization velocity) and power law behaviour,  $\tau_y = 0$ , at gas velocities above  $U_{mf}$ , with  $n$  increasing with higher aeration. The  $U_{mf}$  measured by Bruni et al. (2004) was found to be  $0.36 \text{ cm s}^{-1}$ , which is circa 50% lower than the  $U_{mf}$  measured at POSTEC and the Reference Centre Årdal by the author of this report. The results of Bruni et al. (2004) are shown in Figure 111.

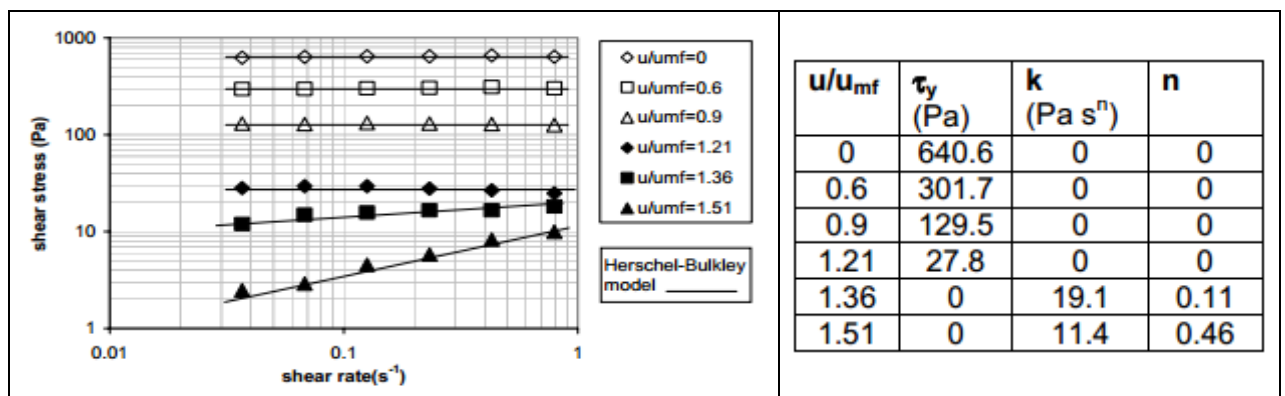


Figure 111 Bruni (2004). Alumina rheogram and calculated values for the Herschel-Bulkley model parameters.

Based on the above literature results, a small rig was built by the author as shown in Figure 112.

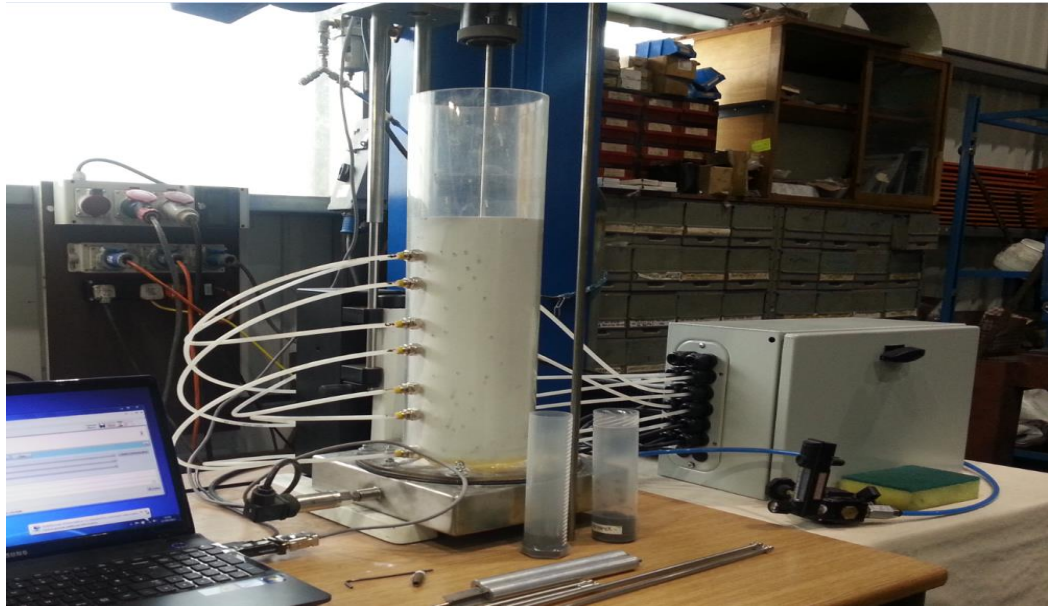


Figure 112 Fluidization column and Brookfield reometer to study the behaviour of alumina.

Three tests were undertaken to study the rheometrical behaviour of the alumina around minimum fluidization velocity. The results, plotted as log shear stress/log rate are shown in Figure 113, Figure 115 and Figure 116.

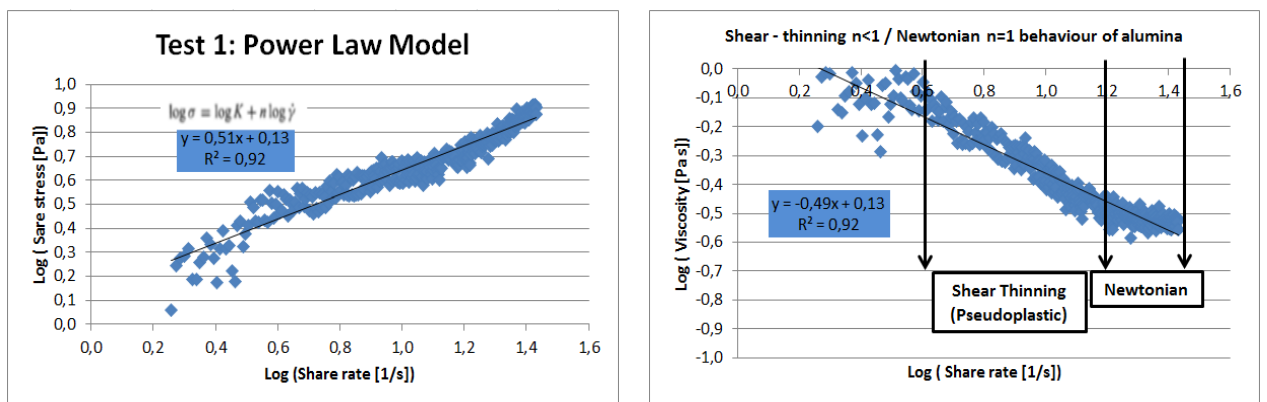


Figure 113 Alumina rheogram. Test 1 Power law model results.

From Figure 113 and Figure 112 following values:  $k = 1.35$  and  $n = 0.51$ ,  $\tau_y \sim 0$  will be used.

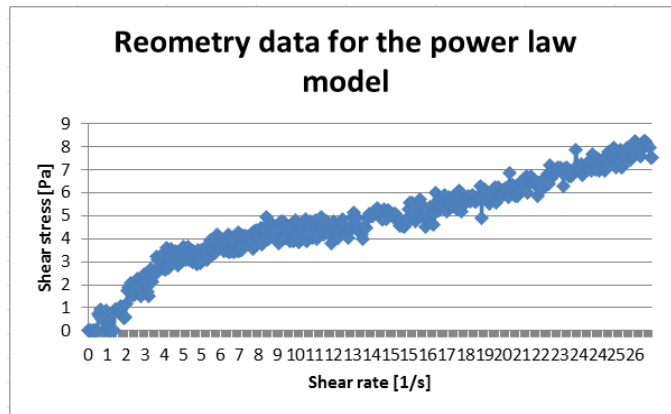


Figure 114 Alumina rheogram. Raw data Test 1.

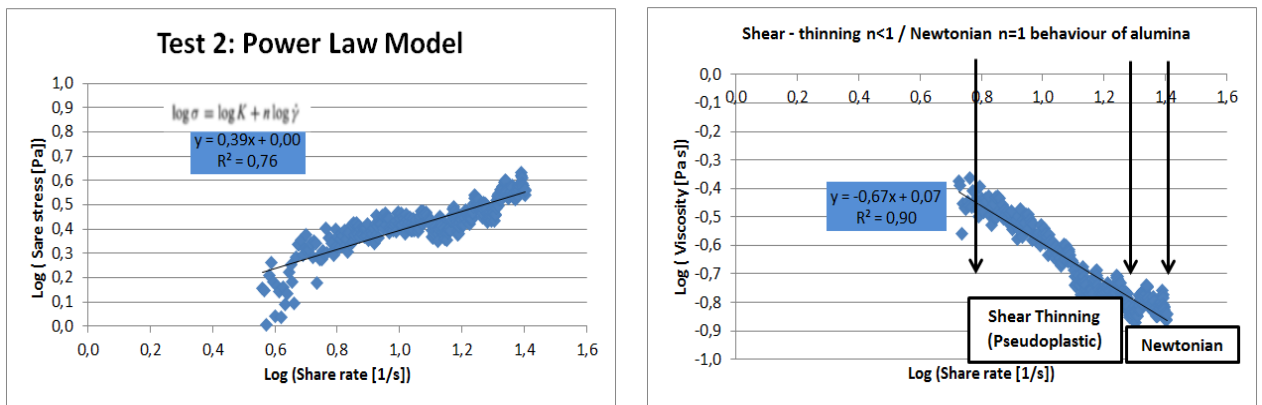


Figure 115 Alumina rheogram. Test 2 Power law model results.

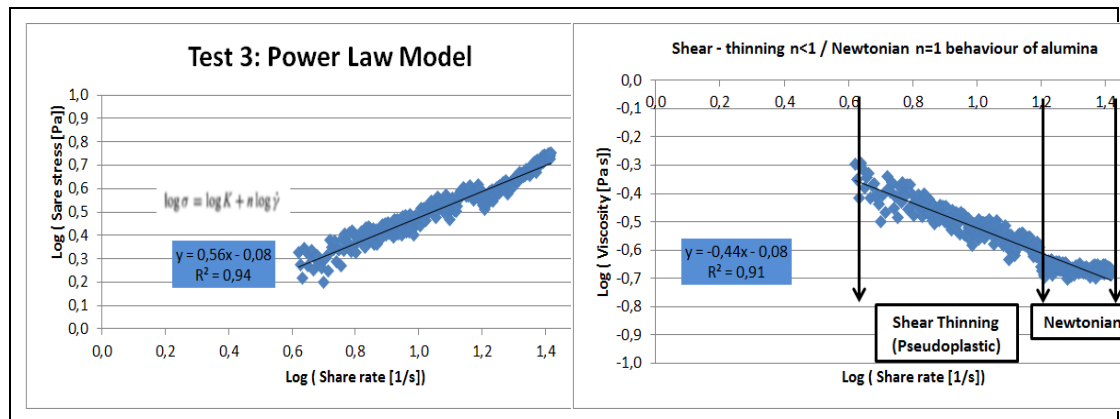


Figure 116 Alumina rheogram. Test 3 Power law model results.

More rheometry tests could have been conducted at different bed heights and different fluidization velocities, since some considerable amount of work had been put into purchasing the Brookfield rheometer, adjusting it to the column, and in commissioning of the fluidization column. The purpose of the measurements at the time they were taken was to gain some modest appreciation of what  $n$ , and  $\tau_y$  could be, and what kind of law they would obey: power law or Herschel-Bulkley law. Bruni et al.'s (2005) findings were interesting in showing that at higher  $U_0/U_{mf}$  the

Herschel-Bulkley model will move towards a power law model. It is the author's belief that a rheometer will not be able to capture the transport mechanisms in an air slide entirely. The author agrees more with Savage and Oger's (2013) affirmations, that the rheometry measurements will serve more as a curve fit to the data. Once the calibration of the model with measured data will give reasonable results or not, then further decisions can be made about the necessity of conducting more experiments.

### 7.2.5 Boundary and initial conditions

To implement the scheme proposed by Agu and Lie (2014) for steady state flow, the initial and boundary conditions must be specified in MATLAB. Only the upstream boundary:  $Q_0$  and  $h_0$  have been specified, where  $Q_0$  is the average capacity from LabView measurements and  $h_0$  is the bed height at the first measurement point situated at ca. 0.5 m from the outlet of the standpipe. This approach corresponds to supercritical flow in Agu and Lie's (2014) work. In addition to  $Q_0$  and  $h_0$ , the length of the air slide segment  $x = L$  needs to be specified.

The steady state solutions implemented in MATLAB are based on the ordinary differential equations (ODE) given by Equation 77. The MATLAB code originally implemented by Agu and Lie (2014) was used. MATLAB has several different built in functions for the numerical solution of the ODE. The ode15 solver has been used with the following syntax:

<b>function</b> Xdx	NNF_rectangular_channel(x,X)	
[x,X]	ode15s	(@NNF_rectangular_channel,x_span,X_0)

- [x,X]: an array, the solution of the system: bed height and average bed velocity at every point in space, at each measurement point along the air slide;
- ode15s: Solver, Matlab algorithm, e.g. ode15s, ode23;
- @NNF\_rectangular\_channel: handle for the function;
- x\_span: space interval;
- X\_0: Initial conditions;

The author of this thesis made some modifications to the code to adapt it for the geometry in this thesis. A cubic spline function was implemented to interpolate the measured values for height and velocity, in order to compare them with simulated values.

### 7.3 MATLAB simulations

To better understand how the shallow water model works, a diagram of the model is shown below in Figure 117:

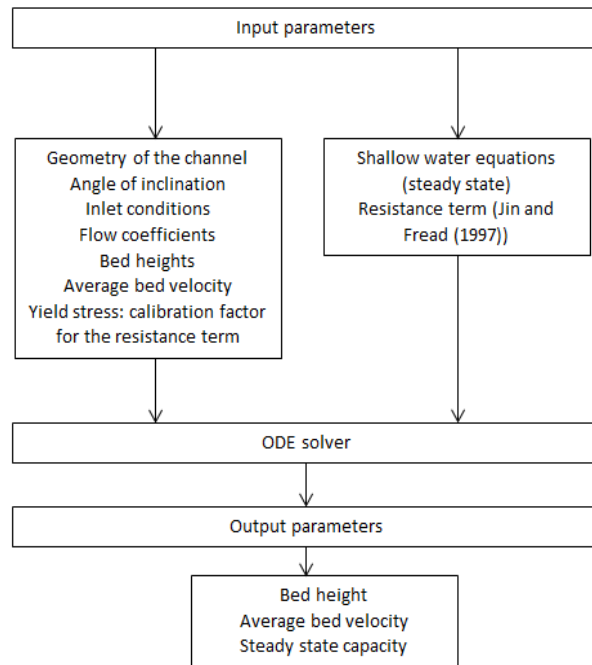
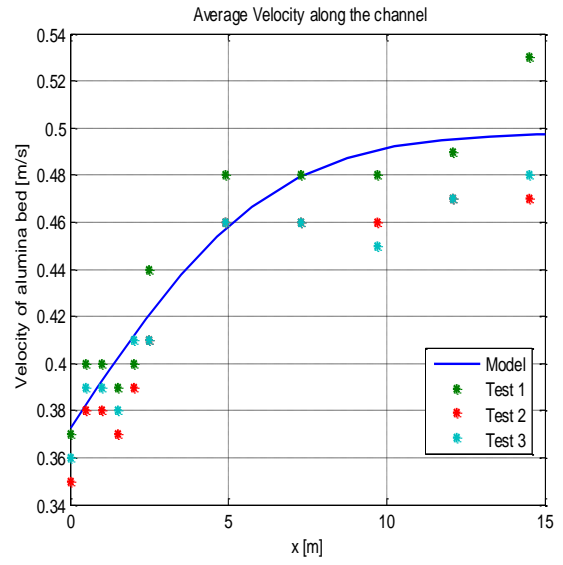
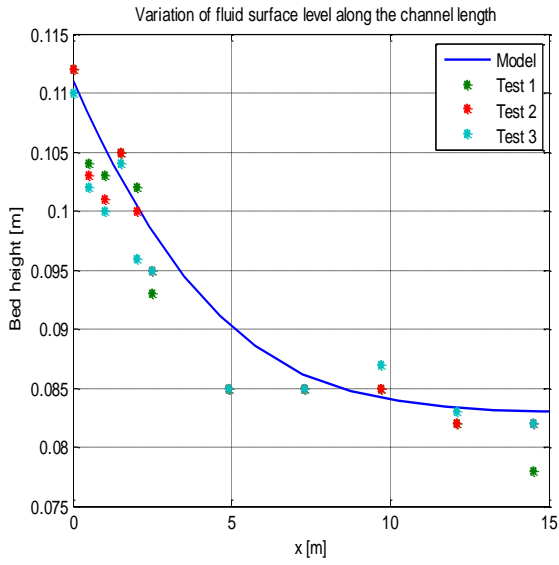


Figure 117 Diagram of the model implemented in MATLAB.

Although this work has been built on a simple model based on a set of nonlinear equations implemented in MATLAB, the huge amount of data generated during the tests was pre-processed in Excel. Some quick simulations of height and velocity for a 15 m air slide segment were made to test the model. The flow coefficients  $K$  and  $n$  obtained from reometry measurements were kept constant in the expression of  $S_f$  representing the friction slope or the flow resistance term. As a starting point, Jin & Fread's (1997) friction factor was used for modelling:

$$S_f = \frac{\tau_y}{\rho g R_h} \left[ 1 + \left( \frac{(\epsilon + 1)(\epsilon + 2)|V|}{(0.74 + 0.65\epsilon) \left(\frac{\tau_y}{k}\right)^\epsilon R_h} \right)^{\frac{1}{\epsilon + 0.15}} \right] = \frac{h_f}{f_D}$$

with following values:  $k = 1.35$   $n = 0.51$  and  $\tau_y \sim 0$  will be used, where  $\epsilon = 1/n$ .



**Figure 118 Flow profiles at 4 bar: a) Bed height measurements compared to model results; b) Velocity measurements compared to model results. Model parameters:  $K = 1.35$ ,  $n = 0.51$ ,  $\theta = 1.1^\circ$ ,  $\tau_y = 12.5e^{-3}$ ,  $h_0 = 0.111m$ ,  $Q_0 = 0.0062 m^3/s$ .**

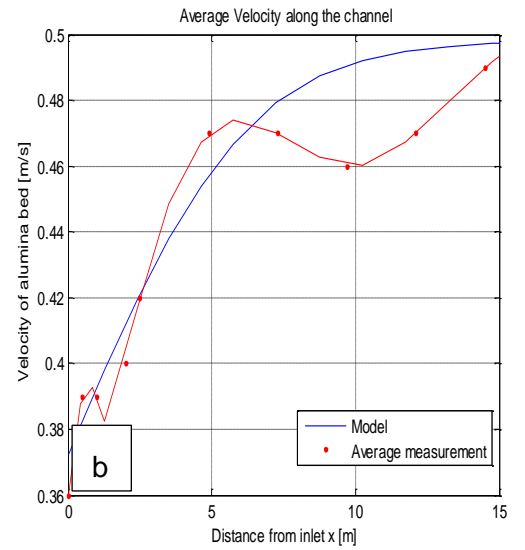
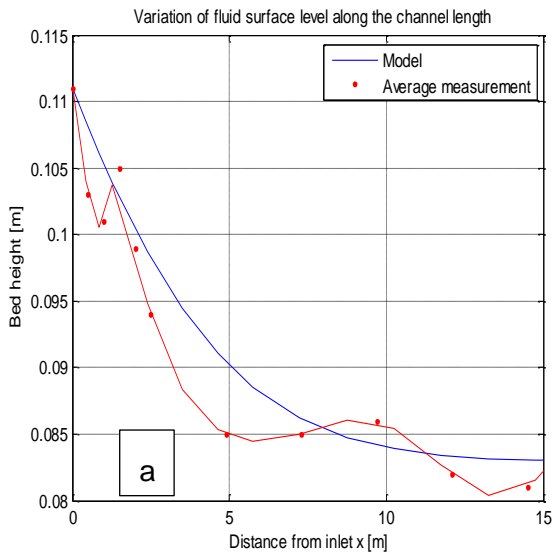


**Figure 119 Flow profiles at 4 bar. Spline function to interpolate the average of three measurements (red) and model results (blue). Model parameters:  $K = 1.35$ ,  $n =$**

0.51,  $\theta = 1.1^\circ$ ,  $\tau_y = 12.5e^{-3}$ ,  $h_0 = 0.111m$ ,  $Q_0 = 0.0062 m^3/s$ . a) Bed heights, b) average velocity profiles.

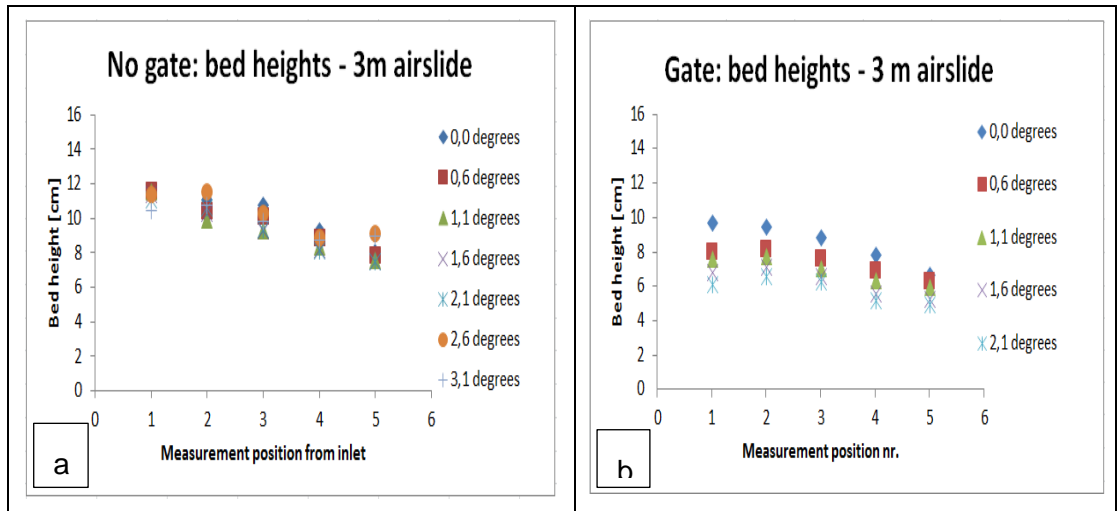


Figure 120 Bed heights profiles a) no gate b) gate.

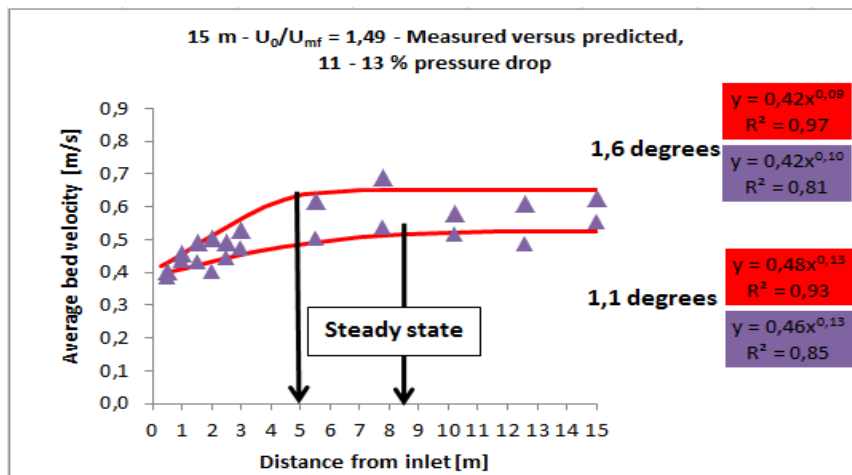
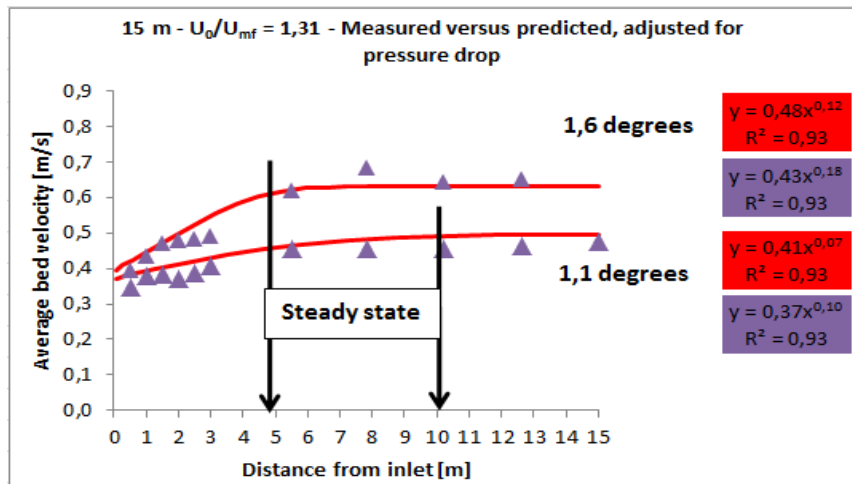
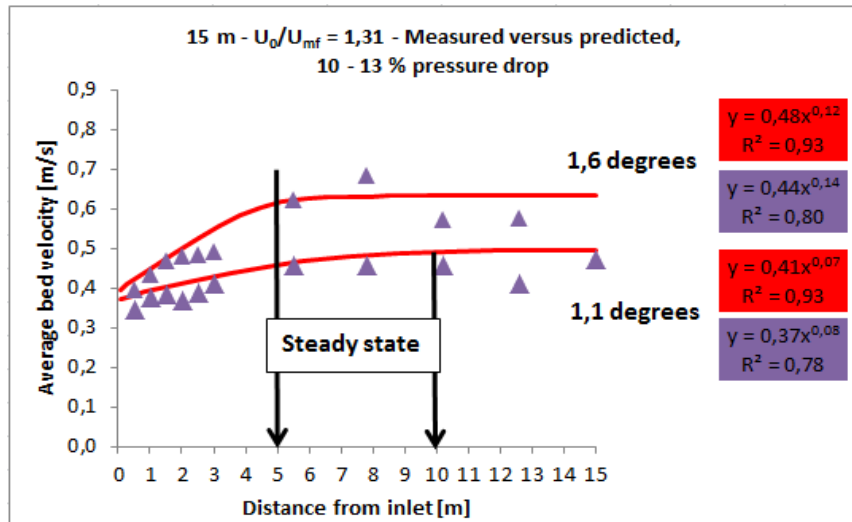
#### 7.4 Simulation results

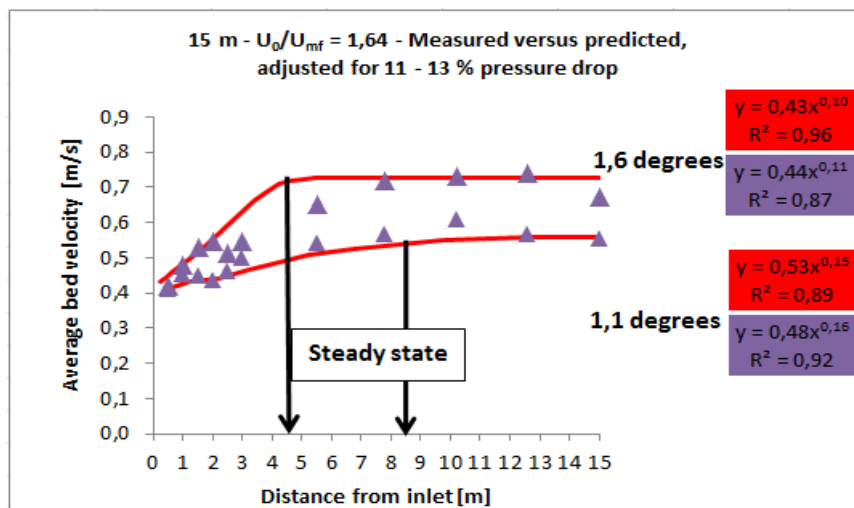
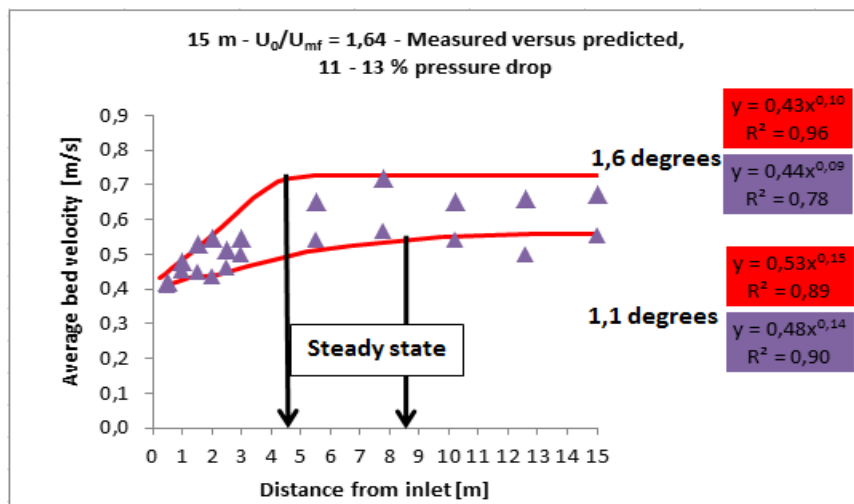
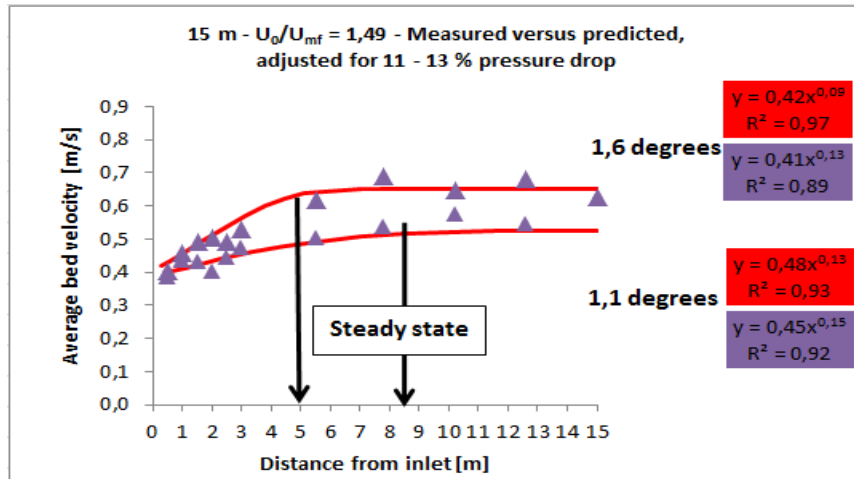
Depending on the friction between the alumina bed conveyed and the bottom/walls of the air slide together with the downward inclination of the air slide the average velocity of the particles within the bed reduces after a certain distance from inlet, reaching steady state. This velocity reduction is dependent on other parameters such as bulk density and air velocity. In this work only one alumina quality has been tested and the bulk density has been assumed constant. One important factor in this velocity reduction is the yield stress,  $\tau_y$  which directly influences the resistance term,  $S_f$ . To calculate the reduction in material velocity, following simplifications have been made: the bed of alumina entering the inlet of the air slide is in a fully accelerated state with negligible slip velocity. In order to achieve steady state the bottom stress is much higher than the yield stress. Results from empirical modelling to predict the average bed velocity carried out in Chapter 6 showed the acceleration zone was 4.5 – 5 m long in a 7 m long air slide segment. Studying bed heights in a 7 m long segment one can see they become constant already after 3 – 3.5 m for inclination angles higher than 0.6 degrees. In the 15 m long segment the acceleration zone is 5 m long; this conclusion was made in the absence of measurements from 3 to 5 m away from inlet. Average bed velocity was best modelled using a power law. This will be a challenge for the shallow water model, whether it will be able to capture the trends seen in Chapter 6 or not.

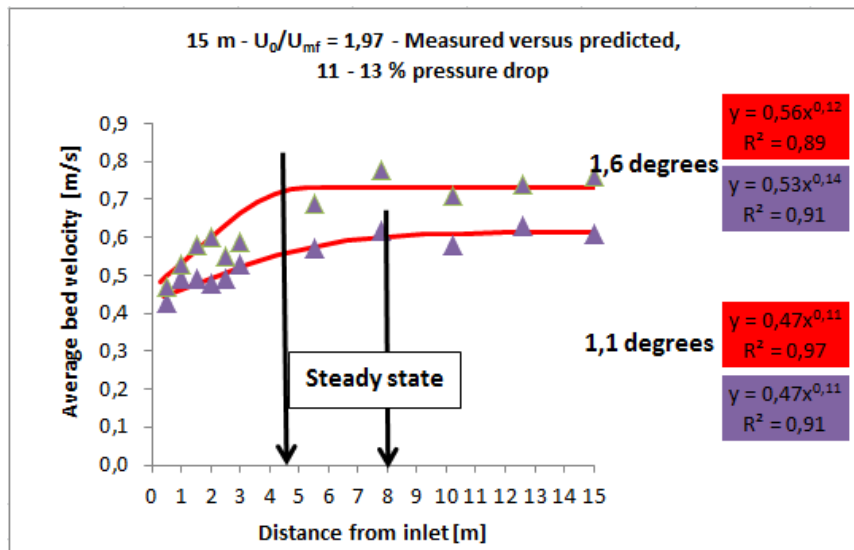
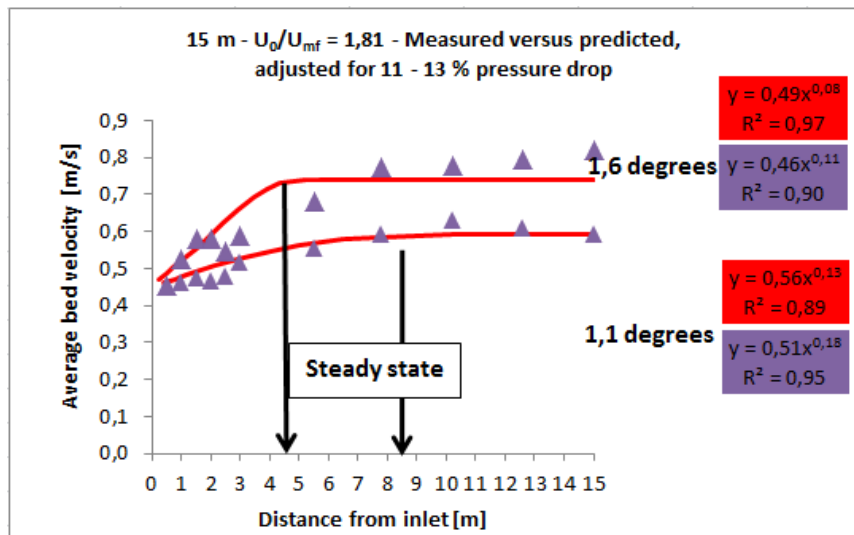
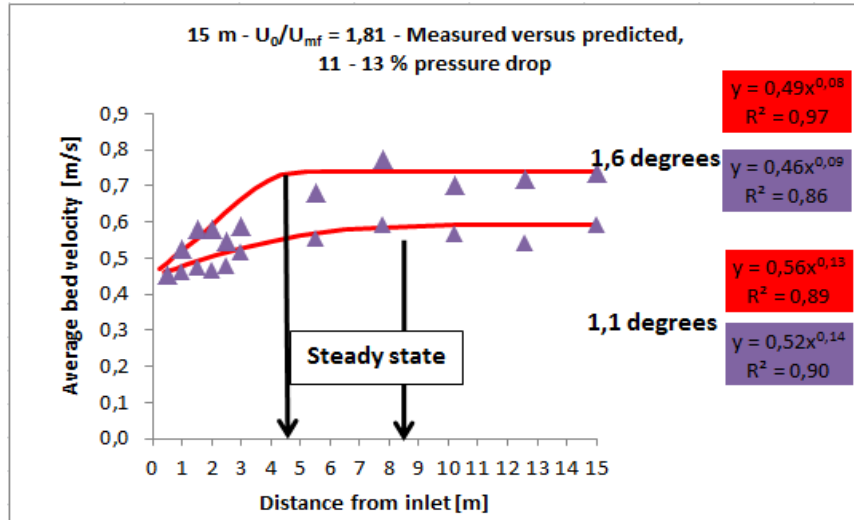


#### 7.4.1 The effects of inclination angle and air velocity on resistance slope

A possible procedure to be followed when attempting to match experimental data to the Saint Venant model was to keep the flow coefficients  $K$  and  $n$  from rheometry measurements constant and vary  $\tau_y$ . The procedure was based on first finding a fixed value of  $\tau_y$  close to zero,  $\tau_y = 0.0125$  starting at the maximal slope of the channel at 1.6 degrees and lowest  $U_0/U_{mf} = 1.31$  as shown in Table 35. Results of shallow water steady state model compared to average bed velocity measured data are shown in Figure 121. The plots in the left columns show the raw data, based on a 10 up to 13 % pressure drop in the pressurized air supply tube. Power law curves were fitted to the shallow water model and to the measured data:  $Y_{measurement} = K(\theta, U_0/U_{mf})x^{P(\theta, U_0/U_{mf})}$ , where  $Y_{measurement}$  is the average bed velocity calculated by the shallow water model,  $\frac{\partial v}{\partial x}$  at each measurement point,  $\partial x$ . The coefficient and the exponent of the power law are a function of both the inclination angle  $\theta$  and the dimensionless coefficient of velocity  $U_0/U_{mf}$ . The red line represents the trend line of the power law behaviour of the shallow water model. The corresponding equations are highlighted in red (model) and purple (measurement). An uneven drop in average bed velocity can be seen for the last three measurement points, at a 10 m distance away from inlet. To compensate for this the values of the average bed velocity at 10 and 12 m away from the inlet have been multiplied by 10 to 13 % according to the pressure drop recorded by the pressure sensors for each  $U_0/U_{mf}$ . The results of the adjustment are shown in the right columns: the values  $R^2$  (purple) have increased from 0.80 to 0.93 for 1.6 degrees inclination. A corresponding increase occurred for all values of  $U_0/U_{mf}$  at both 1.6 and 1.1 degrees downward inclination. In Hydro the standard has been to use  $1.1^0$  downward inclination. The model does not work for 0.0 and 0.6 degrees. As the magnitude of the friction on the bottom, between the moving alumina bed and the fluidization membrane is not known, and it could not be directly measured, the model needs to be calibrated against measured data by adjusting the  $\tau_y$  values.







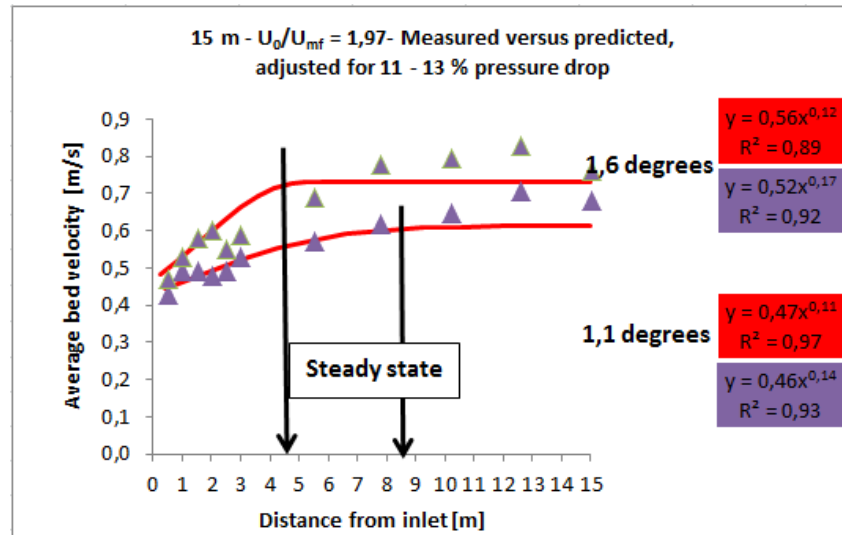


Figure 121 Simulation results for  $\theta = 1.1$  and  $1.6$  degrees, measured versus predicted. Left: 10- 13% pressure drop, right: pressure drop adjusted.

Comparing the results of the model developed from predicted results of the Saint Venant model (red line in Figure 121) with the measurement results (blue) one can see that both follow a power law. The mathematical model manages to capture the lengths of the acceleration zones very well compared to the test data. Results of the model and the raw data from Figure 121 are presented in Table 35. Both operational parameters  $U_0/U_{mf}$  and  $\theta$  influence the length of the acceleration zone,  $\theta$  being the parameter with the highest influence as seen from Table 35. By increasing the inclination angle from  $1.1$  to  $1.6$  degrees, this will decrease the length of the acceleration zone by 50 % at low  $U_0/U_{mf}$  and by 41 % at  $U_0/U_{mf}$  above 1.49. Increasing air velocity further will not influence the acceleration zone length. The results of the curve fit indicate that for an increase in  $U_0/U_{mf}$  to maximum value of 1.97, a decrease by factor 7 is required for a good correlation between the model and the empirical data.

Table 35 Lengths of acceleration zones as a function of  $U_0/U_{mf}$  and  $\theta$  and calibration values of  $\tau_y$ .

$U_0/U_{mf}$	Acceleration zone length [m]				Difference from $1.1^\circ$ to $1.6^\circ$ in acceleration zone length
	$1.6^\circ$		$1.1^\circ$		
		$\tau_y$		$\tau_y$	
1,31	5	0,0125	10	$7,0 * 0,0125 = 0,09$	50 %
1,49	5	$0,0125/1,75 = 0,007$	8,5	$6,5 * 0,0125 = 0,08$	41 %
1,64	4,5	$0,0125/3,5 = 0,004$	8,5	$5,2 * 0,0125 = 0,07$	41 %
1,81	4,5	$0,0125/5,25 = 0,002$	8,5	$4,35 * 0,0125 = 0,05$	41 %
1,97	4,5	$0,0125/7 = 0,002$	8,5	$3,5 * 0,0125 = 0,04$	41 %

A summary with the equations in Figure 121 is presented in Table 36.

Table 36 Summary of Figure 121: power law equations for 1.1 and 1.6 degrees downward inclination at  $U_0/U_{mf} = 1.31 \dots 1.97$ .

$U_0/U_{mf}$	1,6°				Difference		1,1°				Difference	
	Model (predicted)	R <sup>2</sup>	Measured (calculated)	R <sup>2</sup>	Coefficient K	Exponent $\theta$	Model (predicted)	R <sup>2</sup>	Measured (calculated)	R <sup>2</sup>	Coefficient K	Exponent $\theta$
1,31	$y = 0,48x^{0,12}$	0,93	$y = 0,44x^{0,18}$	0,93	-9 %	33 %	$y = 0,41x^{0,07}$	0,93	$y = 0,37x^{0,10}$	0,93	-11 %	30 %
1,49	$y = 0,42x^{0,09}$	0,97	$y = 0,41x^{0,13}$	0,89	-2 %	31 %	$y = 0,48x^{0,13}$	0,93	$y = 0,45x^{0,15}$	0,92	-7 %	13 %
1,64	$y = 0,43x^{0,10}$	0,96	$y = 0,44x^{0,11}$	0,87	2 %	9 %	$y = 0,53x^{0,15}$	0,89	$y = 0,48x^{0,16}$	0,92	-10 %	6 %
1,81	$y = 0,49x^{0,08}$	0,97	$y = 0,46x^{0,11}$	0,90	-7 %	27 %	$y = 0,56x^{0,13}$	0,89	$y = 0,51x^{0,13}$	0,95	-10 %	0 %
1,97	$y = 0,56x^{0,12}$	0,89	$y = 0,52x^{0,17}$	0,92	-8 %	29 %	$y = 0,47x^{0,11}$	0,97	$y = 0,46x^{0,14}$	0,93	-2 %	21 %

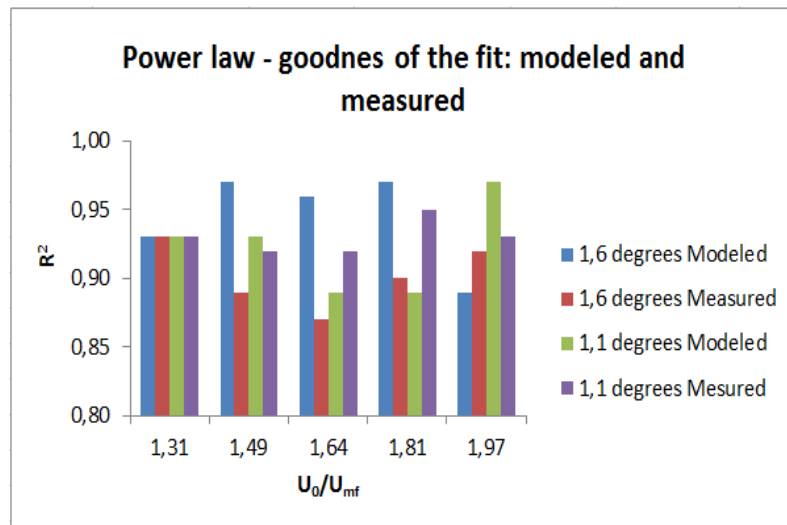
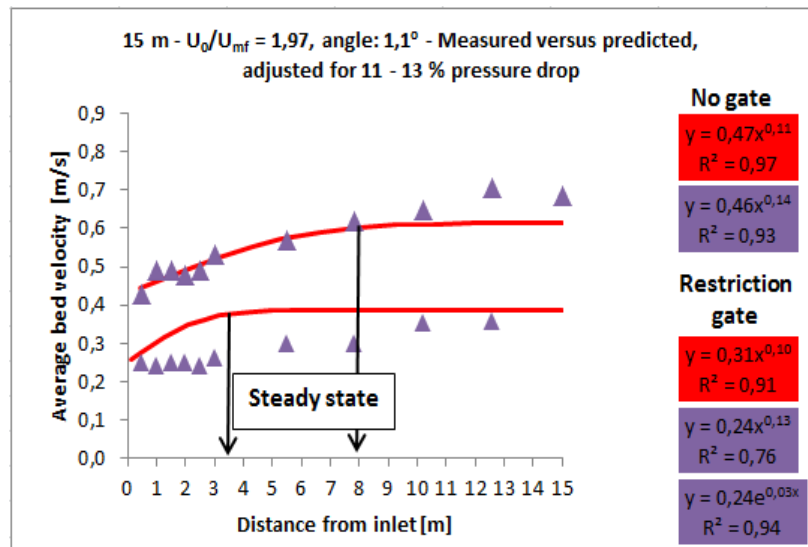
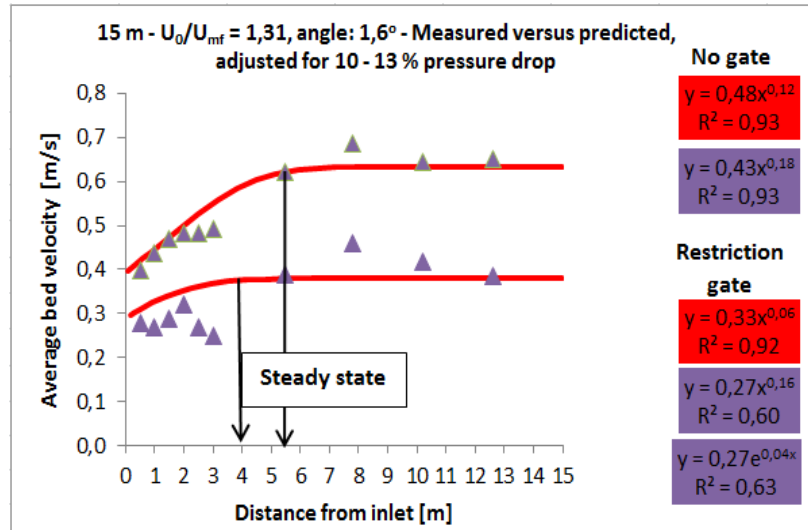
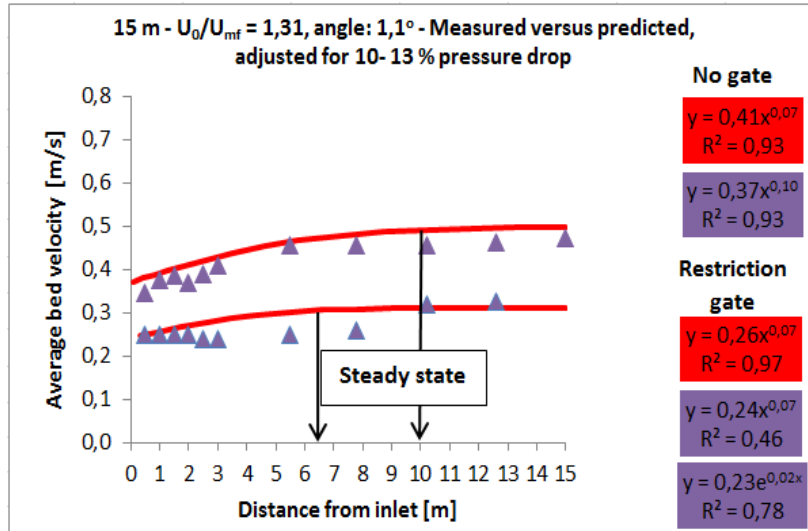


Figure 122 Values of R<sup>2</sup> expressing the goodness of the fit for the power law models.

#### 7.4.2 The effects of inlet configuration on resistance slope

An identical analytical procedure to that described above was followed for the second set of experimental data, test runs conducted with a restriction gate, results are presented in Figure 123. Same values of  $\tau_y$  as presented in Table 35 have been used to simulate the average bed velocity for a modified inlet configuration. A restriction gate was used to minimize the height of the inlet. Tests with no gate and with restriction gate were compared to investigate the sensitivity of the curve fits and how the values of  $\tau_y$  would change with inclination and velocity.



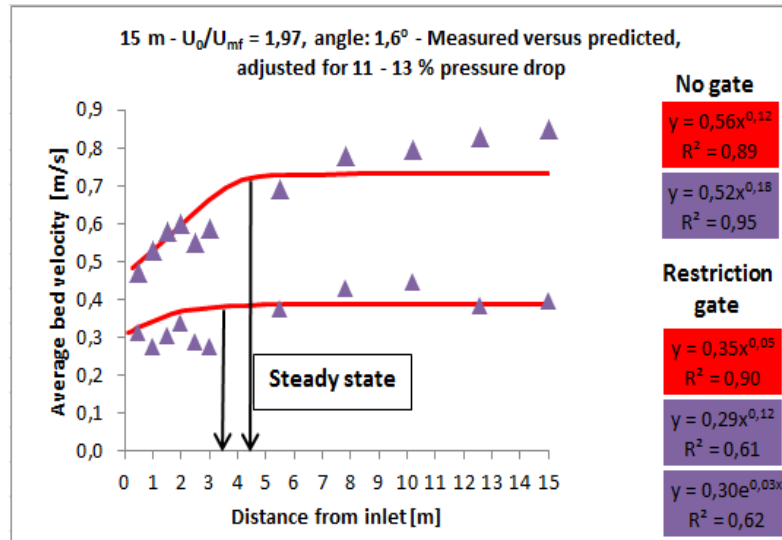


Figure 123 Simulation results for  $\theta = 1.1$  and  $1.6$  degrees, measured versus predicted, gate and no restriction gate.

## 7.5 Conclusions

The shallow water model is a conservative model for predicting bed heights and average bed velocity requiring calibration of the resistance factor through comparison towards measured data. The areas of doubt in the mathematical model surround the bulk density of the flowing bed of alumina as its value taken from fluidised beds that are stationary was kept constant, similar technique as used by Woodcock (1978), and herein lies a weakness of the model. Attention was especially given to the shear stresses at the base of the channel, similar to Woodcock's (1978) approach, in which the shear stress at the side – walls of the channel was assumed constant. Although direct measurements of these stresses could not be made, some indication of the way in which they vary with flow conditions and inclination of the air slide was obtained by applying a curve fit procedure when analysing the correlation between the model and the experimental data. This model could be an effective tool for design purposes and could be used for both long and short air slide systems provided that the standpipe and powder lock are already part of the design and are implemented. For a given geometry: inlet configuration, width, length and inclination of air slide it requires following inputs: mass flow rates measured on line, bed heights (static or dynamic) and flow coefficients. The model needs calibration with any measurement data by adjusting the expression of the resistance term,  $S_f$ . Once the bed heights and average bed velocity have been predicted the steady state capacity can be calculated. One weakness of the model is that it needs rheometry measurements for a range of air velocity and bed heights. In the current state,



based on rheometry measurements taken around minimum fluidization velocity, the prediction accuracy of the model after calibration, compared to the measurement data is between -11 up to +2% for the coefficient values,  $K$  and 0 up to 33 % for the exponent values  $\theta$ . The model follows the trends seen in Chapter 6, where average bed velocity was best predicted by using a power law:  $y_{measurement} = Kx^\theta$ . There is still room for improvement of the accuracy of the model by refining the rheometry measurements or by using the air slide as an on line rheometer device. Refined knowledge of the flow coefficients and how they change as a function of  $U_0/U_{mf}$  and inclination will give more knowledge about the resistance term and how inclination and air velocity affects it. Same material has been used for the tests. It is a strong belief of the author that rheometry tests with different alumina grades and percentage of fines will push the accuracy of the model further.

The mathematical model manages to capture the lengths of the acceleration zones very well compared to the test data, an angle of 1,6 degrees will give a shorter acceleration zone than a 1,1 angle due to increased resistance on the bottom of the air slide, due to increased friction between the bed of material and the bottom of the air slide.

## 8 CONCLUSIONS

The programme of study described in this thesis was aimed to gather as much as possible of the published work addressing air slide gravity conveying of bulk particulate solids. From an analysis of the existing literature and supported by a huge amount of experimental data, an approach to modelling bed velocity of fluidised alumina in an air slide was developed. Prediction of bed velocity in air slides has been a field of powder technology involving considerable amount investigation for the past four decades. Many researchers have suggested predictive models based on open channel flow, yet not so many have managed to incorporate the effect of interfaces and inlet configuration into their models. These developed models either do not take into account the effect of the interfaces on flow stability, or they do not use long enough segments of air slide to achieve steady state. This work was a continuation of Lars Haugland's work started in 1994. Although Haugland did not use a standpipe concept in his work, he highlighted the effect of interfaces on air slide capacity. Haugland's work was based on a Newtonian approach using the model that Woodcock (1976) had developed during his PhD work.

This work has made some valuable contributions to the state of the art of alumina transport modelling and predictions of steady state capacity. A literature review showed that although this thesis is based on existing concepts, no other researcher has previously used a standpipe, the powder lock concept and the shallow water model together, in order to predict capacity in an air slide. For researchers designing air slide systems and using the shallow water models it is therefore important to have a holistic approach to these systems. The conclusions drawn from the work presented in this thesis are presented below in terms of initial and improved objectives of the project presented in Chapter 1, Section 1.4. Feeder operation and performance was initially not an objective of this thesis. It became clear after analysing the results from the first round of air slide capacity tests conducted at POSTEC in 2012, that in order to achieve the initial objectives of the project "Air slide basic modelling", one should include the impact that air slide interfaces: e.g. feeders and feeders outlet design have on the capacity of an air slide. Thus a considerable part of the time allocated to the programme was focused on feeders and spent on trouble shooting and re-design of the original alumina rig. While air slide segments of 3 m, 7 m and 15 m lengths were used for the experiments, only one width of conveying air slide at 150 mm was used in the present

investigation, this was the standard as far as industrial applications in Hydro were concerned.

When it comes to feeder performance, the outputs in this research clearly demonstrated that the dump weights taken from volumetric feeders on the alumina rig in Årdal, presented in Section 3.4, are strongly affected by powder flow properties, amount of pressurized air supplied to the system and mechanical design and feeder/air slide interfaces. Thus feeder parameters should be adjusted according to the flow properties of the powder to be dosed. Feeders are not something the aluminium industry can buy on the market, as they need to be representative in terms of operation that is required and of the flow behaviour of powder mixtures used in the aluminium production. It has taken years and years of multidisciplinary research and development, R&D, to develop and verify the existing technology and yet there is still work to be done in order to optimise feeder performance. A considerable amount of work has been published on both process modelling related topics and on aluminium production in general. Yet the number of publications focusing on alumina flow behaviour and design of feeding equipment is small. This may be due to high price of the measurement programmes to assess the robustness and performance of such equipment or due to intellectual property confidentiality restrictions imposed by the various companies on this type of technology. Although techniques for design of storage vessels, feeders and silos based on the flow characteristics of particulates have been in the public domain since the 1960's, they have been slow to gain acceptance in the aluminium industry. There is a scientific understanding gap that needs to be filled and that has led to:

- limited industrial research in feeder operation and performance correlating both alumina and binary mixtures flow characteristics, mechanical design (interfaces) and repeatability of dump (dose) weights;
- limited understanding of the effect of interfaces between feeders and air slides;
- insufficient measurements and poor control of the dump (dose) weights during operating cycles and especially during shifts in powder quality, that compromise the final dump weight;
- ongoing research work focusing on the development of various feeder operation principles: both dosing and gravity discharge with different interfaces, verified, patented and standardised through trial and error measurement programmes;

The costs of R&D activities concerned with powder technology development could be optimized and variations in dump weights could be at least anticipated and minimized if powder flow properties of the powder and binary mixtures were measured during the concept stage, before huge equipment investments being made, and not after.

There are many available studies of the fluidisation phenomena and formulas for prediction of minimum fluidisation velocity,  $U_{mf}$  (expressed in *cm/s* in this work). For best accuracy of the results and the modelling work the author felt that it would be better to undertake own practical tests on both alumina and binary mixtures of alumina and aluminium fluoride. This thesis studied in depth the feeder operation and performance based on a correlation between chemical analysis and mass balance from a measurement programme conducted on an alumina rig at the Reference Centre in Årdal. The results from this programme were the driving force and provided the motivation throughout the whole period of time it took to shape and complete this thesis. In order to understand the mechanisms that caused the high coefficients of variation in the dump weights from the feeders, literature was reviewed, focusing mainly on powder characterisation and flowability and vessel design for flow. The powder flowability tests on the FTP and rheometry tests undertaken at the Wolfson Centre provided this project with an advanced understanding of the factors affecting the dump weights during feeder operation although rather less time than would have been desirable was left for rheometry measurements. This will be valuable knowledge to take back to the industry.

The literature reviewed provided a good foundation for understanding, eliminating and solving the bottlenecks in the mechanical design of feeder and silo outlet design.

The modelling approach presented in Chapter 7, supported by empirical experience and experimental data, strongly suggests that it should be possible, with further experimental work, to establish a reliable method for predicting the capacity and flow behaviour of fluidized alumina in an air slide. The analytical model proposed by this thesis integrated air slide geometry, operational parameters and powder flow properties in the prediction of steady state capacity. The simulation work in MATLAB showed a good prediction of bed heights and velocities. The extent to which the modelling objectives have been achieved is probably mixed. A limitation of the model is that it needs flow coefficients for each quality of alumina passing through the system to be measured. Another limitation of the Saint Venant model is that it requires the steady

state value of capacity and bed height measurements as inlet conditions. The model has two applications:

1. Full scale feeding systems, with large feeding silos, standpipes, and long air slides attached to them, where monitoring the loss in weight of the silo would be difficult. The steady state capacity needs to be estimated or directly measured on line using a flow meter.
2. Small scale feeders with standpipes, where the loss in weight of the feeder can be monitored on line by using load cells.

Powder samples need to be taken from time to time, for both cases, and measure the flow coefficients by using a rheometer.

When it comes to contribution to existing knowledge, the research work presented in this thesis contributed substantially to the understanding of the feeder operation and clarified the interdependence between a feeder and an air slide, as well as the effect of interfaces on air slide capacity. The contribution has been made by proposing a model which can be applied to a holistic diagnosis of the system. The model has built on the foundation of earlier studies that had focused upon an assessment of air slide performance based on purely upon the output of a relatively short conveying section. However a review of this approach had shown that the model did not fit to an acceptable standard because the consistency and the homogeneity of the input stream had been neglected. A limitation of the model is that it needs flow coefficients to be measured using a rheometer, for each quality of alumina passing through the system. Another limitation of the Saint Venant model is that it requires the steady state value of capacity as inlet condition. The major requirement of future work is to determine the dependence of the measured parameter  $\tau_y$  in the proposed Saint Venant mathematical model on the nature of the powder quality in the air slide at different average bed velocities. Not so much emphasis has been put on the influence of particle size on the behaviour of fluidized powders and its impact on the capacity of an air slide, since Dyrøy (2006) had covered this aspect in his PhD work already. For example it may be well found that there is some correlation between  $\tau_y$ , the flowability and the fluidization behaviour of a powder according to Geldard, then work on the Saint Venant approach in this thesis will have been fully justified.

It can be concluded from this work that operation of air assisted gravity conveyors becomes stable and optimal once the stand pipe and the powder lock concepts are implemented, with the right amount of pressurized air applied to the system and with the right air slide downward inclination. Once the mechanical design has been optimized, one of the main concerns faced by the designers and operators of air slide conveyors should be the optimum quantity of pressurized air to be supplied to the system.

## 9 FURTHER WORK

The following recommendations for further work are made, not only based on what has been learned in this work, but also in terms of what could add further knowledge and benefit to research in the aluminium industry. It is further envisaged that by proving the principles laid out in this programme of work, an additional benefit could be brought to the industry when it comes to optimization of mechanical design of feeders and air slides. It is obvious from the findings presented in this thesis that there are a number of areas where further work could be carried out. The tests conducted on the alumina rig at the Reference Centre in Årdal and on the feeding silo at POSTEC showed the importance of controlled discharge and the need for a system that would be capable of discharging with improved repeatability for a wide range of powders: alumina, alumina fines and binary mixtures. A common cause of flow control problems in the aluminium industry when it comes to feeding alumina to the electrolysis cells has been the application of equipment types without paying attention to interfaces. Another cause of the same problems has been the application of equipment types without fully understanding the flow behaviour of powders. It is a big challenge to optimize the mechanical equipment and interfaces to suit every material to be handled. In the first instance this work was concerned with the alumina flow rates, the air slide inclination, the operational air velocity and the depths of the flowing and stationary alumina bed. Further work should involve the measurements of velocity profiles and shear stresses on the bottom of the fluidizing membrane and walls if possible. Experimental data of this kind would help to further develop the Saint Venant model examined in Chapter 7. Changes in particle size distributions need to be analysed and quantified as part of any design modifications. In order to move this work forward with a view to improve the understanding of powder flowability and its impact on mechanical equipment and drive it towards successful results, some further work is recommended:

- Further develop the mathematical model to be able to predict the transient (dynamic) powder flow in the start-up phase, before it reaches steady state. Some ideas would be dam break approaches used in river modelling and Kalman filter estimation theory.
- Develop an inlet powder flow model by using the Savage-Hutter model based on a Coulomb - type dry friction law (continuum mechanics approach),

applicable for the first 0.5 m of section where flow is very slow due to high friction.

Further topics in air slide modelling can be many and it is anticipated by the author that the following sub topics could be brought together to aid and optimize the development of mechanical design further. The dominant factors related to initiating and supporting reliable discharge rates from a stand pipe (dispensing head), as an interface to the air slide, are the shear properties and gas permeability of a given material. Both of these factors are influenced by the void fraction (particle packing) at a given stress condition. The changes in storage and discharge behaviour resulting from shifts in the proportioning of nominal alumina fines as a function of segregation through handling steps needs to be developed further. The benchmark that could be used to assess and predict the impact of proportional variation in the bulk is:

- the flow function as an indicator of flowability for predictions of packed bed behaviour. (Flow measurements can be performed by using a Brookfield powder flow tester (PFT)).
- gas permeability as complimentary benchmark of changes in bulk behaviour due to its dominance in supporting reliable flow of powders of different qualities. (Gas permeability measurements can be conducted by using a fluidization column).
- particle density, the solid real density by using a Qantachrome Ultrapycnometer.

The voids fraction for a given bulk material reflects the particle packing at a given stress condition and is a function of particle sizes and particle shape as explained by Schulze (2007), and Farnish et al (2006 - 2012). Results of the benchmark can be further used to model the flow behaviour at the inlet of the air slide, by introducing gas permeability and by using the dimensionless velocity coefficient  $U_0/U_{mf}$ . Conduct tests with different alumina qualities and different fines concentrations to investigate the robustness on the new outlet design.

- Initiate a programme of shear testing using the FTP by assessing the impact of fines in the alumina by using the flow function as indicator of flowability and correlate with gas permeability measurements as benchmarking.



- Conduct more rheometry studies to investigate how the flow factors would vary as a function of bed height, air flow rates and spindle position inside the fluidization column;
- Investigate possibilities of reaching higher capacities by conducting air slide tests with a higher filling degree.

Each one of the suggestions mentioned above would form the basis for new industrial – PhD studies and the results will be of great importance, not only from scientific point of view, but also from business/economical point of view.

When it comes to liaison with measurement equipment manufacturers, during the rheometry measurements Brookfield personnel came to Wolfson and provided the necessary support with updating drivers and setting up the rheometer used for this project. The Wolfson Centre has also developed the PFT machine in cooperation with Brookfield and now Hydro has purchased one for further research activities. Both Brookfield and the Wolfson Centre are keen on further collaboration in powder technology research.

## REFERENCES

- Agu, E., C., Model based estimation of drilling mud flow using a Venturi Channel, Master's Thesis 2014, Faculty of Technology, Telemark University College.
- Agu, E., C., Lie, B., Numerical Solution of the Saint Venant Equation for Non – Newtonian Fluid, Proceedings from The 55th Conference on Simulation and Modelling (SIMS 55), 2014, Sweeden.
- Ancey, C., Meunier, M., “Estimating bulk rheological properties of flowing snow avalanches from field data”, Journal of Geophysical Research, Vol.109, F01004, 2004.
- Ancey, C., “Plasticity and geophysical flows: A review”, J. Non-Newtonian Fluid Mech. 142 (2007) 4-35.
- Ancey, C., 2012, “Gravity flow on Steep Slope”. In: Chassignet, E., Cendese, C. (Eds.), Buoyancy Driven Flows. Cambridge University Press, New York.
- Ancey, C., Andreini, N., Epley - Chauvin, G., “Visicoplastic dambreak waves: review of simple computational approaches and comparison with experiments”, Advances in Water Resources, Vol. 48, pp.79 -91, 2012.
- Ancey, C., “Why don't avalanche-dynamics models of higher complexity necessarily lead to better predictions?”, Presentation held at International Snow Science Workshop Grenoble- Chamonix Mont –Blanc – 2013.
- Anjaneyulu P., Khakhar D.V., Rheology of a glas- fluidized bed, Powder Technology 83 (1995) 29-34
- Arnold, P.C., McLean A.G. and Roberts A.W., 1982, “Storage and flow of bulk solids”, paper presented at the seminar: Applications in the storage, flow and handling of bulk solids, Tundra bulk solids handling research associates, The University of New Castle, 4-5 th April.
- ASTM International 2000, Standard Test Method for Shear Testing of Bulk Solids Using the Jenike Shear Cell, West Conshohocken, USA.
- Berry R.J., Bradley M.S.A., Development of the Brookfield Powder Flow Tester. Bulk Solids Europe 2010, Glasgow, September 2010.
- Berry R.J., Bradley M.S.A., McGregor R.J., Development and Commercialisation of a new Powder Flow Tester for Powder Formulation Development, Quality Control and Equipment Design, Bulk Solids India, March 2010.

- Berry R., J., Bradley M., S., A., Farnish R.J., Overview of powder failure property measurements and their uses.
- Botterill, J., S., M., Chandrasekhar, R., v.d. Kolk, M., 1970. Heat transfer and pressure loss for the flow of fluidized solid across banks of tubes. *Br. Chem. Eng.* 15 (1970), 769- 772.
- Botterill, J., S., M., Chandrasekhar, R., v.d. Kolk, M., 1970. The flow of fluidized solids past array of tubes - heat transfer and pressure loss studies. *Chem. Eng. Prog. Symp. Ser.* 66 (1970), 101, 61-69.
- Botterill, J., S., M., v.d. Kolk, M., 1971. The flow properties of fluidized solids. *Chem. Eng. Prog. Symp. Ser.* 67 (1971), 116, 70-76.
- Botterill, J., S., M., v.d. Kolk, M., D., E., Elliott, S., McGuigan, 1971. The flow of fluidized solids. *Proceedings of POWTECH '71: International Powder Technology & Bulk Solids Conference / ed. by A.S. Goldberg*, 215-221.
- Botterill, J., S., M., Bessant, D., J., 1973. The flow properties of fluidized solids. *Powder Technology*, 8 (1973) 213-222.
- Botterill, J., S., M., Bessant, D., J., 1976. The flow properties of fluidized solids. *Powder Technology*, 14 (1976) 131-137.
- Botterill, J., S., M., B.H., Abdul Halim, 1978. The flow of fluidized solids. *Proceedings of the 2nd Engineering Foundation Conference 1978, Cambridge*, 122-127.
- Botterill, J., S., M., B., H., Abdul Halim, 1979. The open channel flow of fluidized solids. *Powder Technology*, 23 (1979) 67-78.
- Bradley M., S., A., Berry R., J., Farnish R., J., Methods for design of hoppers, silos, bins and bunkers for reliable gravity flow, for pharmaceutical, food, mineral and other applications, *Bulk Solids India*, April 2011.
- Bruni, G., Lettieri, P., Elson, T., Yates, J. The effect of process conditions on the fluidization behavior of gas fluidized beds. *Proceedings of Partec 2004, Nuremberg, Germany*
- Bruni G., Barletta D., Poletto M., Lettieri P., 2007a, A rheological model for the flowability of aerated fine powders, *Chemical Engineering Science* 62, 397 – 407.
- Bruni G., Colafigli A., Lettieri P., Elson T., 2005, Torque measurements in aerated

powders using a mechanically stirred Fluidized Bed Rheometer (msFBR), *Chemical Engineering Research and Design* 83, 1311 – 1318.

Bruni G., Lettieri P., Newton D., Barletta D., 2007b, An investigation of the effect of the interparticle forces on the fluidization behaviour of fine powders linked with rheological studies, *Chemical Engineering Science* 62, 387 – 396.

Burger, J., Haldenwang, R., Alderman, N. Experimental database for non-Newtonian flow in four channel shapes. *Journal of Hydraulic Research* Vol. 48, No. 3 (2010), pp.363-370.

Burger, J., Haldenwang, R., Alderman, N. Friction factor - Reynolds number relationship for laminar flow of non-Newtonian fluids in open channels of different cross-sectional shapes. *Chemical Engineering Science* 65 (2010) 3549-3556.

Chan, F.T., August 1979. Flow of cohesionless granular material in inclined fluidized channel. B. Eng. Project Report, Dept. of Civil Engineering and Applied Mechanics, McGill University, Montreal (QC) Canada.

Coussot, P., Meunier, M., "Recognition, classification and mechanical description of debris flows", *Earth-Science Reviews* 40 (1996), 209-227.

DiCristo, C., Iervolino, M., Vacca, A., "Waves Dynamics in a Linearized Mud-Flow Shallow Model", *Applied Mathematical Sciences*, Vol.7, 2013, no.8, 377-393.

Dyrøy, A., 2006. Dr.Ing. Thesis. Norwegian University of Science and Technology/Telemark University College.

Esbensen, K., H., *Multivariate Data Analysis in practice, An Introduction to data analysis and Experimental Design*, 4 th Edition, CAMO ASA.

Faragher, R., "Understanding the basis of the Kalman filter via a simple and intuitive derivation", *IEEE Signal Processing Magazine* [128], Sept. 2012.

Farnish, R., J, Bradley M., S., A. (2006) Consistency and repeatability of gravity discharge of particulates in processes and packages.

Farnish R., J., Berry R., J., Hernandez- Leon E., The effect of Segregation on handling Characteristics, *Bulk Solids Europe*, Germany, October 2012.

- Farnish, R., J. (2006). Effect of flow channel profiles on repeatability of discharge rates from dispensing heads used for flow control of materials in bulk. MPhil Thesis, The University of Greenwich, 2006.
- Fitton, T., Tailings beachslope prediction, PhD Thesis, School of Civil Environmental and Chem. Eng., RMIT University, May 2007.
- Geldart, D., The effect of particle size and size distribution on the behavior of gas-fluidized beds. *Powder Technology* 6 (1972) pp.201-215.
- Geldart, D., Types of gas fluidization. *Powder Technology* 7 (1973) pp.285-292.
- Gerald, C., F., Wheatley P., O., *Applied Numerical Analysis*, Sixth edition, Addison Wesley Longman, 1999.
- Gu, Z., H., Arnold, P., C., McLean, A., G., The use of Standpipes for Increasing Limiting Gravitational Flowrate from Mass Flow Bins, *KONA* No.11 (1993).
- Gupta, S., K., Agarwal, V., K., Singh S.N., Seshadri, V., Mills, D. (2006) An experimental investigation on a fluidized motion conveying system. *Powder Technology*, 167 (2006) 72-84.
- Gupta, S., K., Agarwal, V., K., Singh S., N., Seshadri, V., Mills, D. (2009) Parameters affecting fluidized motion conveying of fly ash. *Particulate Science and technology*, 27:469-487, 2009.
- Gupta, S., K., Agarwal, V., K., Singh S., N., Seshadri, V., Mills, D., Singh, J., Prakash, C., (2009) Prediction of minimum fluidization velocity for fine tailings materials. *Powder Technology*, 196 (2009) 263-271.
- Gupta, S., K., Agarwal, V., K., Mills, D. (2010) A model for fluidized motion conveyor transporting fly ash. *Experimental Thermal and Fluid Science* 34 (2010) 1042-1048.
- Haldenwang, R.,(2003). Flow of non-Newtonian fluids in open channels. PhD thesis, Department of Civil Engineering, Cape Technikon, South Africa.
- Haldenwang, R., Kotze, R., Chhabra, R. Determining the viscous behaviour of non – Newtonian fluids in a flume using a laminar sheet flow model and ultrasonic velocity profiling (UVP) system. 2012, *J. of the Braz. Soc. of Mech. Sci. & Eng.*, vol. XXXIV, No.3, pp. 276-284.
- Haldenwang, R., Slatter, P., Experimental procedure and database for non- Newtonian open channel flow. *Journal of Hydraulic Research* Vol 44, No.2 (2006), pp. 283-287.

- Han, C., D., 2007. Rheology and Processing of Polymeric Materials: Volume 2: Polymer Processing. Oxford University Press.
- Haugland, L. (1998). Transfer document MPhil/PhD, University of Greenwich. Personal correspondence 2012, Word documents, sent by e-mail.
- Hutter, K., Svendsen, B., Rickenman, D., “Debris flow modeling: a review”, Continuum Mech. Termodyn, 8 (1996) 1-35.
- Hutter, K., Wang, Y., Pudasaini, S., P., “The Savage – Hutter avalanche model: how far can it be pushed?”, Phil. Trans. R. Soc. A (2005) 363, 1507-1528.
- Irwin, M. (2006) Course Notes, Generalized Linear Models. Department of Statistics. Harvard University. <http://www.markirwin.net/stat149/lecture.html>.
- Jenike, A., W., “Gravity flow of Bulk Solids” Utah Engineering Experiment Station, University of Utah, Bulletin 108, 1961.
- Jenike, A., W., “Storage and flow of solids” Utah Engineering Experiment Station, University of Utah, Bulletin 123, 1964.
- Janssen, H., A., Zeitschr. d. Vereines deutscher Ingenieure 39, 1045 (1895).
- Jin, M., Fread, D., L., "One-dimensional Modeling of Mud / Debris Unsteady Flows," Journal of Hydraulic Engineering, Vol. 125, No. 8, pp. 827 - 834, 1997.
- Karlsen, M., et al. New Aerated Distribution (ADS) and Anti Segregation (ASS) Systems for Alumina: Essential Readings in Light Metals 2002, p.590-595, 2002.
- Kunii, D., Levenspiel, O., Fluidisation engineering Second Edition: Butterworth-Heinemann, Series in Chemical Engineering, 1991.
- Latkovik, D., Levy, E., K., The flow characteristics of fluidized magnetite powder in an inclined open channel. Powder Technology, 67 (1991) 207-216.
- Leleux, D., P., Claps, R., Chen, W., Tittel, F.K., Harman, T.L., “Applications of Kalman filtering to real-time trace gas concentration measurements”, Appl. Phys. B 74, 85-93 (2002).
- Liot, D., J., April 1979. Transportation of granular materials. B. Eng. Project Report, Dept. of Civil Engineering and Applied Mechanics, McGill University, Montreal (QC) Canada.

- Metzner, A., B., Non-Newtonian fluid flow. Relationships between recent pressure drop correlations. *Industrial and Engineering Chemistry*, vol. 49, No. 9, 1957, pp. 1429-1432.
- Metzner, A., B., Graham Park, M., Turbulent flow characteristics of viscoelastic fluids. *J. Fluid Mech.* (1964), vol.20, part 2, pp. 291-303.
- Metzner, A., B., Reed. J.C., 1955. Flow of non-Newtonian fluids-correlation of the laminar, transitions and turbulent flow regions. *A.I.Ch.E. Journal*, vol.1, No.4, 1955, pp. 434-440.
- Mills, D., *Pneumatic Conveying Design Guide, Second Edition*, Elsevier Butterworth-Heinemann, 2004.
- Moody, L., F., Princeton, N., J., 1944 “Friction factors for pipe flow”, *Trans. ASME*, Nov., pp. 671-684.
- Naef, D., Rickenmann, D., Rutschmann, P., McArdell, B., W., “Comparison of flow resistance relations for debris flows using a one-dimensional finite element simulation model”, *Nat. Hazards Earth Syst. Sci.*, 6, 155-165, 2006.
- Nedderman, R., M., *Statics and kinematics of granular materials*, Cambridge University Press, Great Britain, 1992.
- Karlsen, M., Dyrøy. A., *New Aerated Distribution (ADS) and Anti Segregation (ASS) Systems for Alumina: Essential Readings in Light Metals 2002*, p.590-595, 2002.
- Keuncke, K., *Fluidization and fluidized bed conveyance of small- particle-size solids*, *VDI Forschungsh.*, 509 (1965) 34.
- Kunii, D., Levenspiel, O., *Fluidization Engineering. Second Edition*. Butterworth-Heinemann, Series in Chemical Engineering, 1991.
- Oger, L., Savage S., B., *Flow modelling and comparison with experiments*, *Chemical Engineering Science*, 91 (2013).
- Orgaz-Castro, O., Chanson, H., “Depth- Averaged Specific Energy in Open Channel Flow and Analytical Solution for Critical Irrotational Flow Weirs”, *J.Irrig. Drain Eng.*
- Pinzon, O., A., A., *Modelling of dosator filling and discharge*, PhD Thesis, University of Greenwich, August 2012.
- Pudasaini, S., P., Hutter, K., *Avalanche Dynamics, Dynamics of rapid Flows of Dense Granular Avalanches*, Springer- Verlag Berlin Heidelberg 2007.

- Pouliquen, O., Forterre, Y., “Friction law for dense granular flows: application to the motion of mass down a rough inclined plane”, *J. Fluid. Mech* 2001.
- Rathakrishnan, E., *Applied Gas Dynamics*, John Wiley & Sons (Asia), 2010, pp 485-488.
- Savage S., B., Oger, L., Airslide flows, part 1, experiments, review and extension, *Chemical Engineering Science*, 91 (2013) 35 -43.
- Schulze, D., *Powders and bulk solids. Behaviour, characterization, storage and flow*. Springer-Verlag Berlin Heidelberg 2008.
- Schwedes, J., Review on testers for measuring flow properties of bulk solids (based on an IFPRI- Report 1999), *Granular Matter* 5, 1-43, Springer – Verlag 2003.
- Siemes, W., and Helmer, L., The measurement of viscosity of a fluidized layer with pneumatic trough. *Chem. Eng. Sci.*, 17 (1962), pp. 555-571.
- Singh, B., Calcott, T.G., Rigby, G.R., Flow of fluidized solids and other fluids in open channels. *Powder technology*, 20 (1978) 99-113.
- Szymkiewicz, R. (2010). *Numerical Modeling in Open Channel Hydraulics (Vol. 83)*, Springer, ISBN 978-90-481-3673-5.
- University of Oxford (2002): Introduction to Statistical Modelling: Applications of Generalized Linear Models. [http://www.stats.ox.ac.uk/pub/bdr/IAUL/Modelling Lectures 1-6.pdf](http://www.stats.ox.ac.uk/pub/bdr/IAUL/ModellingLectures1-6.pdf).
- Zaiontz, C. (2013) Real statistical analysis, <http://www.real-statistics.com>.
- Wali, U., G., “Kinetic Energy and Momentum Correction Coefficients for a Small Irrigation Channel”, *Int. J. of Emerging Technology and Advanced Engineering*, Volume 3, Issue 9, September 2013, pp 315-322.
- Woodcock, C., R, *The Flow of Particulate Bulk Solids in an Air-Assisted Gravity Conveyor*, PhD Thesis, School of Mechanical Engineering, Thames Polytechnic, London, October 1978.
- Wilson, K., C., Addie, G., R., Sellgren, A., Clift, R., *Slurry transport using centrifugal pumps*. 2006 Springer, Third edition.
- Woodcock, C., R, Mason, J., S., “Fluidized bed conveying – art or science?” *Proc. Pneumotransport 3, BHRA Conference, Paper E1, Bath, U.K. April 1976*.



Woodcock, C., R, Mason, J., S., “The flow characteristics of a fluidised p.v.c. powder in an inclined channel”. Proc. Int. Powder and Bulk Solids Handling and Processing Conf., Chicago, U.S.A., May 1977, pp 466 - 475.

Woodcock, C., R, Mason, J., S., “ The modelling of air-assisted bulk particulate solids flow in inclined channels”, Proc. Pneumotransport 4, BHRA Conference, Paper D2, Carmel- by- the- Sea, California, U.S.A. , June 1978.

Valciu, S., C., Dyrøy, A., Farnish R., J., Agu, C., E., Lie, B., Mechanical design principles and test results of a small scale airslide rig for alumina transport: Proceedings from The 55th Conference on Simulation and Modelling (SIMS 55), 2014, Sweden.

Versteeg , H., K., and Malalasekera, W. (2007). An Introduction to Computational Fluid Dynamics: Finite Volume Method, 2nd ed., Pearson Education Limited, Edinburgh Gate Harlow Essex CM20 2JE, England.

Øystese, S., Pneumatic Components and alumina feeding equipment HAL4e, M.Sc Thesis, Norwegian University of Science and Technology, June 2015.

## APPENDIX A 3 M AIR SLIDE CAPACITY TESTS

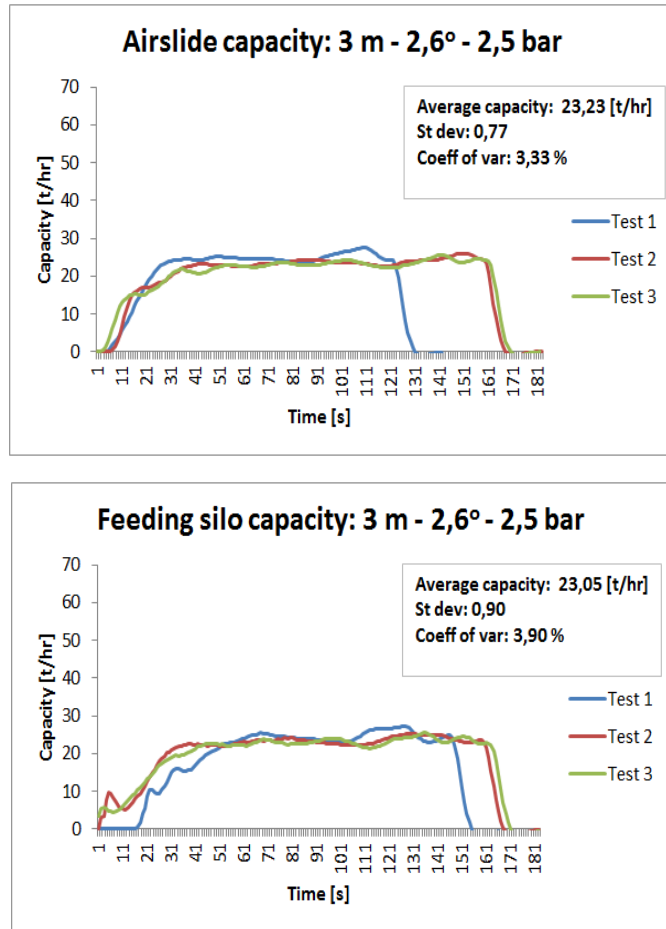


Figure 124 System capacity: 3 m – 2.6 degrees – 2.5 bar

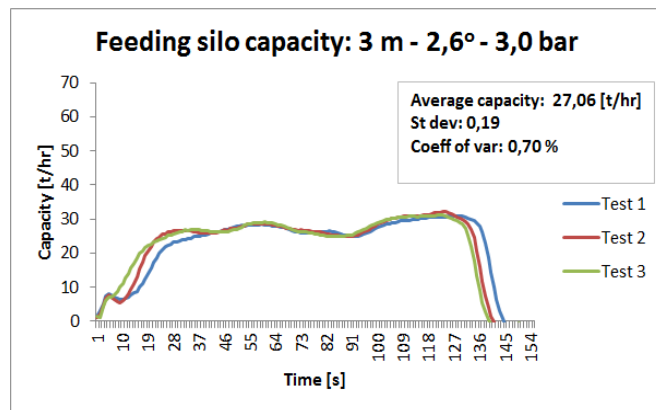
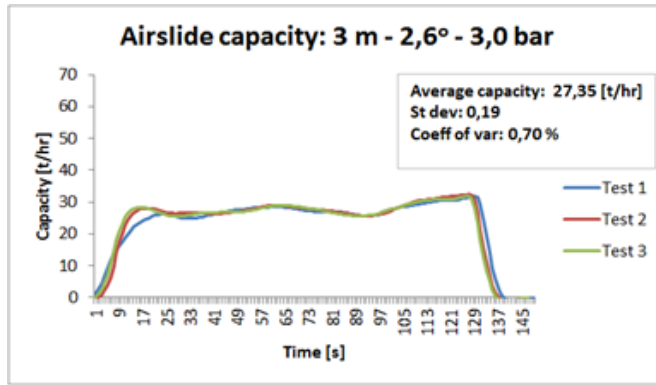


Figure 125 System capacity: 3 m – 2.6 degrees – 3.0 bar

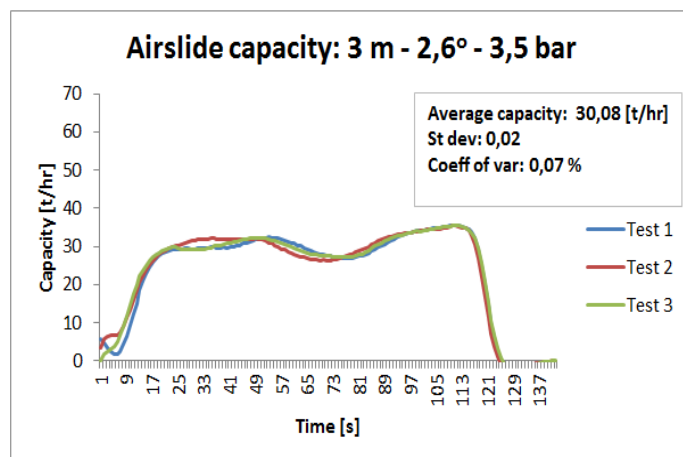
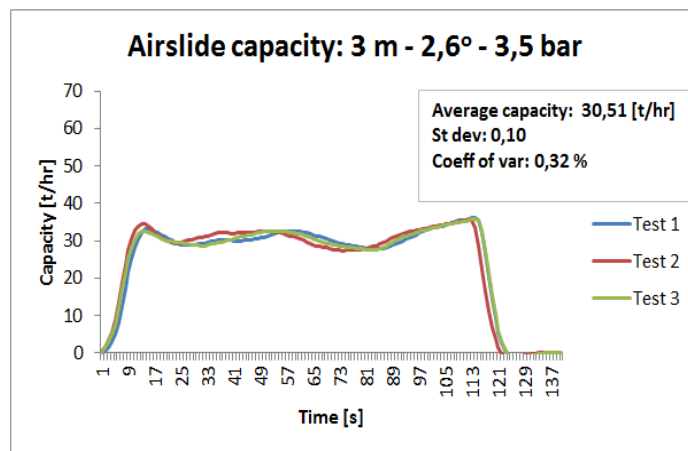


Figure 126 System capacity: 3 m – 2.6 degrees – 3.5 bar

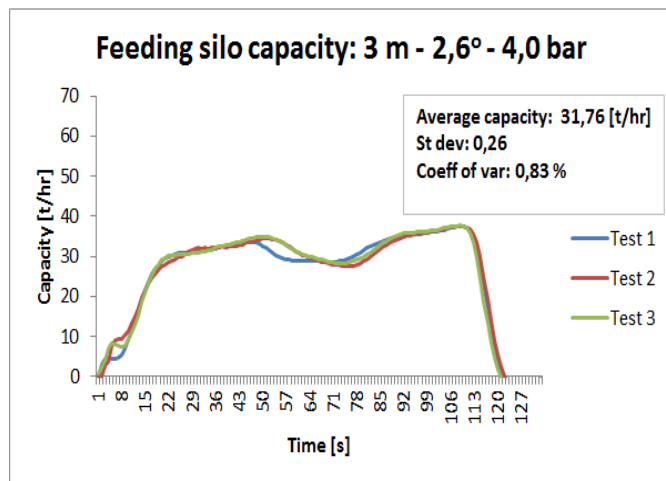
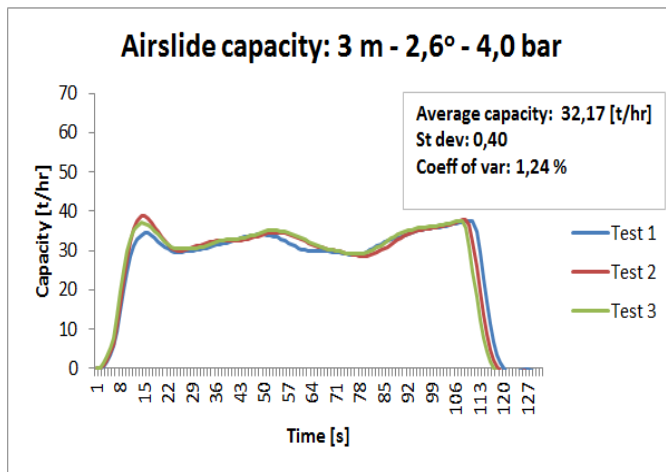


Figure 127 System capacity: 3 m – 2.6 degrees – 4.0 bar

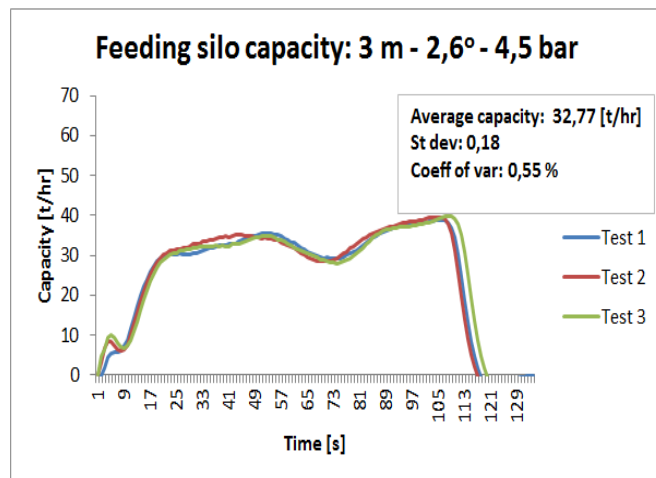
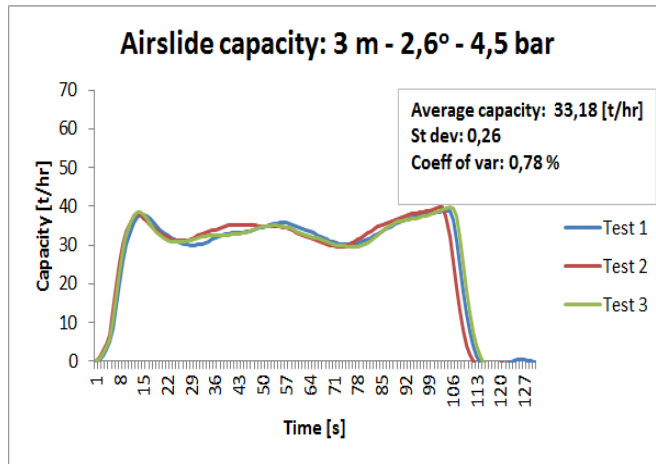


Figure 128 System capacity: 3 m – 2.6 degrees – 4.5 bar

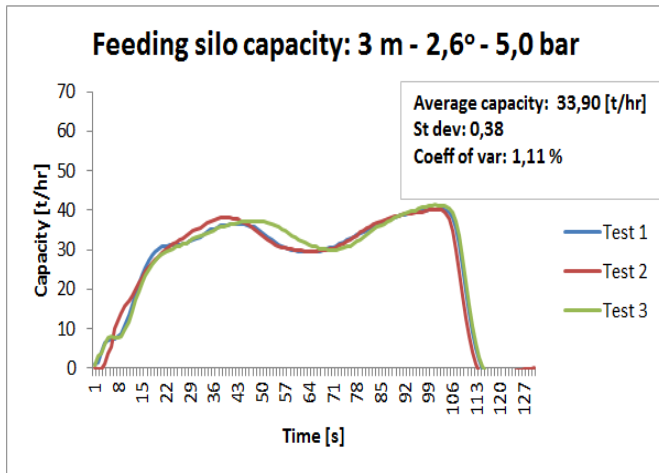
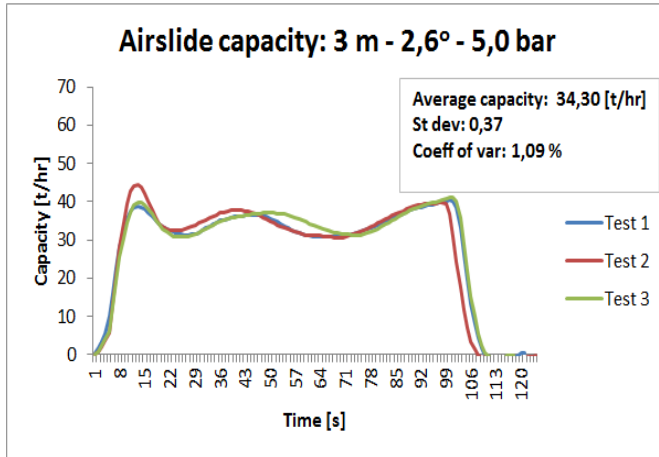


Figure 129 System capacity: 3 m – 2.6 degrees – 5.0 bar

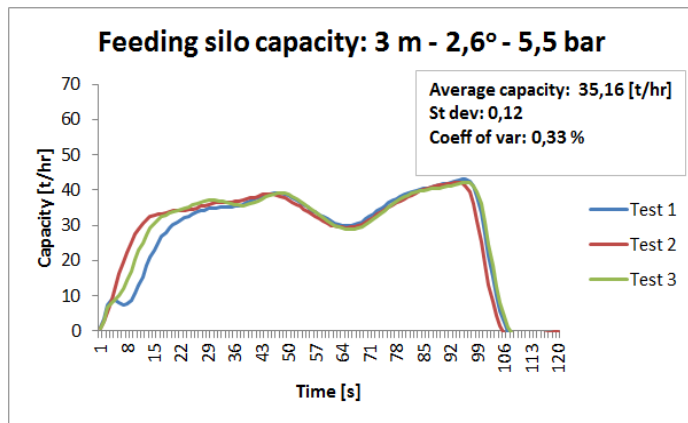
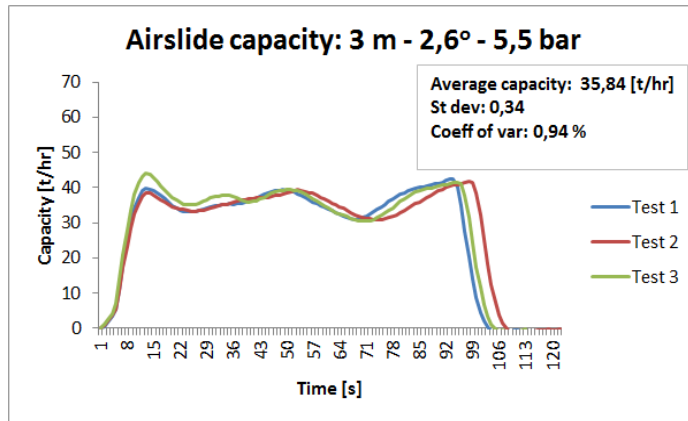


Figure 130 System capacity: 3 m – 2.6 degrees – 5.5 bar

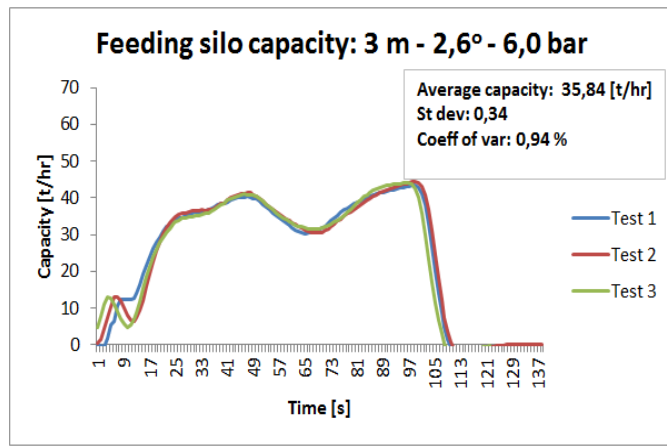
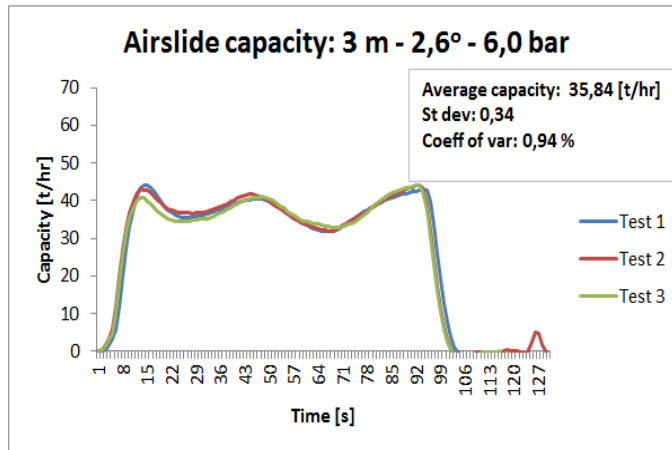


Figure 131 System capacity: 3 m – 2.6 degrees – 6.0 bar



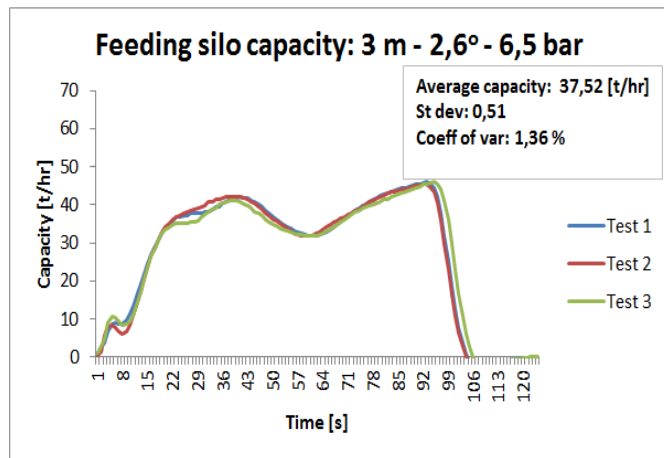
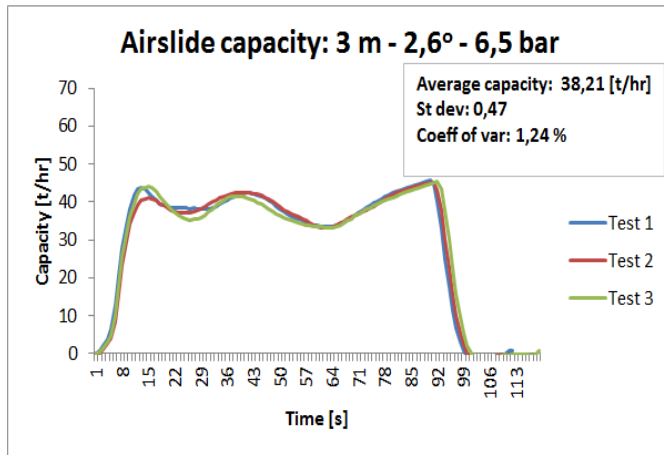


Figure 132 System capacity: 3 m – 2.6 degrees – 6.5 bar

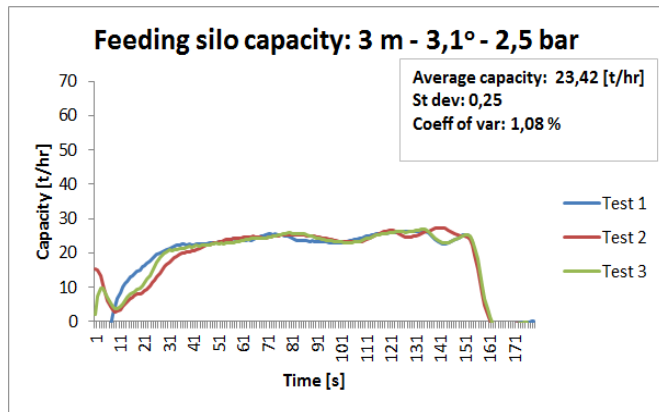
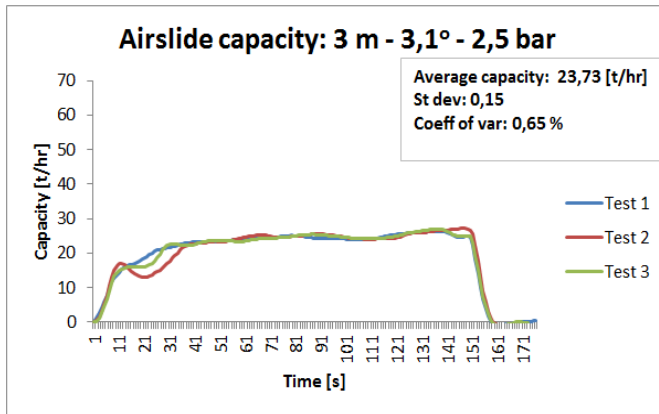


Figure 133 System capacity: 3 m – 3.1 degrees – 2.5 bar

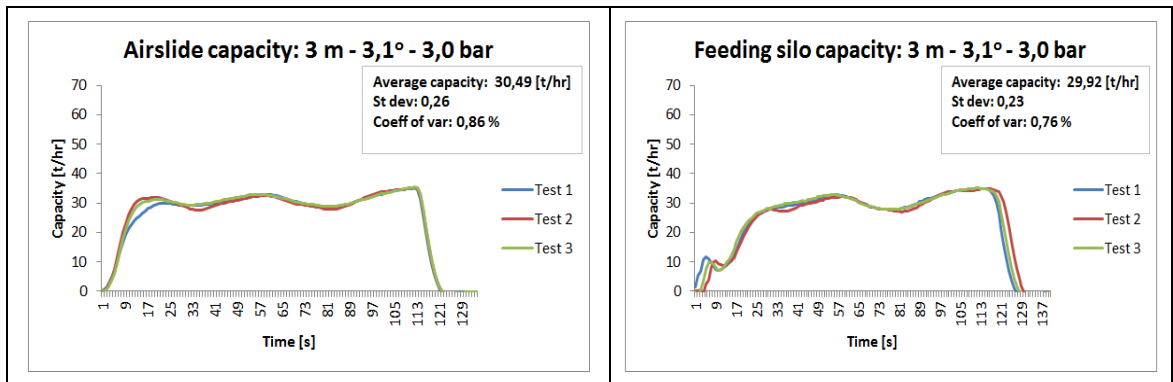


Figure 134 System capacity: 3 m – 3.1 degrees – 3.0 bar

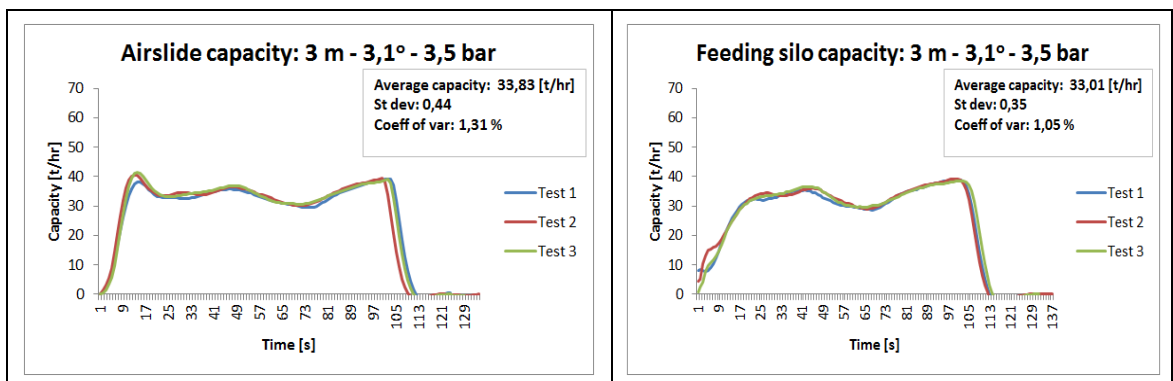


Figure 135 System capacity: 3 m – 3.1 degrees – 3.5 bar

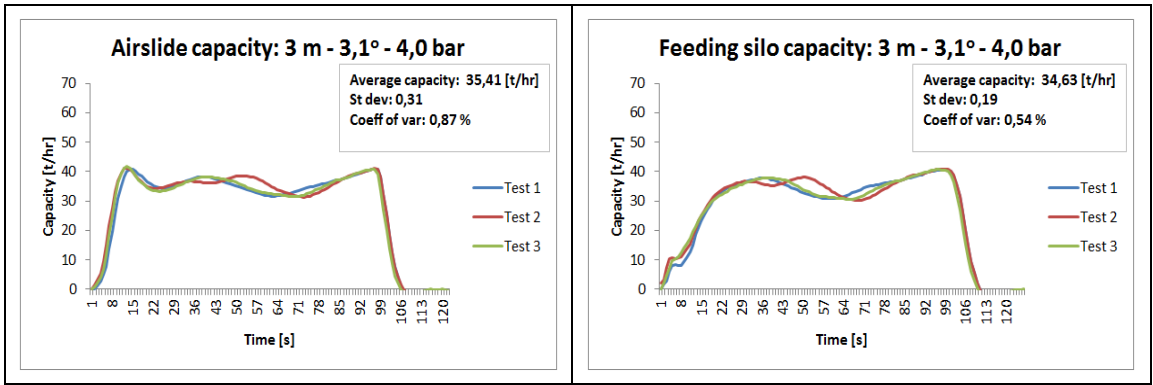


Figure 136 System capacity: 3 m – 3.1 degrees – 4.0 bar

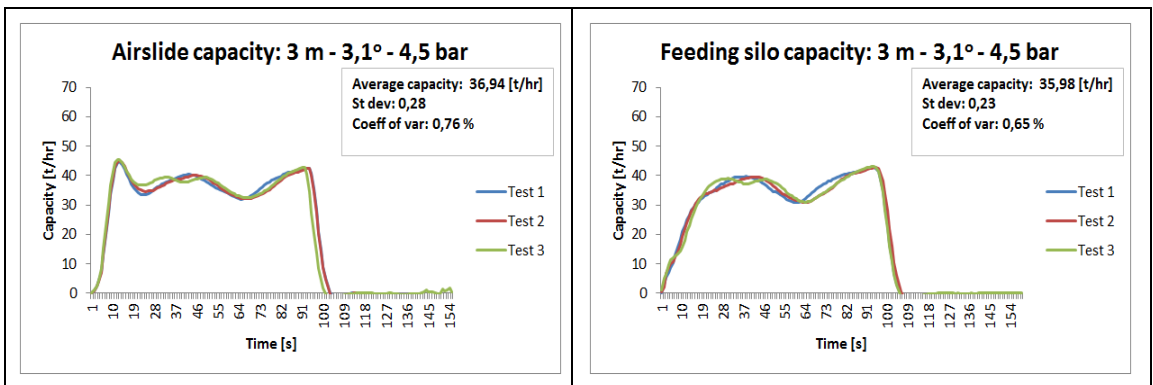


Figure 137 System capacity: 3 m – 3.1 degrees – 4.5 bar

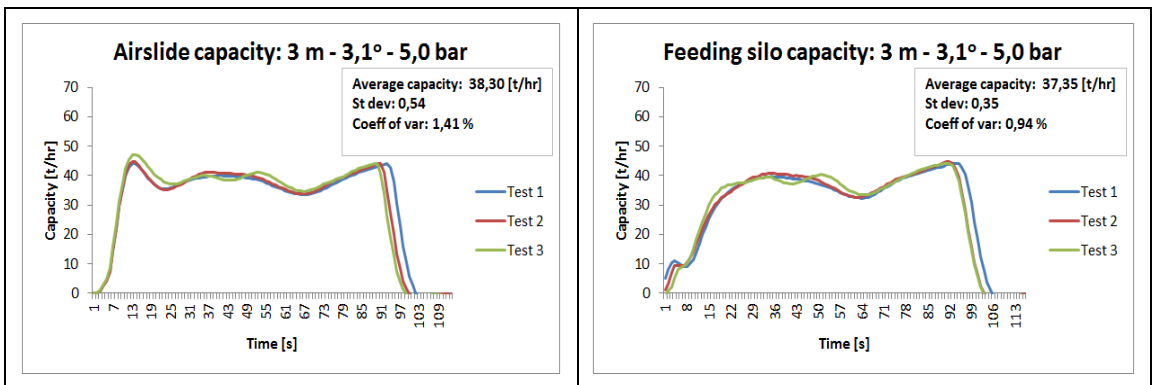


Figure 138 System capacity: 3 m – 3.1 degrees – 5.0 bar

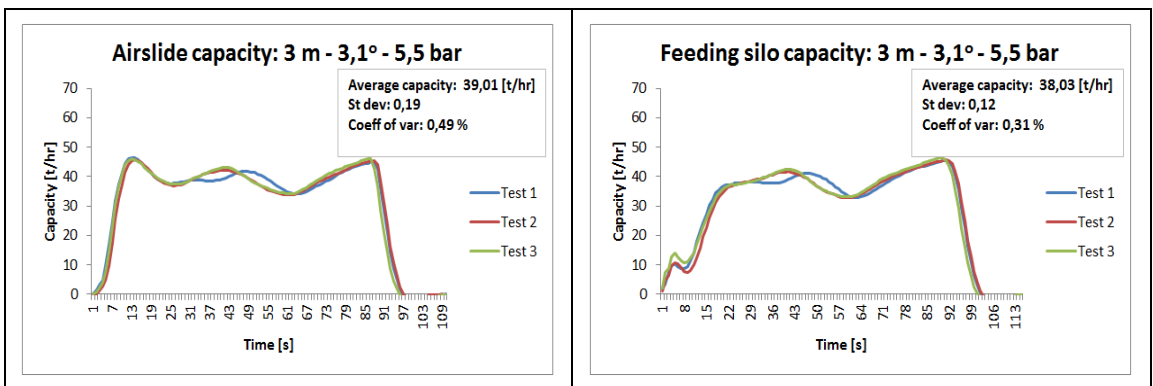


Figure 139 System capacity: 3 m – 3.1 degrees – 5.5 bar

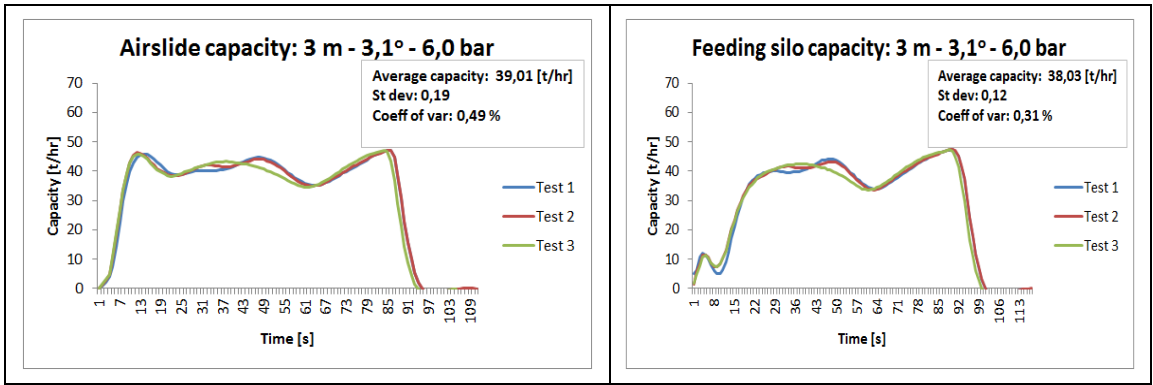


Figure 140 System capacity: 3 m – 3.1 degrees – 6.0 bar

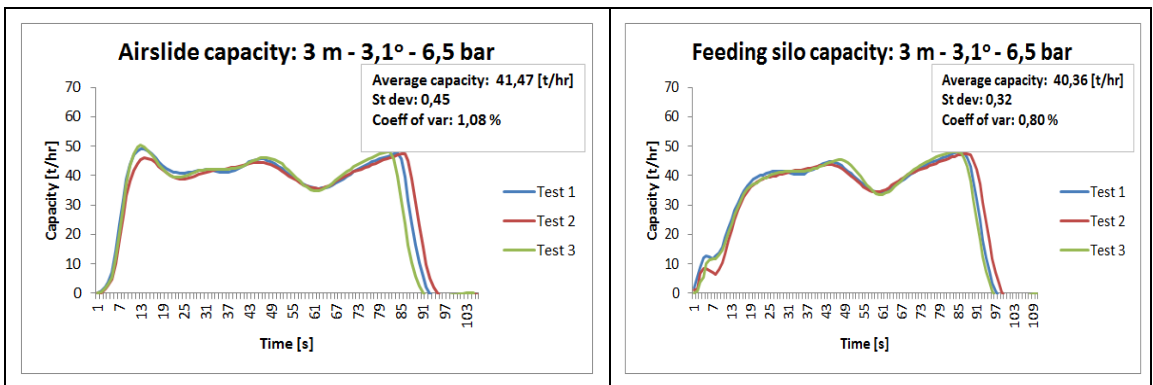


Figure 141 System capacity: 3 m – 3.1 degrees – 6.5 bar

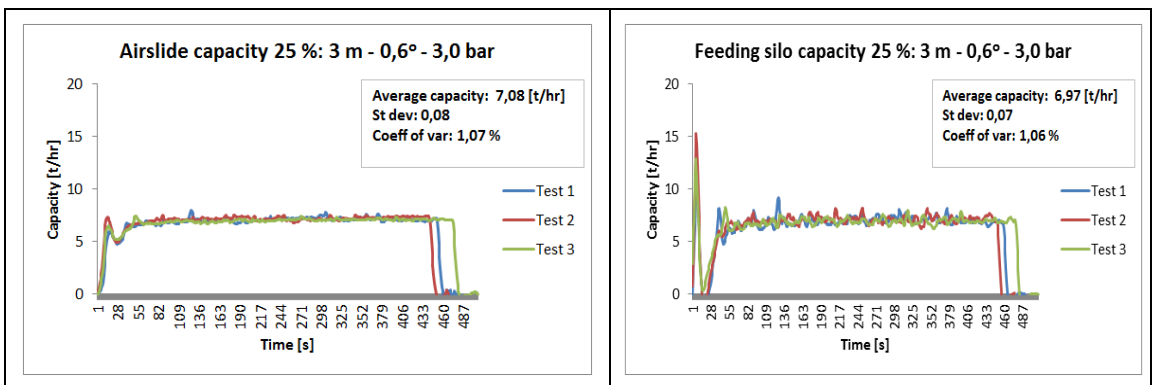


Figure 142 System capacity: 3 m – 0.6 degrees – 3.0 bar

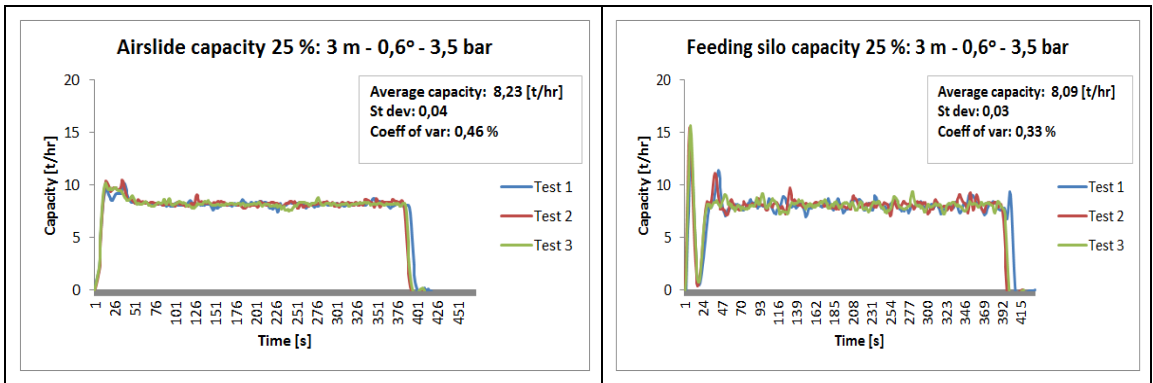


Figure 143 System capacity: 3 m – 0.6 degrees – 3.5 bar

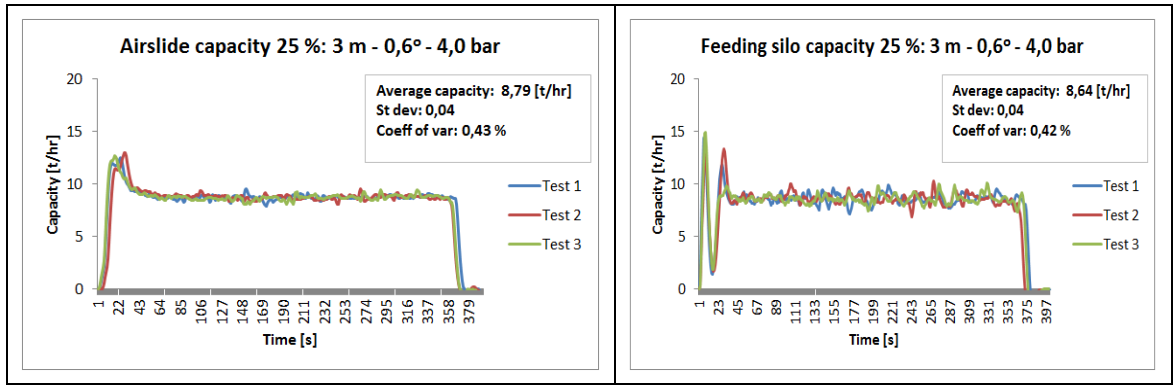


Figure 144 System capacity: 3 m – 0.6 degrees – 4.0 bar

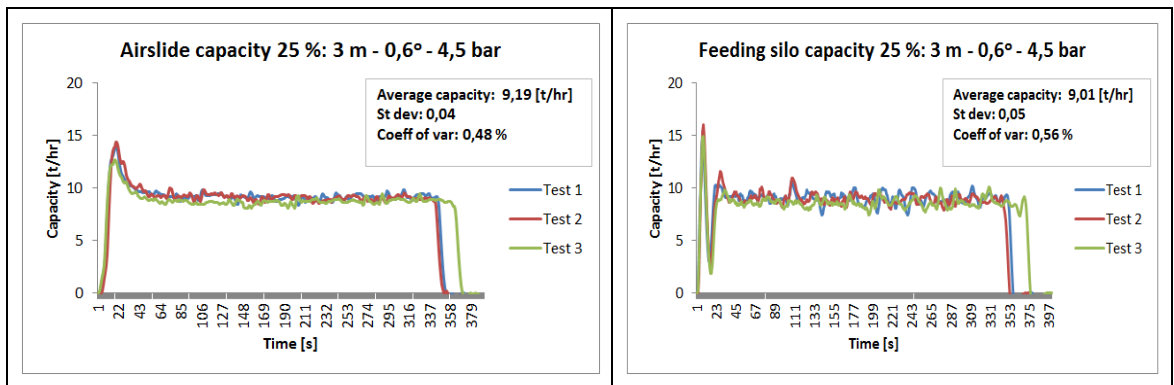


Figure 145 System capacity: 3 m – 0.6 degrees – 4.5 bar

## **APPENDIX B 7 M AIR SLIDE CAPACITY TESTS**

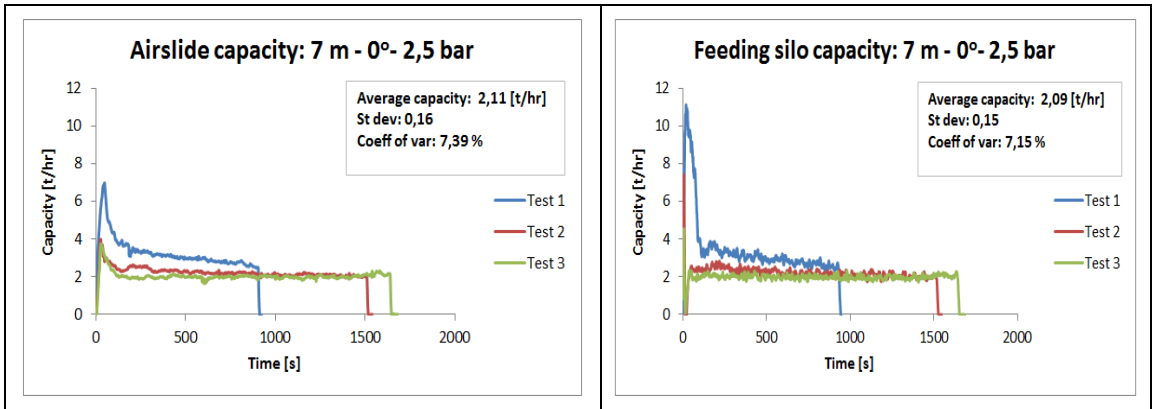


Figure 146 System capacity: 7 m – 0.0 degrees – 2.5 bar

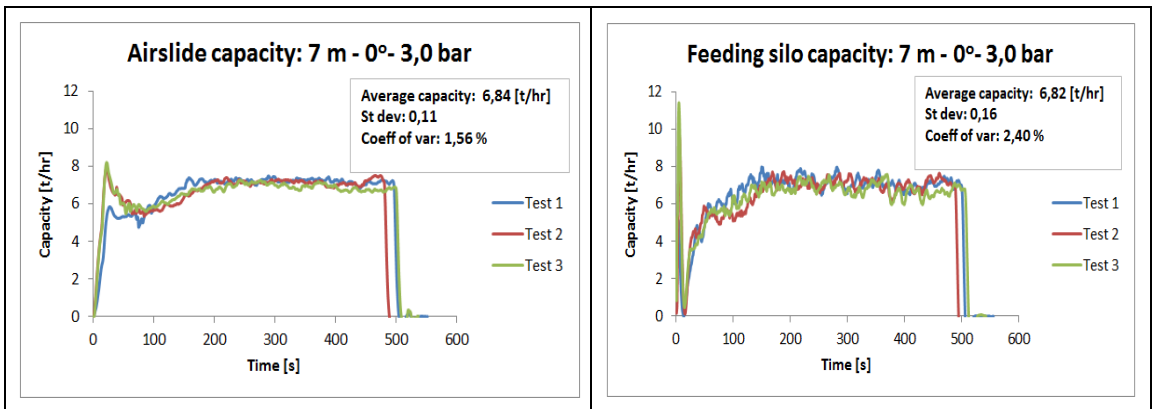


Figure 147 System capacity: 7 m – 0.0 degrees – 3.0 bar

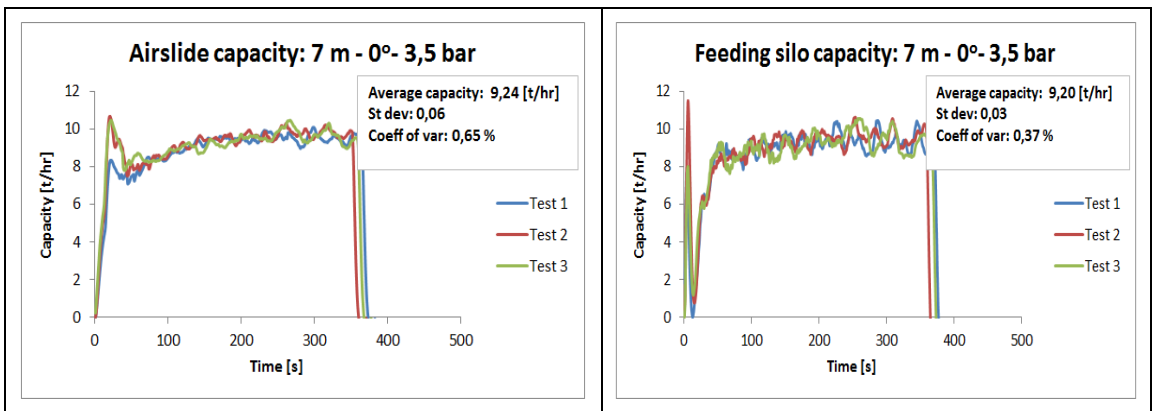


Figure 148 System capacity: 7 m – 0.0 degrees – 3.5 bar

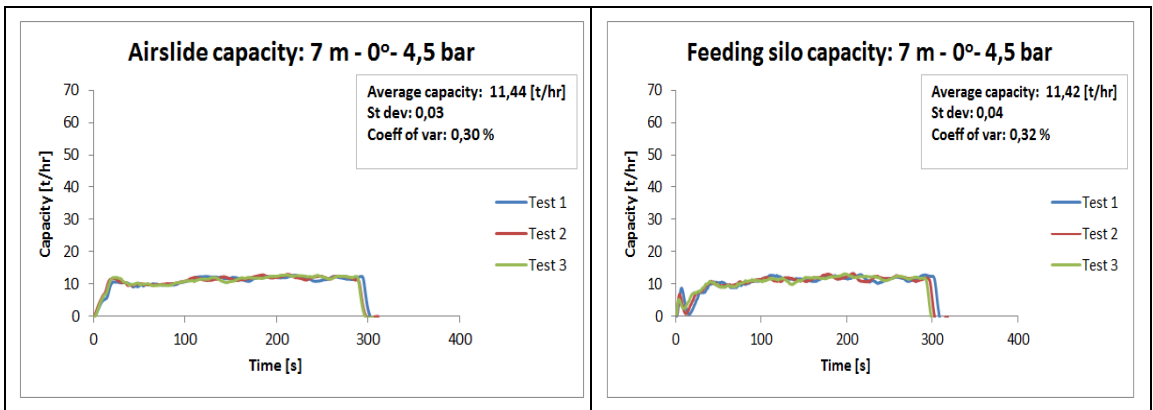


Figure 149 System capacity: 7 m – 0.0 degrees – 4.5 bar

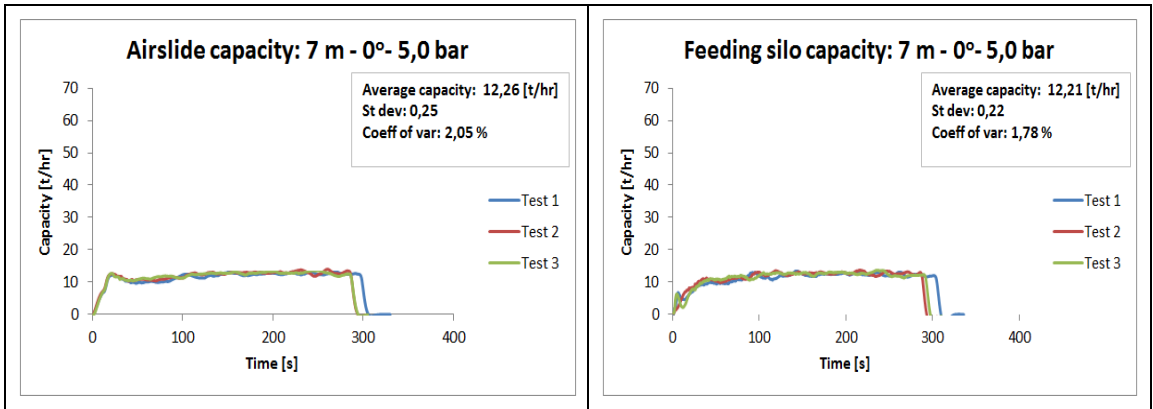


Figure 150 System capacity: 7 m – 0.0 degrees – 5.0 bar

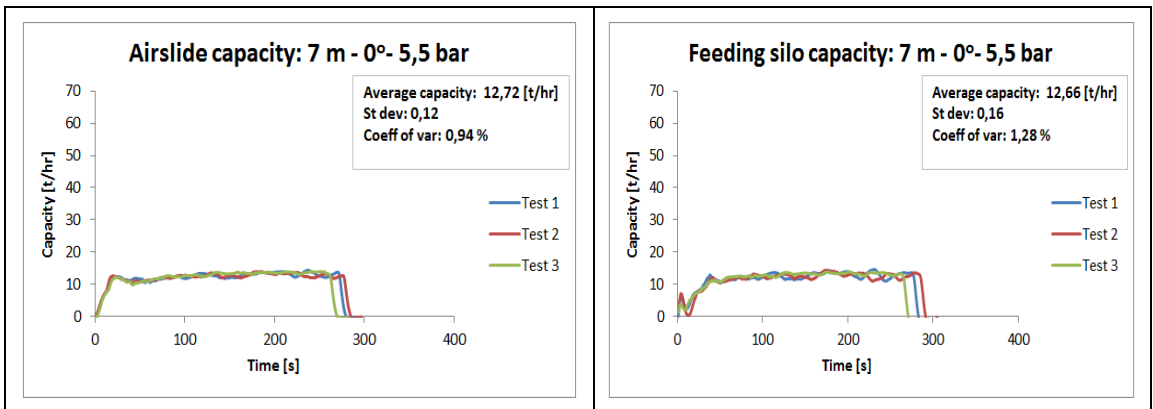


Figure 151 System capacity: 7 m – 0.0 degrees – 5.5 bar

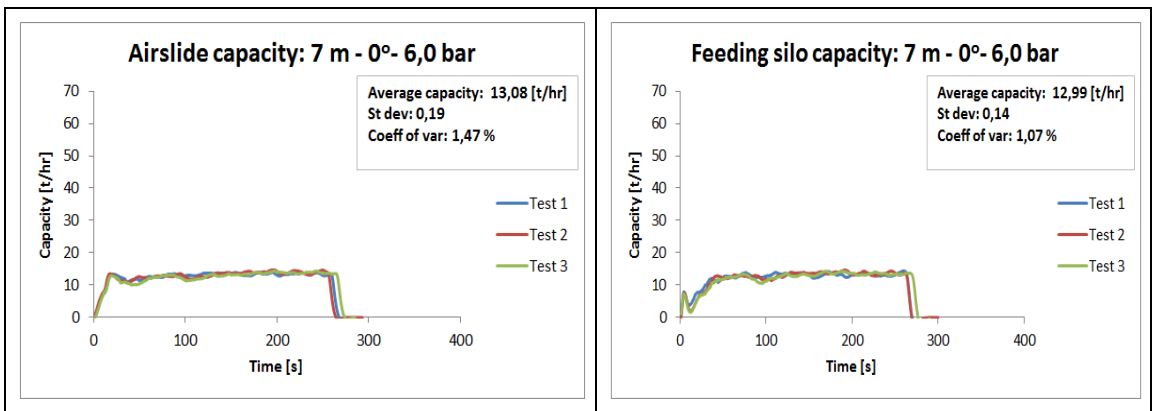


Figure 152 System capacity: 7 m – 0.0 degrees – 6.0 bar

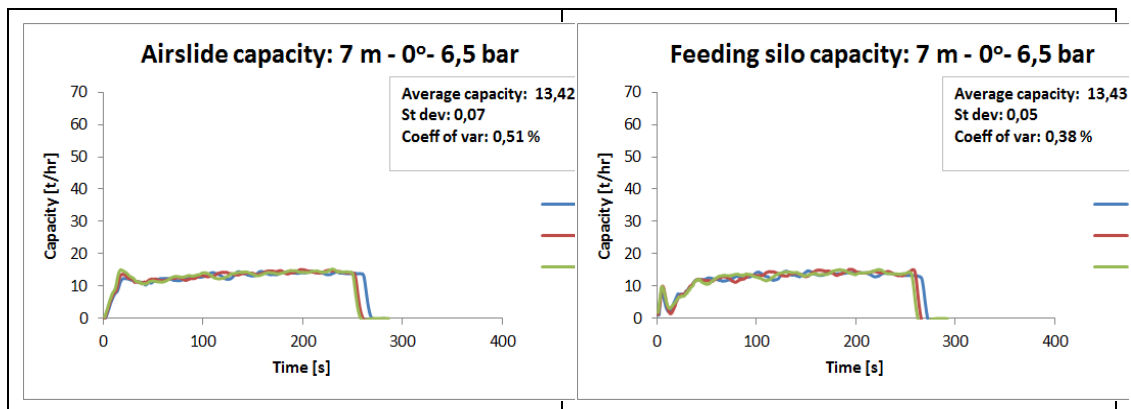


Figure 153 System capacity: 7 m – 0.0 degrees – 6.5 bar



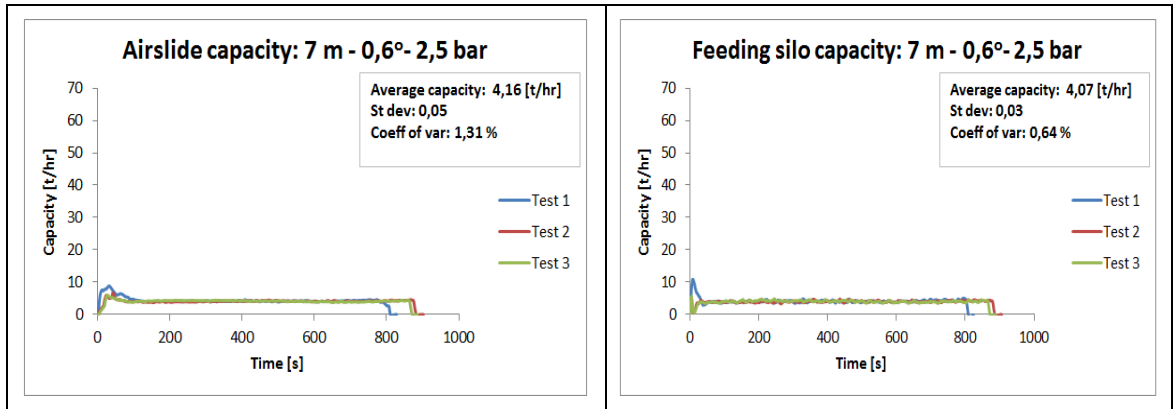


Figure 154 System capacity: 7 m – 0.6 degrees – 2.5 bar

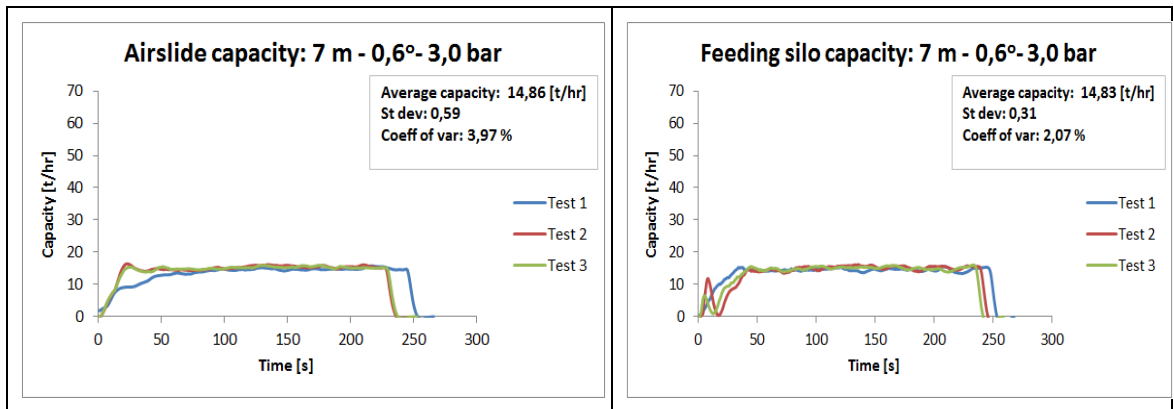


Figure 155 System capacity: 7 m – 0.6 degrees – 3.0 bar

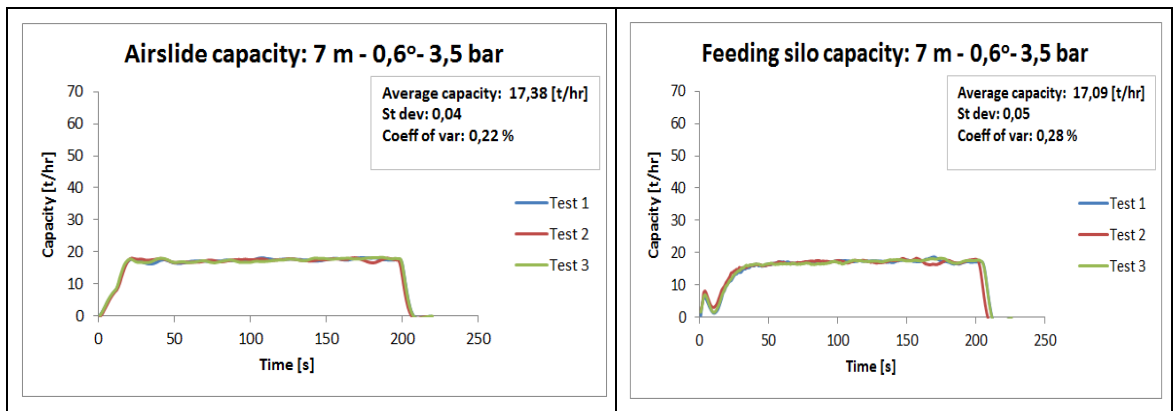


Figure 156 System capacity: 7 m – 0.6 degrees – 3.5 bar

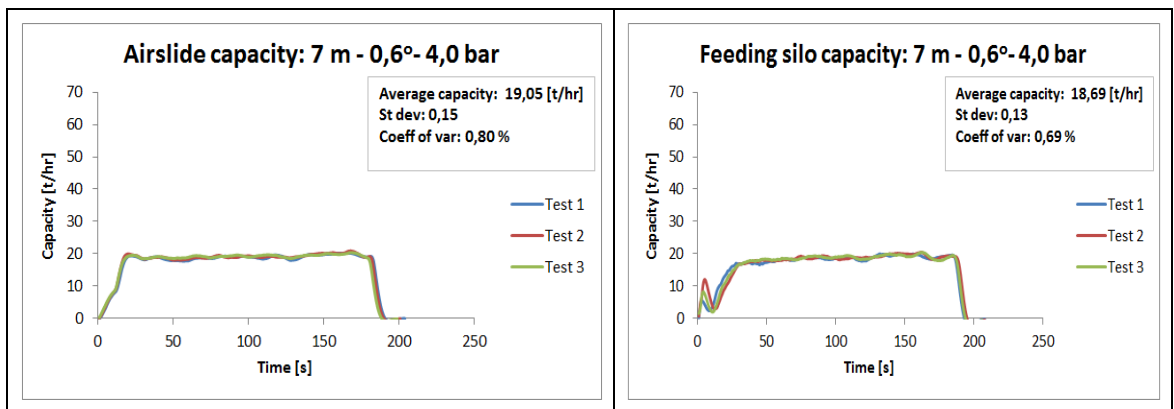


Figure 157 System capacity: 7 m – 0.6 degrees – 4.0 bar

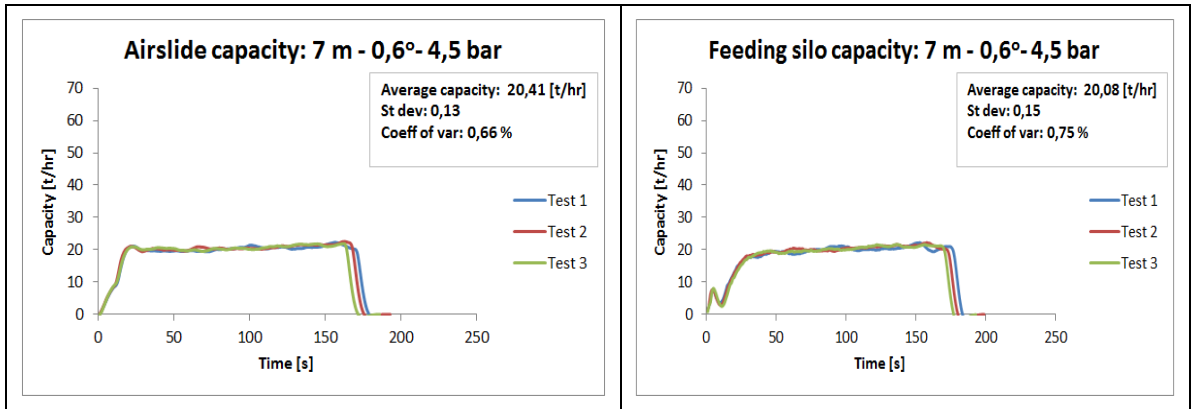


Figure 158 System capacity: 7 m – 0.6 degrees – 4.5 bar

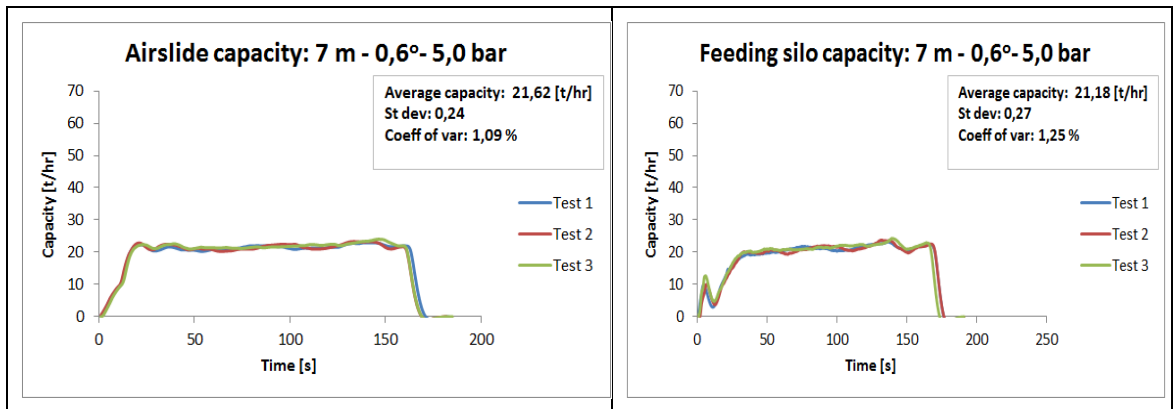


Figure 159 System capacity: 7 m – 0.6 degrees – 5.0 bar

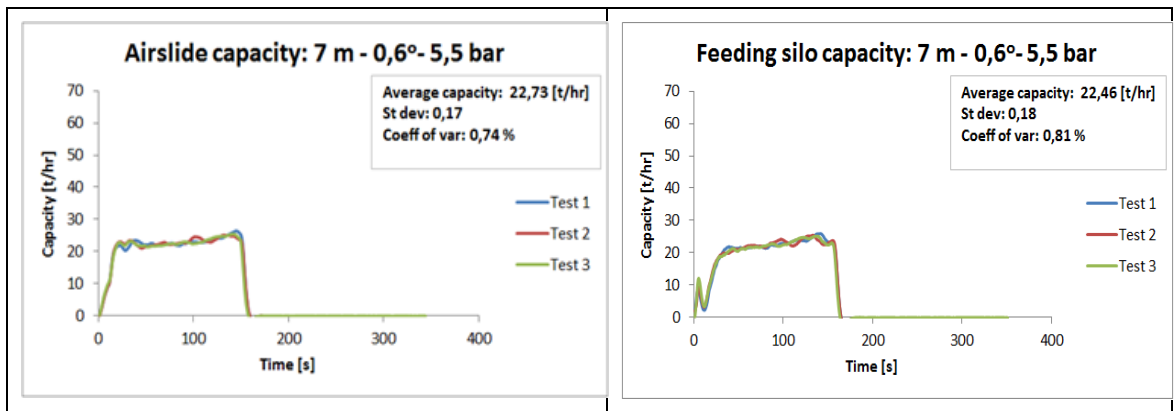


Figure 160 System capacity: 7 m – 0.6 degrees – 5.5 bar

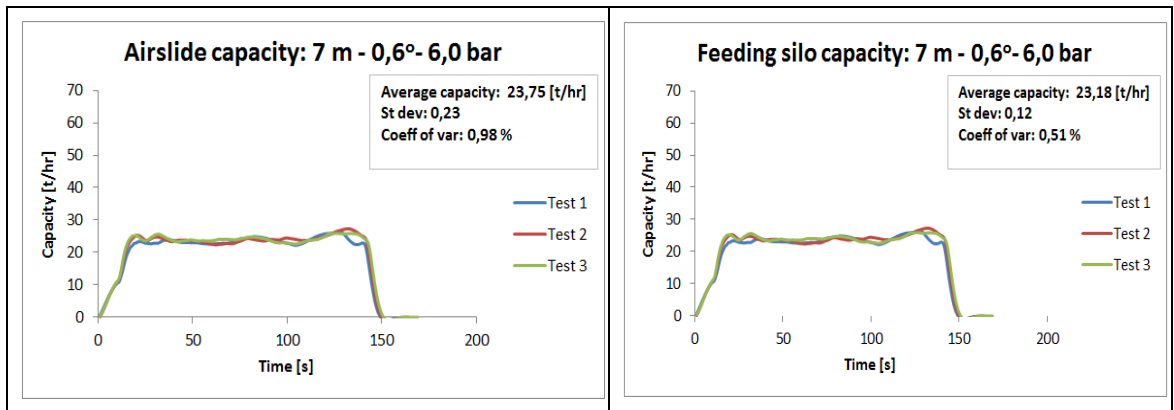


Figure 161 System capacity: 7 m – 0.6 degrees – 6.0 bar

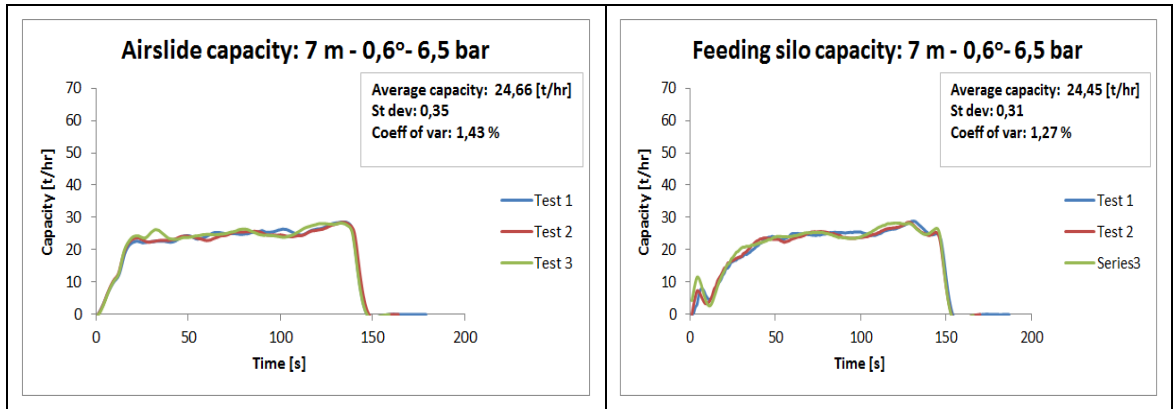


Figure 162 System capacity: 7 m – 0.6 degrees – 6.5 bar

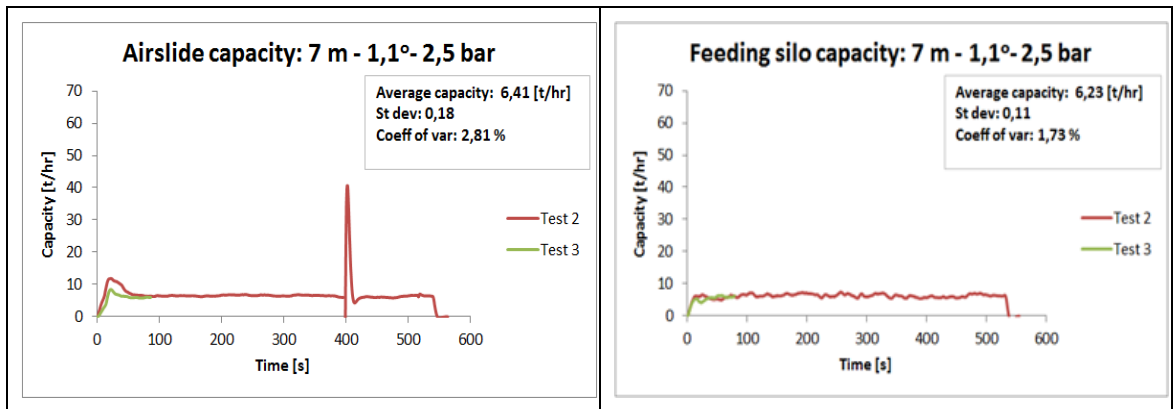


Figure 163 System capacity: 7 m – 1.1 degrees – 2.5 bar

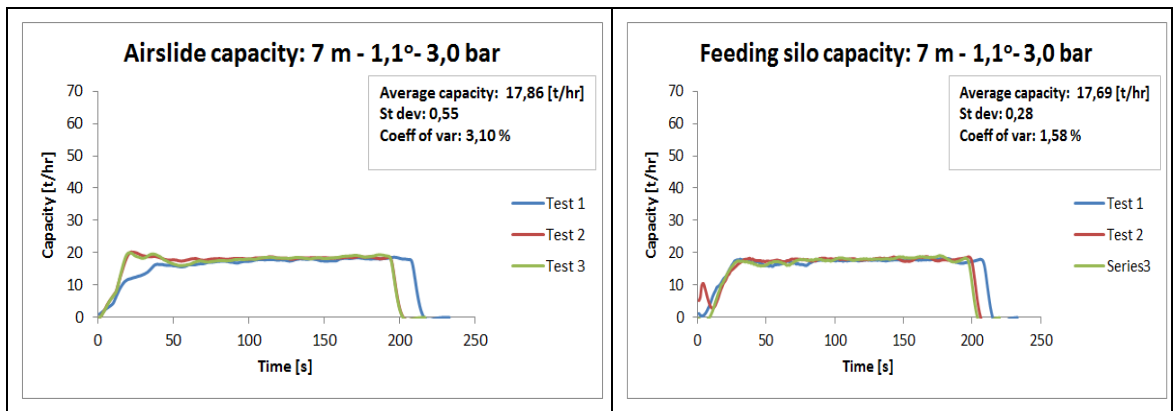


Figure 164 System capacity: 7 m – 1.1 degrees – 3.0 bar

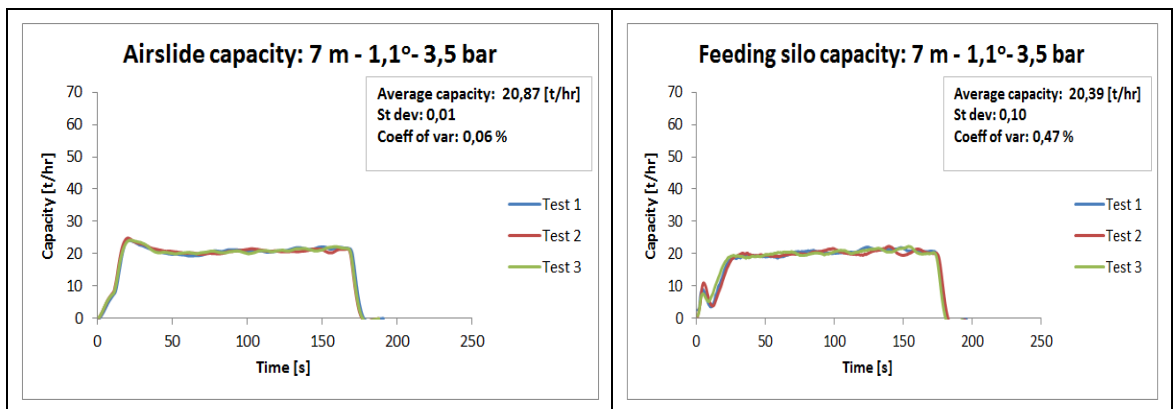


Figure 165 System capacity: 7 m – 1.1 degrees – 3.5 bar

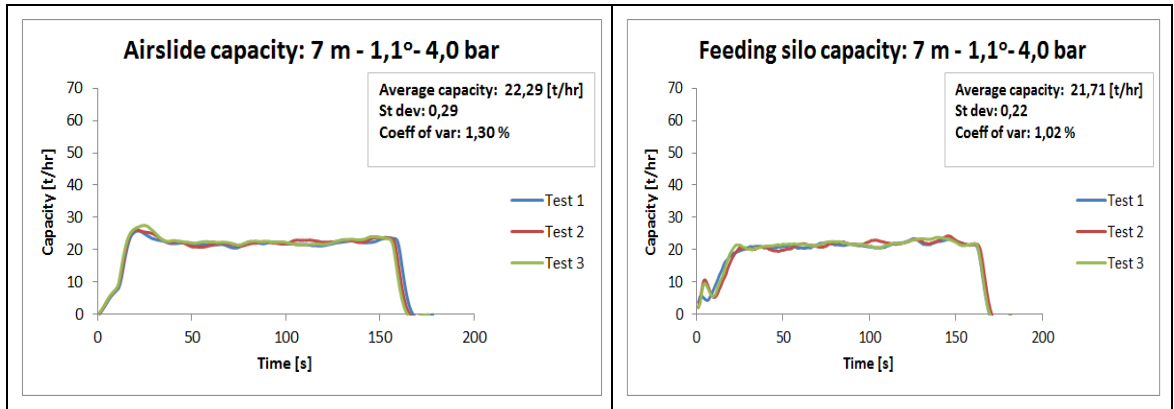


Figure 166 System capacity: 7 m – 1.1 degrees – 4.0 bar

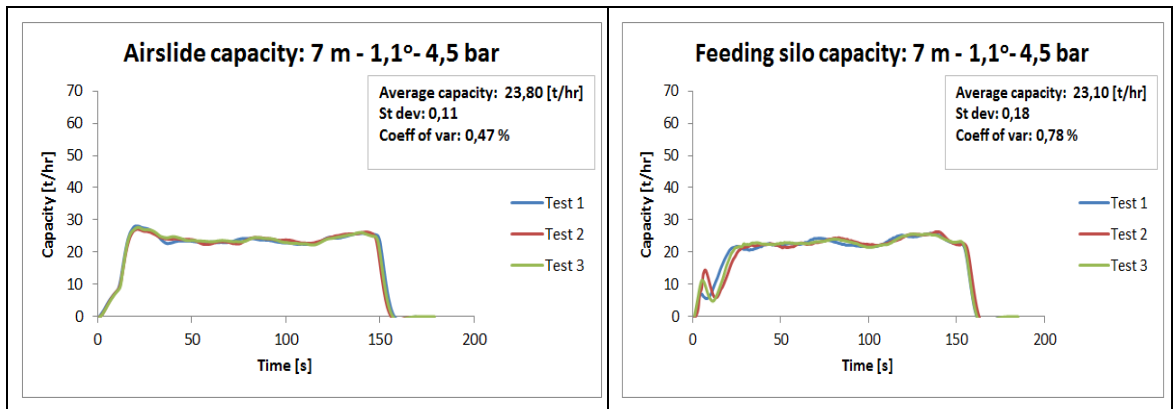


Figure 167 System capacity: 7 m – 1.1 degrees – 4.5 bar

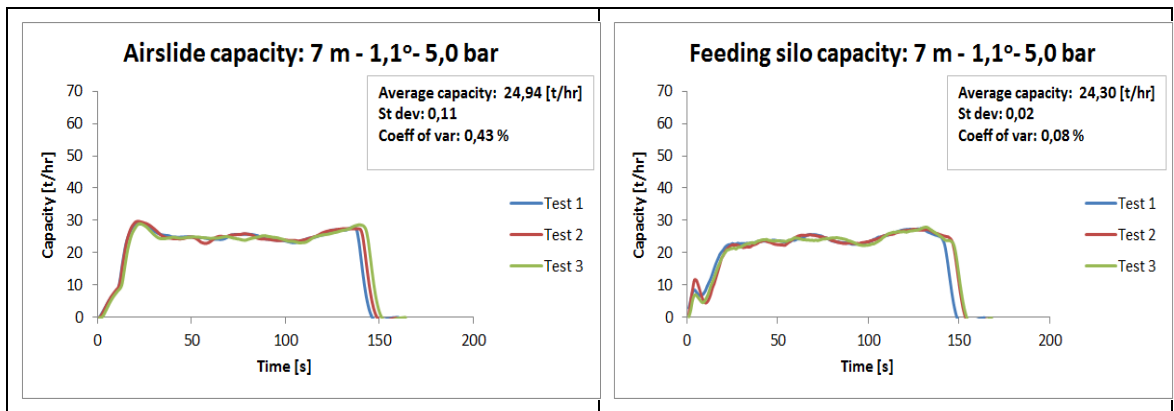


Figure 168 System capacity: 7 m – 1.1 degrees – 5.0 bar

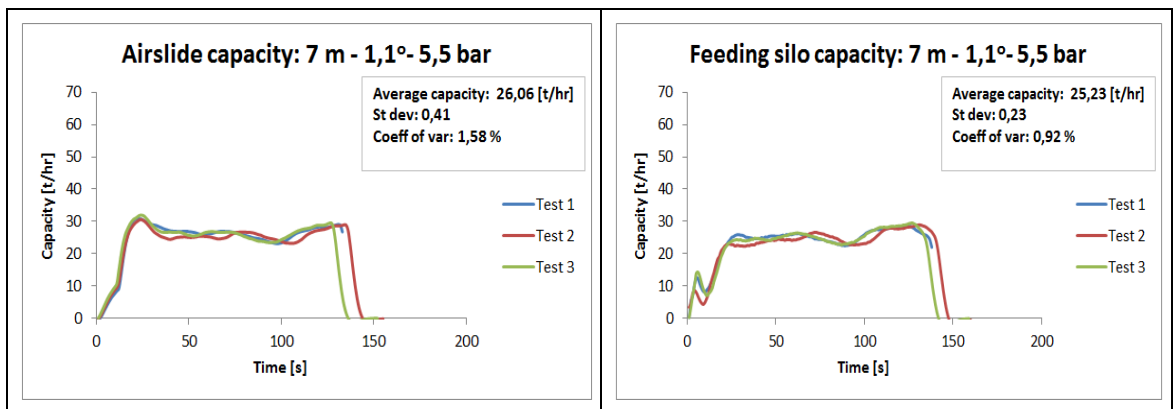


Figure 169 System capacity: 7 m – 1.1 degrees – 5.5 bar

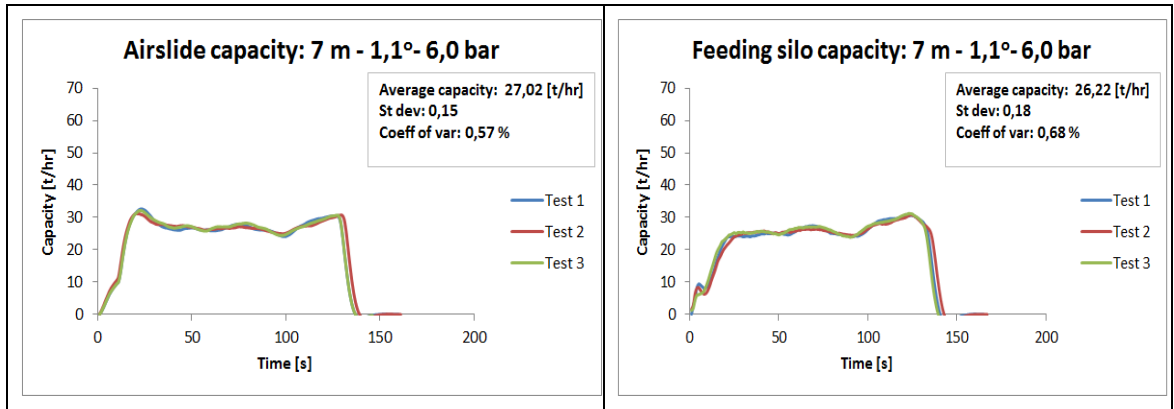


Figure 170 System capacity: 7 m – 1.1 degrees – 6.0 bar

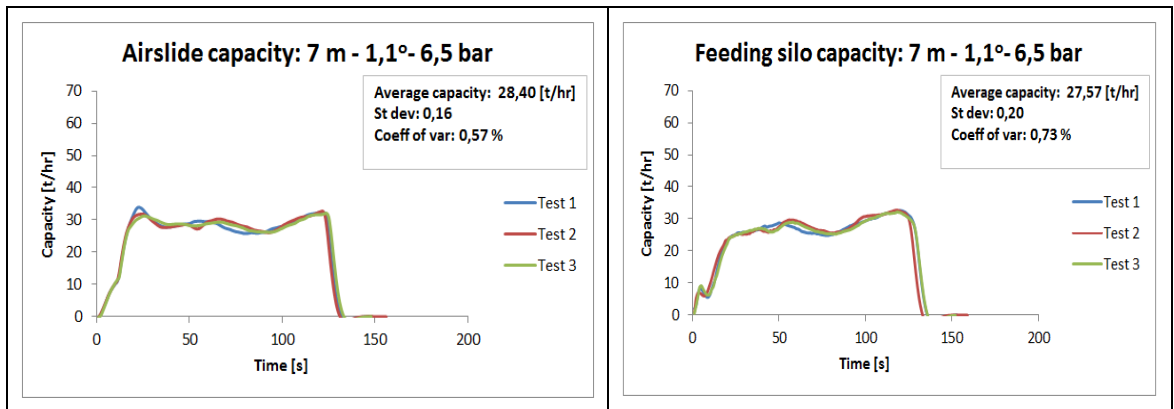


Figure 171 System capacity: 7 m – 1.1 degrees – 6.5 bar

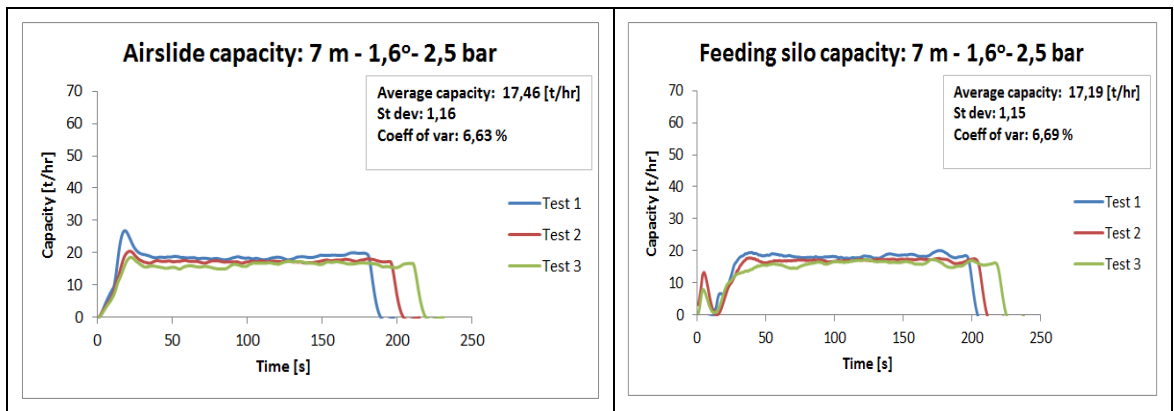


Figure 172 System capacity: 7 m – 1.6 degrees – 2.5 bar

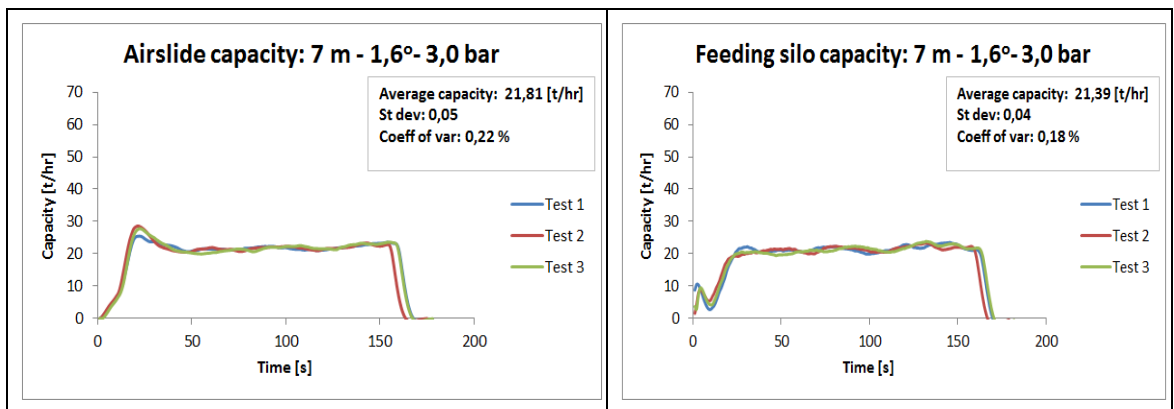


Figure 173 System capacity: 7 m – 1.6 degrees – 3.0 bar

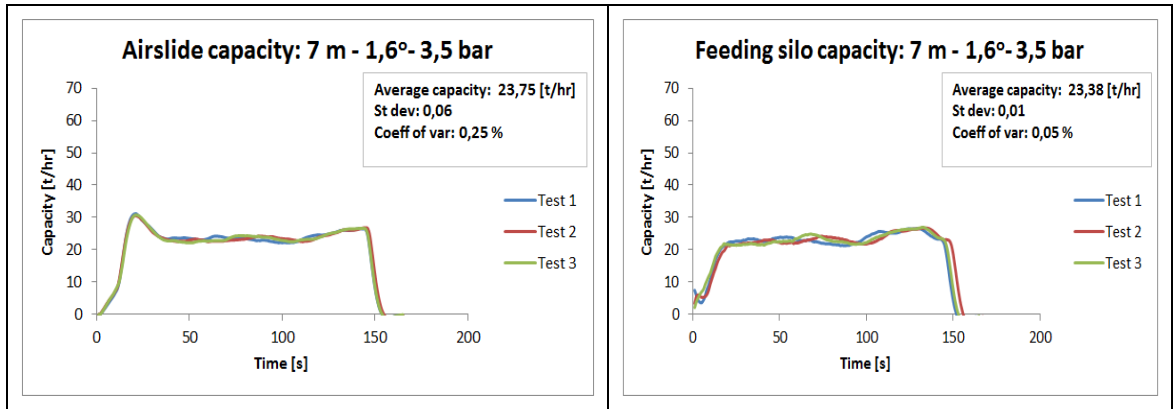


Figure 174 System capacity: 7 m – 1.6 degrees – 3.5 bar

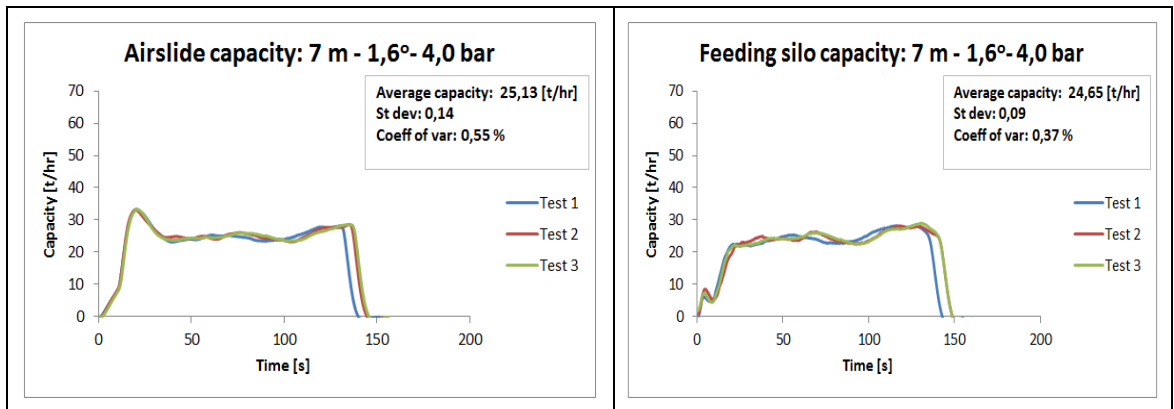


Figure 175 System capacity: 7 m – 1.6 degrees – 4.0 bar

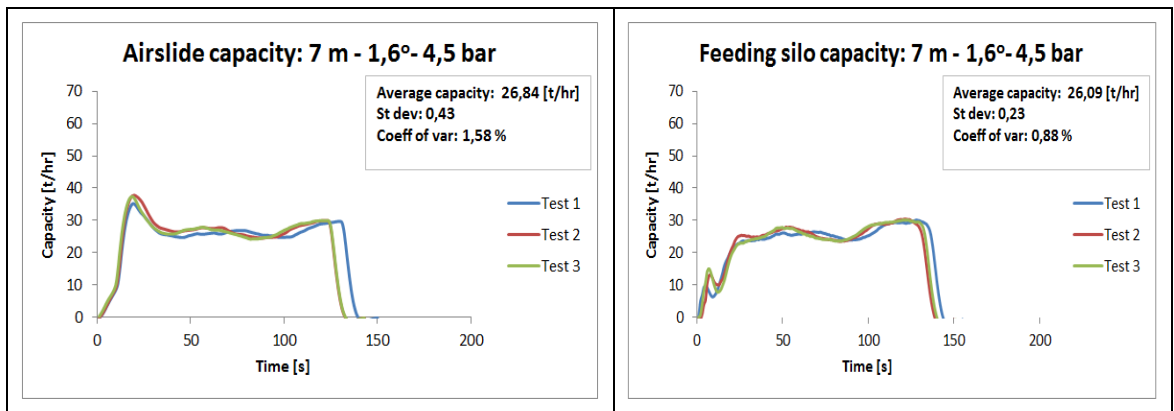


Figure 176 System capacity: 7 m – 1.6 degrees – 4.5 bar

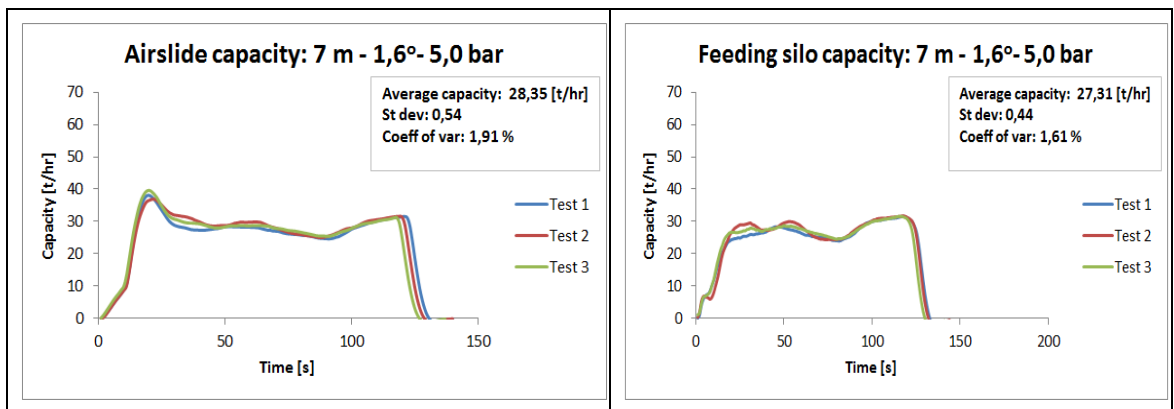


Figure 177 System capacity: 7 m – 1.6 degrees – 5.0 bar

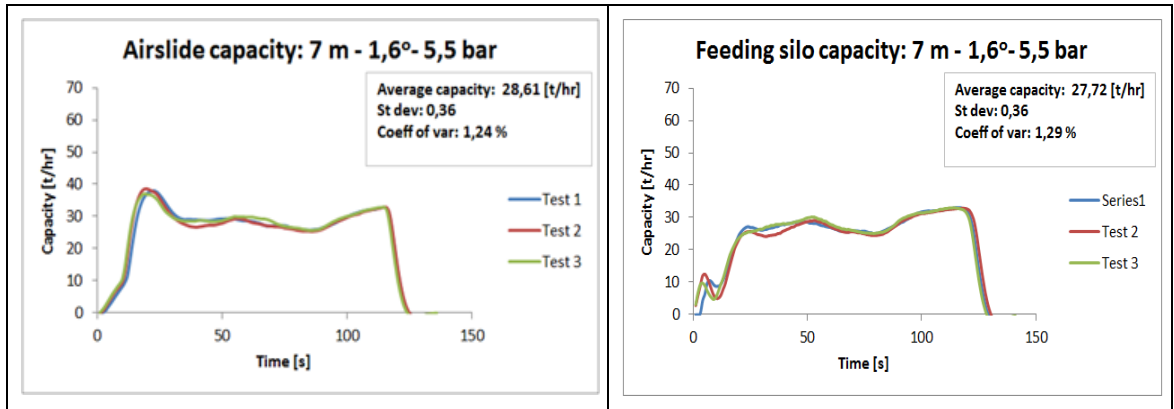


Figure 178 System capacity: 7 m – 1.6 degrees – 5.5 bar

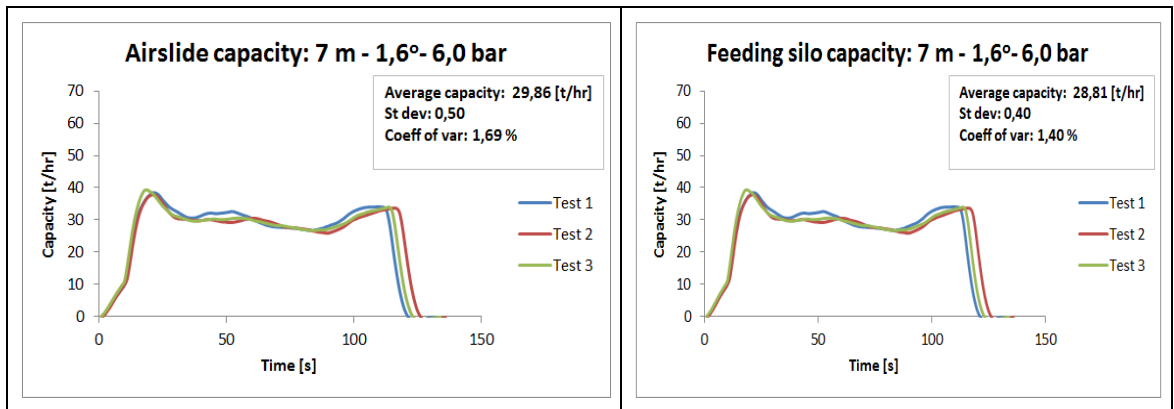


Figure 179 System capacity: 7 m – 1.6 degrees – 6.0 bar

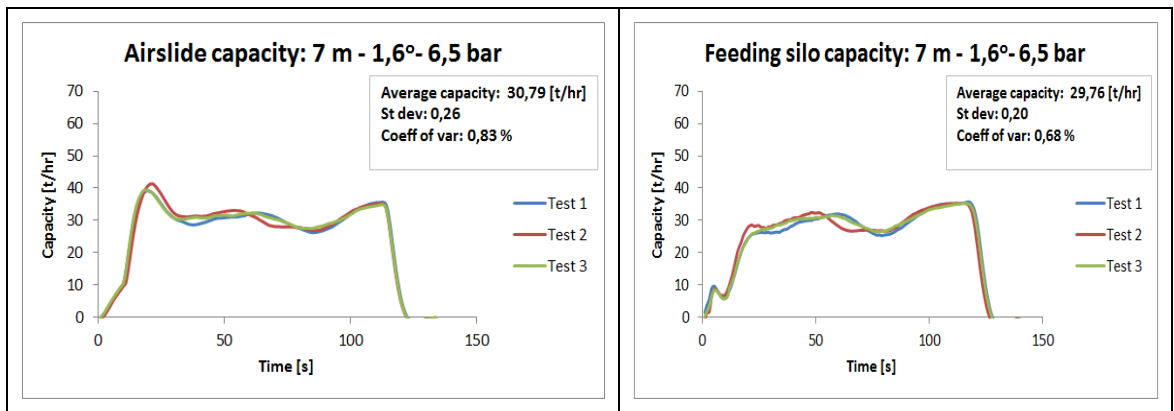


Figure 180 System capacity: 7 m – 1.6 degrees – 6.5 bar

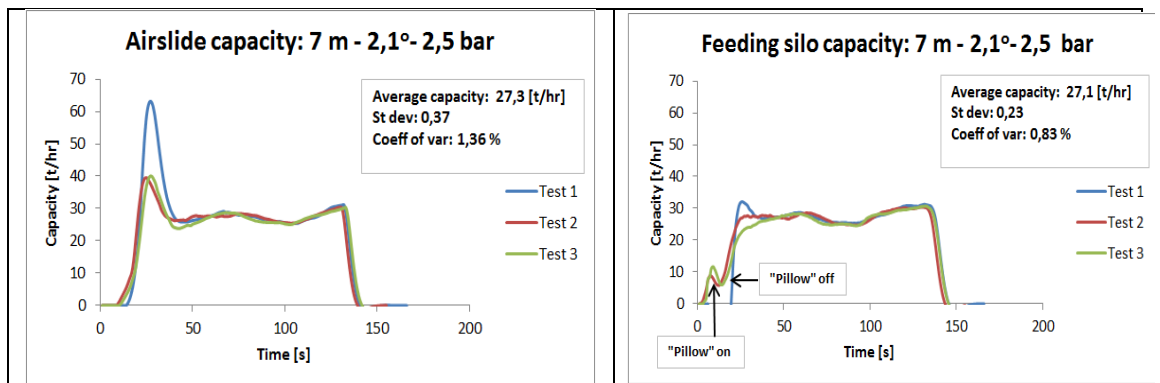


Figure 181 System capacity: 7 m – 2.1 degrees – 2.5 bar

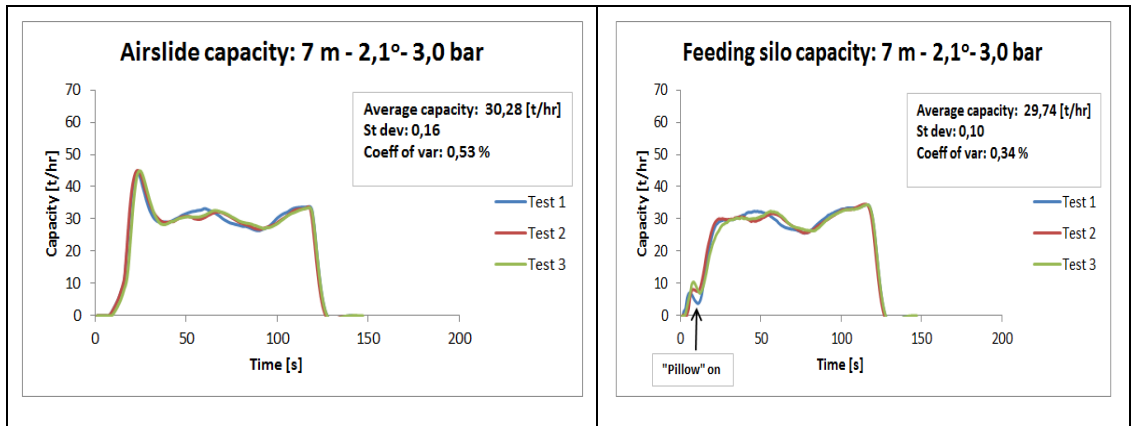


Figure 182 System capacity: 7 m – 2.1 degrees – 3.0 bar

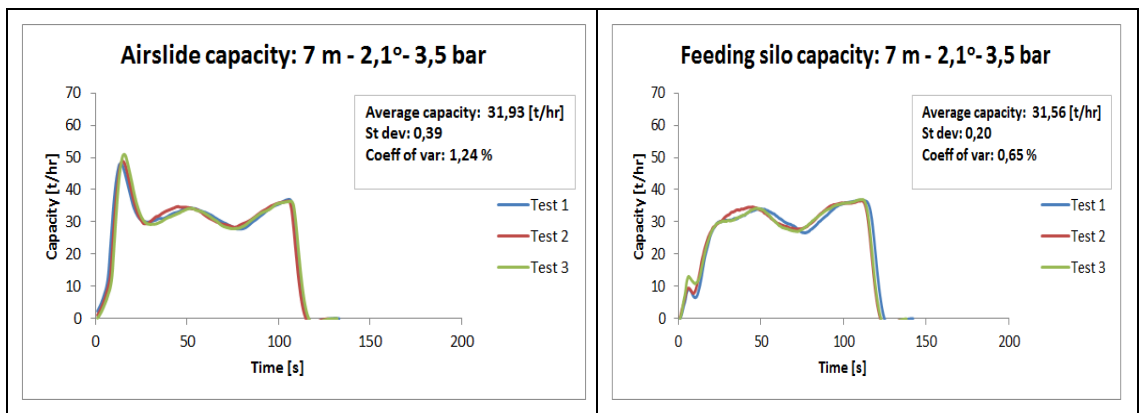




Figure 183 System capacity: 7 m – 2.1 degrees – 3.5 bar

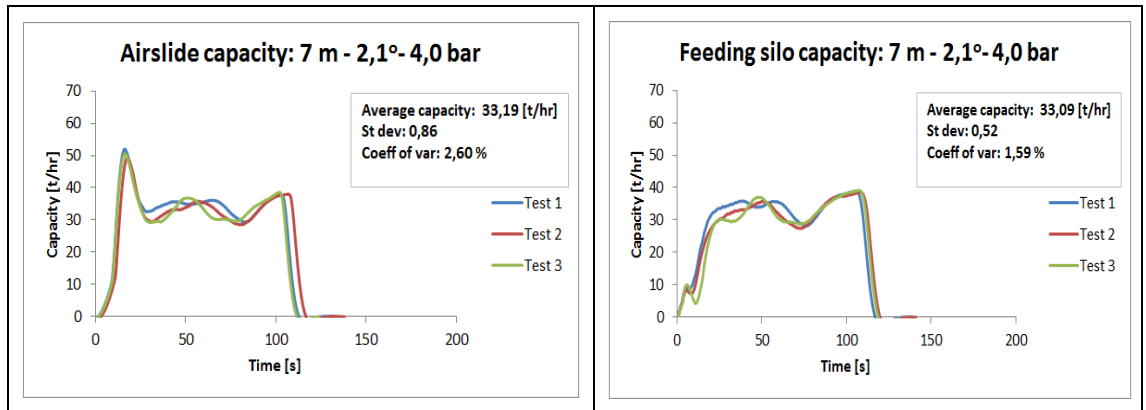


Figure 184 System capacity: 7 m – 2.1 degrees – 4.0 bar

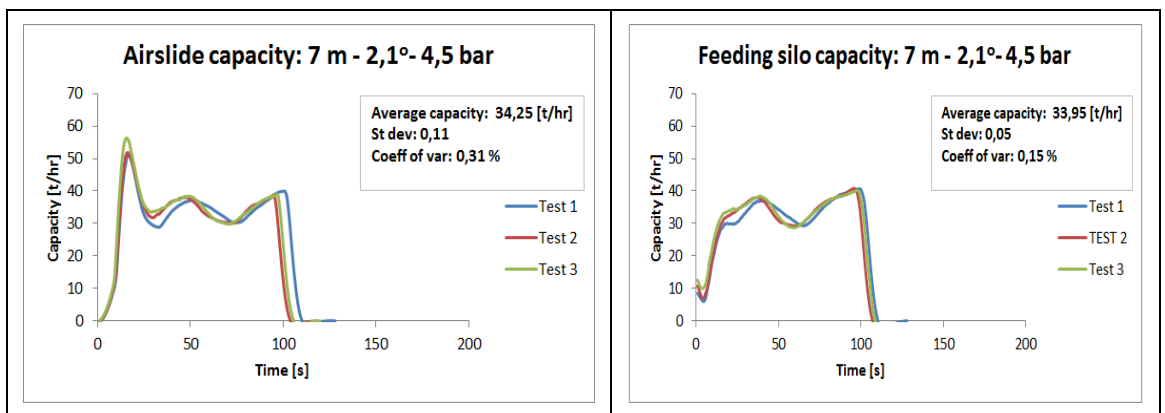


Figure 185 System capacity: 7 m – 2.1 degrees – 4.5 bar

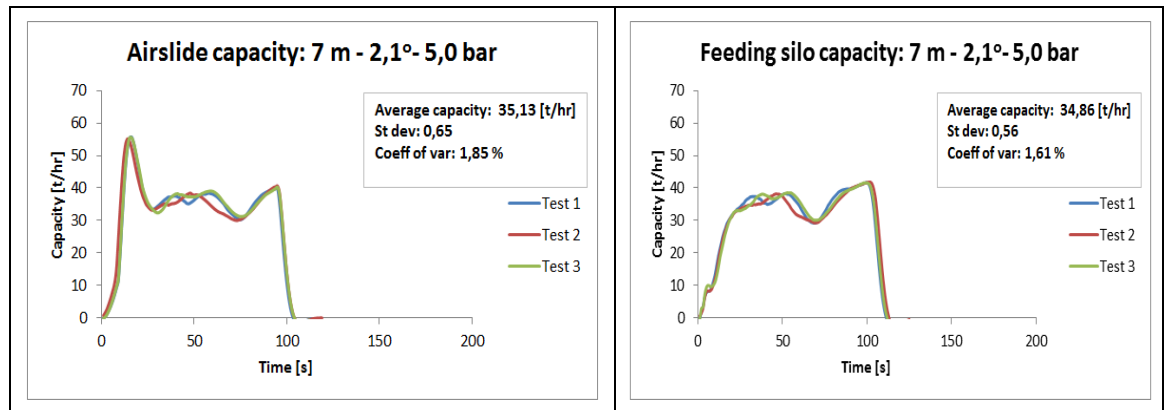


Figure 186 System capacity: 7 m – 2.1 degrees – 5.0 bar



Figure 187 System capacity: 7 m – 2.1 degrees – 5.5 bar

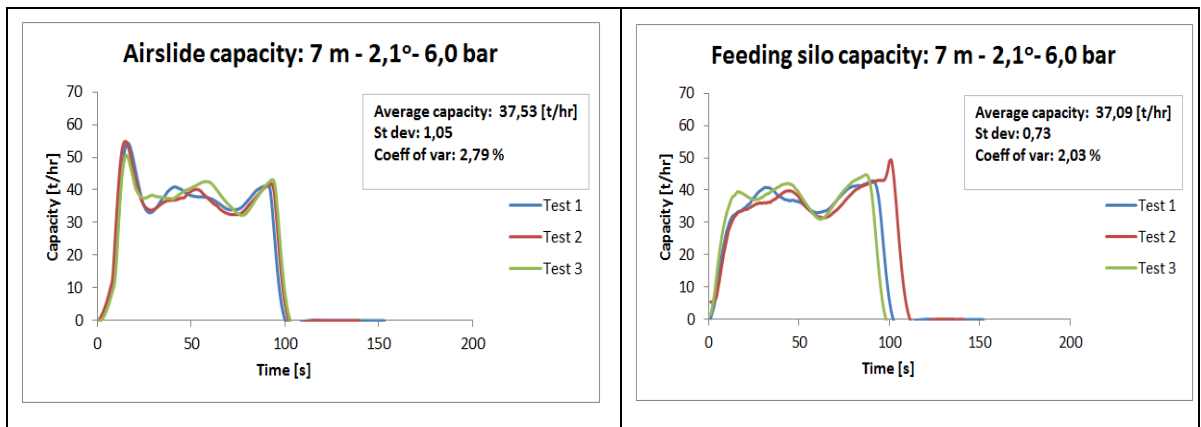


Figure 188 System capacity: 7 m – 2.1 degrees – 6.0 bar

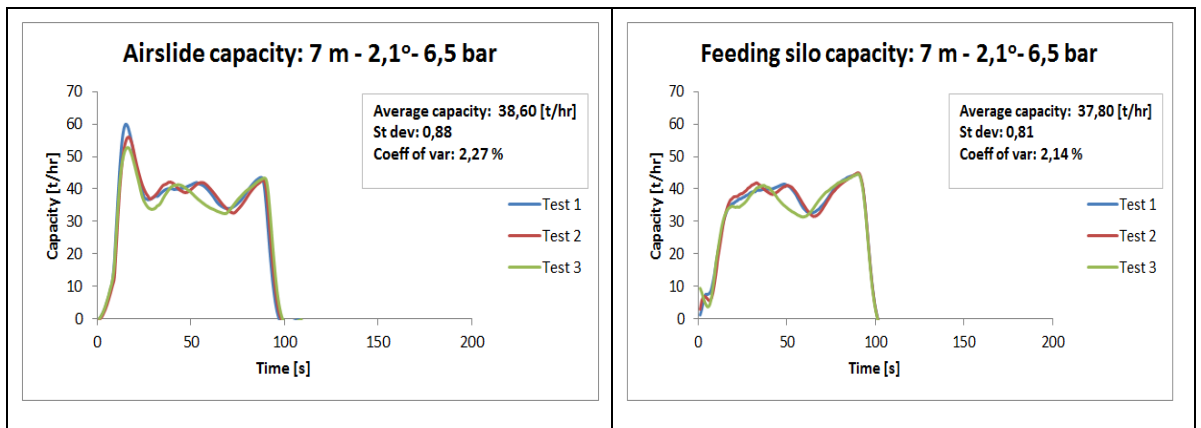


Figure 189 System capacity: 7 m – 2.1 degrees – 6.5 bar

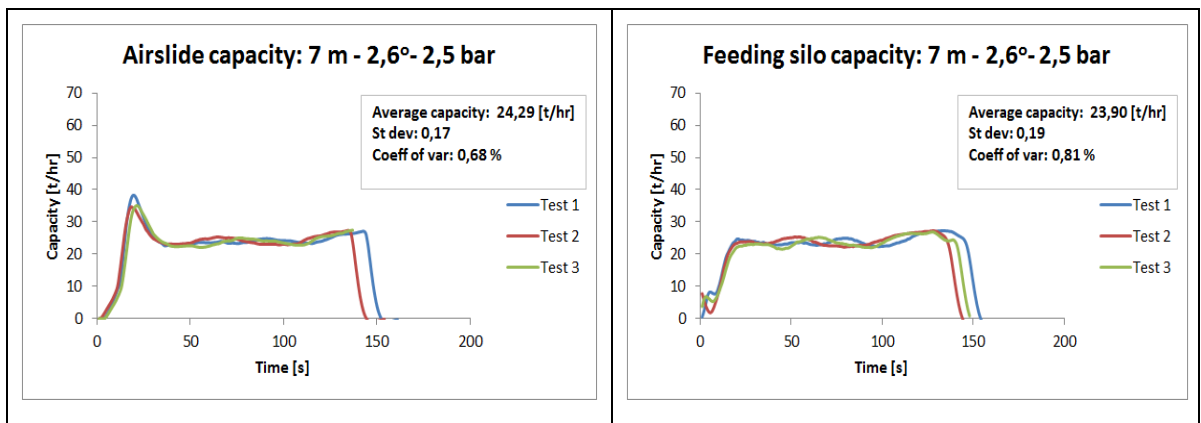


Figure 190 System capacity: 7 m – 2.6 degrees – 2.5 bar

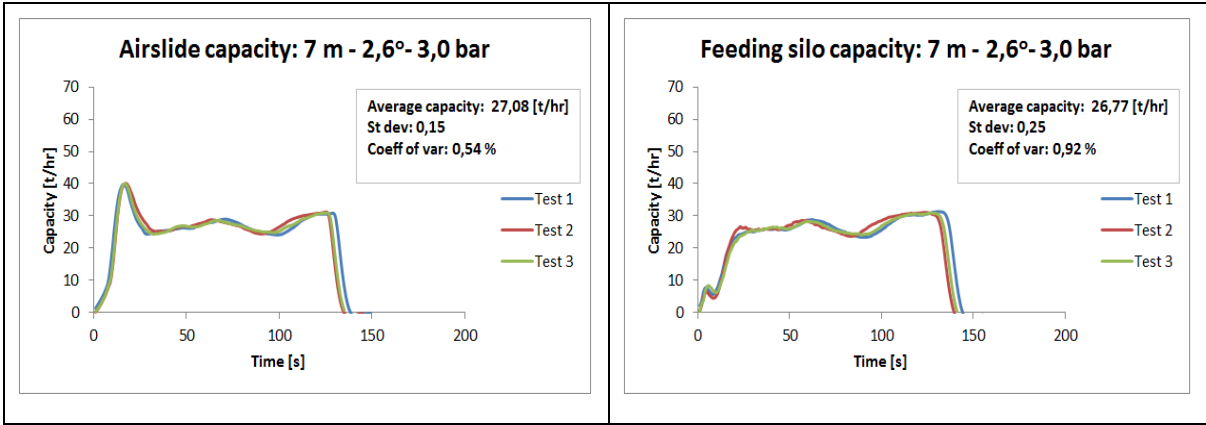


Figure 191 System capacity: 7 m – 2.6 degrees – 3.0 bar

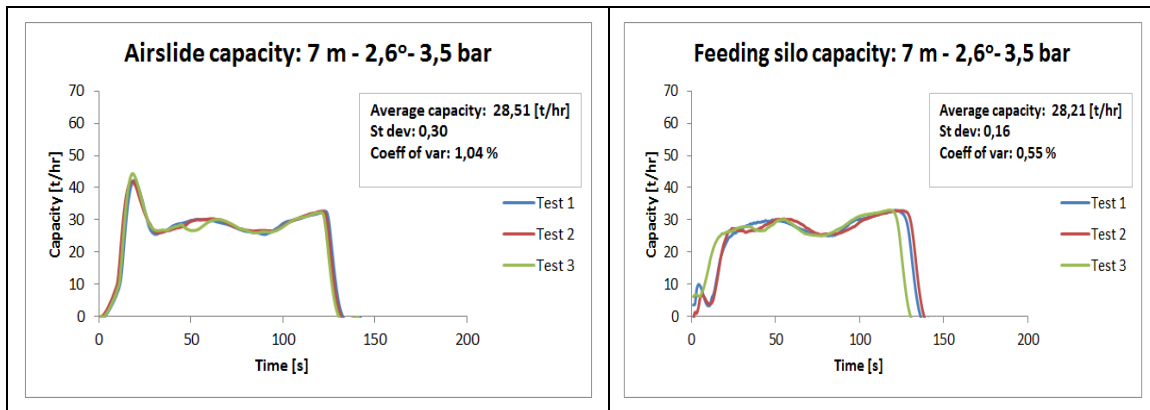


Figure 192 System capacity: 7 m – 2.6 degrees – 3.5 bar

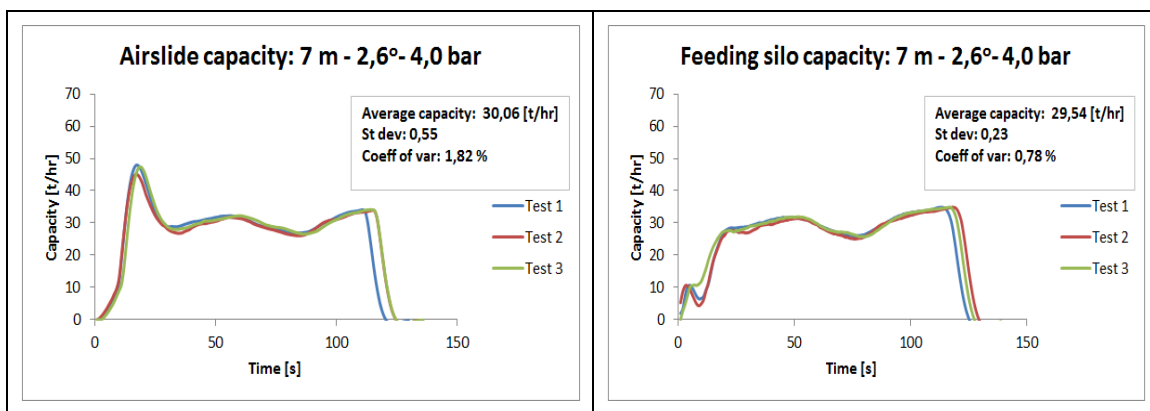


Figure 193 System capacity: 7 m – 2.6 degrees – 4.0 bar

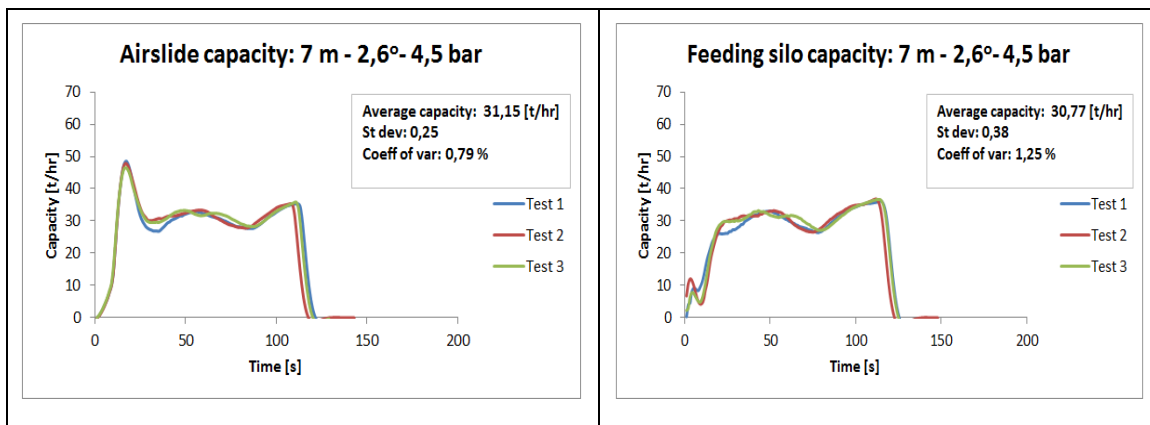


Figure 194 System capacity: 7 m – 2.6 degrees – 4.5 bar

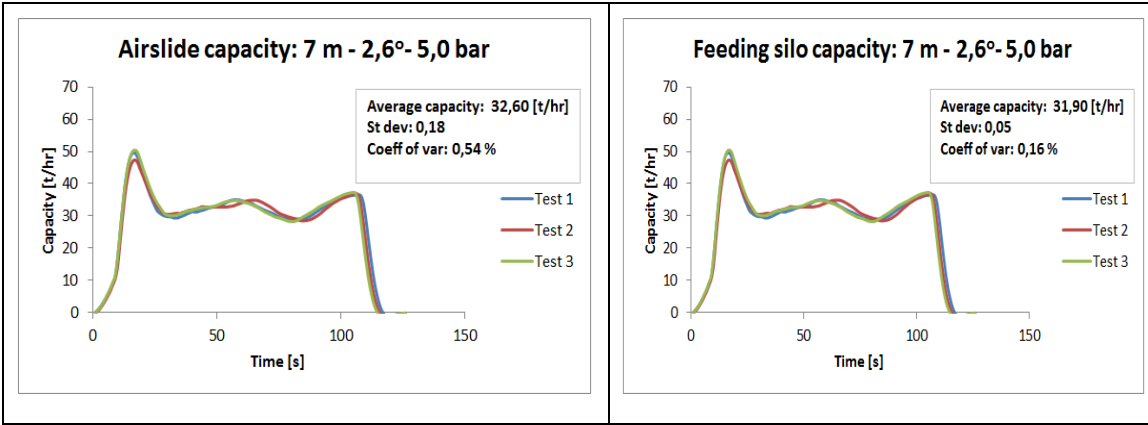


Figure 195 System capacity: 7 m – 2.6 degrees – 5.0 bar

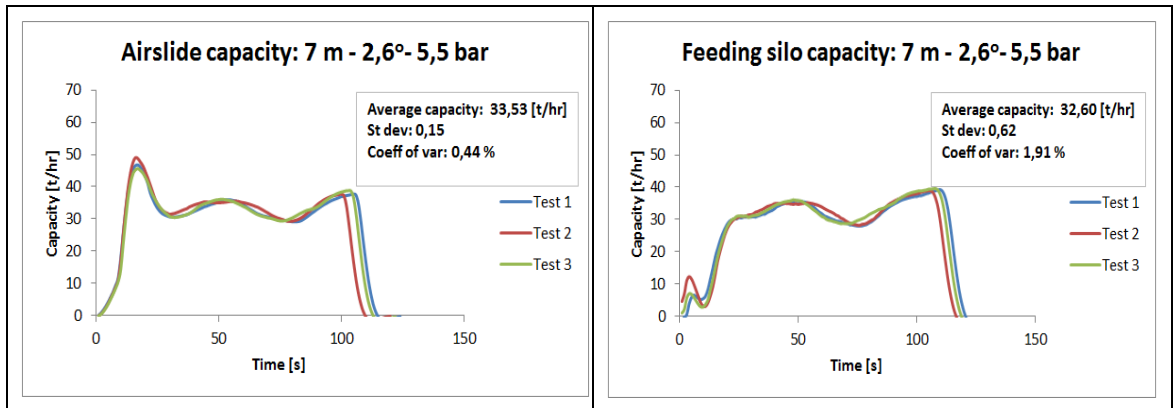


Figure 196 System capacity: 7 m – 2.6 degrees – 5.5 bar

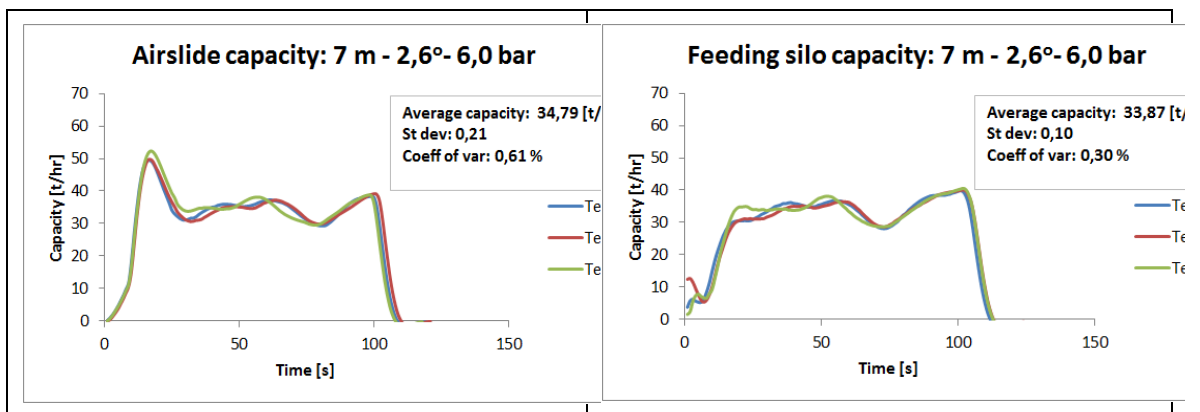


Figure 197 System capacity: 7 m – 2.6 degrees – 6.0 bar

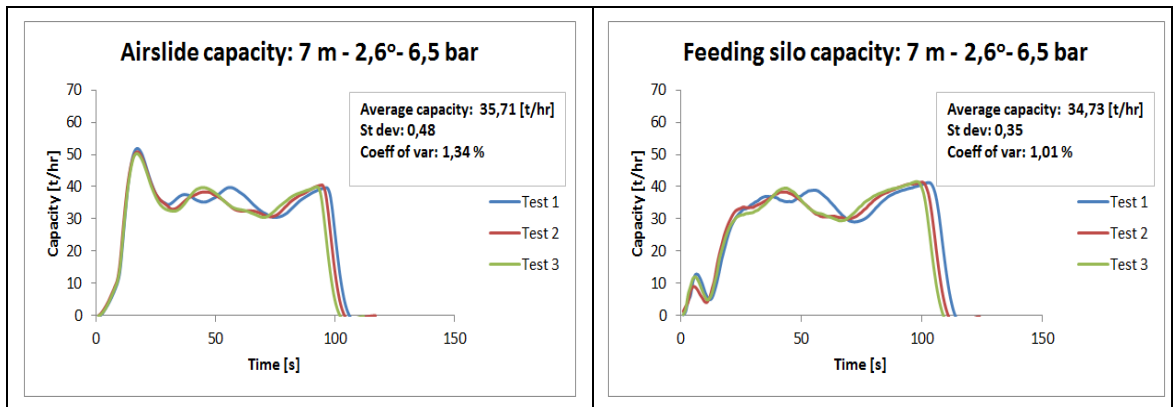


Figure 198 System capacity: 7 m – 2.6 degrees – 6.5 bar

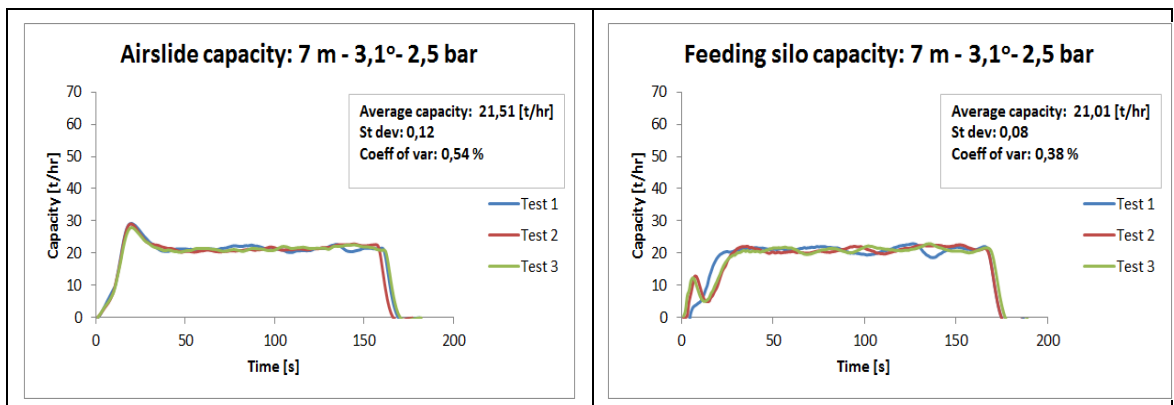


Figure 199 System capacity: 7 m – 3.1 degrees – 2.5 bar

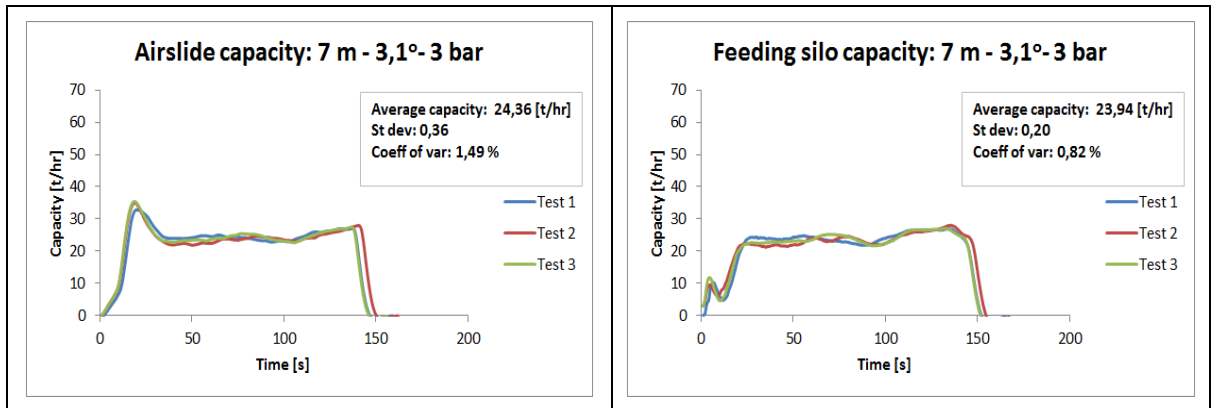


Figure 200 System capacity: 7 m – 3.1 degrees – 3.0 bar

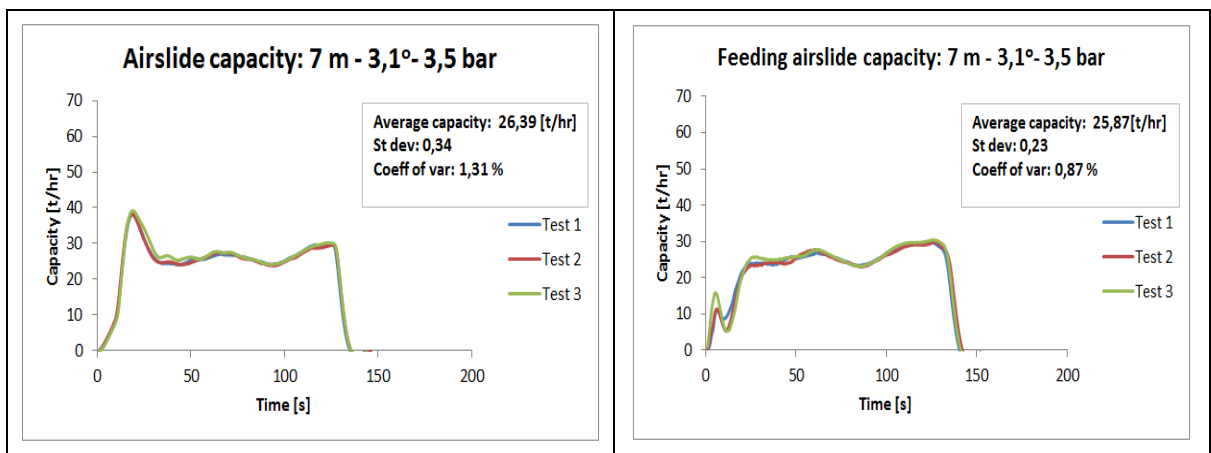


Figure 201 System capacity: 7 m – 3.1 degrees – 3.5 bar

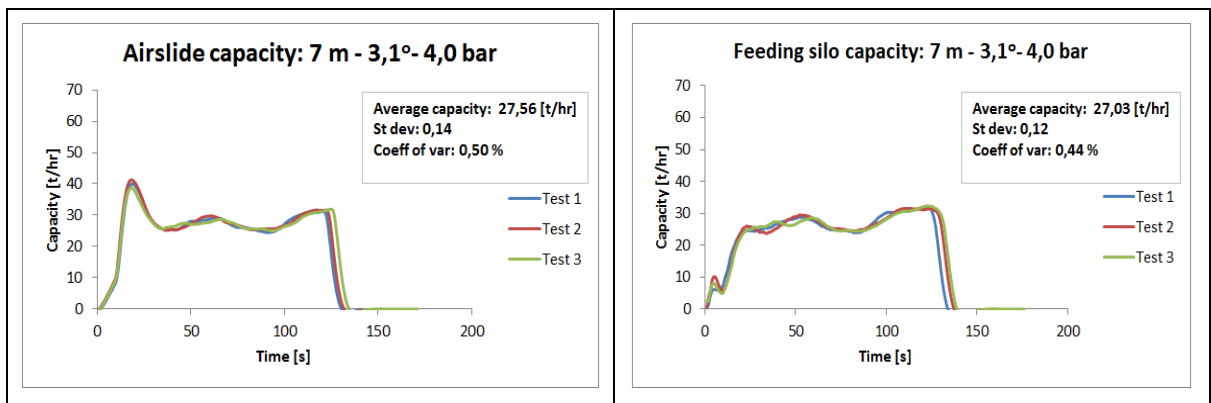


Figure 202 System capacity: 7 m – 3.1 degrees – 4.0 bar

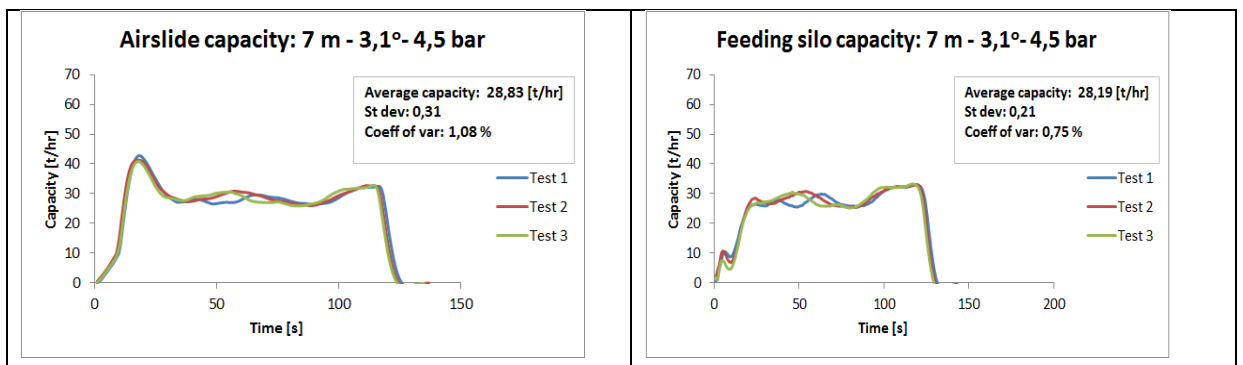


Figure 203 System capacity: 7 m – 3.1 degrees – 4.5 bar

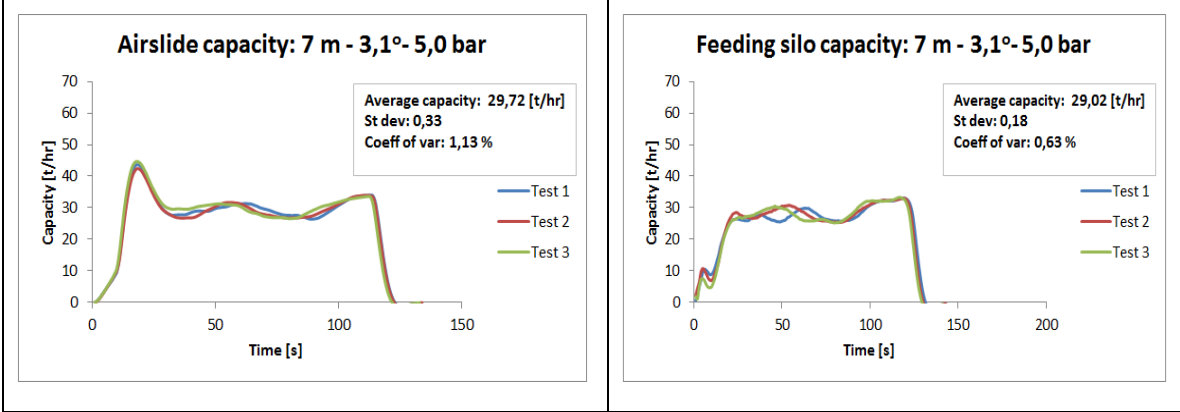




Figure 204 System capacity: 7 m – 3.1 degrees – 5.0 bar

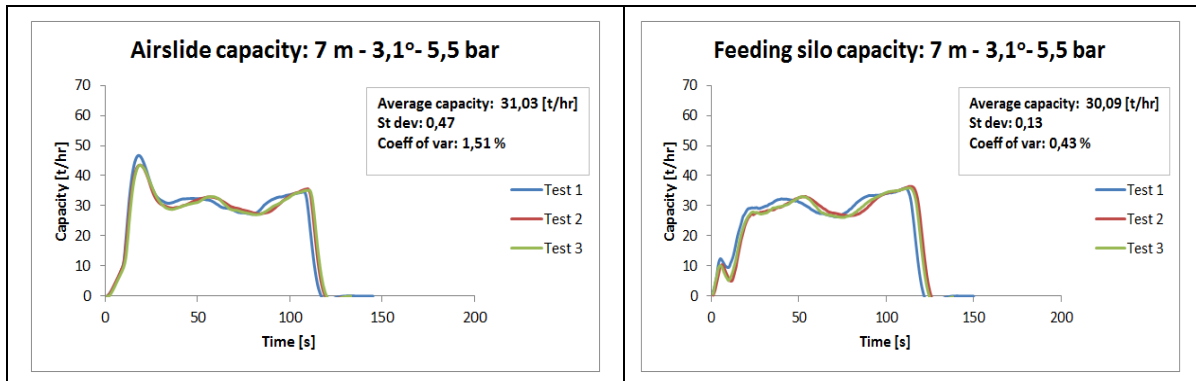


Figure 205 System capacity: 7 m – 3.1 degrees – 5.5 bar

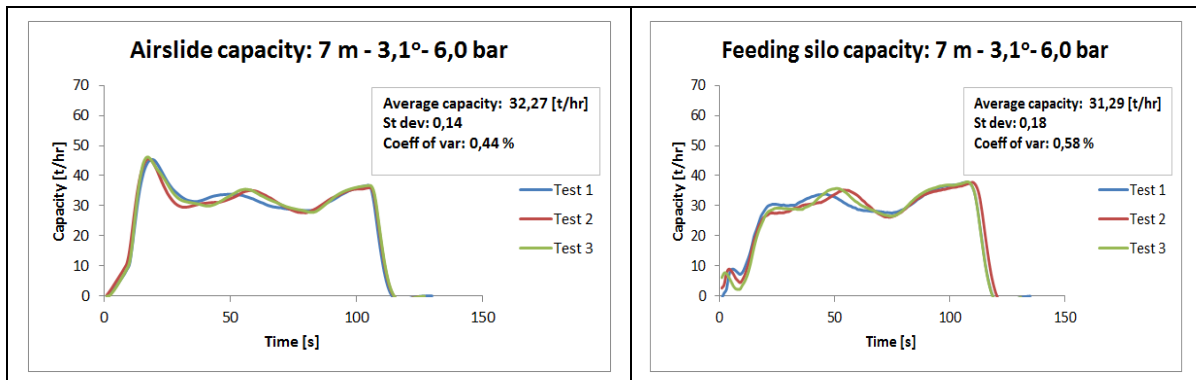


Figure 206 System capacity: 7 m – 3.1 degrees – 6.0 bar

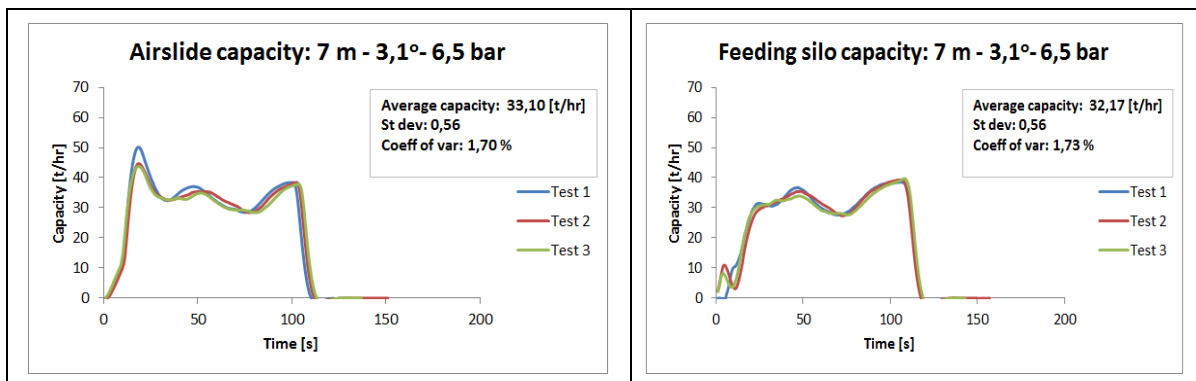


Figure 207 System capacity: 7 m – 3.1 degrees – 6.5 bar

## APPENDIX C 15 M AIR SLIDE CAPACITY TESTS

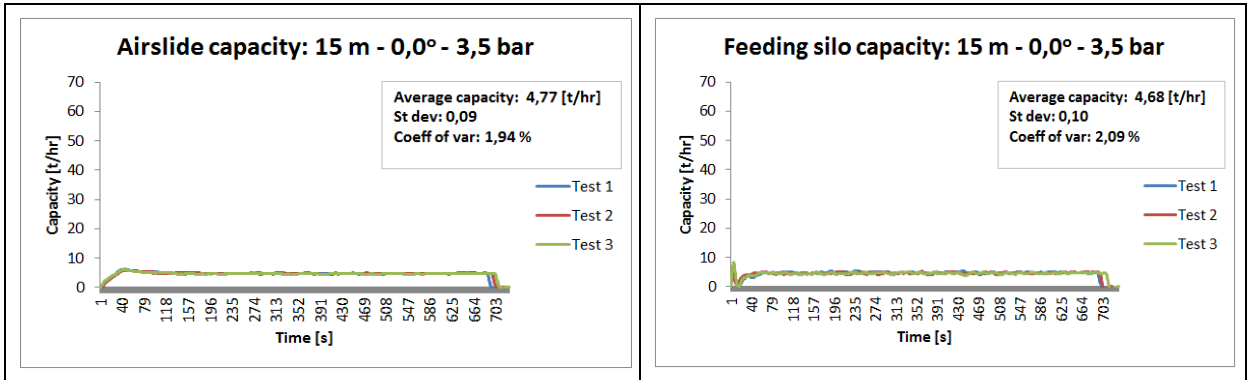


Figure 208 System capacity: 15 m – 0.0 degrees – 3.5 bar

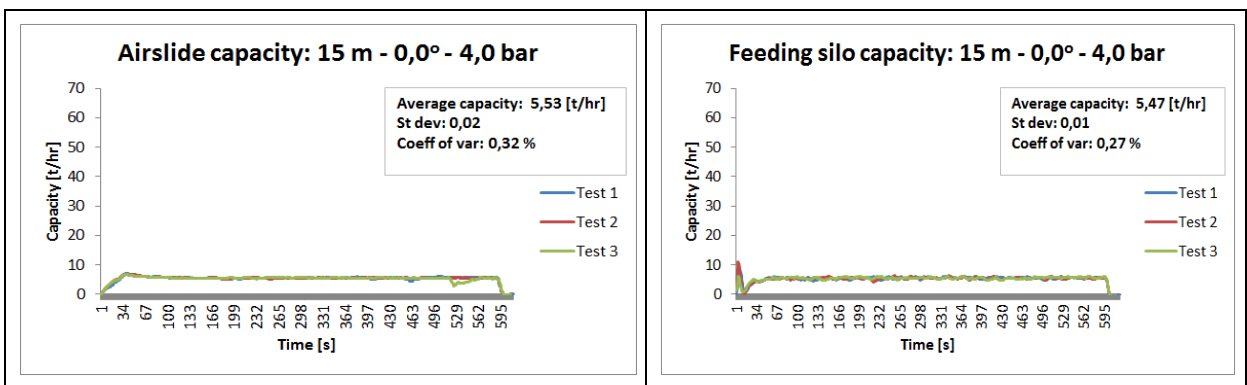


Figure 209 System capacity: 15 m – 0.0 degrees – 4.0 bar

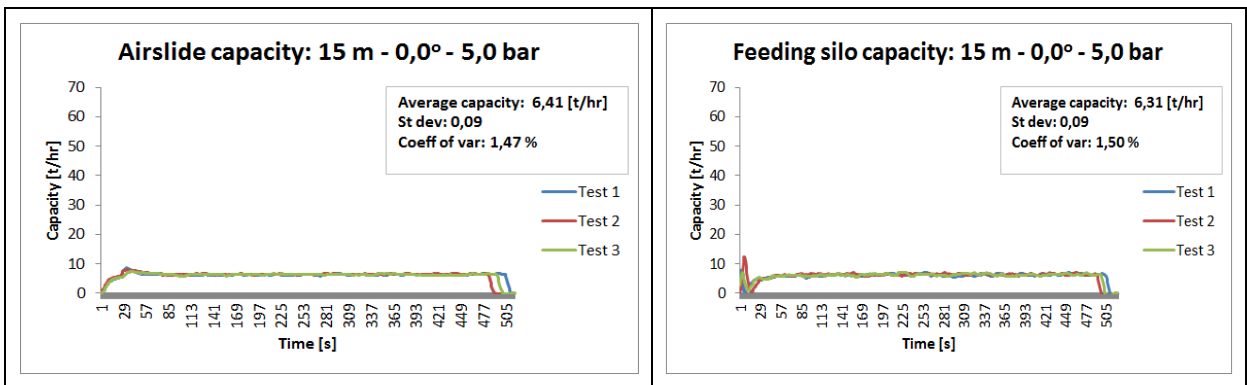


Figure 210 System capacity: 15 m – 0.0 degrees – 5.0 bar

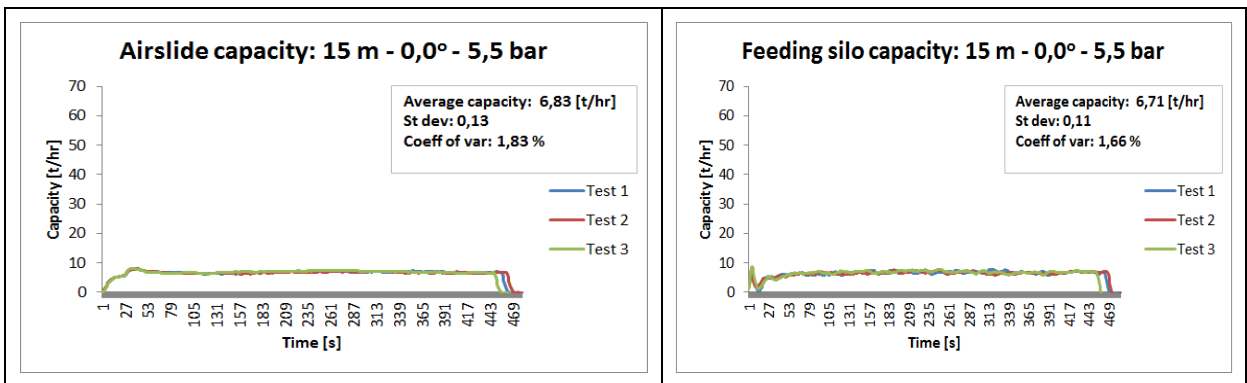


Figure 211 System capacity: 15 m – 0.0 degrees – 5.5 bar

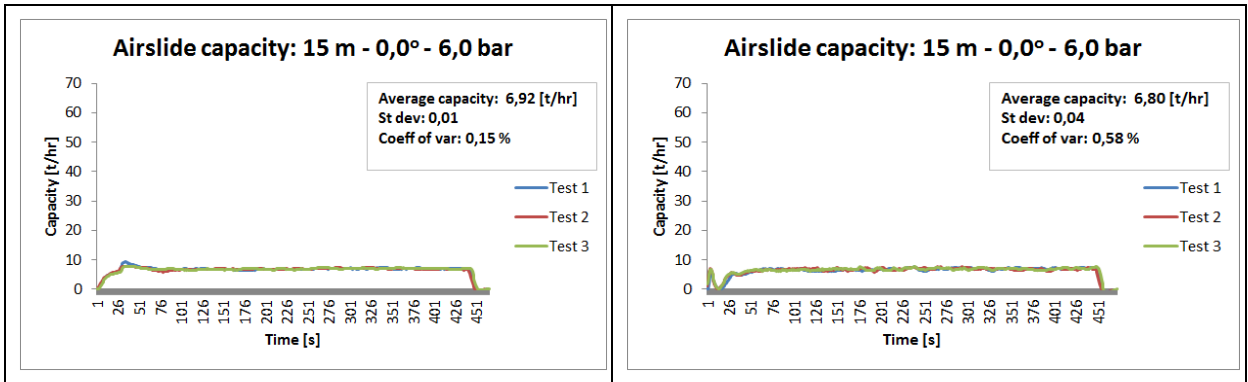


Figure 212 System capacity: 15 m – 0.0 degrees – 6.0 bar

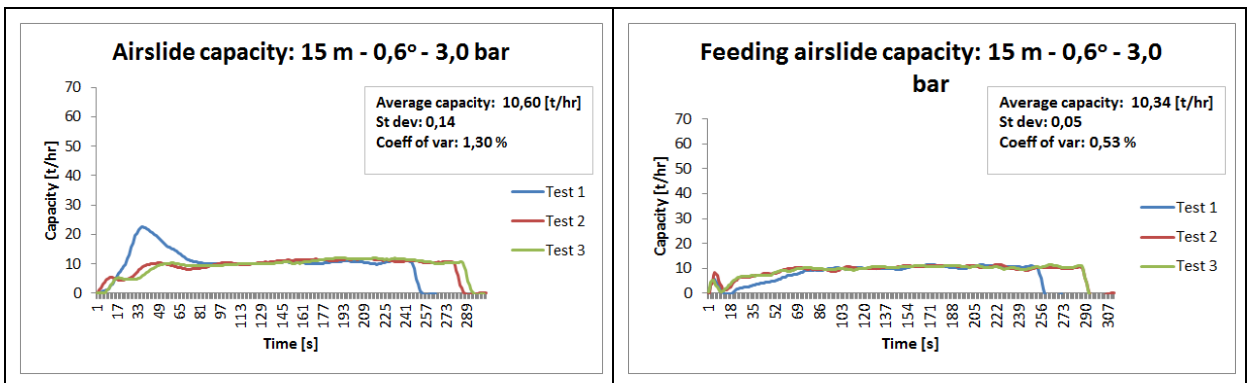


Figure 213 System capacity: 15 m – 0.6 degrees – 3.0 bar

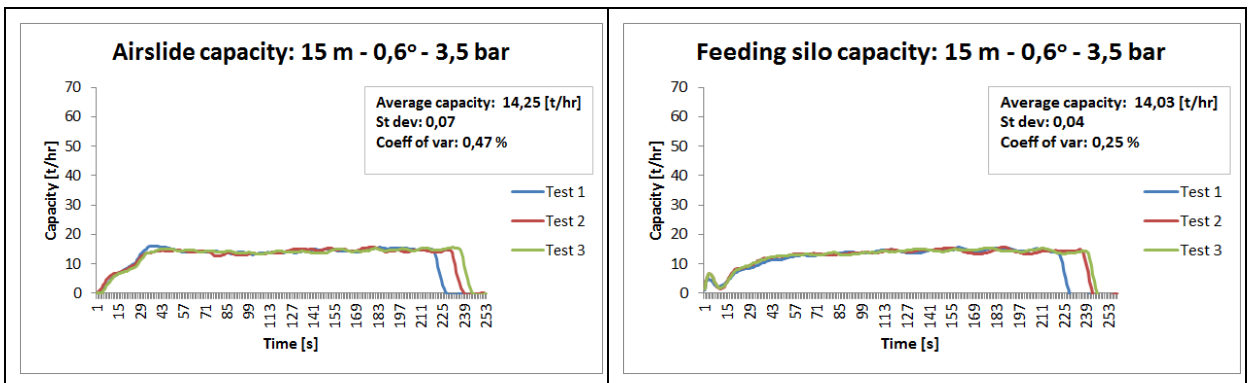


Figure 214 System capacity: 15 m – 0.6 degrees – 3.5 bar

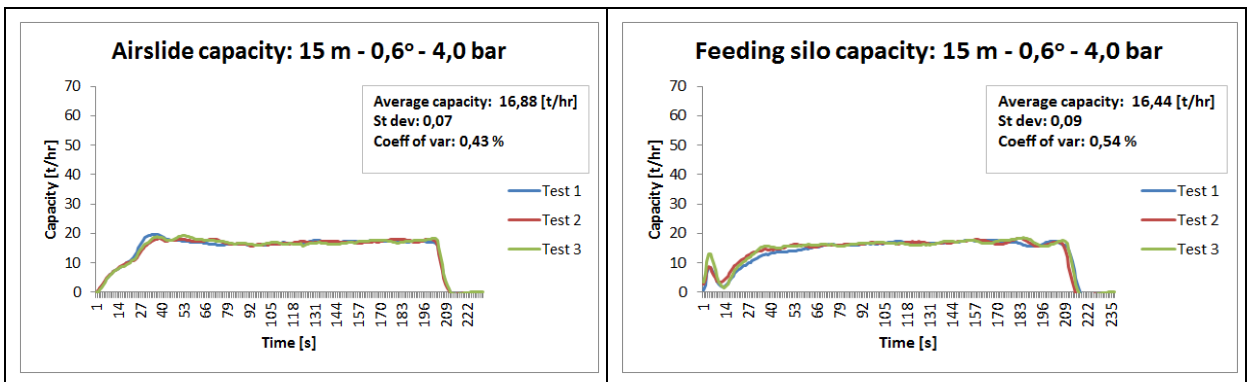


Figure 215 System capacity: 15 m – 0.6 degrees – 4.0 bar

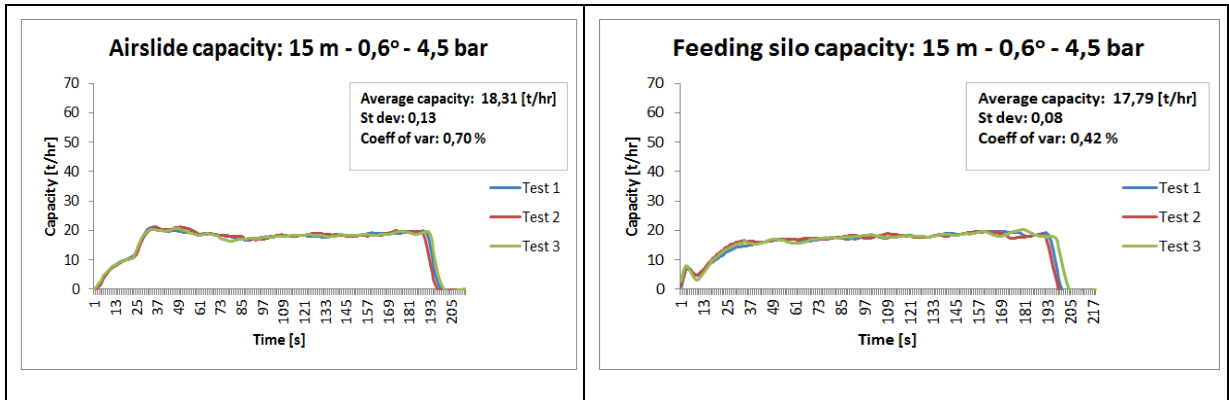


Figure 216 System capacity: 15 m – 0.6 degrees – 4.5 bar

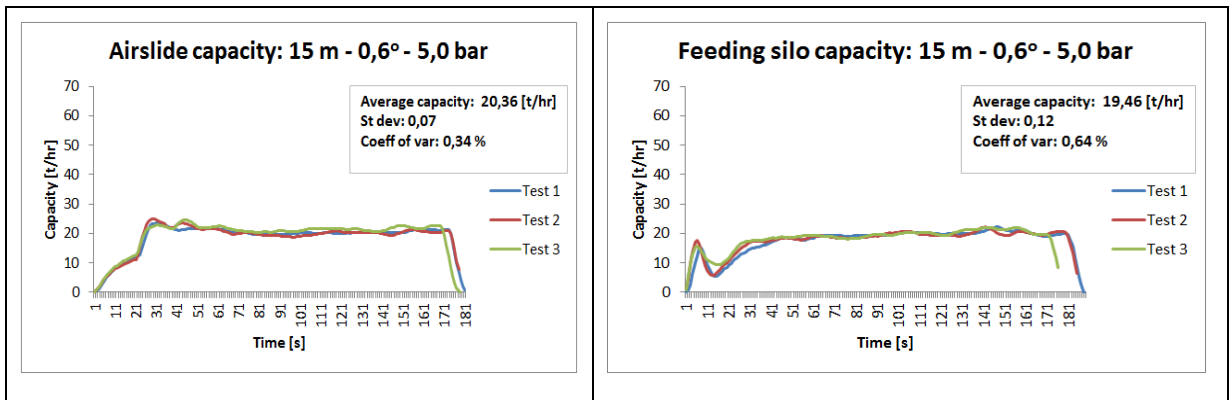


Figure 217 System capacity: 15 m – 0.6 degrees – 5.0 bar

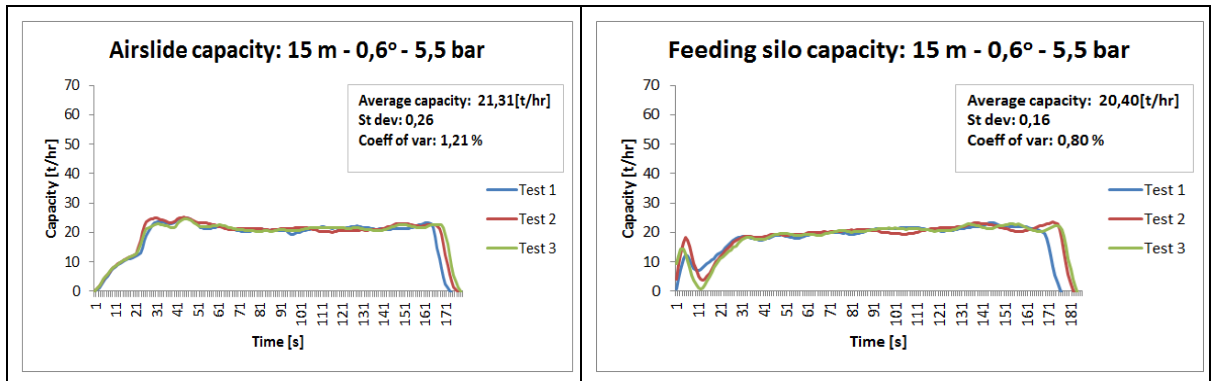


Figure 218 System capacity: 15 m – 0.6 degrees – 5.5 bar

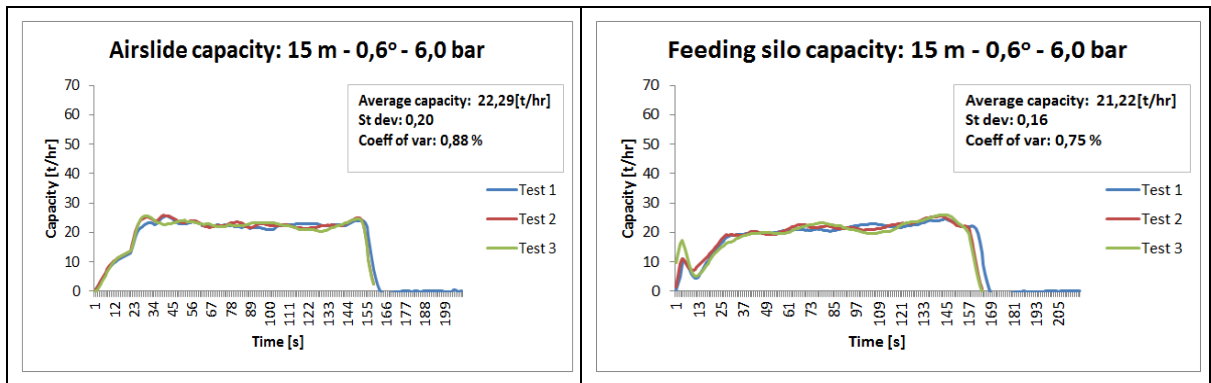


Figure 219 System capacity: 15 m – 0.6 degrees – 6.0 bar

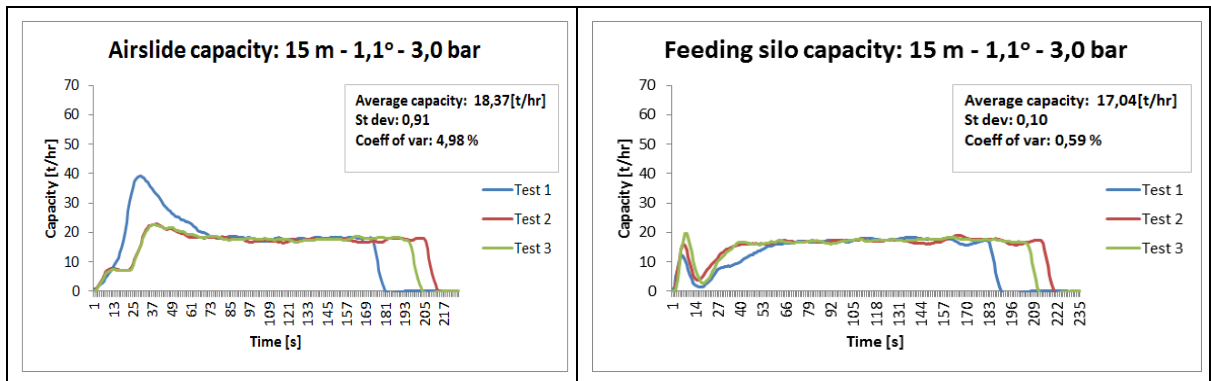


Figure 220 System capacity: 15 m – 1.1 degrees – 3.0 bar

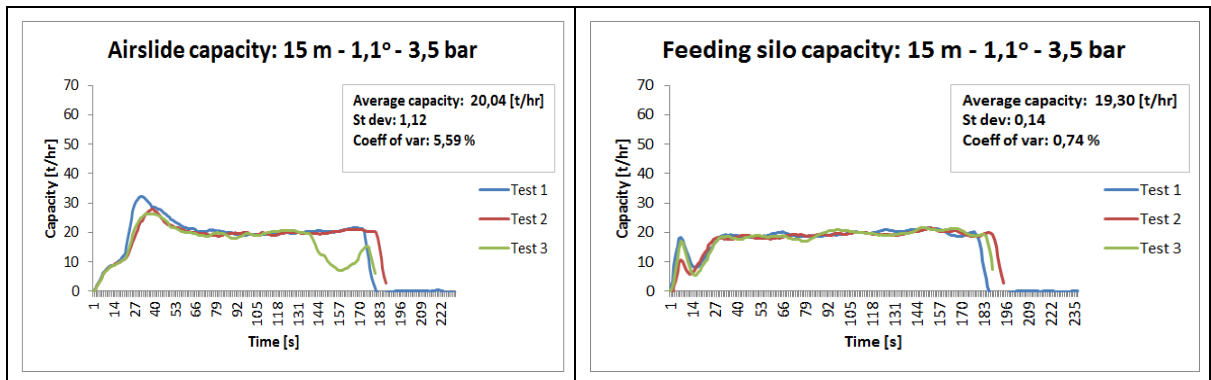


Figure 221 System capacity: 15 m – 1.1 degrees – 3.5 bar

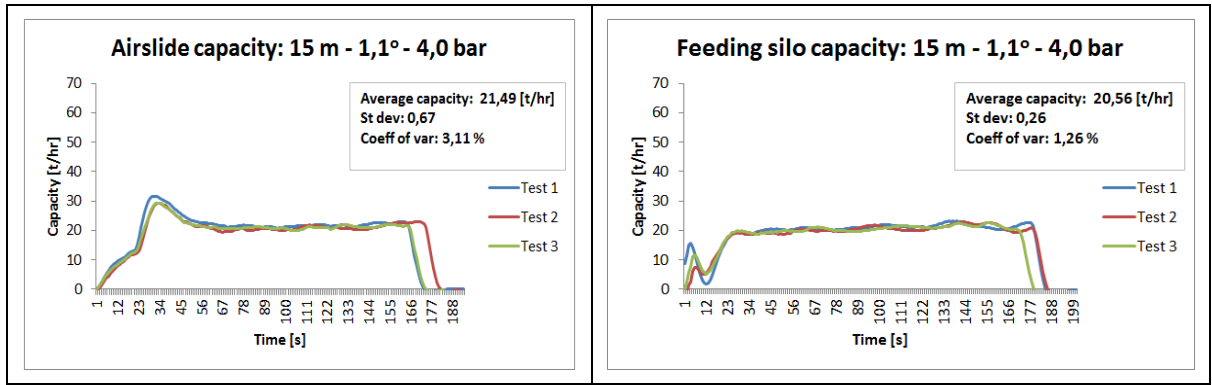


Figure 222 System capacity: 15 m – 1.1 degrees – 4.0 bar

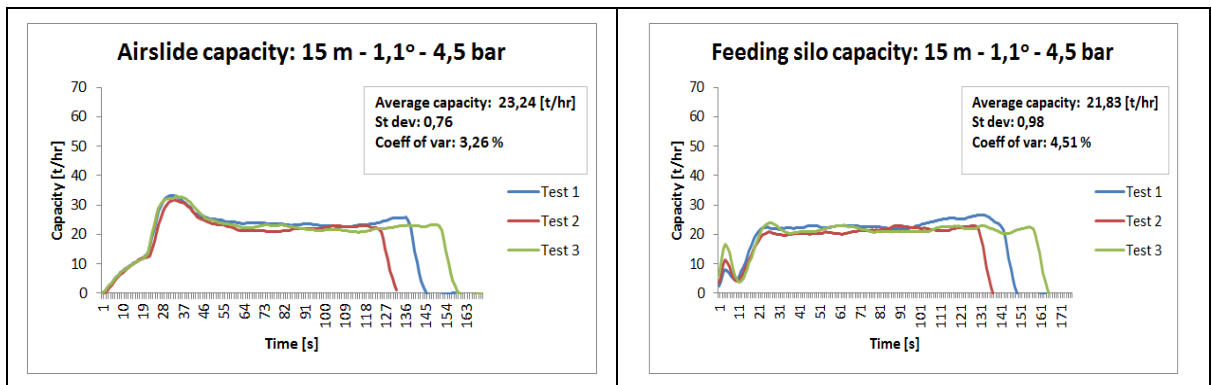


Figure 223 System capacity: 15 m – 1.1 degrees – 4.5 bar

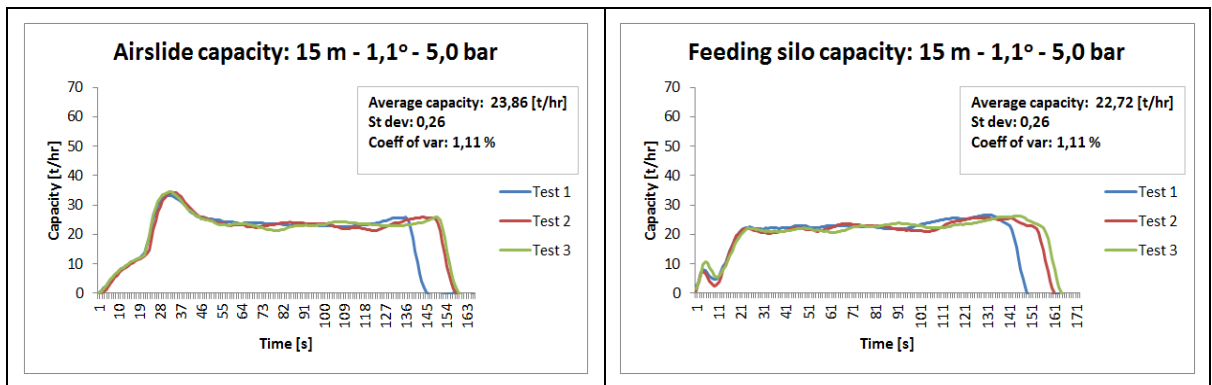


Figure 224 System capacity: 15 m – 1.1 degrees – 5.0 bar

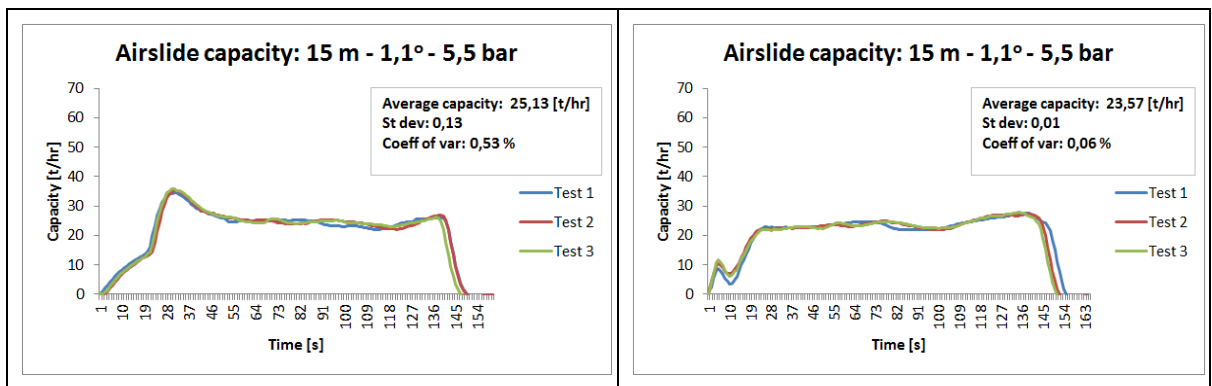


Figure 225 System capacity: 15 m – 1.1 degrees – 5.5 bar

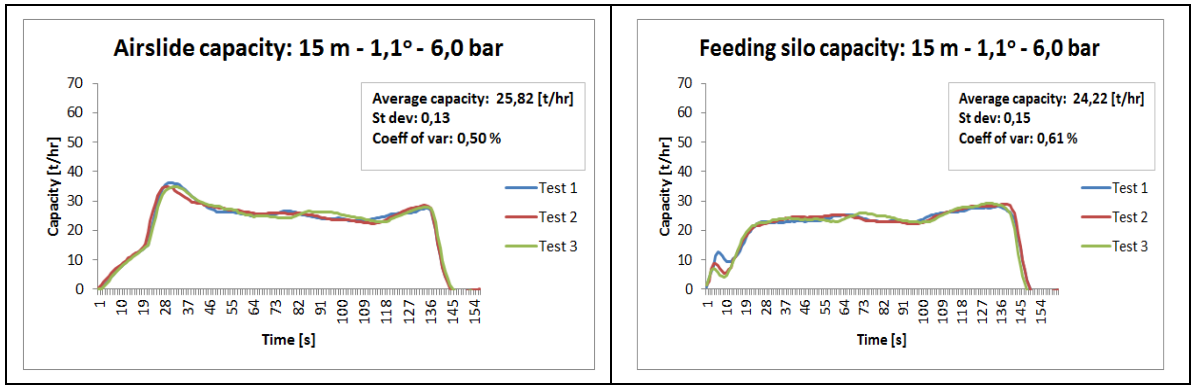


Figure 226 System capacity: 15 m – 1.1 degrees – 6.0 bar

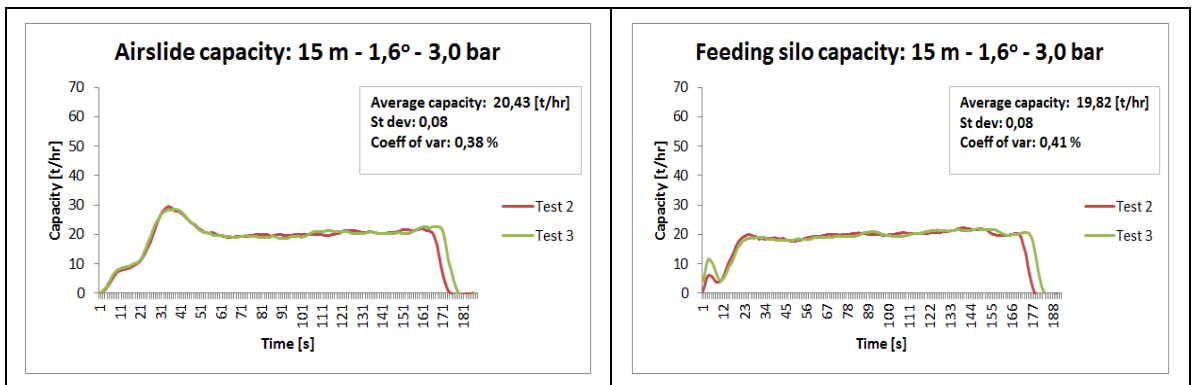


Figure 227 System capacity: 15 m – 1.6 degrees – 3.0 bar

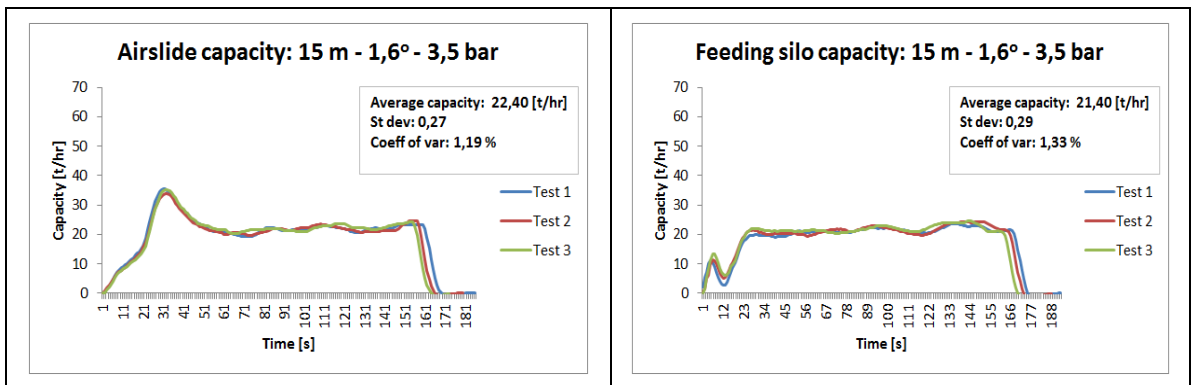


Figure 228 System capacity: 15 m – 1.6 degrees – 3.5 bar

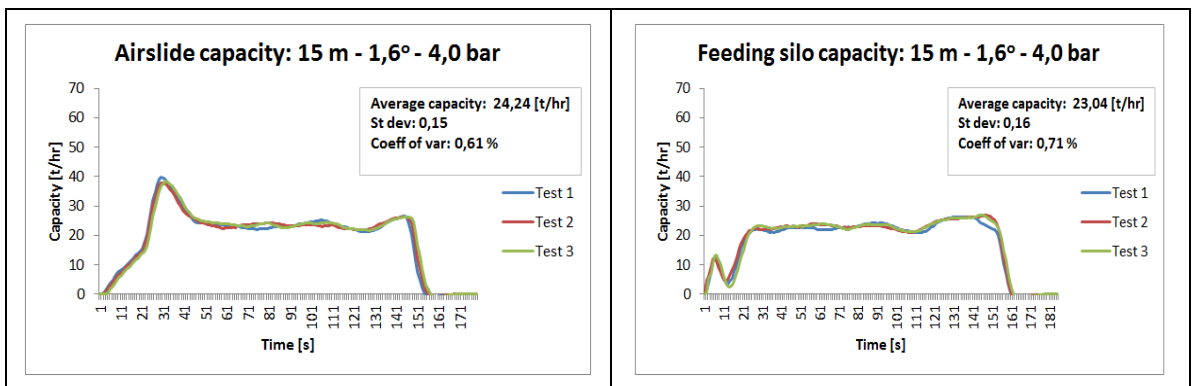


Figure 229 System capacity: 15 m – 1.6 degrees – 4.0 bar

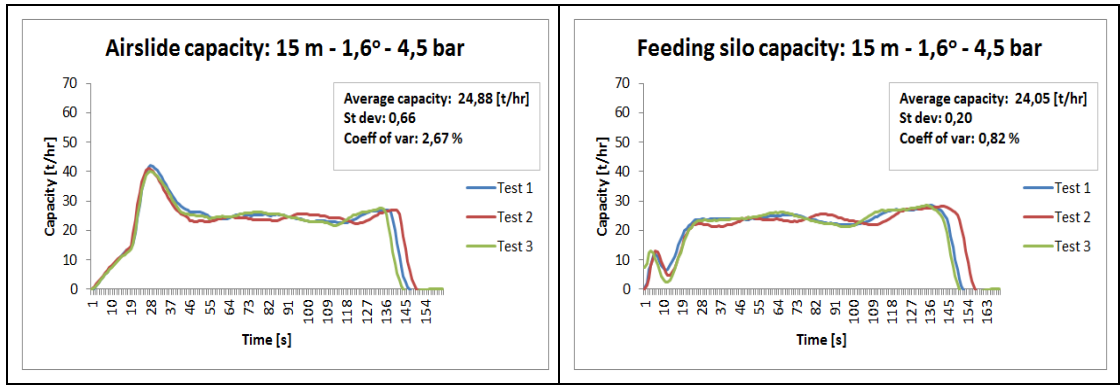


Figure 230 System capacity: 15 m – 1.6 degrees – 4.5 bar

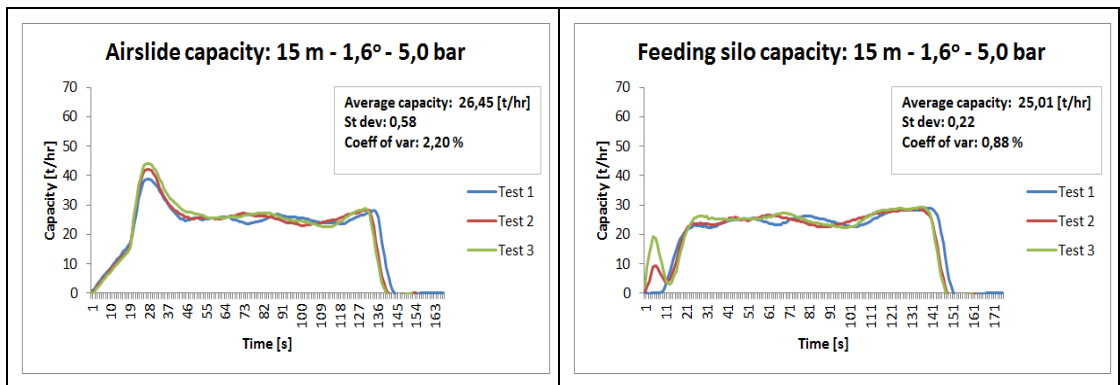


Figure 231 System capacity: 15 m – 1.6 degrees – 5.0 bar

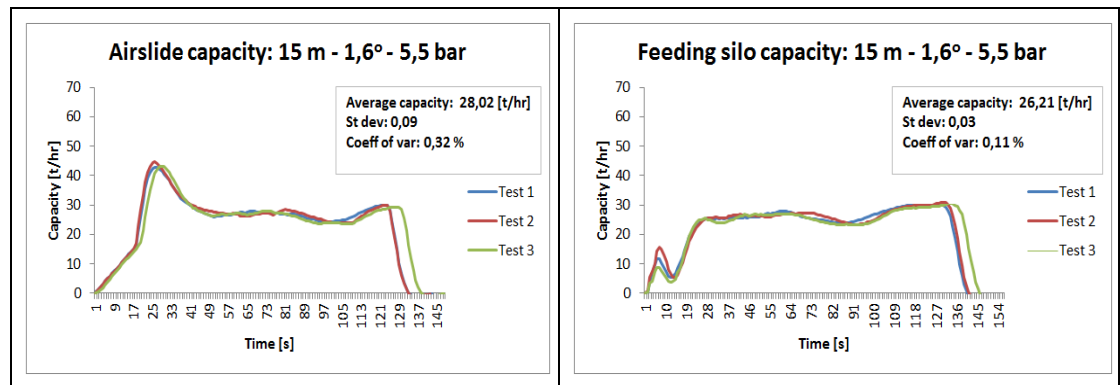


Figure 232 System capacity: 15 m – 1.6 degrees – 5.5 bar

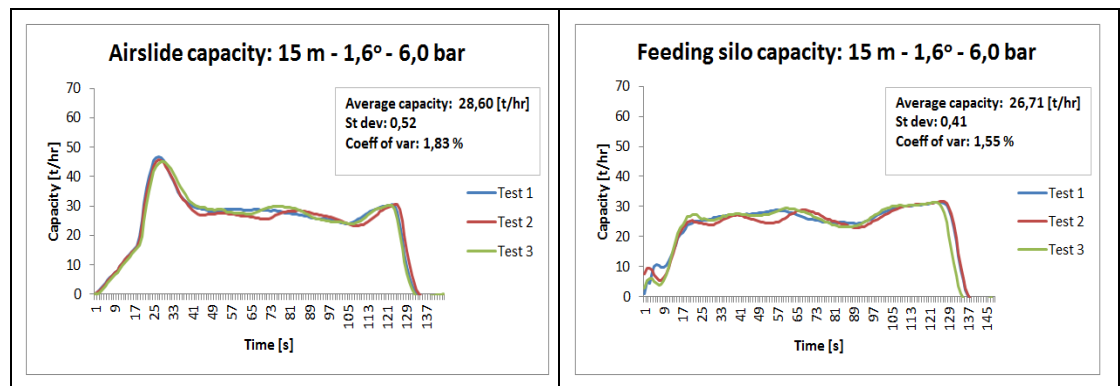


Figure 233 System capacity: 15 m – 1.6 degrees – 6.0 bar



## 15 m – 25% capacity

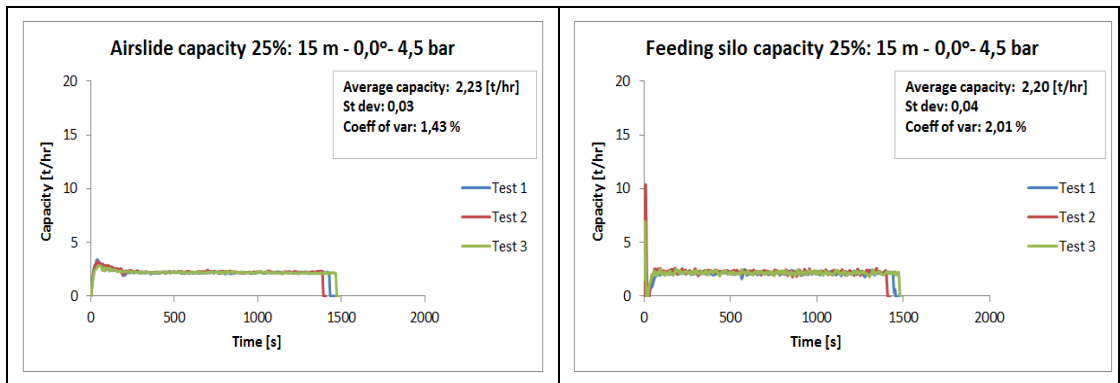


Figure 234 System capacity: 15 m – 0.0 degrees – 4.5 bar

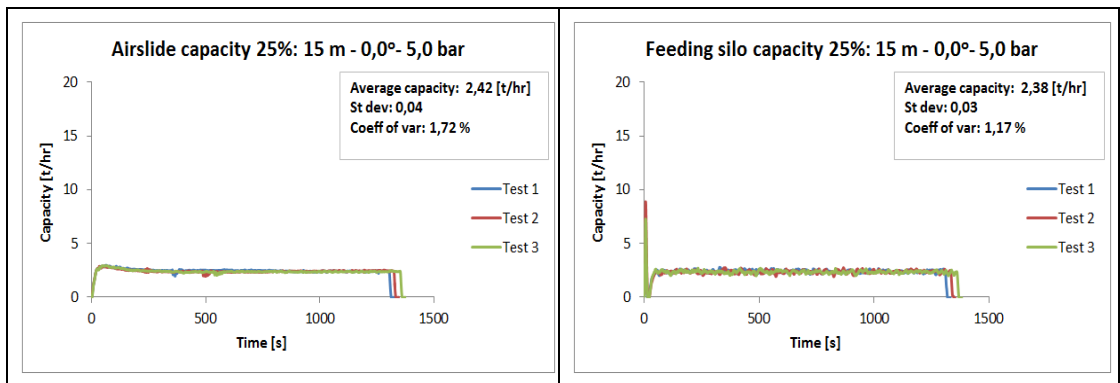


Figure 235 System capacity: 15 m – 0.0 degrees – 5.0 bar

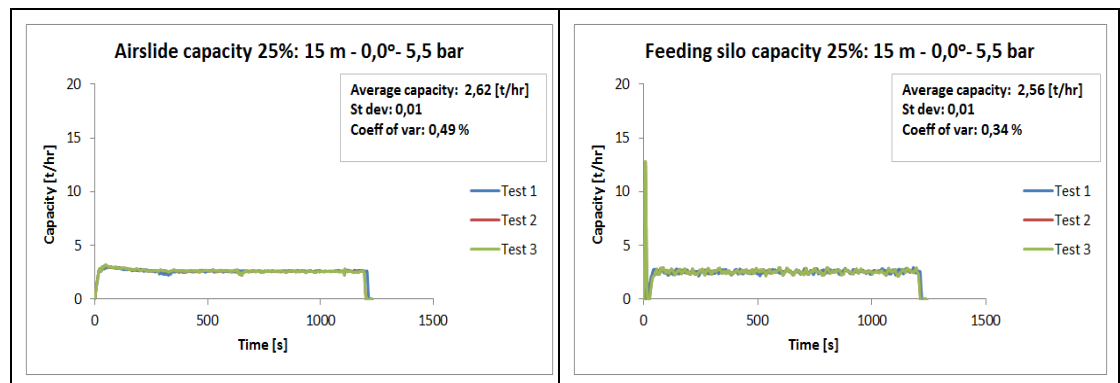


Figure 236 System capacity: 15 m – 0.0 degrees – 5.5 bar

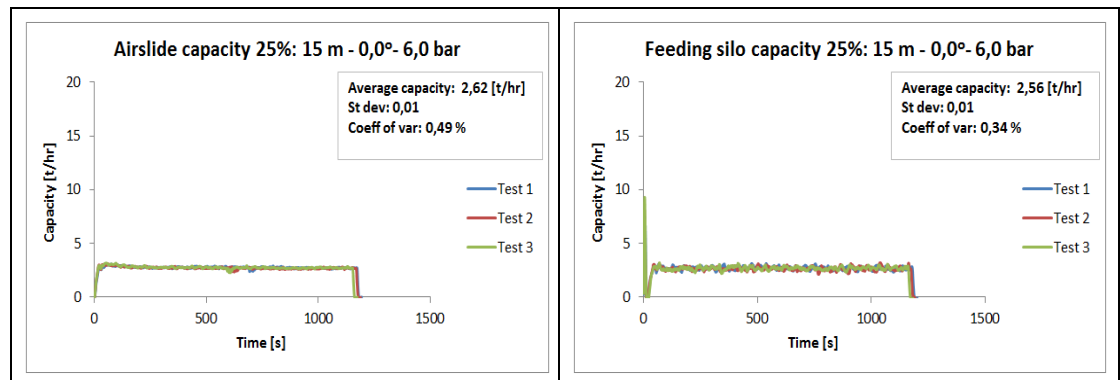


Figure 237 System capacity: 15 m – 0.0 degrees – 6.0 bar

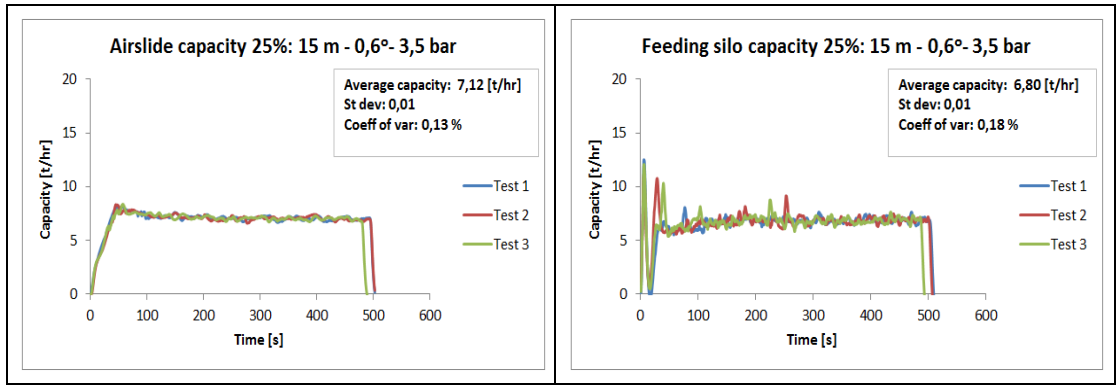


Figure 238 System capacity: 15 m – 0.6 degrees – 3.5 bar

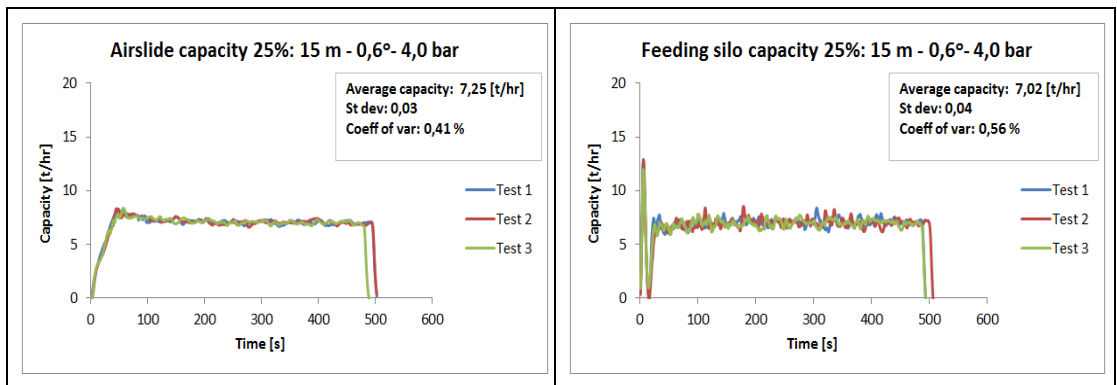


Figure 239 System capacity: 15 m – 0.6 degrees – 4.0 bar

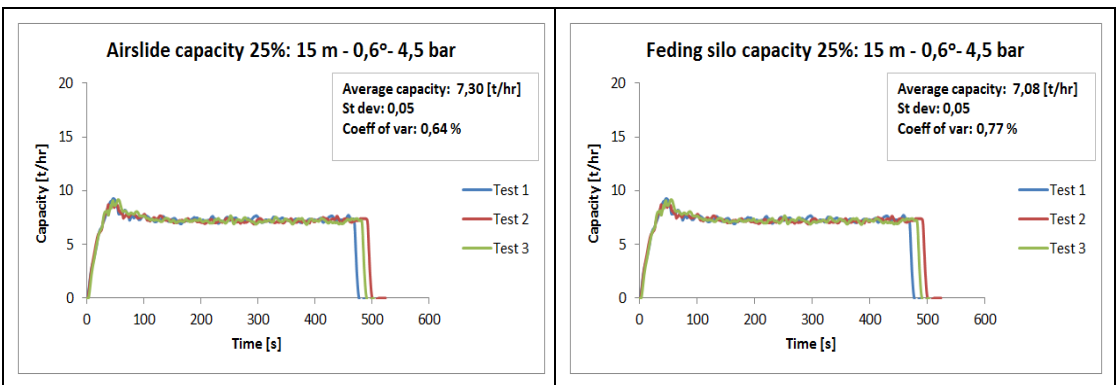


Figure 240 System capacity: 15 m – 0.6 degrees – 4.5 bar

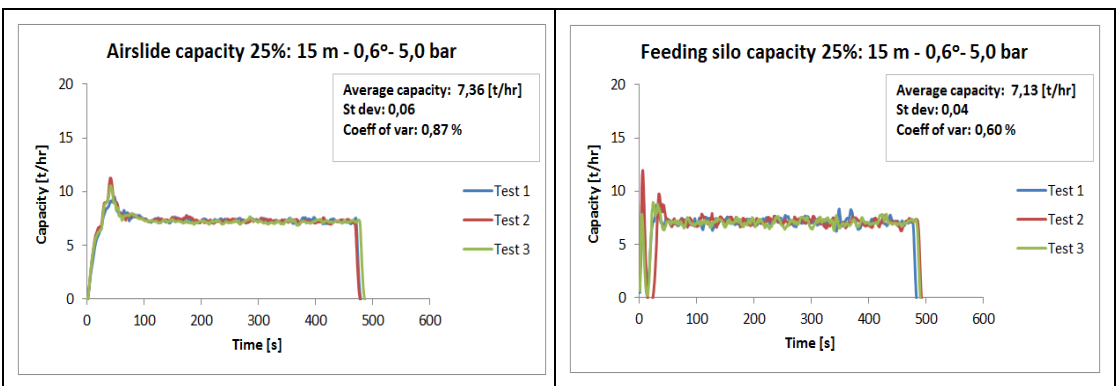


Figure 241 System capacity: 15 m – 0.6 degrees – 5.0 bar

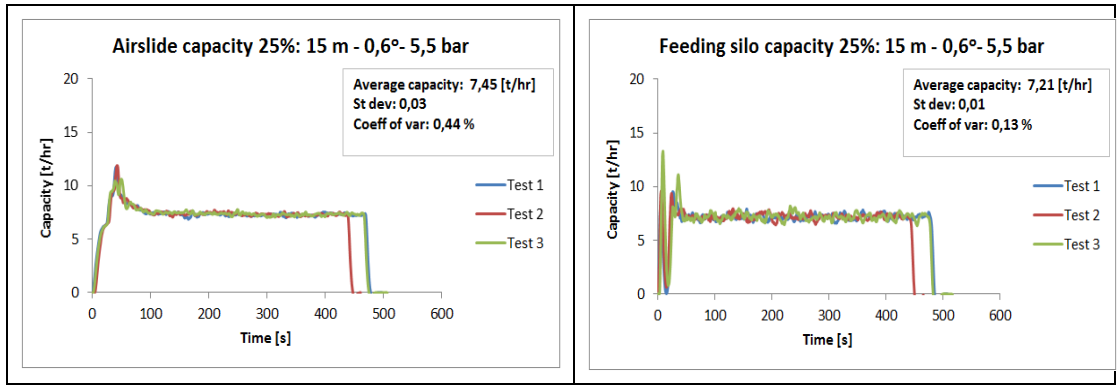


Figure 242 System capacity: 15 m – 0.6 degrees – 5.5 bar

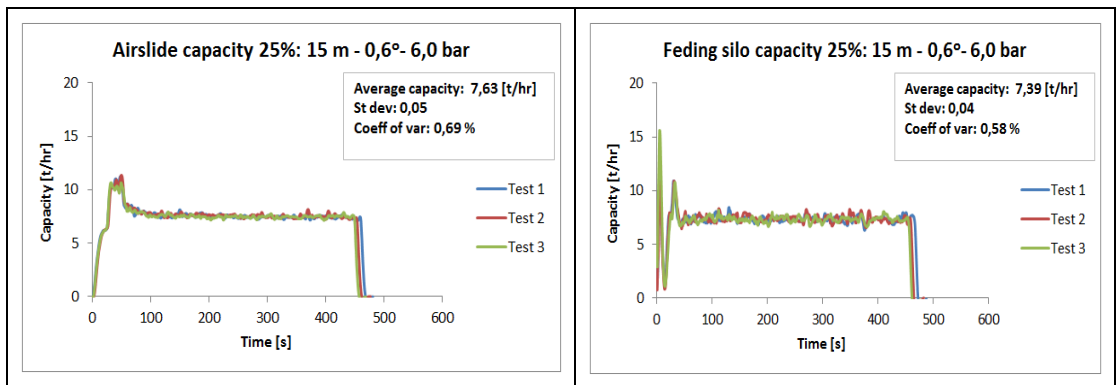


Figure 243 System capacity: 15 m – 0.6 degrees – 6.0 bar

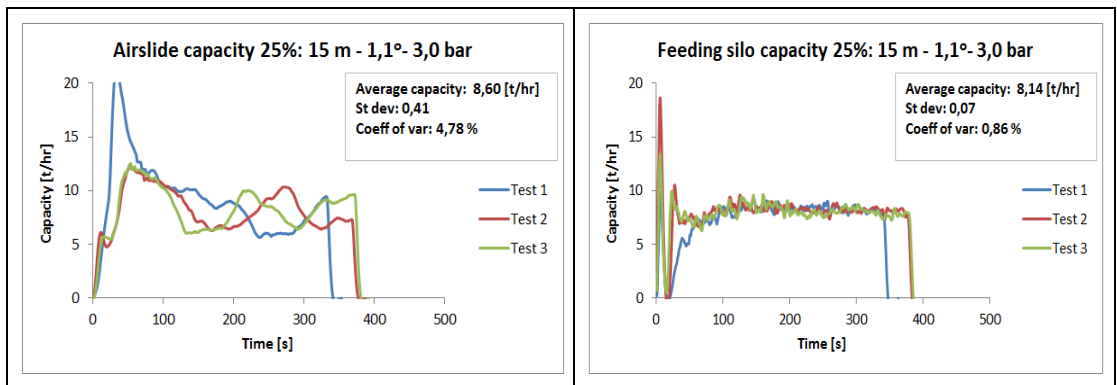


Figure 244 System capacity: 15 m – 1.1 degrees – 3.0 bar

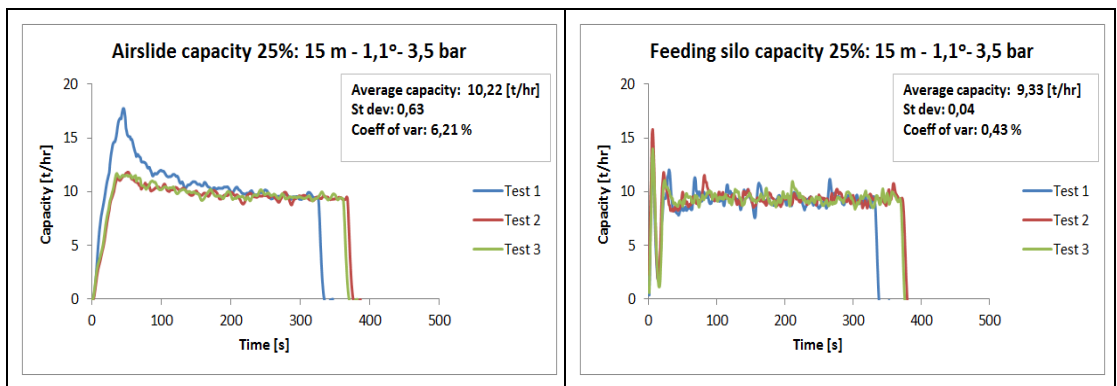


Figure 245 System capacity: 15 m – 1.1 degrees – 3.5 bar

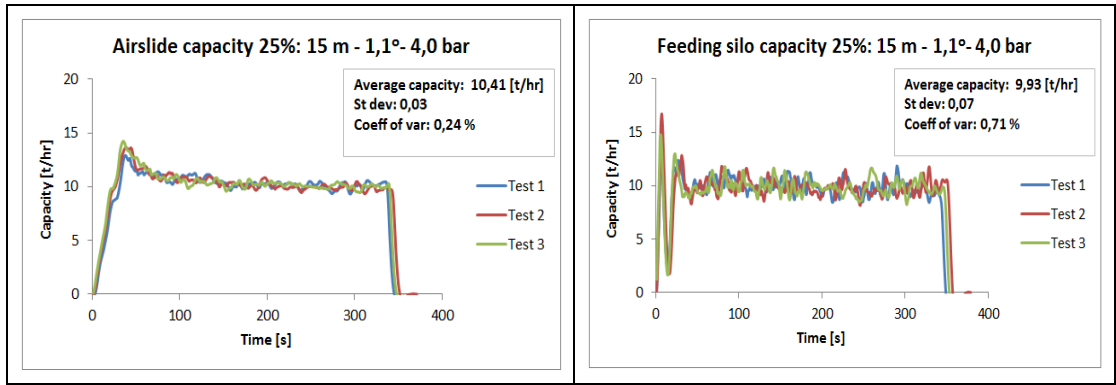


Figure 246 System capacity: 15 m – 1.1 degrees – 4.0 bar

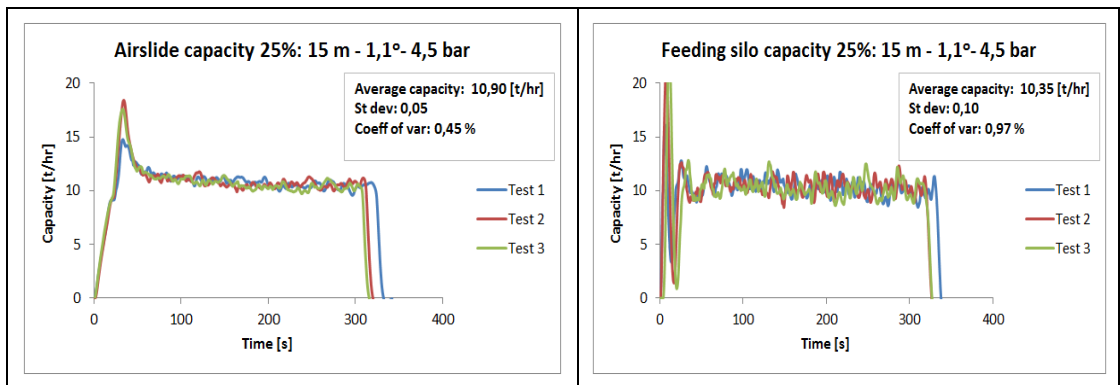


Figure 247 System capacity: 15 m – 1.1 degrees – 4.5 bar

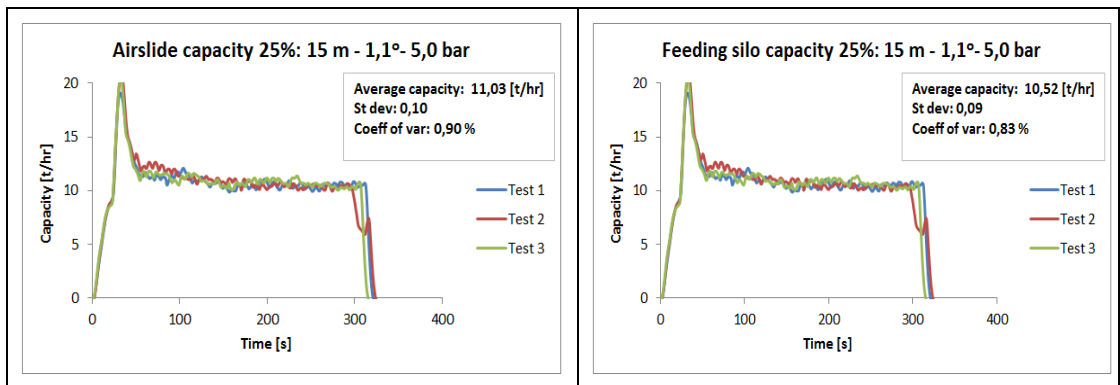


Figure 248 System capacity: 15 m – 1.1 degrees – 5.0 bar

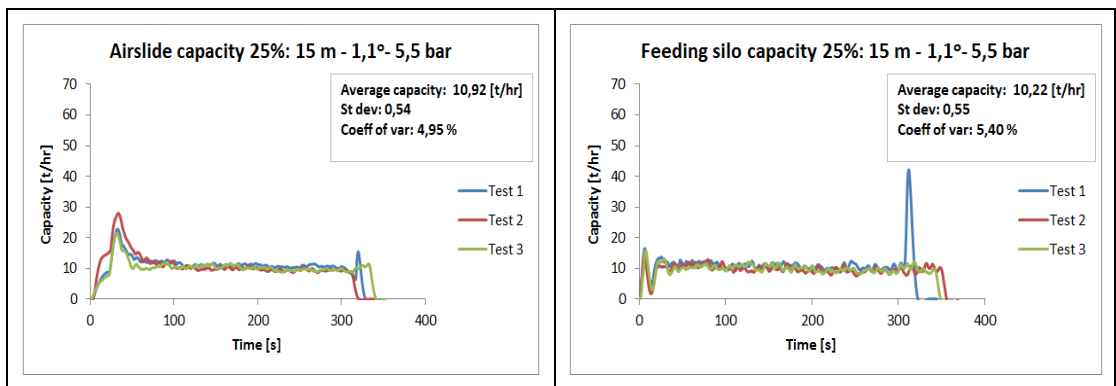


Figure 249 System capacity: 15 m – 1.1 degrees – 5.5 bar

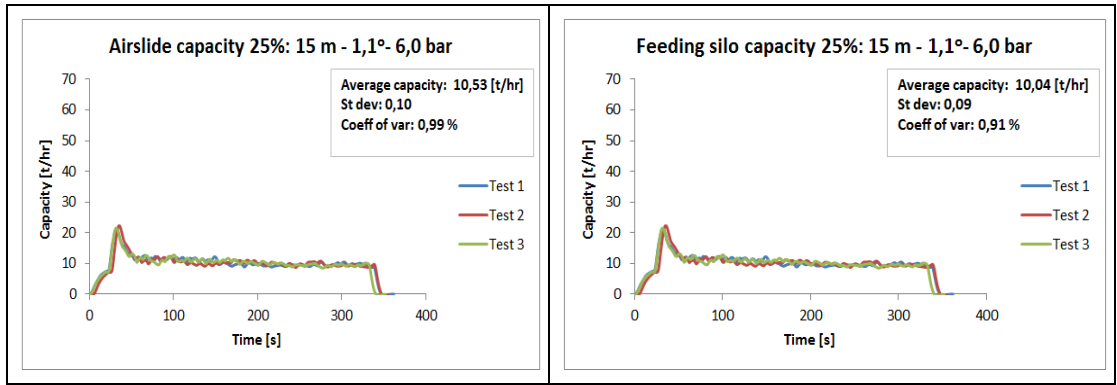


Figure 250 System capacity: 15 m – 1.1 degrees – 6.0 bar

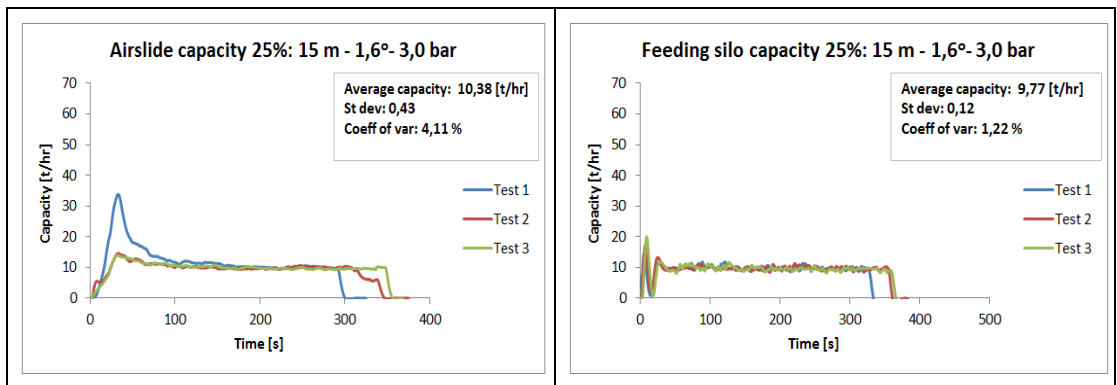


Figure 251 System capacity: 15 m – 1.6 degrees – 3.0 bar

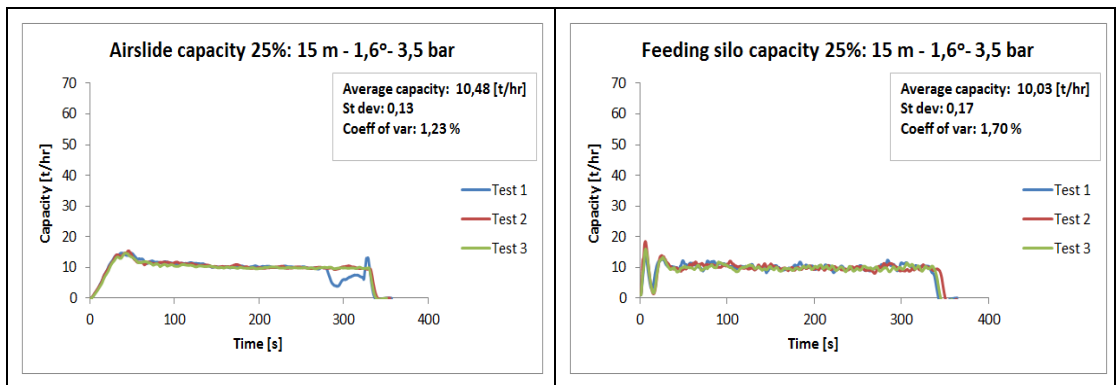


Figure 252 System capacity: 15 m – 1.6 degrees – 3.5 bar

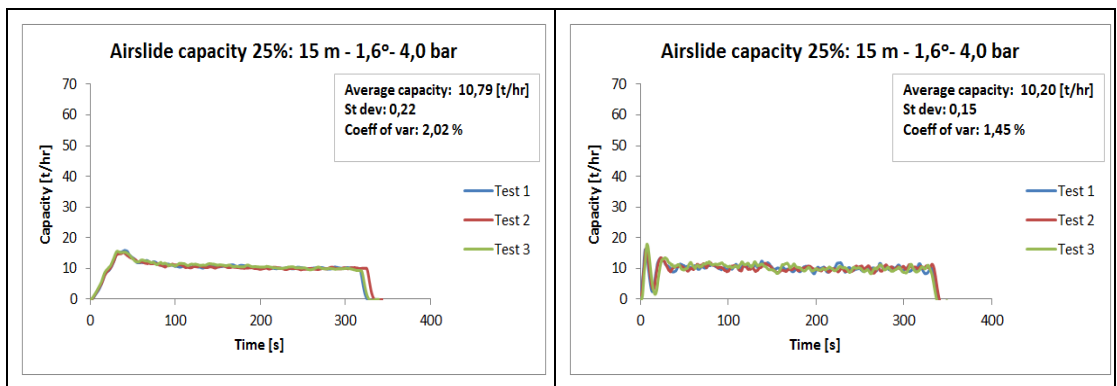


Figure 253 System capacity: 15 m – 1.6 degrees – 4.0 bar

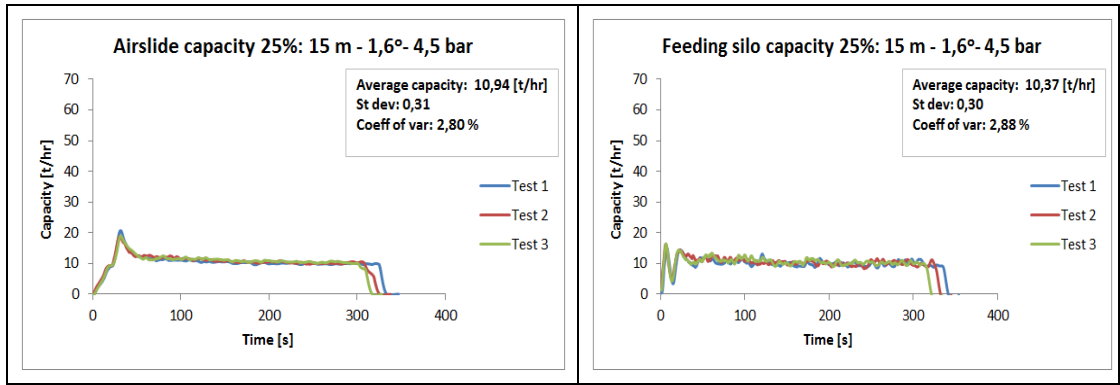


Figure 254 System capacity: 15 m – 1.6 degrees – 4.5 bar

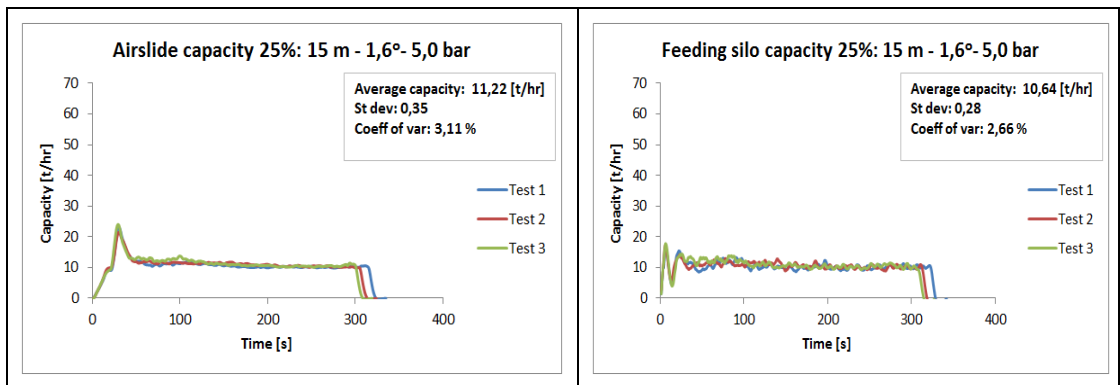


Figure 255 System capacity: 15 m – 1.6 degrees – 5.0 bar

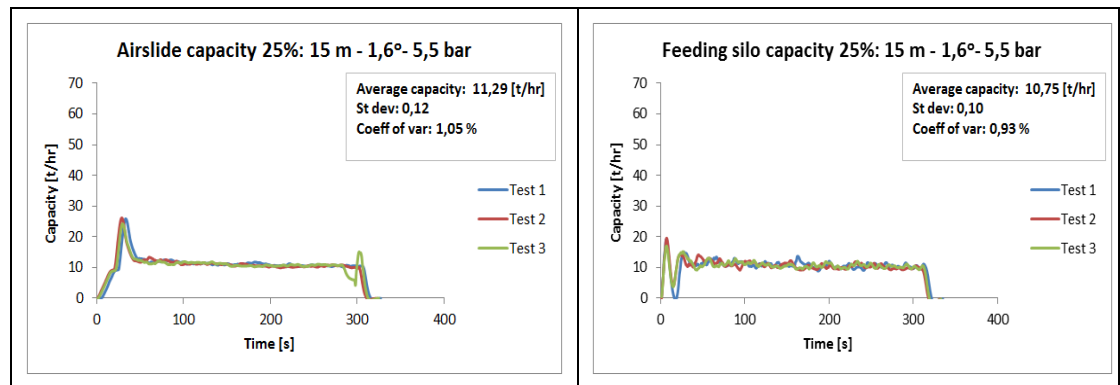


Figure 256 System capacity: 15 m – 1.6 degrees – 5.5 bar

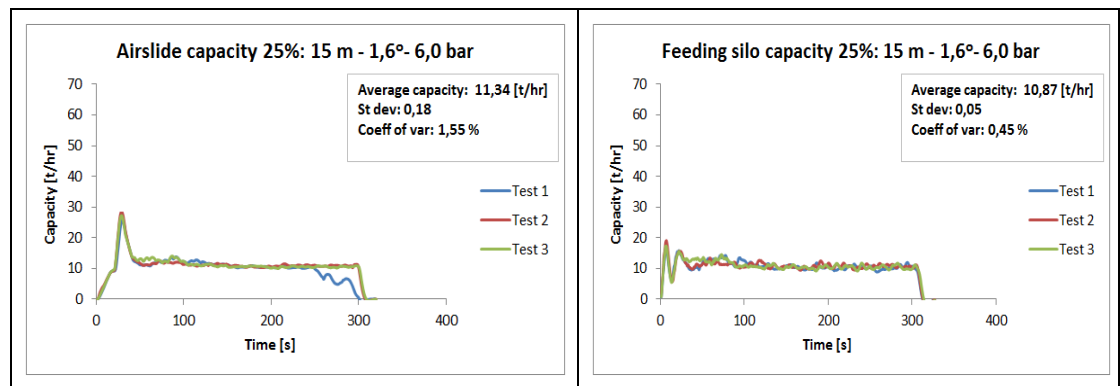


Figure 257 System capacity: 15 m – 1.6 degrees – 6.0 bar

**Table 37 Capacity, 3 m air slide segment, no gate.**

100 %	3 m			
	0,0 degrees			
[bar]	Capacity [t/hr]		Coefficient of variation [%]	
	Airslide	Feeding silo	Airslide	Feeding silo
2,5	0,0	0,0		
3	4,5	4,5	4,8	4,8
3,5	9,9	9,9	0,8	0,9
4	11,7	11,8	0,8	0,8
4,5	13,0	13,2	1,8	1,5
5	14,7	14,8	0,4	0,7
5,5	15,8	15,9	2,2	1,6
6	16,6	16,7	2,7	2,4
6,5	17,3	17,4	1,6	1,5
	0,6 degrees			
[bar]	Capacity [t/hr]		Coefficient of variation [%]	
	Airslide	Feeding silo	Airslide	Feeding silo
2,5	4,1	4,1	3,4	3,7
3	10,4	10,8	6,9	6,9
3,5	14,7	14,9	1,4	1,1
4	16,6	16,7	0,9	1,2
4,5	17,7	17,9	1,3	0,4
5	18,8	18,9	1,1	1,3
5,5	19,5	19,9	1,0	0,5
6	20,8	21,0	1,6	1,3
6,5	22,2	22,3	1,9	1,8

	1,1			
[bar]	Capacity [t/hr]		Coefficient of variation [%]	
	Airslide	Feeding silo	Airslide	Feeding silo
2,5	4,6	4,5	8,7	8,8
3	13,1	13,2	2,1	2,1
3,5	16,8	16,9	1,1	1,1
4	19,3	19,5	1,5	1,7
4,5	20,2	20,3	1,6	1,8
5	21,3	21,4	2,8	2,8
5,5	21,8	21,9	0,4	0,2
6	22,9	22,9	1,0	0,9
6,5	23,1	23,2	2,1	1,2
	1,6			
[bar]	Capacity [t/hr]		Coefficient of variation [%]	
	Airslide	Feeding silo	Airslide	Feeding silo
2,5	5,3	5,2	2,8	3,0
3	18,8	18,9	3,3	3,5
3,5	21,4	21,5	1,2	1,3
4	23,3	23,4	1,1	0,9
4,5	24,6	24,7	0,4	0,4
5	25,4	25,6	0,7	0,6
5,5	26,5	26,7	1,3	1,3
6	27,5	27,8	1,0	0,8
6,5	27,6	27,6	2,1	1,7



2,1 degrees				
	Capacity [t/hr]		Coefficient of variation [%]	
	Airslide	Feeding silo	Airslide	Feeding silo
2,5	4,8	4,7	1,9	1,8
3	21,8	21,7	0,8	0,6
3,5	25,3	25,2	1,1	1,9
4	26,9	26,7	0,9	0,7
4,5	28,1	27,8	0,6	1,0
5	28,8	28,6	0,9	0,7
5,5	29,8	29,6	0,7	0,6
6	31,0	30,8	1,8	1,5
6,5	31,2	30,8	0,6	0,3

2,6 degrees				
	Capacity [t/hr]		Coefficient of variation [%]	
	Airslide	Feeding silo	Airslide	Feeding silo
2,5	23,2	23,1	3,3	3,9
3	27,4	27,1	0,7	0,7
3,5	30,5	30,1	0,3	0,7
4	32,2	31,8	1,2	0,8
4,5	33,2	32,8	0,8	0,6
5	34,3	33,9	1,1	1,1
5,5	35,8	35,2	0,9	0,3
6	37,2	36,5	0,8	0,5
6,5	38,2	37,5	1,2	1,4

3,1 degrees				
	Capacity [t/hr]		Coefficient of variation [%]	
	Airslide	Feeding silo	Airslide	Feeding silo
2,5	23,7	23,4	0,7	1,1
3	30,5	29,9	0,9	0,8
3,5	33,8	33,0	1,3	1,1
4	35,4	34,6	0,9	0,5
4,5	36,9	36,0	0,8	0,7
5	38,3	37,4	1,4	0,9
5,5	39,0	38,0	0,5	0,3
6	40,4	39,4	0,6	0,7
6,5	41,5	40,4	1,1	0,8

## APPENDIX D VELOCITY CALCULATIONS

Table 38 Velocity calculations ( $U_0/U_{mf}$ ), 3 m air slide, 0.5 m from inlet.

Distance from inlet: 0,5 m								
$U_0/U_{mf}$	0,99	1,16	1,31	1,49	1,64	1,81	1,97	2,14
Pressure [barg]	3	3,5	4	4,5	5	5,5	6	6,5
0,0°	0,07	0,16	0,19	0,21	0,24	0,26	0,27	0,28
0,6°	0,15	0,22	0,26	0,29	0,31	0,32	0,35	0,36
1,1°	0,18	0,25	0,30	0,33	0,36	0,37	0,39	0,40
1,6°	0,28	0,34	0,38	0,41	0,42	0,45	0,47	0,48
2,1°	0,33	0,43	0,46	0,50	0,49	0,50	0,51	0,52
2,6°	0,44	0,52	0,53	0,54	0,52	0,59	0,62	0,60
3,1°	0,48	0,57	0,62	0,67	0,70	0,72	0,75	0,77

Table 39 Velocity calculations ( $U_0/U_{mf}$ ), 3 m air slide, 1.0 m from inlet.

Distance from inlet: 1,0 m								
$U_0/U_{mf}$	0,99	1,16	1,31	1,49	1,64	1,81	1,97	2,14
Pressure [barg]	3	3,5	4	4,5	5	5,5	6	6,5
0,0°	0,09	0,17	0,20	0,21	0,24	0,27	0,28	0,28
0,6°	0,19	0,24	0,29	0,31	0,34	0,36	0,37	0,40
1,1°	0,23	0,28	0,34	0,39	0,41	0,44	0,46	0,46
1,6°	0,32	0,37	0,40	0,44	0,49	0,53	0,55	0,55
2,1°	0,37	0,45	0,47	0,51	0,51	0,51	0,53	0,54
2,6°	0,45	0,51	0,52	0,53	0,51	0,57	0,61	0,64
3,1°	0,48	0,57	0,60	0,63	0,67	0,69	0,73	0,76

Table 40 Velocity calculations ( $U_0/U_{mf}$ ), 3 m air slide, 1.5 m from inlet.

Distance from inlet: 1,5 m								
$U_0/U_{mf}$	0,99	1,16	1,31	1,49	1,64	1,81	1,97	2,14
Pressure [barg]	3	3,5	4	4,5	5	5,5	6	6,5
0,0°	0,10	0,19	0,21	0,22	0,25	0,27	0,28	0,29
0,6°	0,21	0,26	0,31	0,32	0,34	0,35	0,38	0,41
1,1°	0,26	0,32	0,37	0,41	0,44	0,45	0,48	0,47
1,6°	0,35	0,40	0,44	0,50	0,52	0,55	0,57	0,56
2,1°	0,41	0,50	0,52	0,57	0,57	0,59	0,62	0,64
2,6°	0,48	0,53	0,55	0,61	0,59	0,65	0,70	0,74
3,1°	0,59	0,64	0,66	0,68	0,72	0,73	0,78	0,81

Table 41 Velocity calculations ( $U_0/U_{mf}$ ), 3 m air slide, 2.0 m from inlet.

Distance from inlet: 2,0 m								
$U_0/U_{mf}$	0,99	1,16	1,31	1,49	1,64	1,81	1,97	2,14
Pressure [barg]	3	3,5	4	4,5	5	5,5	6	6,5
0,0°	0,12	0,22	0,24	0,27	0,30	0,31	0,32	0,32
0,6°	0,26	0,32	0,36	0,35	0,38	0,40	0,42	0,43
1,1°	0,32	0,39	0,36	0,45	0,47	0,47	0,49	0,50
1,6°	0,41	0,47	0,51	0,57	0,56	0,57	0,59	0,60
2,1°	0,50	0,58	0,63	0,66	0,67	0,68	0,71	0,70
2,6°	0,53	0,60	0,67	0,70	0,73	0,77	0,80	0,83
3,1°	0,60	0,69	0,73	0,77	0,83	0,85	0,90	0,91

Table 42 Velocity calculations ( $U_0/U_{mf}$ ), 3 m air slide, 2.5 m from inlet.

Distance from inlet: 2,5 m								
$U_0/U_{mf}$	0,99	1,16	1,31	1,49	1,64	1,81	1,97	2,14
Pressure [barg]	3	3,5	4	4,5	5	5,5	6	6,5
0,0°	0,14	0,25	0,29	0,32	0,35	0,36	0,35	0,35
0,6°	0,28	0,36	0,39	0,42	0,43	0,43	0,48	0,49
1,1°	0,37	0,44	0,50	0,48	0,50	0,50	0,53	0,54
1,6°	0,47	0,52	0,58	0,60	0,60	0,61	0,64	0,64
2,1°	0,54	0,64	0,65	0,71	0,72	0,73	0,74	0,77
2,6°	0,57	0,61	0,64	0,67	0,69	0,72	0,76	0,79
3,1°	0,62	0,67	0,70	0,76	0,81	0,82	0,85	0,88

Table 43 Velocity calculations, 3 m air slide, 0.5 m from inlet.

$K_{0,5m}(\alpha)$	$U_0/U_{mf}$	0	0,6	1,1	1,6	2,1	2,6	3,1
0,14	0,99	0,065	0,152	0,185	0,279	0,333	0,439	0,477
0,14	1,16	0,162	0,220	0,249	0,339	0,429	0,522	0,573
0,14	1,31	0,189	0,262	0,304	0,381	0,460	0,529	0,617
0,14	1,49	0,212	0,293	0,332	0,412	0,498	0,537	0,673
0,14	1,64	0,236	0,311	0,355	0,424	0,486	0,524	0,702
0,15	1,81	0,258	0,320	0,368	0,448	0,497	0,586	0,715
0,15	1,97	0,270	0,346	0,389	0,468	0,509	0,620	0,749
0,14	2,14	0,280	0,357	0,401	0,478	0,521	0,599	0,768

Table 44 Velocity calculations, 3 m air slide, 1. 0 m from inlet.

$K_{1,0m}(\alpha)$	Uo/Umf	0	0,6	1,1	1,6	2,1	2,6	3,1
0,13	0,99	0,088	0,189	0,234	0,316	0,369	0,448	0,477
0,13	1,16	0,172	0,244	0,285	0,365	0,445	0,509	0,566
0,12	1,31	0,197	0,295	0,336	0,399	0,474	0,518	0,596
0,13	1,49	0,210	0,309	0,387	0,439	0,507	0,533	0,626
0,12	1,64	0,244	0,339	0,413	0,493	0,507	0,507	0,674
0,12	1,81	0,267	0,360	0,439	0,534	0,515	0,566	0,686
0,13	1,97	0,283	0,375	0,457	0,550	0,530	0,609	0,727
0,14	2,14	0,285	0,405	0,458	0,547	0,539	0,636	0,758

Table 45 Velocity calculations, 3 m air slide, 1.5 m from inlet.

$K_{1,5m}(\alpha)$	Uo/Umf	0	0,6	1,1	1,6	2,1	2,6	3,1
0,15	0,99	0,101	0,207	0,259	0,347	0,414	0,479	0,592
0,14	1,16	0,186	0,264	0,315	0,401	0,496	0,531	0,637
0,14	1,31	0,210	0,305	0,371	0,442	0,524	0,550	0,660
0,15	1,49	0,220	0,320	0,408	0,497	0,569	0,610	0,684
0,14	1,64	0,252	0,342	0,438	0,520	0,570	0,592	0,719
0,15	1,81	0,267	0,350	0,448	0,545	0,587	0,654	0,732
0,16	1,97	0,281	0,383	0,476	0,573	0,620	0,697	0,777
0,17	2,14	0,287	0,408	0,468	0,559	0,636	0,740	0,808

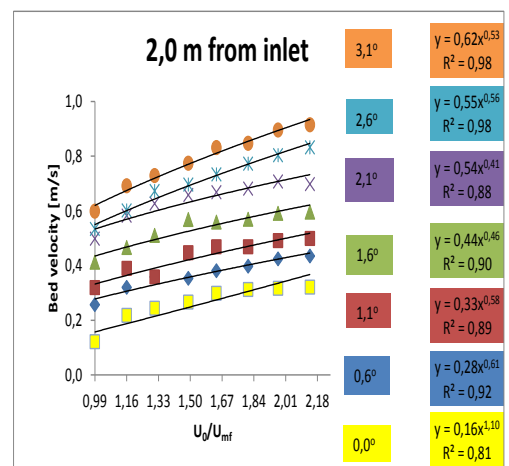
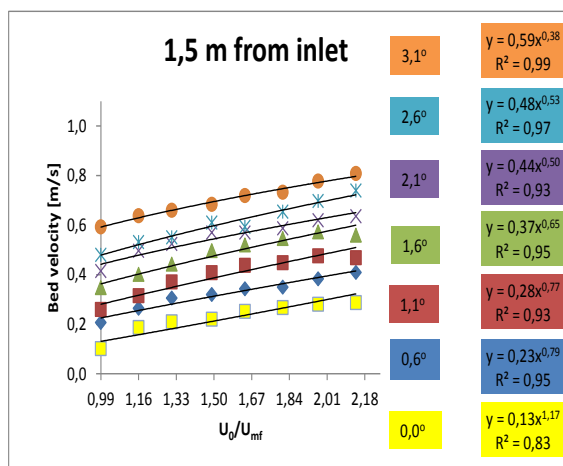
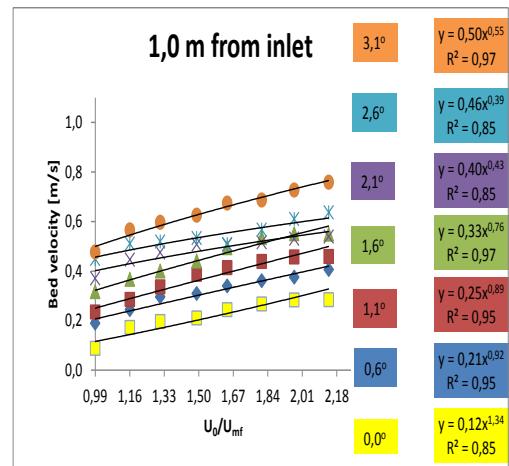
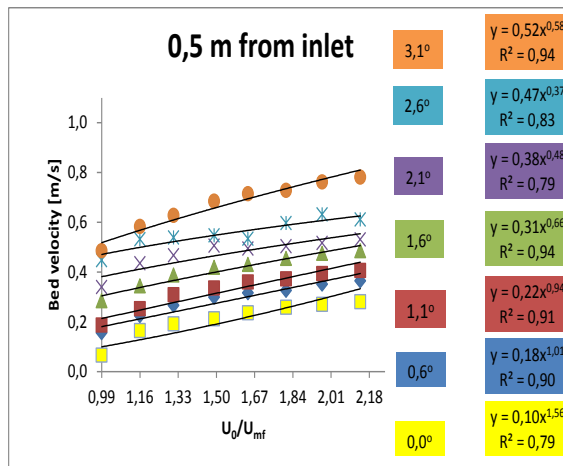
Table 46 Velocity calculations, 3 m air slide, 2. 0 m from inlet.

$K_{2,0m}(\alpha)$	Uo/Umf	0	0,6	1,1	1,6	2,1	2,6	3,1
0,15	0,99	0,121	0,257	0,319	0,412	0,498	0,533	0,599
0,15	1,16	0,218	0,320	0,389	0,466	0,582	0,601	0,691
0,16	1,31	0,244	0,358	0,358	0,510	0,626	0,672	0,728
0,17	1,49	0,266	0,353	0,447	0,568	0,657	0,696	0,774
0,17	1,64	0,298	0,381	0,468	0,559	0,668	0,733	0,831
0,18	1,81	0,312	0,397	0,468	0,569	0,681	0,772	0,847
0,19	1,97	0,316	0,424	0,491	0,591	0,707	0,803	0,895
0,19	2,14	0,321	0,434	0,499	0,595	0,697	0,832	0,914

Table 47 Velocity calculations, 3 m air slide, 2. 5 m from inlet.

$K_{2,5,m}(\alpha)$	$U_0/U_{mf}$	0	0,6	1,1	1,6	2,1	2,6	3,1
0,15	0,99	0,145	0,282	0,374	0,473	0,543	0,571	0,623
0,14	1,16	0,255	0,359	0,439	0,523	0,642	0,606	0,667
0,13	1,31	0,286	0,390	0,499	0,577	0,653	0,643	0,697
0,14	1,49	0,318	0,416	0,481	0,604	0,707	0,665	0,763
0,15	1,64	0,345	0,431	0,499	0,596	0,724	0,685	0,809
0,15	1,81	0,360	0,432	0,504	0,614	0,733	0,721	0,824
0,16	1,97	0,348	0,479	0,529	0,637	0,744	0,762	0,851
0,17	2,14	0,354	0,488	0,539	0,644	0,768	0,786	0,876

3 m - effect of  $U_0/U_{mf}$  on bed velocity at different distances away from inlet and at different angles of inclination,  $\theta$



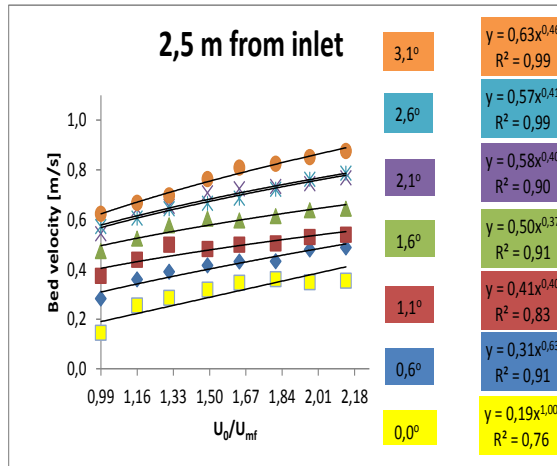


Figure 258 Power law models of average bed velocity as a function of  $U_0/U_{mf} = 0.99 \dots 2.14$  at different angles of inclination,  $\theta = 0. \dots 3.1^\circ$ .

Table 48 3 m air slide, bed velocity slopes.

3 m - $K(U_0/U_{mf})$ - Bed velocity slope [m/s/ $U_0/U_{mf}$ ] ( $\theta$ )									
$\theta$	$R^2$	$K(U_0/U_{mf})_{0,5\text{ m}}$	$P(U_0/U_{mf})_{0,5\text{ m}}$	$R^2$	$K(U_0/U_{mf})_{1,0\text{ m}}$	$P(U_0/U_{mf})_{1,0\text{ m}}$	$R^2$	$K(U_0/U_{mf})_{1,5\text{ m}}$	$P(U_0/U_{mf})_{1,5\text{ m}}$
0,1	0,79	0,10	1,56	0,85	0,12	1,34	0,83	0,13	1,17
0,6	0,90	0,18	1,01	0,95	0,21	0,92	0,95	0,23	0,79
1,1	0,91	0,22	0,94	0,95	0,25	0,89	0,93	0,28	0,77
1,6	0,94	0,31	0,66	0,97	0,33	0,76	0,95	0,37	0,65
2,1	0,79	0,38	0,48	0,85	0,40	0,43	0,93	0,44	0,50
2,6	0,83	0,47	0,37	0,85	0,46	0,39	0,97	0,48	0,53
3,1	0,94	0,52	0,58	0,97	0,50	0,55	0,99	0,59	0,38
Avg $P(U_0/U_{mf})$			<b>0,80</b>			<b>0,75</b>			<b>0,68</b>
Stdev/Avg $P(U_0/U_{mf})$			<b>51 %</b>			<b>44 %</b>			<b>38 %</b>
$\theta$	$R^2$	$K(U_0/U_{mf})_{2,0\text{ m}}$	$P(U_0/U_{mf})_{2,0\text{ m}}$	$R^2$	$K(U_0/U_{mf})_{2,5\text{ m}}$	$P(U_0/U_{mf})_{2,5\text{ m}}$	Avg $P(U_0/U_{mf})$	Stdev/Avg $P(U_0/U_{mf})$	
0,1	0,81	0,16	1,10	0,76	0,19	1,00	<b>1,23</b>	<b>18 %</b>	
0,6	0,92	0,28	0,61	0,91	0,31	0,63	<b>0,79</b>	<b>22 %</b>	
1,1	0,89	0,33	0,58	0,83	0,41	0,40	<b>0,72</b>	<b>31 %</b>	
1,6	0,90	0,44	0,46	0,91	0,50	0,37	<b>0,58</b>	<b>28 %</b>	
2,1	0,88	0,54	0,41	0,90	0,58	0,40	<b>0,44</b>	<b>10 %</b>	
2,6	0,98	0,55	0,56	0,99	0,57	0,41	<b>0,45</b>	<b>19 %</b>	
3,1	0,98	0,62	0,53	0,99	0,63	0,46	<b>0,50</b>	<b>16 %</b>	
Avg $P(U_0/U_{mf})$			<b>0,61</b>			<b>0,52</b>			
Stdev/Avg $P(U_0/U_{mf})$			<b>38 %</b>			<b>43 %</b>			

3 m - bed velocity slope as a function of  $U_0/U_{mf}$ ,  $K(U_0/U_{mf})$ , versus distance from inlet at different angles of inclination,  $\theta$

Table 49 Bed velocity slope coefficients.

Bed velocity slope ( $U_0/U_{mf}(\alpha)$ )					
Angle	$K(\text{air})_{0,5\text{ m}}$	$K(\text{air})_{1,0\text{ m}}$	$K(\text{air})_{1,5\text{ m}}$	$K(\text{air})_{2,0\text{ m}}$	$K(\text{air})_{2,5\text{ m}}$
0,0	0,10	0,12	0,13	0,16	0,19
0,6	0,18	0,21	0,23	0,28	0,31
1,1	0,22	0,25	0,28	0,33	0,41
1,6	0,31	0,33	0,37	0,44	0,50
2,1	0,38	0,40	0,44	0,54	0,58
2,6	0,47	0,46	0,48	0,55	0,57
3,1	0,52	0,50	0,59	0,62	0,63

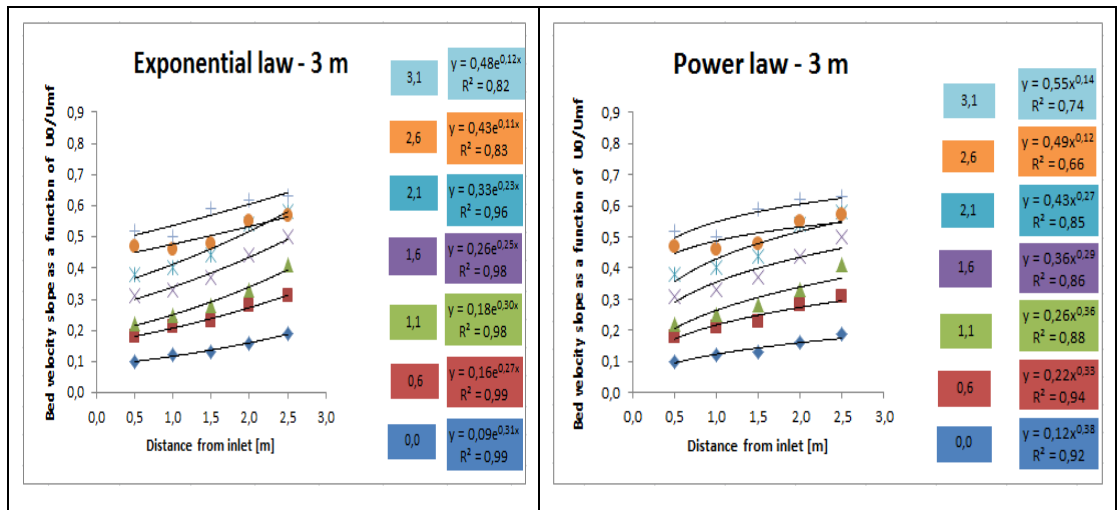


Figure 259 Exponential and power law models fitted to the slope of average bed velocity as a function of  $U_0/U_{mf} = 0.99 \dots 2.14$ ,  $K(U_0/U_{mf})$ , versus distance from inlet, at different angles of inclination,  $\theta = 0 \dots 3.1^\circ$ .

Table 50 Velocity calculations ( $U_0/U_{mf}$ ), 7 m air slide, 0.5 m from inlet.

$K_{0,5m}(\alpha) - 7m$	$U_0/U_{mf}$	0	0,6	1,1	1,6	2,1	2,6	3,1
0,14	0,99	0,085	0,199	0,262	0,342	0,391	0,458	0,543
0,14	1,16	0,120	0,242	0,328	0,382	0,436	0,494	0,591
0,13	1,31	0,151	0,280	0,356	0,407	0,448	0,511	0,600
0,14	1,49	0,154	0,314	0,394	0,430	0,471	0,529	0,639
0,14	1,64	0,160	0,330	0,420	0,462	0,481	0,551	0,651
0,15	1,81	0,168	0,345	0,457	0,458	0,509	0,580	0,688
0,15	1,97	0,170	0,358	0,471	0,469	0,508	0,602	0,726
0,16	2,14	0,170	0,362	0,464	0,469	0,533	0,624	0,732

Table 51 Velocity calculations ( $U_0/U_{mf}$ ), 7 m air slide, 1.0 m from inlet.

$K_{1,0m}(\alpha) - 7m$	$U_0/U_{mf}$	0	0,6	1,1	1,6	2,1	2,6	3,1
0,14	0,99	0,088	0,209	0,278	0,361	0,404	0,462	0,536
0,14	1,16	0,116	0,258	0,347	0,403	0,446	0,489	0,584
0,13	1,31	0,149	0,299	0,386	0,426	0,494	0,508	0,591
0,13	1,49	0,151	0,334	0,441	0,475	0,494	0,526	0,620
0,13	1,64	0,158	0,351	0,475	0,505	0,478	0,552	0,644
0,14	1,81	0,164	0,367	0,504	0,511	0,531	0,588	0,682
0,15	1,97	0,165	0,389	0,509	0,536	0,545	0,620	0,714
0,16	2,14	0,166	0,388	0,510	0,541	0,571	0,642	0,742

Table 52 Velocity calculations ( $U_0/U_{mf}$ ), 7 m air slide, 1.5 m from inlet.

$K_{1,5m}(\alpha) - 7m$	$U_0/U_{mf}$	0	0,6	1,1	1,6	2,1	2,6	3,1
0,15	0,99	0,091	0,217	0,299	0,381	0,437	0,497	0,576
0,15	1,16	0,121	0,259	0,367	0,438	0,485	0,543	0,620
0,15	1,31	0,150	0,293	0,401	0,473	0,534	0,564	0,629
0,15	1,49	0,153	0,319	0,437	0,521	0,564	0,568	0,652
0,15	1,64	0,161	0,344	0,470	0,571	0,583	0,612	0,673
0,16	1,81	0,170	0,364	0,499	0,566	0,619	0,625	0,715
0,18	1,97	0,168	0,378	0,511	0,603	0,651	0,693	0,742
0,18	2,14	0,167	0,383	0,546	0,629	0,660	0,709	0,777

Table 53 Velocity calculations ( $U_0/U_{mf}$ ), 7 m air slide, 2.0 m from inlet.



$K_{2,0m}(\alpha) - 7m$	$U_0/U_{mf}$	0	0,6	1,1	1,6	2,1	2,6	3,1
0,17	0,99	0,101	0,237	0,320	0,401	0,464	0,558	0,660
0,18	1,16	0,128	0,279	0,384	0,440	0,532	0,600	0,704
0,17	1,31	0,158	0,306	0,406	0,513	0,530	0,660	0,703
0,2	1,49	0,160	0,327	0,429	0,533	0,626	0,724	0,767
0,21	1,64	0,165	0,341	0,457	0,577	0,661	0,749	0,820
0,22	1,81	0,169	0,353	0,475	0,584	0,705	0,750	0,858
0,23	1,97	0,171	0,362	0,486	0,624	0,709	0,812	0,879
0,24	2,14	0,172	0,369	0,511	0,638	0,754	0,830	0,901

Table 54 Velocity calculations ( $U_0/U_{mf}$ ), 7 m air slide, 2.5 m from inlet.

$K_{2,5m}(\alpha) - 7m$	$U_0/U_{mf}$	0	0,6	1,1	1,6	2,1	2,6	3,1
0,16	0,99	0,108	0,252	0,363	0,449	0,491	0,558	0,637
0,16	1,16	0,135	0,294	0,423	0,487	0,538	0,568	0,672
0,15	1,31	0,160	0,325	0,442	0,504	0,549	0,605	0,664
0,17	1,49	0,162	0,337	0,464	0,529	0,566	0,643	0,743
0,18	1,64	0,169	0,346	0,485	0,549	0,598	0,684	0,769
0,19	1,81	0,174	0,359	0,491	0,560	0,624	0,709	0,807
0,2	1,97	0,177	0,357	0,519	0,580	0,659	0,747	0,841
0,21	2,14	0,177	0,375	0,516	0,600	0,706	0,790	0,858

Table 55 Velocity calculations ( $U_0/U_{mf}$ ), 7 m air slide, 3.0 m from inlet.

$K_{3,0m}(\alpha) - 7m$	$U_0/U_{mf}$	0	0,6	1,1	1,6	2,1	2,6	3,1
0,19	0,99	0,118	0,271	0,376	0,491	0,540	0,633	0,748
0,2	1,16	0,148	0,312	0,429	0,536	0,600	0,674	0,803
0,21	1,31	0,174	0,344	0,469	0,577	0,628	0,743	0,870
0,22	1,49	0,176	0,360	0,517	0,602	0,670	0,776	0,910
0,23	1,64	0,183	0,372	0,546	0,627	0,703	0,820	0,930
0,24	1,81	0,186	0,383	0,555	0,623	0,751	0,820	0,976
0,26	1,97	0,186	0,390	0,556	0,650	0,766	0,908	0,988
0,26	2,14	0,187	0,390	0,572	0,676	0,810	0,902	1,002

Table 56 Velocity calculations ( $U_0/U_{mf}$ ), 7 m air slide, 3.5 m from inlet.

$K_{3,5m}(\alpha) - 7m$	$U_0/U_{mf}$	0	0,6	1,1	1,6	2,1	2,6	3,1
0,20	0,99	0,129	0,289	0,412	0,531	0,579	0,661	0,779
0,20	1,16	0,159	0,340	0,485	0,566	0,628	0,714	0,818
0,21	1,31	0,185	0,369	0,518	0,599	0,644	0,753	0,874
0,22	1,49	0,186	0,376	0,551	0,616	0,685	0,794	0,915
0,23	1,64	0,191	0,381	0,546	0,659	0,703	0,839	0,948
0,25	1,81	0,193	0,389	0,557	0,657	0,747	0,887	0,985
0,26	1,97	0,194	0,399	0,562	0,664	0,766	0,908	0,993
0,26	2,14	0,196	0,396	0,552	0,668	0,783	0,931	1,021

Table 57 Velocity calculations ( $U_0/U_{mf}$ ), 7 m air slide, 4.0 m from inlet.

$K_{4,0m}(\alpha) - 7m$	$U_0/U_{mf}$	0	0,6	1,1	1,6	2,1	2,6	3,1
0,23	0,99	0,135	0,286	0,439	0,561	0,632	0,773	0,817
0,21	1,16	0,171	0,334	0,509	0,597	0,690	0,744	0,853
0,21	1,31	0,200	0,359	0,527	0,646	0,687	0,773	0,882
0,22	1,49	0,202	0,377	0,533	0,637	0,728	0,805	0,910
0,23	1,64	0,210	0,387	0,542	0,667	0,737	0,851	0,934
0,24	1,81	0,210	0,391	0,546	0,665	0,737	0,875	0,980
0,25	1,97	0,211	0,400	0,556	0,658	0,756	0,883	0,988
0,25	2,14	0,214	0,403	0,572	0,687	0,773	0,910	0,990

Table 58 Velocity calculations ( $U_0/U_{mf}$ ), 7 m air slide, 4.5 m from inlet.

$K_{4,5m}(\alpha) - 7m$	$U_0/U_{mf}$	0	0,6	1,1	1,6	2,1	2,6	3,1
0,22	0,99	0,135	0,276	0,412	0,582	0,623	0,724	0,821
0,22	1,16	0,172	0,326	0,475	0,622	0,694	0,765	0,870
0,22	1,31	0,204	0,359	0,506	0,643	0,725	0,792	0,886
0,23	1,49	0,204	0,374	0,517	0,635	0,725	0,820	0,910
0,23	1,64	0,214	0,388	0,529	0,659	0,737	0,851	0,935
0,24	1,81	0,215	0,391	0,538	0,691	0,763	0,871	0,975
0,25	1,97	0,219	0,393	0,536	0,680	0,760	0,891	0,983
0,25	2,14	0,216	0,405	0,541	0,698	0,779	0,898	1,002

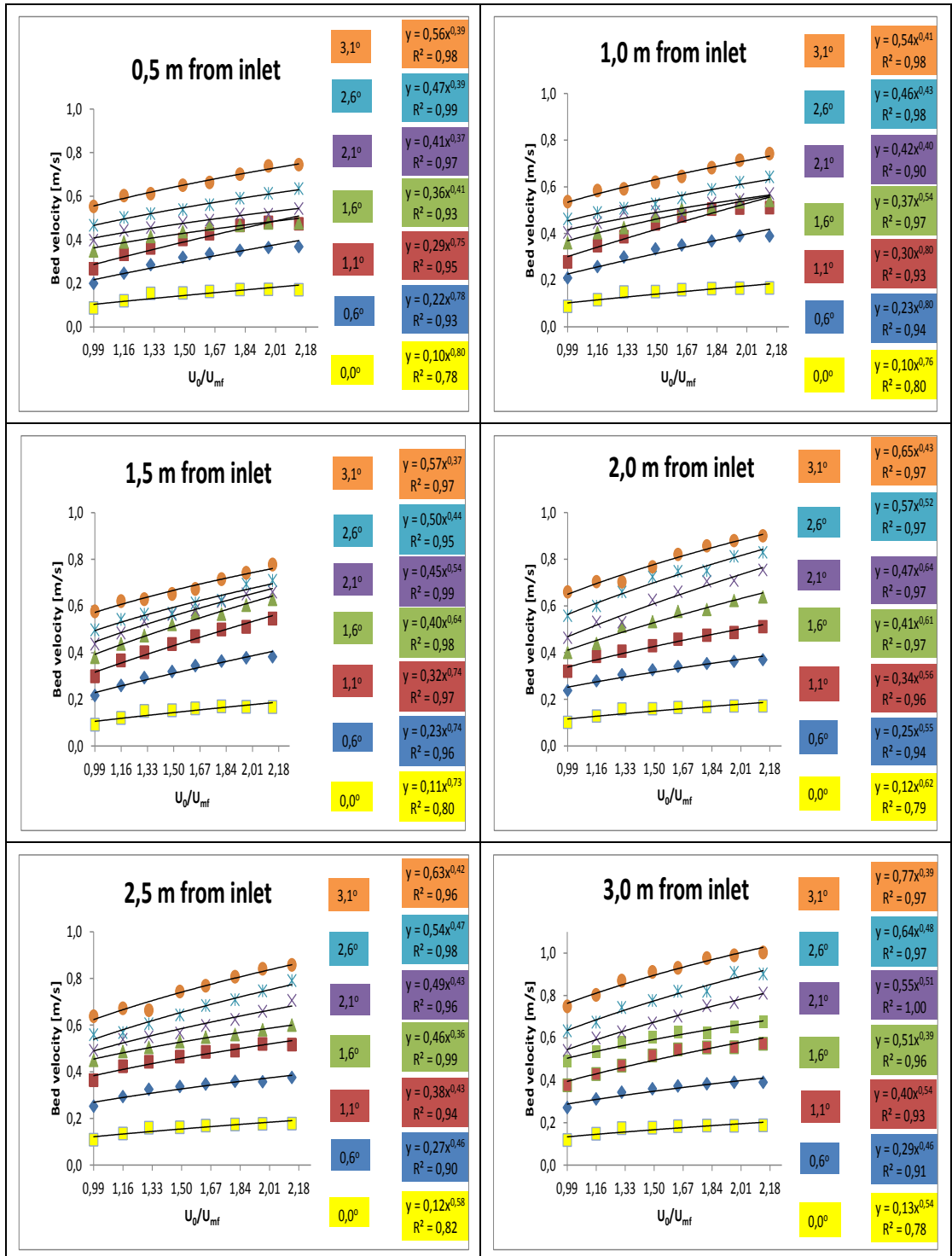
Table 59 Velocity calculations ( $U_0/U_{mf}$ ), 7 m air slide, 5.0 m from inlet.

$K_{5,0m}(\alpha) - 7m$	$U_0/U_{mf}$	0	0,6	1,1	1,6	2,1	2,6	3,1
0,22	0,99	0,169	0,307	0,397	0,577	0,635	0,739	0,837
0,21	1,16	0,211	0,360	0,464	0,597	0,684	0,784	0,861
0,21	1,31	0,243	0,381	0,524	0,649	0,681	0,815	0,913
0,23	1,49	0,245	0,374	0,521	0,621	0,741	0,828	0,942
0,22	1,64	0,254	0,418	0,537	0,659	0,747	0,863	0,944
0,24	1,81	0,246	0,424	0,544	0,662	0,781	0,892	0,990
0,24	1,97	0,259	0,437	0,544	0,666	0,786	0,921	0,997
0,25	2,14	0,262	0,428	0,541	0,693	0,786	0,923	1,021

Table 60 Velocity calculations ( $U_0/U_{mf}$ ), 7 m air slide, 5.5 m from inlet.

$K_{5,5m}(\alpha) - 7m$	$U_0/U_{mf}$	0	0,6	1,1	1,6	2,1	2,6	3,1
0,2	0,99	0,199	0,379	0,463	0,582	0,623	0,757	0,846
0,2	1,16	0,249	0,426	0,522	0,614	0,697	0,800	0,883
0,19	1,31	0,287	0,433	0,573	0,659	0,687	0,823	0,908
0,2	1,49	0,286	0,461	0,568	0,651	0,745	0,857	0,937
0,21	1,64	0,303	0,498	0,566	0,688	0,764	0,888	0,962
0,23	1,81	0,288	0,463	0,575	0,671	0,795	0,905	1,014
0,23	1,97	0,308	0,496	0,573	0,688	0,793	0,925	1,032
0,23	2,14	0,312	0,511	0,584	0,695	0,803	0,927	1,041

**7 m - effect of  $U_0/U_{mf}$  on bed velocity at different distances away from inlet and at different angles of inclination,  $\theta$**



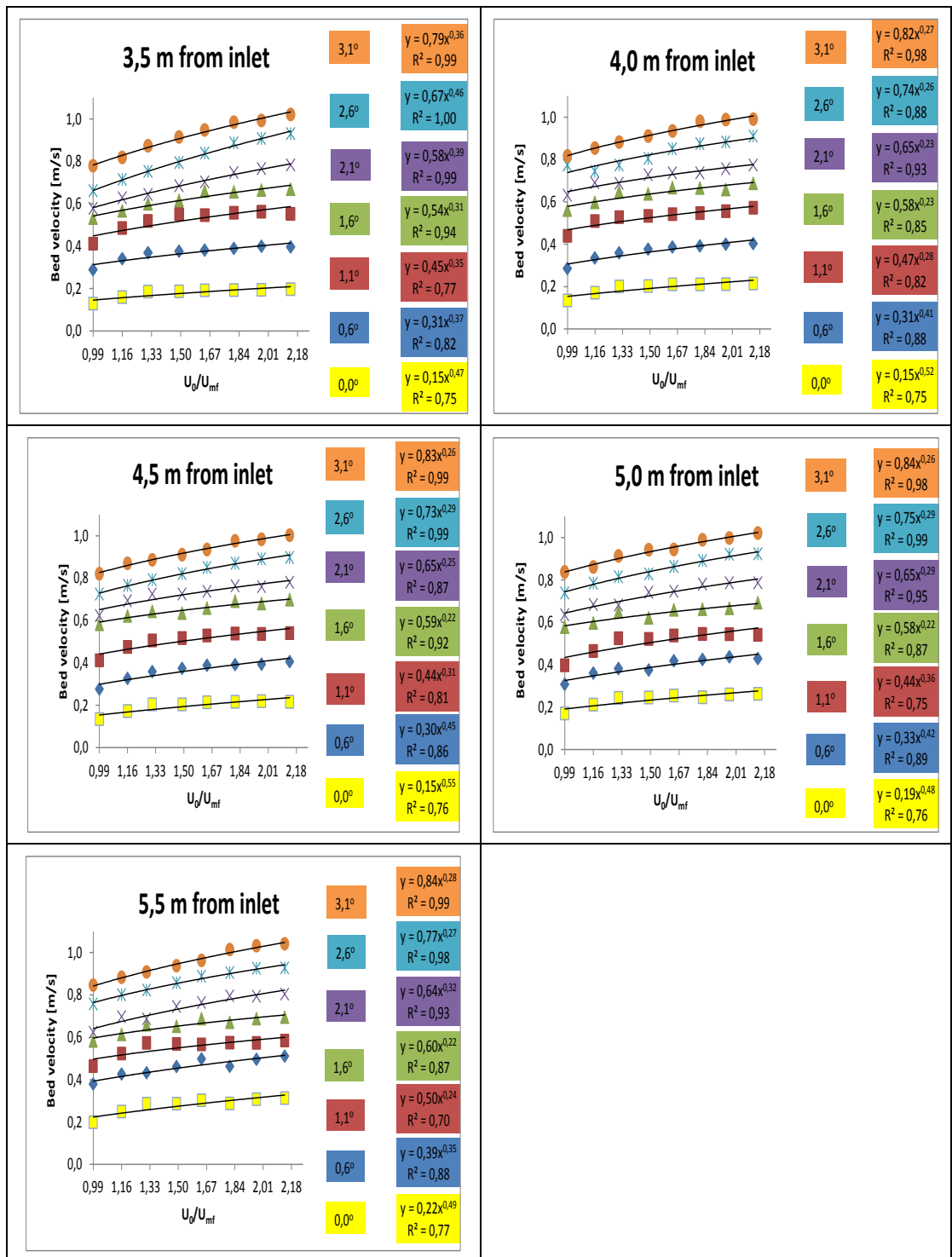


Figure 260 Power law models of average bed velocity as a function of  $U_0/U_{mf} = 0.99 \dots 2.14$  at different angles of inclination,  $\theta = 0..3.1^\circ$ .

**7 m - bed velocity slope as a function of  $U_0/U_{mf}$ ,  $K(U_0/U_{mf})$ , versus distance from inlet at different angles of inclination,  $\theta$**

**Table 61 Bed velocity slopes, 7 m.**

Bed velocity slope ( $U_0/U_{mf}(\alpha)$ )											
Angle	$K(\text{air})_{0,5\text{m}}$	$K(\text{air})_{1,0\text{m}}$	$K(\text{air})_{1,5\text{m}}$	$K(\text{air})_{2,0\text{m}}$	$K(\text{air})_{2,5\text{m}}$	$K(\text{air})_{3,0\text{m}}$	$K(\text{air})_{3,5\text{m}}$	$K(\text{air})_{4,0\text{m}}$	$K(\text{air})_{4,5\text{m}}$	$K(\text{air})_{5,0\text{m}}$	$K(\text{air})_{5,5\text{m}}$
0,0	0,10	0,10	0,11	0,12	0,12	0,12	0,13	0,15	0,15	0,19	0,22
0,6	0,22	0,23	0,23	0,25	0,27	0,29	0,31	0,31	0,30	0,33	0,39
1,1	0,29	0,30	0,32	0,34	0,38	0,40	0,45	0,47	0,44	0,44	0,50
1,6	0,36	0,37	0,40	0,41	0,46	0,51	0,54	0,58	0,59	0,58	0,60
2,1	0,41	0,42	0,45	0,47	0,49	0,55	0,58	0,65	0,65	0,65	0,64
2,6	0,47	0,46	0,50	0,57	0,54	0,64	0,67	0,74	0,73	0,75	0,77
3,1	0,56	0,54	0,57	0,65	0,63	0,77	0,79	0,82	0,83	0,84	0,84

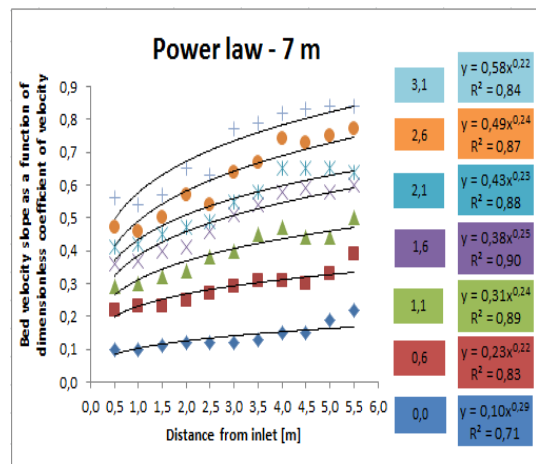
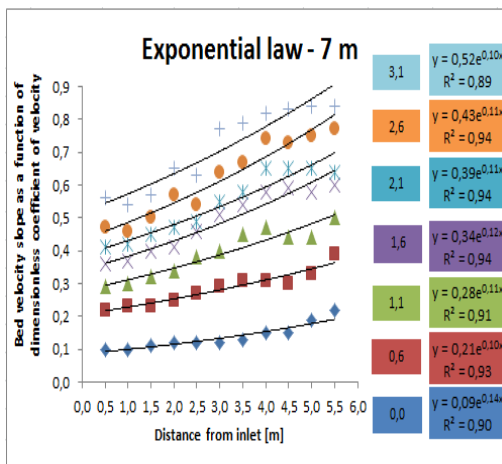


Figure 261 Exponential and power law models fitted to the slope of average bed velocity as a function of  $U_0/U_{mf} = 0.99 \dots 2.14$ ,  $K(U_0/U_{mf})$ , versus distance from inlet, at different angles of inclination,  $\theta = 0..3.1^0$ .

Table 62 Velocity calculations, 7 m air slide, 0.5 m from inlet.

$K_{0,5m}(\alpha) - 15\text{ m}$	$U_0/U_{mf}$	0	0,6	1,1	1,6
0,18	0,99	0,034	0,136	0,274	0,314
0,20	1,16	0,052	0,201	0,314	0,370
0,21	1,31	0,061	0,252	0,357	0,397
0,22	1,49	0,063	0,280	0,385	0,404
0,22	1,64	0,073	0,314	0,412	0,422
0,24	1,81	0,077	0,328	0,448	0,454
0,24	1,97	0,079	0,349	0,430	0,465

Table 63 Velocity calculations, 7 m air slide, 1.0 m from inlet.

$K_{1,0m}(\alpha) - 15\text{ m}$	$U_0/U_{mf}$	0	0,6	1,1	1,6
0,21	0,99	0,036	0,128	0,281	0,358
0,22	1,16	0,052	0,197	0,345	0,390
0,24	1,31	0,062	0,254	0,386	0,436
0,26	1,49	0,063	0,286	0,439	0,458
0,26	1,64	0,073	0,338	0,456	0,479
0,28	1,81	0,077	0,352	0,464	0,524
0,28	1,97	0,078	0,370	0,493	0,532

Table 64 Velocity calculations, 7 m air slide, 1.5 m from inlet.

$K_{1,5m}(\alpha) - 15\text{ m}$	$U_0/U_{mf}$	0	0,6	1,1	1,6
0,21	0,99	0,037	0,129	0,291	0,357
0,24	1,16	0,053	0,190	0,354	0,415
0,26	1,31	0,062	0,249	0,393	0,470
0,27	1,49	0,064	0,280	0,432	0,492
0,29	1,64	0,074	0,321	0,451	0,531
0,31	1,81	0,078	0,339	0,473	0,579
0,31	1,97	0,079	0,350	0,488	0,584

Table 65 Velocity calculations, 7 m air slide, 2.0 m from inlet.

<b>K<sub>2,0m</sub>(alfa) - 15 m</b>	<b>Uo/Umf</b>	<b>0</b>	<b>0,6</b>	<b>1,1</b>	<b>1,6</b>
0,22	<b>0,99</b>	<b>0,039</b>	<b>0,132</b>	<b>0,296</b>	<b>0,371</b>
0,25	<b>1,16</b>	<b>0,055</b>	<b>0,190</b>	<b>0,357</b>	<b>0,432</b>
0,26	<b>1,31</b>	<b>0,064</b>	<b>0,248</b>	<b>0,380</b>	<b>0,481</b>
0,27	<b>1,49</b>	<b>0,066</b>	<b>0,281</b>	<b>0,403</b>	<b>0,503</b>
0,29	<b>1,64</b>	<b>0,076</b>	<b>0,319</b>	<b>0,438</b>	<b>0,546</b>
0,31	<b>1,81</b>	<b>0,081</b>	<b>0,328</b>	<b>0,465</b>	<b>0,579</b>
0,32	<b>1,97</b>	<b>0,082</b>	<b>0,345</b>	<b>0,485</b>	<b>0,602</b>

Table 66 Velocity calculations, 7 m air slide, 2.5 m from inlet.

<b>K<sub>2,5m</sub>(alfa) - 15 m</b>	<b>Uo/Umf</b>	<b>0</b>	<b>0,6</b>	<b>1,1</b>	<b>1,6</b>
0,23	<b>0,99</b>	<b>0,040</b>	<b>0,132</b>	<b>0,301</b>	<b>0,394</b>
0,26	<b>1,16</b>	<b>0,056</b>	<b>0,189</b>	<b>0,361</b>	<b>0,454</b>
0,27	<b>1,31</b>	<b>0,065</b>	<b>0,244</b>	<b>0,401</b>	<b>0,483</b>
0,27	<b>1,49</b>	<b>0,066</b>	<b>0,278</b>	<b>0,445</b>	<b>0,492</b>
0,28	<b>1,64</b>	<b>0,077</b>	<b>0,313</b>	<b>0,464</b>	<b>0,514</b>
0,30	<b>1,81</b>	<b>0,081</b>	<b>0,323</b>	<b>0,480</b>	<b>0,546</b>
0,30	<b>1,97</b>	<b>0,082</b>	<b>0,335</b>	<b>0,493</b>	<b>0,552</b>

Table 67 Velocity calculations, 7 m air slide, 3.0 m from inlet.

<b>K<sub>3,0m</sub>(alfa) - 15 m</b>	<b>Uo/Umf</b>	<b>0</b>	<b>0,6</b>	<b>1,1</b>	<b>1,6</b>
0,22	<b>0,99</b>	<b>0,042</b>	<b>0,140</b>	<b>0,309</b>	<b>0,375</b>
0,24	<b>1,16</b>	<b>0,059</b>	<b>0,199</b>	<b>0,364</b>	<b>0,433</b>
0,27	<b>1,31</b>	<b>0,069</b>	<b>0,255</b>	<b>0,422</b>	<b>0,492</b>
0,29	<b>1,49</b>	<b>0,071</b>	<b>0,295</b>	<b>0,473</b>	<b>0,528</b>
0,30	<b>1,64</b>	<b>0,082</b>	<b>0,339</b>	<b>0,499</b>	<b>0,546</b>
0,32	<b>1,81</b>	<b>0,086</b>	<b>0,346</b>	<b>0,517</b>	<b>0,590</b>
0,32	<b>1,97</b>	<b>0,087</b>	<b>0,361</b>	<b>0,525</b>	<b>0,591</b>

Table 68 Velocity calculations, 7 m air slide, 3.5 m from inlet.

<b>K<sub>5,5m</sub>(alfa) - 15 m</b>	<b>Uo/Umf</b>	<b>0</b>	<b>0,6</b>	<b>1,1</b>	<b>1,6</b>
0,27	<b>0,99</b>	<b>0,047</b>	<b>0,149</b>	<b>0,342</b>	<b>0,470</b>
0,32	<b>1,16</b>	<b>0,067</b>	<b>0,217</b>	<b>0,416</b>	<b>0,568</b>
0,34	<b>1,31</b>	<b>0,078</b>	<b>0,273</b>	<b>0,468</b>	<b>0,621</b>
0,34	<b>1,49</b>	<b>0,080</b>	<b>0,308</b>	<b>0,505</b>	<b>0,617</b>
0,36	<b>1,64</b>	<b>0,091</b>	<b>0,345</b>	<b>0,543</b>	<b>0,650</b>
0,37	<b>1,81</b>	<b>0,097</b>	<b>0,353</b>	<b>0,554</b>	<b>0,680</b>
0,37	<b>1,97</b>	<b>0,097</b>	<b>0,361</b>	<b>0,569</b>	<b>0,682</b>

Table 69 Velocity calculations, 7 m air slide, 4.0 m from inlet.



$K_{7,8\text{ m}}(\alpha) - 15\text{ m}$	$U_0/U_{mf}$	0	0,6	1,1	1,6
0,29	0,99	0,056	0,156	0,332	0,512
0,32	1,16	0,080	0,225	0,410	0,587
0,37	1,31	0,093	0,286	0,468	0,685
0,38	1,49	0,094	0,318	0,538	0,689
0,39	1,64	0,107	0,358	0,569	0,721
0,42	1,81	0,113	0,370	0,594	0,775
0,43	1,97	0,114	0,374	0,621	0,783

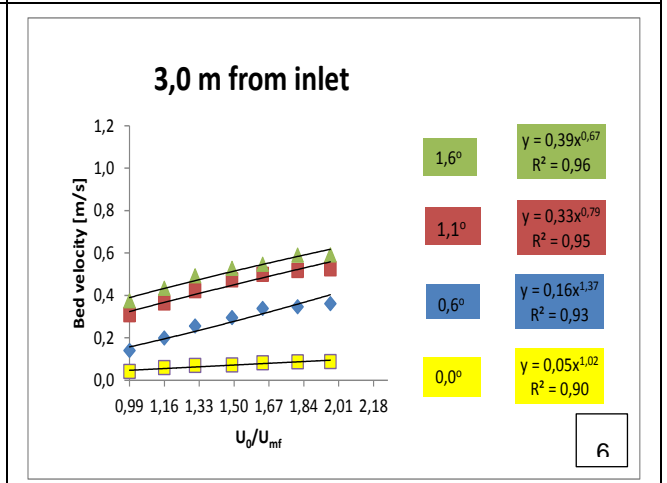
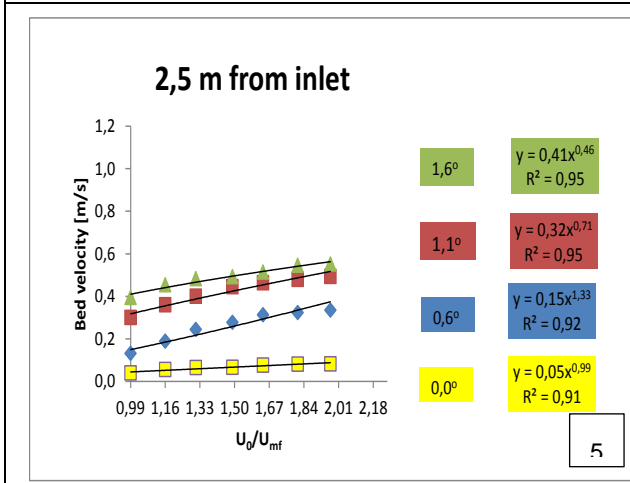
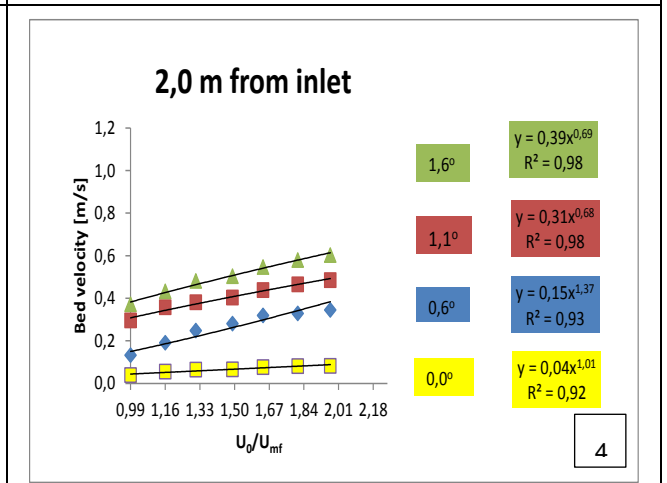
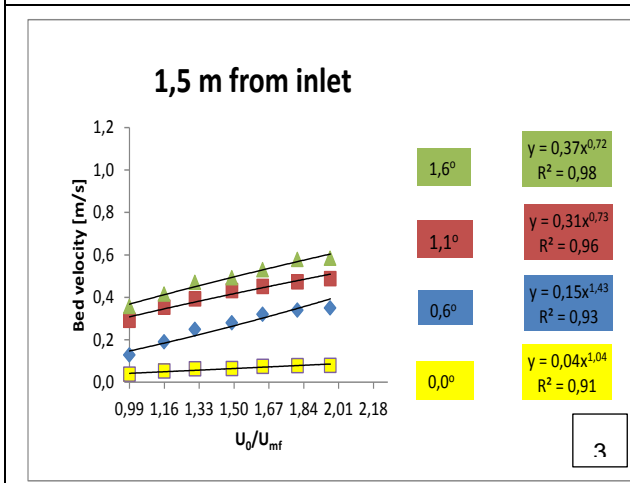
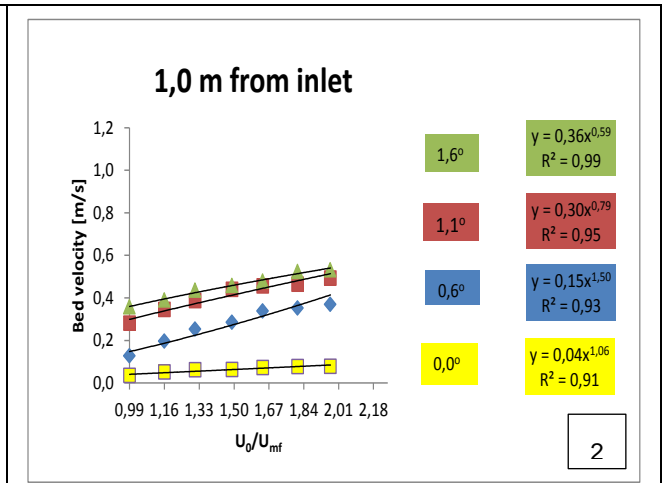
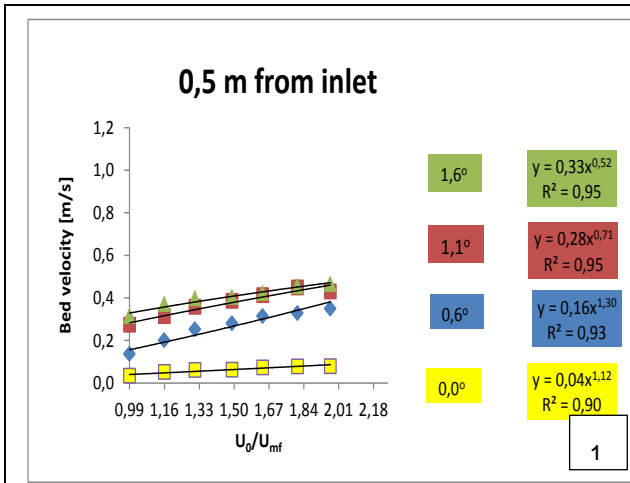
Table 70 Velocity calculations, 7 m air slide, 4.5 m from inlet.

$K_{10,2\text{ m}}(\alpha) - 15\text{ m}$	$U_0/U_{mf}$	0	0,6	1,1	1,6
0,26	0,99	0,070	0,166	0,341	0,473
0,27	1,16	0,098	0,239	0,402	0,521
0,29	1,31	0,113	0,295	0,465	0,571
0,30	1,49	0,111	0,339	0,516	0,578
0,33	1,64	0,126	0,381	0,541	0,653
0,35	1,81	0,136	0,395	0,567	0,701
0,36	1,97	0,139	0,400	0,576	0,706

Table 71 Velocity calculations, 7 m air slide, 5.0 m from inlet.

$K_{12,6\text{ m}}(\alpha) - 15\text{ m}$	$U_0/U_{mf}$	0	0,6	1,1	1,6
0,19	0,99	0,085	0,158	0,303	0,378
0,21	1,16	0,122	0,232	0,360	0,448
0,26	1,31	0,129	0,295	0,416	0,546
0,30	1,49	0,132	0,339	0,486	0,609
0,32	1,64	0,139	0,390	0,501	0,662
0,35	1,81	0,152	0,407	0,543	0,718
0,36	1,97	0,155	0,406	0,562	0,739

15 m - effect of  $U_0/U_{mf}$  on bed velocity at different distances away from inlet and at different angles of inclination,  $\theta$



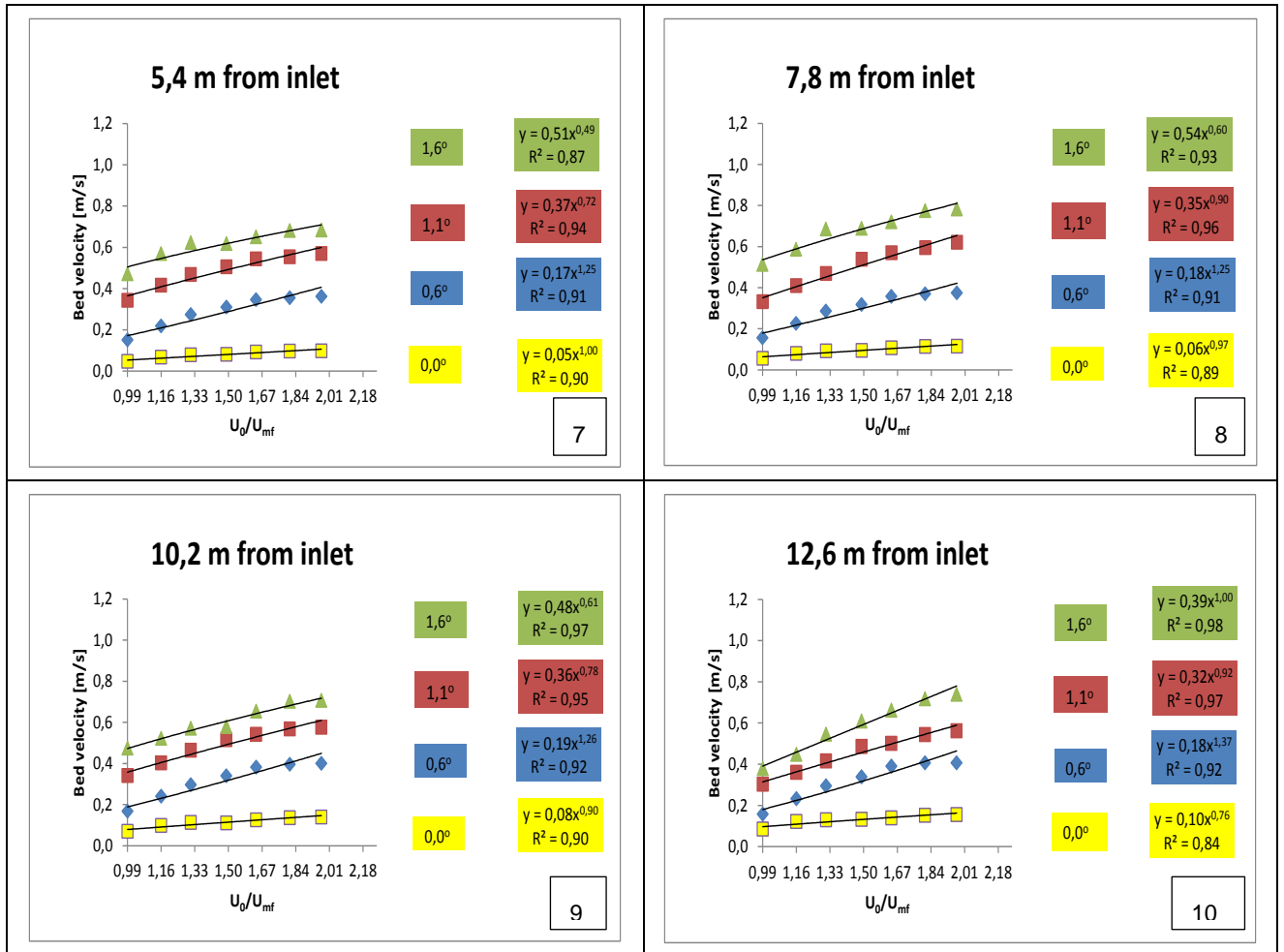


Figure 262 Power law models of average bed velocity as a function of  $U_0/U_{mf} = 0.99 \dots 1.97$  at different angles of inclination,  $\theta = 0 \dots 1.6^\circ$ .

15 m - bed velocity slope as a function of  $U_0/U_{mf}$ ,  $K(U_0/U_{mf})$ , versus distance from inlet at different angles of inclination,  $\theta$

Table 72 15 m air slide, bed velocity slope.

Angle	Bed velocity slope ( $U_0/U_{mf}(\alpha)$ )									
	$K(\alpha)_{0,5\text{ m}}$	$K(\alpha)_{1,0\text{ m}}$	$K(\alpha)_{1,5\text{ m}}$	$K(\alpha)_{2,0\text{ m}}$	$K(\alpha)_{2,5\text{ m}}$	$K(\alpha)_{3,0\text{ m}}$	$K(\alpha)_{5,5\text{ m}}$	$K(\alpha)_{7,8\text{ m}}$	$K(\alpha)_{10,2\text{ m}}$	$K(\alpha)_{12,6\text{ m}}$
0,0	0,04	0,04	0,04	0,04	0,05	0,05	0,05	0,06	0,08	0,10
0,6	0,16	0,15	0,15	0,15	0,15	0,16	0,17	0,18	0,19	0,18
1,1	0,28	0,30	0,31	0,31	0,32	0,33	0,37	0,35	0,36	0,32
1,6	0,33	0,36	0,37	0,39	0,41	0,41	0,51	0,54	0,48	0,39

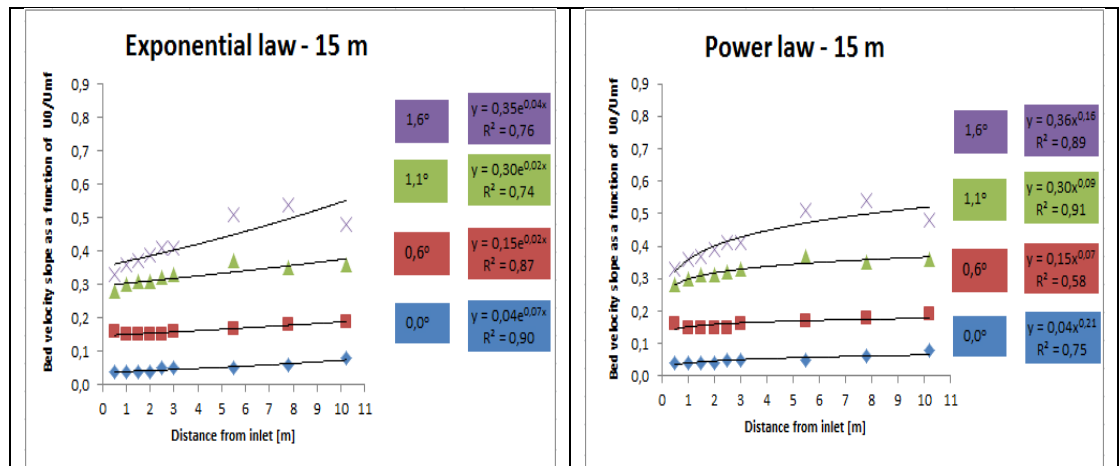


Figure 263 Exponential and power law models fitted to the slope of average bed velocity as a function of  $U_0/U_{mf} = 0.99 \dots 1.97$ ,  $K(U_0/U_{mf})$ , versus distance from inlet, at different angles of inclination,  $\theta = 0 \dots 1.6^\circ$ .

### Calculation of velocity: system input

Velocity has been calculated using gas dynamics theory (Haugland (1998), Rathakrishnan (2010)). Some basic concepts need to be introduced first.

The concept speed of sound, very important in compressible flows (air), is the speed with which an infinitesimal pressure change  $\Delta P$  travels through a compressible medium. The pressure disturbance will create a small density change  $\Delta \rho$  in the medium (air).

The ratio of the speed of the nozzle flow to the speed of sound (about 330 m/s) in the gas is named after Ernst Mach, a late 19<sup>th</sup> century physicist who studied gas dynamics. Thus the Mach number,  $M$ , allows us to define and establish flow regimes with different compressibility effects.

- $M < 1$ : subsonic flow;
- $M = 1$ : sonic flow;
- $1 < M < 5$ : supersonic flow;

$$M = \frac{V}{C} = \frac{V}{\sqrt{KRT}}$$

Mass flow through a nozzle (area change)

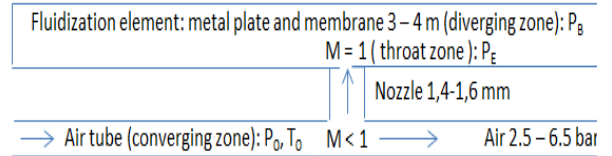


Figure 264 a) Fluidization elements; b) Flow regimes in converging - diverging nozzles based on M number.

Isentropic flow of air is considered through a nozzle. Assuming steady state conditions, air mass flow rate,  $\dot{m}$  will be constant through the nozzle and can be expressed as:

$$\dot{m} = \rho AV$$

$$\frac{\dot{m}}{A} = \rho V = \frac{P}{RT} MC = \frac{PM\sqrt{KRT}}{RT} = PM \sqrt{\frac{K}{RT}}$$

Using the expressions of  $P$  and  $T$  as functions of  $P_0$  and  $T_0$ :

$$T = \frac{T_0}{\left(1 + \frac{K-1}{2} M^2\right)}$$

$$P = \frac{P_0}{\left(1 + \frac{K-1}{2} M^2\right)^{\frac{K}{K-1}}}$$

$$\frac{\dot{m}}{A} = \frac{P_0}{T_0} \sqrt{\frac{K}{R}} \frac{M}{\left(1 + \frac{K-1}{2} M^2\right)^{\frac{K+1}{2(K-1)}}}$$

For  $M = 1$   $\frac{\dot{m}}{A} = \frac{P_0}{T_0} \sqrt{\frac{K}{R}} \frac{1}{\left(\frac{K+1}{2}\right)^{\frac{K+1}{2(K-1)}}$

## APPENDIX E DATA SHEETS

Table 73 Data Sheet HMB RM4220

### RM4220

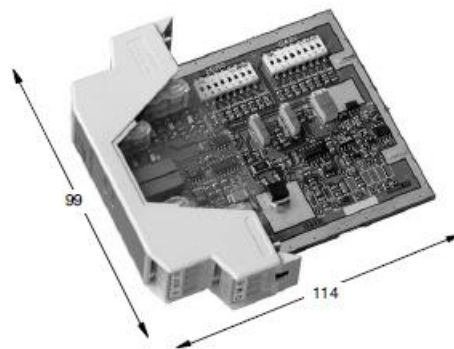
Amplifier for  
SG-Transducers



#### Special features

- Amplifier for up to four 350  $\Omega$  transducers
- To use for mounting on DIN rails
- Output  $\pm 10$  V, 0 ... 10 V and 4 ... 20 mA
- Adjustment via DIP switches and potentiometers
- Service friendly via using plug-in terminal

Dimensions (in mm; 1 mm = 0.03937 inches)



View from above

View of mounting side



## Specifications

Type		RM4220
<b>Accuracy class</b>		0.1
<b>Zero adjustment</b> Maximum for impedance 87 Ω	mV/V	± 2.00
<b>Amplifier gain</b> Maximum Minimum		8500 80
<b>Strain gage full bridge</b> Bridge excitation voltage Strain gage impedance Strain gage sensitivity	V <sub>DC</sub> Ω mV/V	5/10 ≥ 80 0.3 ... 12
<b>Input current</b> Input impedance	nA Ω	5 typ. 10 <sup>10</sup>
<b>Output current</b> Maximum non-linearity Output impedance Load resistance	mA % FSO MΩ Ω	4/20 ± 0.015 typ. 40 max. 800
<b>Output voltage</b> Output short-circuit current Max. non-linearity	V mA % FSO	0/10 or ± 10 ± 22 G = 1000 (± 0.001)
<b>Filter (3rd order)</b> Maximum Minimum / standard	Hz Hz	5000 ± 10 3 ± 10%
<b>Thermal drift</b> Input offset voltage drift Thermal sensitivity drift	V output μV/°C ppm/°C	± 10 typ. ± 0.2 / ± 5 G 150
<b>Max. current consumption</b>	mA	200
<b>Fixture</b>		Mounting rail TS35 as per DIN EN 60750
<b>Connection</b>		Screw terminal
<b>Power supply</b>	V <sub>DC</sub>	24 ± 8
<b>Operating temperature range</b>	°C [°F]	0 ... +70 [32 ... 158]
<b>Storage temperature range</b>	°C [°F]	-40 ... +85 [-40 ... 185]
<b>Temperature stabilization time</b>	min	15
<b>Inflammability</b>		VO (UL94)
<b>Degree of protection</b>		IP 20
<b>Dimensions (L x W x H)</b>	mm	115 x 100 x 23
<b>Housing material</b>		Polyamide PA
<b>Color</b>		grey
<b>Weight, approx.</b>	g	130

Modifications reserved.  
All details describe our products in general form only. They are not to be understood as express warranty and do not constitute any liability whatsoever.

### Hottinger Baldwin Messtechnik GmbH

Im Tiefen See 45 · 64293 Darmstadt · Germany  
Tel. +49 6151 803-0 · Fax: +49 6151 803-9100  
Email: [info@hbm.com](mailto:info@hbm.com) · [www.hbm.com](http://www.hbm.com)

## 2 Application

The RM4220 module is an amplifier for sensors with strain gages. The amplifier offers a very simple and practical setting of the zero point and the full scale with DIP switches and potentiometers. The bridge excitation voltage can be selected: 5 or 10 V. The output signal can be 0 ... 10 V or  $\pm 10$  V and, at the same time 4 ... 20 mA.

The transducer connection can be with four-wire or six-wire configuration. If you are using six-wire configuration, you can ignore the influence of the resistors or the resistance change of the extension cable.

The housing, made of polyamide PA type PHOENIX EM, can be attached to any support rails as per DIN EN 60715. The support rails must be located within an EMC-proof housing, e.g. in a control cabinet.

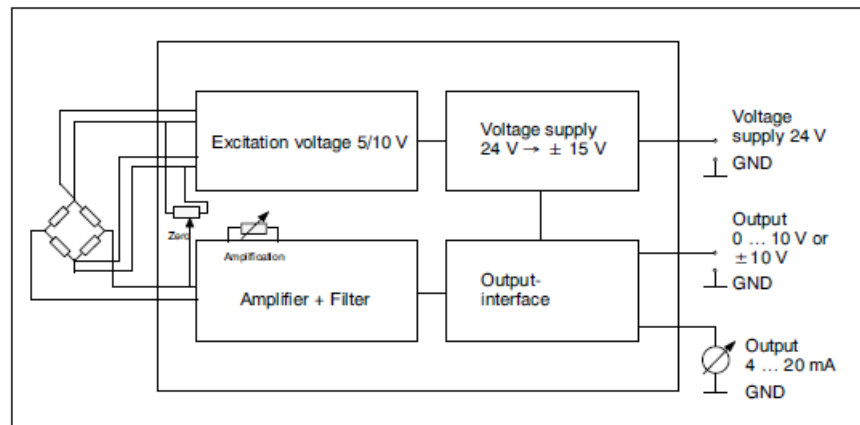


Fig. 2.1: Principle diagram



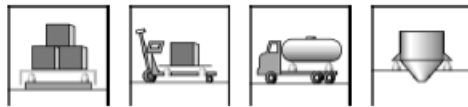


**HLC A1 ...  
HLC B1 ...  
HLC F1 ...**

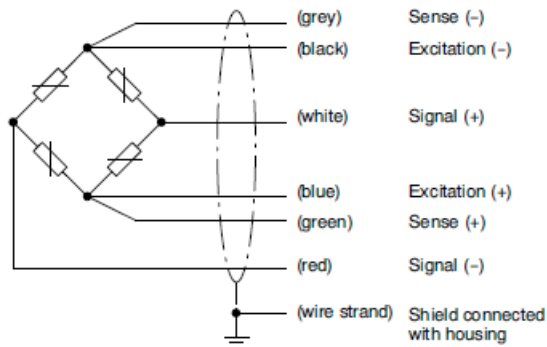
Load cells

**Special features**

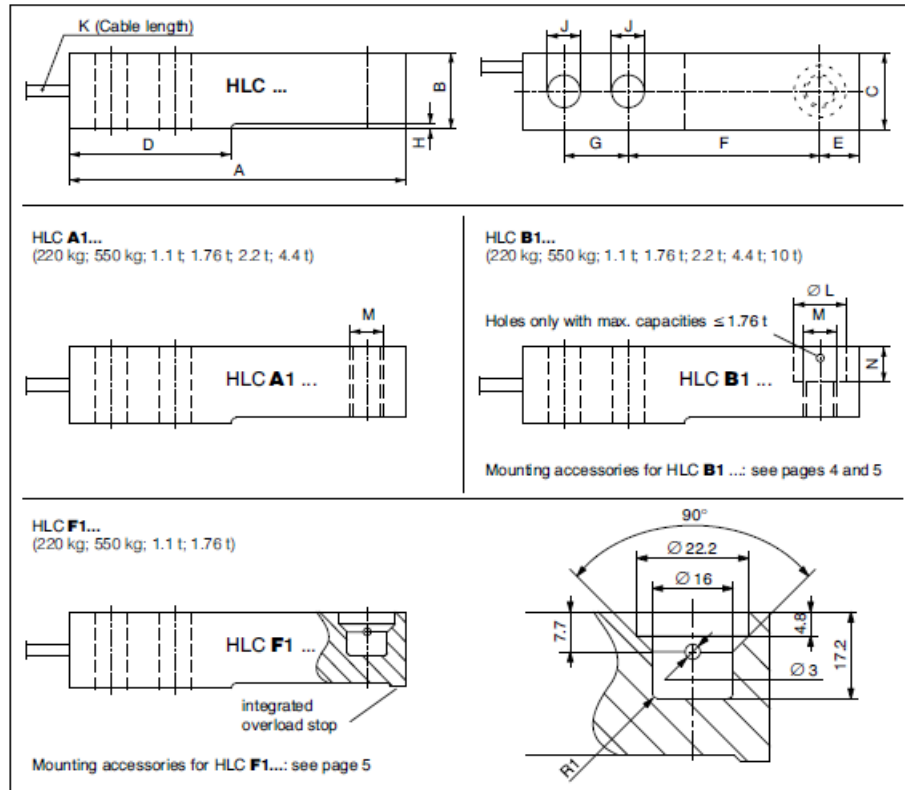
- Hermetically sealed (IP68)
- Max. capacities: 220 kg ... 10 t
- Stainless steel
- Low overall height
- Meets EMC/ESD requirements according to EN 45 501
- Complies with OIML R60 regulations up to 6000d
- Explosion-proof versions according to ATEX 95 optional



**Wiring code (6-wire circuit)**



**Dimensions (in mm; 1 mm = 0.03937 inches)**



Max. capacity	A	B	C	D	E	F	G	H	J	K	ØL	M	N
220 kg; 550 kg; 1.1 t	133.4	30.2	30.7	57.7	15.4	76.2	25.4	1.7	13	3 m	20.6	M12	14.2
1.76 t	133.4	30.2	30.7	51.7	15.4	76.2	25.4	1.7	13	3 m	20.6	M12	14.2
2.2 t <sup>2)</sup>	171.5	36.5	36.8	76.2	19.1	95.3	38.1	2.5	20.5	6 m	30.2	M20	17.0
4.4 t <sup>2)</sup>	171.5	42.9	42.9	76.2	19.1	95.3	38.1	2.5	20.5	6 m	30.2	M20	20.1
10 t <sup>1)</sup>	245.1	72.9	60	119.9	30.2	134.9	50 ± 0.05	11.2	27	6 m	51 +0.2	Ø 32	20

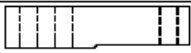
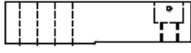
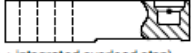
<sup>1)</sup> Maximum capacities 2.2 t and 4.4 t: HLC A1 ... + HLC B1 ... only

<sup>2)</sup> Maximum capacity 10 t: HLC B1 D1 ... only

**Mounting accessories (to be ordered separately)**

In order to minimize error interferences due to load introduction, HBM offers various proven load introductions for the load cell types HLC B1 ... und HLC F1 ..., depending on the mounting situation (see pages 4 and 5)

## Technical Data

<b>Type HLC A1 ...</b> Maximum capacity ( $E_{max}$ )  (Load introduction = thread through)	<b>HLC A1 D1 / ... + HLC A1 C3 / ...</b> 220 kg; 550 kg; 1.1 t; 1.76 t; 2.2 t; 4.4 t			
<b>Type HLC B1 ...</b> Maximum capacity ( $E_{max}$ )  (Load introduction = counterbore + thread) <sup>3)</sup>	<b>HLC B1 D1 / ...</b> 220 kg; 550 kg; 1.1 t; 1.76 t; 2.2 t; 4.4 t; 10 t <b>HLC B1 C3 / ...</b> 220 kg; 550 kg; 1.1 t; 1.76 t; 2.2 t; 4.4 t <b>HLC B1 C4 / ... + HLC B1 C6 / ...</b> 220 kg; 550 kg; 1.1 t			
<b>Type HLC F1 ...</b> Maximum capacity ( $E_{max}$ )  (Load introduction = blind hole + integrated overload stop)	<b>HLC F1 D1 / ... + HLC F1 C3 / ...</b> 220 kg; 550 kg; 1.1 t; 1.76 t			
<b>Accuracy class according to OIML R60</b> <b>Maximum number of load cell intervals (<math>n_{LC}</math>)</b>	D1 1000	C3 3000	C4 <sup>5)</sup> 4000	C6 <sup>5)</sup> 6000
<b>Minimum LC verification interval (<math>v_{min}</math>)</b>	0,0285	0,0100 (220kg; 1.76 t; 2.2 t; 4.4 t) 0,0090 (550 kg + 1.1 t)		
<b>Sensitivity (<math>C_N</math>)</b>	1.94 (10 t = 2.00 mV/V)			
<b>Sensitivity tolerance</b>	± 0.5		± 0.1	
<b>Temperature effect on zero balance (<math>TK_0</math>)</b>	± 0.0140 (220 kg; 1.76 t; 2.2 t; 4.4 t) ± 0.0126 (550 kg + 1.1 t)			
<b>Temperature effect on sensitivity (<math>TK_C</math>) <sup>4)</sup></b>	± 0.0420	± 0.0140	± 0.0105	± 0.0070
<b>Hysteresis error (<math>d_{hy}</math>) <sup>4)</sup></b>	± 0.0500	± 0.0166	± 0.0125	± 0.0083
<b>Non-linearity (<math>d_{lin}</math>) <sup>4)</sup></b>	± 0.0500	± 0.0170	± 0.0166	
<b>Creep (<math>d_{cl}</math>) over 30 min.</b>	± 0.0500	± 0.0166	± 0.0166	± 0.0122
<b>Minimum dead load output return (MDLOR)</b>	± 0.0500	± 0.0166	± 0.0125	± 0.0083
<b>Input resistance (<math>R_{LC}</math>)</b>	350 ... 480			
<b>Output resistance (<math>R_O</math>)</b>	350 ± 2		350 ± 0.12	
<b>Reference excitation voltage (<math>U_{ref}</math>)</b>	5			
<b>Nominal range of excitation voltage (<math>B_U</math>)</b>	0.5 ... 15 ( Ex-Versions max. 12 V !!! )		5 ... 10	
<b>Insulation resistance (<math>R_{is}</math>)</b>	GΩ > 5			
<b>Nominal temperature range (<math>B_T</math>)</b>	-10 ... +40 [-14 ... +104]			
<b>Service temperature range (<math>B_{ts}</math>)</b>	-30 ... +70 [-22 ... +158]			
<b>Storage temperature range (<math>B_{st}</math>)</b>	-50 ... +85 [-58 ... +185]			
<b>Safe load limit (<math>E_L</math>)</b>	150			
<b>Lateral load limit (<math>E_{Lq}</math>)</b>	100			
<b>Breaking load (<math>E_D</math>)</b>	300			
<b>Permissible dynamic load (<math>F_{drel}</math>) (vibration amplitude according to DIN 50100)</b>	70			
<b>Deflection at <math>E_{max}</math> (<math>s_{nom}</math>), approx.</b>	0.5 (1.76 t = 1.4 mm)			
<b>Weight (G), approx.</b>	0.9 (220 kg ... 1.76 t); 1.6 (2.2 t); 2.2 (4.4 t); 6.2 (10 t)			
<b>Protection class to EN 60 529 (IEC 529)</b>	IP68			
<b>Material: Measuring element</b> <b>Cable fitting</b> <b>Cable-sheath</b>	Stainless steel <sup>6)</sup> Stainless steel <sup>6)</sup> / Gasket: Viton <sup>6)</sup> PVC			

<sup>3)</sup> Maximum capacity 10 t: Load introduction = counterbore + hole

<sup>4)</sup> The data for Non-linearity ( $d_{lin}$ ), Hysteresis error ( $d_{hy}$ ) and Temperature effect on sensitivity ( $TK_C$ ) are typical values. The sum of these data meets the requirements according to OIML R60.

<sup>5)</sup> Accuracy classes C4 and C6: HLC B1 ... / 220 kg; 550 kg; 1,1 t only

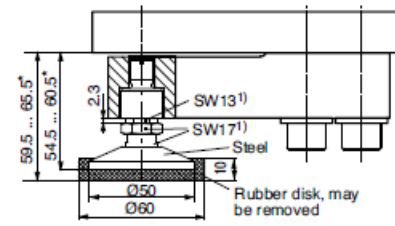
<sup>6)</sup> According to EN 10088-1

### Mounting accessories (to be ordered separately)

In order to minimize error interferences due to load introduction, HBM offers various proven load introductions for the load cell types HLC B1 ... and HLC F1 ..., depending on the mounting situation (see pages 4 and 5)

**Mounting accessories for HLC B ...** (to be ordered separately; Dimensions in mm; 1 mm = 0.03937 inches)

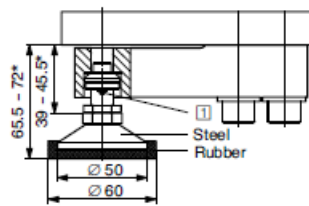
**HLCB/PCX/1.76 t** - Load introduction swivel foot (stainless steel) for HLC B / 220 kg ... 1.76 t, applicable up to accuracy class C6:



1) SW = Width across flats

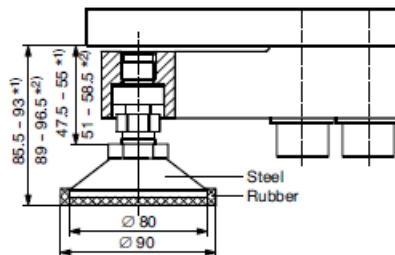
\* High adjustment

**HLCB/ZFP/1.76 T** - Load introduction swivel foot (stainless steel) for HLC B / 220 kg ... 1.76 t



1) Foot fixed in the load cell with the enclosed spring shackle

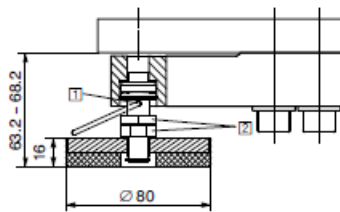
**HLCB/ZFP/4.4 T** - Load introduction swivel foot (stainless steel) for HLC B / 2.2 t + 4.4 t:



\* High adjustment

(1) = Maximum capacity 2.2 t / (2) = Maximum capacity 4.4 t

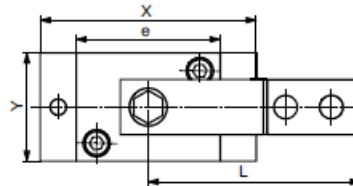
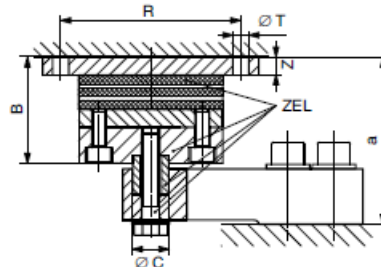
**HLCB/ZAK/1.76 T** - Load introduction swivel foot (stainless steel) for HLC B ≤ 1.76 t



1) Foot fixed in the load cell with the enclosed spring shackle

2) Width across flats 19

**HLCB/...T/ZEL** - Rubber-metal bearing (galvanized material; HLCB/1.76T/ZELR = stainless steel) for HLC B



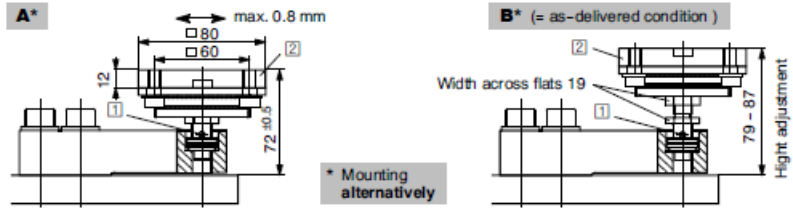
Maximum permissible lateral shift (when loaded with max. capacity):

HLCB/1.76T/ZEL: 4.5 mm  
HLCB/4.4T/ZEL: 8 mm  
HLCB/10T/ZEL: 9.5 mm

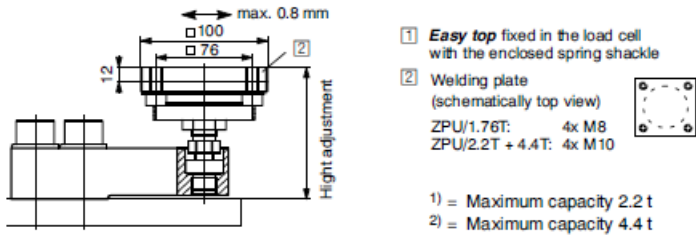
Type	Max capacity	B	∅ C <sub>0.1</sub>	L	R	∅ T	X	Y	Z	a	e
HLCB/1.76T/ZEL HLCB/1.76T/ZELR	220 kg ... 1.76 t	58.8	20	118	100	9	120	60	10	92	80
HLCB/4.4T/ZEL	2.2 t	71.2	30	152.4	125	11	150	100	10	113	100
HLCB/4.4T/ZEL	4.4 t	71.2	30	152.4	125	11	150	100	10	116	100
HLCB/10T/ZEL	10 t	85	50.8	214.9	175	13	200	100	12	167	150

**Accessories for HLC B ... + HLC F ... (to be ordered separately; Dimensions in mm; 1 mm = 0.03937 inches)**

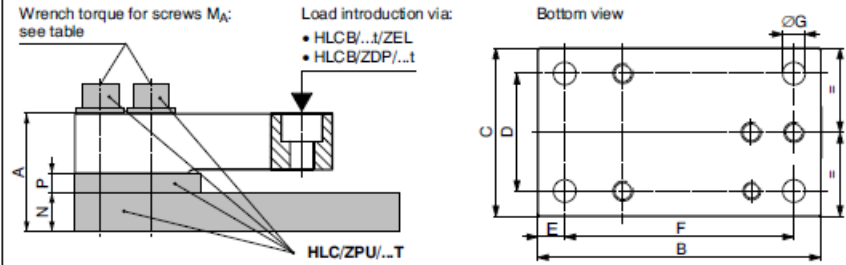
**HLCB/ZDP/1.76 T Easy top** - Rubber-metal bearing for HLC B / 220 kg ... 1.76 t  
(Load introduction: stainless steel, Welding plate: galvanized material)



**HLCB/ZDP/4.4 T Easy top** - Rubber-metal bearing for HLC B / 2.2 t + 4.4 t  
(Load introduction: stainless steel, Welding plate: galvanized material)

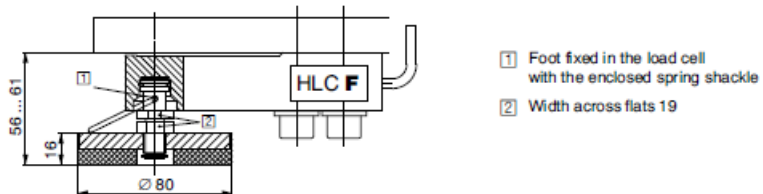


**HLC/ZPU/...T** - Base plate / Mounting kit (galvanized material) for HLC B



Type	Max. capacity	Breaking load	A	B	C	D	E	F	G	N	P	MA
HLC/ZPU/1.76 T	220 kg ... 1.76 t	3.52 t	60.5	168	100	70	16	136	13.5	20	10	130 N·m
HLC/ZPU/2.2 T	2.2 t	4.4 t	81.5	212	120	84	18	175	14	25	20	400 N·m
HLC/ZPU/4.4 T	4.4 t	8.8 t	88	212	120	84	18	175	14	25	20	400 N·m

**HLCF/ZKP/1.76T** - Load introduction swivel foot (stainless steel) for HLC F ≤ 1.76 t







**Australian Government**  
National Measurement  
Institute

Bradfield Road, West Lindfield NSW 2070

## Supplementary Certificate of Approval

### No S498

Issued by the Chief Metrologist under Regulation 60  
of the  
National Measurement Regulations 1999

This is to certify that an approval for use for trade has been granted in respect of the instruments herein described.

HBM Model HLCB1C3 550KG Load Cell

submitted by Hottinger Baldwin Messtechnik GmbH  
Im Tiefen See 45  
D-64293 Darmstadt  
Germany

**NOTE:** This Certificate relates to the suitability of the pattern of the instrument for use for trade only in respect of its metrological characteristics. This Certificate does not constitute or imply any guarantee of compliance by the manufacturer or any other person with any requirements regarding safety.

This approval has been granted with reference to document NMI R 60, *Metrological Regulation for Load Cells*, dated July 2004.

This approval becomes subject to review on 1/08/17, and then every 5 years thereafter.

#### DOCUMENT HISTORY

Rev	Reason/Details	Date
0	Pattern & variant 1 approved – certificate issued	4/07/07
1	Pattern & variant 1 amended, reviewed & updated – certificate issued	16/11/12

## CONDITIONS OF APPROVAL

### General

Instruments purporting to comply with this approval shall be marked with pattern approval number 'NMI S498' and only by persons authorised by the submittor.

Instruments incorporating a component purporting to comply with this approval shall be marked 'NMI S498' in addition to the approval number of the instrument, and only by persons authorised by the submittor.

It is the submittor's responsibility to ensure that all instruments marked with this approval number are constructed as described in the documentation lodged with the National Measurement Institute (NMI) and with the relevant Certificate of Approval and Technical Schedule. Failure to comply with this Condition may attract penalties under Section 19B of the National Measurement Act and may result in cancellation or withdrawal of the approval, in accordance with document NMI P 106.

Signed by a person authorised by the Chief Metrologist  
to exercise his powers under Regulation 60 of the  
*National Measurement Regulations 1999.*

A handwritten signature in black ink, consisting of a series of loops and a long horizontal stroke at the bottom.



TECHNICAL SCHEDULE No S498

**1. Description of Pattern** **approved on 4/07/07**

An HBM model HLCB1C3 550KG load cell of 550 kg maximum capacity (Figure 1 and Table 1).

**1.1 Method of Mounting**

Mounting is to be in accordance with the manufacturer's instructions and as shown in Figure 2.

**1.2 Markings**

Each load cell is marked with the following:

Manufacturer's mark, or name written in full	HBM
Model number	.....
Maximum capacity	..... kg (or t)
Serial number	.....
Pattern approval mark	S498

**1.3 Tables of Specifications**

Specifications for the pattern are given below and in Table 1.

**2. Description of Variant 1** **approved on 16/11/12**

Certain other models and with characteristics and specifications as listed below and in Tables 1 to 6.

In all cases	
mV/V	1.94 mV/V except see Note (b) in Tables 2 to 6
Input imp. (ohms)	350
Voltage (V)	15 V max AC/DC
Cable length	3, 6 or 12 m
Number of leads	6 (plus shield)

Where:

<i>E<sub>max</sub></i>	=	Maximum capacity
nLC	=	Maximum number of verification intervals
<i>V<sub>min</sub></i>	=	Minimum value of verification interval
DR	=	Minimum dead load output return value
mV/V	=	Output rating (nominal)
Input imp.	=	Input impedance (nominal)
Voltage	=	Maximum supply voltage (DC)

TABLE 1  
HBM HLC series load cells of Class C as listed below.

Model	E <sub>max</sub> (kg)	Class	n <sub>LC</sub>	V <sub>min</sub> (g)	Notes
HLCB1C3 220KG	220	C	3000	22	
HLCA1C3 220KG	220	C	3000	22	
HLCF1C3 220KG	220	C	3000	22	
HLCB1C3 550KG	550	C	3000	49.5	
HLCA1C3 550KG	550	C	3000	49.5	
HLCF1C3 550KG	550	C	3000	49.5	
HLCB1C3 1.1T	1100	C	3000	99	
HLCA1C3 1.1T	1100	C	3000	99	
HLCF1C3 1.1T	1100	C	3000	99	
HLCB1C3 1.76T	1760	C	3000	176	
HLCA1C3 1.76T	1760	C	3000	176	
HLCF1C3 1.76T	1760	C	3000	176	
HLCB1C3 2.2T	2200	C	3000	220	(a)
HLCB1C3 4.4T	4400	C	3000	440	(a)
HLCB1C4 220KG	220	C	4000	22	
HLCF1C4 220KG	220	C	4000	22	
HLCB1C4 550KG	550	C	4000	49.5	
HLCF1C4 550KG	550	C	4000	49.5	
HLCB1C4 1.1T	1100	C	4000	99	
HLCF1C4 1.1T	1100	C	4000	99	
HLCB1C6 220KG	220	C	6000	22	
HLCF1C6 220KG	220	C	6000	22	
HLCB1C6 550KG	550	C	6000	49.5	
HLCF1C6 550KG	550	C	6000	49.5	
HLCB1C6 1.1T	1100	C	6000	99	
HLCF1C6 1.1T	1100	C	6000	99	

Notes:

- (a) For this model cable length is 6 m.
- The models HLCA1, HLCB1 and HLCF1 differ according to the load introduction method (see Figure 1).
  - HLCA1 – load introduction through a threaded hole
  - HLCB1 – load introduction through a counter bore and thread
  - HLCF1 – load introduction through a blind hole

TABLE 2  
HBM HLC series load cells of Class D as listed below.

Model	E <sub>max</sub> (kg)	Class	n <sub>LC</sub>	V <sub>min</sub> (g)	Notes
HLCA1D1 220KG	220	D	1000	62.7	
HLCB1D1 220KG	220	D	1000	62.7	
HLCF1D1 220KG	220	D	1000	62.7	
HLCA1D1 550KG	550	D	1000	156.75	
HLCB1D1 550KG	550	D	1000	156.75	
HLCF1D1 550KG	550	D	1000	156.75	
HLCA1D1 1.1T	1100	D	1000	313.5	
HLCB1D1 1.1T	1100	D	1000	313.5	
HLCF1D1 1.1T	1100	D	1000	313.5	
HLCA1D1 1.76T	1760	D	1000	501.6	
HLCB1D1 1.76T	1760	D	1000	501.6	
HLCF1D1 1.76T	1760	D	1000	501.6	
HLCB1D1 2T	2000	D	1000	570	(b)
HLCB1D1 2.2T	2200	D	1000	627	
HLCB1D1 4.4T	4400	D	1000	1254	
HLCB1D1 10T	10 000	D	1000	2850	(b)

Notes:

- (b) For this model sensitivity is 2 mV/V.
- Class D load cells may only be used in a Class 4 (MIP) weighing instrument.
- The models HLCA1, HLCB1 and HLCF1 differ according to the load introduction method (see Figure 1).

HLCA1 – load introduction through a threaded hole  
HLCB1 – load introduction through a counter bore and thread  
HLCF1 – load introduction through a blind hole

TABLE 3  
HBM HLCx1 series load cells of Class C as listed below.

Model	E <sub>max</sub> (kg)	Class	n <sub>LC</sub>	V <sub>min</sub> (g)	Notes
HLCA1C3 2T	2000	C	3000	220	(b)
HLCA1C3 2.2T	2200	C	3000	220	
HLCA1C3 4.4T	4400	C	3000	440	
HLCB1C3 2T	2000	C	3000	220	(b)
HLCF1C3 2T	2000	C	3000	220	(b)

Note (b): For this model sensitivity is 2 mV/V

TABLE 4  
HBM HLCx1 series load cells of Class D as listed below.

Model	E <sub>max</sub> (kg)	Class	n <sub>LC</sub>	V <sub>min</sub> (g)	Notes
HLCA1D1 2T	2000	D	1000	570	(b)
HLCA1D1 2.2T	2200	D	1000	630	
HLCA1D1 4.4T	4400	D	1000	1260	

Note: Class D load cells may only be used in a Class 4 (M) weighing instrument.

TABLE 5  
HBM HLCx2 series load cells of Class C as listed below.

Model	E <sub>max</sub> (kg)	Class	n <sub>LC</sub>	V <sub>min</sub> (g)	Notes
HLCB2C3 220KG	220	C	3000	22	
HLCB2C3 550KG	550	C	3000	49.5	
HLCB2C3 1.1T	1100	C	3000	99	
HLCB2C3 1.76T	1760	C	3000	176	
HLCB2C3 2T	2000	C	3000	220	(b)
HLCB2C3 2.2T	2200	C	3000	220	
HLCB2C3 4.4T	4400	C	3000	440	
HLCF2C3 220KG	220	C	3000	22	
HLCF2C3 550KG	550	C	3000	49.5	
HLCF2C3 1.1T	1100	C	3000	99	
HLCF2C3 1.76T	1760	C	3000	176	
HLCF2C3 2T	2060	C	3000	220	(b)
HLCB2C4 220KG	220	C	4000	22	
HLCB2C4 550KG	550	C	4000	49.5	
HLCB2C4 1.1T	1100	C	4000	99	
HLCF2C4 220KG	220	C	4000	22	
HLCF2C4 550KG	550	C	4000	49.5	
HLCF2C4 1.1T	1100	C	4000	99	
HLCB2C6 220KG	220	C	6000	22	
HLCB2C6 550KG	550	C	6000	49.5	
HLCB2C6 1.1T	1100	C	6000	99	
HLCF2C6 220KG	220	C	6000	22	
HLCF2C6 550KG	550	C	6000	49.5	
HLCF2C6 1.1T	1100	C	6000	99	

Note (b): For this model sensitivity is 2 mV/V

TABLE 6  
HBM HLCx2 series load cells of Class D as listed below.

Model	E <sub>max</sub> (kg)	Class	n <sub>LC</sub>	V <sub>min</sub> (g)	Notes
HLCF2D1 220KG	220	D	1000	62.7	
HLCF2D1 550KG	550	D	1000	156.75	
HLCF2D1 1.1T	1100	D	1000	313.5	
HLCF2D1 1.76T	1760	D	1000	501.6	
HLCB2D1 220KG	220	D	1000	62.7	
HLCB2D1 550KG	550	D	1000	156.75	
HLCB2D1 1.1T	1100	D	1000	313.5	
HLCB2D1 1.76T	1760	D	1000	501.6	
HLCB2D1 2T	2000	D	1000	570	(b)
HLCB2D1 2.2T	2200	D	1000	627	
HLCB2D1 4.4T	4400	D	1000	1254	
HLCB2D1 10T	10 000	D	1000	2850	

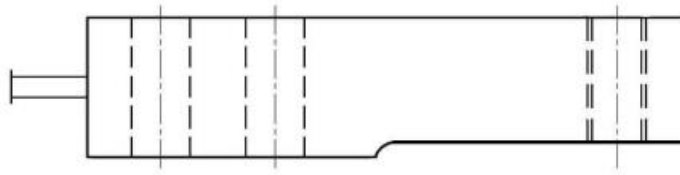
Note: Class D load cells may only be used in a Class 4 (M) weighing instrument.

Note (b): For this model sensitivity is 2 mV/V

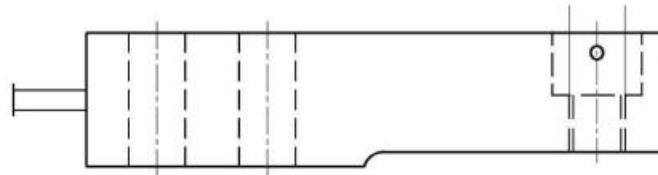
FIGURE S498 – 1



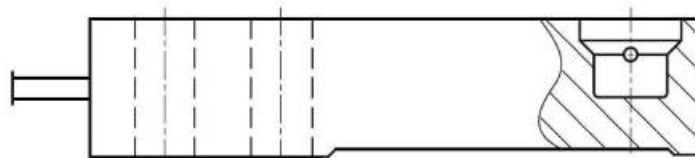
(a) HBM Model HLCB1C3 550KG Load Cell



(b) HBM Model HLCA ...

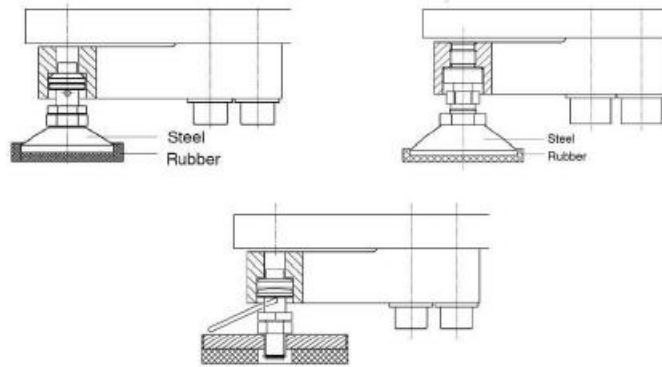


(c) HBM Model HLCB ...

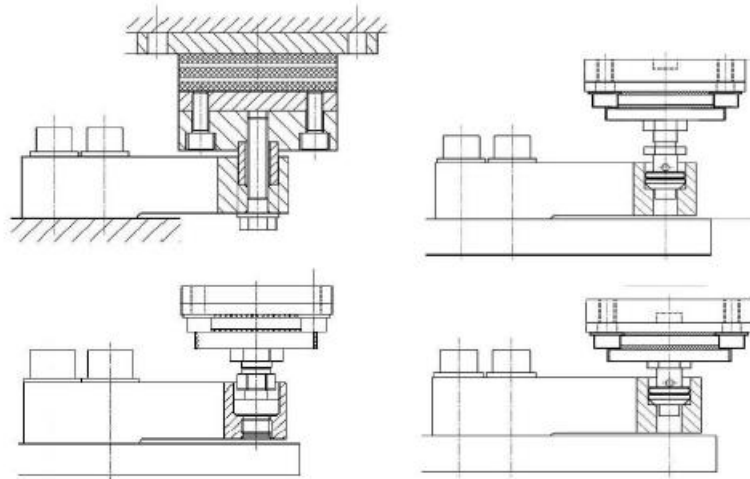


(d) HBM Model HLCF ...

FIGURE S498 – 2



(a) Loading foot – various



(b) Elastomer bearing – various

Mounting Arrangements

Table 76 Technical information flow measuring system

## Technical Information

# Proline Prowirl 72F, 72W, 73F, 73W

Vortex flow measuring system

Reliable flow measurement of gas, steam and liquids



### Application

For the universal measurement of the volume flow of gases, steam and liquids.

The mass flow of steam, water (as per IAPWS-IF97 ASME), natural gas (as per AGA NX-19/AGA8-DC92 detailed method/AGA8 Gross Method 1/SGERC-88), compressed air, other gases and liquids can also be calculated with the aid of integrated temperature measurement and by reading in external pressure values (Prowirl 73).

Maximum range of applications thanks to:

- Fluid temperature range from  $-200$  to  $+400$  °C ( $-328$  to  $+752$  °F)
- Pressure ratings up to PN 250/Class 1500
- Sensor with integrated (optional) diameter reduction by one line size (R Style) or two line sizes (S Style)
- Dualsens version (optional) for redundant measurements with two sensors and electronics

Approvals for:

- ATEX, FM, CSA, TIIS, NEPSI, IEC
- HART, PROFIBUS PA, FOUNDATION Fieldbus
- Pressure Equipment Directive, SIL 2

### Your benefits

The robust **Prowirl sensor**, tried and tested in over 200 000 applications, offers:

- High resistance to vibrations, temperature shocks, contaminated fluids and water hammer
- No maintenance, no moving parts, no zero-point drift ("lifetime" calibration)
- Software initial settings save time and costs

Additional possibilities:

- Complete saturated steam or liquid-mass measuring point in one single device
- Calculation of the mass flow from the measured variables volume flow and temperature in the integrated flow computer
- External pressure value read-in for superheated steam and gas applications
- External temperature value read-in for delta heat measurement

T100070D/06/EN/14.11  
71154560

**Endress+Hauser**   
People for Process Automation



# Input

## Measured variable

### Prowirl 72

- Volumetric flow (volume flow) is proportional to the frequency of vortex shedding after the bluff body.
- The following can be output as the output variable:
  - Volume flow
  - Mass flow or corrected volume flow (if process conditions are constant)

### Prowirl 73

- Volumetric flow (volume flow) is proportional to the frequency of vortex shedding after the bluff body.
- The temperature can be output directly and is used to calculate the mass flow for example.
- The following can be output as the output variable:
  - The measured process variables volume flow and temperature
  - The calculated process variables mass flow, heat flow or corrected volume flow

## Measuring range

The measuring range depends on the fluid and the nominal diameter.

### Start of measuring range

Depends on the density and the Reynolds number ( $Re_{min} = 4000$ ,  $Re_{linear} = 20\,000$ ). The Reynolds number is dimensionless and is the ratio of inertial forces to viscous forces of the fluid. It is used for characterizing the flow. The Reynolds number is calculated as follows:

$$Re = \frac{4 \cdot Q [m^3/s] \cdot \rho [kg/m^3]}{\pi \cdot d_i [m] \cdot \mu [Pa \cdot s]} \quad Re = \frac{4 \cdot Q [ft^3/s] \cdot \rho [lb/ft^3]}{\pi \cdot d_i [ft] \cdot \mu [0.001 \text{ cP}]}$$

$Re = \text{Reynolds number}$ ;  $Q = \text{flow}$ ;  $d_i = \text{internal diameter}$ ;  $\mu = \text{dynamic viscosity}$ ;  $\rho = \text{density}$

$$DN\ 15 \dots 25 \rightarrow v_{min}^* = \frac{6}{\sqrt{\rho [kg/m^3]}} [m/s] \quad DN\ 40 \dots 300 \rightarrow v_{min}^* = \frac{7}{\sqrt{\rho [kg/m^3]}} [m/s]$$

$$\frac{1}{2} \dots 1'' \rightarrow v_{min}^* = \frac{4.92}{\sqrt{\rho [lb/ft^3]}} [ft/s] \quad 1\frac{1}{2} \dots 12'' \rightarrow v_{min}^* = \frac{5.74}{\sqrt{\rho [lb/ft^3]}} [ft/s]$$

\* with amplification 5

### Full scale value

Liquids:  $v_{max} = 9 \text{ m/s}$  (30 ft/s)

Gas/steam: see table

Nominal diameter	$v_{max}$
Standard version: DN 15 (1/2") R Style: DN 25 (1") > DN 15 (1/2") S Style: DN 40 (1 1/2") >> DN 15 (1/2")	40 m/s (151 ft/s) or Mach 0.3 (depending on which value is smaller)
Standard version: DN 25 (1"), DN 40 (1 1/2") R Style: - DN 40 (1 1/2") > DN 25 (1") - DN 50 (2") > DN 40 (1 1/2") S Style: - DN 80 (3") >> DN 40 (1 1/2")	75 m/s (246 ft/s) or Mach 0.3 (depending on which value is smaller)
Standard version: DN 50 to 300 (2 to 12") R Style: - DN 80 (3") > DN 50 (2") - Nominal diameters larger than DN 80 (3") S Style: - DN 100 (4") >> DN 50 (2") - Nominal diameters larger than DN 100 (4")	120 m/s (394 ft/s) or Mach 0.3 (depending on which value is smaller)  Calibrated range: up to 75 m/s (246 ft/s)



### Note!

By using the selection and planning program "Applicator", you can determine the exact values for the fluid you use. You can obtain the Applicator from your Endress+Hauser sales center or on the Internet under [www.endress.com](http://www.endress.com).

**K-factor range**

The table is used for orientation purposes. The range in which the K-factor can be is indicated for individual nominal diameters and designs.

Nominal diameter		K-factor range (pulses/dm <sup>3</sup> )	
DIN/JIS	ANSI	72F / 73F	72W / 73W
DN 15	½"	300 to 450	245 to 280
DN 25	1"	70 to 85	48 to 55
DN 40	1½"	18 to 22	14 to 17
DN 50	2"	8 to 11	6 to 8
DN 80	3"	2.5 to 3.2	1.9 to 2.4
DN 100	4"	1.1 to 1.4	0.9 to 1.1
DN 150	6"	0.3 to 0.4	0.27 to 0.32
DN 200	8"	0.1200 to 0.1400	–
DN 250	10"	0.0677 to 0.0748	–
DN 300	12"	0.0364 to 0.0402	–

**Measuring range for gases [m<sup>3</sup>/h or Nm<sup>3</sup>/h]**

In the case of gases, the start of the measuring range depends on the density. With ideal gases, the density [ρ] or corrected density [ρ<sub>N</sub>] can be calculated using the following formulae:

$$\rho \text{ [kg/m}^3\text{]} = \frac{\rho_N \text{ [kg/Nm}^3\text{]} \cdot P \text{ [bar abs]} \cdot 273.15 \text{ [K]}}{T \text{ [K]} \cdot 1.013 \text{ [bar abs]}}$$

$$\rho_N \text{ [kg/Nm}^3\text{]} = \frac{\rho \text{ [kg/m}^3\text{]} \cdot T \text{ [K]} \cdot 1.013 \text{ [bar abs]}}{P \text{ [bar abs]} \cdot 273.15 \text{ [K]}}$$

$$\rho \text{ [lb/ft}^3\text{]} = \frac{\rho_N \text{ [lb/SCF]} \cdot P \text{ [psia]} \cdot 530 \text{ [}^\circ\text{R]}}{T \text{ [}^\circ\text{F} + 460] \cdot 14.7 \text{ [psia]}}$$

$$\rho_N \text{ [lb/SCF]} = \frac{\rho \text{ [lb/ft}^3\text{]} \cdot T \text{ [}^\circ\text{F} + 460] \cdot 14.7 \text{ [psia]}}{P \text{ [psia]} \cdot 530 \text{ [}^\circ\text{R]}}$$

The following formulae can be used to calculate the volume [Q] or corrected volume [Q<sub>N</sub>] in the case of ideal gases:

$$Q \text{ [m}^3\text{/h]} = \frac{Q_N \text{ [Nm}^3\text{/h]} \cdot T \text{ [K]} \cdot 1.013 \text{ [bar abs]}}{P \text{ [bar abs]} \cdot 273.15 \text{ [K]}}$$

$$Q_N \text{ [Nm}^3\text{/h]} = \frac{Q \text{ [m}^3\text{/h]} \cdot P \text{ [bar abs]} \cdot 273.15 \text{ [K]}}{T \text{ [K]} \cdot 1.013 \text{ [bar abs]}}$$

$$Q \text{ [ft}^3\text{/h]} = \frac{Q_N \text{ [SCF/h]} \cdot T \text{ [}^\circ\text{F} + 460] \cdot 14.7 \text{ [psia]}}{P \text{ [psia]} \cdot 530 \text{ [}^\circ\text{R]}}$$

$$Q_N \text{ [SCF/h]} = \frac{Q \text{ [ft}^3\text{/h]} \cdot P \text{ [psia]} \cdot 530 \text{ [}^\circ\text{R]}}{T \text{ [}^\circ\text{F} + 460] \cdot 14.7 \text{ [psia]}}$$

T = Operating temperature, P = operating pressure

## APPENDIX F ALUMINA RIG

Table 77 Test 1: Closed valve for refilling of alumina from the silo, cycle 1 not weighted, Alumina and fluoride dump weights: [grams] / feeder / cycle. Cycle 1 only alumina, cycle 2 to 7 alumina mixed with fluoride.

Dump nr.	Accumulated	Dump weight	Accumulated	Dump weight	Accumulated	Dump weight
	Feeder 2 / Cycle 2	Feeder 2 / Cycle 2	Feeder 3 / Cycle 3	Feeder 3 / Cycle 3	Feeder 4 / Cycle 4	Feeder 4 / Cycle 4
1		0	690	690	820	820
2		0	1730	1040	1800	980
3		0	2830	1100	2660	860
4		<b>810</b>	3780	<b>950</b>	3620	<b>960</b>
5		0	4830	1050	4560	940
6		0	5850	1020	5480	920
7		0	6870	1020	6380	900
8		0	7830	960	7220	840
9		0	8770	940	8090	870
10		0	9710	940	8940	850
11		0	10750	1040	9780	840
12	8860	0	11730	980	10610	830
13	9680	820	12710	980	11470	860
14	10540	860	13660	950	12330	860
15	11490	950	14680	1020	13180	850
16	12540	1050	15790	1110	14030	850
17	13510	970	16840	1050	14970	940
18	14780	1270	17960	1120	15970	1000
19	15940	1160	19010	1050	17030	1060
20	<b>17820</b>	1880	<b>20370</b>	1360	<b>18950</b>	1920
Average		1086		1066		1033
Stdev		336		127		341
Coeff of var		31 %		12 %		33 %

Accumulated	Dump weight	Accumulated	Dump weight	Accumulated	Dump weight
Feeder 5 / Cycle 5	Feeder 5 / Cycle 5	Feeder 6 / Cycle 6	Feeder 6 / Cycle 6	Feeder 7 / Cycle 7	Feeder 7 / Cycle 7
740	740	670	670	1080	1080
1610	870	1440	770	1910	830
2510	900	2290	850	2850	940
3460	<b>950</b>	3110	<b>820</b>	3740	890
4330	870	3930	820	4620	880
5220	890	4740	810	5520	900
6130	910	5550	810	6390	<b>870</b>
7070	940	6320	770	7280	890
7970	900	7110	790	8190	910
8920	950	7950	840	9030	840
9830	910	8750	800	9880	850
10740	910	9550	800	10780	900
11650	910	10460	910	11680	900
12550	900	11220	760	12550	870
13530	980	12070	850	13450	900
14540	1010	12880	810	14440	990
15700	1160	13720	840	15500	1060
16760	1060	14610	890	16510	1010
17640	880	15660	1050	17300	790
<b>18360</b>	720	<b>18190</b>	2530	<b>17990</b>	690
	952		1051		900
	124		561		113
	13 %		53 %		13 %

**Table 78 Test 1: Closed valve for refilling of alumina from the silo, cycle 1 not weighted, estimated to 145 kg (same as cycle 2). Alumina and fluoride mass balance: [kg] / feeder / cycle.**

Test 1: Alumina & fluoride 20-21 / 09 / 2010						
	Cycle 2	Cycle 3	Cycle 4	Cycle 5	Cycle 6	Cycle 7
Feeder 1	17 670	24510	25880	24570	20950	11010
Feeder 2	<b>17820</b>	22100	23670	24650	24570	7110
Feeder 3	17900	<b>20370</b>	21420	22900	23020	6900
Feeder 4	17850	18760	<b>18950</b>	19400	19730	8730
Feeder 5	17870	18610	18530	<b>18360</b>	18380	19290
Feeder 6	17890	18480	18470	18320	<b>18190</b>	18380
Feeder 7	18860	18810	18680	18380	18270	<b>17990</b>
Feeder 8	18680	19020	19050	18980	18520	12450
Average	18 068	20 083	20 581	20 695	20 204	12 733
Stdev	442	2171	2818	2843	2442	
Coeff of var	2 %	11 %	14 %	14 %	12 %	
Sum [kg]	145	161	165	166	162	132

**Table 79 Test 1: Alumina and fluoride total mass balance: 1074 [kg] material used / test.**

Test 1: Alumina & fluoride mass balance 20 - 21 / 09 / 2010					
Average	Stdev	Coeff of var	Tømming av renne		Høyde alumina målt mellom lukke F5 & F2
22716	3363	15 %	5940	F1+F2+F3+F4	C1: F5:33 cm / F2:23 cm
22562	2843	13 %			C2: F5: 27 cm / F2: 16 cm
21122	2109	10 %			C3: F5: 22 cm / F2: 12 cm
18938	717	4 %			C4: F5: 15 cm / F2: 6 cm
18350	288	2 %	10290	F5+F6+F7+F8	C5: F5: 7 cm / F2: 2.5 cm
18270	244	1 %			C6: F5: 2 cm / F2: 1 cm
18600	262	1 %	7500	F7	Not enough alumina left for C7!!
18850	236	1 %	6500	F8	
			30230		
<b>Total kg alumina &amp; fluoride used for Test 1</b>					
<b>1074</b>					
Cycle 1 not measured, estimated to 145 kg					

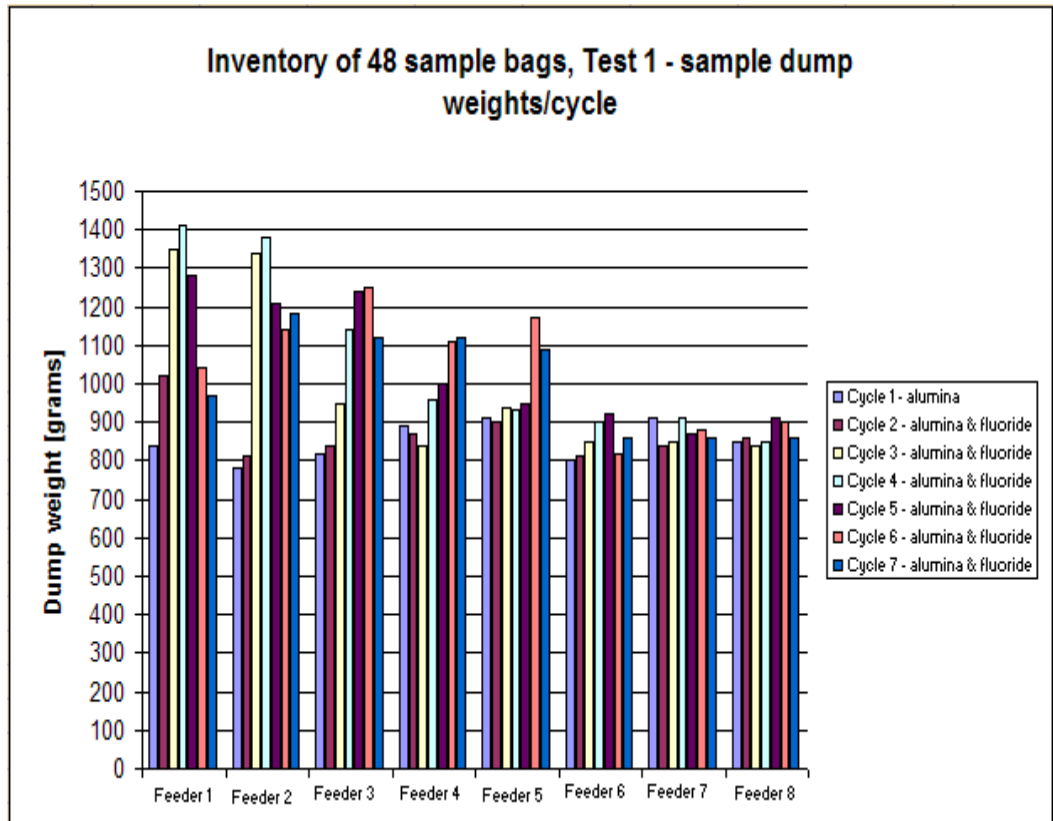


Figure 265 Test 1: Samples inventory

**Table 80 Test 2: Closed valve for refilling of alumina from the silo. Alumina and fluoride accumulated dump weights: [grams] / feeder / cycle. Cycle 1 only alumina, cycle 2 to 7 alumina mixed with fluoride.**

Dump nr.	Accumulated	Dump weight	Accumulated	Dump weight	Accumulated	Dump weight	Accumulated	Dump weight
	Feeder 7 / Cycle 1	Feeder 7 / Cycle 1	Feeder 1 / Cycle 2	Feeder 1 / Cycle 2	Feeder 2 / Cycle 3	Feeder 2 / Cycle 3	Feeder 3 / Cycle 4	Feeder 3 / Cycle 4
1	920	920	1260	1260	830	830	740	740
2	1940	1020	2110	850	1590	760	1560	820
3	2800	860	3040	930	2440	850	2430	870
4	3670	870	3980	940	3385	945	3250	820
5	4560	890	4900	920	4330	945	4050	800
6	5390	830	5820	920	5390	1060	4910	860
7	6270	880	6700	880	6340	950	5740	830
8	7130	860	7630	<b>930</b>	7240	900	6570	830
9	8010	880	8480	850	8180	940	7430	860
10	8890	880	9340	860	9120	940	8260	830
11	9780	890	10210	870	10070	950	9120	860
12	10660	880	11110	900	11120	1050	9970	850
13	11530	870	11940	830	12030	910	10800	830
14	12380	850	12850	910	12940	910	11690	890
15	13230	<b>850</b>	13780	930	13840	900	12540	850
16	14080	850	14790	1010	14770	930	13430	890
17	15040	960	15920	1130	15770	1000	14360	930
18	16100	1060	17030	1110	16910	1140	15360	1000
19	17180	1080	17990	960	18050	1140	16440	1080
20	<b>18790</b>	1610	<b>19150</b>	1160	<b>19780</b>	1730	<b>19090</b>	2650
Average		1000		998		1067		1104
Stdev		246		113		266		586
Coef of var		25 %		11 %		25 %		53 %

Accumulated	Dump weight	Accumulated	Dump weight	Accumulated	Dump weight
Feeder 4 / Cycle 5	Feeder 4 / Cycle 5	Feeder 5 / Cycle 6	Feeder 5 / Cycle 6	Feeder 6 / Cycle 7	Feeder 6 / Cycle 7
740	740	700	700	740	740
1530	790	1540	840	1560	820
2380	850	2400	860	2320	760
3230	850	3260	860	3160	840
4070	840	4150	890	4030	870
4900	830	5030	880	4890	860
5760	860	5920	890	5750	860
6650	890	6830	910	6600	850
7480	830	7740	910	7450	850
8310	830	8610	870	8400	950
9180	870	9540	930	9190	790
10010	830	10390	850	10000	810
10810	800	11280	890	10790	790
11630	820	12230	950	11740	950
12490	860	13230	1000	12620	880
13410	920	14200	970	13540	920
14280	870	15340	1140	14550	1010
15350	1070	16480	1140	15680	1130
16480	1130	17390	910	16660	980
<b>18460</b>	<b>1980</b>	<b>18290</b>	<b>900</b>	<b>18000</b>	<b>1340</b>
	1033		973		982
	372		104		167
	36 %		11 %		17 %

**Table 81 Test 2: Closed valve for refilling of alumina from the silo. Alumina and fluoride mass balance: [kg] / feeder / cycle.**

Test 2: Alumina & fluoride 22-23 / 09 / 2010							
	Cycle 1	Cycle 2	Cycle 3	Cycle 4	Cycle 5	Cycle 6	Cycle 7
Feeder 1	18 630	<b>19150</b>	22510	23830	22830	20450	19250
Feeder 2	18700	18790	<b>19780</b>	20460	21840	22710	8140
Feeder 3	18670	18970	18900	<b>19090</b>	19810	20750	7330
Feeder 4	18610	18650	18700	18530	<b>18460</b>	18460	16410
Feeder 5	18680	18890	18730	18690	18480	<b>18290</b>	18600
Feeder 6	18590	18740	18660	18660	18430	18170	<b>18000</b>
Feeder 7	<b>18790</b>	18890	18830	18770	18600	18360	18100
Feeder 8	19220	18970	19000	19040	18760	18410	18470
Average	18 736	18 881	19 389	19 634	19 651	19 450	
Stdev	205	156	1311	1802	1736	1671	
Coef of var	1 %	1 %	7 %	9 %	9 %	9 %	
Sum	150	151	155	157	157	156	163

**Table 82 Test 2: Alumina and fluoride total mass balance: 1089 [kg] material used / test.**

Test 2: Alumina & fluoride mass balance 22 - 23 / 09 / 2010					
Average	Stdev	Coeff of var	Tømming av renne		Høyde alumina målt mellom lukke F5 & F2
21233	2129	10 %	9810	F1+F2+F3+F4	C1: F5:34 cm / F2:27 cm
20380	1630	8 %			C2: F5: 28 cm / F2: 18 cm
19365	781	4 %			C3: F5: 22 cm / F2: 13 cm
18568	101	1 %			C4: F5: 17 cm / F2: 8 cm
18627	211	1 %	8260	F5+F6	C5: F5: 10 cm / F2: 3 cm
18542	210	1 %			C6: F5: 2.5 cm / F2: 1 cm
18707	196	1 %	12970	F7	Not enough alumina left for C7!!
18900	282	1 %	7600	F8	
			<b>38640</b>		
<b>Total kg alumina &amp; fluoride used for Test 2</b>					
<b>1089</b>					

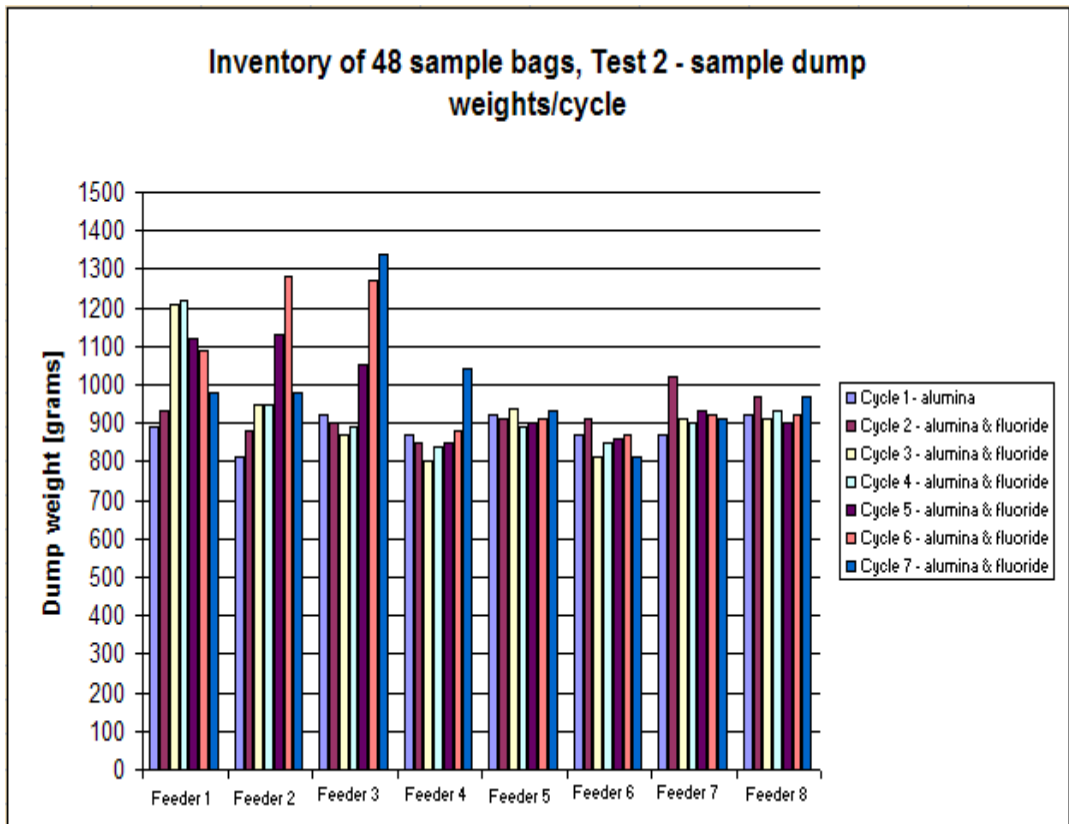


**Figure 266 Test 2: Samples inventory**

**Table 83 Test 3: Closed valve for refilling of alumina from the silo. Alumina and fluoride accumulated and individual dump weights: [grams] / feeder / cycle. Cycle 1 only alumina, cycle 2 to 6 alumina mixed with fluoride.**

Dump nr.	Accumulated	Dump weight	Accumulated	Dump weight	Accumulated	Dump weight
	Feeder 1 / Cycle 1	Feeder 1 / Cycle 1	Feeder 2 / Cycle 2	Feeder 2 / Cycle 2	Feeder 3 / Cycle 3	Feeder 3 / Cycle 3
1	640	640	770	770	760	760
2	1450	810	1540	770	1600	840
3	2330	880	2420	880	2480	880
4	3210	880	3280	860	3400	920
5	4120	910	4150	870	4400	1000
6	5070	950	5000	850	5340	940
7	5980	910	5830	830	6260	920
8	6880	900	6750	920	7090	830
9	7780	900	7660	910	7900	810
10	8670	890	8560	900	8740	840
11	9520	850	9460	900	9610	870
12	10430	910	10300	840	10520	910
13	11290	860	11180	880	11420	900
14	12190	900	12000	820	12290	870
15	13150	960	12860	860	13190	900
16	14150	1000	13770	910	14110	920
17	15410	1260	14740	970	15080	970
18	16510	1100	15770	1030	16220	1140
19	17500	990	16830	1060	17320	1100
20	<b>18650</b>	1150	<b>18620</b>	1790	<b>18950</b>	1630
Average		1011		1020		1039
Stdev		134		300		241
Coeff of var		13 %		29 %		23 %

	Accumulated	Dump weight	Accumulated	Dump weight	Accumulated	Dump weight
	Feeder 4 / Cycle 4	Feeder 4 / Cycle 4	Feeder 5 / Cycle 5	Feeder 5 / Cycle 5	Feeder 6 / Cycle 6	Feeder 6 / Cycle 6
750	750	750	830	830	800	800
1620	870	870	1740	910	1650	850
2440	820	820	2650	910	2490	840
3320	880	880	3600	950	3390	900
4190	870	870	4560	960	4310	920
5040	850	850	5570	1010	5230	920
5890	850	850	6540	970	6110	880
6740	850	850	7490	950	7000	890
7610	870	870	8410	920	7890	890
8480	870	870	9330	920	8760	870
9330	850	850	10280	950	9590	830
10180	850	850	11200	920	10430	840
11050	870	870	12170	970	11280	850
11890	840	840	13210	1040	12160	880
12750	860	860	14210	1000	13060	900
13670	920	920	15350	1140	13990	930
14570	900	900	16430	1080	15060	1070
15650	1080	1080	17330	900	16120	1060
16640	990	990	17910	580	16980	860
<b>18260</b>	1620	1620	<b>18160</b>	250	<b>17940</b>	960
		996		879		934
		246		285		81
		25 %		32 %		9 %



**Table 84 Test 3: Closed valve for refilling of alumina from the silo. Alumina and fluoride mass balance: [kg] / feeder / cycle.**

Test 3: Alumina & fluoride 28 / 09 / 2010							
	Cycle 1	Cycle 2	Cycle 3	Cycle 4	Cycle 5	Cycle 6	Cycle 7
Feeder 1	<b>18 650</b>	18600	23060	24570	23800	8690	
Feeder 2	18600	<b>18620</b>	19940	20950	22300	7590	
Feeder 3	18930	18770	<b>18950</b>	19080	19950	7090	
Feeder 4	18820	18660	18670	<b>18260</b>	18320	14560	
Feeder 5	18820	18750	18620	18320	<b>18160</b>	18240	
Feeder 6	18700	18810	18550	18360	18210	<b>17940</b>	
Feeder 7	18890	18700	18500	18410	18240	17960	
Feeder 8	19370	19110	18920	18600	18450	17030	
Average	18 848	18 753	19 401	19 569	19 679		
Stdev	241	162	1549	2210	2198		
Coeff of var	1 %	1 %	8 %	11 %	11 %		
Sum [kg]	151	150	155	157	157	144	

**Table 85 Test 3: Alumina and fluoride total mass balance: 914 [kg] material used / test.**

Test 3: Alumina & fluoride mass balance 28 / 09 / 2010					
Average	Stdev	Coeff of var	Tømming av renne		Høyde alumina målt mellom lukke F5 & F2
21736	2890	13 %	6800	F1+F2+F3+F4	Start C1: F5:31 cm / F2:22 cm
20082	1583	8 %			C1: F5: 28.5 cm / F2: 18 cm
19136	468	2 %			C2: F5: 22 cm / F2: 14 cm
18546	243	1 %			C3: F5: 16 cm / F2: 7.5 cm
18534	284	2 %	6860	F5	C4: F5: 9 cm / F2: 2.5 cm
18526	244	1 %	7930	F6+F7	C5: F5: 2.5 cm / F2: 1 cm
18548	253	1 %			Not enough alumina left for C6!!
18890	373	2 %	12910	F8	
			<b>34500</b>		
Total kg alumina & fluoride used for Test 3					
<b>914</b>					

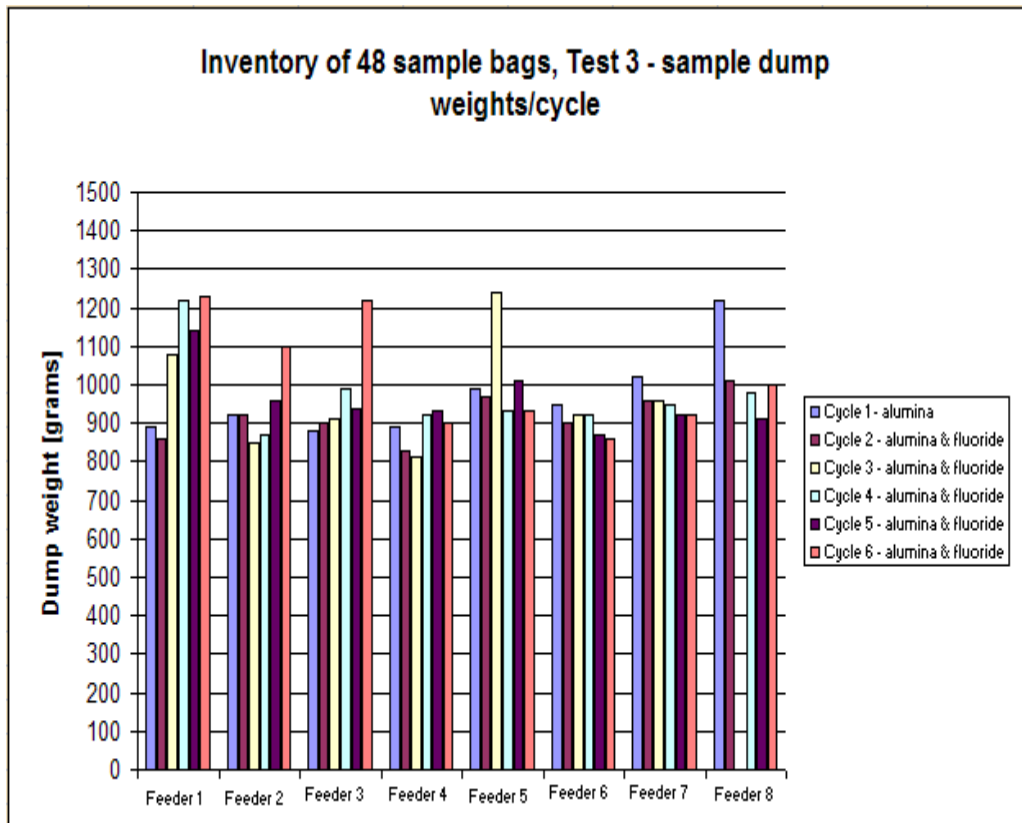


**Figure 267 Test 3: Samples inventory**

**Table 86 Test 4: Closed valve for refilling of alumina from the silo. Alumina and fluoride accumulated and individual dump weights: [grams] / feeder / cycle. Cycle 1 only alumina, cycle 2 to 6 alumina mixed with fluoride.**

Test 4: Alumina/ Cycle 1							
Dump nr.	Accumulated	Dump weight	Accumulated	Dump weight	Accumulated	Dump weight	
	Feeder 1 / Cycle 1	Feeder 1 / Cycle 1	Feeder 2 / Cycle 1	Feeder 2 / Cycle 1	Feeder 3 / Cycle 1	Feeder 3 / Cycle 1	
1	790	790	710	710	860	860	
2	1860	1070	1470	760	1640	780	
3	2790	930	2350	880	2490	850	
4	3730	940	3260	910	3350	860	
5	4670	940	4120	860	4210	860	
6	5710	1040	5040	920	5070	860	
7	6740	1030	5950	910	5970	900	
8	7720	980	6890	940	6850	880	
9	8670	950	7800	910	7730	880	
10	9590	920	8700	900	8570	840	
11	10580	990	8720	20	9460	890	
12	11550	970	10490	1770	10310	850	
13	12610	1060	11380	890	11170	860	
14	13610	1000	12270	890	12070	900	
15	14660	1050	13160	890	12970	900	
16	15850	1190	14150	990	13910	940	
17	17020	1170	15180	1030	14950	1040	
18	18040	1020	16310	1130	16140	1190	
19	18520	480	17380	1070	17260	1120	
20	<b>18810</b>	290	<b>18800</b>	1420	<b>18930</b>	1670	
Average		911		1024		1053	
Stdev		312		173		259	
Coef of var		34 %		17 %		25 %	

Test 4: Alumina + Fluoride / Cycle 2								
Dump nr.	Accumulated	Dump weight	Accumulated	Dump weight	Accumulated	Dump weight	Accumulated	Dump weight
	Feeder 1 / Cycle 2	Feeder 1 / Cycle 2	Feeder 2 / Cycle 2	Feeder 2 / Cycle 2	Feeder 3 / Cycle 2	Feeder 3 / Cycle 2	Feeder 4 / Cycle 2	Feeder 4 / Cycle 2
1	980	980	700	700	950	950	860	860
2	1910	930	1550	850	1860	910	1610	750
3	2960	1050	2440	890	2820	960	2480	870
4	3900	940	3350	910	3760	940	3390	910
5	4870	970	4290	940	4680	920	4290	900
6	5810	940	5250	<b>960</b>	5570	890	5220	930
7	6700	890	6150	900	6460	890	6110	890
8	7600	900	7060	910	7430	<b>970</b>	7060	<b>950</b>
9	8530	930	7960	900	8540	1110	7980	920
10	9470	940	8870	910	9510	970	8890	910
11	10340	870	9810	940	10370	860	9790	900
12	11240	900	10670	860	11290	920	10670	880
13	12160	920	11540	870	12200	910	11600	930
14	13060	900	12430	890	13120	920	12510	910
15	14080	1020	13340	910	14090	970	13430	920
16	15110	1030	14310	970	15320	1230	14410	980
17	16220	<b>1110</b>	15410	1100	16580	1260	15390	980
18	17320	1100	16500	1090	17610	1030	16450	1060
19	18140	820	17480	980	18390	780	17440	990
20	<b>18850</b>	710	<b>18690</b>	1210	<b>18930</b>	540	<b>18910</b>	1470
Average		950		992		953		1017
Stdev		131		116		218		177
Coef of var		14 %		12 %		23 %		17 %

Test 4: Alumina + Fluoride / Cycle 3								
Dump nr.	Accumulated	Dump weight	Accumulated	Dump weight	Accumulated	Dump weight	Accumulated	Dump weight
	Feeder 1 / Cycle 3	Feeder 1 / Cycle 3	Feeder 2 / Cycle 3	Feeder 2 / Cycle 3	Feeder 3 / Cycle 3	Feeder 3 / Cycle 3	Feeder 4 / Cycle 3	Feeder 4 / Cycle 3
1	900	900	840	840	810	810	860	860
2	2130	1230	1830	990	1720	910	1700	840
3	3520	1390	2860	1030	2660	940	2630	930
4	4740	1220	3890	1030	3650	<b>990</b>	3590	960
5	5980	1240	4870	980	4630	980	4560	970
6	7230	1250	5870	1000	5630	1000	5550	<b>990</b>
7	8490	1260	6880	1010	6550	920	6470	920
8	9710	1220	7940	1060	7520	970	7380	910
9	10960	1250	8920	980	8450	930	8310	930
10	12220	1260	9880	960	9380	930	9290	980
11	13460	1240	10840	960	10300	920	10220	930
12	14680	1220	11810	970	11220	920	11120	900
13	15900	1220	12790	980	12160	940	12030	910
14	17140	1240	13780	990	13110	950	12990	960
15	18390	1250	14810	1030	14010	900	13950	960
16	19740	<b>1350</b>	15770	960	15020	1010	14940	990
17	21040	1300	16920	<b>1150</b>	16160	1140	16060	1120
18	22130	1090	18060	1140	17280	1120	17100	1040
19	22770	640	19050	990	18210	930	17980	880
20	<b>23090</b>	320	<b>20220</b>	1170	<b>19100</b>	890	<b>18740</b>	760
Average		1070		1049		986		953
Stdev		351		82		90		101
Coef of var		33 %		8 %		9 %		11 %

Test 4: Alumina + Fluoride / Cycle 4								
Dump nr.	Accumulated	Dump weight	Accumulated	Dump weight	Accumulated	Dump weight	Accumulated	Dump weight
	Feeder 1 / Cycle 4	Feeder 1 / Cycle 4	Feeder 2 / Cycle 4	Feeder 2 / Cycle 4	Feeder 3 / Cycle 4	Feeder 3 / Cycle 4	Feeder 4 / Cycle 4	Feeder 4 / Cycle 4
1	930	930	770	770	760	760	850	850
2	2190	1260	1660	890	1680	920	1730	880
3	3510	1320	2680	1020	2630	950	2680	950
4	4820	1310	3720	1040	3600	<b>970</b>	3620	<b>940</b>
5	6120	1300	4740	1020	4550	950	4610	990
6	7390	1270	5780	1040	5500	950	5580	970
7	8660	1270	6800	1020	6440	940	6530	950
8	9960	1300	7800	1000	7380	940	7440	910
9	11210	1250	8770	970	8330	950	8570	1130
10	12430	1220	9720	950	9300	970	9440	870
11	13600	1170	10750	1030	10260	960	10340	900
12	14820	1220	11780	1030	11220	960	11280	940
13	16140	1320	12770	990	12290	1070	12190	910
14	17440	<b>1300</b>	14010	1240	13300	1010	13090	900
15	18780	1340	15080	1070	14320	1020	14070	980
16	20210	1430	16220	<b>1140</b>	15400	1080	15110	1040
17	21670	1460	17450	1230	16580	1180	16290	1180
18	22980	1310	18660	1210	17740	1160	17310	1020
19	23910	930	19740	1080	18610	870	18020	710
20	<b>24380</b>	470	<b>21140</b>	1400	<b>19340</b>	730	<b>18600</b>	580
Average		1208		1156		1010		918
Stdev		315		127		141		179
Coeff of var		26 %		11 %		14 %		19 %

Test 4: Alumina + Fluoride / Cycle 5								
Dump nr.	Accumulated	Dump weight	Accumulated	Dump weight	Accumulated	Dump weight	Accumulated	Dump weight
	Feeder 1 / Cycle 5	Feeder 1 / Cycle 5	Feeder 2 / Cycle 5	Feeder 2 / Cycle 5	Feeder 3 / Cycle 5	Feeder 3 / Cycle 5	Feeder 4 / Cycle 5	Feeder 4 / Cycle 5
1	1180	1180	950	950	910	910	760	760
2	2430	1250	2030	1080	1920	1010	1620	860
3	3570	1140	3240	1210	2970	1050	2550	930
4	4760	1190	4340	1100	4030	1060	3470	920
5	5870	1110	5510	1170	5170	1140	4400	930
6	7050	1180	6680	1170	6200	1030	5340	940
7	8200	1150	7850	1170	7180	980	6270	930
8	9340	1140	9000	1150	8290	1110	7170	900
9	10520	1180	10170	1170	9350	1060	8050	880
10	11670	1150	11260	1090	10410	1060	8950	900
11	12810	1140	12340	1080	11480	1070	9860	910
12	14010	<b>1200</b>	13470	1130	12570	1090	10780	920
13	15220	1210	14690	1220	13680	1110	11680	900
14	16460	1240	15890	1200	15030	1350	12580	900
15	17670	1210	17080	1190	16490	1460	13470	890
16	19010	1340	18320	1240	17870	<b>1380</b>	14660	1190
17	20520	1510	19640	1320	19080	1210	15890	<b>1230</b>
18	21850	1330	20870	1230	19960	880	16940	1050
19	22740	890	21860	990	20440	480	17800	860
20	<b>23210</b>	470	<b>22670</b>	810	<b>20660</b>	220	<b>18520</b>	720
Average		1154		1144		1017		962
Stdev		305		156		423		164
Coeff of var		26 %		14 %		42 %		17 %

Test 4: Alumina + Fluoride / Cycle 6								
Dump nr.	Accumulated	Dump weight	Accumulated	Dump weight	Accumulated	Dump weight	Accumulated	Dump weight
	Feeder 1 / Cycle 6	Feeder 1 / Cycle 6	Feeder 2 / Cycle 6	Feeder 2 / Cycle 6	Feeder 3 / Cycle 6	Feeder 3 / Cycle 6	Feeder 4 / Cycle 6	Feeder 4 / Cycle 6
1	1180	1180	1160	1160	1160	1160	930	930
2	2270	1090	2330	1170	2320	1160	1870	940
3	3290	1020	3460	1130	3460	1140	2830	960
4	4290	1000	4570	1110	4600	1140	3810	980
5	5280	990	5700	1130	5790	1190	4780	970
6	6260	980	6850	1150	6960	1170	5750	970
7	7250	990	7970	1120	8090	1130	6760	1010
8	8230	980	9130	1160	9240	1150	7720	960
9	9270	1040	10250	1120	10370	1130	8710	990
10	10260	990	11370	1120	11480	1110	9670	960
11	11250	990	12490	1120	12620	1140	10610	940
12	12290	1040	13640	1150	13820	1200	11650	1040
13	13300	1010	14740	1100	15000	1180	12650	1000
14	14340	1040	15830	1090	16230	1230	13630	980
15	15440	1100	17020	1190	17460	1230	14650	1020
16	16640	1200	18350	1330	18840	1380	15830	1180
17	17900	1260	19830	1480	20070	1230	16930	1100
18	19060	1160	21250	1420	20960	890	17830	900
19	19820	760	22390	1140	21420	460	18430	600
20	<b>20180</b>	360	<b>23390</b>	1000	<b>21580</b>	160	<b>18680</b>	250
Average		988		1207		989		890
Stdev		276		165		413		289
Coeff of var		28 %		14 %		42 %		32 %

**Table 87 Test 4: Closed valve for refilling of alumina from the silo. Alumina and fluoride mass balance: [kg] / feeder / cycle.**

Test 4: Alumina & fluoride 29 / 09 - 01 / 10 / 2010							
	Cycle 1	Cycle 2	Cycle 3	Cycle 4	Cycle 5	Cycle 6	Cycle 7
Feeder 1	18 810	18 850	23 090	24 380	23 210	20 180	11 090
Feeder 2	18 800	18 690	20 220	21 140	22 670	23 390	7 769
Feeder 3	18 930	18 930	19 100	19 340	20 660	21 580	6 730
Feeder 4	18 950	18 900	18 740	18 600	18 520	18 680	11 880
Feeder 5	18 950	18 990	18 680	18 450	18 480	18 260	19 090
Feeder 6	18 960	19 020	18 760	18 450	18 510	18 300	18 040
Feeder 7	19 120	19 330	19 040	18 820	18 640	18 480	18 080
Feeder 8	19 690	19 700	19 430	19 300	19 050	18 720	18 400
Average	19 026	19 051	19 633	19 810	19 968	19 699	13 885
Stdev	286	319	1485	2045	1976	1886	5110
Coeff of var	2 %	2 %	8 %	10 %	10 %	10 %	37 %
Sum	152	152	157	158	160	158	111

**Table 88 Test 4: Alumina and fluoride total mass balance: 1082 [kg] material used / test.**

Test 4: Alumina & fluoride 29 / 09 - 01 / 10 / 2010					
Average	Stdev	Coeff of var	Tømming av renne		Høyde alumina målt mellom lukke F5 & F2
21420	2438	11 %	7310	F1+F2+F3	Start C1: F5:34.5 cm / F2:27 cm
20818	1955	9 %	11200	F4+F5+F6	C1: F5: 34 cm / F2: 24 cm
19757	1106	6 %			C2: F5: 28 cm / F2: 18 cm
18732	168	1 %			C3: F5: 22 cm / F2: 12 cm
18635	292	2 %			C4: F5: 15 cm / F2: 6 cm
18667	292	2 %			C5: F5: 8 cm / F2: 2 cm
18905	317	2 %	15070	F7+F8	C6: F5: 2.5 cm / F2: cm
19315	381	2 %			Not enough alumina left for C7!!
			33580		
			Total kg alumina & fluoride used for Test 4		
1 082					

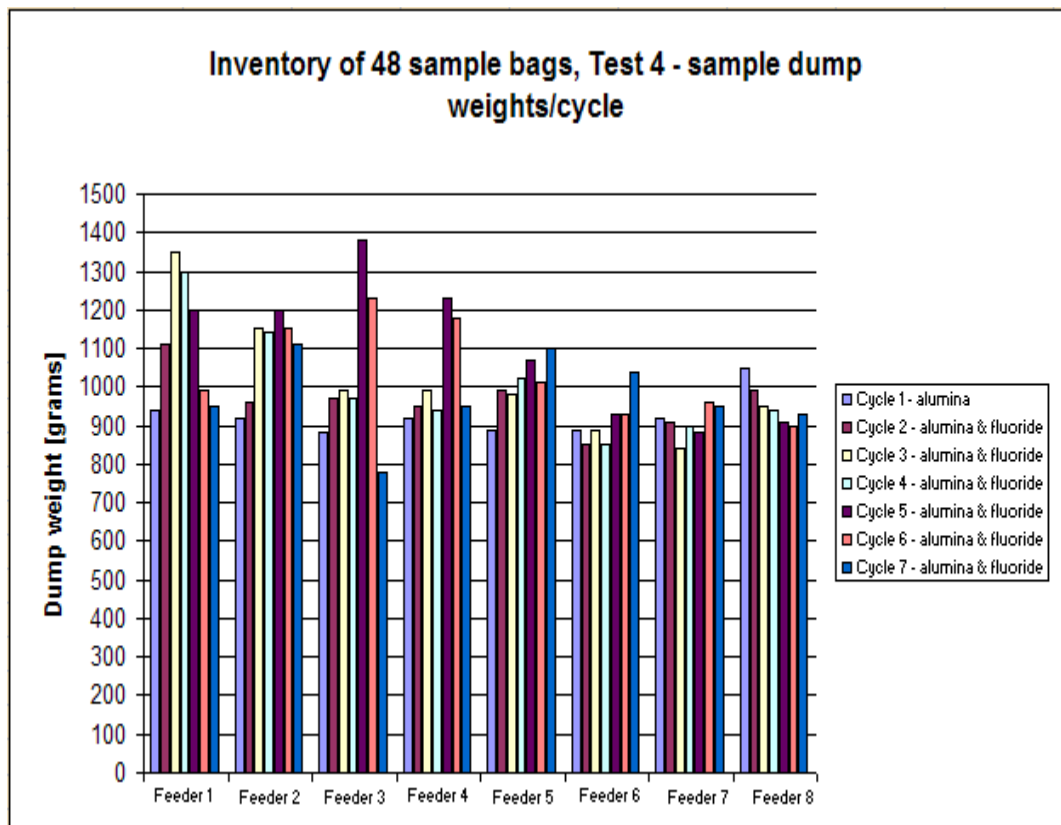


**Figure 268 Test 4: Samples inventory**

Table 89 Test 4 Average alumina and fluoride [kg/feeder/cycle]

Test 4 [kg / feeder / cycle]								
	Feeder 1	Feeder 2	Feeder 3	Feeder 4	Feeder 5	Feeder 6	Feeder 7	Feeder 8
Cycle 1	18.81	18.80	18.93	18.95	18.95	18.96	19.12	19.69
Cycle 2	18.85	18.69	18.93	18.90	18.99	19.02	19.33	19.70
Cycle 3	23.09	20.22	19.10	18.74	18.68	18.76	19.04	19.43
Cycle 4	24.38	21.14	19.34	18.60	18.45	18.45	18.82	19.30
Cycle 5	23.21	22.67	20.66	18.52	18.48	18.51	18.64	19.05
Cycle 6	20.18	23.39	21.58	18.68	18.26	18.30	18.48	18.72
Cycle 7	Empty				19.09	18.04	18.08	18.40

Table 90 Test 4 Method of calculation. Cycle 1, only alumina is considered the 0 line on the X axis.

Difference from average							
Feeder 1	Feeder 2	Feeder 3	Feeder 4	Feeder 5	Feeder 6	Feeder 7	Feeder 8
0.00	0.00	0.00	0.00	0.00	0.00	0.00	0.00
0.04	-0.11	0.00	-0.05	0.04	0.06	0.21	0.01
4.28	1.42	0.17	-0.21	-0.27	-0.20	-0.08	-0.26
5.57	2.34	0.41	-0.35	-0.50	-0.51	-0.30	-0.39
4.40	3.87	1.73	-0.43	-0.47	-0.45	-0.48	-0.64
1.37	4.59	2.65	-0.27	-0.69	-0.66	-0.64	-0.97
Empty				0.14	-0.92	-1.04	-1.29

Table 91 Test 5: Closed valve for refilling of alumina from the silo. Alumina and fluoride accumulated and individual dump weights: [grams] / feeder / cycle. Cycle 1 only alumina, cycle 2 to 6 alumina mixed with fluoride.

Test 5: Alumina/ Cycle 1								
Dump nr.	Accumulated Feeder 1 / Cycle 1	Dump weight Feeder 1 / Cycle 1	Accumulated Feeder 2 / Cycle 1	Dump weight Feeder 2 / Cycle 1	Accumulated Feeder 3 / Cycle 1	Dump weight Feeder 3 / Cycle 1	Accumulated Feeder 4 / Cycle 1	Dump weight Feeder 4 / Cycle 1
1	670	670						
2	1570	900						
3	2520	950						
4	3460	940						
5	4330	870						
6	5250	920						
7	6150	900						
8	7070	920						
9	7960	890						
10	8890	930						
11	9820	930						
12	10800	980						
13	11740	940						
14	12700	960						
15	13670	970						
16	14660	990						
17	15830	1170						
18	16910	1080						
19	17720	810						
20	18290	570						
Average		915						
Stdev		126						
Coeff of var		14 %						

Test 5: Alumina + Fluoride / Cycle 2								
	Accumulated	Dump weight	Accumulated	Dump weight	Accumulated	Dump weight	Accumulated	Dump weight
Dump nr.	Feeder 1 / Cycle 2	Feeder 1 / Cycle 2	Feeder 2 / Cycle 2	Feeder 2 / Cycle 2	Feeder 3 / Cycle 2	Feeder 3 / Cycle 2	Feeder 4 / Cycle 2	Feeder 4 / Cycle 2
1	850	850	780	780		0	900	900
2	1700	850	1625	845		0	1690	790
3	2660	960	2470	845	2600	0	2600	910
4	3620	960	3370	900	3590	990	3600	1000
5	4490	870	4300	930	4610	1020	4580	980
6	5460	970	5200	900	5490	880	5580	1000
7	6440	980	6050	850	6340	850	6530	950
8	7350	910	6950	900	7250	910	7520	990
9	8290	940	7770	820	8100	850	8440	920
10	9200	910	8680	910	9060	960	9410	970
11	10100	900	9590	910	9990	930	10390	980
12	11020	920	10470	880	11110	1120	11320	930
13	11910	890	11350	880	12080	970	12220	900
14	12850	940	12250	900	13000	920	13140	920
15	13800	950	13130	880	13960	960	14100	960
16	14820	1020	14130	1000	15000	1040	15190	1090
17	16010	1190	15170	1040	16240	1240	16390	1200
18	17080	1070	16330	1160	17360	1120	17460	1070
19	17920	840	17400	1070	18300	940	18270	810
20	18580	660	18810	1410	19160	860	18840	570
Average		929		941		828		942
Stdev		103		142		370		126
Coeff of var		11 %		15 %		45 %		13 %

Test 5: Alumina + Fluoride / Cycle 3								
	Accumulated	Dump weight	Accumulated	Dump weight	Accumulated	Dump weight	Accumulated	Dump weight
Dump nr.	Feeder 1 / Cycle 3	Feeder 1 / Cycle 3	Feeder 2 / Cycle 3	Feeder 2 / Cycle 3	Feeder 3 / Cycle 3	Feeder 3 / Cycle 3	Feeder 4 / Cycle 3	Feeder 4 / Cycle 3
1	860	860	700	700	840	840	890	890
2	1870	1010	1550	850	1650	810	1830	940
3	3010	1140	2470	920	2610	960	2810	980
4	4070	1060	3410	940	3480	870	3770	960
5	5140	1070	4310	900	4380	900	4710	940
6	6210	1070	5250	940	5310	930	5680	970
7	7250	1040	6170	920	6200	890	6560	880
8	8380	1130	7080	910	7080	880	7460	900
9	9380	1000	7960	880	7960	880	8490	1030
10	10430	1050	8860	900	8910	950	9390	900
11	11470	1040	9830	970	9810	900	10300	910
12	12500	1030	10710	880	10770	960	11210	910
13	13480	980	11620	910	11800	1030	12170	960
14	14460	980	12570	950	12910	1110	13230	1060
15	15640	1180	13510	940	14010	1100	14360	1130
16	16740	1100	14440	930	15160	1150	15520	1160
17	17790	1050	15440	1000	16490	1330	16500	980
18	18900	1110	16530	1090	17640	1150	17500	1000
19	20130	1230	17730	1200	18440	800	18150	650
20	22880	2750	19900	2170	19050	610	18460	310
Average		1144		995		953		923
Stdev		386		293		158		178
Coeff of var		34 %		29 %		17 %		19 %

Test 5: Alumina + Fluoride / Cycle 4								
	Accumulated	Dump weight	Accumulated	Dump weight	Accumulated	Dump weight	Accumulated	Dump weight
Dump nr.	Feeder 1 / Cycle 4	Feeder 1 / Cycle 4	Feeder 2 / Cycle 4	Feeder 2 / Cycle 4	Feeder 3 / Cycle 4	Feeder 3 / Cycle 4	Feeder 4 / Cycle 4	Feeder 4 / Cycle 4
1	930	930	820	820	810	810	890	890
2	2010	1080	1740	920	1690	880	1850	960
3	3090	1080	2710	970	2600	910	2780	930
4	4190	1100	3640	930	3560	960	3750	970
5	5330	1140	4590	950	4510	950	4690	940
6	6420	1090	5550	960	5450	940	5610	920
7	7480	1060	6520	970	6370	920	6560	950
8	8550	1070	7500	980	7340	970	7450	890
9	9660	1110	8390	890	8270	930	8360	910
10	10750	1090	9330	940	9180	910	9280	920
11	11800	1050	10300	970	10080	900	10230	950
12	12960	1160	11310	1010	11010	930	11160	930
13	14100	1140	12230	920	12030	1020	12090	930
14	15110	1010	13180	950	13000	970	13030	940
15	16440	1330	14130	950	13990	990	14060	1030
16	17600	1160	15090	960	14970	980	15220	1160
17	18820	1220	16100	1010	16150	1180	16360	1140
18	20130	1310	17130	1030	17290	1140	17330	970
19	21640	1510	18260	1130	18230	940	17990	660
20	24260	2620	20860	2600	19100	870	18320	330
Average		1213		1043		955		916
Stdev		355		371		84		169
Coeff of var		29 %		36 %		9 %		18 %

Test 5: Alumina + Fluoride / Cycle 5								
	Accumulated	Dump weight	Accumulated	Dump weight	Accumulated	Dump weight	Accumulated	Dump weight
Dump nr.	Feeder 1 / Cycle 5	Feeder 1 / Cycle 5	Feeder 2 / Cycle 5	Feeder 2 / Cycle 5	Feeder 3 / Cycle 5	Feeder 3 / Cycle 5	Feeder 4 / Cycle 5	Feeder 4 / Cycle 5
1	880	880	860	860	790	790	790	790
2	1940	1060	1890	1030	1840	1050	1780	990
3	2930	990	2880	990	2810	970	2730	950
4	3980	1050	3910	1030	3790	980	3710	980
5	4980	1000	4970	1060	4770	980	4690	980
6	6050	1070	6020	1050	5730	960	5630	940
7	7040	990	7080	1060	6730	1000	6590	960
8	8140	1100	8110	1030	7680	950	7500	910
9	9240	1100	9100	990	8680	1000	8480	980
10	10330	1090	10140	1040	9700	1020	9440	960
11	11400	1070	11110	970	10720	1020	10410	970
12	12490	<b>1090</b>	12020	910	11680	960	11340	930
13	13570	1080	13050	1030	12670	990	12300	960
14	14600	1030	14070	<b>1020</b>	13650	980	13310	1010
15	15690	1090	15060	990	14660	1010	14270	960
16	16830	1140	16160	1100	15690	1030	15410	<b>1140</b>
17	18020	1190	17230	1070	16740	1050	16530	1120
18	19400	1380	18340	1110	17890	1150	17470	940
19	20790	1390	19580	1240	18960	1070	18090	620
20	<b>22750</b>	1960	<b>22270</b>	2690	<b>20110</b>	1150	<b>18380</b>	290
Average		1138		1114		1006		919
Stdev		227		379		75		182
Coeff of var		20 %		34 %		8 %		20 %

Test 5: Alumina + Fluoride / Cycle 6								
	Accumulated	Dump weight	Accumulated	Dump weight	Accumulated	Dump weight	Accumulated	Dump weight
Dump nr.	Feeder 1 / Cycle 6	Feeder 1 / Cycle 6	Feeder 2 / Cycle 6	Feeder 2 / Cycle 6	Feeder 3 / Cycle 6	Feeder 3 / Cycle 6	Feeder 4 / Cycle 6	Feeder 4 / Cycle 6
1	940	940	960	960	940	940	970	970
2	1970	1030	1970	1010	1950	1010	1940	970
3	2960	990	2990	1020	3360	1410	2850	910
4	3910	950	4010	1020	4430	1070	3780	930
5	4900	990	5030	1020	5470	1040	4740	960
6	5870	970	6060	1030	6540	1070	5710	970
7	6860	990	7050	990	7520	980	6680	970
8	7830	970	8040	990	8520	1000	7620	940
9	8760	930	9030	990	9560	1040	8550	930
10	9740	980	10070	1040	10530	970	9490	940
11	10770	1030	11070	1000	11470	940	10640	1150
12	11730	960	12110	1040	12580	1110	11580	940
13	12710	980	13060	950	13660	1080	12560	980
14	13730	<b>1020</b>	14050	990	14660	1000	13500	940
15	14800	1070	15070	1020	15730	1070	14480	980
16	15940	1140	16150	<b>1080</b>	16870	1140	15570	1090
17	17300	1360	17190	1040	18310	<b>1440</b>	16830	<b>1260</b>
18	18520	1220	18360	1170	19590	1280	17710	880
19	19250	730	19690	1330	20610	1020	18290	580
20	<b>19660</b>	410	<b>22660</b>	2970	<b>21500</b>	890	<b>18560</b>	270
Average		983		1133		1075		928
Stdev		183		440		146		200
Coeff of var		19 %		39 %		14 %		22 %

Test 5: Alumina + Fluoride / Cycle 7

**Table 92 Test 5: Closed valve for refilling of alumina from the silo. Alumina and fluoride mass balance: [kg] / feeder / cycle.**

Test 5: Alumina & fluoride ? / 10 / 2010						
	Cycle 1	Cycle 2	Cycle 3	Cycle 4	Cycle 5	Cycle 6
Feeder 1	18 290	18580	22880	24260	22750	19660
Feeder 2	18390	18810	19900	20860	22270	22660
Feeder 3	18530	19160	19050	19100	20110	21500
Feeder 4	18490	18840	18460	18320	18380	18560
Feeder 5	18530	18960	18680	18290	18350	18140
Feeder 6	18300	18960	18640	18430	18380	18010
Feeder 7	18590	19000	18630	18590	18380	18150
Feeder 8	19320	19540	19050	18830	18610	18430
Average	18 555	18 981	19 411	19 585	19 654	19 389
Stdev	328	282	1472	2066	1863	1766
Coeff of var	2 %	1 %	8 %	11 %	9 %	9 %
Sum [kg]	148	152	155	157	157	155

**Table 93 Test 5: Test 5: Alumina and fluoride total mass balance: 1076 [kg] material used / test.**

Test 5: Alumina & fluoride ? / 10 / 2010					
Average	Stdev	Coeff of var	Tømming av renne		Høyde alumina målt mellom lukke F5 & F2
21070	2537	12 %	7280	F1+F2+F3+ F4	Start C1: F5:33 cm / F2:27 cm
20482	1766	9 %	12240	F5+F6	C1: F5: 33 cm / F2: 23 cm
19575	1073	5 %			C2: F5: 27 cm / F2: 17 cm
18508	183	1 %			C3: F5: 22 cm / F2: 12 cm
18492	297	2 %			C4: F5: cm / F2: cm
18453	322	2 %			C5: F5: 6.5 cm / F2: 2.5 cm
18557	283	2 %	8490	F8	C6: F5: cm / F2: cm
18963	423	2 %			Not enough alumina left for C7!!
			28010		
			Total kg alumina & fluoride used for Test 5		
1 076					

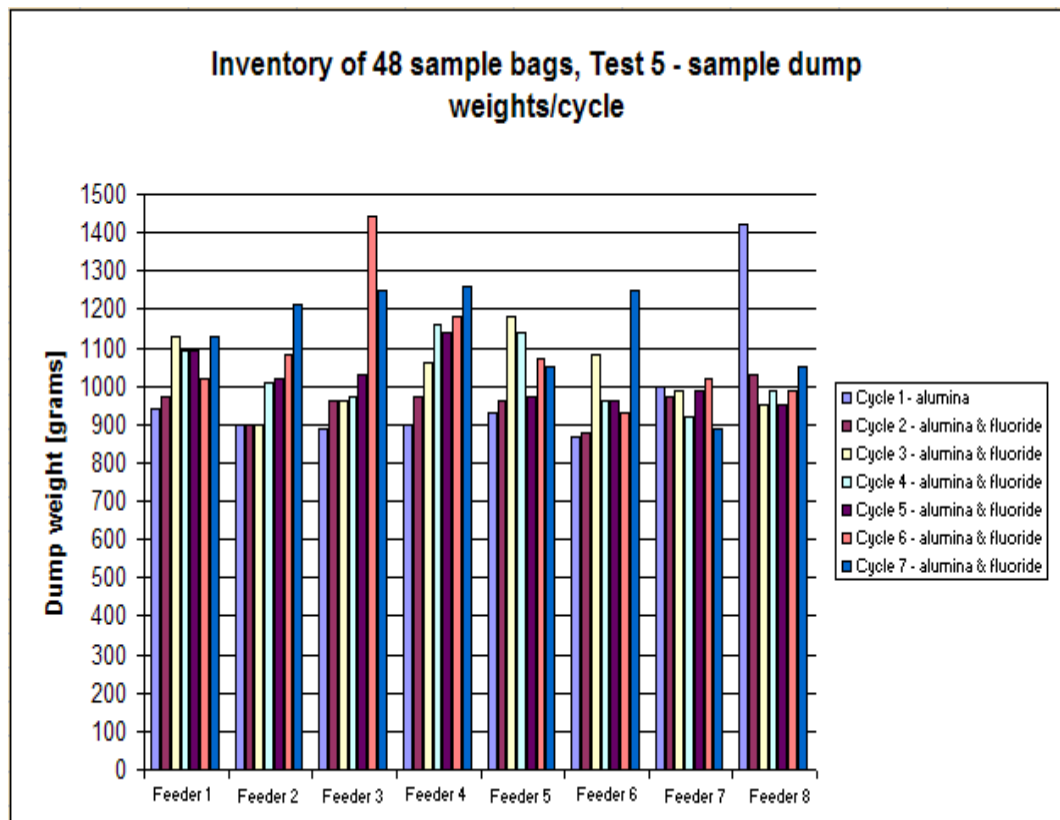


**Figure 269 Test 5: Sample inventory**



**Table 94 Test 6: Closed valve for refilling of alumina from the silo. Alumina and fluoride accumulated and individual dump weights: [grams] / feeder / cycle. Cycle 1 only alumina, cycle 2 to 5 alumina mixed with fluoride.**

Test 6: Alumina / Cycle 1								
	Accumulated	Dump weight	Accumulated	Dump weight	Accumulated	Dump weight	Accumulated	Dump weight
Dump nr.	Feeder 1 / Cycle 1	Feeder 1 / Cycle 1	Feeder 2 / Cycle 1	Feeder 2 / Cycle 1	Feeder 3 / Cycle 1	Feeder 3 / Cycle 1	Feeder 4 / Cycle 1	Feeder 4 / Cycle 1
1	760	760	860	860	860	860	1090	1090
2	1520	760	1900	1040	1700	840	2130	1040
3	2310	790	2800	900	2520	820	3000	870
4	3170	<b>860</b>	3080	280	3390	870	3900	900
5	3940	770	4520	1440	4270	880	4760	860
6	4730	790	5370	850	5040	770	5600	840
7	5560	830	6200	830	5870	<b>830</b>	6690	1090
8	6330	770	6950	750	6730	<b>860</b>	7300	610
9	7190	860	7820	870	7580	850	8280	980
10	8000	810	8650	830	8380	800	9180	<b>900</b>
11	8780	780	9600	950	9210	830	10100	920
12	9540	760	10450	850	10220	1010	10920	820
13	10510	970	11300	850	11160	940	11810	890
14	11340	830	12150	850	12050	890	12680	870
15	12080	740	13020	870	12900	850	13590	910
16	12950	870	13950	930	13800	900	13920	330
17	13840	890	14990	1040	14840	1040	15570	1650
18	14700	860	16040	1050	15860	1020	16620	1050
19	15690	990	17100	1060	17000	1140	17560	940
20	<b>18680</b>	2990	<b>18670</b>	1570	<b>18600</b>	1600	<b>18510</b>	950
Average		934		934		930		926
Stdev		489		255		163		240
Coeff of var		52 %		27 %		20 %		26 %

Test 6: Alumina + Fluoride / Cycle 2								
	Accumulated	Dump weight	Accumulated	Dump weight	Accumulated	Dump weight	Accumulated	Dump weight
Dump nr.	Feeder 1 / Cycle 2	Feeder 2 / Cycle 2	Feeder 2 / Cycle 2	Feeder 2 / Cycle 2	Feeder 3 / Cycle 2	Feeder 3 / Cycle 2	Feeder 4 / Cycle 2	Feeder 4 / Cycle 2
1	740	740	740	740	790	790	890	890
2	1570	830	1530	790	1560	770	1700	810
3	2380	810	2330	800	2380	820	2590	890
4	3250	870	3170	840	3180	800	3490	900
5	4060	810	3980	810	4010	830	4400	910
6	4940	<b>880</b>	4990	1010	4820	810	5290	890
7	5790	850	5910	920	5640	820	6150	860
8	6610	820	6760	<b>850</b>	6500	860	6960	810
9	7420	810	7560	800	7310	810	7810	850
10	8260	840	8330	770	8260	<b>950</b>	8710	900
11	8990	730	9160	830	9110	850	9600	890
12	9830	840	9950	790	9950	840	10510	<b>910</b>
13	10640	810	10830	880	10800	850	11360	850
14	11500	860	11660	830	11660	860	12210	850
15	12330	830	12480	820	12500	840	13110	900
16	13130	800	13390	910	13390	890	14070	960
17	13930	800	14320	930	14390	1000	15120	1050
18	14880	950	15290	970	15580	1190	16330	1210
19	15980	1100	16460	1170	16700	1120	17330	1000
20	<b>18440</b>	2460	<b>18650</b>	2190	<b>18610</b>	1910	<b>18680</b>	1350
Average		922		933		931		934
Stdev		370		312		255		133
Coeff of var		40 %		33 %		27 %		14 %

Test 6: Alumina + Fluoride / Cycle 3								
	Accumulated	Dump weight	Accumulated	Dump weight	Accumulated	Dump weight	Accumulated	Dump weight
Dump nr.	Feeder 1 / Cycle 3	Feeder 1 / Cycle 3	Feeder 2 / Cycle 3	Feeder 2 / Cycle 3	Feeder 3 / Cycle 3	Feeder 3 / Cycle 3	Feeder 4 / Cycle 3	Feeder 4 / Cycle 3
1	680	680	740	740	810	810	900	900
2	1690	1010	1430	690	1600	790	1770	870
3	2780	1090	2210	780	2240	640	2570	800
4	3810	1030	3190	980	3160	920	3490	920
5	4990	1180	4130	940	3950	790	4360	870
6	6160	1170	5050	920	4830	880	5170	810
7	7330	1170	5980	930	5640	810	6020	850
8	8500	<b>1170</b>	6950	970	6430	790	6830	810
9	9650	1150	7890	940	7220	790	7620	790
10	11360	1710	8820	<b>930</b>	8020	800	8460	840
11	11910	550	9740	920	9170	1150	9300	840
12	13030	1120	10690	950	10110	<b>940</b>	10130	830
13	14180	1150	11620	930	10960	850	10980	850
14	15420	1240	12520	900	11810	850	11830	<b>850</b>
15	16660	1240	13500	980	12580	770	12680	850
16	17900	1240	14380	880	13470	890	13620	940
17	19080	1180	15390	1010	14490	1020	14820	1200
18	20420	1340	16450	1060	15540	1050	15930	1110
19	21750	1330	17600	1150	16620	1080	16950	1020
20	<b>23610</b>	1860	<b>20910</b>	3310	<b>19060</b>	2440	<b>18380</b>	1430
Average		1181		1046		953		919
Stdev		282		543		371		160
Coeff of var		24 %		52 %		39 %		17 %

Test 6: Alumina + Fluoride / Cycle 4								
	Accumulated	Dump weight	Accumulated	Dump weight	Accumulated	Dump weight	Accumulated	Dump weight
Dump nr.	Feeder 1 / Cycle 4	Feeder 1 / Cycle 4	Feeder 2 / Cycle 4	Feeder 2 / Cycle 4	Feeder 3 / Cycle 4	Feeder 3 / Cycle 4	Feeder 4 / Cycle 4	Feeder 4 / Cycle 4
1	1160	1160	800	800	800	800	720	720
2	2360	1200	1660	860	1600	800	1600	880
3	3630	1270	2610	950	2430	830	2450	850
4	4980	1350	3600	990	3260	830	3370	920
5	6270	1290	4590	990	4190	930	4260	890
6	7570	1300	5610	1020	5060	870	5130	870
7	8830	1260	6650	1040	5890	830	6010	880
8	10110	1280	7650	1000	6730	840	6890	880
9	11410	1300	8650	1000	7620	890	7700	810
10	12780	<b>1370</b>	9660	1010	8470	850	8530	830
11	13970	1190	10610	950	9370	900	9390	860
12	15240	1270	11670	<b>1060</b>	10290	920	10240	850
13	16530	1290	12690	1020	11140	850	11030	790
14	17810	1280	13690	1000	12040	<b>900</b>	11870	840
15	19160	1350	14620	930	12970	930	12730	860
16	20670	1510	15690	1070	13850	880	13660	<b>930</b>
17	22190	1520	16800	1110	14800	950	14770	1110
18	23500	1310	17890	1090	16040	1240	15950	1180
19	24420	920	19110	1220	17270	1230	16980	1030
20	<b>24910</b>	490	<b>22460</b>	3350	<b>19820</b>	2550	<b>18410</b>	1430
Average		1246		1123		991		921
Stdev		216		532		386		160
Coeff of var		17 %		47 %		39 %		17 %

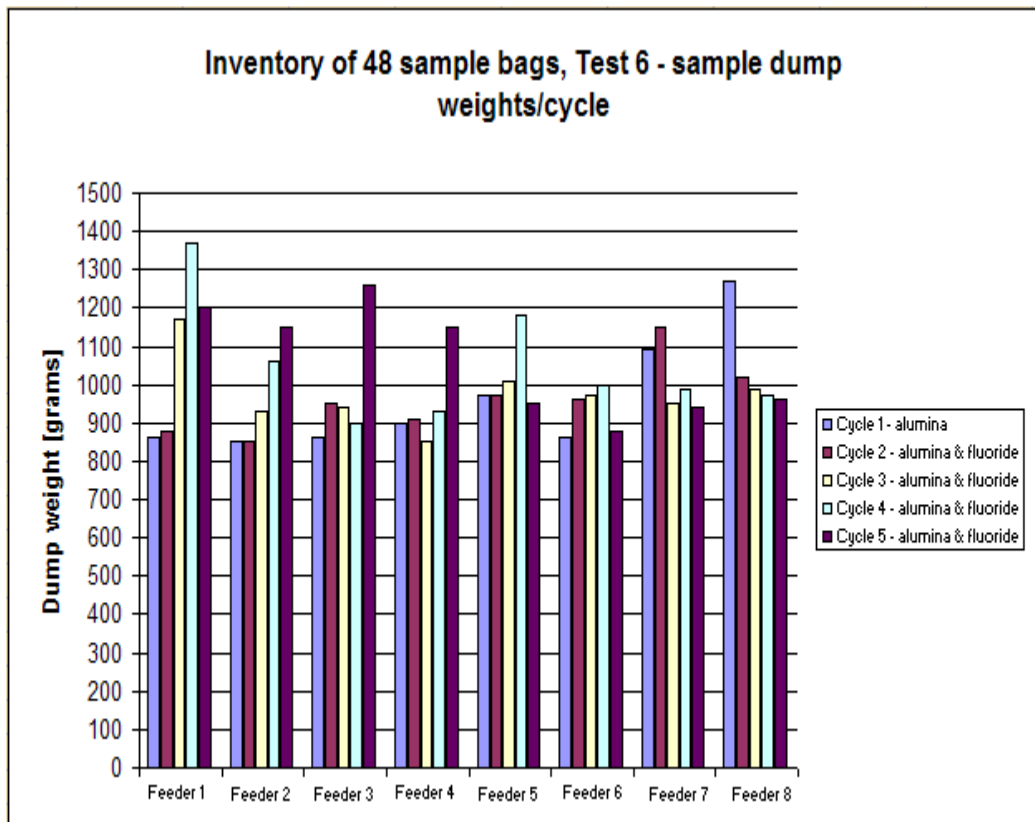
Test 6: Alumina + Fluoride / Cycle 5								
	Accumulated	Dump weight	Accumulated	Dump weight	Accumulated	Dump weight	Accumulated	Dump weight
Dump nr.	Feeder 1 / Cycle 5	Feeder 1 / Cycle 5	Feeder 2 / Cycle 5	Feeder 2 / Cycle 5	Feeder 3 / Cycle 5	Feeder 3 / Cycle 5	Feeder 4 / Cycle 5	Feeder 4 / Cycle 5
1	1470	1470	1120	1120	970	970	900	900
2	2630	1160	2240	1120	1840	870	1820	920
3	3890	1260	3310	1070	2790	950	2690	870
4	5010	1120	4380	1070	3790	1000	3600	910
5	6180	1170	5420	1040	4750	960	4510	910
6	7370	1190	6490	1070	5740	990	5500	990
7	8560	1190	7570	1080	6690	950	6430	930
8	9680	1120	8610	1040	7650	960	7300	870
9	10840	1160	9700	1090	8600	950	8170	870
10	11980	1140	10790	1090	9560	960	9020	850
11	13100	1120	11850	1060	10520	960	9870	850
12	14300	<b>1200</b>	12890	1040	11430	910	10710	840
13	15490	1190	13960	1070	12450	1020	11670	960
14	16710	1220	15110	<b>1150</b>	13420	970	12700	1030
15	17960	1250	16310	1200	14420	1000	13600	900
16	19280	1320	17610	1300	15680	<b>1260</b>	14580	980
17	20780	1500	19050	1440	17040	1360	15730	<b>1150</b>
18	22280	1500	20460	1410	18330	1290	16790	1060
19	23300	1020	21710	1250	19480	1150	17690	900
20	<b>23910</b>	610	<b>23240</b>	1530	<b>20880</b>	1400	<b>18580</b>	890
Average		1196		1162		1044		929
Stdev		189		147		157		79
Coeff of var		16 %		13 %		15 %		9 %

Table 95 Test 6: Closed valve for refilling of alumina from the silo. Alumina and fluoride mass balance: [kg] / feeder / cycle.

Test 6: Alumina & fluoride ? / 10 / 2010						
	Cycle 1	Cycle 2	Cycle 3	Cycle 4	Cycle 5	Cycle 6
Feeder 1	18 680	18440	23610	24910	23910	
Feeder 2	18670	18650	20910	22460	23240	
Feeder 3	18600	18610	19060	19820	20880	
Feeder 4	18510	18680	18380	18410	18580	
Feeder 5	18670	18740	18680	18500	18430	
Feeder 6	18610	18610	18480	18340	18270	
Feeder 7	18620	18770	18500	18410	18290	
Feeder 8	19190	18950	19190	18790	18440	
Average	18 694	18 681	19 601	19 955	20 005	103 640
Stdev	208	148	1815	2441	2372	
Coeff of var	1 %	1 %	9 %	12 %	12 %	
Sum	150	149	157	160	160	104

**Table 96 Test 6: Alumina and fluoride total mass balance: 879 [kg] material used / test.**

Test 6: Alumina & fluoride ? / 10 / 2010					
Average	Stdev	Coef of var	Tømming av renne	F1 + F2 + F3 + F4	Høyde alumina målt mellom lukke F5 & F2
21910	3097	14 %	25460	F5	Start C1: F5: cm / F2: cm
20786	2114	10 %	2380	F6	C1: F5: 29 cm / F2: cm
19394	968	5 %	44970	F7	C2: F5: 19 cm / F2: 10 cm
18512	123	1 %	19740	F8	C3: F5: cm / F2: cm
18604	132	1 %	11090		C4: F5: 13 cm / F2: 4.5 cm
18462	155	1 %			C5: F5: 6 cm / F2: 0.5 cm
18518	186	1 %			
18912	314	2 %			Not enough alumina left for C6!!
			103640		
Total kg alumina & fluoride used for Test 6					
			879		



**Figure 270 Test 6: Sample inventory**

**Table 97 Test 7: Open valve for refilling of alumina from the silo. Alumina and fluoride mass balance: [kg] / feeder / cycle.**

Test 7								
	Cycle 1	Cycle 2	Cycle 3	Cycle 4	Cycle 5	Cycle 6	Cycle 7	Cycle 8
Feeder 1	18 370	18710	22950	24330	20840	18610	18200	18100
Feeder 2	18 450	18760	20010	21090	22780	19620	18320	18090
Feeder 3	18 770	18820	19080	19390	21680	19610	18440	18440
Feeder 4	18 760	18870	18710	18600	18910	20110	18960	18420
Feeder 5	18 940	18910	18720	18560	18460	20320	19300	18590
Feeder 6	18 700	18980	18770	18640	18520	18450	19880	19140
Feeder 7	19 060	19250	18930	18860	18680	18730	18980	19690
Feeder 8	19 700	19690	19540	19270	19120	19100	18940	19210
Average [gram]	<b>18 844</b>	<b>18 999</b>	<b>19 589</b>	<b>19 843</b>	<b>19 874</b>	<b>19 319</b>	<b>18 878</b>	<b>18 710</b>
Stdev	414	325	1433	1994	1665	703	556	576
Coeff of var	2 %	2 %	7 %	10 %	8 %	4 %	3 %	3 %
Sum [kg]	151	152	157	159	159	155	151	150

**Table 98 Test 7: Open valve for refilling of alumina from the silo. Alumina and fluoride accumulated and individual dump weights: [grams] / feeder / cycle. Cycle 1 only alumina, cycle 2 to 8 alumina mixed with fluoride.**

Test 7: Alumina / Cycle 1/08-13 10 - 2010								
Dump nr.	Accumulated	Dump weight	Accumulated	Dump weight	Accumulated	Dump weight	Accumulated	Dump weight
	Feeder 1 / Cycle 1	Feeder 1 / Cycle 1	Feeder 2 / Cycle 1	Feeder 2 / Cycle 1	Feeder 3 / Cycle 1	Feeder 3 / Cycle 1	Feeder 4 / Cycle 1	Feeder 4 / Cycle 1
1	750	750						
2	1530	780	2050		1610		1720	
3	2490	960	2930	880	2460	850	2550	830
4	3390	900	3840	910	3320	860	3380	830
5	4310	920	4740	900	4280	960	4260	880
6	5340	1030	5720	980	5110	830	5100	840
7	6300	960	6600	880	6000	890	5930	830
8	7230	930	7510	910	6880	880	6780	850
9	8260	1030	8420	910	8150	1270	7630	850
10	9230	<b>970</b>	9340	920	9020	870	8500	870
11	10180	950	10250	910	9890	870	9320	820
12	11190	1010	11230	<b>980</b>	10780	<b>890</b>	10170	<b>850</b>
13	12130	940	12150	920	11680	900	11060	890
14	13150	1020	13070	920	12650	970	11890	830
15	14120	970	14040	970	13600	950	12750	860
16	15190	1070	15140	1100	14560	960	13620	870
17	16400	1210	16290	1150	15690	1130	14570	950
18	17400	1000	17310	1020	16820	1130	15650	1080
19	18030	630	18010	700	17790	970	16720	1070
20	<b>18370</b>	340	<b>18450</b>	440	<b>18770</b>	980	<b>18760</b>	2040
Average		919		911		953		947
Stdev		183		151		116		283
Coeff of var		20 %		17 %		12 %		30 %

Test 7: Alumina + Fluoride / Cycle 2								
Dump nr.	Accumulated	Dump weight	Accumulated	Dump weight	Accumulated	Dump weight	Accumulated	Dump weight
	Feeder 1 / Cycle 2	Feeder 1 / Cycle 2	Feeder 2 / Cycle 2	Feeder 2 / Cycle 2	Feeder 3 / Cycle 2	Feeder 3 / Cycle 2	Feeder 4 / Cycle 2	Feeder 4 / Cycle 2
1	810	810	850	850	840	840	950	950
2	1720	910	1690	840	1640	800	1720	770
3	2670	950	2620	930	2490	850	2670	950
4	3630	960	3560	940	3390	900	3630	960
5	4580	950	4530	970	4260	870	4610	980
6	5520	940	5430	900	5150	890	5610	1000
7	6490	970	6290	860	6100	950	6570	960
8	7440	950	7200	910	7330	1230	7480	910
9	8360	920	8140	940	8370	1040	8420	940
10	9280	920	9130	990	9320	950	9360	940
11	10240	960	10020	890	10220	900	10340	980
12	11150	<b>910</b>	10920	900	11200	980	11320	980
13	12080	930	11870	950	12200	1000	12220	900
14	13040	960	12840	<b>970</b>	13190	990	13180	960
15	14070	1030	13800	960	14190	1000	14200	1020
16	15090	1020	14840	1040	15380	<b>1190</b>	15290	1090
17	16230	1140	16060	1220	16610	1230	16450	<b>1160</b>
18	17340	1110	17110	1050	17640	1030	17530	1080
19	18130	790	17980	870	18360	720	18320	790
20	<b>18710</b>	580	<b>18760</b>	780	<b>18820</b>	460	<b>18870</b>	550
Average		936		938		941		944
Stdev		116		94		176		128
Coeff of var		12 %		10 %		19 %		14 %

Test 7: Alumina + Fluoride / Cycle 3								
Dump nr.	Accumulated	Dump weight	Accumulated	Dump weight	Accumulated	Dump weight	Accumulated	Dump weight
	Feeder 1 / Cycle 3	Feeder 1 / Cycle 3	Feeder 2 / Cycle 3	Feeder 2 / Cycle 3	Feeder 3 / Cycle 3	Feeder 3 / Cycle 3	Feeder 4 / Cycle 3	Feeder 4 / Cycle 3
1	860	860	860	860	870	870	910	910
2	1990	1130	1770	910	1820	950	1770	860
3	3130	1140	2780	1010	2730	910	2730	960
4	4270	1140	3780	1000	3660	930	3710	<b>980</b>
5	5430	1160	4770	990	4610	950	4690	980
6	6560	1130	5780	1010	5550	940	5640	950
7	7700	1140	6770	990	6440	890	6580	940
8	8780	1080	7790	1020	7420	980	7520	940
9	9870	1090	8760	970	8330	910	8520	1000
10	10990	1120	9730	970	9240	910	9480	960
11	12040	1050	10650	920	10150	910	10340	860
12	13160	1120	11660	1010	11520	1370	11300	960
13	14280	1120	12600	940	12650	1130	12310	1010
14	15420	<b>1140</b>	13590	990	13710	1060	13300	990
15	16530	1110	14600	1010	14770	1060	14300	1000
16	17660	1130	15750	<b>1150</b>	15910	1140	15470	1170
17	18830	1170	16920	1170	17050	<b>1140</b>	16640	1170
18	20080	1250	18070	1150	18060	1010	17620	980
19	21200	1120	19060	990	18720	660	18280	660
20	<b>22950</b>	1750	<b>20010</b>	950	<b>19080</b>	360	<b>18710</b>	430
Average		1148		1001		954		936
Stdev		159		79		200		159
Coeff of var		14 %		8 %		21 %		17 %

Test 7: Alumina + Fluoride / Cycle 4								
Dump nr.	Accumulated	Dump weight	Accumulated	Dump weight	Accumulated	Dump weight	Accumulated	Dump weight
	Feeder 1 / Cycle 4	Feeder 1 / Cycle 4	Feeder 2 / Cycle 4	Feeder 2 / Cycle 4	Feeder 3 / Cycle 4	Feeder 3 / Cycle 4	Feeder 4 / Cycle 4	Feeder 4 / Cycle 4
1	930	930	1090	1090	880	880	830	830
2	2030	1100	2330	1240	1810	930	1740	910
3	3150	1120	3320	990	2760	950	2690	950
4	4310	1160	4350	1030	3800	<b>1040</b>	3730	1040
5	5420	1110	5410	1060	4830	1030	4700	970
6	6460	1040	6420	1010	5790	960	5670	<b>970</b>
7	7540	1080	7430	1010	6710	920	6570	900
8	8650	1110	8450	1020	7600	890	7460	890
9	9790	1140	9540	1090	8520	920	8390	930
10	10900	1110	10550	1010	9380	860	9660	1270
11	11970	1070	11540	990	10300	920	10590	930
12	13080	1110	12520	980	11180	880	11530	940
13	14190	1110	13540	1020	12170	990	12460	930
14	15320	1130	14570	1030	13140	970	13430	970
15	16420	1100	15610	1040	14170	1030	14380	950
16	17560	1140	16710	1100	15230	1060	15420	1040
17	18750	1190	17990	1280	16300	1070	16580	1160
18	19960	1210	19230	1240	17450	1150	17560	980
19	21320	1360	20180	950	18430	980	18230	670
20	<b>24330</b>	3010	<b>21090</b>	910	<b>19390</b>	960	<b>18600</b>	370
Average		1217		1055		970		930
Stdev		430		97		75		177
Coeff of var		35 %		9 %		8 %		19 %

Test 7: Alumina + Fluoride / Cycle 5								
Dump nr.	Accumulated	Dump weight	Accumulated	Dump weight	Accumulated	Dump weight	Accumulated	Dump weight
	Feeder 1 / Cycle 5	Feeder 1 / Cycle 5	Feeder 2 / Cycle 5	Feeder 2 / Cycle 5	Feeder 3 / Cycle 5	Feeder 3 / Cycle 5	Feeder 4 / Cycle 5	Feeder 4 / Cycle 5
1	1060	1060	880	880	870	870	760	760
2	2070	1010	1940	1060	2010	1140	1660	900
3	3030	960	2950	1010	3030	1020	2620	960
4	4030	<b>1000</b>	4040	<b>1090</b>	4010	980	3560	940
5	5030	1000	5090	1050	5040	1030	4560	1000
6	6030	1000	6130	1040	6140	<b>1100</b>	5520	960
7	7110	1080	7230	1100	7220	1080	6490	970
8	8120	1010	8290	1060	8200	980	7470	980
9	9140	1020	9430	1140	9250	1050	8410	<b>940</b>
10	10160	1020	10480	1050	10320	1070	9290	880
11	11140	980	11530	1050	11400	1080	10250	960
12	12110	970	12580	1050	12450	1050	11150	900
13	13110	1000	13610	1030	13540	1090	12120	970
14	14120	1010	14610	1000	14590	1050	13020	900
15	15250	1130	15670	1060	15600	1010	13990	970
16	16440	1190	16740	1070	16710	1110	14950	960
17	17760	1320	18050	1310	18020	1310	15980	1030
18	19070	1310	19350	1300	19310	1290	17050	1070
19	20120	1050	20700	1350	20400	1090	17990	940
20	<b>20840</b>	720	<b>22780</b>	2080	<b>21680</b>	1280	<b>18910</b>	920
Average		1042		1139		1084		946
Stdev		128		248		108		63
Coeff of var		12 %		22 %		10 %		7 %

Test 7: Alumina + Fluoride / Cycle 6								
Dump nr.	Accumulated	Dump weight	Accumulated	Dump weight	Accumulated	Dump weight	Accumulated	Dump weight
	Feeder 1 / Cycle 6	Feeder 1 / Cycle 6	Feeder 2 / Cycle 6	Feeder 2 / Cycle 6	Feeder 3 / Cycle 6	Feeder 3 / Cycle 6	Feeder 4 / Cycle 6	Feeder 4 / Cycle 6
1	1070	1070	850	850	880	880	840	840
2	1860	790	1810	960	1840	960	1780	940
3	2850	990	2680	870	2730	890	2770	990
4	3850	1000	3610	930	3650	920	3740	970
5	4860	1010	4520	910	4600	950	4740	1000
6	5850	990	5510	990	5520	920	5730	990
7	6860	1010	6500	990	6520	1000	6740	1010
8	7860	1000	7440	940	7470	950	7710	970
9	8810	950	8370	930	8400	930	8700	990
10	9820	1010	9340	970	9330	930	9680	980
11	10830	1010	10250	910	10300	970	10660	980
12	11840	1010	11150	900	11260	960	11610	950
13	12830	990	12140	990	12590	1330	12620	1010
14	13880	1050	13210	1070	13730	1140	13660	1040
15	15030	1150	14210	1000	14780	1050	14680	1020
16	16280	1250	15280	1070	15930	1150	15700	1020
17	17370	1090	16480	1200	17150	1220	16840	1140
18	18160	790	17680	1200	18290	1140	18070	1230
19	18510	350	18720	1040	19100	810	19080	1010
20	18610	100	19620	900	19610	510	20110	1030
Average		931		981		981		1006
Stdev		264		96		170		76
Coeff of var		28 %		10 %		17 %		8 %

Test 7: Alumina + Fluoride / Cycle 7								
Dump nr.	Accumulated	Dump weight	Accumulated	Dump weight	Accumulated	Dump weight	Accumulated	Dump weight
	Feeder 1 / Cycle 6	Feeder 1 / Cycle 6	Feeder 2 / Cycle 6	Feeder 2 / Cycle 6	Feeder 3 / Cycle 6	Feeder 3 / Cycle 6	Feeder 4 / Cycle 6	Feeder 4 / Cycle 6
1	860	860	770	770	840	840	810	810
2	1830	970	1760	990	1880	1040	1700	890
3	2800	970	2780	1020	2870	990	2620	920
4	3790	990	3740	960	3820	950	3570	950
5	4880	1090	4700	960	4770	950	4520	950
6	5860	980	5670	970	5720	950	5490	970
7	6860	1000	6690	1020	6680	960	6450	960
8	7860	1000	7680	990	7640	960	7440	990
9	8820	960	8630	950	8590	950	8420	980
10	9800	980	9690	1060	9440	850	9360	940
11	10760	960	10630	940	10590	1150	10310	950
12	11720	960	11660	1030	11560	970	11290	980
13	12710	990	12680	1020	12500	940	12290	1000
14	13730	1020	13650	970	13480	980	13260	970
15	14860	1130	14670	1020	14510	1030	14270	1010
16	16020	1160	15780	1110	15640	1130	15370	1100
17	17050	1030	16880	1100	16740	1100	16510	1140
18	17790	740	17700	820	17650	910	17590	1080
19	18110	320	18150	450	18180	530	18390	800
20	18200	90	18320	170	18440	260	18960	570
Average		910		916		922		948
Stdev		259		227		202		121
Coeff of var		28 %		25 %		22 %		13 %

Test 7: Alumina + Fluoride / Cycle 8								
Dump nr.	Accumulated	Dump weight	Accumulated	Dump weight	Accumulated	Dump weight	Accumulated	Dump weight
	Feeder 1 / Cycle 6	Feeder 1 / Cycle 6	Feeder 2 / Cycle 6	Feeder 2 / Cycle 6	Feeder 3 / Cycle 6	Feeder 3 / Cycle 6	Feeder 4 / Cycle 6	Feeder 4 / Cycle 6
1	800	800	850	850	800	800	810	810
2	1800	1000	1870	1020	1790	990	1770	960
3	2790	990	2820	950	2770	980	2760	990
4	3800	1010	3790	970	3760	990	3780	1020
5	4800	1000	4720	930	4770	1010	4780	1000
6	5790	990	5690	970	5720	950	5760	980
7	6780	990	6620	930	6620	900	6730	970
8	7750	970	7550	930	7550	930	7710	980
9	8800	1050	8480	930	8520	970	8660	950
10	9790	990	9440	960	9460	940	9660	1000
11	10830	1040	10360	920	10370	910	10600	940
12	11860	1030	11300	940	11320	950	11520	920
13	12960	1100	12250	950	12260	940	12460	940
14	14010	1050	13210	960	13220	960	13420	960
15	15130	1120	14190	980	14220	1000	14450	1030
16	16240	1110	15240	1050	15360	1140	15580	1130
17	17210	970	16370	1130	16500	1140	16710	1130
18	17840	630	17290	920	17460	960	17620	910
19	18050	210	17840	550	18100	640	18180	560
20	18100	50	18090	250	18440	340	18420	240
Average		905		905		922		921
Stdev		287		188		172		198
Coeff of var		32 %		21 %		19 %		22 %

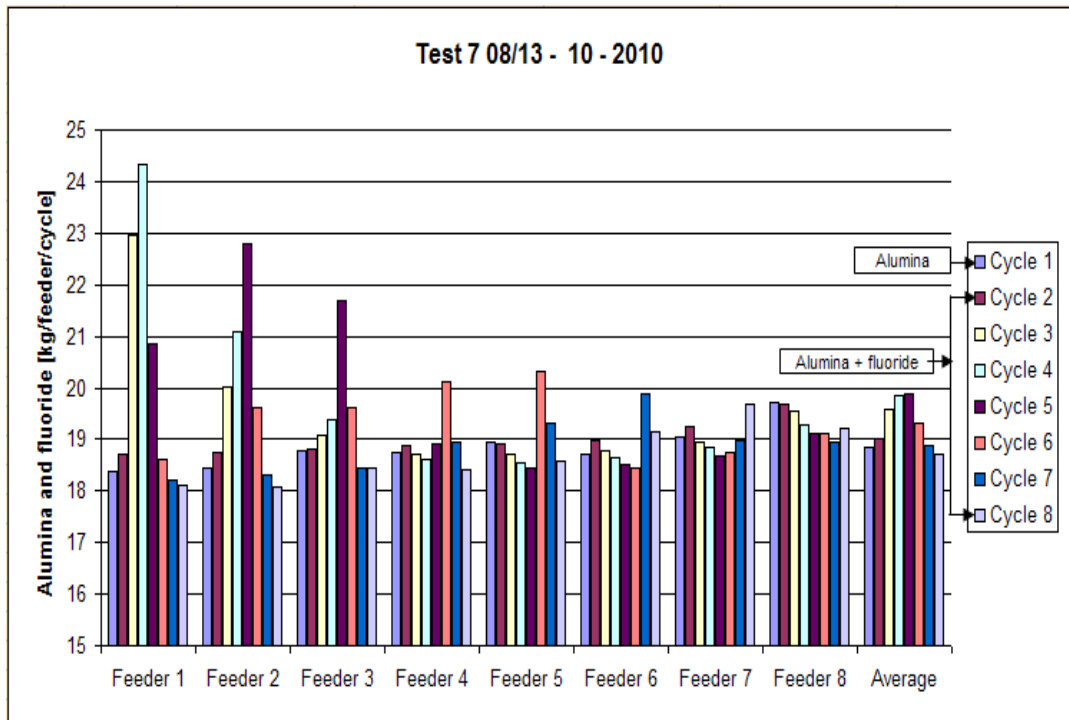


Figure 271 Alumina and fluoride distribution from feeder 1 to 8.

Table 99 Test 8: Open valve for refilling of alumina from the silo. Alumina and fluoride mass balance: [kg] / feeder / cycle.

Test 8								
	Cycle 1	Cycle 2	Cycle 3	Cycle 4	Cycle 5	Cycle 6	Cycle 7	Cycle 8
Feeder 1	18 350	18 790	23 860	20 370	18 200	18 280	17 960	18 170
Feeder 2	18 480	18 760	21 510	22 450	19 350	18 440	18 560	18 260
Feeder 3	18 620	18 760	19 560	22 950	19 980	18 240	18 650	18 500
Feeder 4	18 530	18 510	18 430	19 980	19 310	18 620	18 650	18 580
Feeder 5	18 470	18 470	18 360	18 310	20 690	19 320	18 650	18 430
Feeder 6	18 460	18 550	18 340	18 310	18 740	19 620	18 980	18 520
Feeder 7	18 700	18 650	18 430	18 340	18 340	19 580	19 380	18 810
Feeder 8	19 040	18 820	18 710	18 620	18 650	18 680	19 020	19 360
Average [g]	18 581	18 664	19 650	19 916	19 158	18 848	18 731	18 579
Stdev	214	138	2015	1896	854	572	416	371
Coeff of var	1 %	1 %	10 %	10 %	4 %	3 %	2 %	2 %
Sum [kg]	149	149	157	159	153	151	150	149

**Table 100 Test 8: Open valve for refilling of alumina from the silo. Alumina and fluoride accumulated and individual dump weights: [grams] / feeder / cycle. Cycle 1 only alumina, cycle 2 to 8 alumina mixed with fluoride.**

Test 2E: Alumina / Cycle 1								
	Accumulated	Dump weight	Accumulated	Dump weight	Accumulated	Dump weight	Accumulated	Dump weight
Dump nr.	Feeder 1 / Cycle 1	Feeder 1 / Cycle 1	Feeder 2 / Cycle 1	Feeder 2 / Cycle 1	Feeder 3 / Cycle 1	Feeder 3 / Cycle 1	Feeder 4 / Cycle 1	Feeder 4 / Cycle 1
1	770	770	660	660	730	730	730	730
2	1680	910	1470	810	1510	780	1530	800
3	2620	940	2350	880	2360	850	2620	1090
4	3620	<b>960</b>	3270	920	3240	880	3350	730
5	4510	890	4120	850	4180	940	4250	900
6	5430	920	5120	<b>1000</b>	5120	940	5120	870
7	6400	970	6020	900	6050	930	6060	940
8	7320	920	6940	920	7050	<b>1170</b>	6940	880
9	8240	920	7860	920	7930	880	7860	920
10	9150	910	8720	860	8770	840	8860	<b>910</b>
11	10080	930	9600	880	9660	890	9780	920
12	10970	890	10450	850	10670	1010	10690	910
13	11890	920	11310	860	11580	910	11620	930
14	12860	970	12260	950	12500	920	12530	910
15	13860	1000	13170	910	13430	930	13500	970
16	14890	1030	14100	930	14370	940	14470	970
17	15960	1070	15070	970	15400	1030	15580	1110
18	17010	1050	16140	1070	16540	1140	16740	1160
19	17770	760	17130	990	17510	970	17660	920
20	<b>18350</b>	580	<b>18480</b>	1350	<b>18620</b>	1110	<b>18530</b>	870
Average		916		924		940		922
Stdev		110		130		111		108
Coeff of var		12 %		14 %		12 %		12 %

Test 2E: Alumina + Fluoride / Cycle 2								
	Accumulated	Dump weight	Accumulated	Dump weight	Accumulated	Dump weight	Accumulated	Dump weight
Dump nr.	Feeder 1 / Cycle 2	Feeder 1 / Cycle 2	Feeder 2 / Cycle 2	Feeder 2 / Cycle 2	Feeder 3 / Cycle 2	Feeder 3 / Cycle 2	Feeder 4 / Cycle 2	Feeder 4 / Cycle 2
1	620	620	770	770	880	880	880	880
2	1540	920	1590	820	1770	890	1760	880
3	2490	950	2460	870	2690	920	2690	930
4	3410	920	3360	900	3590	900	3630	940
5	4380	970	4210	850	4510	920	4580	950
6	5380	<b>930</b>	5120	910	5430	920	5520	940
7	6290	910	6020	900	6330	900	6450	930
8	7240	950	7020	<b>920</b>	7230	900	7360	910
9	8200	960	7900	880	8110	880	8260	900
10	9110	910	8760	860	9110	<b>900</b>	9140	880
11	10030	920	9660	900	10080	970	10090	950
12	10900	870	10560	900	11010	930	11090	<b>950</b>
13	11830	930	11420	860	11890	880	11990	900
14	12730	900	12280	860	12820	930	12920	930
15	13670	940	13160	880	13770	950	13860	940
16	14580	910	14080	920	14790	1020	15010	1150
17	15620	1040	15020	940	16010	1220	16220	1210
18	16740	1120	16110	1090	17130	1120	17260	1040
19	17740	1000	17150	1040	18020	890	18020	760
20	<b>18790</b>	1050	<b>18760</b>	1610	<b>18760</b>	740	<b>18510</b>	490
Average		936		934		933		923
Stdev		95		173		98		140
Coeff of var		10 %		19 %		10 %		15 %

Test 2E: Alumina + Fluoride / Cycle 3								
	Accumulated	Dump weight	Accumulated	Dump weight	Accumulated	Dump weight	Accumulated	Dump weight
Dump nr.	Feeder 1 / Cycle 3	Feeder 1 / Cycle 3	Feeder 2 / Cycle 3	Feeder 2 / Cycle 3	Feeder 3 / Cycle 3	Feeder 3 / Cycle 3	Feeder 4 / Cycle 3	Feeder 4 / Cycle 3
1	710	710	800	800	840	840	850	850
2	1720	1010	1830	1030	1730	890	1730	880
3	2870	1150	2790	960	2640	910	2660	930
4	4010	1140	3740	950	3560	920	3570	910
5	5180	1170	4630	890	4480	920	4500	930
6	6310	1130	5560	930	5430	950	5370	870
7	7440	1130	6480	920	6320	890	6280	910
8	8440	<b>1170</b>	7400	920	7210	890	7170	890
9	9600	1160	8320	920	8110	900	8050	880
10	10690	1090	9320	<b>910</b>	8990	880	8940	890
11	11820	1130	10300	980	9900	910	9840	900
12	13050	1230	11240	940	10900	<b>930</b>	10750	910
13	14220	1170	12190	950	11770	870	11640	890
14	15430	1210	13090	900	12700	930	12640	<b>920</b>
15	16580	1150	13990	900	13620	920	13570	930
16	17740	1160	14970	980	14570	950	14550	980
17	18950	1210	15920	950	15580	1010	15630	1080
18	20250	1300	16960	1040	16730	1150	16680	1050
19	21550	1300	18100	1140	17870	1140	17580	900
20	<b>23860</b>	2310	<b>21510</b>	3410	<b>19560</b>	1690	<b>18430</b>	850
Average		1202		1071		975		918
Stdev		288		555		186		59
Coeff of var		24 %		52 %		19 %		6 %



Test 2E: Alumina + Fluoride / Cycle 4								
Dump nr.	Accumulated	Dump weight	Accumulated	Dump weight	Accumulated	Dump weight	Accumulated	Dump weight
	Feeder 1 / Cycle 4	Feeder 1 / Cycle 4	Feeder 2 / Cycle 4	Feeder 2 / Cycle 4	Feeder 3 / Cycle 4	Feeder 3 / Cycle 4	Feeder 4 / Cycle 4	Feeder 4 / Cycle 4
1	980	980	860	860	810	810	810	810
2	1980	1000	1990	1130	1880	1070	1750	940
3	2950	970	3020	1030	3010	1130	2730	980
4	3900	950	4030	1010	4110	1100	3720	990
5	4830	930	5050	1020	5240	1130	4680	960
6	5690	860	6110	1060	6350	1110	5660	980
7	6630	940	7140	1030	7450	1100	6650	990
8	7550	920	8120	980	8510	1060	7650	1000
9	8520	970	9160	1040	9540	1030	8610	960
10	9520	<b>940</b>	10120	960	10640	1100	9560	950
11	10470	950	11150	1030	11730	1090	10530	970
12	11360	890	12150	<b>1050</b>	12840	1110	11620	1090
13	12320	960	13210	1060	13950	1110	12520	900
14	13250	930	14370	1160	14950	<b>1130</b>	13460	940
15	14230	980	15370	1000	15990	1040	14470	1010
16	15290	1060	16410	1040	17110	1120	15470	<b>990</b>
17	16530	1240	17550	1140	18370	1260	16570	1100
18	17880	1350	18830	1280	19780	1410	17690	1120
19	19090	1210	20130	1300	20990	1210	18700	1010
20	<b>20370</b>	1280	<b>22450</b>	2320	<b>22950</b>	1960	<b>19980</b>	1280
Average		1016		1125		1154		999
Stdev		139		299		219		95
Coeff of var		14 %		27 %		19 %		10 %

Test 2E: Alumina + Fluoride / Cycle 5								
Dump nr.	Accumulated	Dump weight	Accumulated	Dump weight	Accumulated	Dump weight	Accumulated	Dump weight
	Feeder 1 / Cycle 5	Feeder 1 / Cycle 5	Feeder 2 / Cycle 5	Feeder 2 / Cycle 5	Feeder 3 / Cycle 5	Feeder 3 / Cycle 5	Feeder 4 / Cycle 5	Feeder 4 / Cycle 5
1	830	830	910	910	910	910	850	850
2	1740	910	1910	1000	1880	970	1790	940
3	2640	900	2770	860	2670	790	2710	920
4	3570	930	3590	820	3500	830	3650	940
5	4500	930	4460	870	4300	800	4560	910
6	5460	960	5310	850	5140	840	5470	910
7	6420	960	6150	840	6020	880	6330	860
8	7310	890	7050	900	6790	770	7230	900
9	8240	930	7940	890	7670	880	8180	950
10	9180	940	8840	900	8530	860	9060	880
11	10100	920	9710	870	9390	860	9980	920
12	11100	<b>930</b>	10600	890	10190	800	10930	950
13	12060	960	11490	890	10990	800	11860	930
14	13000	940	12490	<b>920</b>	11910	920	12790	930
15	13980	980	13400	910	12830	920	13770	980
16	15060	1080	14350	950	13830	<b>960</b>	14860	1090
17	16150	1090	15380	1030	14730	900	15860	<b>910</b>
18	17120	970	16540	1160	15780	1050	17080	1220
19	17780	660	17680	1140	16900	1120	18090	1010
20	<b>18200</b>	420	<b>19350</b>	1670	<b>19980</b>	3080	<b>19310</b>	1220
Average		907		964		997		961
Stdev		143		190		498		103
Coeff of var		16 %		20 %		50 %		11 %

Test 8: Alumina + Fluoride / Cycle 6								
Dump nr.	Accumulated	Dump weight	Accumulated	Dump weight	Accumulated	Dump weight	Accumulated	Dump weight
	Feeder 1 / Cycle 6	Feeder 1 / Cycle 6	Feeder 2 / Cycle 6	Feeder 2 / Cycle 6	Feeder 3 / Cycle 6	Feeder 3 / Cycle 6	Feeder 4 / Cycle 6	Feeder 4 / Cycle 6
1	840	840	740	740	740	740	890	890
2	1850	1010	1650	910	1540	800	1760	870
3	2750	900	2500	850	2390	850	2650	890
4	3650	900	3390	890	3280	890	3650	<b>910</b>
5	4550	900	4230	840	4140	860	4540	890
6	5480	930	5100	870	4950	810	5410	870
7	6360	880	5970	870	5800	850	6300	890
8	7310	950	6820	850	6690	890	7220	920
9	8220	910	7690	870	7570	880	8080	860
10	9140	920	8560	870	8440	870	8960	880
11	10060	920	9450	890	9310	870	9860	900
12	10960	900	10290	840	10200	890	10740	880
13	11890	930	11170	880	11060	860	11620	880
14	12890	<b>960</b>	12050	880	11950	890	12570	950
15	13810	920	12980	930	12820	870	13470	900
16	14860	1050	13980	<b>940</b>	13820	1000	14380	910
17	15930	1070	14970	990	14820	<b>1270</b>	15430	1050
18	16940	1010	16120	1150	15910	1090	16400	970
19	17710	770	17110	990	16990	1080	17330	930
20	<b>18280</b>	570	<b>18440</b>	1330	<b>18240</b>	1250	<b>18620</b>	1290
Average		912		919		926		927
Stdev		106		126		141		96
Coeff of var		12 %		14 %		15 %		10 %

Test 8: Alumina + Fluoride / Cycle 7								
Dump nr.	Accumulated	Dump weight	Accumulated	Dump weight	Accumulated	Dump weight	Accumulated	Dump weight
	Feeder 1 / Cycle 7	Feeder 1 / Cycle 7	Feeder 2 / Cycle 7	Feeder 2 / Cycle 7	Feeder 3 / Cycle 7	Feeder 3 / Cycle 7	Feeder 4 / Cycle 7	Feeder 4 / Cycle 7
1	660	660	710	710	800	800	760	760
2	1500	840	1550	840	1660	860	1600	840
3	2410	910	2410	860	2560	900	2530	930
4	3340	930	3290	880	3560	<b>910</b>	3450	920
5	4250	910	4160	870	4450	890	4340	890
6	5160	910	5030	870	5280	830	5340	<b>890</b>
7	6100	940	5900	870	6110	830	6220	880
8	6940	840	6770	870	6960	850	7080	860
9	7810	870	7650	880	7840	880	7940	860
10	8700	890	8550	900	8680	840	8780	840
11	9610	910	9430	880	9470	790	9680	900
12	10510	900	10340	910	10290	820	10550	870
13	11410	900	11210	870	11120	830	11400	850
14	12320	910	12080	870	11950	830	12230	830
15	13300	980	12930	850	12840	890	13110	880
16	14300	<b>1130</b>	13850	920	13750	910	13990	880
17	15540	1240	14850	<b>1010</b>	14760	1010	14940	950
18	16570	1030	15930	1080	15880	1120	16060	1120
19	17380	810	17020	1090	16920	1040	17170	1110
20	<b>17960</b>	580	<b>18560</b>	1540	<b>18650</b>	1730	<b>18650</b>	1480
Average		905		929		928		927
Stdev		140		166		206		155
Coeff of var		15 %		18 %		22 %		17 %

Test 8: Alumina + Fluoride / Cycle 8								
Dump nr.	Accumulated	Dump weight	Accumulated	Dump weight	Accumulated	Dump weight	Accumulated	Dump weight
	Feeder 1 / Cycle 8	Feeder 1 / Cycle 8	Feeder 2 / Cycle 8	Feeder 2 / Cycle 8	Feeder 3 / Cycle 8	Feeder 3 / Cycle 8	Feeder 4 / Cycle 8	Feeder 4 / Cycle 8
1	670	670	790	790	710	710	710	710
2	1600	930	1660	870	1570	860	1530	820
3	2550	950	2570	910	2430	860	2380	850
4	3490	940	3570	<b>960</b>	3320	890	3290	910
5	4480	990	4510	940	4190	870	4210	920
6	5470	990	5420	910	5190	<b>920</b>	5170	960
7	6430	960	6410	990	6120	930	6110	940
8	7340	910	7290	880	7030	910	7110	<b>890</b>
9	8270	930	8200	910	7940	910	7950	840
10	9210	940	9140	940	8790	850	8790	840
11	10170	960	10010	870	9630	840	9670	880
12	11120	950	10900	890	10580	950	10600	930
13	12130	1010	11790	890	11480	900	11500	900
14	13110	980	12690	900	12370	890	12460	960
15	14180	1070	13670	980	13370	1000	13410	950
16	15310	1130	14680	1010	14360	990	14490	1080
17	16450	1140	15800	1120	15460	1100	15620	1130
18	17450	<b>890</b>	16800	1000	16600	1140	16790	1170
19	17930	480	17610	810	17490	890	17700	910
20	<b>18170</b>	240	<b>18260</b>	650	<b>18500</b>	1010	<b>18580</b>	880
Average		903		911		921		924
Stdev		212		96		94		106
Coeff of var		24 %		11 %		10 %		11 %

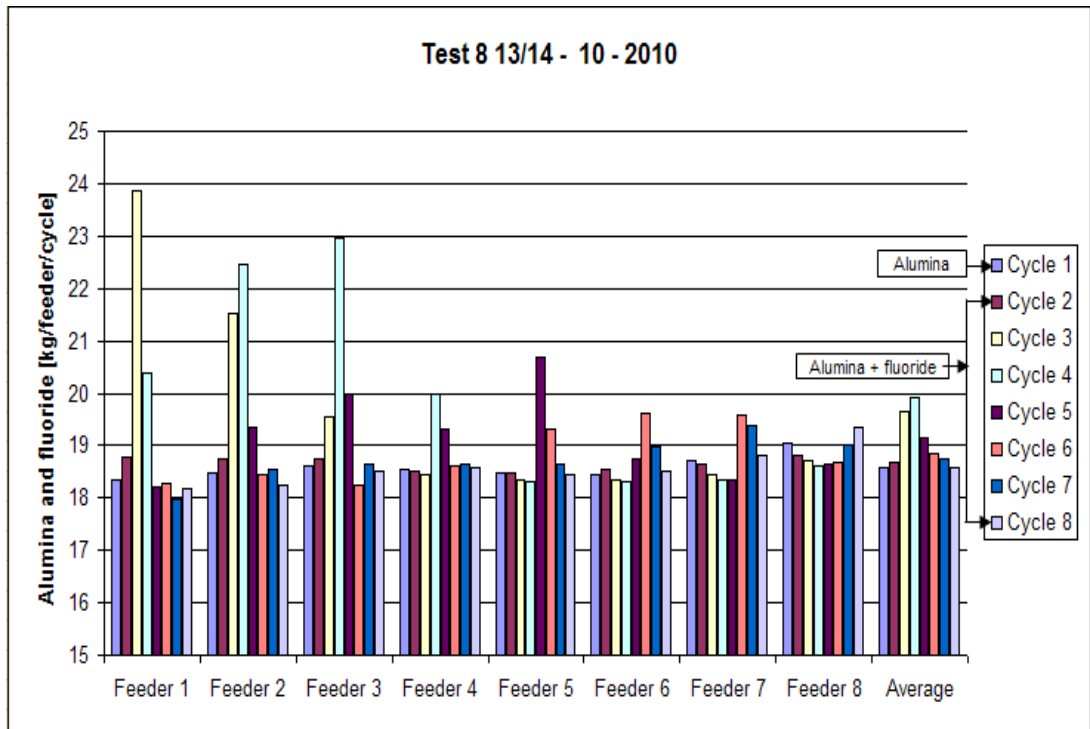


Figure 272 Alumina and fluoride distribution from feeder 1 to 8.

Table 101 Test 9: Open valve for refilling of alumina from the silo. Alumina and fluoride mass balance: [kg] / feeder / cycle.

Test 9								
	Cycle 1	Cycle 2	Cycle 3	Cycle 4	Cycle 5	Cycle 6	Cycle 7	Cycle 8
Feeder 1	18 240	18730	22460	23500	19640	18230	18270	18150
Feeder 2	18340	18930	20520	22290	20000	18230	18300	18140
Feeder 3	18530	18880	19330	20780	19980	18750	18470	18350
Feeder 4	18430	18680	18560	18550	21250	19980	18470	18380
Feeder 5	18460	18730	18560	18420	19830	19520	18250	18360
Feeder 6	18150	18630	18450	18430	18180	20140	19610	18280
Feeder 7	18540	18570	18450	18440	18420	19300	20000	19410
Feeder 8	18650	18860	18890	18910	18660	18830	18920	19540
Average [g]	18 418	18 751	19 403	19 915	19 495	19 123	18 786	18 576
Stdev	166	128	1419	2026	1020	735	672	563
Coeff of var	1 %	1 %	7 %	10 %	5 %	4 %	4 %	3 %
Sum [kg]	147	150	155	159	156	153	150	149

**Table 102 Test 9: Open valve for refilling of alumina from the silo. Alumina and fluoride accumulated and individual dump weights: [grams] / feeder / cycle. Cycle 1 only alumina, cycle 2 to 8 alumina mixed with fluoride.**

Test 9: Alumina / Cycle 1								
Dump nr.	Accumulated	Dump weight	Accumulated	Dump weight	Accumulated	Dump weight	Accumulated	Dump weight
	Feeder 1 / Cycle 1	Feeder 1 / Cycle 1	Feeder 2 / Cycle 1	Feeder 2 / Cycle 1	Feeder 3 / Cycle 1	Feeder 3 / Cycle 1	Feeder 4 / Cycle 1	Feeder 4 / Cycle 1
1	680	680	690	690	640	640	650	650
2	1580	900	1520	830	1410	770	1460	810
3	2540	960	2490	970	2260	850	2420	960
4	3540	<b>1110</b>	3450	960	3120	860	3340	920
5	4470	930	4370	920	4010	890	4270	930
6	5450	980	5370	<b>980</b>	4890	880	5200	930
7	6420	970	6280	910	5790	900	6130	930
8	7400	980	7220	940	6790	<b>940</b>	7030	900
9	8380	980	8130	910	7720	930	7960	930
10	9390	1010	9050	920	8620	900	8960	<b>960</b>
11	10320	930	9940	890	9500	880	9950	990
12	11250	930	10840	900	10390	890	10880	930
13	12240	990	11740	900	11270	880	11810	930
14	13170	930	12650	910	12170	900	12760	950
15	14150	980	13550	900	13070	900	13720	960
16	15190	1040	14520	970	13990	920	14700	980
17	16310	1120	15670	1150	14990	1000	15790	1090
18	17240	930	16780	1110	16070	1080	16830	1040
19	17860	620	17620	840	17080	1010	17690	860
20	<b>18240</b>	380	<b>18340</b>	720	<b>18530</b>	1450	<b>18430</b>	740
Average		918		916		924		920
Stdev		172		105		152		97
Coeff of var		19 %		11 %		16 %		11 %

Test 9: Alumina + Fluoride / Cycle 2								
Dump nr.	Accumulated	Dump weight	Accumulated	Dump weight	Accumulated	Dump weight	Accumulated	Dump weight
	Feeder 1 / Cycle 2	Feeder 1 / Cycle 2	Feeder 2 / Cycle 2	Feeder 2 / Cycle 2	Feeder 3 / Cycle 2	Feeder 3 / Cycle 2	Feeder 4 / Cycle 2	Feeder 4 / Cycle 2
1	800	800	810	810	830	830	920	920
2	1680	880	1570	760	2180	1350	1800	880
3	2590	910	2430	860	3180	1000	2710	910
4	3510	920	3310	880	4090	910	3660	950
5	4440	930	4210	900	4970	880	4590	930
6	5300	860	5050	840	5800	830	5480	890
7	6170	870	5910	860	6660	860	6400	920
8	7170	<b>980</b>	6880	970	7490	830	7300	900
9	8080	910	7780	900	8420	930	8190	890
10	9000	920	8780	<b>900</b>	9280	860	9060	870
11	9900	900	9620	840	10170	890	9960	900
12	10800	900	10440	820	11170	<b>910</b>	10840	880
13	11760	960	11300	860	12060	890	11840	<b>940</b>
14	12700	940	12380	1080	12940	880	12730	890
15	13650	950	13310	930	13830	890	13570	840
16	14650	1000	14210	900	14710	880	14510	940
17	15700	1050	15180	970	15680	970	15580	1070
18	16730	1030	16260	1080	16720	1040	16650	1070
19	17720	990	17300	1040	17700	980	17610	960
20	<b>18730</b>	1010	<b>18930</b>	1630	<b>18880</b>	1180	<b>18680</b>	1070
Average		936		942		940		931
Stdev		62		184		128		67
Coeff of var		7 %		19 %		14 %		7 %

Test 9: Alumina + Fluoride / Cycle 3								
Dump nr.	Accumulated	Dump weight	Accumulated	Dump weight	Accumulated	Dump weight	Accumulated	Dump weight
	Feeder 1 / Cycle 3	Feeder 1 / Cycle 3	Feeder 2 / Cycle 3	Feeder 2 / Cycle 3	Feeder 3 / Cycle 3	Feeder 3 / Cycle 3	Feeder 4 / Cycle 3	Feeder 4 / Cycle 3
1	910	910	740	740	730	730	810	810
2	1700	790	1700	960	1550	820	1670	860
3	3540	1840	2730	1030	2470	920	2610	940
4	4880	1340	3820	1090	3390	920	3530	920
5	6230	1350	4910	1090	4300	910	4480	950
6	7600	1370	6020	1110	5210	910	5420	940
7	9010	1410	7060	1040	6130	920	6310	890
8	10010	<b>1170</b>	8090	1030	7080	950	7180	870
9	11380	1370	9160	1070	7990	910	8420	1240
10	12720	1340	10210	1050	8990	<b>1020</b>	9410	990
11	14090	1370	11190	980	9970	980	10310	900
12	15450	1360	12190	<b>1010</b>	10860	890	11250	940
13	16790	1340	13260	1070	11850	990	12150	900
14	18220	1430	14290	1030	12810	960	13150	<b>980</b>
15	19650	1430	15390	1100	13740	930	14040	890
16	20950	1300	16490	1100	14680	940	14960	920
17	21850	900	17660	1170	15670	990	16030	1070
18	22250	400	18730	1070	16790	1120	17120	1090
19	22410	160	19640	910	17810	1020	17940	820
20	<b>22460</b>	50	<b>20520</b>	880	<b>19330</b>	1520	<b>18560</b>	620
Average		1132		1027		968		927
Stdev		462		96		152		122
Coeff of var		41 %		9 %		16 %		13 %

Test 9: Alumina + Fluoride / Cycle 4								
Dump nr.	Accumulated	Dump weight	Accumulated	Dump weight	Accumulated	Dump weight	Accumulated	Dump weight
	Feeder 1 / Cycle 4	Feeder 1 / Cycle 4	Feeder 2 / Cycle 4	Feeder 2 / Cycle 4	Feeder 3 / Cycle 4	Feeder 3 / Cycle 4	Feeder 4 / Cycle 4	Feeder 4 / Cycle 4
1	1140	1140	960	960	810	810	800	800
2	2660	1520	2190	1230	1850	1040	1730	930
3	4070	1410	3490	1300	2960	1110	2660	930
4	5500	1430	4830	1340	4080	1120	3600	940
5	6900	1400	6130	1300	5180	1100	4540	940
6	8370	1470	7430	1300	6300	1120	5460	920
7	9740	1370	8740	1310	7390	1090	6380	920
8	11090	1350	10130	1390	8810	1420	7370	990
9	12480	1390	11410	1280	9950	1140	8290	920
10	13930	1450	12680	1270	11070	1120	9230	940
11	15330	1400	13950	1270	12160	1090	10150	920
12	16330	1400	15190	1240	13310	1150	11080	930
13	17750	1420	16500	1310	14440	1130	11990	910
14	19210	1460	17500	1340	15530	1090	12900	910
15	20740	1530	18860	1360	16730	1200	13870	970
16	21830	1090	20060	1200	17730	1330	14870	1060
17	22920	1090	21260	1200	19000	1270	15950	1080
18	23220	300	21940	680	19920	920	17040	1090
19	23360	140	22200	260	20500	580	17910	870
20	23500	140	22290	90	20780	280	18550	640
Average		1195		1132		1056		931
Stdev		450		364		254		96
Coeff of var		38 %		32 %		24 %		10 %

Test 9: Alumina + Fluoride / Cycle 5								
Dump nr.	Accumulated	Dump weight	Accumulated	Dump weight	Accumulated	Dump weight	Accumulated	Dump weight
	Feeder 1 / Cycle 5	Feeder 1 / Cycle 5	Feeder 2 / Cycle 5	Feeder 2 / Cycle 5	Feeder 3 / Cycle 5	Feeder 3 / Cycle 5	Feeder 4 / Cycle 5	Feeder 4 / Cycle 5
1	1150	1150	1130	1130	1310	1310	830	830
2	2250	1100	2190	1060	2540	1230	1850	1020
3	3250	1000	3160	970	3500	960	3120	1270
4	4200	950	4020	860	4460	960	4360	1240
5	5120	920	4910	890	5370	910	5610	1250
6	6040	920	5760	850	6280	910	6870	1260
7	6970	930	6640	880	7240	960	8130	1260
8	7900	930	7520	880	8210	970	9280	1150
9	8850	950	8440	920	9180	970	10490	1210
10	9780	930	9310	870	10120	940	11690	1200
11	10720	940	10130	820	11070	950	12930	1240
12	11610	890	10940	810	12040	970	13930	1280
13	12560	950	11810	870	13040	1000	15140	1210
14	13560	980	12610	800	13990	950	16470	1330
15	14540	980	13500	890	15000	1010	17840	1370
16	15490	950	14500	950	16040	1040	19090	1250
17	16600	1110	15440	940	17040	1310	20110	1020
18	17800	1200	16410	970	18240	1200	20810	700
19	18850	1050	17510	1100	19190	950	21130	320
20	19640	790	20000	2490	19980	790	21250	120
Average		981		998		1015		1077
Stdev		97		363		138		337
Coeff of var		10 %		36 %		14 %		31 %

Test 9: Alumina + Fluoride / Cycle 6								
Dump nr.	Accumulated	Dump weight	Accumulated	Dump weight	Accumulated	Dump weight	Accumulated	Dump weight
	Feeder 1 / Cycle 6	Feeder 1 / Cycle 6	Feeder 2 / Cycle 6	Feeder 2 / Cycle 6	Feeder 3 / Cycle 6	Feeder 3 / Cycle 6	Feeder 4 / Cycle 6	Feeder 4 / Cycle 6
1	750	750	830	830	770	770	1250	1250
2	1700	950	1840	1010	1630	860	2370	1120
3	2680	980	2800	960	2560	930	3350	980
4	3610	930	3750	950	3560	950	4350	970
5	4610	1000	4690	940	4480	920	5310	960
6	5610	1000	5670	980	5360	880	6230	920
7	6590	980	6610	940	6280	920	7170	940
8	7550	960	7580	970	7280	1000	8100	930
9	8510	960	8550	970	8220	940	9070	970
10	9490	980	9430	880	9180	960	9930	860
11	10490	1000	10330	900	10110	930	10860	930
12	11490	1000	11270	940	11040	930	11800	940
13	12460	970	12210	940	12010	970	12720	920
14	13450	990	13110	900	12980	970	13640	920
15	14510	1060	14090	980	13970	990	14600	960
16	15510	1010	15100	1010	14970	1000	15620	1020
17	16610	1100	16100	1130	16160	1190	16850	1230
18	17500	890	17060	960	17250	1090	18120	1270
19	18000	500	17770	710	18090	840	19190	1070
20	18230	230	18230	460	18750	660	19980	790
Average		912		918		935		998
Stdev		204		135		109		128
Coeff of var		22 %		15 %		12 %		13 %

Test 9: Alumina + Fluoride / Cycle 7								
Dump nr.	Accumulated	Dump weight	Accumulated	Dump weight	Accumulated	Dump weight	Accumulated	Dump weight
	Feeder 1 / Cycle 7	Feeder 1 / Cycle 7	Feeder 2 / Cycle 7	Feeder 2 / Cycle 7	Feeder 3 / Cycle 7	Feeder 3 / Cycle 7	Feeder 4 / Cycle 7	Feeder 4 / Cycle 7
1	930	930	740	740	730	730	1010	1010
2	1960	1030	1660	920	1590	860	2020	1010
3	2980	1020	2640	980	2560	970	2970	950
4	3970	990	3570	930	3450	890	3960	990
5	5090	1120	4570	<b>990</b>	4410	960	4900	940
6	6170	1080	5550	980	5410	<b>940</b>	5900	<b>940</b>
7	7190	1020	6480	930	6360	950	6820	920
8	8200	1010	7400	920	7260	900	7790	970
9	9180	980	8360	960	8170	910	8940	1150
10	10160	980	9310	950	9070	900	9820	880
11	11100	940	10280	970	9990	920	10720	900
12	12090	990	11190	910	10890	900	11640	920
13	13090	1000	12130	940	11820	930	12550	910
14	14120	1030	13100	970	12680	860	13470	920
15	15270	1150	14100	1000	13590	910	14420	950
16	16380	1110	15070	970	14600	1010	15510	1090
17	17380	<b>1100</b>	16130	1060	15750	1150	16640	1130
18	17940	560	17130	1000	16840	1090	17580	940
19	18150	210	17860	730	17710	870	18180	600
20	<b>18270</b>	120	<b>18300</b>	440	<b>18470</b>	760	<b>18470</b>	290
Average		919		915		921		921
Stdev		284		136		94		186
Coeff of var		31 %		15 %		10 %		20 %

Test 9: Alumina + Fluoride / Cycle 8								
Dump nr.	Accumulated	Dump weight	Accumulated	Dump weight	Accumulated	Dump weight	Accumulated	Dump weight
	Feeder 1 / Cycle 8	Feeder 1 / Cycle 8	Feeder 2 / Cycle 8	Feeder 2 / Cycle 8	Feeder 3 / Cycle 8	Feeder 3 / Cycle 8	Feeder 4 / Cycle 8	Feeder 4 / Cycle 8
1	830	830	750	750	800	800	800	800
2	1870	1040	1720	970	1675	875	1725	925
3	2910	1040	2690	970	2550	875	2650	925
4	3910	<b>920</b>	3640	<b>990</b>	3490	940	3580	930
5	4960	1050	4610	970	4420	930	4540	960
6	5930	970	5610	1000	5350	930	5470	930
7	6890	960	6570	960	6300	950	6380	910
8	7870	980	7500	930	7300	<b>1000</b>	7380	<b>940</b>
9	8860	990	8420	920	8190	890	8300	920
10	9820	960	9340	920	9130	940	9190	890
11	10770	950	10270	930	10080	950	10130	940
12	11720	950	11210	940	10990	910	11040	910
13	12720	1000	12160	950	11920	930	11960	920
14	13790	1070	13120	960	13050	1130	12900	940
15	14960	1170	14130	1010	14110	1060	13860	960
16	16190	1230	15160	1030	15200	1090	14880	1020
17	17150	960	16210	1050	16330	1130	15900	1020
18	17730	580	17150	940	17320	990	16910	1010
19	17940	210	17770	620	17970	650	17720	810
20	<b>18150</b>	210	<b>18140</b>	370	<b>18350</b>	380	<b>18380</b>	660
Average		904		909		918		916
Stdev		269		159		168		82
Coeff of var		30 %		17 %		18 %		9 %

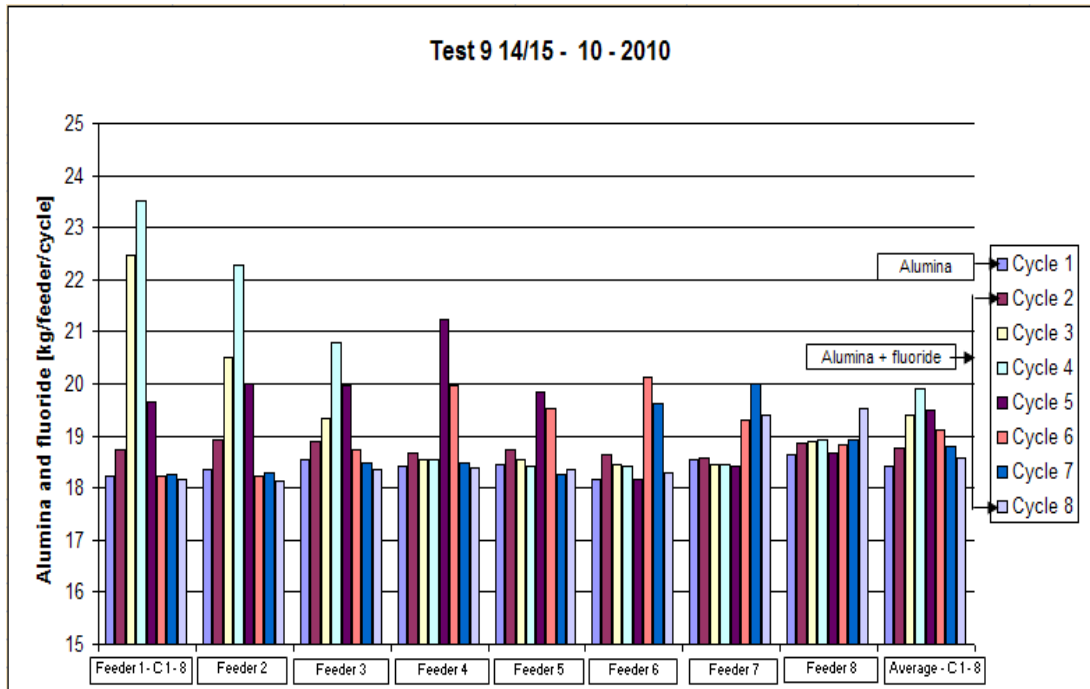


Figure 273 Alumina and fluoride distribution from feeder 1 to 8.

Table 103 Test 10: Open valve for refilling of alumina from the silo. Alumina and fluoride mass balance: [kg] / feeder / cycle.

Test 10								
	Cycle 1	Cycle 2	Cycle 3	Cycle 4	Cycle 5	Cycle 6	Cycle 7	Cycle 8
Feeder 1	18 400	18750	21970	22730	20780	18910	18430	18310
Feeder 2	18570	18730	20310	21300	22220	19640	18440	18370
Feeder 3	18630	18870	19490	19800	21760	19380	18580	18420
Feeder 4	18530	19070	18790	18560	19320	19320	18800	18540
Feeder 5	18600	18930	18610	18660	18740	20210	19600	18730
Feeder 6	18680	18930	18670	18410	18740	19380	20220	19350
Feeder 7	18820	19110	18740	18600	18720	18840	19510	19910
Feeder 8	19110	19290	19190	18920	19240	19020	18950	19200
Average [g]	18 668	18 960	19 471	19 623	19 940	19 338	19 066	18 854
Stdev	216	189	1159	1584	1437	445	647	575
Coeff of var	1 %	1 %	6 %	8 %	7 %	2 %	3 %	3 %
Sum [kg]	149	152	156	157	160	155	153	151

**Table 104 Test 10: Open valve for refilling of alumina from the silo. Alumina and fluoride accumulated and individual dump weights: [grams] / feeder / cycle. Cycle 1 only alumina, cycle 2 to 8 alumina mixed with fluoride.**

Test 10: Alumina / Cycle 1								
Dump nr.	Accumulated	Dump weight	Accumulated	Dump weight	Accumulated	Dump weight	Accumulated	Dump weight
	Feeder 1 / Cycle 1	Feeder 1 / Cycle 1	Feeder 2 / Cycle 1	Feeder 2 / Cycle 1	Feeder 3 / Cycle 1	Feeder 3 / Cycle 1	Feeder 4 / Cycle 1	Feeder 4 / Cycle 1
1								
2								
3								
4								
5								
6								
7								
8								
9								
10				Not measured				
11								
12								
13								
14								
15								
16								
17								
18								
19								
20	18400		18570		18630		18530	
Average								
Stdev								
Coeff of var								

Test 10: Alumina + Fluoride / Cycle 2								
Dump nr.	Accumulated	Dump weight	Accumulated	Dump weight	Accumulated	Dump weight	Accumulated	Dump weight
	Feeder 1 / Cycle 2	Feeder 1 / Cycle 2	Feeder 2 / Cycle 2	Feeder 2 / Cycle 2	Feeder 3 / Cycle 2	Feeder 3 / Cycle 2	Feeder 4 / Cycle 2	Feeder 4 / Cycle 2
1	840	840	800	800	870	870	970	970
2	1870	1030	1750	950	1710	840	1940	970
3	3000	1130	2750	1000	2800	1090	2940	1000
4	4020	1020	3690	940	3760	960	3890	950
5	5000	980	4670	980	4710	950	4890	1000
6	6030	1030	5590	920	5680	970	5760	870
7	7100	1070	6600	1010	6590	910	6600	840
8	8140	1040	7590	990	7530	940	7630	1030
9	9150	1010	8570	980	8490	960	8510	880
10	10260	1110	9550	980	9490	1000	9480	970
11	11230	970	10490	940	10470	980	10420	940
12	12330	1100	11460	970	11440	970	11340	920
13	13340	1010	12470	1010	12440	1000	12280	940
14	14350	1010	13430	960	13490	1050	13210	930
15	15430	1080	14430	1000	14480	990	14150	940
16	16610	1180	15480	1050	15550	1070	15130	980
17	17650	1040	16540	1060	16650	1100	16140	1010
18	18360	710	17470	930	17670	1020	17200	1060
19	18650	290	18220	750	18400	730	18130	930
20	18750	100	18730	510	18870	470	19070	940
Average		938		937		944		954
Stdev		275		124		141		54
Coeff of var		29 %		13 %		15 %		6 %

Test 10: Alumina + Fluoride / Cycle 3								
Dump nr.	Accumulated	Dump weight	Accumulated	Dump weight	Accumulated	Dump weight	Accumulated	Dump weight
	Feeder 1 / Cycle 3	Feeder 1 / Cycle 3	Feeder 2 / Cycle 3	Feeder 2 / Cycle 3	Feeder 3 / Cycle 3	Feeder 3 / Cycle 3	Feeder 4 / Cycle 3	Feeder 4 / Cycle 3
1	900	900	740	740	820	820	880	880
2	2200	1300	1820	1080	1730	910	1770	890
3	3610	1410	2950	1130	2760	1030	2830	1060
4	4920	1310	4100	1150	3760	1000	3730	900
5	6250	1330	5170	1070	4780	1020	4640	910
6	7560	1310	6350	1180	5780	1000	5530	890
7	9130	1570	7450	1100	6820	1040	6430	900
8	10480	1350	8510	1060	7830	1010	7350	920
9	11880	1400	9580	1070	8820	990	8290	940
10	13200	1320	10690	1110	9750	930	9210	920
11	14440	1240	11740	1050	10740	990	10130	920
12	15760	1320	12800	1060	11720	980	11070	940
13	17060	1300	13890	1090	12800	1080	11970	900
14	18410	1350	14940	1050	13800	1000	12880	910
15	19730	1320	16050	1110	14830	1030	13750	870
16	20890	1160	17210	1160	15850	1020	14660	910
17	21630	740	18310	1100	16880	1030	15680	1020
18	21880	250	19310	1000	18000	1120	16710	1030
19	21950	70	19950	640	18820	820	17650	940
20	21970	20	20310	360	19490	670	18790	1140
Average		1099		1016		975		940
Stdev		461		203		103		69
Coeff of var		42 %		20 %		11 %		7 %



Test 10: Alumina + Fluoride / Cycle 4								
Dump nr.	Accumulated	Dump weight	Accumulated	Dump weight	Accumulated	Dump weight	Accumulated	Dump weight
	Feeder 1 / Cycle 4	Feeder 1 / Cycle 4	Feeder 2 / Cycle 4	Feeder 2 / Cycle 4	Feeder 3 / Cycle 4	Feeder 3 / Cycle 4	Feeder 4 / Cycle 4	Feeder 4 / Cycle 4
1	1010	1010	810	810	850	850	910	910
2	2340	1330	1950	1140	1840	990	1900	990
3	3720	1380	3120	1170	2900	1060	2860	960
4	5720	2000	4290	1170	3970	1070	3880	1020
5	6500	780	5520	1230	5090	1120	4890	1010
6	7910	1410	6720	1200	6180	1090	5850	960
7	9210	1300	7810	1090	7180	1000	6740	890
8	10520	1310	8970	1160	8170	990	7640	900
9	11880	1360	10120	1150	9220	1050	8560	920
10	13210	1330	11230	1110	10280	1060	9470	910
11	14510	1300	12360	1130	11300	1020	10360	890
12	15860	1350	13490	1130	12400	1100	11290	930
13	17220	1360	14600	1110	13390	990	12300	1010
14	18650	1430	15600	1000	14620	1230	13240	940
15	20150	1500	16900	1300	15700	1080	14140	900
16	21450	1300	18130	1230	16680	980	15110	970
17	22280	830	19390	1260	17880	1200	16180	1070
18	22550	270	20420	1030	18860	980	17210	1030
19	22660	110	21040	620	19470	610	17990	780
20	22730	70	21300	260	19800	330	18560	570
Average		1137		1065		990		928
Stdev		492		245		201		107
Coeff of var		43 %		23 %		20 %		11 %

Test 10: Alumina + Fluoride / Cycle 5								
Dump nr.	Accumulated	Dump weight	Accumulated	Dump weight	Accumulated	Dump weight	Accumulated	Dump weight
	Feeder 1 / Cycle 5	Feeder 1 / Cycle 5	Feeder 2 / Cycle 5	Feeder 2 / Cycle 5	Feeder 3 / Cycle 5	Feeder 3 / Cycle 5	Feeder 4 / Cycle 5	Feeder 4 / Cycle 5
1	1080	1080	890	890	870	870	730	730
2	3080	2000	2180	1290	1930	1060	1680	950
3	4340	1260	3450	1270	3110	1180	2730	1050
4	5490	1150	4650	1200	4440	1330	3780	1050
5	6680	1190	5880	1230	5620	1180	4800	1020
6	7720	1040	6920	1040	6720	1100	5880	1080
7	9020	1300	8310	1390	8050	1330	6910	1030
8	11200	2180	9110	800	9270	1220	7950	1040
9	11330	130	10740	1630	10570	1300	8960	1010
10	12590	1260	11410	670	11690	1120	9990	1030
11	13800	1210	13110	1700	12890	1200	10960	970
12	14980	1180	14226	1116	14070	1180	11970	1010
13	16200	1220	15420	1194	15210	1140	12990	1020
14	18650	2450	16440	1020	16330	1120	14020	1030
15	19800	1150	17690	1250	17440	1110	14940	920
16	20490	690	18880	1190	18650	1210	15910	970
17	20710	220	20100	1220	19870	1220	16810	900
18	20760	50	21180	1080	20880	1010	18090	1280
19	20760	0	21920	740	21510	630	18890	800
20	20780	20	22220	300	21760	250	19320	430
Average		1039		1111		1088		966
Stdev		697		322		254		167
Coeff of var		67 %		29 %		23 %		17 %

Test 10: Alumina + Fluoride / Cycle 6								
Dump nr.	Accumulated	Dump weight	Accumulated	Dump weight	Accumulated	Dump weight	Accumulated	Dump weight
	Feeder 1 / Cycle 6	Feeder 1 / Cycle 6	Feeder 2 / Cycle 6	Feeder 2 / Cycle 6	Feeder 3 / Cycle 6	Feeder 3 / Cycle 6	Feeder 4 / Cycle 6	Feeder 4 / Cycle 6
1	900	900	950	950	1030	1030	760	760
2	1970	1070	2140	1190	2130	1100	1780	1020
3	3030	1060	3070	930	3030	900	2840	1060
4	4070	1040	4030	960	4010	980	3840	1000
5	5120	1050	4990	960	5030	1020	4830	990
6	6140	1020	5880	890	5970	940	5830	1000
7	7130	990	6750	870	6870	900	6790	960
8	8110	980	7670	920	7850	980	7790	1000
9	9090	980	8580	910	8800	950	9070	1280
10	10060	970	9510	930	9740	940	10140	1070
11	11010	950	10420	910	10670	930	11130	990
12	11960	950	11380	960	11590	920	12140	1010
13	12940	980	12340	960	12520	930	13140	1000
14	14010	1070	13290	950	13490	970	14170	1030
15	15050	1040	14260	970	14460	970	15160	990
16	16230	1180	15250	990	15450	990	16340	1180
17	17400	1170	16330	1080	16430	980	17540	1200
18	18290	890	17520	1190	17630	1200	18530	990
19	18730	440	18620	1100	18690	1060	19100	570
20	18910	180	19640	1020	19380	690	19320	220
Average		946		982		969		966
Stdev		234		91		98		228
Coeff of var		25 %		9 %		10 %		24 %

Test 10: Alumina + Fluoride / Cycle 7								
Dump nr.	Accumulated	Dump weight	Accumulated	Dump weight	Accumulated	Dump weight	Accumulated	Dump weight
	Feeder 1 / Cycle 6	Feeder 1 / Cycle 6	Feeder 2 / Cycle 6	Feeder 2 / Cycle 6	Feeder 3 / Cycle 6	Feeder 3 / Cycle 6	Feeder 4 / Cycle 6	Feeder 4 / Cycle 6
1	800	800	810	810	720	720	850	850
2	1830	1030	1830	1020	1610	890	1860	1010
3	2830	1000	2790	960	2560	950	2830	970
4	3820	990	3730	940	3520	<b>960</b>	3790	960
5	4850	1030	4700	970	4440	920	4720	930
6	5870	1020	5700	1000	5460	1020	5660	<b>940</b>
7	6840	970	6570	870	6350	890	6680	1020
8	7970	1130	7480	910	7260	910	7660	980
9	9030	1060	8410	930	8160	900	8640	980
10	10030	1000	9330	920	9030	870	9590	950
11	11060	1030	10190	860	9960	930	10570	980
12	12060	1000	11090	900	10850	890	11540	970
13	13060	1000	11990	900	11760	910	12470	930
14	14030	<b>970</b>	12930	940	12700	940	13410	940
15	15110	1080	13920	990	13750	1050	14370	960
16	16220	1110	14900	<b>980</b>	14820	1070	15410	1040
17	17280	1060	15970	<b>1070</b>	15960	1140	16520	1110
18	17980	700	17010	1040	17030	1070	17550	1030
19	18300	320	17790	780	17900	870	18280	730
20	<b>18430</b>	130	<b>18440</b>	650	<b>18580</b>	680	<b>18800</b>	520
Average		922		922		929		940
Stdev		259		97		109		125
Coeff of var		28 %		11 %		12 %		13 %

Test 10: Alumina + Fluoride / Cycle 8								
Dump nr.	Accumulated	Dump weight	Accumulated	Dump weight	Accumulated	Dump weight	Accumulated	Dump weight
	Feeder 1 / Cycle 6	Feeder 1 / Cycle 6	Feeder 2 / Cycle 6	Feeder 2 / Cycle 6	Feeder 3 / Cycle 6	Feeder 3 / Cycle 6	Feeder 4 / Cycle 6	Feeder 4 / Cycle 6
1	820	820	830	830	760	760	870	870
2	1780	960	1820	990	1630	870	1890	1020
3	2900	1120	2790	970	2570	940	2850	960
4	3920	1020	3770	<b>980</b>	3530	960	3790	940
5	4970	1050	4710	940	4510	980	4790	1000
6	6030	1060	5640	930	5430	<b>920</b>	5800	1010
7	6990	960	6580	940	6350	920	6720	920
8	7940	950	7470	890	7240	890	7670	<b>950</b>
9	8890	950	8400	930	8130	890	8670	1000
10	9960	1070	9340	940	9020	890	9590	920
11	10960	1000	10240	900	9990	970	10600	1010
12	11930	970	11160	920	10890	900	11550	950
13	12940	1010	12080	920	11790	900	12490	940
14	14000	1060	13000	920	12720	930	13420	930
15	15070	1070	13950	950	13690	970	14440	1020
16	16250	<b>1180</b>	14950	1000	14740	1050	15450	1010
17	17280	1030	16000	1050	15900	1160	16510	1060
18	17960	680	17000	1000	16960	1060	17440	930
19	18230	270	17770	770	17780	820	18110	670
20	<b>18310</b>	80	<b>18370</b>	600	<b>18420</b>	640	<b>18540</b>	430
Average		916		919		921		927
Stdev		276		97		109		142
Coeff of var		30 %		11 %		12 %		15 %

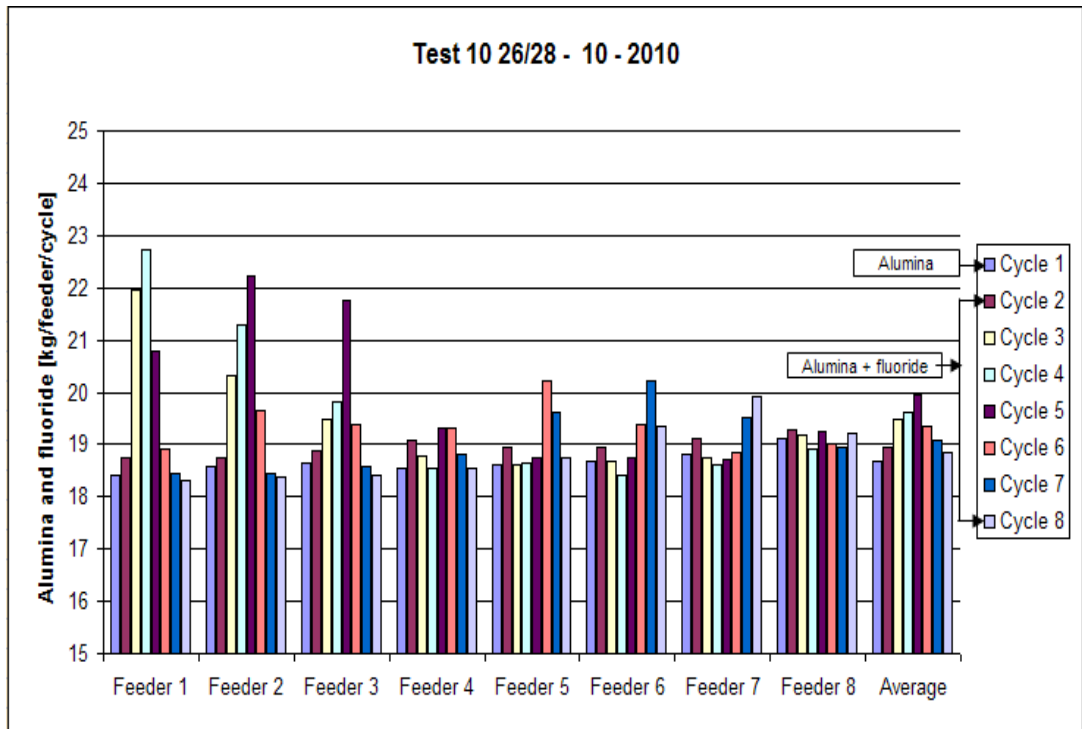


Figure 274 Alumina and fluoride distribution from feeder 1 to 8.

Table 105 Test 11: Open valve for refilling of alumina from the silo. Alumina and fluoride mass balance: [kg] / feeder / cycle.

Test 11								
	Cycle 1	Cycle 2	Cycle 3	Cycle 4	Cycle 5	Cycle 6	Cycle 7	Cycle 8
Feeder 1	18 180	18630	23440	20260	18360	18340	18370	18470
Feeder 2	18 350	19020	21520	21480	18960	18530	18450	18350
Feeder 3	18 330	18940	18980	22450	19710	18660	18370	18260
Feeder 4	18 300	18460	18290	20610	19400	18660	18470	18330
Feeder 5	18 510	18470	18490	18690	19800	19060	18400	18450
Feeder 6	18 460	18480	18290	18330	19450	19360	18600	18510
Feeder 7	18 520	18560	18470	18350	18630	19560	19420	18800
Feeder 8	19 190	19040	18880	18870	18730	19270	19570	19570
Average [g]	18 480	18 700	19 545	19 880	19 130	18 930	18 706	18 593
Stdev	309	256	1899	1559	534	442	494	427
Coeff of var	2 %	1 %	10 %	8 %	3 %	2 %	3 %	2 %
Sum [kg]	148	150	156	159	153	151	150	149

**Table 106 Test 11: Open valve for refilling of alumina from the silo. Alumina and fluoride accumulated and individual dump weights: [grams] / feeder / cycle. Cycle 1 only alumina, cycle 2 to 8 alumina mixed with fluoride.**

Test 11: Alumina / Cycle 1								
Dump nr.	Accumulated	Dump weight	Accumulated	Dump weight	Accumulated	Dump weight	Accumulated	Dump weight
	Feeder 1 / Cycle 1	Feeder 1 / Cycle 1	Feeder 2 / Cycle 1	Feeder 2 / Cycle 1	Feeder 3 / Cycle 1	Feeder 3 / Cycle 1	Feeder 4 / Cycle 1	Feeder 4 / Cycle 1
1	760	760	600	600	630	630	710	710
2	1690	930	1430	830	1360	730	1540	830
3	2610	920	2240	810	2170	810	2350	810
4	3550	<b>940</b>	3070	<b>830</b>	3020	<b>850</b>	3200	850
5	4470	920	3910	840	3870	850	4030	830
6	5380	910	4790	880	4710	840	4860	830
7	6300	920	5870	1080	5520	810	5690	830
8	7280	980	6780	910	6410	890	6550	860
9	8270	990	7630	850	7230	820	7380	830
10	9640	1370	8470	840	8060	830	8230	<b>850</b>
11	10140	500	9320	850	8890	830	9160	930
12	11090	950	10150	830	9700	810	9990	830
13	12020	930	11040	890	10500	800	10820	830
14	12930	910	11890	850	11320	820	11610	790
15	13880	950	12710	820	12210	890	12430	820
16	14880	1000	13580	870	13060	850	13250	820
17	15920	1040	14480	900	13980	920	14210	960
18	16910	990	15430	950	15050	1070	15110	900
19	17620	710	16420	990	16080	1030	16090	980
20	<b>18180</b>	<b>560</b>	<b>18350</b>	<b>1930</b>	<b>18330</b>	<b>2250</b>	<b>18300</b>	<b>2210</b>
Average		909		918		917		915
Stdev		180		255		327		311
Coeff of var		20 %		28 %		36 %		34 %

Test 11: Alumina + Fluoride / Cycle 2								
Dump nr.	Accumulated	Dump weight	Accumulated	Dump weight	Accumulated	Dump weight	Accumulated	Dump weight
	Feeder 1 / Cycle 2	Feeder 1 / Cycle 2	Feeder 2 / Cycle 2	Feeder 2 / Cycle 2	Feeder 3 / Cycle 2	Feeder 3 / Cycle 2	Feeder 4 / Cycle 2	Feeder 4 / Cycle 2
1	900	900	800	800	740	740	820	820
2	1850	950	1660	860	1520	780	1630	810
3	2830	980	2510	850	2430	910	2490	860
4	3820	<b>990</b>	3370	<b>860</b>	3290	860	3380	890
5	4830	1010	4350	980	4180	890	4260	880
6	5830	1000	5290	940	5060	880	5140	880
7	6840	1010	6220	930	5950	890	5990	850
8	7840	1000	7220	1000	6890	940	6830	840
9	8820	980	8170	950	7770	880	7720	890
10	9810	990	9100	930	8690	<b>920</b>	8630	910
11	10730	920	10040	940	9590	900	9500	870
12	11650	920	10970	930	10460	870	10420	<b>920</b>
13	12570	920	11870	900	11710	1250	11290	870
14	13510	940	12800	930	12720	1010	12170	880
15	14480	970	13730	930	13600	880	13050	880
16	15540	1060	14650	920	14570	970	13990	940
17	16680	1140	15650	1000	15560	990	15000	1010
18	17630	950	16640	990	16660	1100	16060	1060
19	18280	650	17630	990	17640	980	17060	1000
20	<b>18630</b>	<b>350</b>	<b>19020</b>	<b>1390</b>	<b>18940</b>	<b>1300</b>	<b>18460</b>	<b>1400</b>
Average		932		951		947		923
Stdev		165		116		137		129
Coeff of var		18 %		12 %		14 %		14 %

Test 11: Alumina + Fluoride / Cycle 3								
Dump nr.	Accumulated	Dump weight	Accumulated	Dump weight	Accumulated	Dump weight	Accumulated	Dump weight
	Feeder 1 / Cycle 3	Feeder 1 / Cycle 3	Feeder 2 / Cycle 3	Feeder 2 / Cycle 3	Feeder 3 / Cycle 3	Feeder 3 / Cycle 3	Feeder 4 / Cycle 3	Feeder 4 / Cycle 3
1	870	870	760	760	780	780	750	750
2	2100	1230	1820	1060	1680	900	1550	800
3	3390	1290	2890	1070	2680	1000	2410	860
4	4700	1310	4040	1150	3730	1050	3320	910
5	6070	1370	5180	1140	4690	960	4200	880
6	7360	1290	6270	1090	5670	980	5080	880
7	8680	1320	7420	1150	6650	980	5990	910
8	10160	<b>1480</b>	8500	1080	7660	1010	6860	870
9	11480	1320	9620	1120	8700	1040	7750	890
10	13130	1650	10760	<b>1140</b>	9740	1040	8620	870
11	14460	1330	11880	1120	10760	1020	9490	870
12	15830	1370	12910	1030	11760	<b>1000</b>	10330	840
13	17220	1390	13960	1050	12730	970	11200	870
14	18580	1360	15020	1060	13720	990	12100	<b>900</b>
15	19970	1390	16150	1130	14710	990	12980	880
16	21330	1360	17270	1120	15750	1040	13930	950
17	22400	1070	18460	1190	16900	1150	14970	1040
18	23060	660	19590	1130	18060	1160	16080	1110
19	23330	270	20570	980	18980	920	17090	1010
20	<b>23440</b>	<b>110</b>	<b>21520</b>	<b>950</b>	<b>18980</b>	<b>0</b>	<b>18290</b>	<b>1200</b>
Average		1172		1076		949		915
Stdev		397		95		238		104
Coeff of var		34 %		9 %		25 %		11 %

Test 11: Alumina + Fluoride / Cycle 4								
Dump nr.	Accumulated	Dump weight	Accumulated	Dump weight	Accumulated	Dump weight	Accumulated	Dump weight
	Feeder 1 / Cycle 4	Feeder 1 / Cycle 4	Feeder 2 / Cycle 4	Feeder 2 / Cycle 4	Feeder 3 / Cycle 4	Feeder 3 / Cycle 4	Feeder 4 / Cycle 4	Feeder 4 / Cycle 4
1	1260	1260	1140	1140	960	960	790	790
2	2320	1060	2380	1240	2110	1150	1730	940
3	3330	1010	3480	1100	3290	1180	2830	1100
4	4290	960	4520	1040	4690	1400	3940	1110
5	5200	910	5550	1030	5910	1220	5070	1130
6	6140	940	6500	950	7170	1260	6210	1140
7	7110	970	7460	960	8590	1420	7270	1060
8	8070	960	8490	1030	9980	1390	8360	1090
9	9020	950	9530	1040	11150	1170	9480	1120
10	10010	990	10520	990	12340	1190	10550	1070
11	10970	960	11520	1000	13520	1180	11610	1060
12	11880	910	12540	1020	14800	1280	12730	1120
13	12770	890	13580	1040	15970	1170	13790	1060
14	13690	920	14590	1010	17260	1290	14910	1120
15	14670	980	15590	1000	18580	1320	15960	1050
16	15690	1020	16750	1160	19960	1380	17100	1140
17	16890	1200	17950	1200	21100	1140	18230	1130
18	18240	1350	19190	1240	21870	770	19240	1010
19	19320	1080	20320	1130	22280	410	19950	710
20	20260	940	21480	1160	22450	170	20610	660
Average		1013		1074		1123		1031
Stdev		123		90		325		144
Coeff of var		12 %		8 %		29 %		14 %

Test 11: Alumina + Fluoride / Cycle 5								
Dump nr.	Accumulated	Dump weight	Accumulated	Dump weight	Accumulated	Dump weight	Accumulated	Dump weight
	Feeder 1 / Cycle 5	Feeder 1 / Cycle 5	Feeder 2 / Cycle 5	Feeder 2 / Cycle 5	Feeder 3 / Cycle 5	Feeder 3 / Cycle 5	Feeder 4 / Cycle 5	Feeder 4 / Cycle 5
1	800	800	880	880	950	950	1030	1030
2	1800	1000	1800	920	1970	1020	2060	1030
3	2650	850	2660	860	2980	1010	3010	950
4	3480	830	3550	890	3860	880	3960	950
5	4320	840	4420	870	4720	860	4900	940
6	5160	840	5300	880	5610	890	5840	940
7	6060	900	6110	810	6510	900	6780	940
8	6980	920	6930	820	7390	880	7700	920
9	7950	970	7770	840	8270	880	8610	910
10	8840	890	8590	820	9180	910	9530	920
11	9740	900	9470	880	10090	910	10440	910
12	10640	900	10330	860	10970	880	11340	900
13	11590	950	11140	810	11870	900	12200	860
14	12480	890	12070	930	12740	870	13050	850
15	13370	890	12920	850	13650	910	13980	930
16	14220	850	13880	960	14600	950	14960	980
17	15220	1000	14890	1010	15560	960	16080	1120
18	16200	980	15940	1050	16670	1110	17320	1240
19	17160	960	17030	1090	17830	1160	18380	1060
20	18360	1200	18960	1930	19710	1880	19400	1020
Average		918		948		986		970
Stdev		88		244		225		92
Coeff of var		10 %		26 %		23 %		10 %

Test 11: Alumina + Fluoride / Cycle 6								
Dump nr.	Accumulated	Dump weight	Accumulated	Dump weight	Accumulated	Dump weight	Accumulated	Dump weight
	Feeder 1 / Cycle 6	Feeder 1 / Cycle 6	Feeder 2 / Cycle 6	Feeder 2 / Cycle 6	Feeder 3 / Cycle 6	Feeder 3 / Cycle 6	Feeder 4 / Cycle 6	Feeder 4 / Cycle 6
1	770	770	940	940	850	850	790	790
2	1730	960	2060	1120	1650	800	1620	830
3	2650	920	2970	910	2480	830	2510	890
4	3530	880	3830	860	3360	880	3430	920
5	4440	910	4700	870	4230	870	4340	910
6	5360	920	5570	870	5180	950	5190	850
7	6320	960	6470	900	6290	1110	6090	900
8	7210	890	7340	870	7240	950	6980	890
9	8130	920	8200	860	8070	830	7820	840
10	9130	1000	9060	860	8870	800	8680	860
11	10040	910	9940	880	9800	930	9520	840
12	10930	890	10800	860	10750	950	10360	840
13	11830	900	11700	900	11560	810	11270	910
14	12770	940	12580	880	12460	900	12150	880
15	13640	870	13490	910	13330	870	13030	880
16	14640	1000	14430	940	14230	900	13980	950
17	15710	1070	15440	1010	15290	1060	14930	950
18	16760	1050	16420	980	16400	1110	16070	1140
19	17580	820	17380	960	17410	1010	17160	1090
20	18340	760	18530	1150	18660	1250	18660	1500
Average		917		927		933		933
Stdev		80		83		121		157
Coeff of var		9 %		9 %		13 %		17 %

Test 11: Alumina + Fluoride / Cycle 7								
Dump nr.	Accumulated	Dump weight	Accumulated	Dump weight	Accumulated	Dump weight	Accumulated	Dump weight
	Feeder 1 / Cycle 6	Feeder 1 / Cycle 6	Feeder 2 / Cycle 6	Feeder 2 / Cycle 6	Feeder 3 / Cycle 6	Feeder 3 / Cycle 6	Feeder 4 / Cycle 6	Feeder 4 / Cycle 6
1	780	780	750	750	910	910	880	880
2	1700	920	1580	830	1910	1000	1790	910
3	2620	920	2430	850	2710	800	2640	850
4	3530	910	3300	870	3570	<b>860</b>	3490	850
5	4480	950	4200	900	4420	850	4390	900
6	5400	920	5030	830	5280	860	5260	870
7	6340	940	5960	930	6140	860	6130	870
8	7230	890	6800	840	6990	850	7020	890
9	8120	890	7660	860	7860	870	7930	910
10	9040	920	8490	830	8730	870	8820	890
11	9930	890	9360	870	9670	940	9710	890
12	10840	910	10160	800	10540	870	10570	860
13	11720	880	10950	790	11410	870	11420	850
14	12630	<b>910</b>	11760	810	12270	860	12270	850
15	13560	930	12590	830	13190	920	13150	880
16	14550	990	13420	830	14210	1020	14080	930
17	15620	1070	14320	<b>900</b>	15300	1090	15040	960
18	16710	1090	15240	920	16410	1110	16170	1130
19	17530	820	16240	1000	17320	910	17170	1000
20	<b>18370</b>	840	<b>18450</b>	2210	<b>18370</b>	1050	<b>18470</b>	1300
Average		919		923		919		924
Stdev		72		308		88		110
Coeff of var		8 %		33 %		10 %		12 %

Test 11: Alumina + Fluoride / Cycle 8								
Dump nr.	Accumulated	Dump weight	Accumulated	Dump weight	Accumulated	Dump weight	Accumulated	Dump weight
	Feeder 1 / Cycle 6	Feeder 1 / Cycle 6	Feeder 2 / Cycle 6	Feeder 2 / Cycle 6	Feeder 3 / Cycle 6	Feeder 3 / Cycle 6	Feeder 4 / Cycle 6	Feeder 4 / Cycle 6
1	1090	1090	750	750	760	760	810	810
2	1760	670	1680	930	1590	830	1700	890
3	2640	880	2610	930	2410	820	2565	865
4	3520	880	3490	<b>880</b>	3230	820	3430	865
5	4440	920	4310	820	4080	850	4250	820
6	5390	950	5150	840	5020	<b>940</b>	5110	<b>860</b>
7	6260	870	6000	850	5930	910	5930	820
8	7220	960	6880	880	6770	840	6820	890
9	8100	880	7720	840	7590	820	7700	880
10	9040	940	8580	860	8400	810	8580	880
11	9920	880	9620	1040	9210	810	9430	850
12	10770	850	10510	890	10070	860	10280	850
13	11700	930	11360	850	10940	870	11150	870
14	12770	1070	12240	880	11830	890	12000	850
15	13740	970	13110	870	12740	910	12870	870
16	14800	1060	14000	890	13710	970	13780	910
17	15860	<b>1060</b>	14880	880	14760	1050	14770	990
18	16880	1020	15840	960	15960	1200	15900	1130
19	17600	720	16750	910	16980	1020	16950	1050
20	<b>18470</b>	870	<b>18350</b>	1600	<b>18260</b>	1280	<b>18330</b>	1380
Average		924		918		913		917
Stdev		109		171		134		135
Coeff of var		12 %		19 %		15 %		15 %

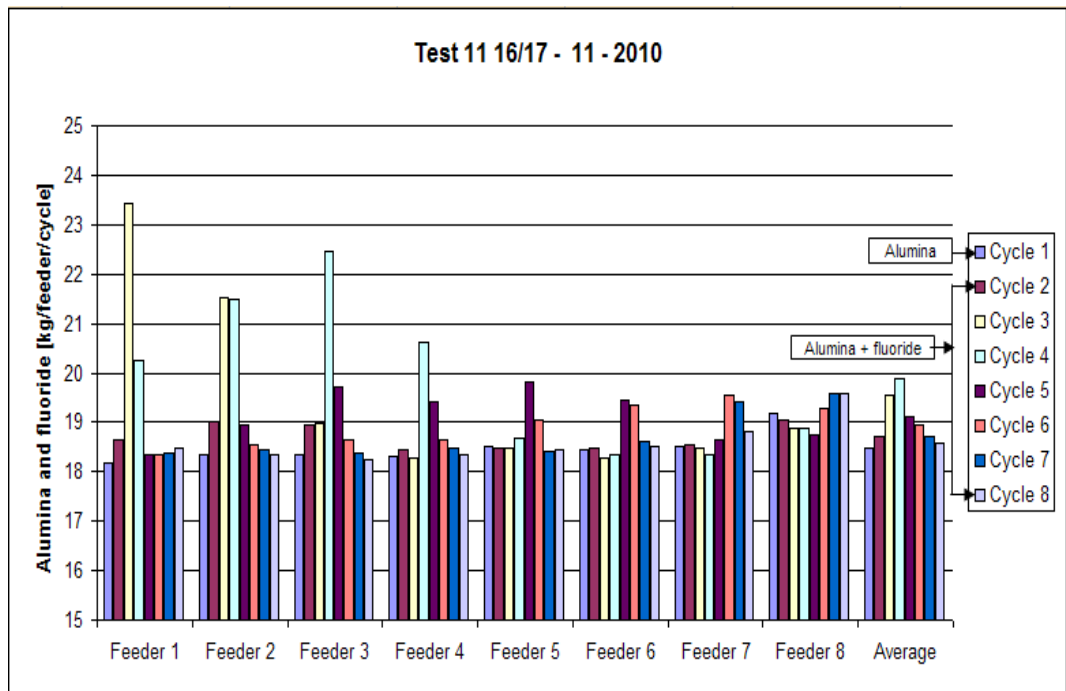


Figure 275 Alumina and fluoride distribution from feeder 1 to 8.

Table 107 Test 12: Open valve for refilling of alumina from the silo. Alumina and fluoride mass balance: [kg] / feeder / cycle.

Test 12								
	Cycle 1	Cycle 2	Cycle 3	Cycle 4	Cycle 5	Cycle 6	Cycle 7	Cycle 8
Feeder 1	18 810	19420	21700	22380	21960	20200	18240	18370
Feeder 2	18130	19160	20280	20500	20850	20920	18990	18100
Feeder 3	18500	19580	19540	19620	20190	20630	19150	18190
Feeder 4	18600	19410	18870	18680	18630	18830	19320	18430
Feeder 5	18590	20210	19010	18510	18540	18490	19990	18990
Feeder 6	18570	19310	18720	18820	18410	18520	18540	19140
Feeder 7	18790	18870	18830	18700	18490	18400	18750	19180
Feeder 8	19080	19110	19230	18810	18920	18900	18630	18380
Average [g]	18 634	19 384	19 523	19 503	19 499	19 361	18 951	18 598
Stdev	276	400	1015	1338	1340	1044	544	436
Coeff of var [kg]	1 %	2 %	5 %	7 %	7 %	5 %	3 %	2 %
Sum	149	155	156	156	156	155	152	149

**Table 108 Test 12: Open valve for refilling of alumina from the silo. Alumina and fluoride accumulated and individual dump weights: [grams] / feeder / cycle. Cycle 1 only alumina, cycle 2 to 8 alumina mixed with fluoride.**

Test 12: Alumina / Cycle 1								
Dump nr.	Accumulated	Dump weight	Accumulated	Dump weight	Accumulated	Dump weight	Accumulated	Dump weight
	Feeder 1 / Cycle 1	Feeder 1 / Cycle 1	Feeder 2 / Cycle 1	Feeder 2 / Cycle 1	Feeder 3 / Cycle 1	Feeder 3 / Cycle 1	Feeder 4 / Cycle 1	Feeder 4 / Cycle 1
1	840	840	710	710	1080	1080	770	770
2	1760	920	1540	830	1540	460	1700	930
3	2620	860	2340	800	2340	800	2540	840
4	3600	<b>980</b>	3170	830	3110	770	3450	910
5	4520	920	3940	770	3910	800	4340	890
6	5840	1320	4890	<b>950</b>	4680	770	5190	850
7	6810	970	5330	440	5470	790	6090	900
8	7750	940	6190	860	6410	<b>940</b>	6990	900
9	8710	960	7080	890	7250	840	7890	900
10	9570	860	7910	830	7970	720	8860	<b>970</b>
11	10420	850	8790	880	8710	740	9740	880
12	11350	930	9620	830	9460	750	10600	860
13	12290	940	10390	770	10270	810	11440	840
14	13200	910	11200	810	11020	750	12310	870
15	14110	910	12070	870	11830	810	13150	840
16	15090	980	12960	890	12680	850	14020	870
17	16180	1090	13830	870	13550	870	15010	990
18	17260	1080	14780	950	14420	870	16080	1070
19	18110	850	15680	900	15220	800	17020	940
20	<b>18810</b>	700	<b>18130</b>	2450	<b>18500</b>	3280	18600	1580
Average		941		907		925		930
Stdev		124		379		566		166
Coeff of var		13 %		42 %		61 %		18 %

Test 12: Alumina + Fluoride / Cycle 2								
Dump nr.	Accumulated	Dump weight	Accumulated	Dump weight	Accumulated	Dump weight	Accumulated	Dump weight
	Feeder 1 / Cycle 2	Feeder 1 / Cycle 2	Feeder 2 / Cycle 2	Feeder 2 / Cycle 2	Feeder 3 / Cycle 2	Feeder 3 / Cycle 2	Feeder 4 / Cycle 2	Feeder 4 / Cycle 2
1	970	970	1000	1000	1200	1200	1230	1230
2	1900	930	1800	800	2160	960	2100	870
3	2840	940	2700	900	3090	930	3050	950
4	3820	980	3570	870	3980	890	4030	980
5	4780	960	4460	890	4880	900	5000	970
6	6080	<b>1300</b>	5420	960	5770	890	5970	970
7	7040	960	6340	920	6690	920	6860	890
8	7950	910	7500	<b>1160</b>	7600	910	7730	870
9	8880	930	8410	910	8480	880	8640	910
10	9880	1000	9340	930	9540	<b>1060</b>	9570	930
11	10780	900	10210	870	10420	880	10480	910
12	11690	910	11130	920	11290	870	11570	<b>1090</b>
13	12670	980	12050	920	12130	840	12470	900
14	13610	940	12930	880	13010	880	13360	890
15	14540	930	13950	1020	13940	930	14380	1020
16	15470	930	15000	1050	14820	880	15360	980
17	16590	1120	16070	1070	15750	930	16400	1040
18	17720	1130	17270	1200	16760	1010	17510	1110
19	18600	880	18170	900	17850	1090	18450	940
20	<b>19420</b>	820	<b>19160</b>	990	<b>19580</b>	1730	<b>19410</b>	960
Average		971		958		979		971
Stdev		105		101		197		91
Coeff of var		11 %		11 %		20 %		9 %

Test 12: Alumina + Fluoride / Cycle 3								
Dump nr.	Accumulated	Dump weight	Accumulated	Dump weight	Accumulated	Dump weight	Accumulated	Dump weight
	Feeder 1 / Cycle 3	Feeder 1 / Cycle 3	Feeder 2 / Cycle 3	Feeder 2 / Cycle 3	Feeder 3 / Cycle 3	Feeder 3 / Cycle 3	Feeder 4 / Cycle 3	Feeder 4 / Cycle 3
1	1060	1060	910	910	970	970	1030	1030
2	2360	1300	1750	840	1810	840	1840	810
3	3980	1620	2640	890	2720	910	2740	900
4	5420	1440	3560	920	3670	950	3630	890
5	6750	1330	4490	930	4620	950	4530	900
6	8070	1320	5490	1000	5510	890	5410	880
7	9330	1260	6500	1010	6440	930	6300	890
8	10410	<b>1080</b>	7430	930	7490	1050	7170	870
9	11630	1220	8360	930	8370	880	8030	860
10	12890	1260	9710	<b>1350</b>	9250	880	8880	850
11	14150	1260	10660	950	10160	910	9750	870
12	15310	1160	11620	960	11320	<b>1160</b>	10650	<b>900</b>
13	16550	1240	12540	920	12260	940	11540	890
14	17900	1350	13430	890	13200	940	12560	1020
15	19260	1360	14410	980	14240	1040	13460	900
16	20360	1100	15400	990	15310	1070	14440	980
17	21020	660	16400	1000	16450	1140	15530	1090
18	21290	270	17450	1050	17590	1140	16700	1170
19	21650	360	18560	1110	18560	970	17710	1010
20	<b>21700</b>	50	<b>20280</b>	1720	<b>19540</b>	980	<b>18870</b>	1160
Average		1085		1014		977		944
Stdev		417		198		93		103
Coeff of var		38 %		19 %		10 %		11 %



Test 12: Alumina + Fluoride / Cycle 4								
Dump nr.	Accumulated	Dump weight	Accumulated	Dump weight	Accumulated	Dump weight	Accumulated	Dump weight
	Feeder 1 / Cycle 4	Feeder 1 / Cycle 4	Feeder 2 / Cycle 4	Feeder 2 / Cycle 4	Feeder 3 / Cycle 4	Feeder 3 / Cycle 4	Feeder 4 / Cycle 4	Feeder 4 / Cycle 4
1	1080	1080	960	960	940	940	1020	1020
2	2320	1240	1970	1010	1840	900	1910	890
3	3560	1240	3000	1030	2740	900	2850	940
4	4790	1230	4020	1020	3720	980	3860	1010
5	6020	1230	5000	980	4640	920	4810	950
6	7290	1270	6040	1040	5600	960	5760	950
7	8540	1250	7110	1070	6580	980	6700	940
8	9810	1270	8060	950	7550	970	7640	940
9	11030	1220	9100	1040	8530	980	8570	930
10	12300	<b>1270</b>	10110	1010	9490	960	9520	950
11	12540	240	11160	1050	10490	1000	10470	950
12	14870	2330	12260	<b>1100</b>	11450	960	11430	960
13	16110	1240	13200	940	12390	940	12370	940
14	17500	1390	14220	1020	13660	<b>1270</b>	13330	960
15	18980	1480	15280	1060	14680	1020	14350	1020
16	20390	1410	16340	1060	15760	1080	15460	1110
17	21440	1050	17520	1180	16890	1130	16600	1140
18	22000	560	18730	1210	18000	1110	17580	980
19	22170	170	19660	930	18920	920	18270	690
20	<b>22380</b>	210	<b>20500</b>	840	<b>19620</b>	700	<b>18680</b>	410
Average		1119		1025		981		934
Stdev		499		83		112		151
Coeff of var		45 %		8 %		11 %		16 %

Test 12: Alumina + Fluoride / Cycle 5								
Dump nr.	Accumulated	Dump weight	Accumulated	Dump weight	Accumulated	Dump weight	Accumulated	Dump weight
	Feeder 1 / Cycle 5	Feeder 1 / Cycle 5	Feeder 2 / Cycle 5	Feeder 2 / Cycle 5	Feeder 3 / Cycle 5	Feeder 3 / Cycle 5	Feeder 4 / Cycle 5	Feeder 4 / Cycle 5
1	1100	1100	1010	1010	900	900	1040	1040
2	2300	1200	2240	1230	1880	980	2060	1020
3	3640	1340	3360	1120	2890	1010	2960	900
4	5000	1360	4450	1090	3900	1010	3840	880
5	6290	1290	5520	1070	4890	990	4790	950
6	7640	1350	6650	1130	6000	1110	5780	990
7	8960	1320	7720	1070	7160	1160	6680	900
8	10260	1300	8750	1030	8170	1010	7510	830
9	11590	1330	9820	1070	9190	1020	8430	920
10	12860	1270	10900	1080	10170	980	9410	980
11	14080	1220	11950	1050	11190	1020	10290	880
12	15350	<b>1270</b>	12970	1020	12200	1010	11260	970
13	16640	1290	14030	1060	13160	960	12140	880
14	17970	1330	15050	<b>1020</b>	14150	990	13060	920
15	19440	1470	16160	1110	15270	1120	13990	930
16	20660	1220	17260	1100	16180	<b>910</b>	14980	990
17	21510	850	18530	1270	17330	1150	16180	<b>1200</b>
18	21850	340	19630	1100	18260	930	17190	1010
19	21950	100	20390	760	18780	520	18010	820
20	<b>21960</b>	10	<b>20850</b>	460	<b>20190</b>	1410	<b>18630</b>	620
Average		1098		1043		1010		932
Stdev		430		168		162		112
Coeff of var		39 %		16 %		16 %		12 %

Test 12: Alumina + Fluoride / Cycle 6								
Dump nr.	Accumulated	Dump weight	Accumulated	Dump weight	Accumulated	Dump weight	Accumulated	Dump weight
	Feeder 1 / Cycle 6	Feeder 1 / Cycle 6	Feeder 2 / Cycle 6	Feeder 2 / Cycle 6	Feeder 3 / Cycle 6	Feeder 3 / Cycle 6	Feeder 4 / Cycle 6	Feeder 4 / Cycle 6
1	1150	1150	1000	1000	1020	1020	940	940
2	2370	1220	2160	1160	2200	1180	1880	940
3	3430	1060	3340	1180	3430	1230	2840	960
4	4440	1010	4480	1140	4640	1210	3730	890
5	5510	1070	5610	1130	5840	1200	4700	970
6	6580	1070	6750	1140	6950	1110	5660	960
7	7590	1010	7910	1160	8130	1180	6590	930
8	8610	1020	9070	1160	9250	1120	7520	930
9	9610	1000	10190	1120	10370	1120	8490	970
10	10610	1000	11350	1160	11510	1140	9460	970
11	11600	990	12460	1110	12630	1120	10380	920
12	12560	960	13540	1080	13720	1090	11360	980
13	13620	1060	14680	1140	14870	1150	12310	950
14	14920	<b>1300</b>	15780	1100	16080	1210	13250	940
15	16210	1290	16950	1170	17280	1200	14280	1030
16	17650	1440	17920	<b>970</b>	18460	1180	15370	1090
17	18960	1310	19170	1250	19390	<b>930</b>	16520	1150
18	19830	870	20160	990	20230	840	17580	1060
19	20170	340	20790	630	20630	400	18380	800
20	<b>20200</b>	30	<b>20920</b>	130	<b>20630</b>	0	<b>18830</b>	450
Average		1010		1046		1032		942
Stdev		320		251		307		137
Coeff of var		32 %		24 %		30 %		15 %

Test 12: Alumina + Fluoride / Cycle 7								
Dump nr.	Accumulated	Dump weight	Accumulated	Dump weight	Accumulated	Dump weight	Accumulated	Dump weight
	Feeder 1 / Cycle 6	Feeder 1 / Cycle 6	Feeder 2 / Cycle 6	Feeder 2 / Cycle 6	Feeder 3 / Cycle 6	Feeder 3 / Cycle 6	Feeder 4 / Cycle 6	Feeder 4 / Cycle 6
1	840	840	950	950	930	930	870	870
2	1880	1040	1930	980	1920	990	1870	1000
3	2870	990	2890	960	2870	950	2870	1000
4	3880	1010	3800	910	3780	<b>910</b>	3830	960
5	4860	980	4700	900	4720	940	4800	970
6	5830	970	5570	870	5590	870	5770	<b>970</b>
7	6850	1020	6490	920	6460	870	6800	1030
8	7830	980	7350	860	7680	1220	7720	920
9	8800	970	8260	910	8830	1150	8700	980
10	9790	990	9220	960	9710	880	9670	970
11	10790	1000	10100	880	10680	970	10620	950
12	11790	1000	10960	860	11650	970	11570	950
13	12820	1030	11870	910	12580	930	12500	930
14	13920	1100	12810	940	13510	930	13460	960
15	15260	1340	13720	910	14450	940	14500	1040
16	16210	<b>950</b>	14700	980	15500	1050	15560	1060
17	17240	1030	15700	<b>1000</b>	16700	1200	16810	1250
18	17870	630	16960	1260	17850	1150	17930	1120
19	18090	220	18010	1050	18690	840	18750	820
20	<b>18240</b>	150	<b>18990</b>	980	<b>19150</b>	460	<b>19320</b>	570
Average		912		950		958		966
Stdev		278		89		162		129
Coeff of var		31 %		9 %		17 %		13 %

Test 12: Alumina + Fluoride / Cycle 8								
Dump nr.	Accumulated	Dump weight	Accumulated	Dump weight	Accumulated	Dump weight	Accumulated	Dump weight
	Feeder 1 / Cycle 6	Feeder 1 / Cycle 6	Feeder 2 / Cycle 6	Feeder 2 / Cycle 6	Feeder 3 / Cycle 6	Feeder 3 / Cycle 6	Feeder 4 / Cycle 6	Feeder 4 / Cycle 6
1	760	760	850	850	820	820	840	840
2	1730	970	2040	1190	1770	950	1840	1000
3	2780	1050	2990	950	2730	960	2790	950
4	3770	990	3820	<b>830</b>	3780	1050	3730	940
5	4790	1020	4830	1010	4820	1040	4730	1000
6	5810	1020	5790	960	5710	<b>890</b>	5680	950
7	6840	1030	6770	980	6620	910	6640	960
8	7870	1030	7720	950	7530	910	7560	920
9	8820	950	8720	1000	8490	960	8480	<b>920</b>
10	9820	1000	9620	900	9440	950	9460	980
11	10810	990	10520	900	10400	960	10370	910
12	11810	1000	11480	960	11370	970	11420	1050
13	12850	1040	12470	990	12390	1020	12330	910
14	13890	1040	13490	1020	13410	1020	13320	990
15	15060	1170	14570	1080	14540	1130	14360	1040
16	16210	1150	15630	1060	15740	1200	15420	1060
17	17140	930	16650	1020	16810	1070	16500	1080
18	18080	<b>940</b>	17470	820	17630	820	17480	980
19	18310	230	17920	450	18040	410	18180	700
20	<b>18370</b>	60	<b>18100</b>	180	<b>18190</b>	150	<b>18430</b>	250
Average		919		905		910		922
Stdev		278		224		238		179
Coeff of var		30 %		25 %		26 %		19 %

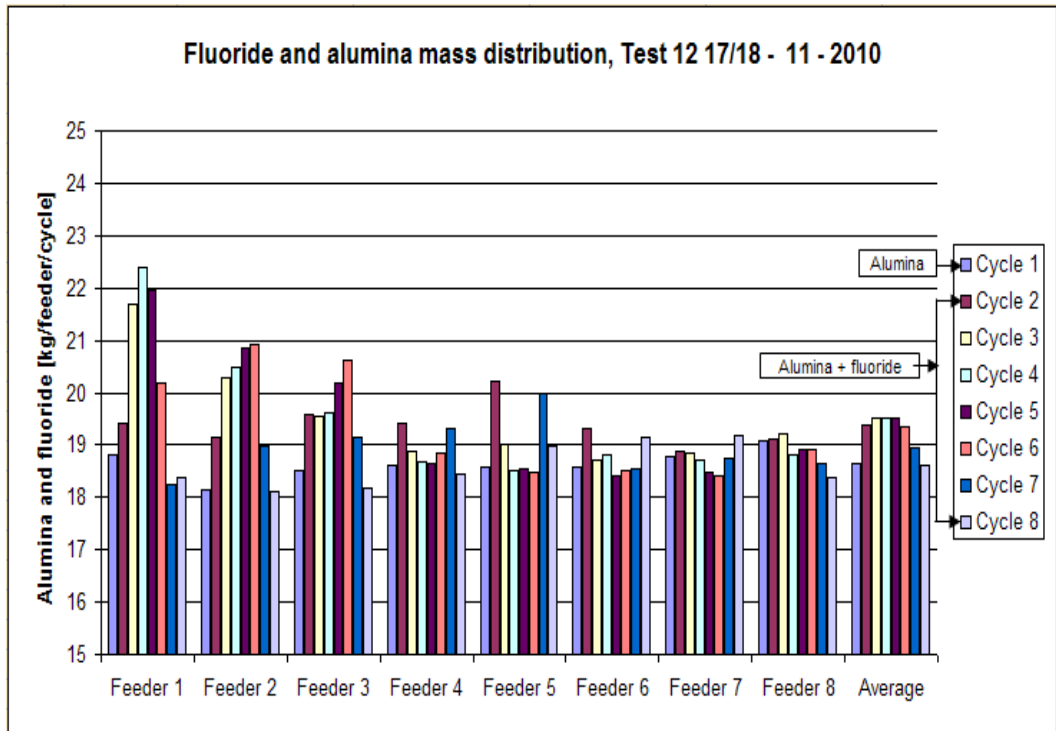


Figure 276 Alumina and fluoride distribution from feeder 1 to 8.

**Recommendations for further rheometry work: experimental procedure**

Much of the work planned for this fluidization rig has not been conducted in this project. The work has potential in better understanding the fluidization behaviour of powders and binary mixtures, and is planned to be conducted as a separate project. Four two – flat – bladed spindles at two lengths: 465 and 185 mm with two different geometries of the spindles in each length: 60 mm (length) and 13 mm (width) and 40 mm (length) and 8 mm (width) are available for further measurements measurements. Cylindrical ones at the same lengths of spindles have been ordered from Brookfield.

## APPENDIX G FURTHER WORK RHEOMETRY

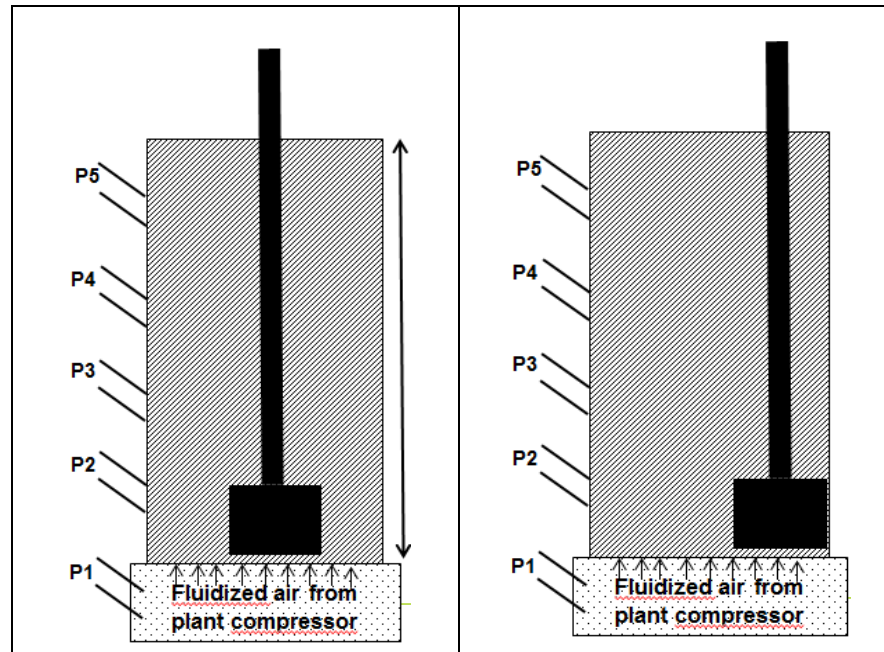


Figure 277 Position of the spindle a) bottom - middle of the column b) bottom – wall.

The experimental procedure to be used is as follows: for given flow rates, spindle lengths and geometry and three ranges of immersion of the spindle into the fluidized bed, place the spindle in the middle of the column and at the wall, as shown in Figure 277, Figure 278, and Figure 279 . Record pressure drops and torque readings taken at different rotational speeds of the spindle and for different bed heights.

Make plots of experimentally measured:

### Torque data

- 5 tests: shear stress at the wall as a function of the rotational speed; curves at different air velocities to be plotted in the same graph;
- 5 tests: shear stress at the bottom as a function of the rotational speed; curves at different air velocities to be plotted in the same graph;
- 5 tests: shear stress at the wall as a function of the rotational speed; curves at different air velocities to be plotted in the same graph;

### Viscosity data

- 5 tests: viscosity at the wall as a function of air flow rates; curves at different depths (range 0 - 150, 150 - 300, 300 - 450 mm) to be plotted in the same graph;
- 5 tests: viscosity at the bottom as a function of air flow rates; curves at different depths to be plotted in the same graph;

- 5 tests: viscosity at the wall as a function of air flow rates; curves at different depths to be plotted in the same graph;

**Yield stress data**

- 5 tests: yield stress at the wall as a function of air flow rates; curves at different depths (range 0 - 150, 150 - 300, 300 - 450 mm) to be plotted in the same graph;
- 5 tests: yield stress at the bottom as a function of air flow rates; curves at different depths to be plotted in the same graph;
- 5 tests: yield stress at the wall as a function of air flow rates; curves at different depths to be plotted in the same graph;

It is important to record the expansion of the bed for each air flow rate; calculate the bulk density and porosity of the bed, for individual components and binary mixtures.

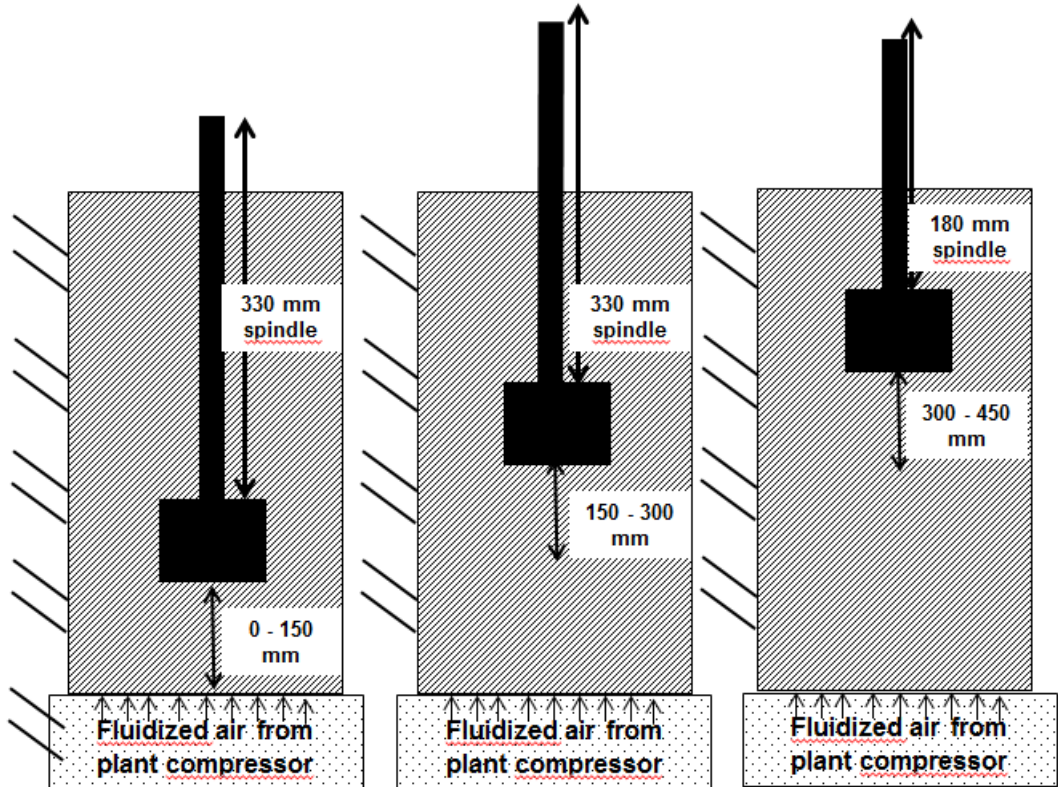


Figure 278 Middle of the column measurements with two spindle lengths: 330 and 180 mm.

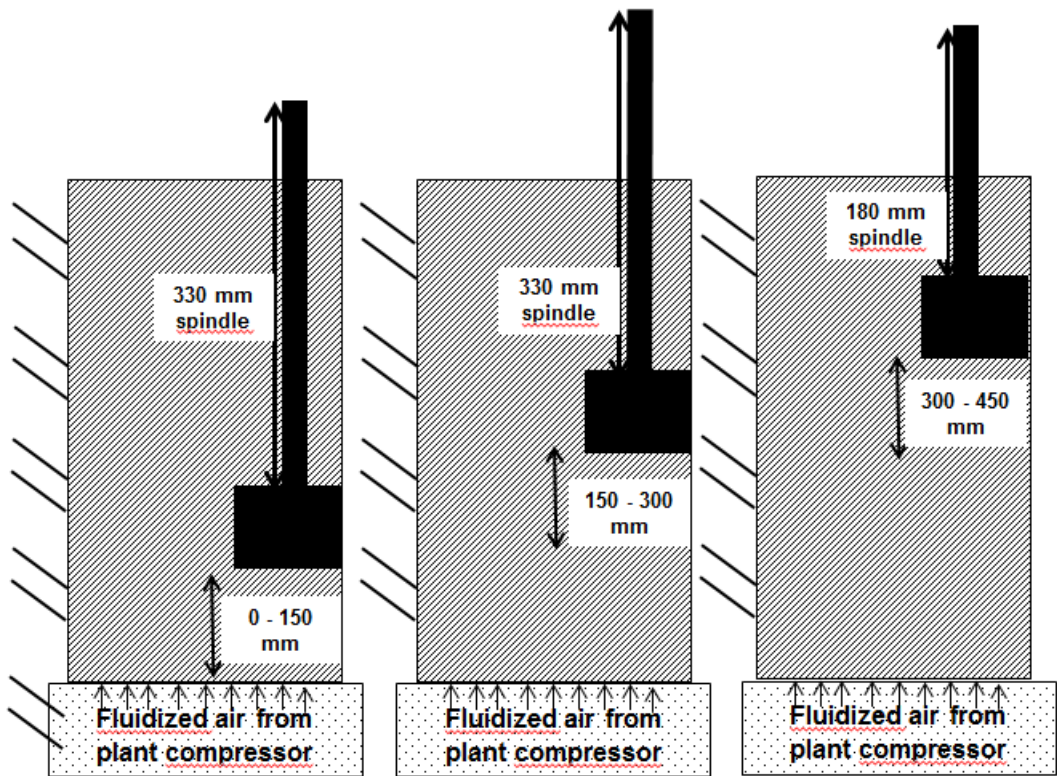


Figure 279 At the wall of the column measurements with two spindle lengths: 330 and 180 mm.